AD_____

Award Number: DAMD17-99-1-9402

TITLE: Training Program in the Molecular Basis of Breast Cancer Research

PRINCIPAL INVESTIGATOR: Wen-Hwa Lee, Ph.D.

CONTRACTING ORGANIZATION: The University of Texas Health Science Center at San Antonio
San Antonio, Texas 78284-7828

REPORT DATE: August 2002

TYPE OF REPORT: Annual Summary

PREPARED FOR: U.S. Army Medical Research and Materiel Command
Fort Detrick, Maryland 21702-5012

DISTRIBUTION STATEMENT: Approved for Public Release;
Distribution Unlimited

REPORT DOCUMENTATION PAGE

Form Approved
OMB No. 074-0188

1. AGENCY USE ONLY (Leave blank)	2. REPORT DATE	3. REPORT TYPE AND DATES COVERED
	August 2002	Annual Summary (1 Aug 2001 - 31 Jul 2002)

4. TITLE AND SUBTITLE
Training Program in the Molecular Basis of Breast Cancer Research

5. FUNDING NUMBERS
DAMD17-01-1-0304

6. AUTHOR(S)
Wen-Hwa Lee, M.D.

7. PERFORMING ORGANIZATION NAME(S) AND ADDRESS(ES)
The University of Texas Health Science Center at San Antonio
San Antonio, Texas 78284-7828

E-Mail: ting@uthscsa.edu

8. PERFORMING ORGANIZATION REPORT NUMBER

9. SPONSORING / MONITORING AGENCY NAME(S) AND ADDRESS(ES)
U.S. Army Medical Research and Materiel Command
Fort Detrick, Maryland 21702-5012

10. SPONSORING / MONITORING AGENCY REPORT NUMBER

11. SUPPLEMENTARY NOTES

12a. DISTRIBUTION / AVAILABILITY STATEMENT
Approved for Public Release; Distribution Unlimited

12b. DISTRIBUTION CODE

13. ABSTRACT (Maximum 200 Words)
The objective of the program is to train highly qualified doctoral students in the genetic, cellular, and molecular basis of Breast Cancer. The training program, conducted within the Molecular Medicine Ph.D. Program, was administered by a select group of faculty whose research projects were intimately involved in breast cancer. An additional goal of the program was to promote synergistic interactions between the various laboratories engaged in breast cancer research. Breast cancer meetings, Molecular Medicine Distinguished Seminar Series were integral parts of the training program for students supported by the Breast Cancer Training Program. The major strengths of the program were the high quality of the Program faculty, and the interactive nature of the Breast Cancer research community in San Antonio. The program faculty encompassed scientists and physicians studying different aspects of breast cancer and cancer therapy, as well as fundamental mechanisms of DNA repair, cell growth and cell differentiation. Key research accomplishments during the 2001-2002 reporting period were: **1)** publication of 14 peer-reviewed articles by students in the program; **2)** DOD BCRP pre-doctoral grants awarded to four students in the program, and a postdoctoral training grant to a fellow in a faculty member's laboratory; **3)** the addition of one new highly qualified faculty; and **4)** six faculty awarded DOD BCRP Idea and/or Career Development grants; **5)** five Ph.D. students supported by the program graduated.

14. SUBJECT TERMS
Breast cancer, research training, cancer therapy, DNA repair and tumor suppressor genes, cell growth regulation and cell differentiation

15. NUMBER OF PAGES
178

16. PRICE CODE

17. SECURITY CLASSIFICATION OF REPORT	18. SECURITY CLASSIFICATION OF THIS PAGE	19. SECURITY CLASSIFICATION OF ABSTRACT	20. LIMITATION OF ABSTRACT
Unclassified	Unclassified	Unclassified	Unlimited

Table of Contents

INTRODUCTION

Brief Description of the Training Program and Its Objectives

The goal of the program is to establish at the University of Texas Health Science Center in San Antonio an in-depth training program in the Molecular Genetics of Breast Cancer. The most important goal of the program is to train highly qualified Ph.D. students in the genetic, cellular, and molecular basis of Breast Cancer. Toward these ends, the program has been extremely successful. Based on the publication record of our trainees, our expectation for significant discoveries is being realized. During the reporting period, students supported by the training program achieved a total of 14 publications relevant to breast cancer.

The training program was conducted within the Molecular Medicine Ph.D. Program by a select group of faculty whose research projects are relevant to breast cancer. An additional goal of the program was to promote synergistic interactions between the various laboratories engaged in breast cancer research. An important meeting was the Annual Breast Cancer Symposium held in San Antonio. All students supported by the program were required to attend. Finally, an outstanding Molecular Medicine Seminar Series sponsored by the Department of Molecular Medicine was also a requirement for all trainees. The following seminars in this series were pertinent to breast cancer:

- **Fall Semester: 2001**

James L. Roberts	"Novel Mechanisms of Regulation of Gonadotropin-Releasing-Hormone" Function"
Thomas A. Kunkel	"Recent Studies of DNA Replication Fidelity"
Jun Qin	"Network Analysis Proteomics"
Myles A. Brown	"Coregulator Dynamics in Steroid Receptor Action"
Lewis A. Chodosh	"Microarray and Transgenic Approaches to Mammary Development and Carcinogenesis"
Thomas Ellenberger	"Structures of a DNA Replication Assembly"
Curtis C. Harris	"p53, Nitric Oxide and Genomic Instability Diseases"
George F. Vande Woude	"Met-HGF/SF: Tumorigenesis & Metastasis"
Wei Yang	"DNA Mismatch Repair: A Tale of Two ATPases"
George N. DeMartino	"Function and Regulation of the Proteasome: Nature's Most Interesting and Complex Protease"
Bik K. Tye	"Coordination of Genome Expression and DNA Replication in Proliferating Cells: The Multiple Roles of the MCM Proteins in Eukaryotes"

Spring Semester: 2002

Nahum Sonenberg	Signaling to Translation Factors in Control of Cell Growth and Proliferation"
Kun Ping Lu	"Pinning Down Proline-Directed Phosphorylation Signaling"
Lynne E. Maquat	"Nonsense-mediated mRNA Decay: Evidence for a Pioneer Round of mRNA Translation"
David Toczynski	"Visualizing the DNA Damage Checkpoint in Yeast"
Karen Vasquez	"DNA Repair Mechanisms are Involved in Triplex-induced Mutagenesis"
Stuart Yuspa	"Interacting Signaling Pathways in the Pathogenesis of Experimental Squamous Cell Cancer"
James L. Maller	"Biochemistry of Cell Cycle Checkpoints at the G2/M and Metaphase/Anaphase Transitions"
Rodney Rothstein	"Formation of DNA Repair & Recombination Centers In Vivo"
Sue Jinks-Robertson	"Mechanisms of Spontaneous Mutagenesis in Yeast"
Michael Liskay	"DNA Mismatch Repair and Cancer"
Zhijian Chen	"Roles of Ubiquitin in NF-KB Signaling"

Breast Cancer Research Programs and Faculty.

One of the major strengths of the program is the high quality of the Program faculty, and the interactive nature of the Breast Cancer research community in San Antonio, which encompass scientists and physicians studying different aspects of breast cancer and cancer therapy, as well as fundamental mechanisms of to maintain genomic stability, cell growth, differentiation and molecular genetics. These faculty groupings are listed below; detailed descriptions of individual research programs were included in the original application.

Breast Cancer Research Training Faculty

W.-H. Lee, Ph.D. (Director)
C. Kent Osborne, M.D. (Co-Director)
Powell H. Brown, M.D., Ph.D.
Peter O'Connell, Ph.D.
Gary M. Clark, Ph.D.
Suzanne Fuqua, Ph.D.
Alan Tomkinson, Ph.D.
E. Lee, Ph.D.
W.-H. Lee, Ph.D.
Z. Dave Sharp, Ph.D.

Patrick Sung, Ph.D.
Greg R. Mundy
Bettie Sue Masters, Ph.D.
Bandana Chatterjee, Ph.D.
Arun K. Roy, Ph.D.
Judy M. Teale, Ph.D.
Peter M. Ravdin, M.D. Ph.D.
Phang-Lang Chen, Ph.D
Renee Yew, Ph.D.
Tom Boyer, Ph.D.
Maria Gazynska, Ph.D.
Paul Hasty, DVM
Jan Vijg, Ph.D.
Tadayoshi Bessho, Ph.D.
Sang Eun Lee, Ph.D.
**Hai Rao, Ph.D., Assistant Professor, Department of Molecular Medicine

** New faculty additions

Relationship between the Breast Cancer Training Program and the Molecular Medicine Graduate Ph.D. Program

The Breast Cancer Training Program was implemented within the context of the Molecular Medicine Graduate Ph.D. Program. The Molecular Medicine Ph.D. Program is an interdisciplinary Ph.D. training program in the Graduate School of Biomedical Sciences at the UTHSCSA. For the academic year 2001-02, there were a total of 42 Ph.D. students enrolled in the Molecular Medicine Program.

The Breast Cancer Training program takes advantage of the internationally recognized breast cancer research programs existing in the institution for many years, and offers a unique opportunity for students interested in starting careers in breast cancer research. The participating scientists in this breast cancer program represent diverse departments including the Divisions of Medical Oncology and Endocrinology in the Department of Medicine, and the Departments of Cellular and Structural Biology, and Biochemistry. In addition, the University of Texas Institute of Biotechnology and the San Antonio Cancer Institute (SACI), an NIH-designated Cancer Center, represent outstanding resources for training opportunities in clinical and basic science research. The national and international reputation of the participating faculty serve to attract a large number of excellent applicants to the breast cancer research track in the Molecular Medicine program.

The rationale for administering the breast cancer training program in the Molecular Medicine Ph.D. program remains based on several important criteria: (1) The Molecular Medicine curriculum is specifically designed to provide basic science training while integrating fundamental principles of molecular biology with modern medicine. A Molecular Medicine Core course provides students with the mechanisms underlying human disease and provides intensive review of specific diseases (including breast cancer) that may serve as models for how human diseases can be studied at the molecular genetic level. (2) The Molecular Medicine program requires the participation of both clinical and basic scientists in the training process. The inclusion of MDs on all student advisory committees insures that every graduate of the program has a clear perspective on the clinical relevance of the basic research in their program that, in most instances, will serve as a guide for the project. (3) The Molecular Medicine program is an interdepartmental, interdisciplinary program that offers flexibility to students in terms of research laboratories, advisors and committee members. This arrangement offers a

real potential for synergism in breast cancer research not possible in traditional department-bound programs. In summary, the Ph.D. program in Molecular Medicine offers a near perfect environment for Ph.D. training in breast cancer and has attracted many well-qualified applicants.

Research Support for Program Faculty

An essential component of maintaining a successful and aggressive training program in Breast Cancer Research is the continued research funding of the individual Program Faculty laboratories. The faculty have been extremely successful in obtaining research funding, including over $15 million in total direct costs for the 2001-2002 reporting period.

Key Research Accomplishments:

Research grants awarded to members of the faculty by the Defense Department's Breast Cancer Research Program (BCRP).

Tom Boyer, Ph.D., Career Development Award

Project Title: Regulation of BRCA1 function by DNA damage-induced site-specific phosphorylation.

Project Period: 05/15/02 - 06/15/06

Project Total: $176,516 Total for entire project

Considerable evidence implicates DNA-damage-induced site-specific phosphorylation of BRCA1 as a critical regulator of its caretaker properties. Dr. Boyer hypothesizes that DNA damage-induced site-specific phosphorylation of BRCA1 regulates its transcription and/or DNA double-strand break repair activities.

Tom Boyer, Ph.D., Idea Award

Project Title: Regulation of BRCA1 function by DNA damage-induced site-specific phosphorylation.

Project Period: 04/01/01 - 03/31/04

Project Total: $414,599 Total for entire project

Considerable evidence implicates DNA-damage-induced site-specific phosphorylation of BRCA1 as a critical regulator of its caretaker properties. Dr. Boyer hypothesizes that DNA damage-induced site-specific phosphorylation of BRCA1 regulates its transcription and/or DNA double-strand break repair activities.

Phang-Lang Chen, Ph.D., Idea Award

Project Title: BRCA2 and the DNA double strand break repair machinery

Project Period: 10/01/99 – 10/31/02 (obtained one-year no cost extension to 10/31/03)

Project Total: $304,500

To understand the cellular function of BRCA2, and to elucidate its role in the development and progression of breast cancer.

Phang-Lang Chen, Ph.D., Idea Award

Project Title: Small chemical molecules disrupt BRCA2 and Rad51 interaction for adjuvant BC

Project Period: 04/01/01 – 05/31/04

Project Total: $433,500

To isolate small molecules which disrupt the interactions between BRCA2 and Rad51 using reverse yeast two-hybrid screening. To evaluate the ability of the identified molecules to sensitize cultured breast cancer cells to the genotoxic and cytotoxic effects of ionizing radiation; and to assess the efficacy of the small molecules as adjuvant.

Maria Gaczynska, Ph.D., Idea Award

Project Title: Molecular characteristics of multicorn, a new large proteolytic assembly and potential anticancer drug target in human breast cancer cells

Project Period: 04/01/01 – 03/31/04

Project Total: $324,056

The goal of this project is to clone and express the gene of human multicorn monomer, study the mechanism controlling the multicorn activity through its oligomerization and phosphorylation, and test molecular characterization of the multicorn at different stages of the cell cycle.

Paul Hasty, DVM, Idea Award

Project Title: Development of anti-cancer therapeutics that modulate the RAD51-BRCA2 complex.

Project Period: 02/15/02 - 02/14/05

Project Total: $436,500

RAD51 is important for repairing double-strand breaks in DNA by recombination; interestingly, this function is likely to be essential since mammalian cells deleted for RAD51 exhibit chromosomal instability, are unable to sustain proliferation and senesce or die. Our specific aims are: characterize antp-26mer for biological activity on tissue culture cells, perform a deletion and substitution analysis on the antp-26mer, and test peptides for potential as anti-cancer therapeutics in mice.

Patrick Sung, Ph.D., Career Development Award

Project Title: Interactions among BRCA1, BRCA2 & components of the recombination machinery

Project Period: 06/01/98 – 05/31/03

Project Total: $200,000

The main goal of this project is to purify BRCA1 and BRCA2 and study their biochemical properties.

Patrick Sung, Ph.D., Idea Award

Project Title: BRCA2 & components of the recombination machinery

Project Period: 06/01/98 – 05/31/03

Project Total: $303,311

The main goal of this project is to purify BRCA1 and BRCA2 and study their biochemical properties.

Renee Yew, Ph.D., Career Development Award

Project Title: The role of BRCA1-dependent ubiquitination in Breast Cancer

Project Period: 06/01/02 - 05/31/04

Project Total: $181,960

Mutational inactivation of the BRCA1 gene accounts for a large percentage of hereditary breast cancer. Although the BRCA1 gene product has been implicated to function in a number of different cellular processes including DNA repair and transcription, it is still unclear how BRCA1 biochemically mediates its cellular function as a tumor suppressor protein. It has been suggested that the BRCA1 gene product functions as an ubiquitin protein ligase or E3 enzyme in a manner similar to a growing number of proteins that comprise a family of ring finger proteins. If this putative E3 activity of BRCA1 can be shown to be a physiological function of full length BRCA1 in the cell, this could greatly aid in determining the molecular mechanisms by which BRCA1 mediates its cellular function.

Renee Yew, Ph.D., Idea Award

Project Title: The role of BRCA1-dependent ubiquitination in Breast Cancer

Project Period: 04/01/01 - 03/31/04

Project Total: $411,006

Mutational inactivation of the BRCA1 gene accounts for a large percentage of hereditary breast cancer. Although the BRCA1 gene product has been implicated to function in a number of different cellular processes including DNA repair and transcription, it is still unclear how BRCA1 biochemically mediates its cellular function as a tumor suppressor protein. It has been suggested that the BRCA1 gene product functions as an ubiquitin protein ligase or E3 enzyme in a manner similar to a growing number of proteins that comprise a family of ring finger

proteins. If this putative E3 activity of BRCA1 can be shown to be a physiological function of full length BRCA1 in the cell, this could greatly aid in determining the molecular mechanisms by which BRCA1 mediates its cellular function.

Postdoctoral Breast Cancer Research Awards to Supported Trainees

Postdoctoral training grants awarded to current postdoctoral fellows by the Defense Department's Breast Cancer Research Program (BCRP):

Qing Gao, Ph.D., Postdoctoral Traineeship Award
(Fellow in the laboratory of Dr. Wen-Hwa Lee)

Project Title: Involvement of BRCA2 BRC repeats in RAD51 mediated DNA repair

Project Period: 12/01/00 – 11/30/03 (obtained one-year no cost extension to 11/30/04)

Project Total: $141,330

To test the importance of BRC repeats in BRCA2 for binding to RAD51 in response to DNA damage. To determine the critical residues in the BC repeats of BRCA2 and the significance of these residues for BRCA2/RAD51 interactions. To determine if BRCA2, through BRC repeats, directly affects DNA repair mechanisms mediated by RAD51; and to test small BRC repeat peptides in vivo for their ability to overcome tumor resistance to DNA damaging agents.

Predoctoral Breast Cancer Research Awards to Supported Trainees

Predoctoral training grants awarded to current trainees by the Defense Department's Breast Cancer Research Program (BCRP):

Karen Block, training in Dr. Renee Yew's laboratory.

Project Title: The role of Ubiquitin-Mediated Proteolysis of cyclin D in Breast Cancer

Project Period: 04/01/02-3/31/04

Project Total: $65,636

Recent studies have indicated that cyclin D protein levels are modulated post-transcriptionally by the ubiquitin-mediated protein degradation pathway. The specific E2 and E3 enzymes postulated to target cyclin D for ubiquitination are the ubiquitin conjugating enzyme, CDC34, and the ubiquitin protein ligase called SCF (Skp1, cullin, F-box, ring protiein). We will define and characterize how the regulation of CDC34-SCF activity modulates cyclin D proteolysis during the normal cell cycle and in breast cancer cells.

Sean Post, training in Dr. E. Lee's laboratory.

Project Title: Phosphorylation of hRad17 by ATR is required for cell cycle checkpoint activation

Project Period: 04/01/02 - 03/31/04

Total Award: $61,342

The goal of this study is to determine the relationship between ATR, hRad17, Chk2, and BRCA1 and demonstrate how these potential protein networks regulate checkpoint activation. Based on the reuqirement of SpRad3 and SpRad17 for checkpoint activation through SpCds1 in fission yeast and the ability of Chk2 to phosphorylate BRCA2 Ser988 in humans, it is my hypothesis that ATR mediated phosphorylation of hRad17 is required to activate cell cycle checkpoints, through Chk2 and BRCA1.

Stefan Sigurdsson, training in Dr. Patrick Sung's laboratory.

Project Title: Functions of Human Rad51 and Other Recombination Factors In DNA Double-Strand Break Repair.

Project Period: 06/01/01 - 05/31/04

Total Award: $66,000

Homologous recombination and recombinational repair of DNA double-strand breaks are mediated by proteins of the *RAD52* epistasis group. Rad51 is a key factor in these processes and the protein can assemble on ssDNA substrates to form a nucleoprotein filament. With the help from other factors, the Rad51-ssDNA nucleoprotein filament searches for a DNA homlog and catalyzes formation of a heteroduplex DNA joint with the homolog. The biochemical reaction that forms heteroduplex DNA joints is called □homologous DNA pairing and strand exchange. A number of Rad51-like proteins are known in human cells, but their function in recombination and DNA repair is currently unknown. I have shown that two of these Rad51-like proteins, Rad51B and Rad51C, are associated in a stable heterodimer. I will further define the homologous DNA pairing and strand exchange activity of human Rad51. In addition, a variety of experiments will be conducted to test the hypothesis that the Rad51B-Rad51C complex promotes the assembly of the Rad51-ssDNA nucleoprotein filament and enhances the efficiency of Rad51-mediate d homologous DNA pairing and strand exchange. The information garnered from this study should contribute significantly to our understanding of how DNA double-strand breaks are repaired in human cells.

Stephen Van Komen, training in Dr. Patrick Sung's laboratory.

Project Title: Functional interactions of HRAD54 with the RAD51 recombinase

Project Period: 04/01/01 - 03/31/03

Total Award: $65,173

Homologous recombination is essential for the accurate repair of DNA double-strand breaks. Products of the BRCA1 and BRCA2 breast and ovarian susceptibility genes have recently been shown to associate with key members of the recombinational machinery including the Rad51 recombinase. Rad51 is homologous to the bacterial homologous DNA pairing and strand exchange enzyme, RecA. Unlike RecA, yeast Rad51 has little ability to promote pairing between homologous linear ssDNA and covalently closed duplex to form an important recombination intermediate known as a D-loop. Importantly, yeast Rad54, another recombination factor, promotes robust D-loop formation by Rad51. Recently, I have shown that yeast Rad54 uses the free energy from ATP hydrolysis to remodel DNA structure in a fashion that generates both

positively and negatively supercoiled domains in the DNA template, and that DNA supercoiling by Rad54 is important for the D-loop reaction. Given the conservation between yeast and human recombination factors, I hypothesize that human Rad54 supercoils DNA and promotes D-loop formation with human Rad51 in a similar manner. Using highly purified human Rad51 and Rad54 proteins, I will study the functional interactions between these two factors in D-loop formation and in supercoiling DNA. The results from these studies will be important for understanding the human recombinational machinery and may provide a system for dissecting the role of BRCA1, BRCA2, and other tumor suppressors in recombination and DNA double-strand break repair.

Graduates During the Reporting Period (A description of supported student's research and future plans is below)

Ling Chen, Ph.D.
David Levin, Ph.D.
Ernesto Salcedo, Ph.D.
Jill Gilroy, Ph.D.
Kelly Trujillo, Ph.D.

Reportable Outcomes

Supported Trainees, Research Description and Publications

The following outstanding group of trainees was supported on the Breast Cancer Training Program during the final reporting period.

Reporting Period 8/1/01 – 7/31/02

1. Sean Post – 5th year, supported August 1-31, 2001, or 1 month. Mr. Post received a DOD BCRP predoctoral fellowship from which he is currently supported.
2. Teresa Motycka – 5th year
3. Deanna Jansen – 3rd year, supported August 1-31 or for one month prior to her withdrawal from the program (See below and previous year's report).
4. Horng-Ru Lin – 4th year
5. Song Zhao – 6th year
6. Guikai Wu – 5th year
7. Xianzhi Jiang – 3rd year, supported from 09/01/01 to 07/31/02, or 11 months.
8. Yi-Tzu Lin – 3rd year, supported from 09/01/01 to 07/31/02, or 11 months.
9. Chang-Ching Liu – 4th year, supported 08/01/01 to 05/31/02, or 10 months.
10. Wei Tan – 4th year, supported from 09/01/01 to 07/31/02, or 11 months.
11. Ahmad Utomo – 8th year.
12. Sangeetha Vijayakumar – 4th year, supported from 03/01/02 to 07/31/02, or 5 months.

The accomplishments of these students and their mentors are outstanding examples of how small investments in student training can be amplified in programs grounded in excellence.

The 2001-2002 academic year marks the ninth full year of operation for the Molecular Medicine Ph.D. Program, and is the seventh year for the Training Program in the Molecular Basis of Breast Cancer Research. The availability of highly qualified applicants to the Molecular

Medicine Program was excellent. Overall, 55 applications were received for admission to the Fall 2001 entering class. Fourteen new students began classes in August of 2001. The total number of students at the start of the Fall semester 2001 in the Molecular Medicine Ph.D. Program at all levels was 42, which includes 22 women, and 1 underrepresented minority.

Project Summaries and Publications of Ph.D. Trainees (past and present supported by the currently active grant)

Note that the Program Director's comments regarding each student's research are in italics below each description.

David Levin ***Mentor -- Dr. Alan Tomkinson***

DNA joining events are required to maintain the integrity of the genome. Three human genes encoding DNA ligases have been identified. David is identifying the cellular functions involving the product of the LIG1 gene. Previous studies have implicated DNA ligase I in DNA replication and some pathways of DNA repair. During DNA replication, DNA ligase I presumably functions to join Okazaki fragments. However, under physiological salt conditions, DNA ligase I does not interact with DNA. It is Mr. Levin's working hypothesis that DNA ligase I involvement in different DNA metabolic pathways is mediated by specific protein-protein interactions which serve to recruit DNA ligase I to the DNA substrate. To detect proteins that bind to DNA ligase I, David has fractionated a HeLa nuclear extract by DNA ligase I affinity chromatography. PCNA was specifically retained by the DNA ligase I matrix. To confirm that DNA ligase I and PCNA interact directly, Mr. Levin found that in vitro translated and purified recombinant PCNA bind to the DNA ligase I matrix. In similar experiments, he has shown that DNA ligase I interacts with a GST (glutathione S transferase)-PCNA fusion protein but not with GST. Using in vitro translated deleted versions of DNA ligase I, Mr. Levin determined that the amino terminal 120 residues of this polypeptide are required for the interaction with PCNA. During DNA replication PCNA acts as a homotrimer that encircles DNA and tethers the DNA polymerase to its template. He showed that DNA ligase I forms a stable complex with PCNA that is topologically linked to a DNA duplex. Thus, it appears that PCNA can also tether DNA ligase I to its DNA substrate. A manuscript describing these studies has been published
in the Proc. Natl. Acad. Sci. U.S.A.

In addition to interacting with PCNA, the amino terminal domain of DNA ligase I also mediates the localization of this enzyme to replication foci. To determine whether these are separable functions David fine mapped the region that interacts with PCNA and, in collaboration with Dr. Montecucco's group, the region required for recruitment to replication foci. Since the same 19 amino acids are necessary and sufficient for both functions and the same changes in amino acid sequence inactivate both functions, we conclude that DNA ligase I is recruited to replication foci by its interaction with PCNA. A manuscript describing these studies has been published in the EMBO Journal.

In recent studies, Mr. Levin has a constructed a mutant version of DNA ligase I that does not interact with PCNA. Importantly the amino acid substitutions do not affect the catalytic activity of DNA ligase I. By transfecting cDNAs encoding the mutant and wild type DNA ligase I into a DNA ligase I-mutant cell line, he has demonstrated the biological significance of the DNA ligase I/PCNA interaction in DNA replication and long patch base excision repair.

This project was relevant to breast cancer since problems with DNA replication and repair undoubtedly underlie the genomic instability associated with tumor formation.

Dr. Levin earned his Ph.D. in Molecular Medicine in the summer of 2000, and is currently a staff scientist at GeneTex, Inc., in San Antonio, Texas.

- ***John Leppard*** ***Mentor -- Alan Tomkinson***

Three genes, *LIG1*, *LIG3* and *LIG4*, encoding DNA ligases have been identified in the mammalian genome. Unlike the *LIG1* and *LIG4* genes, there are no homologues of the *LIG3* gene in lower eukaryotes such as yeast. Biochemical and genetic studies suggest that DNA ligase III participates in base excision repair and the repair of DNA single-strand break. A feature of DNA ligase III that distinguishes it from other eukaryotic DNA ligases is a zinc finger. In published studies we have shown that this zinc finger binds preferentially to nicks in duplex DNA and allows DNA ligase III to efficiently ligate nicks at physiological salt concentrations. These studies will be extended by determining how the zinc finger of DNA ligase III binds to DNA single-strand breaks but does not hinder access of the catalytic domain of DNA ligase III to ligatable nicks. Furthermore, we will reconstitute the base excision and single-strand break repair pathways mediated by DNA ligase III and elucidate the functional consequences of interactions between DNA ligase III and other DNA repair proteins such as Xrcc1, DNA polymerase beta and poly (ADP-ribose) polymerase that participate in these repair pathways.

Mr. Leppard's research is relevant to breast cancer since genomic instability is likely to be involved at several stages during the progression to malignant breast cancer. Methods to intervene and stabilize the genome could prevent progression and spread of the disease. In addition, information about DNA repair processes in normal and cancer cells may lead to the development of treatment regimes that more effectively kill cancer cells and minimize damage to normal tissues and cells.

Publications:

Tomkinson AE, Chen L, Dong Z, **Leppard JB**, Levin DS, Mackey ZB, Motycka TA. Completion of base excision repair by mammalian DNA ligases. Prog Nucleic Acid Res Mol Biol. 2001;68:151-64.

- ***Teresa Motycka*** ***Mentor -- Alan Tomkinson***

DNA double-strand break repair is important for maintaining genomic stability. If left unrepaired, these lesions may cause cell death. The cell has evolved two major pathways for dealing with these lesions, nonhomologous end-jo ining and homologous recombination. Nonhomologous end-joining fuses the ends of broken DNA irrespective of the sequence at the site of the break, whereas homologous recombination preserves the sequence at the damaged site by using a sister chromatid as a template to copy the genetic information. Genetic studies in the budding yeast Saccharomyces cerevisiae have identified a number of genes important in this pathway, collectively named the RAD52 epistasis group. Of all of these genes, a del etion in rad52 produces the most severe phenotype. Mammalian homologs of RAD52 have been identified and the biochemical activity of the protein products is conserved from yeast to human. In order to gain further understanding of Rad52 function in higher eukaryotes, Ms. Motycka looked for interacting proteins by affinity chromatography and identified those polypeptides that were specifically bound by the resin. She has shown a direct interaction between XPF, a component of a multifunctional DNA structu re-specific endonuclease, with the N-terminus of hRad52. Complex formation between hRad52 and XPF/ERCC1 concomitantly stimulates the DNA structure-specific endonuclease activity of XPF/ERCC1 and attenuates the DNA strand annealing activity of hRad52. These results are consistent with previous genetic studies and provide a novel role for hRad52 in the modulation of XPF/ERCC1 activity. We are currently

examining the biological significance of a second protein-protein interaction identified in our screen. Hypersensitivity to DNA damage results from the deletion of the respective gene, suggesting we may have identified a novel player in Rad52-dependent DNA repair.

An understanding of the mechanisms of DSB in mammalian cells is relevant to breast cancer because the accumulating evidence linking the products of the breast cancer susceptibility genes, BRCA1 and BRCA2, with DSB repair.

- ***Suh-Chin(Jackie) Lin*** ***Mentor -- Dr. Eva Lee***

The tumor suppressor gene, p53, is frequently mutated in human tumors, including breast carcinoma. P53 null mice develop multiple spontaneous tumors, predominantly lymphoma and sarcoma, within the first 6 months of age. To establish a mouse model of p53-mediated mammary tumor development, Ms. Lin initiated a bigenetic approach employing the cre-loxp system. Through gene targeting in embryonic stem (ES) cells, mice carrying floxed p53 genes in which exons 5 and 6 are flanked by the loxp sequence were generated. A second mouse line carrying a cre transgene under the control of mouse mammary tumor virus LTR (MMTV-cre) has also been generated. Floxed p53 mice were mated with MMTV-cre transgenic mice to produce mice with p53 inactivation in mammary tissue. Indeed, we observed p53 excision in the tissues of double transgenic mice. In addition, adenoviral vectors carrying cre recombinase are being used to inactivate p53. These approaches should provide a mouse mammary tumor model for studies of mammary tumor progression resulting from p53 mutation and for testing therapeutic interventions of mammary tumorigenesis. The resulting mice have demonstrated interesting patterns of tumor development including those of the mammary gland. These animals will be valuable models for testing new approaches to breast cancer treatment and understanding its etiology.

Upon DNA damage, p53 protein becomes phosphorylated and stabilized, leading to subsequent activation of cell cycle checkpoints. It has been shown that ATM is required for IR induced phosphorylation on Ser15 residue of p53. Based on the involvement of p53 in mammary tumorigenesis and on the higher risk of ATM carriers for breast cancer, we have carried out studies to address the cancer susceptibility of ATM heterozygous and ATM null mammary epithelial cells by transplanting mammary gland to wild-type sibling mice. Initial studies have indicated differential checkpoint and apoptotic responses in cells harboring ATM mutation. These studies will establish whether ATM plays important roles in mammary tumorigenesis.

Both of these projects are highly relevant to breast cancer, especially the Ms. Lin's animal models which hold promise in terms of new therapies for breast cancer and its metastases.

Publications:

Skapek SX, **Lin SC**, Jablonski MM, McKeller RN, Tan M, Hu N, Lee EY (2001) Persistent expression of cyclin D1 disrupts normal photoreceptor differentiation and retina development. *Oncogene* **20**:6742-51.

Ms. Lin successfully defended her dissertation on December 18, 2000, and continues as a post-doctoral fellow in Dr. Lee's laboratory extending her work on the development of important animal models for human cancer.

- ***Sean Post*** ***Mentor -- Dr. Eva Lee***

Recent studies indicate that breast cancer susceptibility genes,BRCA1 and BRCA2, are involved in DNA repair. Cells harboring mutations in either gene are hypersensitive to ionizing radiation (IR). Extensive genetic evidence in yeast indicates that DNA double-stranded breaks are processed by Rad50/Mre11 nuclease complex. It has also been shown that in response to IR, Rad50 assembles into nuclear foci. In mammalian cells, such IR-induced Rad50 foci are not observed in cells established from Nijmegen breakage syndrome (NBS). We and others have shown that the protein product of gene mutated in NBS, Nibrin, forms a stable complex with Rad50/Mre11 and the complex possesses nuclear activity. The E. Lee laboratory demonstrated that IR-induced Rad50 redistribution requires ATM kinase activity. Rad50 is phosphorylated upon IR. Their preliminary studies indicate that such IR-induced Rad50 foci formation and phosphorylation are defective in A-T cells. In addition, IR-induced Rad50 foci formation is aberrant in some sporadiac cancers that express normal ATM, Rad50, Mre11, nibrin, BRCA1 and BRCA2 suggesting involvement of additional protein in this DNA damage response.

Mr. Post is a fifth year graduate student who is characterizing IR-induced Rad50 phosphorylation. How phosphorylation affects Rad50 function will be studied. In addition, cross-linking experiments will be carried out to investigate whether there is defective Rad50 protein complex formation in breast cancer cells. These studies will provide insights into the role of ATM kinase cascade in the assembly of double-stranded breakage repair protein. Furthermore, characterization of components in the repair protein complex may lead to the identification of additional players involved in breast carcinoma.

These projects are highly relevant to breast cancer since genomic instability is a hallmark of cancer and is thought to be a major contributor to the tumorigenic process. Mr. Post's research will contribute toward a greater understanding of the mechanisms responsible for maintaining genomic integrity that is undoubtedly involved in breast cancer development and progression.

Mr. Post is scheduled to defend his dissertation research in July of 2003, and is in the process of revising his last paper for publication.

- ***Song Zhao*** ***Mentor -- Dr. Eva Lee***

Mr. Zhao is working on the functional interactions between ATM and DNA repair proteins with a focus on NBS1. Ataxia-telangiectasia (A-T) and Nijmegen breakage syndrome (NBS) are recessive genetic disorders with susceptibility to cancer and similar cellular phenotypes. The protein product of the gene responsible for A-T, designated ATM, is a member of a family of kinases characterized by a carboxy-terminal phosphatidylinositol 3-kinase-like domain. The NBS1 protein is specifically mutated in patients with Nijmegen breakage syndrome and forms a complex with the DNA repair proteins Rad50 and Mrel1. Mr. Song has shown that phosphorylation of NBS1, induced by ionizing radiation, requires catalytically active ATM. Complexes containing ATM and NBS1 exist in vivo in both untreated cells and cells treated with ionizing radiation. He, along with others in the lab, have identified two residues of NBS1, Ser 278 and Ser 343 that are phosphorylated in vitro by ATM and whose modification in vivo is essential for the cellular response to DNA damage. This response includes S-phase checkpoint activation, formation of the NBS1/Mrel1/Rad50 nuclear foci and rescue of hypersensitivity to ionizing radiation. Together, these results demonstrate a biochemical link between cell-cycle checkpoints activated by DNA damage and DNA repair in two genetic diseases with overlapping phenotypes

These projects have clear and compelling relevance to breast cancer since all of the proteins described are vital to the "caretaker" function of the DNA repair and response systems of all

cells, to which mammary cells are especially dependent. Dr. Zhao made significant contributions as a graduate student and will undoubtedly continue this level of contribution as a postdoctoral fellow.

Song Zhao was recently obtained his Ph.D., and is continuing his training as a postdoctoral fellow in Dr. Thomas Kelly's laboratory at the Memorial Sloan Kettering Institute. Dr. Zhao will be working to understand the regulation of DNA replication.

Publications:

Yuan SS, Su JH, Hou MF, Yang FW, **Zhao S**, Lee EY. (2002) Arsenic-induced Mre11 phosphorylation is cell cycle-dependent and defective in NBS cells. DNA Repair (Amst). 1:137-42.

Zhao S, Renthal W, Lee EY. (2002) Functional analysis of FHA and BRCT domains of NBS1 in chromatin association and DNA damage responses. Nucleic Acids Res. 30:4815-22.

Yazdi PT, Wang Y, **Zhao S**, Patel N, Lee EY, Qin J. (2002) SMC1 is a downstream effector in the ATM/NBS1 branch of the human S-phase checkpoint. Genes Dev. 16:571-82.

- ***Shang Li*** ***Mentor -- Dr. Wen-Hwa Lee***

Mutations of the *BRCA1* gene predispose women to the development of breast cancer. The *BRCA1* gene product [BRCA1] is a nuclear phosphoprotein whose cellular function is poorly understood. The C-terminal region of the BRCA1 protein contains an activation domain and two repeats termed BRCT (for BRCA1 C-terminal). In his recent work, Mr. Li identified a BRCT-interacting protein previously identified as CtIP, a protein that interacts with the C-terminal-binding protein (CtBP) of E1A. Together, CtIP and CtBP are postulated to form a transcription corepressor complex. The ability of BRCA1 to transactivate the p21 promoter can be inactivated by mutation of the C-terminal conserved BRCT domains. To explore the mechanisms of this BRCA1 function, the BRCT domains were used as bait in a yeast two-hybrid screen. A known protein, CtIP, a co-repressor with CtBP, was found. CtIP interacts specifically with the BRCT domains of BRCA1, both *in vitro* and *in vivo*, and tumor-derived mutations abolished these interactions. The association of BRCA1 with CtIP was also abrogated in cells treated with DNA-damaging agents including UV, γ-irradiation and adriamycin, a response correlated with BRCA1 phosphorylation. The transactivation of the p21 promoter by BRCA1 was diminished by expression of exogenous CtIP and CtBP. These results suggest that the binding of the BRCT domains of BRCA1 to CtIP/CtBP is critical in mediating transcriptional regulation of p21 in response to DNA damage.

This project was directly relevant to breast cancer since it involves the study of a protein whose function appears to central to the mobilizing the response of cells to DNA damage. Perturbations in the systems that maintain genomic integrity underlie initiation and progression of most cancers, including those of the breast.

Dr. Li defended his dissertation in Fall of 2000. He continues his training as a post doctoral fellow in the laboratory of Dr. Elizabeth Blackburn in the department of biochemistry and biophysics at the UCSF. He is working on a novel cancer therapy involving a mutated telomere RNA template.

- ***Qing Zhong*** ***Mentor -- Dr. Wen-Hwa Lee***

One of Mr. Zhong's project in Dr. Lee's laboratory is a study of the tumor suppressor protein, TSG101. *tsg101* was identified as a tumor susceptibility gene by homozygous function inactivation of allelic loci in mouse 3T3 fibroblasts. To confirm its relevance to breast cancer that was originally reported, antibodies specific for the putative gene product were prepared and used to identify cellular 46 kDa TSG101 protein. A full size 46 kDa TSG101 protein was detected in a panel of 10 breast cancer cell lines and 2 normal breast epithelial cell lines with the same antibodies. A full-length *TSG101* mRNA was also detected using rtPCR. These results indicate that homozygous intragenic deletion of *TSG101* is rare in breast cancer cells. In more recent work, Mr. Zhong demonstrated that TSG101 is a cytoplasmic protein that translocates to the nucleus during S phase of the cell cycle. Interestingly, TSG101 is distributed mainly around the chromosomes during M phase. Microinjection of antibodies selective for TSG101 during G1 or S results in cell cycle arrest and overexpression leads to cell death. These data indicate that neoplastic transformation due to lack of TSG101 could be due to a bypass of cell cycle checkpoints.

Another more recent interest of Mr. Zhong is the role of the breast tumor suppressor BRCA1 in cancer formation. *BRCA1*, encodes a tumor suppressor that is mutated in familial breast and ovarian cancers. Mr. Zhong's work showed that BRCA1 interacts *in vitro* and *in vivo* with human Rad50, which forms a complex with hMre11 and p95/nibrin. BRCA1 was detected in discrete foci in the nucleus that colocalize with hRad50 after irradiation. Formation of irradiation-induced foci positive for BRCA1, hRad50, hMre11 or p95 were dramatically reduced in HCC1937 breast cancer cells carrying a homozygous mutation in *BRCA1*, but was restored by transfection of wild-type *BRCA1*. Ectopic expression of wild-type, but not mutated *BRCA1* in these cells rendered them less sensitive to the DNA damage agent, methyl methanesulfonate. These data suggest that BRCA1 is important for the cellular responses to DNA damage that are mediated by the hRad50-hMre11-p95 complex.

Dr. Zhong's work on BRCA1 was highly relevant for breast cancer research. By understanding the interaction and functional role of BRCA1 in the DNA repair process could lead to a greater understanding of its role in tumorigenesis and to new forms of cancer therapy aimed at interactions with the repair proteins.

Publications:

Zhong Q, Boyer TG, Chen PL, Lee WH. (2002) Deficient nonhomologous end-joining activity in cell-free extracts from Brca1-null fibroblasts. *Cancer Res.* 62(14):3966-70.

Zhong Q, Chen CF, Chen PL, Lee WH. (2002) BRCA1 facilitates microhomology-mediated end joining of DNA double strand breaks. J Biol Chem. 277:28641-7.

Dr. Zhong successfully defended his dissertation in November, 2000, and obtained his Ph.D. He recently published additional work related to his doctoral research as a postdoctoral fellow in Dr. Wen-Hwa Lee's laboratory. Dr. Zhong is currently continuing his training in Xiaodong Wang's laboratory at the University of Texas Southwestern Medical Center at Dallas, where he is working on the biochemistry and cell biology of apoptosis.

- ***Lei Zheng*** ***Mentor -- Dr.Wen-Hwa Lee***

Lei accomplished a significant amount of work during this training period. His main goal was to elucidate the molecular basis of genomic instability that occurs in most of human cancers including breast cancer. He started working on a novel mitotic phase specific protein, Hec1, by demonstrating that Hec1 interacts with retinoblastoma protein for maintaining the genomic stability that was published in Mol. Cell. Biol. (1999). He then developed a method to examine the level of chromosome instability by using retrovirus carrying both positive and negative selectable marker that integrated randomly into individual chromosomes, and the frequency of loss of this selectable chromosomal marker (LOM) was measured. The results showed that normal mouse embryonic stem cells had a very low frequency of LOM, which was less than 10-8/cell/generation. In Rb-/- mouse ES cells, the frequency was increased to approximately 10-5/cell/generation, while in Rb+/- ES cells, the frequency was approximately 10-7/cell/generation. LOM was mainly mediated through chromosomal mechanisms and not due to point mutations.

These results revealed that RB haploinsufficiency plays a critical role in the maintenance of chromosome stability. The mystery of why RB heterozygous carriers have early onset tumor formation with high penetrance can be, at least, partially explained by this novel activity. Dr. Lei Zheng made very significant contributions toward this novel aspect with RB function.

Publications:

Chen Y, Riley DJ, **Zheng L**, Chen PL, Lee WH. (2002) Phosphorylation of the mitotic regulator protein Hec1 by Nek2 kinase is essential for faithful chromosome segregation. J Biol Chem. 277:49408-16.

Zheng L, Lee WH. (2002) Retinoblastoma tumor suppressor and genome stability. Adv Cancer Res.;85:13-50.

Peng H, **Zheng L**, Lee WH, Rux JJ, Rauscher FJ 3rd. (2002) A common DNA-binding site for SZF1 and the BRCA1-associated zinc finger protein, ZBRK1. Cancer Res. 62:3773-81.

Zheng L, Andrea Flesken-Nikitin, Phang-Lang Chen and Wen-Hwa Lee. (2002) Deficiency of Retinoblastoma gene in mouse embryonic stem cells leads to genetic instability. Cancer Research 62:2498-502.

Dr. Zheng successfully defended his Ph.D. dissertation in Novermber, 2000. Lei is currently working on a project involving regulators of gene transcription in Dr. Robert Roeder's at the I Laboratory of Biochemistry and Molecular Biology, The Rockefeller University, New York. After completing his postdoctoral training in Dr. Roeder's laboratory, Dr. Zheng will begin an internal medicine residency program of Albert Einstein Medical College in New York, beginning in July, 2003. After that he is planning to do an Oncology subspecialty fellowship, all the while using his protected research time in Dr. Roeder's laboratory. Dr. Zheng will undoubtedly continue make major contributions in both basic and clinical science of breast cancer.

- ***Horng-Ru Lin***

BRCA1 or BRCA2 germline mutations predispose women to early onset, familial breast cancer. Current studies on BRCA1 and BRCA2 suggest their roles in the maintenance of genome integrity. However, in contrast to the clear studies of BRCA1, there has been very little characterization of the BRCA2 protein and evidence that speaks to a dynamic function of BRCA2 in this regard. That is, the intrinsic biological nature of the BRCA2 protein remains

enigmatic. Therefore, this project is to try to reveal the physiological function of the BRCA2 protein by characterizing its posttranslational processing, such as phosphorylation.

The novelty of the work lies in the following. First, it demonstrates BRCA2 is a phosphoprotein in vivo. Second, BRCA2 is hyperphosphorylated specifically in mitosis. Third, dephosphorylation of BRCA2 corresponds to the timing of cells' exit from mitosis. These findings imply that BRCA2 may play an important role in mitosis. To further characterize the phosphorylated amino acids of BRCA2 will provide fresh insights into functional study of BRCA2, which has obvious relevance to breast cancer.

- ***Stephen Van Komen*** ***Mentor – Dr. Patrick Sung***

In yeast homologous recombination, Rad54, a member of Swi2/Snf2 family of proteins, functionally cooperates with the Rad51 recombinase in making D-loop, the first DNA joint formed between recombining chromosomes. Our biochemical studies have indicated that yeast Rad54 modulates DNA topology at the expense of ATP hydrolysis, producing extensive unconstrained supercoils in DNA. This supercoiling ability is likely to be indispensable for D-loop formation. Given the high degree of structural and functional conservation among yeast and human recombination factors, we hypothesize that human Rad51 and Rad54 also function together to make D-loop. This hypothesis is being tested with human Rad51 and Rad54 proteins purified from insect cells infected with recombinant baculoviruses. In addition, whether human Rad54 has ATP hydrolysis-driven DNA supercoiling ability is also being examined. Our work is directly relevant to breast cancer, since recent studies have implicated the breast tumor suppressor BRCA2 in modulating the activities of the recombination machinery via Rad51.

Mr. Van Komen's research is directly relevant to breast cancer since double strand breaks in DNA and their repair is an issue pertinent to breast cancer. Since the tumor suppressor, BRCA2, interacts with Rad51, it is critically important to understand the biochemistry of this important enzyme in DNA repair.

Van Komen S, Petukhova G, Sigurdsson S, Sung P. (2002) Functional cross-talk among Rad51, Rad54, and replication protein A in heteroduplex DNA joint formation. J Biol Chem. 277:43578-87.

Sigurdsson S, **Van Komen S**, Petukhova G, Sung P. (2002) Homologous DNA pairing by human recombination factors Rad51 and Rad54. J Biol Chem. 277:42790-4.

Sigurdsson S, **Van Komen S**, Bussen W, Schild D, Albala JS, Sung P. (2001) Mediator function of the human Rad51B-Rad51C complex in Rad51/RPA-catalyzed DNA strand exchange. Genes Dev. 15:3308-18.

- **Deanna Jansen**

Ms. Jansen's husband was transferred to a new military base and, for family reasons, she decided to withdraw from the program. At some point, she plans to complete her Ph.D. training.

- **Stefan Sigurdsson** **Mentor – Dr. Patrick Sung**

The RAD51 encoded product exhibits structural and functional similarities to the Escherichia coli recombination protein RecA. RecA promotes the pairing and strand exchange between homologous DNA molecules to form heteroduplex DNA. We have shown that hRad51 also

makes DNA joints avidly and promotes highly efficient DNA strand exchange. Two Rad51-like proteins, Rad51B and Rad51C, are found associated in a heterodimeric complex. We have co-expressed the Rad51B and Rad51C proteins in insect cells and purified the Rad51B-Rad51C complex to near homogeneity. Biochemical experiments have revealed that Rad51B-Rad51C binds DNA and enhances the recombinase activity of the Rad51 protein. This recombination mediator function of Rad51B-Rad51C is likely indispensable for efficient recombination in vivo. Recently, hRad51 was shown to interact with the breast tumor suppressor BRCA2. The biochemical studies by Mr. Sigurdsson should be useful for understanding the molecular basis of breast tumor suppression by the recombination machinery.

Genomic caretaking by the recombination systems is vital to the "health" of the information residing in DNA. Corruption of the information by insults arising from internal and external sources is known to be involved in genesis of cancer. Thus, the system elucidated by Mr. Sigurdsson is very important for all cancers including those of the mammary glands.

Publications:

Van Komen S, Petukhova G, **Sigurdsson S**, Sung P. (2002) Functional cross-talk among Rad51, Rad54, and replication protein A in heteroduplex DNA joint formation. J Biol Chem. 277:43578-87.

Sigurdsson S, Van Komen S, Petukhova G, Sung P. (2002) Homologous DNA pairing by human recombination factors Rad51 and Rad54. J Biol Chem. 277:42790-4.

Sigurdsson S, Van Komen S, Bussen W, Schild D, Albala JS, Sung P. (2001) Mediator function of the human Rad51B-Rad51C complex in Rad51/RPA-catalyzed DNA strand exchange. Genes Dev. 15:3308-18.

Guikai Wu **Mentor – Dr. Phang-Lang Chen**

Immortalized cells maintain telomere length through either a telomerase-dependent process or a telomerase-independent pathway termed alternative lengthening of telomeres (ALT). Homologous recombination is implicated in the ALT pathway in both yeast and human ALT cells. In ALT cells, two types of DNA double-strand break repair and homologous recombination factors, the Rad50/Mre11/NBS1 complex and Rad51/Rad52 along with replication factors (RPA) and telomere binding proteins (TRF1 and TRF2), are associated with the ALT-associated PML body (APB). DNA synthesis in late S-G(2) is associated with APBs, which contain telomeric DNA and, are therefore, potential sites for telomere length maintenance. Mr. Gu showed that the breast cancer susceptibility gene product, breast cancer susceptibility gene 1, and the human homologue of yeast Rap1, hRap1, are also associated with APBs specifically during late S-G(2) phase of the cell cycle. He additionally show that the localization of the double-strand break repair factors with APBs is distinct from their association with ionizing radiation-induced nuclear foci. To systematically explore the mechanism involved in the assembly of APBs, we examine the role of Nijmegen breakage syndrome 1 (NBS1) and TRF1 in this process, respectively. He demonstrated that NBS1 plays a key role in the assembly and/or recruitment of Rad50, Mre11, and breast cancer susceptibility gene 1, but not Rad51 or TRF1, to APBs. The NH(2) terminus of NBS1, specifically the BRCA1 COOH-terminal domain, is required for this activity. Although TRF1 interacts with NBS1 directly, it is dispensable for the association of either Rad50/Mre11/NBS1 or Rad51 with APBs. Perturbation of the interactions between NBS1/Mre11 and APBs correlates with reduced BrdUrd incorporation associated with APBs, consistent with decreased DNA synthesis at these sites. Taken together, these results support a model in which NBS1 has a vital role in the assembly of APBs, which function to maintain telomeres in human ALT cells.

All of the proteins in Mr. Wu's project are vital to the DNA repair and response systems of normal and cancer cells. Telomeres are essential for the maintenance of chromosome length and are a target of both cancer and aging research. Accordingly, Mr. Wu's project could have important relevance to the age-related onset of cancer including those of the mammary gland.

Publications: At the time of writing this report, Mr. Wu just published a paper in *Cancer Research* entitled "Assembly of Functional ALT-associated Promyelocytic Leukemia Bodies Requires Nijmegen Breakage Syndrome 1."

Xianzhi Jiang **Mentor – Dr. Phang-Lang Chen**

Since joining Dr. Chen's lab, Mr. Jiang has been participating in the following two research projects: (I) A systematic study of the mechanism involved in the assembly of the ALT-associated promyelocytic leukemia body (APB), and (II) the characterization of a novel non-selenocysteine containing phospholipid hydroperoxide glutathione peroxidase (NPGPx). Regarding the first project, it has been known that NBS1 and TRF1 are associated with ALT-associated PML body (APB). NBS1 physically interacts with TRF1, a telomere-specific binding protein. In order to understand the potential roles of NBS1 and TRF1 in the assembly of APBs, Mr. Jiang made adenovirus constructs that expressed GFP-TRF1Dmyb fusion protein, which lacks the NBS1 interaction region. Overexpressed TRF1Dmyb protein can form a TRF1Dmyb/TRF1 dimer and thus acts as a dominant negative by depleting endogenous TRF1 from telomere DNA. In collaboration with Guikai Wu, Mr. Jiang demonstrated that NBS1 plays a key role in the assembly and/or recruitment of RAD50, MRE11, and BRCA1, but not RAD51 or TRF1, to APBs. Although TRF1 interacts with NBS1 directly, it is dispensable for the association of either RAD50/MRE11/NBS1 or RAD51 with APBs.

In the second project, Mr. Jiang identified a novel non-selenocysteine containing phospholipid hydroperoxide glutathione peroxidase named as NPGPx. In collaboration with Ahmad Utomo, Mr. Jiang demonstrated that ectopic expression of NPGPx in Brca1-null cells that were sensitive to oxidative stress induce by hydrogen peroxide conferred a similar resistance level to that of the wild-type cells, suggesting the importance of this enzyme in reducing oxidative stress. Unlike mammary gland and other normal tissues, the majority of breast cancer cell lines studied (11 out of 12) expressed very low or undetectable levels of NPGPx irrespective of BRCA1 status. Re-expression of NPGPx in breast cancer lines, MCF-7 and HCC1937, induced resistance to eicosapentaenoic acid (an omega-3 type of polyunsaturated fatty acid) mediated cell death and abrogated proliferative stimulation by linoleic acid (an omega-6 type). Thus NPGPx plays an essential role in breast cancer cells in alleviating oxidative stress generated from polyunsaturated fatty acid metabolism.

Mr. Jiang's projects are clearly important to breast cancer research. The proteins in project one are of obvious importance to DNA repair and genomic stability. Project two is novel and offers fresh insights into the role of oxidative damage and the proteins that participate in assuaging it. Thus the research plan of Mr. Jiang will be important in combating breast cancer on two critically important fronts.

Publications: At the time this report was written, Mr. Jiang's study has just recently been published in *Cancer Research* report entitled "Assembly of Functional ALT-associated Promyelocytic Leukemia Bodies Requires Nijmegen Breakage Syndrome 1." The second project is being prepared for publication under the title "Identification of a Non-selenocysteine Containing Phospholipid Hydroperoxide Glutathione Peroxidase (NPGPx) Essential for alleviating Oxidative Stress Generated from polyunsaturated Fatty Acids in Breast Cancer Cells."

Yi-Tzu Lin **Mentor – Dr. Wen-Hwa Lee**

Accurate chromosome segregation, a process essential for maintenance of genomic integrity, requires coordination between centrosomes, kinetochores, and chromosomes during M phase progression. Previously, we discovered a novel coil-coiled kinetochore protein, Hec1, which is essential for faithful chromosome segregation. Hec1 interacts directly with Hint1/HZWint1, which in turn binds to Zw10 at the kinetochore to facilitate spindle attachment. Ms. Lin showed that when Hec1 expression is down regulated by a small inhibitory RNA, localization of both Hec1 and Hint1 at kinetochores is abolished. When Hint1 expression is similarly down regulated by siRNA, Hec1 remains at kinetochores. Thus Hec1 is required for the recruitment of Hint1 to kinetochores. Down regulation of Hec1 expression resulted in chromosome missegregation characterized by lagging chromosomes during metaphase, and incomplete segregation during anaphase. These aberrations in turn lead to formation of micronuclei and multiple nuclei. Similar albeit less severe phenotypes were observed in cells treated with Hint1 siRNA. M phase is prolonged in cells treated with Hec1 siRNA, but not completely arrested since cytokinesis occurs. The cells in which Hec1 expression is down regulated fail to activate the spindle checkpoint: they do not accumulate in metaphase after treatment with nocodazole, nor is BubR1 phosphorylated. Taken together, Ms. Lin's results suggest that Hec1 recruits Hint1/Zw10 to the kinetochore for spindle attachment and may serve as a platform for control of the spindle checkpoint. The findings thus provide a molecular mechanism by which Hec1 plays a crucial role in chromosome segregation.

Cells from solid tumors typically display chromosomal aberrations attributed to problems with their segregation during cell division. Ms. Lin's research is especially relevant to breast cancer since these tumors often demonstrate these types of chromosomal defects, which may contributed to their progression.

Ahmad Utomo **Mentor – Dr. Wen-Hwa Lee**

A drastic reduction in the expression of a novel phospholipid hydroperoxide glutathione peroxidase (PHGPx), which incorporates cysteine instead of selenocysteine in the conserved catalytic motif was observed in a microarray analysis using cDNAs amplified from mRNA of Brca1-null mouse embryonic fibroblasts (MEFs). This non-selenocysteine PHGPx named as NPGPx is a cytoplasmic protein with a molecular weight of approximately 22 kDa. Ectopic expression of NPGPx in Brca1-null cells, which are sensitive to oxidative stress induced by hydrogen peroxide, conferred a similar resistance level equal to that of the wild-type cells, suggesting the importance of this enzyme in reducing oxidative stress. Expression of NPGPx was found in many tissues, including developing mammary gland. However, the majority of breast cancer cell lines studied (11 out of 12) expressed very low or undetectable levels of NPGPx irrespective of BRCA1 status. Re-expression of NPGPx in breast cancer lines, MCF-7 and HCC1937, induced resistance to eicosapentaenoic acid (an omega-3 type of polyunsaturated fatty acid) mediated cell death, and abrogated proliferative stimulation by linoleic acid (an omega-6 type). Thus, NPGPx plays an essential role in breast cancer cells in alleviating oxidative stress generated from polyunsaturated fatty acid metabolism.

The data and novel insights derived from Mr. Utomo's research might help explain breast cancer development due to defects in responding to oxidative damage. If true, affected family members of families carrying alterations in BRCA1 might benefit from avoidance of situations where oxidative damage is increased.

Dr. Utomo successfully defended his dissertation and was awarded his Ph.D., prior to preparation of this report. He is continuing his training as a postdoctoral fellow at the Harvard Medical School in the laboratory of Dr. Tanya Mayadas.

Chang-Ching Liu **Mentor – Dr. Wen-Hwa Lee**

The Rad50/MRE11/NBS 1 complex is involved in a variety of cellular processes, including both non-homologous end-joining and homologous recombination pathways involved in DNA double-strand breaks repair, cell cycle checkpoint activation, telomere maintenance, and meiosis. In order to understand the mechanism underlying the function of this repair complex, a novel Rad50-interacting protein (RINT-1) was identified by a yeast two-hybrid screen in our laboratory. RINT-1, an evolutionarily conserved protein from Drosophila to human beings, has been shown to interact with Rad50 preferentially at late S and G2/M phases through its central and c-terminal conserved region. To further explore the function of interaction between RINT-1 and Rad50, several stable MCF7 clonal cell lines that express GFP fusions containing only the Rad50 binding region of RINT-1 were established. Overexpression of the fusion protein leads to a defective radiation-induced G2/M checkpoint. This observation is related to the repair function of Rad50 and another Rad50-interacting protein, BRCA1, which is also thought to play a role in radiation-induced G2/M checkpoint control. Like Rad50 and BRCA1, inactivation of RINT-1 causes early embryonic lethality. Blastocysts were isolated at day 3.5 of pregnancy from Rint-1+/- intercross and were cultured in vitro for 7 days. Unlike wild type and Rint-1+/- embryos, whose inner cell mass continued to expand and differentiate, Rint-1-/- cells stop their expansion subsequent to day 4 and died.

To study the cellular function of RINT-1 besides its roles in response to DNA damage, Ms. Liu established an U2OS cell line expressing full-length RINT-1 protein coupled with GFP and discovered that RINT-1 localizes to the centrosome in a microtubule-independent manner. GFP-RINT-1 proteins localize at the centrosomes throughout the cell cycle and move to the midbody along with the mother centrosome before cytokinesis. Endogenous RINT-1 proteins reside in the centrosomal fractions isolated from LEM cells, and are found in purified centrosomes. Interestingly, GFP fusions with either the N-terminal coiled-coil domain or the conserved Rad50 binding region of RINT-1 are recruited to the centrosome. Using the N-terminal coiled-coil domain of RINT-1 as bait in a yeast two-hybrid screen, Ms. Liu found two centrosomal proteins potentially interacting with RINT-1; PA28b and p150glued. Similar to the p150glued component of the dynactin complex, adenovirally overexpressed N-terminal RINT-1 polypeptides decorated the entire length of interphase microtubules. Overexpressed N-terminal RINT-1 polypeptides also resulted in the formation of cytoplasmic dots outside the centrosome, a phenomenon also observed when peptides of a coiled-coil centrosomal protein, Cep135, were overexpressed. The centrosome is a major microtubule-organizing center in animal cells. It duplicates only once during the cell cycle and ensures the formation of bipolar spindles, which distribute replicated chromosomes equally to daughter cells. Defective centrosomes, exemplified by an excess number of centrioles and pericentriolar material, are characteristic of solid tumors in general and breast tumors in particular, and may contribute to their genomic instability by the formation of multipolar mitotic spindles. Recent molecular evidence suggests that centrosomes are also involve in stress response mechanisms, cell cycle checkpoint control, and cell cycle progression. It has been shown that inactivation of the other Rad50-interacting proteins, MRE11 and Brca1, lead to centrosome amplification and embryonic lethality. Future studies of the roles played by RINT-1 in regulation of centrosomal activities may provide insight about how DNA repair pathways coordinate with the cell cycle progression and the regulation of centrosome function.

This on the basic biology of centrosomes and their roles in cells division is applicable to all cells including those that form tumors. It is especially relevant to breast tumors since they often display chromosomal aberrations attributed to defects involving centrosomal proteins.

Note: Miss. Liu withdrew from the graduate program to return to home to assist with a critically ill member of her immediate family.

Wei Tan **Mentor – Dr. Thomas Boyer**

The breast and ovarian-specific tumor suppressor BRCA1 has been implicated in both activation and repression of gene transcription by virtue of its direct interaction with sequence-specific DNA-binding transcription factors. However, the mechanistic basis by which BRCA1 mediates the transcriptional activity of these regulatory proteins remains largely unknown. Mr. Tan has been studying the functional interaction between BRCA1 and ZBRK1, a BRCA1-dependent KRAB-zinc finger transcriptional repressor as a model system to understand the mechanistic basis by which BRCA1 mediates sequence-specific transcription control. During the reporting period, Mr. Tan succeeded in identifying and initiating the molecular characterization of a portable BRCA1-dependent transcriptional repression domain within the ZBRK1 C-terminus. Mr. Tan found that this C-terminal repression domain functions in a BRCA1-, HDAC-, and promoter-specific manner, and is thus functionally distinguishable from the N-terminal KRAB repression domain in ZBRK1, which exhibits no BRCA1 dependency and broad promoter specificity. Significantly, Mr. Tan also found that the BRCA1-dependent transcriptional repression domain modulates sequence-specific DNA-binding by the minimal ZBRK1 DNA-binding domain. These findings thus reveal a dual function for the BRCA1-binding domain on ZBRK1 in sequence-specific DNA-binding and transcriptional repression by DNA-bound ZBRK1. Mr. Tan is currently engaged in experiments to complete the functional characterization of this BRCA1-dependent repression domain, and he is in the process of writing up his results in manuscript form.

This project is applicable to breast cancer since all of these proteins are involved in the transcriptional response to DNA damage medicated by BRCA1. Understanding this response system, which includes the ZBRK1 protein, is critical to preventing and treating breast cancer.

Sangeetha Vijayakumar **Mentor – Dr. Wen-Hwa Lee**

The Suv3 helicase of yeast *Saccharomyces cerevisiae* has been classified as a mitochondrial RNA helicase. Yeast genetic studies revealed that suv3-null yeast fails to grow in glycerol media and forms petite colonies, implicating a role in energy metabolism. Because the helicase domains in both yeast and human Suv3 vary considerably from typical RNA helicase motifs, homogenously purified Suv3 was required by Ms. Vijayakumar in order to verify its putative enzymatic activities. Ms. Vijayakumar expressed a form of human Suv3 carrying an N-terminal deletion of 46 amino acids (ΔNhSuv3) in yeast suv3 null mutants and demonstrated that ΔNhSuv3 fully complements the null phenotype. Through a five-step chromatographic procedure, ΔNhSuv3 (83 kDa) and its partially degraded 70 kDa protein (hSuv3-70), which constitutes amino acids 68 to 685, were purified to homogeneity. Both proteins have ATPase activities, but mutants with an invariant lysine in the ATP binding site, K213, changed to alanine (A) or arginine (R) lose activity. At pH 7.5, ΔNhSuv3 unwinds only RNA/DNA hetero duplex, while hSuv3-70, which retains all the core catalytic domains, can unwind multiple substrates including homoduplexes of RNA and DNA and heteroduplexes of RNA-DNA. However, under low pH (≤ 5.0) reaction conditions, ΔNhSuv3 also exhibits ATP-dependent multi-substrate specificity similar to that of hSuv3-70. Consistently, ΔNhSuv3 binds to homo duplexes of both RNA and DNA at pH 5.0, but not at pH 7.5, Moreover, data from circular dichroism analysis suggests that at pH 5.0, ΔNhSuv3 adopts a similar conformation to that of hSuv3-70, which in turn may govern its differential substrate specificity.

Human Suv3 is likely to be involved in critical functions in both normal and breast cancer cells. Knowledge regarding its function will, therefore, be a significant contribution toward understanding the development and/or maintenance of the tumorigenic state.

Changes to the Program Faculty:

Removals: None

Additions: The following investigators have been added to the faculty. All have expertise and funded research programs relevant to breast cancer as indicated by their descriptions below and appended NIH Biosketches.

Hai Rao, Ph.D., Assistant Professor, Department of Molecular Medicine.

Dr. Rao is investigating fundamental mechanisms of the Ub-proteasome system, and its functions in signal transduction and DNA repair. Ubiquitin (Ub) is a 76-residue polypeptide that is highly conserved in eukaryotes. In addition to its classical role in protein degradation, Ub is also emerging as a signal for protein transport and processing. Ubiquitylation — the covalent conjugation of Ub to other intracellular proteins — regulates a broad range of basic cellular processes, including cell growth and differentiation, DNA repair, signal transduction, inflammation, transcription, and stress responses. Many proteins involved in cancer development and progression, including p53, cyclins, β-catenin, are targets of the Ub-proteasome system. Not surprisingly, defects in the Ub-proteasome system can lead to diseases ranging from cancer to neurodegenerative disorders. Recent findings that both BRCA1, a protein involved in breast cancer, and Parkin, a crucial protein involved in Parkinson's disease, function as the E3 components in the Ub-mediated pathway indicate that studies of the Ub-proteasome system are essential for the understanding the pathogenesis of human diseases.
Specifically, Dr. Rao wishes to understand how proteins modified by Ub are degraded by the proteasome. It is proposed that adaptor molecules, which selectively recognize ubiquitylated substrates, facilitate the proteolysis of substrates. He is focusing on Rad23-like proteins, Rad23, Dsk2, and Ddi1 that are candidate adaptor molecules involved in delivering ubiquitylated substrates to the proteasome. He will use a variety of molecular and biochemical approaches to dissect the role of these adaptor molecules in substrate proteolysis. He expects these studies will have important implications with respect to the treatment of cancers. The components of the Ub-proteasome system are attractive drug targets, as illustrated with the efficacy of some proteasome inhibitors in the treatment of multiple myeloma and other cancers of blood cells.

Changes in the Program Courses: None during the last funding period.

SUMMARY: The Breast Cancer Training Program made excellent progress toward attracting and retaining excellently qualified students in breast cancer research. The students received a high level of training in the modern research methods and theory. A total of 14 publications on breast cancer was achieved by students supported by the program. Six of the faculty, one postdoctoral fellow and 4 students in the program were funded by Defense Department's Breast Cancer Research Program. There was a new faculty addition that will substantially expanded the training opportunities in Breast Cancer Research in the area of regulated protein stability, a fundamental property of all cells, including mammary cells. Combined with the basic instruction they receive in the Molecular Medicine Ph.D. Program, students will graduate as highly skilled researchers who will be competitive for post doctoral positions in the premiere breast cancer laboratories in the world.

Appendix: NIH Biosketches and Reprints of Trainee Publications.

BIOGRAPHICAL SKETCH

Provide the following information for the key personnel in the order listed for Form Page 2.
Follow the sample format for each person. **DO NOT EXCEED FOUR PAGES.**

NAME	POSITION TITLE
Hai Rao, Ph.D.	Principal Investigator

EDUCATION/TRAINING *(Begin with baccalaureate or other initial professional education, such as nursing, and include postdoctoral training.)*

INSTITUTION AND LOCATION	DEGREE *(if applicable)*	YEAR(s)	FIELD OF STUDY
Wuhan University, China	B.S.	1989	Chemistry
Boston University, Boston, MA	M.S.	1991	Chemistry
State University of New York at Stony Brook	Ph.D.	1996	Biochemistry
California Institute of Technology, Pasadena, CA	Postdoc	2002	Biology

A. Positions and Honors

Positions and Employment

1989-1991 Graduate Research Assistant, Boston University, Boston, CA.

1991-1996 Graduate Research Assistant, State University of New York at Stony Brook and the Cold Spring Harbor Laboratory.

1997-2002 Postdoctoral Fellow, California Institute of Technology

2002-present Assistant Professor, Department of Molecular Medicine/Institute of Biotechnology
The University of Texas Health Science Center at San Antonio

Honors and Awards

1998-2001 Postdoctoral Scholarship, Leukemia & Lymphoma Society of America.
1996 Graduate Research Award, State University of New York at Stony Brook.

B. Selected peer-reviewed publications (in chronological order)

Rao, H., Mohr, S.C., Fairhead, H., Setlow, P. (1992). Synthesis and characterization of a 29-amino acid residue DNA-binding peptide derived from α/β-type small acid soluble spore proteins (SASP) of bacteria. *FEBS letter*. 305: 115-120.

Bell, S.P., Marhrens, Y., **Rao, H.**, and Stillman, B. (1993). The replicon model and eukaryotic chromosomes. *Cold Spring Harbor Symp. Quant. Biol.* 58: 435-442.

Rao, H., Marhrens, Y., and Stillman, B. (1994). Functional conservation of modular elements in yeast chromosomal replicators. *Mol. Cell. Biol.* 14: 7643-7651.

Rao, H., and Stillman, B. (1995). The origin recognition complex (ORC) interacts with a bipartite DNA binding site within yeast replicators. *Proc. Natl. Acad. Sci.* USA 92: 2224-2228.

Rao, H., Uhlmann, F., Nasmyth, K., and Varshavsky, A. (2001). Degradation of a cohesin subunit by the N-end rule pathway is essential for chromosome stability. *Nature* 410, 955-959.

Rao, H., and Sastry, A.(2002). Recognition of specific ubiquitin conjugates is important for the proteolytic functions of the UBA domain proteins Dsk2 and Rad23. *J. Biol. Chem.* 277: 11691-11695.

C. Research Support:

NONE

Completion of Base Excision Repair by Mammalian DNA Ligases

ALAN E. TOMKINSON, LING CHEN, ZHIWAN DONG, JOHN B. LEPPARD, DAVID S. LEVIN, ZACHARY B. MACKEY, AND TERESA A. MOTYCKA

Department of Molecular Medicine
Institute of Biotechnology
The University of Texas Health Science Center at San Antonio
San Antonio, Texas 78245

Three mammalian genes encoding DNA ligases—*LIG1*, *LIG3*, and *LIG4*—have been identified. Genetic, biochemical, and cell biology studies indicate that the products of each of these genes play a unique role in mammalian DNA metabolism. Interestingly, cell lines deficient in either DNA ligase I (46BR.1G1) or DNA ligase III (EM9) are sensitive to simple alkylating agents. One interpretation of these observations is that DNA ligases I and III participate in functionally distinct base excision repair (BER) subpathways. In support of this idea, extracts from both DNA ligase-deficient cell lines are defective in catalyzing BER *in vitro* and both DNA ligases interact with other BER proteins. DNA ligase I interacts directly with proliferating cell nuclear antigen (PCNA) and DNA polymerase β

Progress in Nucleic Acid Research and Molecular Biology, Vol. 68

0079-6603/01 $35.00

(Pol β), linking this enzyme with both short-patch and long-patch BER. In somatic cells, DNA ligase IIIα forms a stable complex with the DNA repair protein Xrcc1. Although Xrcc1 has no catalytic activity, it also interacts with Pol β and poly(ADP-ribose) polymerase (PARP), linking DNA ligase IIIα with BER and single-strand break repair, respectively. Biochemical studies suggest that the majority of short-patch base excision repair events are completed by the DNA ligase IIIα/Xrcc1 complex. Although there is compelling evidence for the participation of PARP in the repair of DNA single-strand breaks, the role of PARP in BER has not been established.

I. Introduction

Phosphodiester bond formation is a common step in many DNA metabolic pathways, including DNA replication, DNA excision repair, and DNA strand-break repair. All the DNA ligation events in the prokaryote *Escherichia coli* are catalyzed by a single species of DNA ligase in an NAD-dependent reaction (*1*). In contrast, mammalian cells contain several distinct species of ATP-dependent DNA ligases (2). Except for the different nucleotide cofactor, prokaryotic and eukaryotic DNA ligases employ the same basic three-step reaction mechanism (*1, 2*). Initially, the enzyme reacts with the nucleotide cofactor to form a covalent enzyme–AMP complex, in which the AMP moiety is linked to a specific lysine residue. Next, the AMP group is transferred from the polypeptide to the 5′-phosphate terminus of a DNA nick. Finally, the nonadenylated enzyme catalyzes phosphodiester bond formation between the 3′-hydroxyl and 5′-phosphate termini of the nick, releasing AMP.

Based on their different biochemical properties, it was predicted that the mammalian DNA ligase activities were encoded by different genes (*3, 4*). This has been validated by the identification of three mammalian *LIG* genes: *LIG1*, *LIG3*, and *LIG4* (*5–7*). It seems reasonable to assume that the increased size and complexity of the eukaryotic genome provided the evolutionary driving force for multiple DNA ligases with distinct functions in cellular DNA metabolism. The presence of a conserved catalytic domain within the polypeptides encoded by the mammalian *LIG* genes supports the notion that these genes were generated by duplication events. Insights into the cellular roles of the mammalian *LIG* gene products have been gleaned both from the phenotype of DNA ligase-deficient cell lines and from the identification of proteins that specifically interact with the unique regions that flank the conserved catalytic domain.

In the yeast *Saccharomyces cerevisiae*, the *CDC9* and *DNL4* genes are homologous with the mammalian *LIG1* and *LIG4* genes, respectively (*5, 8–10*). Elegant genetic and biochemical studies have shown that, in addition to its essential role in DNA replication, Cdc9 DNA ligase completes nucleotide and base excision repair pathways (*11, 12*). The assignment of DNA ligases to excision repair pathways in mammalian cells is complicated by the presence

of the *LIG3* gene. Here we will focus on the products of the mammalian *LIG* genes with particular emphasis on the contribution of these enzymes to base excision repair (BER).

II. Mammalian *LIG* Genes and Their Protein Products

The relationship between the mammalian *LIG* genes and their products is shown in Table I and described below.

A. *LIG1*

A full-length cDNA encoding DNA ligase I was identified by screening for human cDNAs that complemented the conditional lethal phenotype of a *S. cerevisiae cdc9* DNA ligase mutant (*5*). The relationship between the 919-amino acid polypeptide encoded by the cDNA and DNA ligase I was confirmed by the alignment of peptide sequences from purified bovine DNA ligase I with sequences within the open reading frame encoded by the cDNA (*5*). A notable feature of the DNA ligase I polypeptide is its high proline content, which causes aberrant mobility during SDS-PAGE. Thus, DNA ligase I has a molecular mass of 125 kDa when measured by SDS-PAGE compared with a calculated molecular weight of 102,000 (*5, 13*).

When compared with other eukaryotic DNA ligases, mammalian DNA ligase I is most closely related to the replicative DNA ligases of *S. cerevisiae* and *Schizosaccharomyces pombe* encoded by the *CDC9* and *CDC17* genes, respectively (*5*). However, the amino acid homology is restricted to the C-terminal catalytic domains of these enzymes. The noncatalytic N-terminal domain of DNA ligase I contains sequences that target this polypeptide to the nucleus and to specific subnuclear locations (*14, 15*). In addition, this domain is phosphorylated *in vivo* and mediates specific protein–protein interactions (*16–18*).

The association of DNA ligase I with DNA replication is further supported by several other observations: (1) The level of DNA ligase I correlates with cell proliferation (*19, 20*); (2) DNA ligase I colocalizes with other replication

TABLE I
MAMMALIAN *LIG* GENES AND THEIR PRODUCTS

Gene	Enzyme
LIG1	DNA ligase I
LIG3	DNA ligase IIIα-nucl
	DNA ligase IIIα-mito
	DNA ligase IIIβ
LIG4	DNA ligase IV

proteins at the sites of DNA synthesis, termed replication foci, in replicating cells (*21*); (3) DNA ligase I copurifies with a high-molecular-weight replication complex (22).

B. *LIG3*

This gene was cloned at about the same time by two different approaches—searching an EST database with a motif conserved among eukaryotic DNA ligases, and a conventional cDNA cloning strategy based on partial amino acid sequences from purified bovine DNA ligase III (*6, 7*). The absence of *LIG3* homologs in the genomes of *S. cerevisiae, Drosophila melanogaster,* and *Caenorhabditis elegans* suggests that this gene was a relatively recent addition to the genome of mammals during evolution. In contrast to the *LIG1* and *LIG4* genes, the *LIG3* gene encodes several polypeptides that appear to have distinct cellular functions. Two forms of DNA ligase III, α and β, are produced by an alternative splicing event that results in proteins with different C termini (23). The C-terminal 77 amino acids of human DNA ligase IIIα are replaced by a unique 17-amino acid sequence in human DNA ligase IIIβ. The sequence of the C-terminal 100 amino acids of DNA ligase IIIα exhibits homology with the BRCT motif, a putative protein–protein interaction domain that was first identified in the product of the breast cancer susceptibility gene, *BRCA1* (*24, 25*). DNA ligase IIIα mRNA is expressed in all tissues and cells, whereas DNA ligase IIIβ mRNA expression is restricted to male germ cells, specifically pachytene spermatocytes and round spermatids (23). The differential expression profiles suggest that DNA ligase IIIα is a housekeeping enzyme, whereas DNA ligase IIIβ participates either in meiotic recombination or postmeiotic DNA repair.

Although the human DNA ligase IIIα open reading frame encodes a 949-amino acid polypeptide, the second in-frame ATG was chosen as the most likely *in vivo* translation initiation site based on homology with the Kozak consensus sequence (*6, 7*). More recently, it was noticed that the preceding 87-amino acid sequence contained a putative mitochondrial targeting signal (*26*). It was assumed that DNA ligase IIIα was a nuclear protein, as this enzyme was purified from nuclear extracts and immunocytochemistry experiments indicated that the majority of DNA ligase IIIα protein is located within the nucleus (*23, 27*). However, fusion of the putative targeting sequence to a heterologous protein resulted in mitochondrial localization of the fusion protein (*26*). Therefore, it appears that mitochondrial and nuclear forms of DNA ligase IIIα are produced in somatic cells by alternative translation initiation. Presumably, mitochondrial DNA ligase IIIα participates in the replication and repair of the mitochondrial genome. At present the mechanism underlying the nuclear localization of DNA ligase IIIα is unknown.

A zinc finger motif at the N terminus of DNA ligase III distinguishes the products of the *LIG3* gene from other eukaryotic DNA ligases. Intriguingly,

the DNA ligase III zinc finger is most closely related to the two zinc fingers located at the N terminus of poly(ADP-ribose) polymerase (PARP) (*7*). PARP is a relatively abundant nuclear protein whose avid binding to both single- and double-strand breaks is mediated by its zinc fingers. DNA binding activates the polymerase activity of PARP, resulting in the ADP-ribosylation of itself and other nuclear proteins (*28*). The single zinc finger of DNA ligase III has similar DNA binding properties in that it mediates the binding of this enzyme to DNA strand breaks with a preference for single-strand breaks (*29*). Although the zinc finger is not required for catalytic activity *in vitro* or for functional complementation of a temperature-sensitive *E. coli lig* mutant, it has a significant effect on the DNA-binding and DNA-joining activities of DNA ligase III at physiological salt concentrations (*29*).

C. *LIG4*

This gene, which was cloned by searching an EST database with a motif conserved among eukaryotic DNA ligases, was identified prior to the detection of the enzyme activity in mammalian cell extracts (*7, 30*). There are several reasons why DNA ligase IV activity escaped detection in the earlier enzyme purification studies: (1) In extracts from proliferating cells, DNA ligase IV is a minor contributor to cellular DNA ligase activity (*30*); (2) both the *LIG3* and *LIG4* genes encode polypeptides with similar electrophoretic mobility (*7, 30*); (3) unlike DNA ligases I and III, a significant fraction of DNA ligase IV remains adenylated during fractionation, making it difficult to label with [α^{32}P]ATP in the adenylation assay (*30*). A unique feature of the *LIG4* gene product compared with the *LIG1* and *LIG3* gene products is its long C-terminal extension beyond the conserved catalytic domain. Furthermore, this C-terminal region contains two BRCT motifs (*7*).

III. DNA Ligase-Associated Proteins

The identification of specific protein partners for each of the DNA ligases (Table II) has provided insights into both the molecular mechanisms by which these enzymes recognize interruptions in the phosphodiester backbone and their cellular functions.

A. DNA Ligase I

Using affinity chromatography with either DNA Pol β antibody or Pol β as the ligand, a multiprotein complex that catalyzed the repair of a uracil-containing DNA substrate was partially purified from a bovine testis nuclear extract (*31*). Subsequent studies revealed that DNA ligase I was a component of this BER complex and that DNA ligase I interacts directly with Pol β (*18, 31*). This interaction occurs between the noncatalytic N-terminal domain of DNA ligase I and

TABLE II
DNA LIGASE INTERACTING PROTEINS[a]

Enzyme	Interacting protein
DNA ligase I	PCNA
	DNA Pol β
DNA ligase IIIα	XRCC1
DNA ligase IIIβ	?
DNA ligase IV	XRCC4

[a]Biochemical and genetic studies indicate that the majority of short-patch BER events are completed by the DNA ligase IIIα/Xrcc1 complex. The contribution of DNA ligase I to short-patch BER via its interaction with Pol β is not known. The interaction of DNA ligase I with PCNA suggests that this enzyme completes the PCNA-dependent long-patch BER subpathway.

the 8-kDa N-terminal domain of Pol β that has DNA binding and 5′-deoxyribose phosphate diesterase activities (*32*, *33*).

Intuitively, an association between two enzymes that catalyze consecutive steps in a reaction pathway suggests that the interaction should enhance the overall rate of the reaction. In Figure 1, we show that gap-filling synthesis and ligation of a DNA substrate with a single nucleotide gap by the concerted action of Pol β and DNA ligase I occurs more rapidly than ligation of a DNA substrate with a single ligatable nick. It should be noted that this experiment does not demonstrate that the increased ligation rate is a direct consequence of the binding of DNA ligase I to Pol β. Nonetheless, it is intriguing that DNA ligase I, which transfers the AMP group to the 5′-phosphate terminus at a nick, interacts with the domain of Pol β that binds to and can modify the 5′ terminus at a nick or short gap in duplex DNA (*32*, *33*).

An association between DNA ligase I and proliferating cell nuclear antigen (PCNA) was also detected by affinity chromatography, in this case using DNA ligase I as the ligand (*17*). The direct interaction of these proteins is mediated by the noncatalytic N-terminal domain of DNA ligase I. Cell biology studies had demonstrated that this region of the protein was required both for nuclear localization and for subnuclear targeting to replication foci (*14*). Subsequent studies mapped these targeting activities to two distinct regions within the N-terminal region of DNA ligase I (*15*). Interestingly, the sequence required for targeting to replication foci was coincident with that required for PCNA binding (*15*). The replication foci targeting/PCNA binding sequence of DNA ligase I exhibits homology with a PCNA binding motif initially identified in the cell division kinase inhibitor p21 and subsequently found in several PCNA binding proteins (*34*). Although these observations indicate that the stable association of

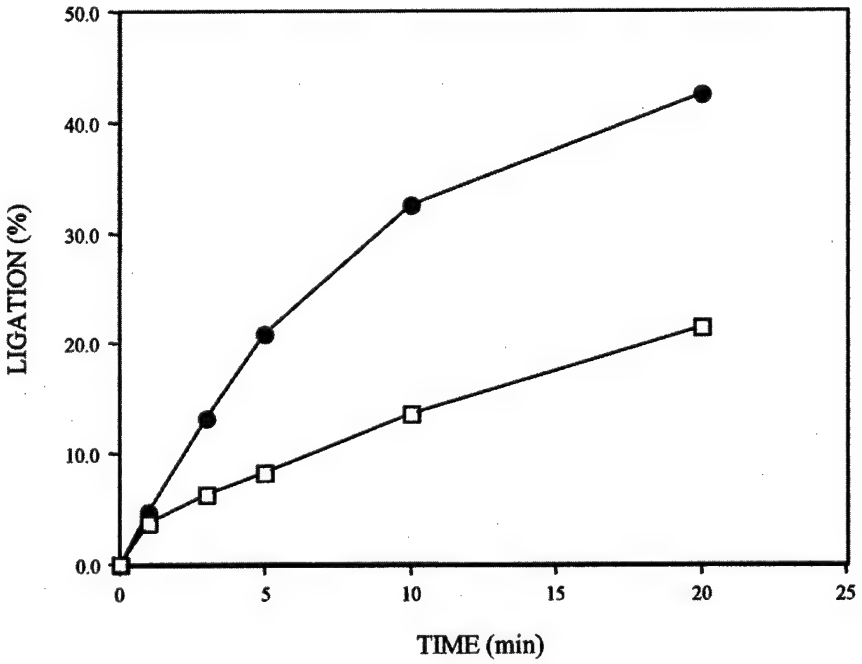

FIG. 1. Repair of a one-nucleotide gap by Pol β and DNA ligase I. DNA ligase I (0.06 pmol) and Pol β (0.12 pmol) were incubated with a labeled linear duplex DNA substrate (4 pmol) containing a one-nucleotide gap in the presence of the 4 dNTPs (filled circles). DNA ligase I (0.06 pmol) was incubated with a labeled linear duplex DNA substrate (4 pmol) containing a single ligatable nick in the presence of the 4 dNTPs (open squares). Aliquots were removed at the times indicated. After separation by denaturing gel electrophoresis, ligated product was detected and quantitated by PhosphorImager analysis. The inclusion of Pol β in assays with the nicked DNA substrate had no effect on the rate of ligation.

DNA ligase I with replication foci is mediated by PCNA binding, they do not address the direct role of PCNA binding in cellular ligation events catalyzed by DNA ligase I. In this regard, the inclusion of PCNA in DNA ligase assays does not stimulate DNA joining by DNA ligase I. However, DNA ligase I will bind to a PCNA molecule that is topologically linked to a circular DNA duplex so PCNA binding could serve to tether DNA ligase I to DNA substrates (*17*).

B. DNA Ligase III

DNA ligase III was identified as a protein that bound specifically to a tagged version of the DNA repair protein Xrcc1 (*35*). The human *XRCC1* gene was identified by its ability to complement the DNA damage hypersensitivity of a mutant Chinese hamster cell line, EM9 (*36*), which is described in more

detail below. Following the discovery of the different forms of DNA ligase III generated by alternative splicing, it was demonstrated that DNA ligase IIIα but not DNA ligase IIIβ formed a complex with Xrcc1 (*23, 37*). Interestingly, complex formation is mediated by an interaction between BRCT motifs present at the C termini of both Xrcc1 and DNA ligase IIIα (*37*). Although Xrcc1 has no catalytic activity, the reduced level of DNA ligase IIIα in the *xrcc1* mutant cell line indicates that Xrcc1 is important for the stability of DNA ligase IIIα (*38*). Moreover, protein–protein interactions between Xrcc1 and both Pol β and PARP have been characterized (*39, 40*). Each of these binding events involves different regions of Xrcc1 that are also distinct from the DNA ligase IIIα binding site, suggesting that Xrcc1 may act as a scaffold for the assembly of a multiprotein complex (*39, 40*).

C. DNA Ligase IV

DNA ligase IV was identified as a protein that specifically coimmunoprecipitated with a tagged version of the DNA repair protein Xrcc4 (*41*). The human *XRCC4* gene was identified by its ability to complement the DNA damage hypersensitivity of a mutant Chinese hamster cell line XR1 (*42*). In contrast to the interaction between DNA ligase IIIα and Xrcc1, the interaction between DNA ligase IV and Xrcc4 is not mediated by BRCT motifs, but instead Xrcc4 binds to the region between the two C-terminal BRCT motifs of DNA ligase IV (*43*). The reduced level of DNA ligase IV protein in *xrcc4* mutant cells suggests that the interaction with Xrcc4 stabilizes DNA ligase IV (*44*). Since Xrcc4 binds to DNA, it is possible that this protein mediates the binding of DNA ligase IV to its DNA substrate (*45*).

IV. Phenotype of DNA Ligase-Deficient Cell Lines

Our understanding of the cellular functions of the mammalian DNA ligases has been greatly enhanced by the isolation of mammalian cell lines deficient in each of the DNA ligases. The phenotypes of these cell lines are summarized below.

A. DNA Ligase I-Deficient Cell Lines

The fibroblast cell line 46BR and an SV40-immortalized derivative 46BR.1G1 were established from an immunodeficient individual who inherited different point mutations in each *LIG1* allele (*46, 47*). One of the mutations abolishes DNA ligase activity, whereas the other mutant allele encodes a polypeptide that is 10- to 20-fold less active than the wild-type enzyme. As expected, the DNA ligase I deficiency results in abnormal joining of Okazaki fragments (*48, 49*). The cell lines are also hypersensitive to the cytotoxic effects of monofunctional

DNA alkylating agents and are moderately sensitive to ultraviolet and ionizing radiation (*50*). These observations are consistent with DNA ligase I participating in strand-break and excision-repair pathways. In support of this idea, 46BR.1G1 extracts are defective in the repair of circular duplex DNA containing a single uracil residue (*48*). Specifically, the DNA ligase I deficiency resulteds in reduced levels of repaired circular product and increased levels of DNA repair synthesis.

B. DNA Ligase III-Deficient Cell Lines

The mutant Chinese hamster ovary cell line EM9 was isolated based on its hypersensitivity to DNA alkylating agents (*51*). Further analysis revealed that this cell line was also moderately sensitive to ionizing radiation and exhibited elevated levels of sister chromatid exchange when grown in the presence of bromodeoxyuridine (*52*). As mentioned previously, expression of the human *XRCC1* gene complemented the DNA damage-sensitive phenotype of the mutant CHO cell line (*36*). Analysis of DNA repair in EM9 cells revealed a defect in events after DNA damage-incision. The interactions of Xrcc1 with both Pol β and DNA ligase IIIα provide a molecular explanation for the participation of Xrcc1 in the DNA synthesis and ligation reactions that complete base excision repair (*35, 40*). In further support of the idea that Xrcc1 plays an important role in BER, extracts from EM9 cells are defective in this type of repair (*53*).

It should be noted that Xrcc1 may function independently of DNA ligase IIIα. As mentioned previously, Xrcc1 interacts with PARP, an enzyme that is not required for the reconstitution of BER *in vitro* (*39*). In addition, a recent study with *xrcc1* mutant cells reported evidence that the DNA ligase IIIα/Xrcc1 complex plays an important role in DNA repair within the G_1 phase of the cell cycle whereas Xrcc1 alone mediates DNA repair events within the DNA synthesis phase of the cell cycle (*54*). The construction and characterization of *lig3* mutant cell lines will facilitate further analysis of the cellular functions of DNA ligase III and Xrcc1.

C. DNA Ligase IV-Deficient Cell Lines

The mutant Chinese hamster cell line XR1 is hypersensitive to ionizing radiation and defective in V(D)J recombination (*42*). Interestingly, the DNA damage hypersensitivity is most pronounced in the G_1 phase of the cell cycle. As noted above, both the repair and V(D)J recombination defects in XR1 cells are complemented by the human *XRCC4* gene whose product forms a stable complex with the *LIG4* gene product (*41, 55*). More recently, the *XRCC4* gene has been deleted in mouse embryonic cells by gene targeting and embryonic fibroblast cell lines established from the resultant *xrcc4*$^{-/-}$ embryos. These cell lines reiterate the phenotype of the XR1 cells (*56*).

Cell lines with mutations in the *LIG4* gene are also available. A radiosensitive human cell line 180BR was established from a leukemia patient who had

severe reactions to both radiotherapy and chemotherapy (*57*). Subsequently, a point mutation was identified within the *LIG4* gene of the 180BR cells (*58*). Interestingly, the leukemia patient did not appear to be immunodeficient, and the 180BR cells, when activated for V(D)J recombination, had no obvious defect in this type of site-specific recombination (*58*). It is possible that the mutant allele encodes a product that retains sufficient activity to complete V(D)J recombination, but not for the repair of DNA damage-induced double-strand breaks. The *LIG4* gene has been deleted in mouse embryonic cells by gene targeting, and embryonic fibroblast cell lines have been established from the resultant *lig4*$^{-/-}$ embryos. These cell lines exhibit the same phenotype as the *xrcc4* mutant cell line in that they are hypersensitive to ionizing radiation and defective in V(D)J recombination (*59*). Based on the results described above and comparable studies in the yeast *S. cerevisiae* (*8–10*), it appears that DNA ligase IV plays a major role in the repair of DNA double-strand breaks by nonhomologous end joining but does not contribute significantly to BER and other excision repair pathways.

V. Involvement of Mammalian DNA Ligases in BER

Biochemical studies using cell-free extracts and purified proteins have identified two pathways of BER that can be distinguished both by the extent of DNA repair synthesis and the requirement for PCNA (*40, 60–63*). At the present time, the spectrum of DNA base lesions repaired *in vivo* by the short-patch (single-nucleotide repair patch, PCNA-independent) and long-patch (repair patches of 2–11 nucleotides, PCNA-dependent) BER subpathways is not known. Thus it is possible that certain base lesions can be repaired by only one of the BER subpathways, whereas other lesions can be effectively repaired by either subpathway.

As mentioned above, cell lines defective in either DNA ligase I or DNA ligase III are hypersensitive to killing by monofunctional alkylating agents such as methyl methanesulfonate (MMS) (*50, 52*). Since the base lesions caused by MMS are thought to be repaired by BER, one explanation of these observations is that there are two functionally distinct BER subpathways, one involving DNA ligase I and the other involving DNA ligase III, that repair different cytotoxic lesions induced by MMS exposure (Fig. 2). In support of this model, extracts from cell lines defective in either DNA ligase I or DNA ligase III exhibit abnormalities in BER assays (*48, 53*). The extracts with reduced DNA ligase III activity are defective in short-patch BER but proficient in long-patch BER (*53*). This suggests that the interaction between Pol β and the Xrcc1 subunit of the Xrcc1/DNA ligase IIIα complex is critical for the completion of short-patch BER (Fig. 2).

Although the interactions of DNA ligase I with both Pol β and PCNA suggest that this enzyme could function in both short- and long-patch BER (*17, 18*), the

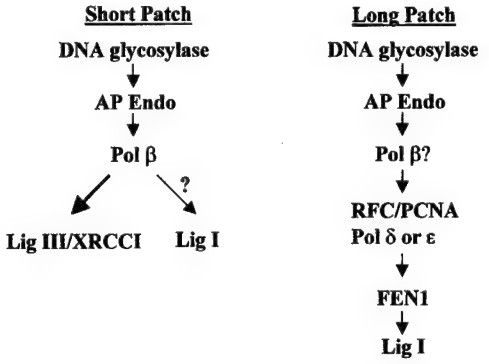

FIG. 2. A model illustrating the participation of DNA ligases I and III in BER.

effect of DNA ligase I deficiency on these subpathways has not been determined. Since DNA ligase III deficiency effects short- but not long-patch BER, it is conceivable that DNA ligase I deficiency will have the opposite effect, causing a defect in long-patch, but not short-patch BER (Fig. 2). If this is the case, the DNA ligase III- and DNA ligase I-deficient cell lines should be useful reagents to determine the spectrum of base lesions repaired *in vivo* by short- and long-patch BER.

VI. Concluding Remarks

Genetic and biochemical studies suggest that both the DNA ligase IIIα/Xrcc1 complex and DNA ligase I play biologically significant roles in BER. Based on currently available evidence, it appears that the DNA ligase IIIα/Xrcc1 complex completes the majority of short-patch BER events (*40, 53*). The interaction of DNA ligase I with PCNA makes this species of DNA ligase the most likely candidate for the long-patch BER subpathway (*17, 60, 63*). Further studies are required to determine the *in vivo* roles of these BER subpathways. At the present time, the biological significance of the interaction between DNA ligase I and Pol β is unclear. Since the 180-kDa BER complex containing these proteins was isolated from extracts of bovine testes (*31*), it is possible that the involvement of DNA ligase I and DNA ligase IIIα/Xrcc1 in short-patch BER is cell type-specific. Further studies are required to elucidate the functional consequence of the interactions between the DNA ligases and Pol β and/or PCNA on the coordination of the reactions that complete BER.

The role of the nuclear protein PARP in BER is controversial. Although both the short- and long-patch BER pathways can be reconstituted *in vitro* without PARP (*40, 60, 61*), the results of BER assays with extracts from parp$^{-/-}$

cells and the interaction between PARP and Xrcc1 suggest that PARP may contribute to the completion of BER (39, *64*). The involvement of PARP in BER does not appear to be compatible with the current model of BER, in which pairwise interactions between BER proteins mediate the handover of repair intermediates. In fact, this model predicts that PARP would be actively excluded from DNA undergoing BER by the coordinate action of the BER proteins. It is possible that the DNA ligase IIIα/Xrcc1 complex participates in both PARP-dependent repair of DNA single-strand breaks and PARP-independent short-patch BER. Further biochemical and molecular genetic studies are required to clarify the complex relationships between these DNA repair proteins.

ACKNOWLEDGMENTS

Studies in A.E.T.'s laboratory were supported by grants from the Department of Health and Human Services (GM47251 and GM57479), the Nathan Shock Aging Center, and the San Antonio Cancer Institute. D.S.L. and Z.B.M. were supported by the Training Program in the Molecular Basis of Breast Cancer. D.S.L. is supported by the Training Program in the Molecular Basis of Aging. Z.B.M is a UNCF-MERCK fellow.

REFERENCES

1. I. R. Lehman, *Science* **186,** 790–797 (1974).
2. A. E. Tomkinson and Z. B. Mackey, *Mutat. Res.* **407,** 1–9 (1998).
3. A. E. Tomkinson, E. Roberts, G. Daly, N. F. Totty, and T. Lindahl, *J. Biol. Chem.* **286,** 21728–21735 (1991).
4. J. E. Arrand, A. E. Willis, I. Goldsmith, and T. Lindahl, *J. Biol. Chem.* **261,** 9079–9082 (1986).
5. D. E. Barnes, L. H. Johnston, K. Kodama, A. E. Tomkinson, D. D. Lasko, and T. Lindahl, *Proc. Natl. Acad. Sci. U.S.A.* **87,** 6679–6683 (1990).
6. J. Chen, A. E. Tomkinson, W. Ramos, Z. B. Mackey, S. Danehower, C. A. Walter, R. A. Schultz, J. M. Besterman, and I. Husain, *Mol. Cell. Biol.* **15,** 5412–5422 (1995).
7. Y.-F. Wei, P. Robins, K. Carter, K. Caldecott, D. J. C. Pappin, G.-L. Yu, R.-P. Wang, B. K. Shell, R. A. Nash, P. Schär, D. E. Barnes, W. A. Haseltine, and T. Lindahl, *Mol. Cell. Biol.* **15,** 3206–3216 (1995).
8. P. Schär, G. Herrman, G. Daly, and T. Lindahl, *Genes Dev.* **11,** 1912–1924 (1997).
9. S. H. Teo and S. P. Jackson, *EMBO J.* **16,** 4788–4795 (1997).
10. T. E. Wilson, U. Grawunder, and M. R. Lieber, *Nature (London)* **388,** 495–498 (1997).
11. X. Wu, E. Braithwaite, and Z. Wang, *Biochemistry* **38,** 2628–2635 (1999).
12. D. R. Wilcox and L. Prakash, *J. Bacteriol.* **148,** 618–623 (1981).
13. A. E. Tomkinson, D. D. Lasko, G. Daly, and T. Lindahl, *J. Biol. Chem.* **265,** 12611–12617 (1990).
14. A. Montecucco, E. Savini, F. Weighardt, R. Rossi, G. Ciarrocchi, A. Villa, and G. Biamonti, *EMBO J.* **14,** 5379–5386 (1995).
15. A. Montecucco, R. Rossi, D. S. Levin, R. Gary, M. S. Park, T. A. Motycka, G. Ciarrocchi, A. Villa, G. Biamonti, and A. E. Tomkinson, *EMBO J.* **17,** 3786–3795 (1998).

16. C. Prigent, D. D. Lasko, K. Kodama, J. R. Woodgett, and T. Lindahl, *EMBO J.* **11,** 2925–2933 (1994).
17. D. S. Levin, W. Bai, N. Yao, M. O'Donnell, and A. E. Tomkinson, *Proc. Natl. Acad. Sci. U.S.A.* **94,** 12863–12868 (1997).
18. E. K. Dimitriadis, R. Prasad, M. K. Vaske, L. Chen, A. E. Tomkinson, M. S. Lewis, and S. H. Wilson, *J. Biol.Chem.* **273,** 20540–20550 (1998).
19. J. H. J. Petrini, K. G. Huwiler, and D. T. Weaver, *Proc. Natl. Acad. Sci. U.S.A.* **88,** 7615–7619 (1991).
20. S. Soderhall, *Nature (London)* **260,** 640–642 (1976).
21. D. Wilcock and D. P. Lane, *Nature (London)* **349,** 429–431 (1991).
22. C. Li, J. Goodchild, and E. F. Baril, *Nucleic Acids Res.* **22,** 632–638 (1994).
23. Z. B. Mackey, W. Ramos, D. S. Levin, C. A. Walter, J. R. McCarrey, and A. E. Tomkinson, *Mol. Cell. Biol.* **17,** 989–998 (1996).
24. I. Callebaut and J. P. Mornon, *FEBS Lett.* **400,** 25–30 (1997).
25. E. V. Koonin, S. F. Alschul, and P. Bork, *Nature Genet.* **13,** 266–267 (1996).
26. U. Lakshmipathy and C. Campbell, *Mol. Cell. Biol.* **19,** 3869–3876 (1999).
27. I. Husain, A. E. Tomkinson, W. A. Burkhart, M. B. Moyer, W. Ramos, Z. B. Mackey, J. M. Besterman, and J. Chen, *J. Biol. Chem.* **270,** 9683–9690 (1995).
28. G. de Murcia and J. M. de Murcia, *Trends Biochem. Sci.* **19,** 172–176 (1994).
29. Z. B. Mackey, C. Niedergang, J. M. Murcia, J. Leppard, K. Au, J. Chen, G. de Murcia, and A. E. Tomkinson, *J. Biol. Chem.* **274,** 21679–21687 (1999).
30. P. Robins and T. Lindahl, *J. Biol. Chem.* **271,** 24257–24261 (1996).
31. R. Prasad, R. K. Singhal, D. K. Srivastava, J. T. Molina, A. E. Tomkinson, and S. H. Wilson, *J. Biol. Chem.* **271,** 16000–16007 (1996).
32. Y. Matsumoto and K. Kim, *Science* **269,** 699– 702 (1995).
33. R. Prasad, W. A. Beard, and S. H. Wilson, *J. Biol. Chem.* **269,** 18096–18101 (1994).
34. E. Warbrick, *Bioessays* **20,** 195– 199 (1998).
35. K. W. Caldecott, C. K. McKeown, J. D. Tucker, S. Ljunquist, and L. H. Thompson, *Mol. Cell. Biol.* **14,** 68–76 (1994).
36. L. H. Thompson, K. W. Brookman, N. J. Jones, S. A. Allen, and A. V. Carrano, *Mol. Cell. Biol.* **10,** 6160–6171 (1990).
37. R. A. Nash, K. Caldecott, D. E. Barnes, and T. Lindahl, *Biochemistry* **36,** 5207– 5211 (1997).
38. S. Ljungquist, K. Kenne, L. Olsson, and M. Sandstrom, *Mutat. Res.* **314,** 177–186 (1994).
39. M. Masson, C. Niedergang, V. Schreiber, S. Muller, J. M. de Murcia, and G. de Murcia, *Mol. Cell. Biol.* **18,** 3563–3571 (1998).
40. Y. Kubota, R. A. Nash, A. Klungland, P. Schär, D. E. Barnes, and T. Lindahl, *EMBO J.* **15,** 6662–6670 (1996).
41. U. Grawunder, M. Wilm, X. Wu, P. Kulesza, T. E. Wilson, M. Mann, and M. R. Lieber, *Nature (London)* **388,** 492–495 (1997).
42. Z. Li, T. Otevrel, Y. Gao, H.-L. Cheng, B. Seed, T. D. Stamato, G. E. Taccioli, and F. W. Alt, *Cell (Cambridge, Mass.)* **83,** 1079–1089 (1995).
43. U. Grawunder, D. Zimmer, and M. R. Leiber, *Curr. Biol.* **8,** 873–876 (1998).
44. M. Bryans, M. C. Valenzano, and T. Stamato, *Mutat. Res.* **433,** 53–58 (1999).
45. M. Modesti, J. E. Hesse, and M. Gellert, *EMBO J* **18,** 2008–2017 (1999).
46. D. E. Barnes, A. E. Tomkinson, A. R. Lehmann, A. D. B. Webster, and T. Lindahl, *Cell (Cambridge, Mass.)* **69,** 495–503 (1992).
47. A. D. B. Webster, D. E. Barnes, C. F. Arlett, A. R. Lehmann, and T. Lindahl, *Lancet* **339,** 1508–1509 (1992).
48. C. Prigent, M. S. Satoh, G. Daly, D. E. Barnes, and T. Lindahl, *Mol. Cell. Biol.* **14,** 310–317 (1994).

49. V. J. Mackenney, D. E. Barnes, and T. Lindahl, *J. Biol. Chem.* **272,** 11550–11556 (1997).
50. I. A. Teo, C. F. Arlett, S. A. Harcourt, A. Priestly, and B. C. Broughton, *Mutat. Res.* **107,** 371–386 (1983).
51. L. H. Thompson, T. Shiomi, E. P. Salazar, and S. A. Stewart, *Somat. Cell Mol. Genet.* **14,** 605–612 (1988).
52. L. H. Thompson, K. W. Brookman, L. E. Dillehay, A. V. Carrano, J. A. Mazrimas, C. L. Mooney, and J. L. Minkler, *Mutat. Res.* **95,** 247–254 (1982).
53. E. Cappelli, R. Taylor, M. Cevasco, A. Abbondandolo, K. Caldecott, and G. Frosina, *J. Biol. Chem.* **272,** 23970–23975 (1997).
54. R. M. Taylor, D. J. Moore, J. Whitehouse, P. Johnson, and K. W. Caldecott, *Mol. Cell. Biol.* **20,** 735–740 (2000).
55. S. E. Critchlow, R. P. Bowater, and S. P. Jackson, *Curr. Biol.* **7,** 588–598 (1997).
56. Y. Gao, Y. Sun, K. M. Frank, P. Dikkes, Y. Fujiwara, K. J. Seidl, J. M. Sekiguchi, G. A. Rathbun, W. Swat, J. Wang, R. T. Bronson, B. A. Malynn, M. Bryans, C. Zhu, J. Chaudhuri, L. Davidson, R. Ferrini, T. Stamato, S. H. Orkin, M. E. Greenberg, and F. W. Alt, *Cell (Cambridge, Mass.)* **95,** 891–902 (1998).
57. P. N. Plowman, B. A. Bridges, C. F. Arlett, A. Hinney, and J. E. Kingston, *Br. J. Radiol.* **63,** 624–628 (1990).
58. E. Riballo, S. E. Critchlow, S.-H. Teo, A. J. Doherty, A. Priestly, B. Broughton, B. Kysela, H. Beamish, N. Plowman, C. F. Arlett, A. R. Lehmann, S. P. Jackson, and P. A. Jeggo, *Curr. Biol.* **9,** 699–702 (1999).
59. K. M. Frank, J. M. Sekiguchi, K. J. Seidl, W. Swat, G. A. Rathbun, H. L. Cheng, L. Davidson, L. Kangaloo, and F. W. Alt, *Nature (London)* **396,** 173–176 (1998).
60. A. Klungland and T. Lindahl, *EMBO J.* **16,** 3341–3348 (1997).
61. Y. Matsumoto, K. Kim, J. Hurwitz, R. Gary, D. S. Levin, A. E. Tomkinson, and M. Park, *J. Biol. Chem.* **274,** 33703–33708 (1999).
62. D. K. Srivastava, B. J. Vande Berg, R. Prasad, J. T. Molina, W. A. Beard, A. E. Tomkinson, and S. H. Wilson, *J. Biol. Chem.* **273,** 21203–21209 (1998).
63. G. Frosina, P. Fortini, O. Rossi, F. Carrozzino, G. Raspaglio, L. S. Cox, D. P. Dane, A. Abbondandolo, and E. Dogliotti, *J. Biol. Chem.* **271,** 9573–9578 (1996).
64. C. Trucco, F. J. Oliver, G. de Murcia, and J. Menissier-de Murcia, *Nucleic Acids Res.* **26,** 2644–2649 (1998).

Oncogene (2001) 20, 6742–6751

www.nature.com/onc

Persistent expression of cyclin D1 disrupts normal photoreceptor differentiation and retina development

Stephan X Skapek*[,1], Suh-Chin J Lin[2], Monica M Jablonski[3,4], Robyn N McKeller[1], Ming Tan[5], Nanpin Hu[2] and Eva Y-HP Lee*[,2]

[1]*Department of Hematology–Oncology, St. Jude Children's Research Hospital, Memphis, Tennessee, TN 38105, USA;* [2]*Department of Molecular Medicine, University of Texas Health Science Center at San Antonio, San Antonio, Texas, TX 78245, USA;* [3]*Department of Ophthalmology, University of Tennessee, Memphis, Memphis, Tennessee TN 38163, USA;* [4]*Department of Anatomy and Neurobiology, University of Tennessee, Memphis, Memphis, Tennessee TN 38163, USA;* [5]*Department of Biostatistics, St. Jude Children's Research Hospital, Memphis, Tennessee TN 38105, USA*

The differentiation of neuronal cells in the developing mammalian retina is closely coupled to cell cycle arrest and proceeds in a highly organized manner. Cyclin D1, which regulates cell proliferation in many cells, also drives the proliferation of photoreceptor progenitors. In the mouse retina, cyclin D1 protein normally decreases as photoreceptors mature. To study the importance of the down-regulation of cyclin D1 during photoreceptor development, we generated a transgenic mouse in which cyclin D1 was persistently expressed in developing photoreceptor cells. We observed numerous abnormalities in both photoreceptors and other nonphotoreceptor cells in the retina of these transgenic mice. In particular, we observed delayed opsin expression in developing photoreceptors and alterations in their number and morphology in the mature retina. These alterations were accompanied by disorganization of the inner nuclear and plexiform layers. The expression of cyclin D1 caused excess photoreceptor cell proliferation and apoptosis. Loss of the *p53* tumor suppressor gene decreased cyclin D1-induced apoptosis and led to microscopic hyperplasia in the retina. These findings are distinct from other mouse models in which the retinoblastoma gene pathway is disrupted and suggest that the *IRBP–cyclin D1* mouse model may recapitulate an early step in the development of retinoblastoma. *Oncogene* (2001) **20,** 6742–6751.

Keywords: cyclin D1; retina; *RB*; photoreceptors; retinoblastoma

Introduction

The mammalian retina consists of six major types of neuronal cells and one type of glial cell, all of which are derived from a neuroepithelial evagination of the ventricular layer of the developing brain (reviewed in Reh and Levine, 1998; Cepko *et al.*, 1996). A number of mouse studies have demonstrated that (1) these distinct retinal cells are derived from a pool of homogeneous, multipotent progenitor cells (Cepko *et al.*, 1996; Turner *et al.*, 1990) and (2) the differentiation process in the retina is closely coupled with irreversible cell cycle arrest (Reh and Levine, 1998; Cepko *et al.*, 1996). Importantly, when cell cycle arrest is disrupted *in vitro* or *in vivo*, neuronal differentiation does not proceed normally (Dobashi *et al.*, 1995; Poluha *et al.*, 1996; Lee *et al.*, 1994). In order to study its importance *in vivo* in the retina, we sought to generate a transgenic mouse in which this normal cell cycle arrest would be disrupted.

The close coupling of cell cycle arrest with differentiation in neuronal cells has been previously shown to involve the *Rb* gene (Lee *et al.*, 1992, 1994; Jacks *et al.*, 1992; Clarke *et al.*, 1992). The *Rb* gene encodes a protein RB that belongs to a family of related proteins, which includes p107 and p130 (Weinberg, 1995; DiCiommo *et al.*, 2000; Riley *et al.*, 1994). RB, p107, and p130 directly or indirectly control cell proliferation, differentiation, and apoptosis in a variety of cell types, including neuronal cells (Lin *et al.*, 1996). It has become clear that abnormalities in the control of the cell cycle, particularly those involving *Rb*, contribute to pathologic processes in the retina. For example, uncontrolled cell proliferation in retinal progenitor cells is a primary feature of retinoblastoma, the most common form of malignant eye tumor in children, which is caused by mutation of the retinoblastoma tumor suppressor gene *RB* (DiCiommo *et al.*, 2000; Riley *et al.*, 1994).

Cyclins, a family of cell cycle regulated proteins, and their catalytic partners, cyclin-dependent kinases (cdks), are direct regulators of RB function (Sherr, 1996; Dynlacht, 1997). Cyclin/cdk complexes phosphorylate RB, disrupt its interaction with other proteins, and drive the cell cycle transition from the G1 phase to the DNA synthesis (S) phase. Therefore, in order to disrupt the normal cell proliferation arrest in developing photoreceptor cells, we made a transgenic mouse in which the *I*nterphotoreceptor *r*etinoid *b*inding *p*rotein (IRBP) promoter drove the ectopic expression of cyclin D1 in these cells. Cyclin D1 is

*Correspondence: SX Skapek or EY-HP Lee;
E-mail: steve.skapek@stjude.org
Received 9 April 2001; revised 31 July 2001; accepted 1 August 2001

normally expressed in these cells during embryonic development (Sicinski *et al.*, 1995), but it decreases as they differentiate (see below). We hypothesized that the persistent expression of cyclin D1 in developing photoreceptors would alter their differentiation and potentially lead to photoreceptor-derived tumors by disrupting the function of RB. In this manuscript we describe these abnormalities, which, surprisingly, seem to be different from those observed in other models in which the RB pathway is disrupted.

Results

Expression of endogenous cyclin D1 decreases as photoreceptor cells mature

Cyclin D1 is expressed in proliferating cells in the neural retina at embryonic day 14.5 of mouse development (Sicinski *et al.*, 1995). Because photoreceptors cease to proliferate as they differentiate, we hypothesized that endogenous cyclin D1 expression would decrease concurrently. The proliferation of cells that are destined to become photoreceptors peaks at postnatal day P0, and few proliferating cells are detected after P5 (Young, 1985). Consistent with our hypothesis, at P4 when photoreceptors are beginning to differentiate (see below), few cells in the outer retina expressed cyclin D1 (Figure 1a). At P6 and P10, although some cyclin D1-positive cells were detected within the developing inner nuclear layer (INL), no positive cells were detected in the outer nuclear layer (ONL) (Figure 1c and data not shown). The temporal correlation between decreased cyclin D1 expression and the morphologic changes in post-mitotic, differentiating photoreceptor cells may be consistent with cyclin D1-dependent coordination of cell cycle arrest and differentiation in photoreceptor cells.

Establishment of IRBP-cyclin D1 transgenic mice

Six transgenic mouse founder lines, which demonstrated germ line transmission of the *IRBP–cyclin D1* transgene, were studied. All founder mice and their

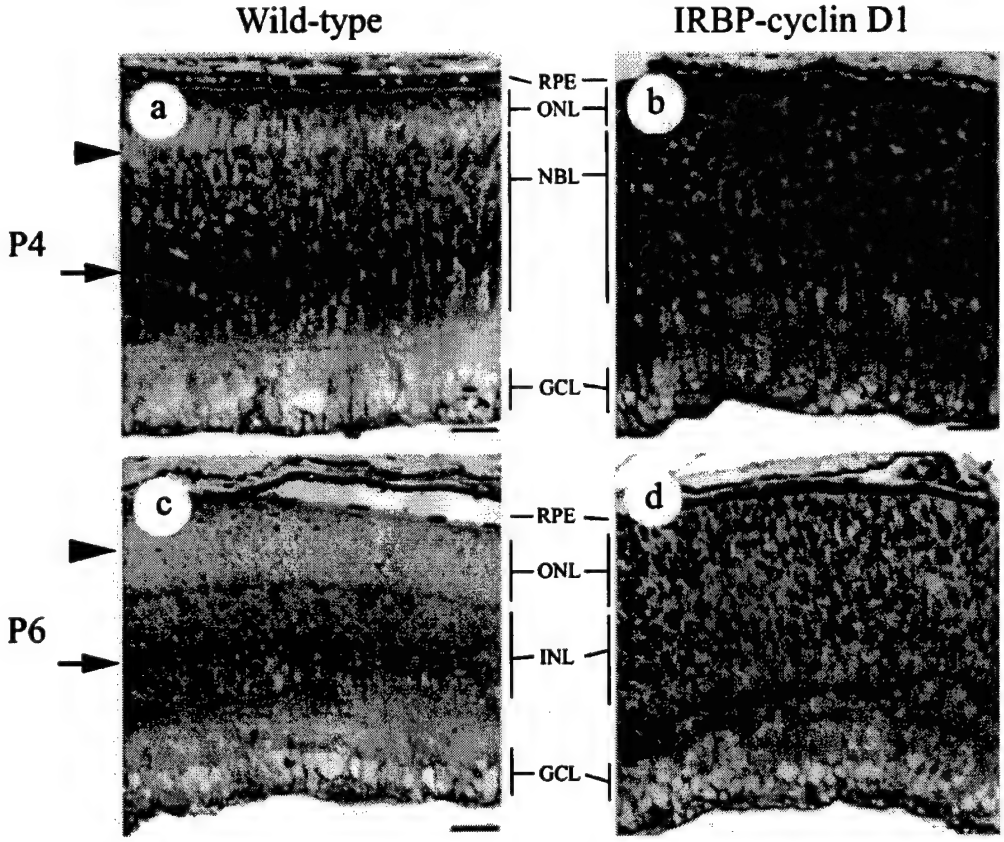

Figure 1 Expression of endogenous and ectopic cyclin D1 during mouse retina development. Immunohistochemical staining for cyclin D1 in the retinas of wild-type and *IRBP–cyclin D1* transgenic littermates at postnatal day (P) 4 (**a, b**), and P6 (**c, d**). Cyclin D1-positive cells are present in the neuroblastic layer which develops into the inner nuclear layer of retinas of wild-type and transgenic mice (arrow) and are present in the outer nuclear layer in transgenic mice (arrowhead). Photomicrographs of the central retina were taken at 200 × magnification and are oriented with the outer surface of the retina upward. Scale bar: 50 μm. RPE, retina pigment epithelium; NBL, neuroblastic layer; ONL and INL, outer and inner nuclear layers, respectively; OPL, IPL, outer and inner plexiform layers, respectively; GCL, ganglion cell layer

offspring appeared to be healthy with no overt phenotype. Morphologic changes in the eyes of 2–3-month-old progeny of these founder mice were analysed by light microscopy (data not shown). Mice from two of these transgenic lines (D15 and D40) which showed similar microscopic eye abnormalities were used in the remainder of the studies. To validate our transgenic model, we confirmed that ectopic cyclin D1 protein was expressed in these mice. At P4, P6 and P10, cyclin D1 was detectable throughout the cells in the developing ONL of the retinas of transgenic mice, whereas its expression was largely excluded from these cells in wild-type mice (Figure 1a–d and data not shown).

Ectopic expression of cyclin D1 in photoreceptors alters their development

Because cyclin D1 is known to drive cell proliferation (Hinds *et al.*, 1992), we hypothesized that the ectopic expression of cyclin D1 would increase the number of photoreceptors in the mature retina of *IRBP–cyclin D1* mice. However, retinas of mature transgenic mice appeared to contain fewer photoreceptor cells: the mature ONL, which normally contains approximately ten rows of photoreceptor cell nuclei, typically contained only two to five rows in transgenic mice (Figure 2A). In contrast to the focal loss of photoreceptors in mice that lack cyclin D1 (Ma *et al.*, 1998), the loss of photoreceptors in *IRBP–cyclin D1* mice was observed throughout the retina.

To determine whether the *IRBP–cyclin D1* transgene alters the development of individual photoreceptor cells, we performed histologic studies of retinas taken from mice at various times during the first two weeks of life. In these studies, we evaluated the expression of the photoreceptor-specific protein opsin (Morrow *et al.*, 1998). Although opsin was detected in many ONL cells in wild-type mice at P4, it was only detected in scattered cells in transgenic littermates at this age (Figure 2B, top). At P14, opsin was detected in most cells in the ONL of both transgenic and wild-type mice (Figure 2B, bottom). Interestingly, though, numerous opsin-positive cells were detected in the INL in P14 transgenic mice but not in wild-type mice (Figure 2B, bottom). Furthermore, higher magnification indicated that photoreceptor cells in *IRBP–cyclin D1* mice appeared to lack outer segments (Figure 2C). Taken together, these findings indicate that the ectopic expression of cyclin D1 in developing photoreceptor cells does not strictly prevent differentiation, but it does alter morphology, delay the expression of opsin, and potentially cause aberrant localization of these cells within the retina.

Abnormal retina anatomy in transgenic mice

Because cell-to-cell signaling and the timing of cellular differentiation are important during retina development (Cepko *et al.*, 1996; Reh and Levine, 1998; Ross, 1996), we determined whether cyclin D1-mediated changes in photoreceptor cells might affect other retinal cells. A number of abnormalities were observed in non-photoreceptor cells in *IRBP–cyclin D1* mice after P4, at which time the retina appeared morphologically normal (Figure 3a,b). First, the separation of the INL and ONL by the developing outer plexiform layer was delayed in *IRBP–cyclin D1* mice (compare Figure 3c with d). By P10, the outer plexiform layer was evident in transgenic mice, but it was irregular and poorly developed (compare Figure 3e and f). Second, the INL appeared to be expanded and disorganized in transgenic mice (Figures 2A and 3e,f). Third, cells were frequently observed within the normally acellular inner plexiform layer (Figures 2A and 3c,d). Finally, ganglion cells, which are normally arranged in a single row in the innermost layer of the retina, were in disarray (Figures 2A and 3c,d). It is not known whether the non-photoreceptor cell abnormalities were due to low level expression of cyclin D1 in these cells or due to indirect effects of aberrant cyclin D1 in photoreceptor cells. It is also possible that some of these effects, such as delayed INL–ONL separation, may contribute to certain photoreceptor-specific abnormalities, such as their aberrant localization within the INL.

Ectopic expression of cyclin D1 causes excess cell proliferation and apoptosis in maturing photoreceptors

As noted above, we hypothesized that persistent cyclin D1 expression would increase photoreceptor proliferation. To test this, we identified retinal cells that were synthesizing DNA at specific times during the postnatal period in both normal and transgenic mice. By P6, the few BrdU-labeled cells in wild-type mouse retinas were located in the peripheral retina whereas many more BrdU-labeled cells were observed in both the central and peripheral retina in *IRBP–cyclin D1* littermates at P6 and P10 (Figure 4A,a,b). It is interesting to note that the number of BrdU-labeled cells in both regions of the retina decreased from P6 to P10. Thus, although persistent expression of cyclin D1 in developing photoreceptors drove excess DNA synthesis, a mechanism to eventually decrease the number of BrdU-positive cells in the transgenic mice seemed to be intact.

Because the number of photoreceptors in mature mice appeared to be decreased despite increased DNA synthesis in photoreceptor precursors and because the number of BrdU-positive cells decreased from P6 to P10, we suspected that ectopic cyclin D1 expression might cause apoptosis. A small degree of apoptosis normally occurs in the mouse retina during development (Young, 1984). Consistent with this, we detected cells stained using terminal deoxyribonucleotidyl transferase-mediated dUTP-biotin nick end labeling (TUNEL) in the INL and ONL through P13–14 in wild-type mice (Figure 4Ba,b). In the retinas of *IRBP–cyclin D1* mice, more TUNEL-labeled cells were observed in both the INL and ONL and in both the central and peripheral retina at P9–10 and P13–14 (Figure 4Bb). These findings indicate that ectopic

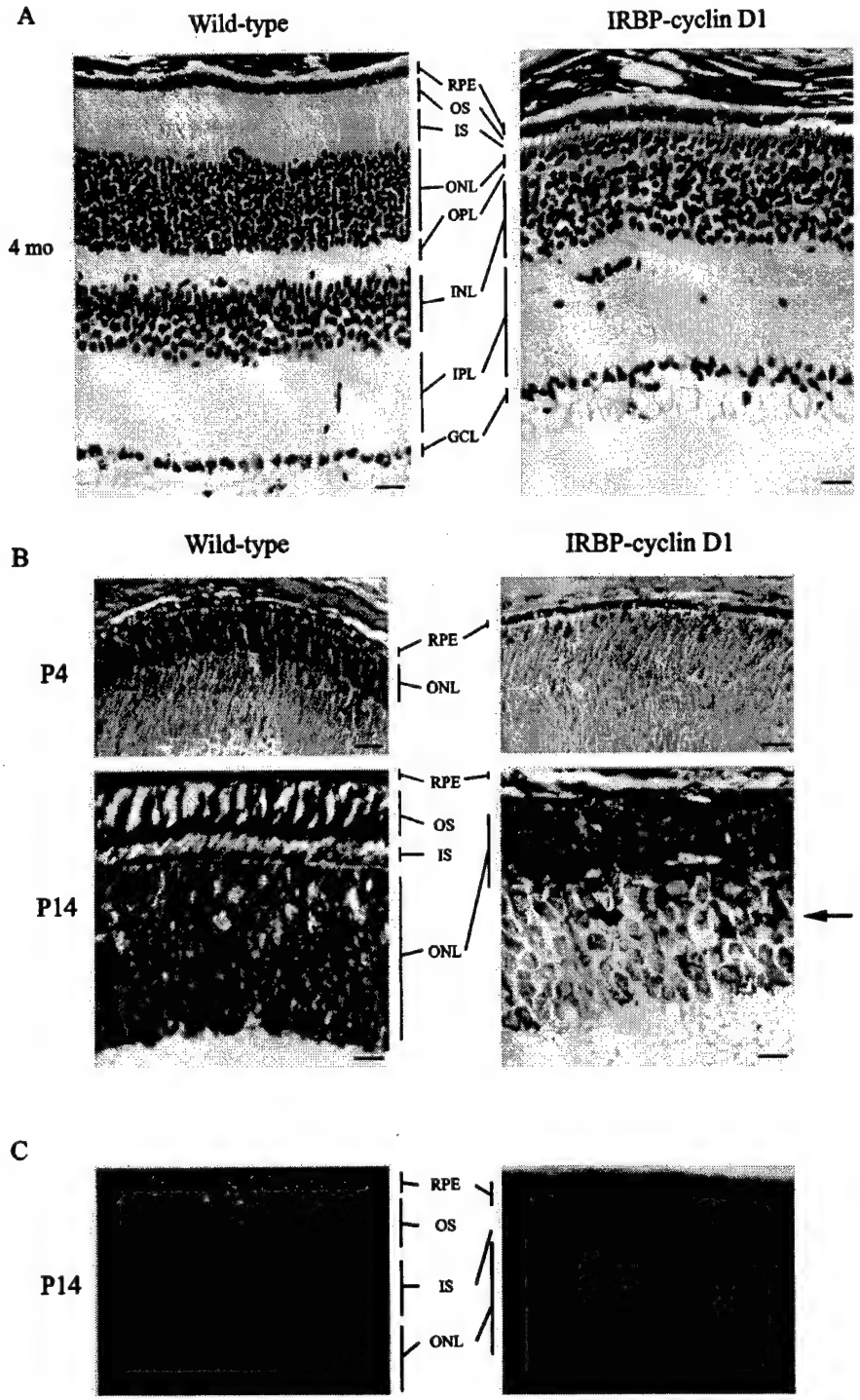

Figure 2 Ectopic expression of cyclin D1 disrupts photoreceptor development. **(A)** Photomicrographs of H and E-stained central retinas of four-month-old wild-type mouse (left) and *IRBP–cyclin D1* littermate (right), taken at 400 × magnification. **(B)** Photomicrographs of retinas of wild-type (left) and transgenic (right) littermates at P4 and P14, taken at 400 × (P4) and 600 × (P14) magnification following immunohistochemical staining for opsin. Note that opsin-positive cells are seen within the inner nuclear layer in IRBP-cyclin D1 mouse retinas at P14 (arrow). **(C)** Photomicrographs of photoreceptors in wild-type (left) and transgenic (right) mice, taken at 1000 × magnification following toluidine blue-O stain. Note the absence of outer segments in the transgenic mice. Scale bars: 25 μm (**A, B** top), 16 μm (**B** bottom). RPE, retina pigment epithelium; OS and IS, outer and inner segments, respectively; ONL and INL, outer and inner nuclear layers, respectively; OPL, IPL, outer and inner plexiform layers, respectively; GCL, ganglion cell layer

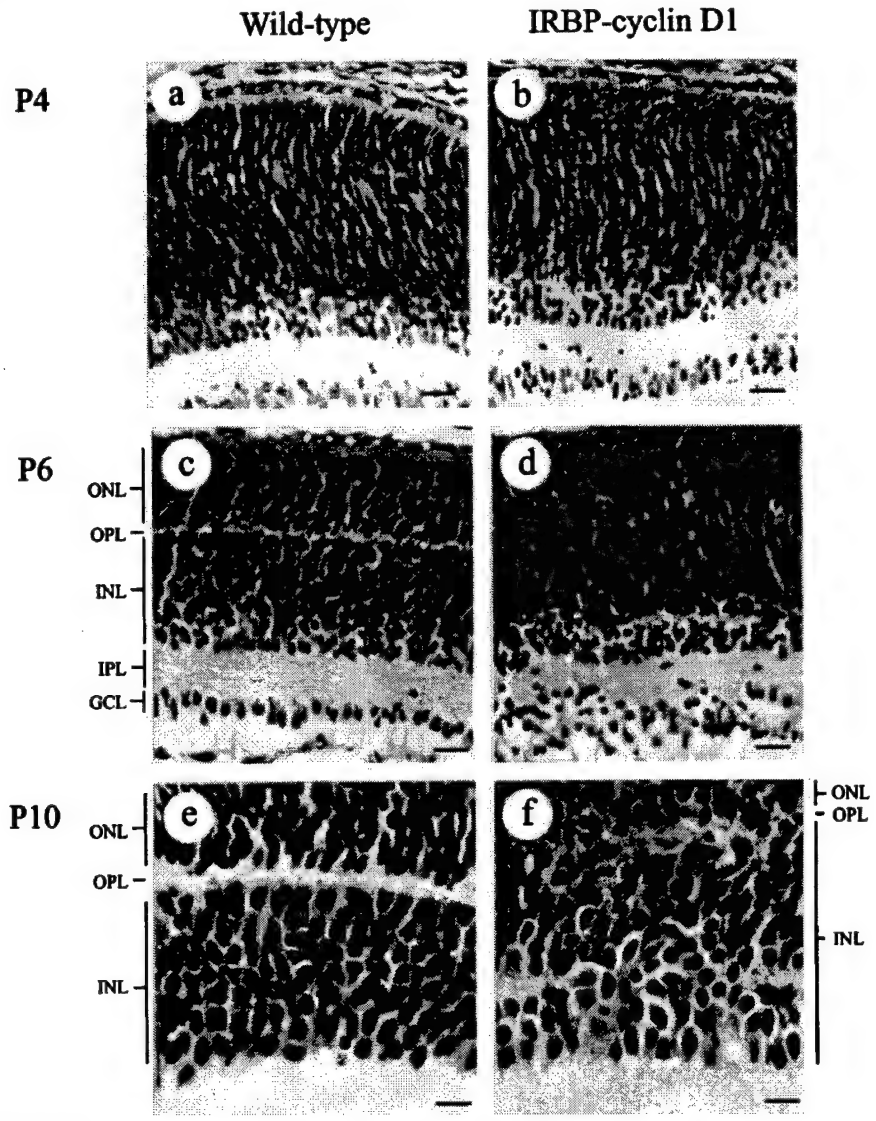

Figure 3 Multiple abnormalities in non-photoreceptor cells in the retinas of *IRBP–cyclin D1* mice. Photomicrographs of the central retinas of wild-type and *IRBP–cyclin D1* mice at P4 (**a, b**), P6 (**c, d**), and P10 (**e, f**) are shown. Tissue was stained with hematoxylin and eosin and photographed at 400 × magnification (**a–d**) or 1000 × magnification (**e, f**). The outer surface of the retina is oriented upward. Scale bars: 25 μm (**a–d**), 10 μm (**e, f**). ONL and INL, outer and inner nuclear layers, respectively; OPL, IPL, outer and inner plexiform layers, respectively; GCL, ganglion cell layer

expression of cyclin D1 in developing photoreceptors increases apoptosis in both photoreceptor and non-photoreceptor cells in the developing retina.

Loss of p53 *decreases apoptosis and allows focal hyperplasia in IRBP–cyclin D1 mice*

Normal cells possess a *p53*-dependent mechanism to detect abnormal proliferation signals and activate a pro-apoptotic response (Sherr, 1998). To determine whether the apoptosis observed in the retina of *IRBP–cyclin D1* transgenic mice was dependent on *p53*, we bred the transgenic mice into a $p53^{-/-}$ background. The loss of *p53* was associated with a decrease (but not an absence) of apoptosis in retinas of transgenic mice at P6 and P13–14 (Figure 4Bb and data not shown). Despite this decrease, there was no change in the average width of the ONL at P13–14 in *IRBP–cyclin D1* with *p53* versus those that lacked *p53* [26.7 (standard error (s.e.) 2.3) μm versus 28.2 (se 1.7) μm, ($P=0.61$), respectively]. Other *IRBP–cyclin D1*-induced abnormalities–such as abnormal photoreceptor cell localization, loss of outer segments, INL disorganization, and cells within the inner plexiform layer–

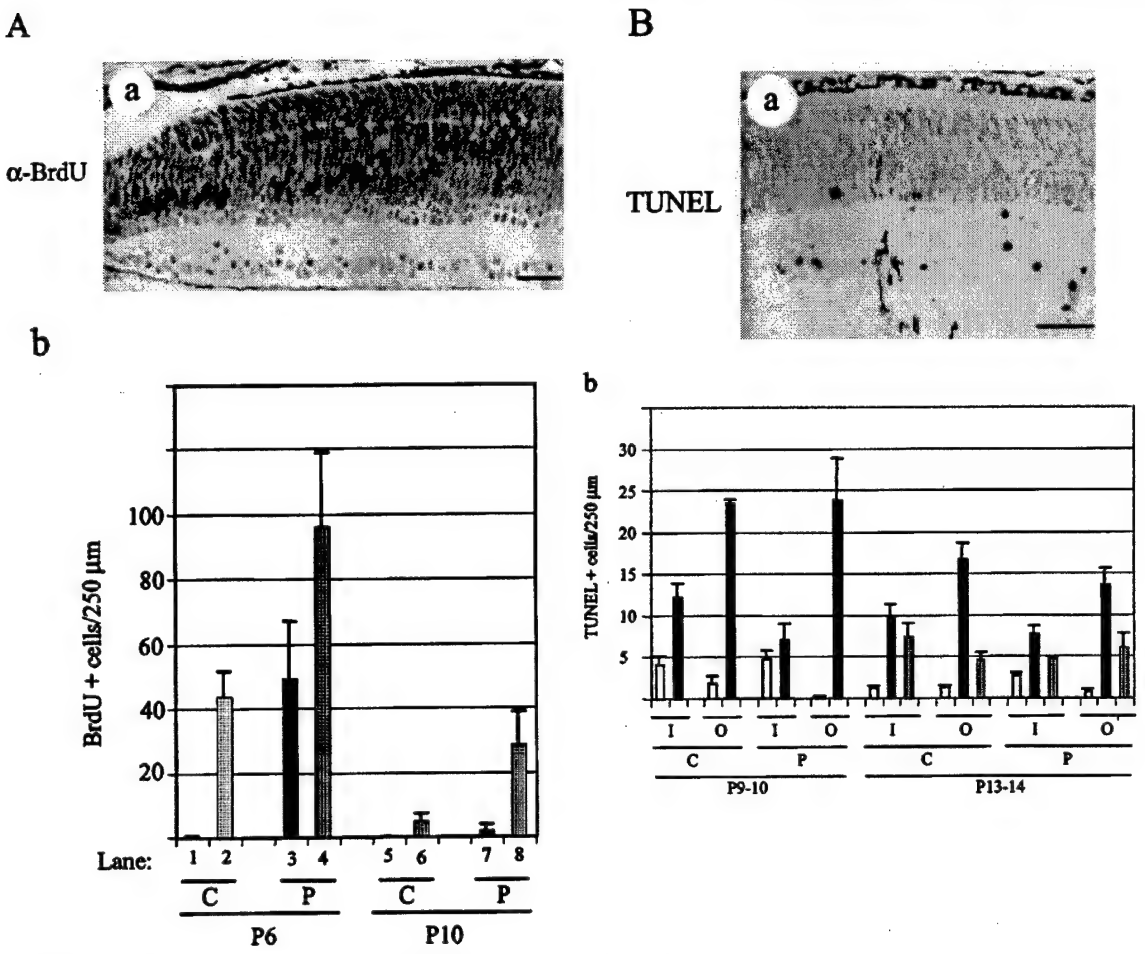

Figure 4 Increased DNA synthesis and apoptosis in retinas of *IRBP–cyclin D1* mice. (**A**) Representative photomicrograph of BrdU labeled cells in wild-type P6 mouse (**a**) (original magnification 200×, scale bar: 50 μm) and quantitation of BrdU labeled cells (**b**) in the central (C) and peripheral (P) retinas from wild-type (black bars) and IRBP-cyclin D1 (gray bars) mice at P6 and P10 as indicated. Values are mean number of BrdU-stained cells within 250 μm of optic nerve (C) or most peripheral retina (P). Error bars represent standard deviation. (**B**) Representative photomicrograph of TUNEL stained cells in wild-type P9 mouse (**a**) (original magnification 200×, scale bar: 50 μm) and quantitation of TUNEL stained cells (**b**) in the INL (I) and ONL (O) of central (C) and peripheral (P) retina from wild-type mice (white bars), *IRBP-cyclin D1* mice with wild-type p53 (black bars) or *IRBP-cyclin D1* mice without wild-type *p53* (gray bars) at P9-10 and P13-14 as indicated. Values are mean number of TUNEL-stained cells within 250 μm of optic nerve (C) or most peripheral retina (P). Error bars represent standard error of the mean. Overall comparisons by genotype were significant at the $P=0.05$ level

were also observed in *IRBP-cyclin D1, p53*$^{-/-}$ mice (compare Figure 5a and b with Figures 2 and 3, and data not shown). Although the presence of these abnormalities was strictly *p53*-independent, our analyses do not exclude the possibility that their severity may be subtly altered in the absence of *p53*.

One expectation was that loss of *p53* in *IRBP–cyclin D1* mice would cause photoreceptor-derived tumors. Serial sections through the entire eye of several *IRBP–cyclin D1, p53*$^{-/-}$ mice only demonstrated two foci of apparent hyperplasia (Figure 5c,d). The microscopic appearance of these foci suggested that they were not derived from photoreceptor cells (Figure 5d and data not shown). Consistent with this, quantitative measurements indicated that the loss of *p53* allowed slight expansion of the non-photoreceptor INL in *IRBP–cyclin D1, p53*$^{-/-}$ mice versus *IRBP–cyclin D1, p53*+ mice [mean INL width: 83.0 (se 4.5) μm versus 66.1 (se 3.3) μm, respectively ($P=0.013$)]. Larger retinal tumors were not observed in 1–4-month-old *IRBP–cyclin D1, p53*$^{-/-}$ mice ($n=7$), nor were they observed in transgenic mice with at least one normal *p53* allele ($n=11$). Hence, *p53* prevents microscopic hyperplasia in the INL of *IRBP–cyclin D1* mice. However, loss of *p53* does not seem to be sufficient to induce macroscopic retina tumors.

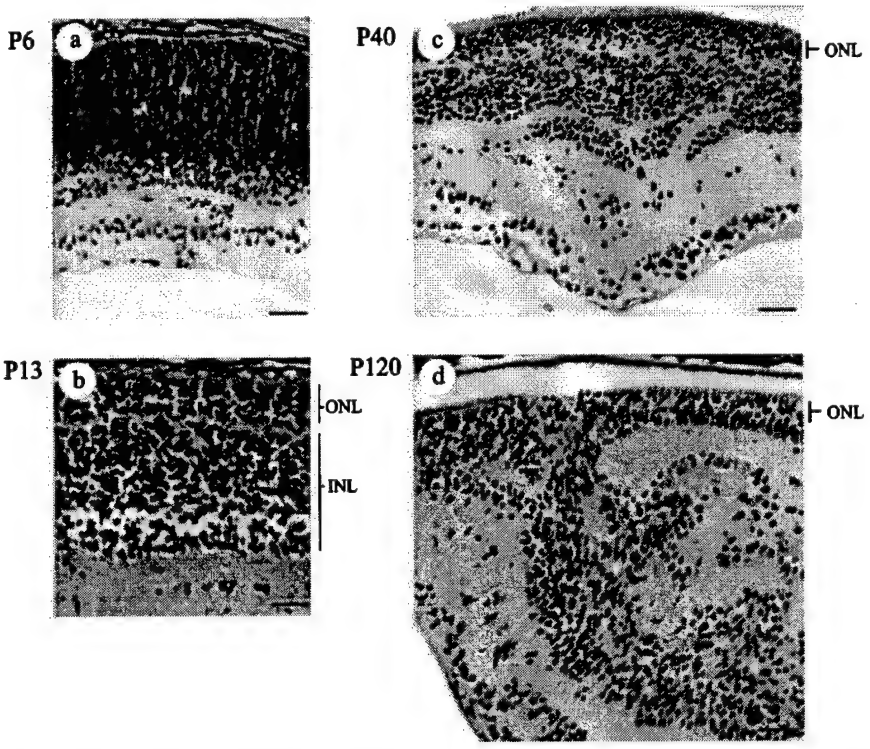

Figure 5 Absence of *p53* causes focal hyperplasia in retina of *IRBP–cyclin D1* mice without altering other retina abnormalities. Photomicrographs of H and E-stained retinas of *IRBP–cyclin D1*, $p53^{-/-}$ mice harvested at P6 (**a**), P13 (**b**), P40 (**c**), and P120 (**d**) were taken at 200 × magnification. The outer surface of the retina is oriented upward. Scale bars: 50 μm. ONL and INL, outer and inner nuclear layer, respectively

Discussion

This study was undertaken to evaluate the relationship between cell cycle arrest and photoreceptor differentiation using a model in which a gene that normally drives cell proliferation in photoreceptor progenitors is persistently expressed. We observed that the persistent expression of cyclin D1 (1) disrupts photoreceptor differentiation as manifested by delayed expression of opsin and lack of outer segments, (2) alters overall retina anatomy, and (3) causes excess proliferation and apoptosis in developing photoreceptor cells. However, this genetic defect is not sufficient to cause macroscopic retina tumors, even in the absence of the tumor suppressor gene, *p53*. These findings offer new insight into how genes in the RB pathway influence photoreceptor differentiation and retina development and they advance our understanding of genetic events that are required for photoreceptor-derived tumor formation.

Ectopic expression of cyclin D1 may alter photoreceptor cell differentiation and retina development by two general mechanisms: by primarily affecting the cell cycle or by influencing processes that are independent of the cell cycle. With respect to the former possibility, cyclin D1 causes hyperphosphorylation and inactivation of RB (Ewen *et al*., 1993; Dowdy *et al*., 1993; Hinds *et al*., 1992), which augments E2F-1 activity and enhances cell proliferation (Dyson, 1998; Harbour and Dean, 2000). Primary alterations of cell cycle exit might disrupt retina development by either altering neuronal cell fate decisions or by decreasing the efficiency of the differentiation process. Either mechanism could explain the observed abnormal photoreceptor morphology, inappropriate localization of photoreceptor cells into the INL, and the apparent expansion and disorganization of non-photoreceptor cells. Although this cell cycle-dependent model is reasonable, it is important to note that our findings are different from those of previous reports in which the RB-E2F-1 pathway is disrupted in photoreceptors. First, in transgenic mouse models in which the *IRBP* promoter drives the expression of either human papilloma virus (HPV) *E7* or *E2F-1*, the most prominent phenotypes are retinal dysplasia, manifested by rosette formation, and massive apoptosis (Howes *et al*., 1994b; Lin *et al*., 2001). Similarly, retinal dysplasia is a prominent finding in mice that are deficient in both *Rb* and the related *p107* gene (Lee *et al*., 1996). Altered photoreceptor cell localization and abnormal inner retinal layers were not reported in those studies, and we did not observe dysplastic photoreceptor rosettes in

the *IRBP–cyclin D1* mice. Given these differences, we must consider that cyclin D1 may have effects that are independent of the RB–E2F-1 pathway and the cell cycle.

There are different mechanisms by which cyclin D1 could regulate photoreceptor differentiation in a manner that is independent of the cell cycle. For example, as has been suggested for myogenic transcription factors (Skapek *et al.*, 1995; Rao *et al.*, 1994), cyclin D1-associated cdk activity may alter the function of a transcription factor that influences retinal cell fate or photoreceptor-specific gene expression. Alternatively, cyclin D1 could exert its effects by shifting the relative levels of other cyclin/cdk complexes and CKIs (Sherr and Roberts, 1999). This mechanism is particularly interesting given the role of certain CKIs in retinogenesis. For example, mice lacking $p27^{Kip1}$ show retinal dysplasia and apparent expansion of the INL similar to that observed in our *IRBP–cyclin D1* mice (Nakayama *et al.*, 1996). Others have shown that loss of $p27^{Kip1}$ or $p57^{Kip2}$ in the mouse retina or forced expression of $p27^{Xic1}$ in the *Xenopus* retina alters cell cycle exit and development of specific retinal cell types (Levine *et al.*, 2000; Dyer and Cepko, 2000; Ohnuma *et al.*, 1999). However, the effects of $p27^{Xic1}$ appear to be separable from its function as a formal cdk regulator (Ohnuma *et al.*, 1999). Further experiments will be required to clarify the mechanism by which persistent expression of cyclin D1 in developing photoreceptor precursors alters retina development.

Another prominent phenotype in *IRBP–cyclin D1* mice was the decreased number of photoreceptor cells in the retinas of mature mice, likely because of both *p53*-dependent and *p53*-independent apoptosis. There are several mechanisms by which cyclin D1 may induce apoptosis in the developing photoreceptors. For example, loss of RB (Jacks *et al.*, 1992; Lee *et al.*, 1992, 1994; Clarke *et al.*, 1992; Lin *et al.*, 2001) or transgenic expression of HPV *E7* to disrupt RB function (Howes *et al.*, 1994b) enhances apoptosis in neuronal cells, including the mouse retina. Secondly, dysregulated cyclin D1 may signal to the $p19^{ARF}$ tumor suppressor to induce apoptosis in response to abnormal proliferation signals (Sherr, 1998). A final mechanism to account for cyclin D1-induced apoptosis in photoreceptors may be related to its effects on photoreceptor differentiation. It is established that even subtle abnormalities in photoreceptor development, such as expression of mutated forms of the light-sensing protein rhodopsin can lead to photoreceptor loss by apoptosis (Chang *et al.*, 1993, Humphries *et al.*, 1997). Whether the apoptosis observed in the *IRBP–cyclin D1* mice is due to disruption of the RB-like protein function, due to a $p19^{ARF}$-dependent pathway that responds to abnormal proliferative signals or due to abnormal photoreceptor differentiation will require further studies.

A final issue raised by these studies is the tumorigenic capacity of cyclin D1 and the role of *p53* as a tumor suppressor in photoreceptor cells that express cyclin D1. In our studies, occasional microscopic hyperplastic foci were found in the INL of the retinas of $p53^{-/-}$ transgenic mice.

Interestingly, the morphology of the cells in these foci suggests that they are not composed of photoreceptor cells. A similar finding has been observed in *IRBP–E2F-1*, $p53^{-/-}$ mice (Lin *et al.*, 2001), and in chimeric mice in which retina cells were derived from $Rb^{-/-}$, $p107^{-/-}$ mice which developed tumors of amacrine cell origin (Robanus-Maandag *et al.*, 1998). These findings are in contrast to those of previous work in which mice expressing *IRBP*-simian virus 40 large T antigen (SV40–*Tag*) and *IRBP*–HPV *E7*, $p53^{-/-}$ mice, both of which caused large photoreceptor-derived tumors (Howes *et al.*, 1994a,b). The differences in retinal tumor formation in these transgenic models suggest that the *p53* tumor suppressor prevents microscopic foci of hyperplasia induced by cyclin D1, but further genetic mutations are probably required for the development of macroscopic retinal tumors. These additional changes either may not be required or may accumulate more readily in photoreceptor cells expressing SV40–*Tag* or HPV *E7*. Identifying these additional genetic changes may offer a useful insight into mechanisms driving retina tumor development when the cyclin-RB–E2F pathway is disrupted.

Materials and methods

Animals and animal maintenance

Wild-type C57BL6 mice and $p53^{-/-}$ mice (Donehower *et al.*, 1992) were maintained in isolator cages according to standard husbandry practice. Animal studies were approved by the relevant institutional review boards at the University of Texas Health Science Center and St. Jude Children's Research Hospital.

IRBP–cyclin D1 transgene construction

The *pIRBP–cyclin D1* transgene was made by using the *pBS/pKCR3* plasmid modified from *pKCR3* (Howes *et al.*, 1994b) (provided by J Windle, University of Texas Health Science Center at San Antonio, USA). The plasmid contained 1.9 kb of DNA from the mouse *IRBP* promoter, which includes the transcription start site, and a portion of the rabbit *β-globin* gene, which provides splicing elements and a polyadenylation signal (Howes *et al.*, 1994b). Human *cyclin D1* cDNA, which contained a translation initiation codon and a hemagglutinin (HA) tag at the COOH terminus, was obtained by *Bam*HI and *Not*I digestion of the *pRC/cyclin D1* plasmid (Dowdy *et al.*, 1993, Hinds *et al.*, 1992) (provided by P. Hinds, Harvard Medical School, USA). The ends of this restriction fragment were filled in with Klenow DNA polymerase and then subcloned into the *Eco*RI enzyme site (also filled in with Klenow DNA polymerase) within exon 3 of the *β-globin* gene (as previously described Howes *et al.*, 1994b) to generate the *pIRBP–cyclin D1* plasmid. Restriction enzyme digests confirmed the correct orientation of the cDNA insert.

Transgenic mouse production and analysis

The purified *pIRBP–cyclin D1* plasmid was digested with *Xho*I enzyme to release a ~4.0 kb cDNA fragment that

contained the *IRBP* promoter and *cyclin D1* cDNA, which included the polyadenylation signal. This fragment was gel-purified and injected into the pronuclei of fertilized eggs derived from CB6 F1 × C57BL6 intercrosses, according to standard protocols.

To determine the genotype of the offspring, genomic DNA was isolated from either tail biopsy samples or tail vein blood samples and analysed by either Southern blotting or PCR. Southern blotting was performed by digesting genomic DNA with NcoI enzyme and probing the blot with a gel-purified, ^{32}P-dCTP-labeled cDNA probe containing the *IRBP–cyclin D1* cDNA. PCR was performed by using 5′-gATCCACTAg-TAACggCCgC as the 5′ primer (complementary to sequence from the *pRC/CMV* plasmid polylinker immediately adjacent to the *cyclin D1* cDNA) and 5′-ACACATTTgAAgTAggA-CACCg as the 3′ primer taken from the human *cyclin D1* cDNA. PCR reactions were performed by using 35 cycles at the following conditions: 94°F × 30 sec to denature the samples, 63°F × 30 sec for annealing the DNA, and 72°F × 1 minute for extension. The expected 350-bp PCR product was visualized by ethidium bromide staining after it had been subjected to agarose gel electrophoresis.

Histologic studies

Morphological studies were performed on mouse retina tissue at P4, P6, P10, P13, P14, P40 and P120. For these studies, mice were killed by cervical dislocation immediately before surgical removal of the eyes. Eyes were fixed for 18–24 h in 4% paraformaldehyde in phosphate-buffered saline and then embedded in paraffin blocks, according to standard techniques. Sections 4 μm or 5 μm thick were stained for (1) cell type distinction with hematoxylin and eosin, (2) presence of cyclin D1 and opsin, or (3) apoptosis with TUNEL. Thin sections (0.75 μm) were stained with Toluidine blue-O. In a separate set of experiments, proliferation of retinal cells was examined. In those studies, mice received an intraperitoneal injection of bromodeoxyuridine (BrdU) at a dose of 100 μg per g of body weight 2–3 h before their eyes were harvested, fixed, and processed, as described above.

For immunohistochemical staining, the following antibodies were used: mouse anti-cyclin D1 (1:400, Zymed Laboratories, San Francisco, CA, USA), mouse anti-opsin (obtained from D Papermaster), and mouse anti-BrdU (1:200, Becton Dickinson, San Jose, CA, USA). After the cells were stained with primary antibody, secondary antibody staining was performed by using the Vectastain Elite ABC kit (Vector Laboratories, Burlingame, CA, USA) with Vector VIP or DAB substrates and methyl green or hematoxylin counterstain, according to the manufacturer's recommendations. TUNEL staining was performed as previously described (Howes *et al.*, 1994b; Gavrieli *et al.*, 1992).

For quantitative data, the average number of BrdU- or TUNEL-labeled cells, and the average width of the ONL and INL were determined using a light microscope. Measurements in the central retina and peripheral retina were within 250 μm of the optic nerve or the most anterior aspect of the neuroretina, respectively. Two to six stained sections from 1 (BrdU at P6), or 2–4 (all other variables) mice of each genotype were analysed to obtain quantitative data. The values are expressed as mean and standard error of the mean. Statistical analyses were performed for ONL and INL thickness, BrdU labeling at P10, and TUNEL labeling at P9-10 and P13-14 using a repeated measures model for normal outcome (Diggle *et al.*, 1994), with the Bonferroni procedure to adjust for multiple comparisons within each age group.

Photomicrography was performed by using an Olympus BX60 microscope (Olympus, Melville, NY, USA) equipped with an Olympus PM-30 camera to produce 35-mm slides. Digital images were captured by using a Nikon Coolscan III LS-30 film scanner (Nikon, Inc., Melville, NY, USA) and the Adobe Photoshop 5.0 software program.

Acknowledgments

The authors gratefully acknowledge the plasmid reagents provided by P Hinds and J Windle; technical assistance provided by S Lampkin in the Histology Laboratory at University of Texas Health Science Center at San Antonio and Ms L Rhodes; helpful discussions with Drs J Cunningham, D Rice and D Papermaster; statistical assistance by C Billups; and editorial assistance by Dr A McArthur. This work was supported, in part, by the American Lebanese Syrian Associated Charities (ALSAC).

References

Cepko CL, Austin CP, Yang X, Alexiades M and Ezzeddine D. (1996). *Proc. Natl. Acad. Sci. USA*, **93**, 589–595.

Chang G-Q, Hao Y and Wong F. (1993). *Neuron*, **11**, 595–605.

Clarke AR, Maandag ER, van Roon M, van der Lugt NMT, van der Valk M, Hooper ML, Berns A and te Riele H. (1992). *Nature*, **359**, 328–330.

DiCiommo D, Gallie BL and Bremner R. (2000). *Sem. Cancer Biol.*, **10**, 255–269.

Diggle P, Liang K-Y and Zeger S. (1994). *Analysis of longitudinal data*. Clarendon Press: Oxford, England. pp. 63–77.

Dobashi Y, Kudoh T, Matsumine A, Toyoshima K and Akiyama T. (1995). *J. Biol. Chem.*, **270**, 23031–23037.

Donehower LA, Harvey M, Slagle BL, McArthur MJ, Montgomery Jr. CA, Butel JS and Bradley A. (1992). *Nature*, **356**, 215–221.

Dowdy SF, Hinds PW, Louie K, Reed SI, Arnold A and Weinberg RA. (1993). *Cell*, **73**, 499–511.

Dyer MA and Cepko CL. (2000). *Development*, **127**, 3593–3605.

Dynlacht BD. (1997). *Nature*, **389**, 149–152.

Dyson N. (1998). *Genes Dev.*, **12**, 2245–2262.

Ewen ME, Sluss HK, Sherr CJ, Matsushime H, Kato JY and Livingston DM. (1993). *Cell*, **73**, 487–497.

Gavrieli Y, Sherman Y and Ben-Sasson SA. (1992). *J. Cell Biol.*, **119**, 493–501.

Harbour JW and Dean DC. (2000). *Genes Dev.*, **14**, 2393–2409.

Hinds PW, Mittnacht S, Dulic V, Arnold A, Reed SI and Weinberg RA. (1992). *Cell*, **70**, 993–1006.

Howes KA, Lasudry JGH, Albert DM and Windle JJ. (1994a). *Invest. Ophthalmol. Vis. Sci.*, **35**, 342–351.

Howes KA, Ransom N, Papermaster DS, Lasudry JGH, Albert DM and Windle JJ. (1994b). *Genes Dev.*, **8**, 1300–1310.

Humphries MM, Rcourt D, Farrar GJ, Kenna P, Hazel M, Bush RA, Sieving PA, Sheils DM, McNally N, Creighton P, Erven A, Boros A, Gulya K, Capecchi MR and Humphries P. (1997). *Nature Genet.*, **15,** 216–219.

Jacks T, Fazeli A, Schmitt EM, Bronson RT, Goodell MA and Weinberg RA. (1992). *Nature,* **359,** 295–300.

Lee EY, Chang CY, Hu N, Wang YJ, Lai CC, Herrup K, Lee WH and Bradley A. (1992). *Nature,* **359,** 288–294.

Lee EY-HP, Hu N, Yuan SF, Cox LA, Bradley A, Lee W-H and Herrup K. (1994). *Genes Dev.*, **8,** 2008–2021.

Lee N-H, Williams BO, Mulligan G, Mukai S, Bronson RT, Dyson N, Harlow E and Jacks T. (1996). *Genes Dev.*, **10,** 1621–1632.

Levine EM, Close J, Fero M, Ostrovsky A and Reh TA. (2000). *Devel. Biol.*, **219,** 299–314.

Lin S-C, Skapek SX and Lee EY-HP. (1996). *Sem. Cancer Biol.*, **7,** 279–289.

Lin S-C J, Skapek SX, Papermaster DS, Hankin M, Lee EY-HP. (2001). *Oncogene,* in press.

Ma C, Papermaster D and Cepko CL. (1998). *Proc. Natl. Acad. Sci. USA,* **95,** 9938–9943.

Morrow EM, Belliveau MJ and Cepko CL. (1998). *J. Neurosci.*, **18,** 3738–3748.

Nakayama K, Ishida N, Shirane M, Inomata A, Inoue T, Shishido N, Horii A, Loh DY and Nakayama K-I. (1996). *Cell,* **85,** 707–720.

Ohnuma S-I, Philpott A, Wang K, Holt CE and Harris WA. (1999). *Cell,* **99,** 499–510.

Poluha W, Poluha DK, Chang B, Crosbie NE, Schonhoff CM, Kilpatrick DL and Ross AH. (1996). *Mol. Cell. Biol.*, **16,** 1335–1341.

Rao SS, Chu C and Kohtz DS. (1994). *Mol. Cell. Biol.*, **14,** 5259–5267.

Reh TA and Levine EM. (1998). *J. Neurobiol,* **36,** 206–220.

Riley DJ, Lee EYHP and Lee W-H. (1994). *Ann. Rev. Cell Biol.*, **10,** 1–29.

Robanus-Maandag E, Dekker M, van der Valk M, Carrozza M-L, Jeanny J-C, Dannenberg J-H, Berns A and te Riele H. (1998). *Genes Dev.*, **12,** 1599–1609.

Ross ME. (1996). *Trends Neurosci.*, **19,** 62–68.

Sherr CJ. (1996). *Science,* **274,** 1672–1677.

Sherr CJ. (1998). *Genes Dev.*, **12,** 2984–2991.

Sherr CJ and Roberts JM. (1999). *Genes Dev.*, **13,** 1501–1512.

Sicinski P, Donaher JL, Parker SB, Li T, Faxeli A, Gardner H, Haslam SZ, Bronson RT, Elledge SJ and Weinberg RA. (1995). *Cell,* **82,** 621–630.

Skapek SX, Rhee J, Spicer DB and Lassar AB. (1995). *Science,* **267,** 1022–1024.

Turner DL, Snyder EY and Cepko CL. (1990). *Neuron,* **4,** 833–845.

Weinberg RA. (1995). *Cell,* **81,** 323–330.

Young RW. (1984). *J. Comp. Neurol.*, **229,** 362–373.

Young RW. (1985). *Anat. Rec.*, **212,** 199–205.

ELSEVIER

DNA Repair 1 (2002) 137–142

DNA REPAIR

www.elsevier.com/locate/dnarepair

Arsenic-induced Mre11 phosphorylation is cell cycle-dependent and defective in NBS cells

Shyng-Shiou F. Yuan[a,*], Jinu-Huang Su[a], Ming-Feng Hou[b], Fei-Wen Yang[a], Song Zhao[c], Eva Y.-H.P Lee[c]

[a] *Department of Obstetrics and Gynecology, Kaohsiung Medical University Hospital, Kaohsiung 807, Taiwan, ROC*
[b] *Department of Surgery, Kaohsiung Medical University Hospital, Kaohsiung 807, Taiwan, ROC*
[c] *Department of Molecular Medicine/Institute of Biotechnology, University of Texas Health Science Center, San Antonio, TX 78245-3207, USA*

Received 19 July 2001; received in revised form 20 October 2001; accepted 29 October 2001

Abstract

Cancer-prone diseases ataxia-telangiectasia (AT), Nijmegen breakage syndrome (NBS) and ataxia-telangiectasia-like disorder (ATLD) are defective in the repair of DNA double-stranded break (DSB). On the other hand, arsenic (As) has been reported to cause DSB and to be involved in the occurrence of skin, lung and bladder cancers. To dissect the repair mechanism of As-induced DSB, wild type, AT and NBS cells were treated with sodium arsenite to study the complex formation and post-translational modification of Rad50/NBS1/Mre11 repair proteins. Our results showed that Mre11 went through cell cycle-dependent phosphorylation upon sodium arsenite treatment and this post-translational modification required NBS1 but not ATM. Defective As-induced Mre11 phosphorylation was rescued by reconstitution with full length NBS1 in NBS cells. Although As-induced Mre11 phosphorylation was not required for Rad50/NBS1/Mre11 complex formation, it might be required for the formation of Rad50/NBS1/Mre11 nuclear foci upon DNA damage.

Keywords: Ataxia-telangiectasia; Nijmegen breakage syndrome; Ataxia-telangiectasia-like disorder; DNA double-stranded breaks; Arsenic; Phosphorylation

1. Introduction

The maintenance of genomic integrity is essential for the cell surviving and functioning [1]. Ataxia-telangiectasia (AT), Nijmegen breakage syndrome (NBS) and ataxia-telangiectasia-like disorder (ATLD), caused by mutations in *ATM*, *NBS1* and *Mre11*, respectively, share the similar phenotypes of defective DNA double-stranded break (DSB) repair and aberrant checkpoint activation when treated with ionizing radiation (IR) or radio-mimetic drugs [2–4]. A function link between repair proteins ATM and NBS1 was demonstrated recently [5–8]. Furthermore, IR-induced Mre11 phosphorylation is abrogated in NBS cell lines [9]. All these results suggest that ATM, NBS1 and Mre11 may play important roles in DNA repair through protein–protein interaction and post-translational modification.

Arsenic (As) is a naturally occurring metalloid and broadly present in water, soil, air and food. Chronic As exposure has a strong correlation to the occurrence of bladder, lung and skin cancers [10]. However, the molecular basis for the carcinogenesis of As is mostly unclear. As treatment leads to DNA mutations, DSBs,

* Corresponding author. Tel.: +886-7-3805228; fax: +886-7-3110947.
E-mail address: yuanssf@ms33.hinet.net (S.-S.F. Yuan).

1568-7864/02/$ – see front matter
PII: S1568-7864(01)00009-X

chromosome breaks and deletions, micronuclei induction and aneuploidy in the cells, events frequently observed in cancer cells [11–14]. As also induces cell proliferation and aberrant expression of genes involved in cell growth or cell cycle control [15–18].

To study the genetic requirement for the repair of As-induced DNA damage, cultured wild type, AT and NBS cells were treated with sodium arsenite to analyze post-translational modification of Rad50/NBS1/Mre11 protein complex and formation of Rad50/NBS1/Mre11 nuclear foci. Here, we showed that As-induced Mre11 phosphorylation required NBS1, not ATM. Although As-induced Mre11 phosphorylation was present in all phases of cell cycle, it was most dominant at M phase.

2. Materials and methods

2.1. Cell culture and treatment

Human AT fibroblast cell lines (GM05849C, and GM09607B) and NBS fibroblast cell lines (GM07166A and GM15989) were received from Coriell Institute and cultured in DMEM with 10% FBS. Human NBS fibroblast NBS-LBI, VA13 human fibroblast and T24 human bladder transitional cell carcinoma cell lines were all grown in DMEM with 10% FBS. NBS-LBI-V and NBS-LBI-WT stable cell lines were derived from NBS-LBI, a NBS cell line, after infection with pLXIN retroviral vector (Clontech) and retroviral vector expressing wild type NBS1, respectively. Both stable cell lines were selected under 500 μg/ml G418 (Sigma) and maintained in DMEM supplemented with 10% FBS and 200 μg/ml G418. Various cell cycle phases T24 cells were retrieved by density arrest accordingly [19] and cell cycle distribution of T24 cells was analyzed by EPICS flow cytometer (Beckman Coulter). M phase-enriched T24 cells were achieved by treating the cells, which were 32 h released from density arrest, with 0.4 μg/ml nocodazole (Sigma) for 10 h.

2.2. Immunoblotting and immunoprecipitation

The cultured cells were treated with sodium arsenite (Sigma) or γ-irradiation, harvested and lysed in EBC buffer (50 mM Tris, pH7.6, 120 mM NaCl, 0.5% Nonidet P-40, 1 mM EDTA, 1 mM β-mercaptoethanol, 50 mM NaF, and 1 mM Na_3VO_4) plus protease inhibitors. The detailed procedures for immunoblotting and immunoprecipitation were followed accordingly [20]. Phosphatase and phosphatase inhibitor (New England BioLab) were incubated with the Mre11 immunoprecipitate to study the As-induced Mre11 phosphorylation [7]. Rad50, NBS1 and Mre11 proteins were detected by enhanced chemiluminence (Amersham Pharmacia Biotech).

2.3. Immunofluorescent staining

The cultured cells were grown in 35 mm petri dish, treated with sodium arsenite and fixed for NBS1 nuclear foci study. Cell treatment and immunofluorescent staining were carried out as described [20]. In this assay, NBS1 monoclonal antibody and FITC-conjugated goat anti-mouse IgG (Jackson Immunochemicals) were used as the primary and secondary antibodies, respectively.

3. Results

3.1. The effect of cell cycle on arsenic-induced Mre11 phosphorylation

The cellular responses to As are complex and include DNA damage, aberrant cell growth and apoptosis ([10] for review). To study how As affects the DSB repair machinery, T24 cells were treated with sodium arsenite and Rad50/NBS1/Mre11 repair proteins were analyzed. Interestingly, exposure of T24 cells to sodium arsenite for 3 h at the concentration of 10 μM or more, before obvious cell death was noticed by morphology, resulted in the formation of a slower migrating form of Mre11 (Fig. 1A). This mobility shift was abolished after phosphatase treatment (Fig. 1B), suggesting it was caused by protein phosphorylation. As-induced Mre11 phosphorylation appeared 2 h after treatment and persisted for at least 8 h (Fig. 1C). For comparison, the dosage effect (Fig. 1A) and time course of IR-induced Mre11 phosphorylation (Fig. 1C) was also analyzed. In our study, IR-induced Mre11 phosphorylation was observed as early as 10 min after 20 Gy γ-irradiation treatment and decreased at 8 h after treatment (Fig. 1C).

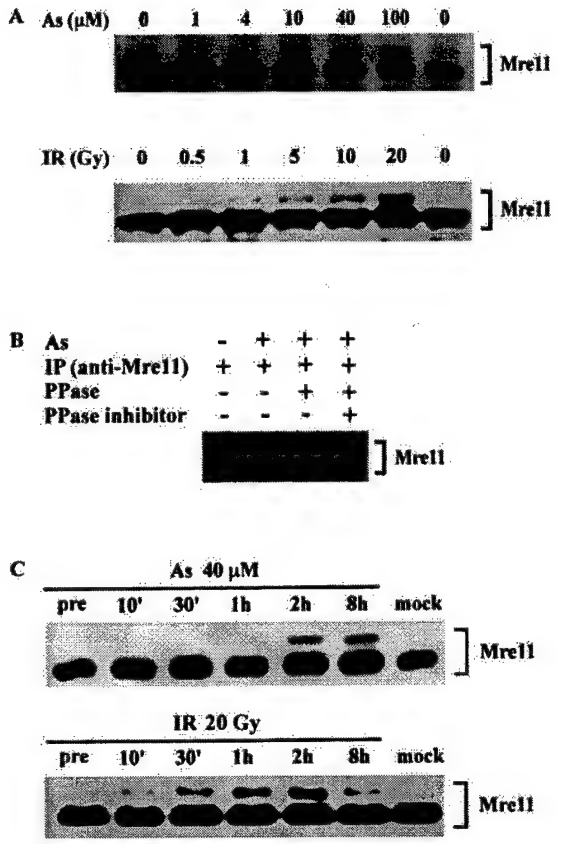

Fig. 1. Arsenic-induced Mre11 mobility shift was caused by phosphorylation. (A) Mobility shift of Mre11. Unsynchronized T24 cells were treated with various dosages of sodium arsenite (As) for 3 h or γ-irradiation (IR) and then subjected for immunoblotting analysis. (B) Phosphorylation of Mre11. Arsenic-treated T24 cell lysates were immunoprecipitated (IP) with anti-Mre11 antibody and the immunoprecipitate was incubated with phosphatase (PPase) in the absence or presence of phosphatase inhibitor. (C) The time course of arsenic-induced and IR-induced Mre11 phosphorylation. T24 cells were treated with 40 μM sodium arsenite or 20 Gy γ-irradiation and the kinetics of Mre11 phosphorylation was analyzed at different time points after treatment. (−) Without treatment; (+) with treatment; (pre) before sodium arsenite treatment; (mock) in arsenic-free medium or without γ-irradiation for 8 h.

To examine the effect of cell cycle progression on As-induced Mre11 phosphorylation, T24 cells of different cell cycle phases were obtained by density arrest [19] or nocodazole treatments. T24 cells of various phases were harvested for Mre11 immunoblotting analysis after As exposure for 3 h. Although the As-induced Mre11 phosphorylation was observed in T24 cells of all cell cycle phases, it was more significant at M phase (Fig. 2). This result was somewhat different from the IR-induced Mre11 phosphorylation, which is at similar levels in all cell cycle phases (Fig. 2).

3.2. The effect of arsenic on Rad50/NBS1/Mre11 protein complex maintenance and NBS1 nuclear focus formation

To study the functional significance of As-induced Mre11 phosphorylation on DSB repair, the effect of As on the maintenance of Rad50/NBS1/Mre11 protein complex and formation of NBS1 nuclear foci was analyzed. Although sodium arsenite treatment induced Mre11 phosphorylation in cultured cells, Rad50/NBS1/Mre11 complex remained unchanged before and after treatment (Fig. 3A), suggesting Mre11 phosphorylation was not required for Rad50/NBS1/Mre11 complex maintenance. However, the NBS1 nuclear foci formation is prompt in response to As (Fig. 3B). In our preliminary study, about 8% of the unsynchronized T24 cells showed NBS1 foci at 5 h after 40 μM sodium arsenite treatment, in comparison to 2% before treatment (data not shown).

3.3. The requirement of NBS1 for arsenic-induced Mre11 phosphorylation

It has been well documented that ATM and NBS1 are the key players in DSB repair ([21] for review). To study the requirement of ATM and NBS1 for the As-induced Mre11 phosphorylation, wild type, AT cells and NBS cells were treated with 40 μM sodium arsenite for 3 h and subjected for Mre11 analysis. The As-induced Mre11 phosphorylation was observed in wild type and AT cells but not NBS cell lines we analyzed (Fig. 4B). However, this post-translational modification reappeared in the NBS cells when they were reconstituted with full length NBS1 (Fig. 4B), suggesting NBS1 was required for As-induced Mre11 phosphorylation. Interestingly, an elevated basal level of Mre11 phosphorylation was observed frequently in GM09607B AT cells and less frequently in other AT and NBS cell lines we tested. The reason for this constitutive phosphorylation is unclear, but suggests certain ATM-independent kinase(s) may be involved [9].

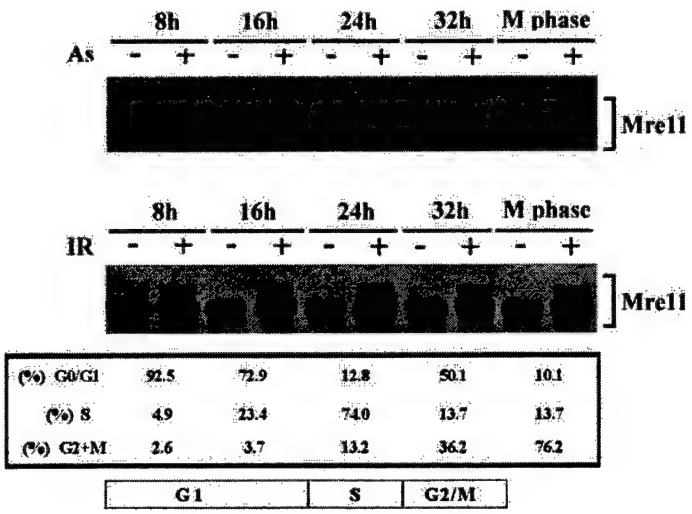

Fig. 2. Arsenic-induced Mre11 phosphorylation was cell cycle-dependent. T24 cells of various cell cycle phases were retrieved after releasing from density arrest for 8, 16, 24, and 32 h. M phase-enriched cells (M phase) were retrieved by treating the T24 cells, which were 32 h released from density arrest, with 0.4 μg/ml nocodazole for 10 h. Cell cycle distribution of T24 cells was analyzed by flow cytometer. T24 cells of different phases were treated with 40 μM sodium arsenite for 3 h or 20 Gy γ-irradiation and the cell lysates were subjected for immuoblotting analysis.

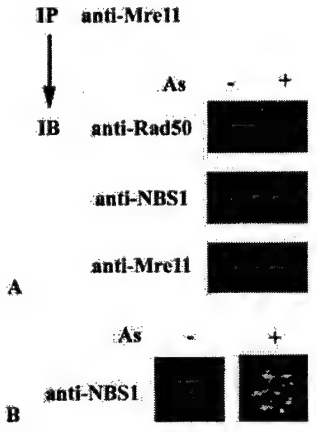

Fig. 3. The effect of arsenic-induced Mre11 phosphorylation on Rad50/NBS1/Mre11 complex maintenance and NBS1 nuclear focus formation. (A) For Rad50/NBS1/Mre11 complex study, unsynchronized T24 cells were treated with 40 μM sodium arsenite for 3 h and the cell lysates were immunoprecipitated (IP) with anti-Mre11 antibody, followed by immunoblotting (IB) using anti-Rad50, anti-NBS1 and anti-Mre11 antibodies, respectively. (B) For NBS1 nuclear foci analysis, unsynchronized T24 cells were treated with 40 μM sodium arsenite for 5 h and the cells were fixed and subjected for immunofluorecent staining.

ATM and NBS1 dependency of Mre11 phosphorylation following IR was also analyzed for comparison. Although As-induced Mre11 phosphorylation is NBS1-dependent but ATM-independent (Fig. 4B), both ATM and NBS1 are required for IR-induced Mre11 phosphorylation (Fig. 4C).

4. Discussion

As is a well documented environmental carcinogen [10]. Although it causes DSBs in the exposed cells, the role of DSB repair proteins in the repair process of As-induced DNA damage is not clear. To the best of our knowledge, this is the first report demonstrating the involvement of Rad50/NBS1/Mre11 DSB repair complex in As-induced DNA damage.

It has been reported that As-treated cells arrested at G1 and G2/M phases and then went through apoptosis eventually [22,23]. It was intriguing to notice that the As-induced Mre11 phosphorylation was dominant at M phase (Fig. 2). Since T24 cells were harvested 3 h after 40 μM sodium arsenite treatment, before cell apoptosis was observed, the functional significance of this M phase-dominant event remains to be explored.

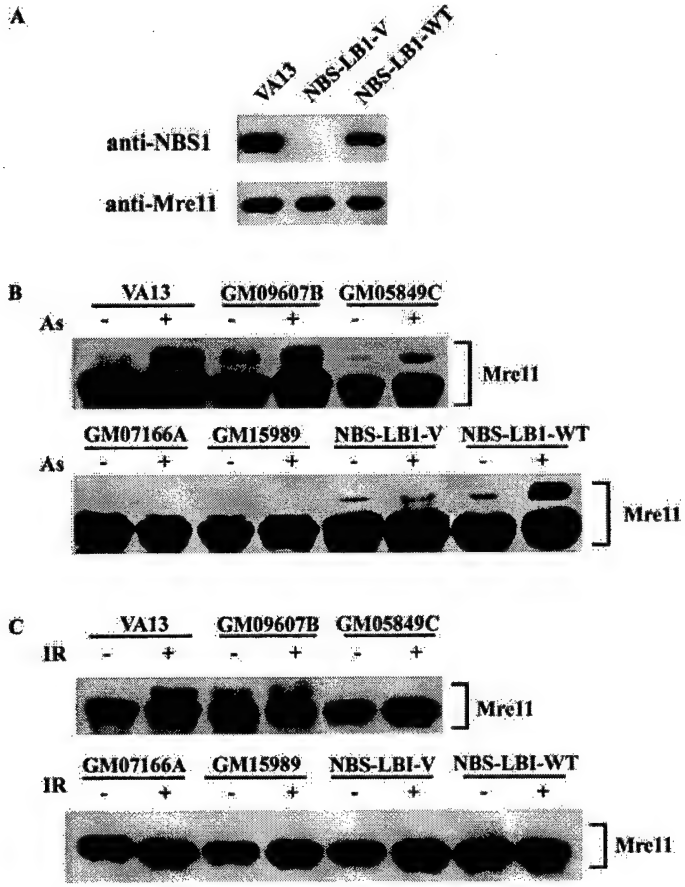

Fig. 4. The requirement of ATM and NBS1 for arsenic-induced Mre11 phosphorylation. (A) The expression of NBS1 and Mre11 in wild type fibroblasts (VA13), NBS fibroblasts (NBS-LBI-V) and NBS1-reconstituted NBS fibroblasts (NBS-LBI-WT). (B) VA13, AT fibroblasts (GM09607B and GM05849C), NBS fibroblasts (GM07166A, GM15989 and NBS-LBI-V) and NBS-LBI-WT were treated with 40 μM sodium arsenite for 3 h and the cell lysates were subjected for immunoblotting analysis. (C) The cells were treated with 20 Gy γ-irradiation, harvested at 3 h after treatment and subjected for immunoblotting analysis.

The involvement of Rad50/NBS1/Mre11 protein complex in DSB repair is well documented ([21] for review). In our study, As-induced Mre11 phosphorylation was observed at earlier time points than the formation of NBS1 foci. Although the Rad50/NBS1/Mre11 protein complex status was not affected by As treatment, the prompt NBS1 nuclear foci formation suggested a possible link between Mre11 phosphorylation and As-induced foci formation.

NBS1 is a downstream target for ATM and is phosphorylated upon IR in an ATM-dependent manner [5–8]. However, in our study, the As-induced Mre11 phosphorylation only required NBS1 but not ATM (Fig. 4B), suggesting that, in the repair of As-induced DNA damage, an ATM-independent but NBS1-dependent pathway, which linked Mre11 phosphorylation and downstream repair processes together, might exist. Further studies are required to rule out this possibility.

In agreement with the recent paper by Stewart et al. [24], we did not observe IR-induced Mre11 phosphorylation in any of the classical AT cell lines we tested. Nevertheless, As-, UV- or MMS-induced Mre11 phosphorylation is intact in the classical AT cell lines (Fig. 4B and [9]). More efforts are required to define the detailed mechanisms and biological

significance of Mre11 phosphorylation in response to DNA damages caused by different genotoxic agents.

Acknowledgements

This work is supported by grant from National Science Committee, Taiwan, ROC to S.S.Y. (NSC89-2320-B-037-070).

References

[1] D.C. van Gent, J.H. Hoeijmakers, R. Kanaar, Chromosomal stability and the DNA double-stranded break connection, Nat. Rev. Genet. 2 (2001) 196–206.

[2] Y. Shiloh, Ataxia-telangiectasia and the Nijmegen breakage syndrome: related disorders but genes apart, Ann. Rev. Genet. 31 (1997) 635–662.

[3] G. Rotman, Y. Shiloh, ATM: from gene to function, Hum. Mol. Genet. 7 (1998) 1555–1563.

[4] G.S. Stewart, R.S. Maser, T. Stankovic, D.A. Bressan, M.I. Kaplan, N.G. Jaspers, A. Raams, P.J. Byrd, J.H. Petrini, A.M. Taylor, The DNA double-strand break repair gene hMRE11 is mutated in individuals with an ataxia-telangiectasia-like disorder, Cell 99 (1999) 577–587.

[5] D.S. Lim, S.T. Kim, B. Xu, R.S. Maser, J. Lin, J.H. Petrini, M.B. Kastan, ATM phosphorylates p95/nbs1 in an S-phase checkpoint pathway, Nature 404 (2000) 613–617.

[6] M. Gatei, D. Young, K.M. Cerosaletti, A. Desai-Mehta, K. Spring, S. Kozlov, M.F. Lavin, R.A. Gatti, P. Concannon, K Khanna, ATM-dependent phosphorylation of nibrin in response to radiation exposure, Nat. Genet. 25 (2000) 115–119.

[7] S. Zhao, Y.C. Weng, S.S. Yuan, Y.T. Lin, H.C. Hsu, S.C. Lin, E. Gerbino, M.H. Song, M.Z. Zdzienicka, R.A. Gatti, J.W. Shay, Y. Ziv, Y. Shiloh, E.Y. Lee, Functional link between ataxia-telangiectasia and Nijmegen breakage syndrome gene products, Nature 405 (2000) 473–477.

[8] X. Wu, V. Ranganathan, D.S. Weisman, W.F. Heine, D.N. Ciccone, T.B. O'Neill, K.E. Crick, K.A. Pierce, W.S. Lane, G. Rathbun, D.M. Livingston, D.T. Weaver, ATM phosphorylation of Nijmegen breakage syndrome protein is required in a DNA damage response, Nature 405 (2000) 477–482.

[9] Z. Dong, Q. Zhong, P.L. Chen, The Nijmegen breakage syndrome protein is essential for Mre11 phosphorylation upon DNA damage, J. Biol. Chem. 274 (1999) 19513–19516.

[10] NRC (National Research Council), Arsenic in Drinking Water, National Academy Press, Washington, DC, 1999.

[11] A.N. Jha, M. Noditi, R. Nilsson, A.T. Natarajan, Genotoxic effects of sodium arsenite on human cells, Mutat. Res. 284 (1992) 215–221.

[12] M.E. Gonsebatt, L. Vega, A.M. Salazar, R. Montero, P. Guzman, J. Blas, L.M. Del Razo, G. Garcia-Vargas, A. Albores, M.E. Cebrian, M. Kelsh, P. Ostrosky-Wegman, Cytogenetic effects in human exposure to arsenic, Mutat. Res. 386 (1997) 219–228.

[13] L.E. Moore, A.H. Smith, C. Hopenhayn-Rich, M.L. Biggs, D.A. Kalman, M.T. Smith, Decreased in bladder cell micronucleus prevalence after intervention to lower the concentration of arsenic in drinking water, Cancer Epidemiol. Biomarkers Prev. 12 (1997) 1051–1056.

[14] T.K. Hei, S.X. Liu, C. Waldren, Mutagenicity of arsenic in mammalian cells: role of reactive species, Proc. Natl. Acad. Sci. U.S.A. 95 (1998) 8103–8107.

[15] D.R. Germolec, J. Spalding, G.A. Boorman, J.L. Wilmer, T. Yoshida, P.P. Simeonova, A. Bruccoleri, F. Kayama, K. Gaido, R. Tennant, F. Burleson, W. Dong, R.W. Lang, M.I. Luster, Arsenic can mediate skin neoplasia by chronic stimulation of keratinocyte-derived growth factors, Mutat. Res. 386 (1997) 209–218.

[16] D.R. Germolec, J. Spalding, H.S. Yu, G.S. Chen, P.P. Simeonova, M.C. Humble, A. Bruccoleri, G.A. Boorman, J.F. Foley, T. Yoshida, M.I. Luster, Arsenic enhancement of skin neoplasia by chronic stimulation of growth factors, Am. J. Pathol. 153 (1998) 1775–1785.

[17] P.P. Simeonova, S. Wang, W. Toriuma, V. Kommineni, J. Matheson, N. Unimye, F. Kayama, D. Harki, M. Ding, V. Vallyathan, M.I. Luster, Arsenic-mediated cell proliferation and gene expression in the bladder epithelium: association with activating protein-1 transactivation, Cancer Res. 60 (2000) 2445–2453.

[18] K.J. Trouba, E.M. Wauson, R.L. Vorce, Sodium arsenite-induced dysregulation of proteins involved in proliferative signaling, Toxicol. Appl. Pharmacol. 164 (2000) 161–179.

[19] P.L. Chen, P. Scully, J.Y. Shew, J.Y. Wang, W.H. Lee, Phosphorylation of the retinoblastoma gene product is modulated during the cell cycle and cellular differentiation, Cell 58 (1989) 1193–1198.

[20] S.S. Yuan, S.Y. Lee, G. Chen, M. Song, G.E. Tomlinson, E.Y. Lee, BRCA2 is required for ionizing radiation-induced assembly of Rad51 complex in vivo, Cancer Res. 59 (1999) 3547–3551.

[21] G.K. Dasika, S.C. Lin, S. Zhao, P. Sung, A. Tomkinson, E.Y. Lee, DNA damage-induced cell cycle checkpoints and DNA strand break repair in development and tumorigenesis, Oncogene 18 (1999) 7883–7899.

[22] W.H. Park, J.G. Seol, E.S. Kim, J.M. Hyun, C.W. Jung, C.C. Lee, B.K. Kim, Y.Y. Lee, Arsenic trioxide-mediated growth inhibition in MC/CAR myeloma cells via cell cycle arrest in association with induction of cyclin-dependent kinase inhibitor, p21, and apoptosis, Cancer Res. 60 (2000) 3065–3071.

[23] S.C. Huang, C.Y. Huang, T.C. Lee, Induction of mitosis-mediated apoptosis by sodium arsenite in HeLa S3 cells, Biochem. Pharmacol. 60 (2000) 771–780.

[24] G.S. Stewart, J.I. Last, T. Stankovic, N. Haites, A.M. Kidd, P.J. Byrd, A.M. Taylor, Residual ataxia-telangiectasia mutated protein function in cells from ataxia-telangiectasia patients, with 5762ins137 and 7271T → G mutations, showing a less severe phenotype, J. Biol. Chem. 276 (2001) 30133–30141.

Nucleic Acids Research, 2002, Vol. 30 No. 22 4815–4822

Functional analysis of FHA and BRCT domains of NBS1 in chromatin association and DNA damage responses

Song Zhao, William Renthal and Eva Y.-H. P. Lee*

Department of Molecular Medicine/Institute of Biotechnology, University of Texas Health Science Center, San Antonio, TX 78245, USA

Received August 19, 2002; Revised and Accepted September 13, 2002

ABSTRACT

Rad50/Mre11/NBS1 (R/M/N) is a multi-functional protein complex involved in DNA repair, cell cycle checkpoint activation, DNA replication and replication block-induced responses. Ionizing radiation (IR) induces the phosphorylation of NBS1 and nuclear foci formation of the complex. Although it has been suggested that the R/M/N complex is associated with DNA damage sites, we present here biochemical evidence for chromatin association of the complex. We show that the chromatin association of R/M/N is independent of IR and ataxia telangiectasia mutated (ATM). We also demonstrate that optimal chromatin association of the Rad50/Mre11/NBS1 proteins requires both the conserved forkhead-associated (FHA) and breast cancer C-terminus (BRCT) domains of NBS1. Moreover, both these domains of NBS1 are required for its phosphorylation on Ser343 but not on Ser278. Importantly, both the FHA and BRCT domains are essential for IR-induced foci (IRIF) formation of R/M/N and S phase checkpoint activation, but only the BRCT domain is needed for cell survival after IR. These data demonstrate that the FHA and BRCT domains of NBS1 are crucial for the functions of the R/M/N complex.

INTRODUCTION

A number of intricate networks have evolved in eukaryotic cells to respond to endogenous and exogenous genotoxic stresses. Cell cycle checkpoint control and DNA repair processes play crucial roles in maintaining genomic stability (1,2). A defect in either of these processes often results in hypersensitivity to DNA-damaging agents, chromosomal instability and predisposition to cancer. For example, the inherited cancer-prone syndromes ataxia telangiectasia (A-T), Nijmegen breakage syndrome (NBS) and A-T like disorder (A-TLD) are characterized by radiation sensitivity, chromosomal instability and defects in both checkpoint control and DNA repair.

One of the genes mutated in NBS, NBS1, encodes a 95 kDa protein (NBS1 or nibrin) that is a component of the Rad50/Mre11/NBS1 (R/M/N) complex (3–5). This complex plays important roles in checkpoint activation and repair of DNA double-strand breaks (DSBs) (6,7). Purified Mre11 displays 3′→5′ exonuclease and endonuclease activities (8–10) and, in the presence of Rad50 and NBS1, DNA duplex unwinding and hairpin cleavage activities (11). It has been shown that the R/M/N complex forms nuclear foci after ionizing radiation (IR) (4), suggesting that this complex is directly associated with DSB sites. Although Mre11 exhibits a DNA-binding activity *in vitro* (9,11–13), it is not yet clear if the R/M/N complex is directly associated with chromatin *in vivo*. Recently, Maser *et al.* (14) reported that the R/M/N complex co-localizes with proliferating cell nuclear antigen (PCNA) during S phase, while Franchitto and Pichierri (15) demonstrated that it also assembles into nuclear foci after replication blockage. These studies suggest that the R/M/N complex is associated with DNA replication sites and that this complex plays a regulatory role during DNA synthesis.

In response to IR, NBS1 becomes phosphorylated at Ser278 and Ser343 in an ataxia telangiectasia mutated (ATM)-dependent manner (16–19), which is important for activating the S phase checkpoint. Recent studies have suggested that the ATM/NBS1-dependent activation of the S phase checkpoint is partly through regulating the phosphorylation of structural maintenance of chromosome (SMC) proteins (20,21).

NBS1 contains a forkhead-associated (FHA) domain and a breast cancer C-terminal (BRCT) domain (22). The FHA domain is a phosphoserine/threonine specific protein–protein interaction motif (23), whereas the BRCT domain is also predicted to be a protein–protein interaction domain. His45 of NBS1 is one of the few invariant residues within the FHA domain (22). In *Saccharomyces cerevisiae* mutation of this conserved histidine in the FHA2 domain of Rad53 abolishes not only the interaction between Rad53 and Rad9, but also DNA damage responses such as the induction of *RNR3*

*To whom correspondence should be addressed at present address: Department of Biological Chemistry and Department of Developmental and Cell Biology, University of California–Irvine, Sprague Hall, Room 122, 839 Medical Science Court, Irvine, CA 92697, USA. Tel: +1 949 824 9766; Fax: +1 949 824 9767; Email: elee@uci.edu
Present address:
William Renthal, Department of Chemistry and Biochemistry, The University of Texas, Austin, TX 78712, USA

transcription and the G_2/M checkpoint arrest (24). These observations suggest that this conserved histidine plays a crucial role in the biological activity of the FHA domain. In this study, we have examined chromatin association of the R/M/N complex and analyzed the functional importance of both the FHA and BRCT domains of NBS1. We show that the conserved histidine within the NBS1 FHA domain is critical for its function, and that both the FHA and BRCT domains are required for optimal chromatin association of the R/M/N complex, IR-induced phosphorylation of NBS1 and S phase checkpoint activation.

MATERIALS AND METHODS

Cell culture and retroviral gene expression

The simian virus 40 (SV40)-transformed human fibroblast cell line NBS1-LBI (25), the HeLa S3 cell line and human bladder carcinoma cell line T24 were grown in Dulbecco's modified Eagle's medium (DMEM) (Life Technologies Inc.) supplemented with 10% fetal calf serum (FCS) (Life Technologies Inc.). A-T cells (AT22IJE-T/pEBS7) and A-T cells complemented with ATM (AT22IJE-T/pEBS7-YZ5) were grown in DMEM supplemented with 10% FCS and 100 μg/ml hygromycin B (Life Technologies Inc.). T24 cells were synchronized by density arrest and collected as described (26). Cells were irradiated with 10 Gy γ-irradiation and harvested 1 h later unless otherwise specified. NBS1-LBI cell lines with retroviral expression of $NBS1^{WT}$, $NBS1^{S278A}$, $NBS1^{S343A}$, $NBS1^{S278A/S343A}$, $NBS1^{H45A}$, $NBS1^{\Delta FHA}$ or $NBS1^{\Delta BRCT}$ were established as previously described (20). Briefly, 29310A1 retroviral packaging cells (Imgenex, CA) were transfected with pLXIN vector or pLXIN vectors containing cDNA encoding wild-type NBS1 or mutants. Retroviral supernatants were collected 48 h post-transfection. NBS1-LBI cells were incubated in retroviral supernatant plus fresh DMEM supplemented with 10% FCS (1:1 v/v) for at least 24 h. Seventy-two hours after infection, infected cells were selected with 500 μg/ml G418 (Life Technologies Inc.). Clones with ectopic expression of NBS1 or mutants were identified and maintained in DMEM supplemented with 10% FCS and 400 μg/ml G418.

Flow cytometric analysis

For each time point after release from density arrest, ~2×10^6 cells were trypsinized, washed with phosphate-buffered saline (PBS) and fixed with ice-cold 70% ethanol. After at least 2 h fixation at 4°C, cells were collected, washed once with PBS, and incubated in 1 ml staining solution (25 μg/ml propidium iodide and 200 μg/ml DNase-free RNase in PBS) for 30 min at 37°C. Cells were then analyzed with a FACScan (Becton-Dickinson, CA). 10 000 events were counted for each sample.

Plasmids

Full-length cDNAs encoding wild-type NBS1 were generated and cloned into a pCMV vector as described (17). The $NBS1^{S278A}$, $NBS1^{S343A}$, $NBS1^{S278A/S343A}$ and $NBS1^{H45A}$ mutants were generated by site-specific mutagenesis using the QuickChange site-directed mutagenesis kit (Stratagene) and confirmed by DNA sequencing. $NBS1^{WT}$, $NBS1^{S278A}$, $NBS1^{S343A}$, $NBS1^{S278A/S343A}$ and $NBS1^{H45A}$ were subcloned from vector pCMV into the *Xho*I site of the pLXIN retroviral vector (Clontech). Deletions of the FHA and BRCT domains were achieved by ligating cDNA fragments flanking the FHA domain (nucleotides 1–60 and 300–2265) or fragments flanking the BRCT domain (nucleotides 1–300 and 570–2265) and subcloning into the *Xho*I site of the pLXIN retroviral vector.

Antibodies

The mouse monoclonal antibodies against human NBS1, Mre11, Rad50 and ATM were generated as previously described (10,17,27). Rabbit polyclonal anti-NBS1S278-P and anti-NBS1S343-P phosphoserine-specific antibodies were raised against the following KLH-conjugated peptides: TGITNpSQTLPDCQ (Ser278) and CTPGPSLpSQGVSV (Ser343). The phosphorylated peptide:unphosphorylated peptide reactivity ratio of affinity purified phosphoserine278- and phosphoserine343-specific antibodies were >99:1 and 98.5:1.5, respectively, as determined by ELISA (Bethyl Laboratories Inc.). Rabbit polyclonal anti-hOrc2 antibodies were a gift from Dr B. Stillman (Cold Spring Harbor Laboratory). Mouse anti-MEK2 IgG (catalog no. 610235) was obtained from BD Biosciences Inc. FITC-conjugated anti-mouse and Texas Red-conjugated anti-mouse antibodies were from Jackson Research Laboratories.

Chromatin fractionation

Whole cell extracts (WCE) were obtained by lysis of cells directly in SDS sample buffer and sonication. To isolate chromatin, cells were lysed and fractionated as described by Mendez and Stillman (28). Approximately 2×10^6 cells were washed with PBS and resuspended in 200 μl buffer A (10 mM HEPES, pH 7.9, 10 mM KCl, 1.5 mM $MgCl_2$, 0.34 M sucrose, 10% glycerol, 1 mM DTT, 5 μg/ml aprotinin, 5 μg/ml leupeptin, 0.5 μg/ml pepstatin A and 0.1 mM phenylmethylsulfonyl fluoride). Triton X-100 (0.1%) was added, mixed gently by inversion and the mixture was incubated on ice for 5 min. Nuclei were collected in pellet 1 (P1) by centrifugation at low speed (1300 *g*, 5 min, 4°C). The supernatant (S1) was clarified by high speed centrifugation (20 000 *g*, 15 min, 4°C) to obtain the soluble fraction (S2). Nuclei were then washed once in buffer A, resuspended in 200 μl buffer B (3 mM EDTA, 0.2 mM EGTA, 1 mM DTT, 5 μg/ml aprotinin, 5 μg/ml leupeptin, 0.5 μg/ml pepstatin A and 0.1 mM phenylmethylsulfonyl fluoride) and incubated on ice for 30 min. Insoluble chromatin was collected by centrifugation (1700 *g*, 5 min, 4°C), washed once in buffer B, and centrifuged at 1700 *g* for 5 min. The final chromatin-enriched pellet (P3) was resuspended in SDS sample buffer and subjected to sonication. To release chromatin-bound proteins, nuclei (P1) were digested with 0.2 U of micrococcal nuclease (Sigma) in buffer A plus 1 mM $CaCl_2$. After 1 min incubation at 37°C, the nuclease reaction was stopped by addition of 1 mM EGTA. Nuclei were then lysed and fractionated as above.

Immunoblotting, immunoprecipitation and immunostaining

Protein concentration was determined by Bradford assay (Bio-Rad, CA). For immunoprecipitation (IP), cell lysates were incubated with 5 μg antibodies for 4 h followed by addition of 20 μl protein G–Sepharose™ 4 Fast Flow beads (Amersham Pharmacia Biotech Inc., Sweden) for 2 h at 4°C.

Cell lysates or IP samples were mixed with SDS sample buffer and analyzed using a SDS–8% polyacrylamide gel. Quantitative analysis of immunoblots was performed using a Personal Densitometer SI (Molecular Dynamics, CA). For immunofluorescence, cells were fixed with 4% paraformaldehyde in PBS (pH 7.2) and permeabilized with 0.5% Triton X-100 in PBS. After 30 min incubation in blocking buffer (10% FCS in PBS), cells were incubated with primary antibodies overnight at 4°C. After being washed three times with PBS, the cells were incubated with FITC- or Texas Red-conjugated secondary antibodies for 2 h at room temperature. The cells were then washed with PBS, counterstained with 0.05 μg/ml 4′,6′-diamidino-2-phenylindole (DAPI) in PBS and mounted in Immunon™ mountant (Shandon, PA). All antibodies were diluted in PBS supplemented with 5% FCS.

Radio-resistant DNA synthesis (RDS) assay

IR-induced inhibition of DNA synthesis was measured as previously described (25,29,30). In brief, 3×10^4 cells were seeded into 35 mm dishes and grown for at least 48 h, and then prelabeled with 10 nCi/ml [^{14}C]thymidine (NEN Life Science Products Inc., Boston, MA) in DMEM for ~48 h. The cells were subsequently incubated in non-radioactive DMEM for 24 h before treatment with 0, 5, 10 or 15 Gy γ-irradiation. After incubation for 30 min at 37°C, the cells were labeled with 2.5 μCi/ml [^{3}H]thymidine (NEN Life Science Products Inc.) for 30 min. The cells were then washed and incubated in non-radioactive DMEM for 45 min. Then the cells were washed with PBS and lysed with 0.5 ml 0.2 M NaOH. The radioactivity was measured in a liquid scintillation counter. The ratio [^{3}H]:[^{14}C] was calculated and compared with the ratio for non-irradiated cells to determine the rate of inhibition of DNA synthesis.

Colony survival assay

Cells were exposed to 0, 2, 4 or 6 Gy γ-irradiation at 2.44 Gy/min (J.L. Shepherd & Associates, CA) and immediately plated at 800 cells/100 mm diameter dish in triplicate. After incubation at 37°C for 2 weeks, cells were washed with PBS, fixed in ice-cold methanol for 15 min and then stained with Giemsa stain (Sigma Diagnostics, St Louis, MO) for 30 min. Colonies per plate were counted and the means ± standard errors were determined. At least two independent experiments were performed on each cell line.

RESULTS

Rad50/Mre11/NBS1 proteins are chromatin-associated *in vivo*

The R/M/N complex forms nuclear foci at DNA damage sites after IR treatment (4,31). It has also been shown that R/M/N foci in replicating cells co-localize with PCNA foci (14). Thus, it seems plausible that the R/M/N complex may become chromatin associated after IR treatment and during S phase. However, there is as yet no biochemical evidence to support chromatin association of the R/M/N complex. Using a biochemical fractionation scheme recently described by Mendez and Stillman (28), we examined the chromatin association of the R/M/N complex. Asynchronously growing HeLa S3 cells were fractionated into a cytoplasmic fraction (S2) and a nuclear fraction (P2). The P2 fraction was then divided into a soluble nuclear fraction (S3) and an insoluble chromatin-enriched nuclear fraction (P3). The P2 fraction was also subjected to digestion with micrococcal nuclease to release the insoluble chromatin-bound protein into a soluble fraction (S3′), while the nuclease-resistant fraction (P3′) remained insoluble (Fig. 1A). The subunits of the R/M/N complex were mainly found in the P3 and S3′ fractions, indicating that the R/M/N complex is chromatin-bound. The chromatin association of R/M/N increases moderately following entry into S phase (Fig. 1B and Table 1), which may reflect its interaction with replication factors such as E2F1 and PCNA (14). It is also noteworthy that the chromatin-associated R/M/N decreases significantly during G_2/M phases. Chromatin association of the R/M/N complex during the normal cell cycle is consistent with its role in the surveillance of chromosomal integrity.

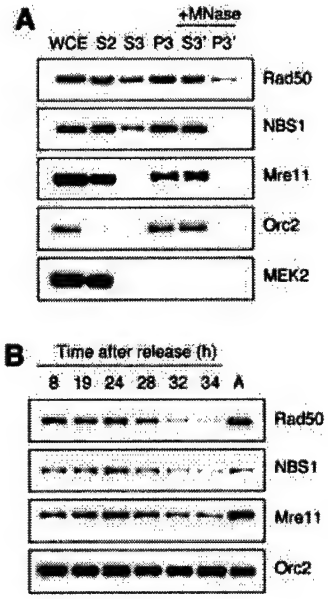

Figure 1. Chromatin association of Rad50/Mre11/NBS1. (**A**) Asynchronous HeLa S3 cells were subjected to biochemical fractionation as described in Materials and Methods. Five different fractions were obtained: soluble cytoplasmic fraction (S2), soluble nuclear fraction (S3), insoluble chromatin-enriched nuclear fraction (P3), nuclease-solubilized chromatin-bound fraction (S3′) and insoluble nuclease-resistant nuclear fraction (P3′). Whole cell extract (WCE) was included as a control. Orc2, a replication initiating factor known to be chromatin bound throughout the cell cycle regardless of DNA damage, served as a control for the chromatin-enriched fractions P3 and S3′. MEK2, a cytoplasmic kinase, was used as a control for the cytoplasmic fraction S2. (**B**) Cell cycle-dependent chromatin association of R/M/N complex. Cells collected at different time points after release from density arrest were subjected to fractionation. The chromatin-enriched fraction (P3) is shown.

Chromatin association of R/M/N is independent of IR and ATM

Since the chromatin association of R/M/N may be important for its functions in response to DNA damage, we next tested whether IR treatment could enhance its association with

Table 1. The percentage of cells in each phase of the cell cycle as determined by the CellQuest analysis program

	T8	T19	T24	T28	T32	T34	Asynchronous cells
G_1	96.3	72.9	13.1	5.24	14.5	16.9	64.6
S	0.67	21.4	74.1	44.7	18.6	5.84	14.4
G_2/M	1.36	2.1	12.0	48.5	65.6	75.2	19.6

chromatin. Surprisingly, no significant increase in the amount of R/M/N in the P3 fraction was detected after IR (Fig. 2). Since NBS1 is phosphorylated by ATM after IR on several residues, including Ser278 and Ser343 (16–19), we also examined whether ATM deficiency affects the ability of R/M/N to associate with chromatin. Again, the chromatin association of R/M/N is comparable between A-T cells and A-T cells complemented with ATM, regardless of DNA damage (Fig. 2). Taken together, these data suggest that the chromatin association of R/M/N is not affected by IR or deficiency of ATM.

The FHA and BRCT domains of NBS1 are required for optimal chromatin association of R/M/N

Since NBS1 is crucial for both nuclear localization and formation of IR-induced foci (IRIF) of Rad50 and Mre11 (4), we examined the chromatin association of Rad50 and Mre11 in NBS cells. In NBS1-deficient cells Rad50 and Mre11 were only minimally associated with chromatin, while the majority of them were found in the soluble fractions S2 and S3 (Fig. 3C). The nuclear localization and chromatin association of R/M were fully restored by expression of wild-type NBS1 as well as $NBS1^{S278A/S343A}$ (Fig. 3C, Table 2 and data not shown). These results not only demonstrate that NBS1 is essential for the chromatin-binding activities of the R/M/N but also confirm that the IR-induced phosphorylations of Ser278 and Ser343 by ATM are not required for the chromatin association of R/M/N.

To examine the significance of the FHA and BRCT domains of NBS1 in chromatin association, we constructed mutants with a single deletion of either the FHA or BRCT domain, as well as a substitution of the invariant His45 residue with Ala (Fig. 3A and B). Consistent with previous reports that deletion of the N-terminal region of NBS1 does not affect nuclear localization of R/M/N (32,33), nuclear localization of Mre11 and Rad50 can be fully restored by expression of $NBS1^{H45A}$, $NBS1^{\Delta FHA}$ or $NBS1^{\Delta BRCT}$ (data not shown). However, even with restored nuclear localization of R/M, the levels of chromatin-associated R/M/N are significantly lower in NBS cells expressing $NBS1^{H45A}$, $NBS1^{\Delta FHA}$ or $NBS1^{\Delta BRCT}$ than those in cells expressing $NBS1^{WT}$ (Fig. 3D and Table 2). For example, only 10.9–24.2% of $NBS1^{\Delta BRCT}$ is chromatin bound compared to >90% of wild-type NBS1. Therefore, optimal chromatin association of R/M/N requires intact FHA and BRCT domains.

The FHA and BRCT domains are required for IR-induced phosphorylation of Ser343 of NBS1

Using antibodies specifically against phosphorylated Ser278 or Ser343, we examined the IR-induced phosphorylation of NBS1 and its mutants. The phosphorylation of Ser343 and Ser278 was readily detectable in cells expressing $NBS1^{S278A}$ and $NBS1^{S343A}$, respectively, indicating that these modifications can occur independently (Fig. 4A). However, while the phosphorylation of Ser278 is normal in $NBS1^{H45A}$, $NBS1^{\Delta FHA}$ and $NBS1^{\Delta BRCT}$, the phosphorylation of Ser343 is greatly diminished (Fig. 4B and C). Therefore, the FHA and BRCT domains play an important role in the phosphorylation of NBS1 at Ser343 *in vivo*.

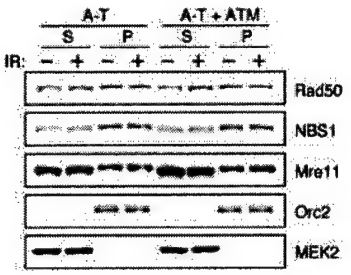

Figure 2. Chromatin association of R/M/N in A-T cells. A-T cells and A-T cells complemented with ATM were fractionated as described. Both soluble fraction S (S2 + S3) and chromatin-enriched fraction P (P3) from IR-treated and non-treated cells are shown.

The FHA and BRCT domains are essential for formation of IRIF of R/M/N and S phase checkpoint activation

To determine the importance of the FHA and BRCT domains in other biological functions of NBS1, we examined the IRIF of R/M/N in different NBS cell lines. Both Mre11 and NBS1 (data not shown) antibodies were used to test IRIF to eliminate the possibility that the different expression levels of $NBS1^{WT}$, $NBS1^{S278A/S343A}$, $NBS1^{H45A}$, $NBS1^{\Delta FHA}$ and $NBS1^{\Delta BRCT}$ may affect foci formation. As shown in Figure 5A, IRIF formation with Mre11 was defective in cells expressing $NBS1^{H45A}$, $NBS1^{\Delta FHA}$ and $NBS1^{\Delta BRCT}$.

NBS cells exhibit RDS due to a defective S phase checkpoint (34). While NBS cells expressing $NBS1^{WT}$ were able to inhibit DNA synthesis upon IR, cells expressing the mutant forms of NBS1 failed to do so (Fig. 5B). Taken together, both IRIF and S phase checkpoint activation rely on the FHA and BRCT domains.

The BRCT but not FHA domain is important for cell survival after IR

By measuring cell survival 2 weeks after exposure of cells to a sub-lethal dose of γ-irradiation, we investigated whether the various forms of NBS1 could complement the IR sensitivity of NBS cells. We found that neither His45 nor the FHA domain is essential to complement cell sensitivity to IR. However, the $NBS1^{\Delta BRCT}$ allele is less effective in complementing the IR sensitivity of NBS cells, in comparison with other NBS alleles (Fig. 5C).

DISCUSSION

We report here that the R/M/N complex is tightly associated with chromatin *in vivo*. Moreover, chromatin association is increased following entry into S phase, but is not dependent on IR or ATM kinase, suggesting that this complex plays a role in

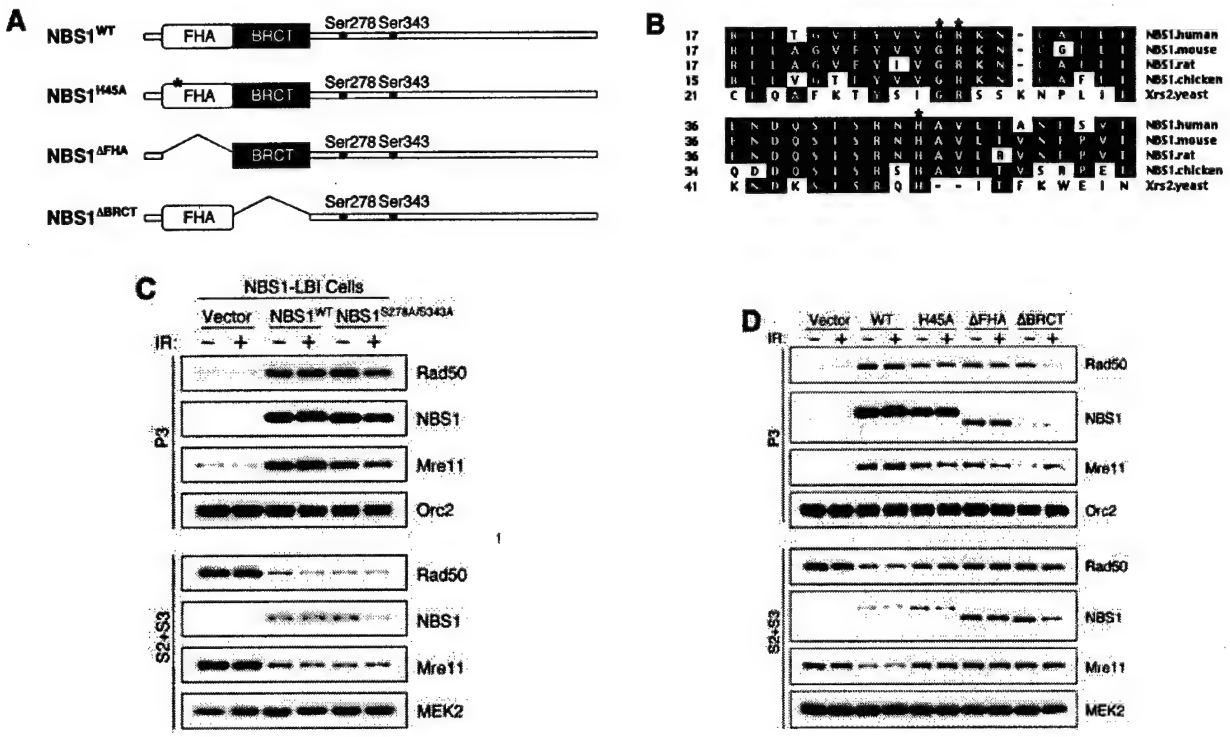

Figure 3. Chromatin association of R/M/N in NBS cells. (**A**) Diagram of wild-type NBS1, NBS1^{H45A}, NBS1$^{\Delta FHA}$ and NBS1$^{\Delta BRCT}$ proteins. Locations of the FHA domain, BRCT domain and phosphorylation sites on Ser278 and Ser343 are shown. The asterisk represents single residue substitution (His→Ala). (**B**) Alignment of part of the FHA domain of NBS1 among different species. The shaded boxes indicate the regions of identity. The invariant Gly·Arg (GR) pair and His45 (H) are marked with asterisks. (**C**) Chromatin association of R/M/N in different NBS1-LBI cell clones (with vector only, with expression of NBS1^{WT}, and with expression of NBS1$^{S278A/S343A}$). (**D**) Comparison of chromatin association of R/M/N in NBS cells expressing NBS1^{H45A}, NBS1$^{\Delta FHA}$ or NBS1$^{\Delta BRCT}$. The soluble fraction (S2 + S3) and chromatin-enriched fraction P (P3) from IR-treated and non-treated cells are shown. MEK2 and Orc2 serve as controls for the soluble fraction and chromatin fraction, respectively.

Table 2. Percentages of chromatin-associated fraction of R/M/N in different NBS cell lines (mean ± SD)

		Vector	Wild-type	S278A/S343A	H45A	ΔFHA	ΔBRCT
Rad50	–IR	9.7 ± 4.7	78.0 ± 5.1	90.6 ± 3.6	61.8 ± 8.7	45.2 ± 1.9	33.1 ± 7.8
	+IR	10.9 ± 6.9	80.2 ± 5.6	92.5 ± 3.3	45.8 ± 4.2	35.6 ± 5.4	29.0 ± 9.3
NBS1	–IR	NA	90.2 ± 1.3	87.6 ± 8.5	70.6 ± 3.2	60.2 ± 6.4	10.9 ± 6.4
	+IR	NA	91.0 ± 4.8	89.2 ± 8.1	68.3 ± 5.8	56.7 ± 7.2	24.2 ± 10.5
Mre11	–IR	8.4 ± 2.3	71.0 ± 3.9	81.8 ± 4.3	47.0 ± 2.7	46.4 ± 8.0	20.6 ± 2.5
	+IR	4.9 ± 2.1	82.0 ± 5.7	74.4 ± 3.9	26.8 ± 4.9	27.5 ± 2.5	19.8 ± 3.3

In three independent experiments, the protein levels of R/M/N in the soluble fraction and chromatin fraction were quantitatively analyzed; the ratios (%) of P:(S + P) were obtained to indicate the percentage of chromatin-associated R/M/N in the whole cell extract.

the maintenance of chromosomal stability even during the normal cell cycle. This suggestion is further supported by the observation that NBS1 forms nuclear foci and interacts with E2F1 and replication origins during S phase (14). The decreased level of chromatin-associated R/M/N during G_2/M phases is likely due to its dissociation from replication regions after exit from S phase. However, there may be other mitosis-related mechanisms involved, since the chromatin association of R/M/N in G_2/M phases is less than in G_1 phase.

As several lines of evidence have suggested that the R/M/N complex is recruited to DNA damage sites, it is puzzling that no increase in chromatin association of the complex was observed after IR. We propose two possible mechanisms by which a change of localization actually occurs without a detectable change in the chromatin-bound fraction of R/M/N. First, there may be a translocalization among chromatin-bound proteins, i.e. similar to the *S.cerevisiae* Ku and Sir proteins, from telomeric regions to DNA damage sites (35–38). Second, the soluble and chromatin-bound fractions of the R/M/N complex might undergo constant exchange so that relocalization of R/M/N is not necessarily reflected by the relative amounts of protein in each fraction.

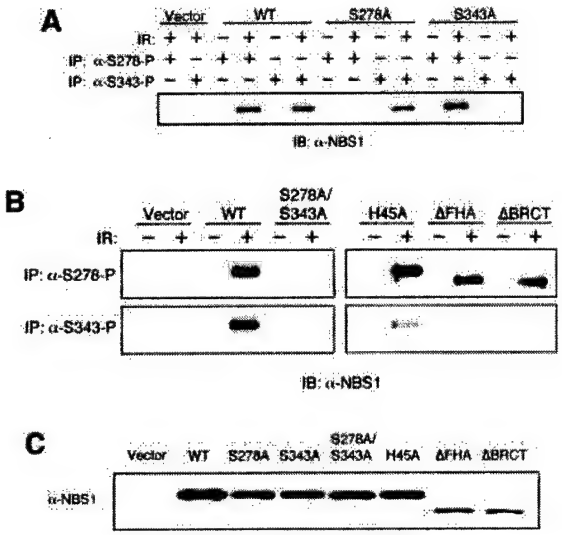

Figure 4. Phosphorylation of Ser278 and Ser343 in wild-type NBS1 and mutants. **(A)** Immunoprecipitation of $NBS1^{WT}$, $NBS1^{S278A}$ and $NBS1^{S343A}$ with anti-phosphoserine specific antibodies, α-S278-P and α-S343-P. **(B)** Immunoprecipitation of $NBS1^{WT}$, $NBS1^{S278A/S343A}$, $NBS1^{H45A}$, $NBS1^{\Delta FHA}$ and $NBS1^{\Delta BRCT}$ with anti-phosphoserine specific antibodies, α-S278-P and α-S343-P. **(C)** Comparison of expression levels of wild-type NBS1 and different NBS1 mutants. Immunoblotting of whole cell extracts from different NBS cell clones. All immunoblots were probed with α-NBS1 monoclonal antibody MHN1.

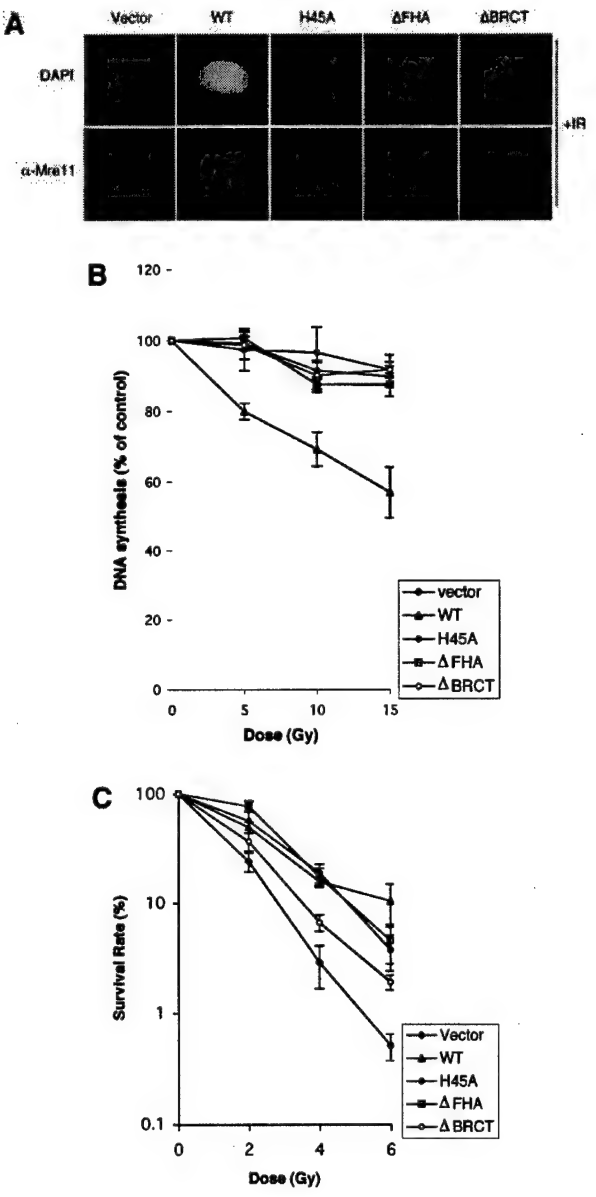

Figure 5. IRIF formation, S phase checkpoint activation and radiation sensitivity of NBS cells expressing $NBS1^{WT}$, $NBS1^{H45A}$, $NBS1^{\Delta FHA}$ and $NBS1^{\Delta BRCT}$. **(A)** IRIF formation of Mre11. Four hours after IR (15 Gy), cells were fixed and probed with anti-Mre11 monoclonal antibody, 13H1, followed by FITC-conjugated anti-mouse antibody. Nuclei were counter-stained with DAPI. **(B)** DNA synthesis was measured 30 min after 0, 5, 10 or 15 Gy γ-irradiation. See Materials and Methods for details. **(C)** Cells were exposed to 0, 2, 4 or 6 Gy γ-irradiation and incubated for 2 weeks before colonies per plate were counted. Post-irradiation survival was assessed by comparison with the non-irradiated control. Experiments were performed in triplicate at least twice. Error bars represent standard deviation.

Since Rad50 and Mre11 (R/M) are localized in both the cytoplasm and nucleus in NBS cells (4), it is conceivable that the R/M complex fails to bind to chromatin in the absence of NBS1. However, the defective chromatin association cannot be fully corrected by simply restoring nuclear localization of R/M. In fact, intact FHA and BRCT domains seem necessary for not only directing NBS1 itself onto chromatin but also stabilizing the chromatin association of the whole complex. On the other hand, chromatin association of the R/M/N is comparable in NBS cells expressing $NBS1^{WT}$ and $NBS1^{S278A/S343A}$, suggesting that the phosphorylations at Ser278 and Ser343 of NBS1 are dispensable for its chromatin association. It has been shown that the BRCT regions of the putative DNA-binding proteins TopBP1 and BRCA1 directly bind to DNA breaks and ends (39). Therefore, it is possible that the BRCT domain of NBS1 plays a similar role in the chromatin-binding activity of R/M/N.

Since the FHA and BRCT domains are required for phosphorylation of NBS1 at Ser343 but not Ser278, it appears that there are different levels of regulation of these two phosphorylation events. Moreover, since $NBS1^{H45A}$, $NBS1^{\Delta FHA}$ and $NBS1^{\Delta BRCT}$ are defective in binding to chromatin, we speculated that Ser343 may be phosphorylated only when NBS1 is bound to chromatin. However, on immunoprecipitating phosphorylated NBS1 with phosphoserine-specific antibodies, we could not detect a significant difference between the distribution of phosphorylated Ser278 and phosphorylated Ser343 in the soluble and chromatin-bound fractions (data not shown). We therefore hypothesize that there may be a constant exchange between soluble and chromatin-bound fractions of NBS1. Since we could not prevent wild-type NBS1 from binding onto chromatin *in vivo*,

how the FHA and BRCT domains dictate phosphorylation of Ser343 and where phosphorylation occurs remain unknown.

The FHA and BRCT domains are also essential for other DNA damage responses, including IRIF formation and S phase checkpoint activation. Since these mutants are also unable to effectively bind to chromatin *in vivo*, it seems very likely that the chromatin association of R/M/N is necessary for IRIF formation. However, the precise cause of the defective S phase checkpoint in the $NBS1^{H45A}$, $NBS1^{\Delta FHA}$ and $NBS1^{\Delta BRCT}$ mutants remains elusive. Since $NBS1^{S278A/S343A}$ can restore chromatin association of the R/M/N complex but not the S phase checkpoint, chromatin association of the R/M/N is not sufficient for activation of the S phase checkpoint. Therefore, the defective S phase checkpoint observed in the $NBS1^{H45A}$, $NBS1^{\Delta FHA}$ and $NBS1^{\Delta BRCT}$ mutants could be simply due to a deficiency in phosphorylation of Ser343 (16–19) or deficiencies in both phosphorylation of Ser343 and chromatin association.

Finally, our results have revealed that the BRCT but not the FHA domain plays a crucial role in cell survival after IR. The lack of correlation between a checkpoint defect and radiosensitivity in the $NBS1^{H45A}$ and $NBS1^{\Delta FHA}$ mutants is supported by a previous report that radiosensitivity of NBS cells is not due to a defective S phase checkpoint but rather DNA repair defects (40). Given that multiple checkpoint pathways, i.e. the G_1/S checkpoint, G_2/M checkpoint and a parallel Chk2-dependent S phase checkpoint (41), can be activated upon DNA damage, abrogation of one checkpoint may not be sufficient to cause hypersensitivity to IR. It has been reported that the N-terminal region (amino acids 1–152) of NBS1, which includes the FHA domain and part of the BRCT domain (amino acids 108–152), is not essential for radiation resistance (32). However, we found that deletion of the entire BRCT domain (amino acids 108–196) results in increased cell sensitivity to IR. The discrepancy is likely due to the fact that different deletion mutants were used in these two studies. We believe that deletion of the BRCT domain may cause additional defects in compensatory checkpoint pathways and/or repair of DNA lesions, thereby sensitizing cells to IR. Since NBS1657del5, the most common mutation found in NBS patients, results in deletion of the BRCT domain, it will be informative to further characterize its function in detail.

ACKNOWLEDGEMENTS

We thank Drs Alan Tomkinson and Patrick Sung for critical reading and comments on the manuscript, Mr Sean M. Post and Drs Juan Mendez, David Levine and Malgorzata Zdzienicka for technical advice, Dr Bruce Stillman for providing anti-hOrc2 antibody, Mei-Hua Song for producing antibodies and Stefan Sigurdsson for constructing the pCMV-$NBS1^{\Delta BRCT}$ plasmid. S.Z. is the recipient of a Susan G. Komen Breast Cancer Foundation predoctoral fellowship. E.Y.-H.P.L. is supported by National Cancer Institute grant 1P01CA81020.

REFERENCES

1. Dasika,G.K., Lin,S.C., Zhao,S., Sung,P., Tomkinson,A. and Lee,E.Y. (1999) DNA damage-induced cell cycle checkpoints and DNA strand break repair in development and tumorigenesis. *Oncogene*, **18**, 7883–7899.
2. Zhou,B.B. and Elledge,S.J. (2000) The DNA damage response: putting checkpoints in perspective. *Nature*, **408**, 433–439.
3. Varon,R., Vissinga,C., Platzer,M., Cerosaletti,K.M., Chrzanowska,K.H, Saar,K., Beckmann,G., Seemanova,E., Cooper,P.R., Nowak,N.J *et al.* (1998) Nibrin, a novel DNA double-strand break repair protein, is mutated in Nijmegen breakage syndrome. *Cell*, **93**, 467–476.
4. Carney,J.P., Maser,R.S., Olivares,H., Davis,E.M., Le Beau,M., Yates,J.R.,III, Hays,L., Morgan,W.F. and Petrini,J.H. (1998) The hMre11/hRad50 protein complex and Nijmegen breakage syndrome: linkage of double-strand break repair to the cellular DNA damage response. *Cell*, **93**, 477–486.
5. O'Driscoll,M., Cerosaletti,K.M., Girard,P.M., Dai,Y., Stumm,M., Kysela,B., Hirsch,B., Gennery,A., Palmer,S.E., Seidel,J. *et al.* (2001) DNA ligase IV mutations identified in patients exhibiting developmental delay and immunodeficiency. *Mol. Cell*, **8**, 1175–1185.
6. Haber,J.E. (1998) The many interfaces of Mre11. *Cell*, **95**, 583–586.
7. D'Amours,D. and Jackson,S.P. (2002) The mre11 complex: at the crossroads of DNA repair and checkpoint signalling. *Nature Rev. Mol. Cell. Biol.*, **3**, 317–327.
8. Paull,T.T. and Gellert,M. (1998) The 3′ to 5′ exonuclease activity of Mre 11 facilitates repair of DNA double-strand breaks. *Mol. Cell*, **1**, 969–979.
9. Usui,T., Ohta,T., Oshiumi,H., Tomizawa,J., Ogawa,H. and Ogawa,T. (1998) Complex formation and functional versatility of Mre11 of budding yeast in recombination. *Cell*, **95**, 705–716.
10. Trujillo,K.M., Yuan,S.S., Lee,E.Y. and Sung,P. (1998) Nuclease activities in a complex of human recombination and DNA repair factors Rad50, Mre11 and p95. *J. Biol. Chem.*, **273**, 21447–21450.
11. Paull,T.T. and Gellert,M. (1999) Nbs1 potentiates ATP-driven DNA unwinding and endonuclease cleavage by the Mre11/Rad50 complex. *Genes Dev.*, **13**, 1276–1288.
12. Furuse,M., Nagase,Y., Tsubouchi,H., Murakami-Murofushi,K., Shibata,T. and Ohta,K. (1998) Distinct roles of two separable *in vitro* activities of yeast Mre11 in mitotic and meiotic recombination. *EMBO J.*, **17**, 6412–6425.
13. Trujillo,K.M. and Sung,P. (2001) DNA structure-specific nuclease activities in the *Saccharomyces cerevisiae* Rad50*Mre11 complex. *J. Biol. Chem.*, **276**, 35458–35464.
14. Maser,R.S., Mirzoeva,O.K., Wells,J., Olivares,H., Williams,B.R., Zinkel,R.A., Farnham,P.J. and Petrini,J.H. (2001) Mre11 complex and DNA replication: linkage to E2F and sites of DNA synthesis. *Mol. Cell. Biol.*, **21**, 6006–6016.
15. Franchitto,A. and Pichierri,P. (2002) Bloom's syndrome protein is required for correct relocalization of RAD50/MRE11/NBS1 complex after replication fork arrest. *J. Cell Biol.*, **157**, 19–30.
16. Lim,D.S., Kim,S.T., Xu,B., Maser,R.S., Lin,J., Petrini,J.H. and Kastan,M.B. (2000) ATM phosphorylates p95/nbs1 in an S-phase checkpoint pathway. *Nature*, **404**, 613–617.
17. Zhao,S., Weng,Y.C., Yuan,S.S., Lin,Y.T., Hsu,H.C., Lin,S.C., Gerbino,E., Song,M.H., Zdzienicka,M.Z., Gatti,R.A. *et al.* (2000) Functional link between ataxia-telangiectasia and Nijmegen breakage syndrome gene products. *Nature*, **405**, 473–477.
18. Wu,X., Ranganathan,V., Weisman,D.S., Heine,W.F., Ciccone,D.N., O'Neill,T.B., Crick,K.E., Pierce,K.A., Lane,W.S., Rathbun,G. *et al.* (2000) ATM phosphorylation of Nijmegen breakage syndrome protein is required in a DNA damage response. *Nature*, **405**, 477–482.
19. Gatei,M., Young,D., Cerosaletti,K.M., Desai-Mehta,A., Spring,K., Kozlov,S., Lavin,M.F., Gatti,R.A., Concannon,P. and Khanna,K. (2000) ATM-dependent phosphorylation of nibrin in response to radiation exposure. *Nature Genet.*, **25**, 115–119.
20. Yazdi,P.T., Wang,Y., Zhao,S., Patel,N., Lee,E.Y. and Qin,J. (2002) SMC1 is a downstream effector in the ATM/NBS1 branch of the human S-phase checkpoint. *Genes Dev.*, **16**, 571–582.
21. Kim,S.T., Xu,B. and Kastan,M.B. (2002) Involvement of the cohesin protein, Smc1, in Atm-dependent and independent responses to DNA damage. *Genes Dev.*, **16**, 560–570.
22. Featherstone,C. and Jackson,S.P. (1998) DNA repair: the Nijmegen breakage syndrome protein. *Curr. Biol.*, **8**, R622–R625.
23. Durocher,D., Henckel,J., Fersht,A.R. and Jackson,S.P. (1999) The FHA domain is a modular phosphopeptide recognition motif. *Mol. Cell*, **4**, 387–394.

24. Sun,Z., Hsiao,J., Fay,D.S. and Stern,D.F. (1998) Rad53 FHA domain associated with phosphorylated Rad9 in the DNA damage checkpoint. *Science*, **281**, 272–274.
25. Kraakman-van der Zwet,M., Overkamp,W.J., Friedl,A.A., Klein,B., Verhaegh,G.W., Jaspers,N.G., Midro,A.T., Eckardt-Schupp,F., Lohman,P.H. and Zdzienicka,M.Z. (1999) Immortalization and characterization of Nijmegen Breakage syndrome fibroblasts. *Mutat. Res.*, **434**, 17–27.
26. Chen,P.L., Scully,P., Shew,J.Y., Wang,J.Y. and Lee,W.H. (1989) Phosphorylation of the retinoblastoma gene product is modulated during the cell cycle and cellular differentiation. *Cell*, **58**, 1193–1198.
27. Chen,G. and Lee,E. (1996) The product of the ATM gene is a 370-kDa nuclear phosphoprotein. *J. Biol. Chem.*, **271**, 33693–33697.
28. Mendez,J. and Stillman,B. (2000) Chromatin association of human origin recognition complex, cdc6 and minichromosome maintenance proteins during the cell cycle: assembly of prereplication complexes in late mitosis. *Mol. Cell. Biol.*, **20**, 8602–8612.
29. Painter,R.B. and Young,B.R. (1980) Radiosensitivity in ataxia-telangiectasia: a new explanation. *Proc. Natl Acad. Sci. USA*, **77**, 7315–7317.
30. Morgan,S.E., Lovly,C., Pandita,T.K., Shiloh,Y. and Kastan,M.B. (1997) Fragments of ATM which have dominant-negative or complementing activity. *Mol. Cell. Biol.*, **17**, 2020–2029.
31. Nelms,B.E., Maser,R.S., MacKay,J.F., Lagally,M.G. and Petrini,J.H. (1998) *In situ* visualization of DNA double-strand break repair in human fibroblasts. *Science*, **280**, 590–592.
32. Tauchi,H., Kobayashi,J., Morishima,K., Matsuura,S., Nakamura,A., Shiraishi,T., Ito,E., Masnada,D., Delia,D. and Komatsu,K. (2001) The forkhead-associated domain of NBS1 is essential for nuclear foci formation after irradiation but not essential for hRAD50·hMRE11·NBS1 complex DNA repair activity. *J. Biol. Chem.*, **276**, 12–15.
33. Desai-Mehta,A., Cerosaletti,K.M. and Concannon,P. (2001) Distinct functional domains of nibrin mediate Mre11 binding, focus formation and nuclear localization. *Mol. Cell. Biol.*, **21**, 2184–2191.
34. Young,B.R. and Painter,R.B. (1989) Radioresistant DNA synthesis and human genetic diseases. *Hum. Genet.*, **82**, 113–117.
35. Martin,S.G., Laroche,T., Suka,N., Grunstein,M. and Gasser,S.M. (1999) Relocalization of telomeric Ku and SIR proteins in response to DNA strand breaks in yeast. *Cell*, **97**, 621–633.
36. Mills,K.D., Sinclair,D.A. and Guarente,L. (1999) MEC1-dependent redistribution of the Sir3 silencing protein from telomeres to DNA double-strand breaks. *Cell*, **97**, 609–620.
37. Wu,G., Lee,W.H. and Chen,P.L. (2000) NBS1 and TRF1 colocalize at promyelocytic leukemia bodies during late S/G2 phases in immortalized telomerase-negative cells. Implication of NBS1 in alternative lengthening of telomeres. *J. Biol. Chem.*, **275**, 30618–30622.
38. Zhu,X.D., Kuster,B., Mann,M., Petrini,J.H. and Lange,T. (2000) Cell-cycle-regulated association of RAD50/MRE11/NBS1 with TRF2 and human telomeres. *Nature Genet.*, **25**, 347–352.
39. Yamane,K. and Tsuruo,T. (1999) Conserved BRCT regions of TopBP1 and of the tumor suppressor BRCA1 bind strand breaks and termini of DNA. *Oncogene*, **18**, 5194–5203.
40. Girard,P.M., Foray,N., Stumm,M., Waugh,A., Riballo,E., Maser,R.S., Phillips,W.P., Petrini,J., Arlett,C.F. and Jeggo,P.A. (2000) Radiosensitivity in Nijmegen Breakage Syndrome cells is attributable to a repair defect and not cell cycle checkpoint defects. *Cancer Res.*, **60**, 4881–4888.
41. Falck,J., Petrini,J.H., Williams,B.R., Lukas,J. and Bartek,J. (2002) The DNA damage-dependent intra-S phase checkpoint is regulated by parallel pathways. *Nature Genet.*, **30**, 290–294.

SMC1 is a downstream effector in the ATM/NBS1 branch of the human S-phase checkpoint

Parvin T. Yazdi,[1] Yi Wang,[1] Song Zhao,[2] Nimitt Patel,[1] Eva Y.-H.P. Lee,[2] and Jun Qin[1,3]

[1]Verna and Marrs McLean Department of Biochemistry and Molecular Biology and Department of Molecular and Cellular Biology, Baylor College of Medicine, Houston, Texas 77030, USA; [2]Department of Molecular Medicine/Institute of Biotechnology, The University of Texas Health Science Center at San Antonio, San Antonio, Texas 78245, USA

Structural maintenance of chromosomes (SMC) proteins (SMC1, SMC3) are evolutionarily conserved chromosomal proteins that are components of the cohesin complex, necessary for sister chromatid cohesion. These proteins may also function in DNA repair. Here we report that SMC1 is a component of the DNA damage response network that functions as an effector in the ATM/NBS1-dependent S-phase checkpoint pathway. SMC1 associates with BRCA1 and is phosphorylated in response to IR in an ATM- and NBS1-dependent manner. Using mass spectrometry, we established that ATM phosphorylates S957 and S966 of SMC1 in vivo. Phosphorylation of S957 and/or S966 of SMC1 is required for activation of the S-phase checkpoint in response to IR. We also discovered that the phosphorylation of NBS1 by ATM is required for the phosphorylation of SMC1, establishing the role of NBS1 as an adaptor in the ATM/NBS1/SMC1 pathway. The ATM/CHK2/CDC25A pathway is also involved in the S-phase checkpoint activation, but this pathway is intact in NBS cells. Our results indicate that the ATM/NBS1/SMC1 pathway is a separate branch of the S-phase checkpoint pathway, distinct from the ATM/CHK2/CDC25A branch. Therefore, this work establishes the ATM/NBS1/SMC1 branch, and provides a molecular basis for the S-phase checkpoint defect in NBS cells.

[*Key Words*: DNA damage response; S-phase checkpoint; phosphorylation; SMC1; ATM; NBS1]

Received December 18, 2001; revised version accepted January 16, 2002.

Cells have an intricate signaling network that deals with genomic insults (Weinert 1998; Zhou and Elledge 2000). This signaling network in response to DNA damage is composed of interacting signal transduction pathways, each consisting of sensors, transducers, and effectors. Sensors detect damaged DNA and signal to transducers. Transducers amplify and relay the signal to effectors. Effectors then execute the cellular response to elicit cell cycle checkpoint activation, DNA repair or apoptosis. Many tumor suppressor proteins are components of the DNA damage signaling network, underscoring the importance of this network to cancer development.

Proteins that serve as sensors are not well defined. Prime candidates are three groups of proteins that contain functional motifs: (1) PCNA-like proteins Rad1/Rad9/Hus1, (2) RFC-like proteins Rad17/RFC2–5, and (3) BRCT domain-containing proteins Rad9/DPB11 in *Saccharomyces cerevisiae* and Crb2/Rhp9/Cut5 in *Schizosaccharomyces pombe* (the mammalian counterparts are not known, but the breast cancer tumor suppressor protein BRCA1 and a protein called 53BP1 are candidates; Zhou and Elledge 2000). The double-stranded break (DSB) repair protein complex MRE11/RAD50/NBS1 (M/R/N) is also hypothesized to be a sensor, as it localizes to the region of DSBs in response to ionizing radiation (IR) (Maser et al. 1997; Nelms et al. 1998; Mirzoeva and Petrini 2001). The central signal transducer in response to IR is the checkpoint kinase ATM, the protein product of the gene mutated in ataxia-telangiectasia (A-T) (Shiloh and Rotman 1996). ATM is responsible for the activation of the G_1, S, and G_2/M checkpoints (Shiloh 2001). Tumor suppressor proteins p53 and CHK2 serve as effectors and are phosphorylated and activated by ATM to induce G_1 and G_2/M cell cycle arrest (Banin et al. 1998; Canman et al. 1998; Matsuoka et al. 1998).

The defective S-phase checkpoint is defined by radioresistant DNA synthesis (RDS). In S-phase checkpoint proficient cells, the rate of DNA synthesis decreases in response to IR. This decrease occurs to a lower extent in S-phase checkpoint defective cells. A-T and NBS (derived from the Nijmegen breakage syndrome) cells were first noted for this defect (Painter and Young 1980). One pathway involved in the activation of the S-phase checkpoint is ATM/CHK2/CDC25A (Falck et al. 2001). ATM activates CHK2, and CHK2 phosphorylates the cell cycle

[3]Corresponding author.
E-MAIL jqin@bcm.tmc.edu; FAX (713) 798-1625.
Article and publication are at http://www.genesdev.org/cgi/doi/10.1101/gad.970702.

regulator CDC25A, leading to its degradation through the polyubiquitination-mediated proteolysis pathway. ATM also phosphorylates NBS1 to activate the S-phase checkpoint (Gatei et al. 2000; Lim et al. 2000; Wu et al. 2000; Zhao et al. 2000), but the downstream effectors are not known, and the relationship between the NBS1 pathway and the ATM/CHK2/CDC25A pathway is not clear. BRCA1, which is believed to function in DNA damage response and transcription regulation, is also required for activation of the S-phase checkpoint (Xu et al. 2001), and is also phosphorylated by ATM in response to IR (Cortez et al. 1999).

Structural maintenance of chromosomes (SMC) proteins are evolutionarily conserved chromosomal proteins. SMC proteins contain coiled-coil domains flanked by globular N- and C-terminal domains, and are divided in the central region by a flexible hinge domain. SMC1 and SMC3 are components of the cohesin complex, which is necessary for sister chromatid cohesion (Guacci et al. 1997; Michaelis et al. 1997; Losada et al. 1998). SMC1 and SMC3 are believed to form a heterodimer in an antiparallel fashion, in which the C-terminal coiled-coil domain of SMC1 interacts with the N-terminal coiled-coil domain of SMC3 (Strunnikov and Jessberger 1999). Cohesion between sister chromatids must be coordinated with DNA replication because cohesion is established during DNA replication (Uhlmann and Nasmyth 1998). The cohesin complex also functions in DNA repair, and is required for postreplicative DSB repair in *S. cerevisiae* (Sjogren and Nasmyth 2001). A mutation in one subunit of the cohesin complex in *S. pombe*, Rad21, renders cells sensitive to DNA damage (Birkenbihl and Subramani 1992).

We report here that SMC proteins are components of the DNA damage response network. ATM phosphorylates SMC1 in response to IR in an NBS1-dependent manner, and the phosphorylation of SMC1 is required for S-phase checkpoint activation. Our data show that SMC1 is a downstream effector in the ATM/NBS1 branch of the S-phase checkpoint pathway. We also show that NBS1 serves as an adaptor in the ATM/NBS1/SMC1 pathway. The ATM/CHK2/CDC25A pathway is intact in NBS cells. Therefore, the ATM/NBS1/SMC1 pathway defines a separate branch of the S-phase checkpoint that is distinct from the ATM/CHK2/CDC25A pathway.

Results

SMC1 associates with BRCA1 and is phosphorylated in response to IR

We recently partially purified and identified a BRCA1-containing protein complex, BASC, which contains several components of the DNA damage response network, including ATM, NBS1, and BLM, the protein product of the gene mutated in Bloom syndrome (Wang et al. 2000). We speculated that BASC functions as a human genome surveillance complex. We report here that SMC1 and SMC3 are two additional proteins that associate with BRCA1 (data not shown). To confirm the association, we immunoprecipitated SMC1 from HeLa nuclear extracts (NE) and detected BRCA1 by Western blotting. An irrelevant antibody against SGT1 did not coimmunoprecipitate BRCA1 (Fig. 1a). This protein interaction is not mediated by DNA, as SMC1 coimmunoprecipitated BRCA1 from NE that were treated with 1.2 μg/mL ethidium bromide to disrupt protein–DNA interactions (Fig. 1a, last lane).

Because BASC contains many proteins that function in DNA damage signaling, we examined whether SMC1 was posttranslationally modified in cells that were treated with IR. A slower-migrating band was observed for SMC1 (Fig. 1b, lane 3), indicating that SMC1 may be phosphorylated in response to IR. Phosphatase treatment of the cell lysate eliminated the top band (Fig. 1b, lane 4), showing that SMC1 was, indeed, phosphorylated. SMC1 can also be phosphorylated in response to a DNA replication block (HU treatment), but with much slower kinetics than BRCA1 (Fig. 1b; data not shown), suggesting that different kinases are involved. These observations support the notion that SMC1 may be a component of the DNA damage response network.

SMC1 phosphorylation is defective in ATM- and NBS1-deficient cells

To delineate the interrelationship between SMC1 and the components of the BRCA1 network, we studied the phosphorylation of SMC1 in cell lines that are wild type or defective in the individual components of the BRCA1 network. Phosphorylation of SMC1 was detected in both

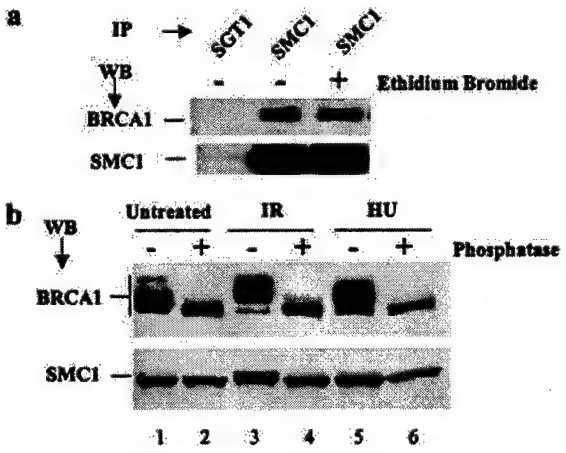

Figure 1. SMC1 associates with BRCA1 and is phosphorylated in response to IR. (*a*) Coimmunoprecipitation of BRCA1 and SMC1 in HeLa NE and NE treated with 1.2 μg/mL ethidium bromide. SGT1 is an irrelevant antibody serving as a negative control. (*b*) Phosphorylation of SMC1 in response to IR. T24 cells were left untreated, irradiated with 10 Gy of IR and incubated for 2 h, or treated with 1 mM hydroxyurea (HU) for 8 h. Cell lysates before and after treatment with 20 U/μL λ protein phosphatase were analyzed by Western blotting.

human cancer and primary cell lines as early as 15 min after IR treatment (Fig. 2a; data not shown). The A-T cell line GM05849 was defective in SMC1 phosphorylation in response to IR (Fig. 2a,b).

Because NBS1 functions in the ATM pathway, we examined the dependence of SMC1 phosphorylation on NBS1. Defective phosphorylation of SMC1 was also observed in cells defective in NBS1 (GM 07166 and JS; Fig.

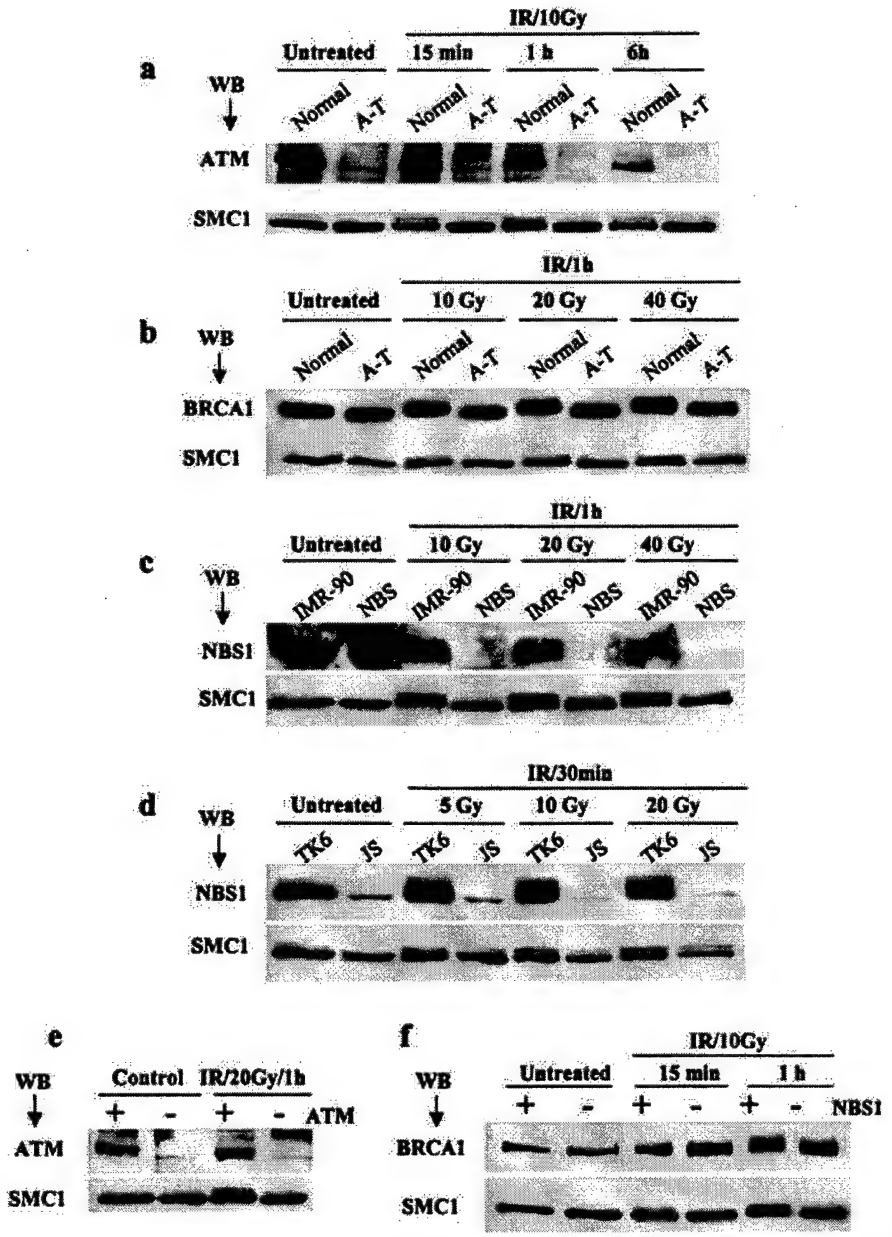

Figure 2. Phosphorylation of SMC1 in response to IR is ATM- and NBS1-dependent. (*a*) Comparison of SMC1 phosphorylation kinetics in normal (GM00637) and A-T (GM05849) cell lines. Cells were irradiated with 10 Gy and incubated for indicated time periods. Cell lysates were analyzed by Western blotting. (*b*) Comparison of SMC1 phosphorylation in normal and A-T cells as a function of IR dosage. After receiving the indicated IR dosages, cells were incubated for 1 h. (*c,d*) Comparison of SMC1 phosphorylation in normal (IMR-90 and TK6) and NBS1-defective cells (GM07166 and JS). (*e*) Dependence of SMC1 phosphorylation on ATM. ATM fibroblasts FT169A and their ATM cDNA-complemented derivative cell line YZ5 were irradiated and analyzed for SMC1 phosphorylation. (*f*) Dependence of SMC1 and BRCA1 phosphorylation on NBS1. A GM07166 TERT cell line and its NBS1 cDNA-complemented derivative cell line were irradiated and analyzed for SMC1 and BRCA1 phosphorylation.

2c,d) as compared with NBS1 wild-type cells (IMR-90 and TK6; Fig. 2c,d). Interestingly, the defect in SMC1 phosphorylation was better observed at a lower IR dosage, particularly in the lymphoblast cell line JS.

Defective SMC1 phosphorylation in A-T cells was corrected by the introduction of ATM cDNA; therefore, SMC1 phosphorylation is indeed ATM-dependent (Fig. 2e). Phosphorylation of SMC1 and BRCA1 was restored with the introduction of NBS1 cDNA in NBS fibroblasts (Fig. 2f), thus showing that the phosphorylation of SMC1 and BRCA1 in response to IR is NBS1-dependent. Together, these observations suggest that SMC1 and BRCA1 function in the ATM and NBS1 signaling pathway in response to IR.

S957 and S966 of SMC1 are phosphorylated in vivo in response to IR, and ATM phosphorylates SMC1 in vitro

We used mass spectrometry to identify in vivo phosphorylation sites in SMC1. SMC1 was immunoprecipitated from NE prepared from irradiated cells, immunoprecipitates were resolved on SDS-PAGE, and SMC1 was analyzed with mass spectrometry (Zhang et al. 1998). Trypsin digestion of the bottom band of SMC1 identified a phosphopeptide, and mass spectrometric sequencing of the phosphopeptide was used to identify the exact phosphorylation site. The observation of the y_{10} ion, which corresponds to amino acid residues 959–968 without phosphorylation, and the y_{12} ion, which corresponds to residues 957–968 with a phosphate group, unambiguously identified one of the three SQ sites present in the phosphopeptide, S957, as the site of phosphorylation (Fig. 3a). The masses of other fragment ions all agree with this assignment. Asp-N digest of the top band identified another phosphopeptide (Fig. 3b). Mass spectrometric sequencing of this phosphopeptide confirmed phosphorylation and unambiguously identified it as spanning amino acids 961–984 of SMC1 (data not shown). However, owing to the low amount of phosphorylated SMC1 and the lesser propensity of Asp-N peptides to break randomly along the peptide backbone compared with tryptic peptides, we were unable to pinpoint the precise phosphorylation site in this phosphopeptide. Given that this phosphopeptide contains one SQ motif, which confers to the ATM phosphorylation consensus (Kim et al. 1999; O'Neill et al. 2000), and that phosphorylation of SMC1 is ATM-dependent, we tentatively assigned S966 as the phosphorylation site. Because the phosphopeptide recovered from the bottom band contains unphosphorylated S966 (Fig. 3a), and the phosphopeptide recovered from the top band contains phosphorylated S966, the phosphorylation of S966 is likely to contribute to the SDS-PAGE mobility shift.

We raised phosphorylation site-specific antibodies against pS957 and pS966 of SMC1 and affinity-purified them. To show the specificity of these antibodies, we made S957A, S966A, and S957A/S966A mutations in SMC1, transiently expressed Flag-tagged wild-type (WT) and mutant SMC1 in 293T cells, irradiated the cells with 10 Gy of IR, and let them recover for 1 h. Flag-SMC1 proteins were immunoprecipitated and analyzed by Western blotting using phospho-SMC1 antibodies. Phospho-specific antibody against pS957 did not recognize Flag-SMC1-S957A or Flag-SMC1-S957A/S966A, in which S957 was mutated, but recognized Flag-SMC1-WT and Flag-SMC1-S966A (Fig. 3c), showing that the phospho-specific antibody against pS957 specifically recognized S957. Similarly, the phospho-specific antibody against pS966 specifically recognized S966. We then used these antibodies to examine SMC1 phosphorylation in vivo in 293T and HeLa cells in response to IR. Both S957 and S966 were phosphorylated in vivo in response to IR (Fig. 3d; data not shown).

To determine whether ATM directly phosphorylates SMC1 in vitro, we expressed a fragment of SMC1 (amino acids 890–1233) containing the in vivo phosphorylation sites as a GST fusion protein. Wild-type Flag-tagged ATM, immunoprecipitated either by an ATM antibody or a Flag antibody from transiently transfected 293T cells following IR treatment, phosphorylated GST-SMC1, whereas kinase-dead ATM did not (Fig. 3e; data not shown). We conclude that ATM phosphorylates SMC1 in vitro.

Dependence of S957 and S966 phosphorylation on ATM and NBS1

To examine whether ATM is required for the phosphorylation of S957 and S966 in response to IR, we used the A-T fibroblast cell line FT169 that was complemented with either wild-type *ATM* cDNA or the vector. Cycling cells were irradiated with 10 Gy of IR and allowed to recover for different times. Figure 4a shows that both S957 and S966 phosphorylation depended on ATM. To examine whether NBS1 is required for S957 and S966 phosphorylation, we used NBS fibroblasts that were complemented with either wild-type NBS1 or the vector (Fig. 4b, lanes 1–8). Phosphorylation of S957 and S966 both depended on the presence of NBS1. Quantification of the pS966 blot relative to the SMC1 blot indicated that at 1 h after IR, complementation with wild-type NBS1 resulted in a threefold increase in the phosphorylation of S966, whereas at 2 and 4 h after IR, this increase was only about twofold.

It is hypothesized that the M/R/N complex may function as a sensor for DSB (Mirzoeva and Petrini 2001). ATM phosphorylates NBS1 in response to IR on S278 and S343. This phosphorylation is required for the activation of the S-phase checkpoint (Zhao et al. 2000). If the M/R/N complex functions as a sensor, phosphorylation of proteins that are downstream of NBS1 will be defective in NBS cells. This is, indeed, the case for SMC1, which supports the sensor model. The sensor model also predicts that the phosphorylation of ATM substrates should not depend on NBS1 phosphorylation. We tested this prediction using NBS cells that were complemented with S278A/S343A mutant NBS1 (Fig. 4b, lanes 9–12). Phosphorylation of S957 clearly depended on NBS1 phos-

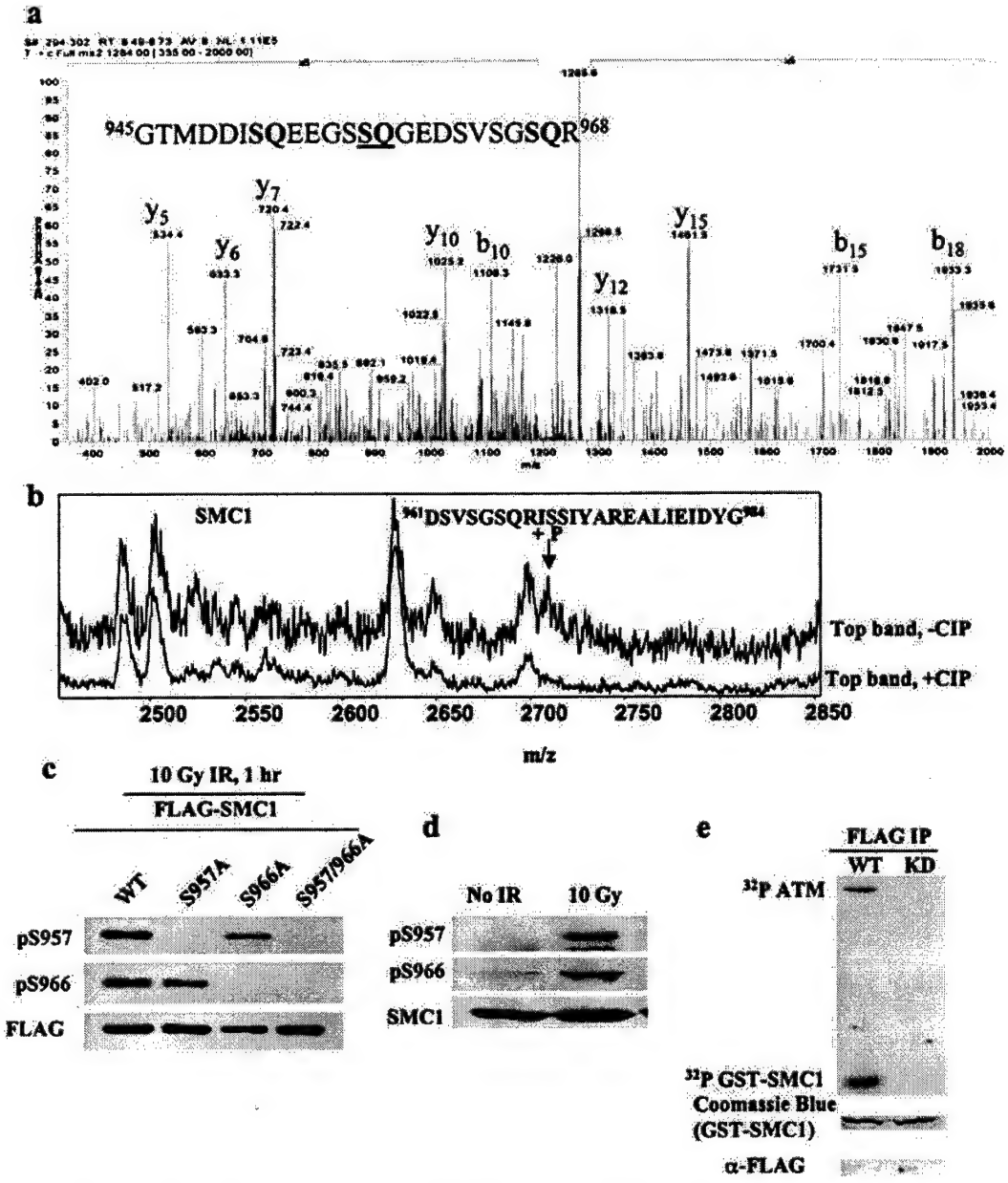

Figure 3. S957 and S966 of SMC1 are phosphorylated in vivo in response to IR. SMC1 was immunoprecipitated from HeLa NE prepared from cells that were irradiated with 20 Gy of IR, recovered for 2 h, and resolved on a 6% SDS-PAGE gel. The top and bottom bands of SMC1 were cut out and analyzed separately. Identification of phosphopeptides was carried out as described using mass spectrometry (Zhang et al. 1998). (*a*) The MS/MS spectrum of the tryptic phosphopeptide amino acids 945–968 of SMC1 from the bottom band. The spectrum identifies the site of phosphorylation as S957. (*b*) A portion of the MALDI-TOF spectra of the Asp-N digests of the top band of SMC1 that were treated with (*bottom* panel) and without (*top* panel) calf intestine phosphatase (CIP). The arrow marks the phosphopeptide, in which S966 is tentatively assigned as the site of phosphorylation. (*c*) Test of the specificity of phospho-specific antibodies. Flag-SMC1 WT, S957A, S966A, and S957A/S966A were expressed in 293T cells. Cells were treated with 10 Gy of IR and allowed to recover for 1 h. Flag-SMC1 proteins were immunoprecipitated with a Flag antibody, and Western blotted with phospho-specific antibodies against pS957 and pS966. (*d*) In vivo phosphorylation of S957 and S966 of SMC1 in response to IR. Untreated and IR-treated 293T cells were analyzed by Western blotting using phospho-specific antibodies against pS957 and pS966. (*e*) In vitro phosphorylation of SMC1 by ATM. A GST–SMC1 fragment (amino acids 890–1233) and Flag-tagged ATM (wild-type or kinase dead) immunoprecipitated by Flag antibody from transiently transfected 293T cells following 20 Gy of IR and 1 h of recovery were used to perform the kinase assay.

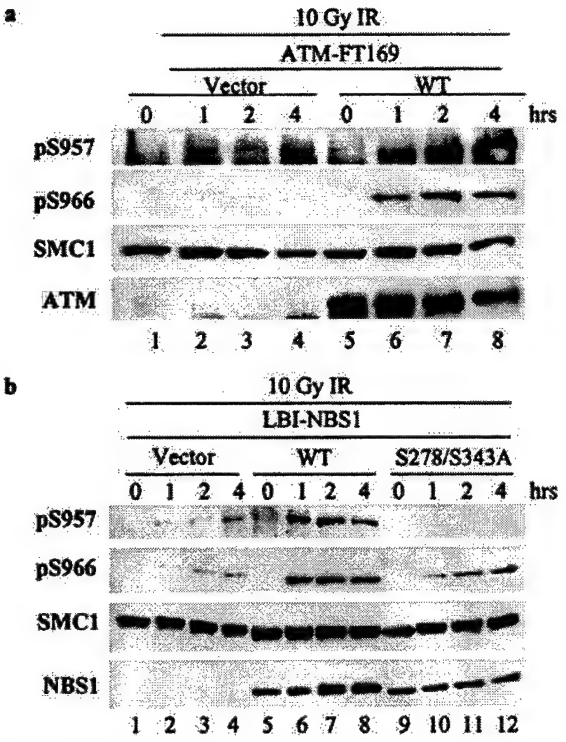

Figure 4. Phosphorylation of S957 and S966 of SMC1 depends on ATM and NBS1. (*a*) Vector and wild-type ATM cDNA-complemented A-T cells were irradiated with 10 Gy of IR and allowed to recover for the indicated times. Phosphorylation of S957 and S966 of SMC1 was examined by Western blotting using phospho-specific antibodies against pS957 and pS966 of SMC1. Two identical gels were run, one for blotting pS957, and the other for blotting pS966. Care was taken to load the two gels equally. (*b*) Vector, wild-type NBS1, and phosphorylation mutant S278A/S343A NBS1 cDNA-complemented NBS cells were irradiated with 10 Gy of IR and allowed to recover for the indicated times. Phosphorylations of S957 and S966 of SMC1 were examined by Western blotting using phospho-specific antibodies against pS957 and pS966 of SMC1.

phorylation. However, the dependence of S966 phosphorylation on NBS1 phosphorylation was not as clear. Quantification of the data indicated a nearly twofold difference in S966 phosphorylation 1 h after IR between cells complemented with wild-type and/or S278A/S343A mutant NBS1. Although small, this difference was consistently observed in three different sets of experiment. At 2 and 4 h after IR, no significant difference in S966 phosphorylation was observed between the two cell lines. Therefore, the phosphorylation of S966 depends on NBS1 phosphorylation in the early response (1 h after IR), but not in the late response (2 and 4 h after IR). These observations contradict the prediction of the sensor model. Therefore, the sensor model cannot be strictly correct and needs to be modified. We propose that the M/R/N complex can serve as a sensor, but that NBS1 functions as an adaptor after IR for the phosphorylation of SMC1 in the ATM/NBS1/SMC1 pathway (see below).

Phosphorylation of SMC1 is BRCA1- and BLM-independent

To test the hypothesis that BRCA1 plays an organizer or adaptor role in BASC, we examined the dependence of SMC1 phosphorylation on BRCA1. SMC1 was phosphorylated on S957 and S966 in response to 10 Gy of IR in HCC1937 cells that were complemented with wild-type *BRCA1* cDNA or the vector (Fig. 5a). Quantification of phosphorylated bands relative to total SMC1 indicated a maximum 1.5-fold increase in the phosphorylation of S957 and S966 in the presence of wild-type BRCA1 at 1 and 4 h after IR. We observed no significant difference in the SDS-PAGE mobility shift of SMC1 in the two cell lines after IR treatment (Fig. 5b). Moreover, the phosphorylation of S957 and S966 was independent of BRCA1 when studied in mouse embryonic fibroblasts (MEF) that

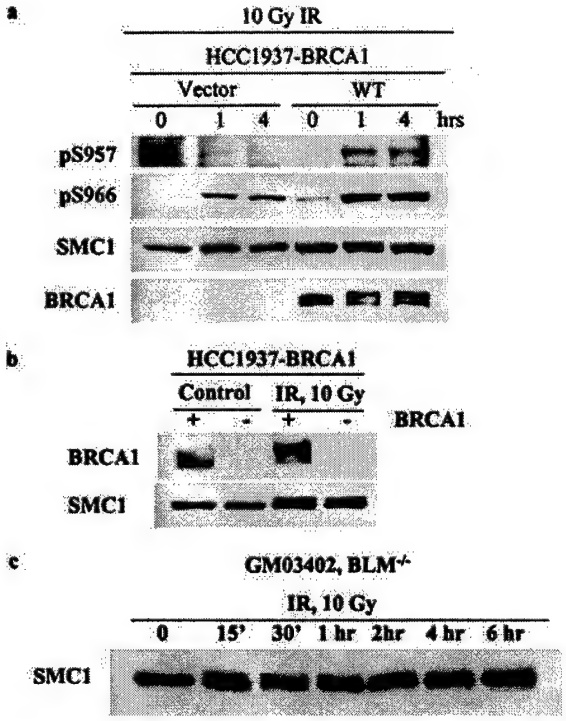

Figure 5. Phosphorylation of S957 and S966 of SMC1 does not depend on BRCA1 or BLM. (*a*) Vector and wild-type *BRCA1* cDNA-complemented HCC1937 cells were irradiated with 10 Gy of IR and allowed to recover for the indicated times. Phosphorylation of S957 and S966 of SMC1 was examined by Western blotting using phospho-specific antibodies against pS957 and pS966 of SMC1. (*b*) Phosphorylation of SMC1 was examined by SDS-PAGE mobility shift in the HCC1937 cells that were complemented with vector and wild-type BRCA1 cDNA. (*c*) The BLM-deficient cell line GM03402 was used to examine the kinetics of SMC1 phosphorylation in response to 10 Gy of IR.

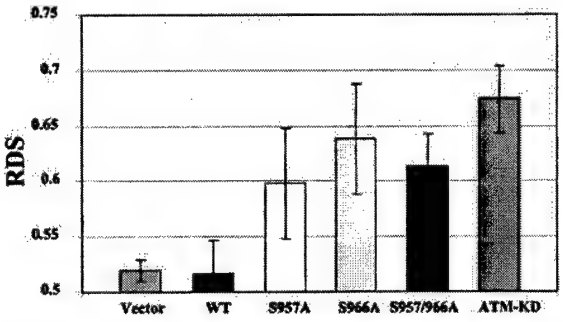

Figure 6. Phosphorylation of S957 and/or S966 of SMC1 is required for IR-induced S-phase checkpoint activation. RDS in 293T cells that were transiently transfected with pCDNA3-Flag vector, pCNDA3-Flag–SMC1-WT, S957A, S966A, S957A/S966A, and pCDNA3-Flag–ATM-KD. Incorporated [^{3}H]thymidine was measured following 20 Gy of IR and 1 h of incubation. Data were normalized with respect to untreated (control) cells. Error bars represent the standard deviation. Five independent experiments were carried out.

were either wild type for BRCA1 or contained a BRCA1 exon 11 deletion (data not shown). Therefore, phosphorylation of SMC1 appears to be BRCA1-independent, and BRCA1 does not seem to play an adapter/organizer role in the phosphorylation of SMC1 in response to IR. However, HCC1937 cells are not completely null for BRCA1, and the BRCA1 exon 11 deletion MEF has a truncated BRCA1 protein. Hence, it is formally possible that BRCA1 plays a role in this pathway. Sgs1 of *S. cerevisiae* is required for DNA damage checkpoint activation (Frei and Gasser 2000), and its human homolog, the BLM helicase, is a component of the BASC. BLM also associates with SMC1 (data not shown). The above findings led us to question whether SMC1 phosphorylation depends on BLM. SMC1 was phosphorylated in the BLM-defective cell line GM03402 in response to IR with kinetics similar to those in IMR-90 cells (Fig. 5c). Therefore, SMC1 phosphorylation does not depend on BLM.

Phosphorylation of S957 and/or S966 is required for activation of the S-phase checkpoint

As SMC1 phosphorylation is both ATM- and NBS1-dependent, we tested whether SMC1 phosphorylation participates in the ATM/NBS1-dependent S-phase checkpoint pathway in response to IR. We transiently transfected 293T cells with Flag-epitope-tagged wild-type or mutant S957A, S966A, or S957A/S966A SMC1, and measured RDS 1 h after 20 Gy of IR. Cells expressing both vector and Flag-SMC1-WT showed inhibition of DNA synthesis, but those expressing Flag-SMC1-S957A, Flag-SMC1-S966A, and Flag-SMC1-S957A/S966A showed RDS (Fig. 6). The extent of RDS in the three SMC1 mutant cell lines was intermediate to those in Flag-SMC1-WT and ATM-KD cells (ATM-KD is a kinase-dead mutant of ATM that functions as a dominant negative, interfering with wild-type ATM functions.) Similar amounts of Flag-SMC1 were expressed in 293T cells (data not shown; similar to Fig. 3c). Therefore, phosphorylation of S957 and/or S966 is required for the activation of the S-phase checkpoint.

Cohesion per se is not sufficient for the phosphorylation of SMC1

To help understand the molecular mechanism of SMC1-dependent S-phase checkpoint activation, we examined whether the phosphorylation of SMC1 has an effect on its binding to chromosomes. Untreated or IR-treated U2OS cells were fractionated according to the chromatin fractionation protocol developed in the Stillman laboratory (Mendez and Stillman 2000), and cytoplasmic, nucleoplasmic, and chromatin-bound fractions were analyzed by Western blotting (Fig. 7a). SMC1 was largely chromatin-bound (P3 fraction) before and after IR, and the phosphorylation of S966 did not affect chromatin binding. We could not detect pS957, as the pS957 antibody is significantly weaker than the pS966 antibody.

Because SMC1 is a component of the cohesin complex, it is important to study its phosphorylation in relation to its function in sister chromatid cohesion. The cohesin

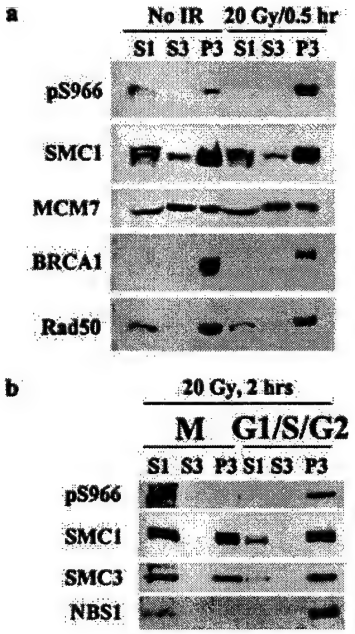

Figure 7. Characterization of SMC1 phosphorylation. (*a*) Phosphorylation of S966 does not affect SMC1 chromatin binding. U2OS cells were fractionated into the cytoplasmic (S1), nucleoplasmic (S2), and chromatin (P3) fractions and analyzed by Western blotting. (*b*) Cohesion per se is not sufficient for S966 phosphorylation. U2OS cells were blocked in mitosis with nocodazole, irradiated with 20 Gy of IR, and allowed to recover for 2 h. Cells were then separated into the mitotic fraction (M) and $G_1/S/G_2$ fraction by mitotic shake-off. M and $G_1/S/G_2$ cells were subject to chromatin fractionation.

complex is present on chromosomes in interphase cells even before sister chromatids are made. Most of the cohesin, however, dissociates from chromosomes in prometaphase, leaving only a small fraction of the cohesin on chromosomes to hold the sister chromatids together until the metaphase–anaphase transition (Losada et al. 1998; Hirano 2000). Only this small fraction that is still chromatin-bound in metaphase technically functions as cohesin. To examine the relationship between SMC1 phosphorylation and sister chromatid cohesion, we blocked the cell cycle in mitosis using nocodazole, irradiated the cells with 20 Gy of IR, and allowed cells to recover for 2 h. We then separated the mitotic cells from the rest by mitotic shake-off, and chromatin-fractionated the two cell populations. As shown in Figure 7b, S966 is not phosphorylated in the mitotic population, although a significant amount of SMC1 is still chromatin-bound. In the $G_1/S/G_2$ population, however, the chromatin-bound SMC1 (P3) is phosphorylated on S966. Therefore, cohesion per se is not sufficient for S966 phosphorylation. Consistent with this finding, NBS1 dissociates from chromatin in the mitotic population, but is chromatin-bound in the $G_1/S/G_2$ population. Therefore, the phosphorylation of SMC1 is not likely to regulate cohesion in mitosis, suggesting other functions for SMC1 besides sister chromatid cohesion.

The ATM/NBS1/SMC1 S-phase checkpoint pathway is distinct from the ATM/CHK2/CDC25A pathway

The molecular mechanism for the ATM/NBS1-dependent S-phase checkpoint is not known. Because the ATM/CHK2/CDC25A pathway is known to regulate the S-phase checkpoint in response to IR, we investigated whether the ATM/NBS1 pathway converges to the ATM/CHK2/CDC25A pathway. NBS cells complemented with vector, wild-type NBS1, or S287A/S343A mutant were treated with 10 Gy of IR and analyzed for CDC25A. As shown in Figure 8a, CDC25A is degraded in all three cell lines in response to IR. Therefore, the ATM/CHK2/CDC25A pathway is intact in NBS cells. This is consistent with the activation of CHK2 in the three cell lines (Fig. 8b). In wild-type NBS1-complemented cells, CDC25A starts to accumulate 3 h after IR. In vector and mutant NBS1-complemented cells, however, CDC25A is not detected up to 4 h after IR. This observation implies that the signal that leads to CDC25A degradation is removed shortly after IR in wild-type cells, but persists in the absence of NBS1 or the presence of a phosphorylation-defective mutant. These data suggest that the ATM/NBS1/SMC1 pathway of the S-phase checkpoint is distinct from the ATM/CHK2/CDC25A pathway (Fig. 8c).

Discussion

In this study, we established that SMC1 of the structural maintenance of chromosomes proteins is a component of the DNA damage response network. Data presented here show that SMC1 is a downstream effector of ATM and NBS1 in the activation of the IR-induced S-phase checkpoint. We also discovered that the phosphorylation of NBS1 by ATM is required for the phosphorylation of SMC1, establishing the role of NBS1 as an adaptor in the ATM/NBS1/SMC1 pathway. The ATM/CHK2/CDC25A pathway is also involved in S-phase checkpoint activation (Falck et al. 2001). We found that this pathway is intact in NBS cells. Our results indicate that the ATM/NBS1/SMC1 pathway is a separate branch of the S-phase checkpoint pathway, distinct from the ATM/CHK2/CDC25A branch (Fig. 8c). Thus, this work establishes the ATM/NBS1/SMC1 branch of the S-phase checkpoint

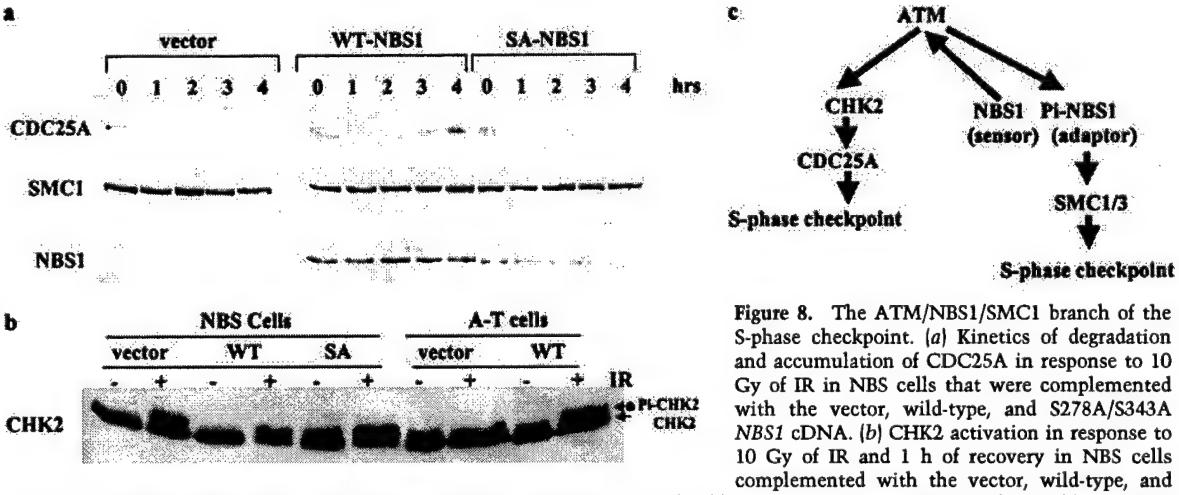

Figure 8. The ATM/NBS1/SMC1 branch of the S-phase checkpoint. (*a*) Kinetics of degradation and accumulation of CDC25A in response to 10 Gy of IR in NBS cells that were complemented with the vector, wild-type, and S278A/S343A *NBS1* cDNA. (*b*) CHK2 activation in response to 10 Gy of IR and 1 h of recovery in NBS cells complemented with the vector, wild-type, and S278A/S343A *NBS1* cDNA and A-T cells complemented with the vector and wild-type *ATM* cDNA. CHK2 was detected by Western blotting. The slowly migrating form marked with an arrow is labeled with Pi-CHK2. (*c*) A simplified S-phase checkpoint pathway in response to DSBs in mammalian cells. Phosphorylated NBS1 (Pi-NBS1) is depicted as an adaptor.

in response to IR, and provides a molecular basis for the S-phase checkpoint defect in NBS cells.

The distinction between the ATM/CHK2/CDC25A pathway and the ATM/NBS1/SMC1 pathway

The kinetics of CDC25A degradation and accumulation in response to IR in NBS cells complemented with the vector, wild-type NBS1, or the phosphorylation mutant NBS1 are intriguing. CDC25A is degraded in the early response to IR in the three cell lines, suggesting that the ATM/CHK2/CDC25A pathway is intact in NBS cells (Fig. 8a). Consistently, CHK2 is activated in response to IR in all three cell lines (Fig. 8b). Therefore, NBS1 is not required for the activation of CHK2, at least in response to 10 Gy of IR. This conclusion is in contrast with Delia's results (Buscemi et al. 2001). Whereas Delia and coworkers used an IR dosage of 4 Gy, we used a dosage of 10 Gy. Possibly, different pathways are used for the response to DNA damage of different severity. Moreover, CDC25A does not accumulate to detectable levels after IR in the absence of NBS1 or if NBS1 cannot be phosphorylated by ATM. Therefore, NBS cells are defective in the late stage of the response to IR, possibly in the recovery phase. In the presence of wild-type NBS1, the signal that leads to CDC25A degradation is eliminated in 3 h, whereas in the absence of NBS1 or NBS1 phosphorylation by ATM, this signal is not removed in 3 h, leading to a relatively late accumulation of CDC25A. NBS1 must participate in the elimination of the signal that results in the degradation of CDC25A. This scenario agrees with a role for the M/R/N complex in DNA replication and repair (Maser et al. 2001). Phosphorylated SMC1 may also play a role in removing the signal, perhaps by homologous recombinational repair. Homologous recombinational repair requires the presence of an undamaged copy of the chromosome as a template. Sister chromatids are the preferred partners for this purpose. SMC1, as a subunit of the cohesin complex, may provide the structural scaffold for DSB repair by homologous recombination. This is consistent with the requirement of sister chromatid cohesion for postreplicative DSB repair in *S. cerevisiae* (Sjogren and Nasmyth 2001) and the finding that SMC1 is a component of the recombination complex RC-1 (Jessberger et al. 1996). It has been shown that postreplicative repair requires cohesion that is established only during S phase. When the cohesin complex is expressed after the S phase, despite the fact that the cohesin complex is chromatin-bound, the cells are defective in DNA repair. This finding is in agreement with our observation that the fraction of SMC1 that is still chromatin-bound in mitosis, providing cohesion between sister chromatids, is not phosphorylated. Taken together, it is likely that phosphorylated SMC1 is required for efficient postreplicative repair in human cells. Functionally, the two branches of ATM-dependent S-phase checkpoint pathways diverge to allow the CHK2/CDC25A branch to directly communicate with the cell cycle machinery, and the NBS1/SMC1 branch to directly communicate with the replication/repair machinery.

Phosphorylation of SMC1 is required for activation of the S-phase checkpoint

The exact molecular mechanism by which phosphorylated SMC1 prevents radio-resistant DNA synthesis is not known. CDC25A is degraded and CHK2 is activated in NBS cells. Considering the above observations, phosphorylated SMC1 is not likely to function toward the suppression of the firing of origins in line for firing before encountering DSB, a pathway that is largely controlled by RAD53 (the human counterpart is CHK2) and the cell cycle machinery (Tercero and Diffley 2001). Phosphorylation of SMC1 may participate in the replication elongation process by interfering with the establishment of cohesion between the template and the sister chromatid that is being elongated, thus slowing down the progression of the replication fork. Phosphorylated SMC1 binds tightly to chromosomes in $G_1/S/G_2$. Structurally, SMC1 is phosphorylated within the C-terminal coiled-coil domain, and SMC3, the partner of SMC1, is phosphorylated in the N-terminal coiled-coil domain (P. Yazdi and J. Qin, unpubl.). These coiled-coil domains of SMC1 and SMC3 are in the same position of the antiparallel heterodimer of SMC1/3. Hence, phosphorylation of SMC1 and SMC3 may result in a large conformational change, modulating protein–protein interactions, presumably with the replication machinery. The heart of future research in the NBS1 branch of the S-phase checkpoint will be at the identification of the components of the replication machinery that are subject to regulation by the ATM/NBS1 pathway.

NBS1 may be an adaptor in response to IR in the ATM/NBS1/SMC1 pathway

The identities of sensors that detect DNA damage have been elusive. The proposal that the human M/R/N complex functions as a sensor is supported by the observation that in response to DSB, checkpoint activation and *S. cerevisiae* Rad9 phosphorylation, an early event in checkpoint activation, require the Mre11/Rad50/Xrs2 complex (the *S. cerevisiae* counterpart of the human M/R/N complex; D'Amours and Jackson 2001; Grenon et al. 2001). Our finding that SMC1 phosphorylation (as well as BRCA1 phosphorylation) in response to IR depends on ATM and NBS1 may suggest that NBS1 lies upstream of ATM, serving as a sensor for DSB as proposed previously (Mirzoeva and Petrini 2001), or modifying DSB to a form recognizable by ATM. ATM is known to phosphorylate NBS1 in response to IR, suggesting that ATM lies upstream of NBS1. To resolve this paradox, we suggest an alternative model in which the M/R/N complex initially serves as a sensor, leading to the activation of ATM. ATM, in turn, phosphorylates its substrates, including NBS1. Phosphorylation of NBS1 effectively terminates the function of NBS1 as a sensor and

converts NBS1 into an adaptor by conformational change. The adaptor NBS1 then positions NBS1-binding proteins such that ATM can phosphorylate them. This model is consistent with our finding that SMC1 phosphorylation depends on NBS1 phosphorylation. Within this model, the role of NBS1 can be more accurately described as an adaptor that brings the substrate, SMC1, to ATM. This also agrees with the observation that a small population of NBS1 interacts with a small population of SMC1, as shown by coimmunoprecipitation (P. Yazdi and J. Qin, unpubl.). Our duo sensor/adaptor model also imposes specificity on DNA damage response, that is, the transducers can only transduce signals to downstream effectors that bind to the duo sensor/adaptor proteins. This specificity can explain why specific forms of DNA damage elicit specific responses although they all may work through the same transducer. The specificity is imposed by the sensor/adaptor/effector combination.

SMC1 phosphorylation is independent of BLM, suggesting that BLM does not function in the ATM/NBS1/SMC1 pathway. A definitive conclusion is difficult to make for the role of BRCA1 as an organizer or adaptor in the ATM/NBS1/SMC1 signaling pathway. The small increase in SMC1 phosphorylation after stable complementation of HCC1937 cells with *BRCA1* cDNA may be attributable to the low expression level of wild-type BRCA1 in this cell line. A definitive result would be obtained if the HCC1937 cell line could be complemented with higher, yet physiological amounts of BRCA1. The relationship between SMC1 and BRCA1 is not clear. BRCA1 may function as a downstream effector in this pathway, in which its putative E3 ubiquitin ligase activity (Hashizume et al. 2001; Ruffner et al. 2001) is regulated by DNA damage. Many BRCA1-interacting proteins can thus serve as substrates for the E3 activity of BRCA1. We speculate that SMC1 is such a substrate. Therefore, it is conceivable that the BASC, as a genome-surveillance complex, assembles sensors/adaptors, transducers, and effectors in a position to respond promptly to insults on the genome. Understanding the functional relationships among ATM, NBS1, BRCA1, SMC1/3, and other proteins in the BASC complex will provide insights into the mechanism of DNA damage response and the role of each individual protein.

Materials and methods

Antibodies

Rabbit polyclonal SMC1 antibody was raised against peptide sequence DLTKYPDANPNPNEQ and affinity-purified (Bethyl Laboratories). ATM and NBS1 antibodies were from GeneTex. Monoclonal mouse CDC25A antibody (F-6) was from Santa Cruz Biotechnology. BRCA1 antibody was described before (Wang et al. 2000). Phosphorylation site-specific SMC1 antibodies were raised against QEEGSpSQGEDS (S957 of SMC1), and DSVSGpSQRISS (S966 of SMC1). Affinity-purified phosphorylation site-specific antibodies recognize phosphorylated and unphosphorylated peptides with ratios >99:1 by ELISA (Bethyl Laboratories). Immunoprecipitation and Western blotting were carried out as described (Wang et al. 2000).

Plasmids, recombinant proteins, transient transfection, and in vitro kinase assays

Fragments of SMC1 cDNA were generated by polymerase chain reaction with reverse transcription (RT–PCR) using RNA isolated from HeLa cells and cloned in pCR-Blunt II-TOPO vectors (Invitrogen). Full-length *SMC1* cDNA was assembled by ligation of SMC1 fragments in pCDNA3.1(–). A GST–SMC1 fusion protein (amino acids 890–1233) plasmid was generated by PCR and cloned in PGEX-4T-2. The fusion protein was expressed and purified according to the standard procedures. Site-specific mutagenesis was performed using a QuickChange site-directed mutagenesis kit (Stratagene), and the results were verified by sequencing. Wild-type, S957A, S966A, and S957A/S966A mutant SMC1 were subcloned in the pCDNA3-Flag vector. Transient transfection of these plasmids was carried out using Lipofectamine 2000 (Invitrogen) according to the manufacturer's suggested protocol. In vitro kinase assays were carried out as described (Cortez et al. 1999).

Cell culture

Control (IMR-90, GM00637, TK6, 293T, and HeLa), A-T (GM05849), NBS (GM07166 and JS), BLM (GM03402), and BRCA1 (HCC1937) cell lines were purchased from either the Coriell Human Mutant cell repository or ATCC and cultured according to directions from the source. Wild-type or mutant S279A/S343A NBS1 was expressed in NBS1-LBI fibroblasts (Zhao et al. 2000) using the retroviral vector pLXIN (Clontech). The 29310A1 retroviral packaging cells (Imgenex) were transfected with pLXIN vector (as a negative control) or pLXIN vectors containing cDNA encoding wild-type NBS1 or mutant S279A/S343A NBS1. Retroviral supernatants were collected 48 h posttransfection. NBS1-LBI cells were incubated in retroviral supernatant plus fresh D-MEM supplemented with 10% fetal calf serum (volume ratio 1:1) for at least 24 h. NBS1-LBI cells were selected with 500 μg/mL G418 72 h after infection. Clones with ectopic expression of NBS1 were tested by Western blotting and immunostaining and maintained in D-MEM supplemented with 10% FCS and 200 μg/mL G418. FT169A ATM fibroblasts and their derivative YZ5 (ATM cDNA-complemented) were provided by Y. Shiloh (Department of Human Genetics and Molecular Medicine, Sackler School of Medicine, Tel Aviv University, Israel); GM07166 telomerase catalytic subunit (TERT) cells and the NBS1 cDNA-complemented GM07166 TERT cell line were provided by D. Livingston (The Dana-Farber Cancer Institute and the Harvard Medical School, Boston, MA); and the BRCA1 cDNA-complemented HCC1937 cell line was provided by J. Chen (Division of Oncology Research, Mayo Clinic, Rochester, MN).

Radio-resistant DNA synthesis

RDS assay was carried out as described (Morgan et al. 1997). Briefly, 293T cells were labeled with 10 nCi/mL of [^{14}C]thymidine for 48 h to control for the total DNA content of different samples. Cells were then transfected with plasmids encoding wild-type and mutant Flag-SMC1. Transfection efficiency was estimated to be ~60%–70% using a GFP–SMC1 plasmid and FACS analysis. Sixty hours after transfection, cells were irradiated with 20 Gy of IR and incubated for 1 h. They were then pulse-labeled with 1 μCi/mL [^{3}H]thymidine for 30 min, washed twice with PBS, fixed with methanol, and filtered on a GF/C

fiberglass filter. Filters were counted in a liquid scintillation counter. DNA synthesis was calculated using the ratio of $^{3}H/^{14}C$. Overlapping ^{3}H and ^{14}C emissions were corrected with quenched ^{3}H and ^{14}C standards. Three replicas were measured for each sample, and five independent experiments were performed to collect data for statistical analysis.

Mass spectrometry for the identification of phosphorylation sites

Identification of phosphorylation sites with mass spectrometry was carried out as described previously (Zhang et al. 1998).

Acknowledgments

We thank Y. Shiloh, D. Livingston, and J. Chen for distribution of cell lines; Z. Songyang for teaching J.Q. molecular biology; and D. Cortez and S. Elledge for discussion and critical reading of the manuscript. This work was supported by grants from the A-T Children Project and NCI (CA84199). J.Q. is a recipient of a career development award from the U.S. Department of Defense Breast Cancer Research program (DAMD17-00-1-0146), and P.T.Y. is a postdoctoral fellow of the U.S. Department of Defense Breast Cancer Research Program (DAMD17-01-1-0148).

The publication costs of this article were defrayed in part by payment of page charges. This article must therefore be hereby marked "advertisement" in accordance with 18 USC section 1734 solely to indicate this fact.

References

Banin, S., Moyal, L., Shieh, S., Taya, Y., Anderson, C.W., Chessa, L., Smorodinsky, N.I., Prives, C., Reiss, Y., Shiloh, Y., et al. 1998. Enhanced phosphorylation of p53 by ATM in response to DNA damage. *Science* **281:** 1674–1677.

Birkenbihl, R.P. and Subramani, S. 1992. Cloning and characterization of rad21, an essential gene of *Schizosaccharomyces pombe* involved in DNA double-strand-break repair. *Nucleic. Acids. Res* **20:** 6605–6611.

Buscemi, G., Savio, C., Zannini, L., Micciche, F., Masnada, D., Nakanishi, M., Tauchi, H., Komatsu, K., Mizutani, S., Khanna, K., et al. 2001. Chk2 activation dependence on Nbs1 after DNA damage. *Mol. Cell. Biol.* **21:** 5214–5222.

Canman, C.E., Lim, D.S., Cimprich, K.A., Taya, Y., Tamai, K., Sakaguchi, K., Appella, E., Kastan, M.B., and Siliciano, J.D. 1998. Activation of the ATM kinase by ionizing radiation and phosphorylation of p53. *Science* **281:** 1677–1679.

Cortez, D., Wang, Y., Qin, J., and Elledge, S.J. 1999. Requirement of ATM-dependent phosphorylation of brca1 in the DNA damage response to double-strand breaks. *Science* **286:** 1162–1166.

D'Amours, D. and Jackson, S.P. 2001. The yeast Xrs2 complex functions in S phase checkpoint regulation. *Genes & Dev.* **15:** 2238–2249.

Falck, J., Mailand, N., Syljuasen, R.G., Bartek, J., and Lukas, J. 2001. The ATM-Chk2-Cdc25A checkpoint pathway guards against radioresistant DNA synthesis. *Nature* **410:** 842–847.

Frei, C. and Gasser, S.M. 2000. The yeast Sgs1p helicase acts upstream of Rad53p in the DNA replication checkpoint and colocalizes with Rad53p in S-phase-specific foci. *Genes & Dev.* **14:** 81–96.

Gatei, M., Young, D., Cerosaletti, K.M., Desai-Mehta, A., Spring, K., Kozlov, S., Lavin, M.F., Gatti, R.A., Concannon, P., and Khanna, K. 2000. ATM-dependent phosphorylation of nibrin in response to radiation exposure. *Nat. Genet.* **25:** 115–119.

Grenon, M., Gilbert, C., and Lowndes, N.F. 2001. Checkpoint activation in response to double-strand breaks requires the Mre11/Rad50/Xrs2 complex. *Nat. Cell Biol.* **3:** 844–847.

Guacci, V., Koshland, D., and Strunnikov, A. 1997. A direct link between sister chromatid cohesion and chromosome condensation revealed through the analysis of MCD1 in *S. cerevisiae*. *Cell* **91:** 47–57.

Hashizume, R., Fukuda, M., Maeda, I., Nishikawa, H., Oyake, D., Yabuki, Y., Ogata, H., and Ohta, T. 2001. The RING heterodimer BRCA1–BARD1 is a ubiquitin ligase inactivated by a breast cancer-derived mutation. *J. Biol. Chem.* **276:** 14537–14540.

Hirano, T. 2000. Chromosome cohesion, condensation, and separation. *Annu. Rev. Biochem.* **69:** 115–144.

Jessberger, R., Riwar, B., Baechtold, H., and Akhmedov, A.T. 1996. SMC proteins constitute two subunits of the mammalian recombination complex RC-1. *EMBO J.* **15:** 4061–4068.

Kim, S.T., Lim, D.S., Canman, C.E., and Kastan, M.B. 1999. Substrate specificities and identification of putative substrates of ATM kinase family members. *J. Biol. Chem.* **274:** 37538–37543.

Lim, D.S., Kim, S.T., Xu, B., Maser, R.S., Lin, J., Petrini, J.H., and Kastan, M.B. 2000. ATM phosphorylates p95/nbs1 in an S-phase checkpoint pathway. *Nature* **404:** 613–617.

Losada, A., Hirano, M., and Hirano, T. 1998. Identification of *Xenopus* SMC protein complexes required for sister chromatid cohesion. *Genes & Dev.* **12:** 1986–1997.

Maser, R.S., Monsen, K.J., Nelms, B.E., and Petrini, J.H. 1997. hMre11 and hRad50 nuclear foci are induced during the normal cellular response to DNA double-strand breaks. *Mol. Cell. Biol.* **17:** 6087–6096.

Maser, R.S., Mirzoeva, O.K., Wells, J., Olivares, H., Williams, B.R., Zinkel, R.A., Farnham, P.J., and Petrini, J.H. 2001. Mre11 complex and DNA replication: Linkage to E2F and sites of DNA synthesis. *Mol. Cell. Biol.* **21:** 6006–6016.

Matsuoka, S., Huang, M., and Elledge, S.J. 1998. Linkage of ATM to cell cycle regulation by the Chk2 protein kinase. *Science* **282:** 1893–1897.

Mendez, J. and Stillman, B. 2000. Chromatin association of human origin recognition complex, cdc6, and minichromosome maintenance proteins during the cell cycle: Assembly of prereplication complexes in late mitosis. *Mol. Cell. Biol.* **20:** 8602–8612.

Michaelis, C., Ciosk, R., and Nasmyth, K. 1997. Cohesins: Chromosomal proteins that prevent premature separation of sister chromatids. *Cell* **91:** 35–45.

Mirzoeva, O.K. and Petrini, J.H. 2001. DNA damage-dependent nuclear dynamics of the Mre11 complex. *Mol. Cell. Biol.* **21:** 281–288.

Morgan, S.E., Lovly, C., Pandita, T.K., Shiloh, Y., and Kastan, M.B. 1997. Fragments of ATM which have dominant-negative or complementing activity. *Mol. Cell. Biol.* **17:** 2020–2029.

Nelms, B.E., Maser, R.S., MacKay, J.F., Lagally, M.G., and Petrini, J.H. 1998. In situ visualization of DNA double-strand break repair in human fibroblasts. *Science* **280:** 590–592.

O'Neill, T., Dwyer, A.J., Ziv, Y., Chan, D.W., Lees-Miller, S.P., Abraham, R.H., Lai, J.H., Hill, D., Shiloh, Y., Cantley, L.C., et al. 2000. Utilization of oriented peptide libraries to identify substrate motifs selected by ATM. *J. Biol. Chem.* **275:** 22719–22727.

Painter, R.B. and Young, B.R. 1980. Radiosensitivity in ataxia-telangiectasia: A new explanation. *Proc. Natl. Acad. Sci.* **77:** 7315–7317.

Ruffner, H., Joazeiro, C.A., Hemmati, D., Hunter, T., and Verma, I.M. 2001. Cancer-predisposing mutations within the RING domain of BRCA1: Loss of ubiquitin protein ligase activity and protection from radiation hypersensitivity. *Proc. Natl. Acad. Sci.* **98:** 5134–5139.

Shiloh, Y. 2001. ATM and ATR: Networking cellular responses to DNA damage. *Curr. Opin. Genet. Dev.* **11:** 71–77.

Shiloh, Y. and Rotman, G. 1996. Ataxia-telangiectasia and the ATM gene: Linking neurodegeneration, immunodeficiency, and cancer to cell cycle checkpoints. *J. Clin. Immunol.* **16:** 254–260.

Sjogren, C. and Nasmyth, K. 2001. Sister chromatid cohesion is required for postreplicative double-strand break repair in *Saccharomyces cerevisiae*. *Curr. Biol.* **11:** 991–995.

Strunnikov, A.V. and Jessberger, R. 1999. Structural maintenance of chromosomes (SMC) proteins: Conserved molecular properties for multiple biological functions. *Eur. J. Biochem.* **263:** 6–13.

Tercero, J.A. and Diffley, J.F. 2001. Regulation of DNA replication fork progression through damaged DNA by the Mec1/Rad53 checkpoint. *Nature* **412:** 553–557.

Uhlmann, F. and Nasmyth, K. 1998. Cohesion between sister chromatids must be established during DNA replication. *Curr. Biol.* **8:** 1095–1101.

Wang, Y., Cortez, D., Yazdi, P., Neff, N., Elledge, S.J., and Qin, J. 2000. BASC, a super complex of BRCA1-associated proteins involved in the recognition and repair of aberrant DNA structures. *Genes & Dev.* **14:** 927–939.

Weinert, T. 1998. DNA damage and checkpoint pathways: Molecular anatomy and interactions with repair. *Cell* **94:** 555–558.

Wu, X., Ranganathan, V., Weisman, D.S., Heine, W.F., Ciccone, D.N., O'Neill, T.B., Crick, K.E., Pierce, K.A., Lane, W.S., Rathbun, G., et al. 2000. ATM phosphorylation of Nijmegen breakage syndrome protein is required in a DNA damage response. *Nature* **405:** 477–482.

Xu, B., Kim, S., and Kastan, M.B. 2001. Involvement of Brca1 in S-phase and G(2)-phase checkpoints after ionizing irradiation. *Mol. Cell. Biol.* **21:** 3445–3450.

Zhang, X., Herring, C.J., Romano, P.R., Szczepanowska, J., Brzeska, H., Hinnebusch, A.G., and Qin, J. 1998. Identification of phosphorylation sites in proteins separated by polyacrylamide gel electrophoresis. *Anal. Chem.* **70:** 2050–2059.

Zhao, S., Weng, Y.C., Yuan, S.S., Lin, Y.T., Hsu, H.C., Lin, S.C., Gerbino, E., Song, M.H., Zdzienicka, M.Z., Gatti, R.A., et al. 2000. Functional link between ataxia-telangiectasia and Nijmegen breakage syndrome gene products. *Nature* **405:** 473–477.

Zhou, B.B. and Elledge, S.J. 2000. The DNA damage response: Putting checkpoints in perspective. *Nature* **408:** 433–439.

[CANCER RESEARCH 62, 3966–3970, July 15, 2002]

Deficient Nonhomologous End-Joining Activity in Cell-free Extracts from Brca1-null Fibroblasts[1]

Qing Zhong, Thomas G. Boyer, Phang-Lang Chen, and Wen-Hwa Lee[2]

Department of Molecular Medicine/Institute of Biotechnology, University of Texas Health Science Center at San Antonio, San Antonio, Texas 78245

ABSTRACT

BRCA1 ensures genomic stability, at least in part, through a functional role in DNA damage repair. BRCA1 interacts with the Rad50/Mre11/Nbs1 complex that occupies a central role in DNA double-strand break repair mediated by homologous recombination and nonhomologous end joining (NHEJ). NHEJ can be catalyzed by mammalian whole cell extract in a reaction dependent upon DNA ligase IV, Xrcc4, Ku70, Ku80, and DNA-PKcs. Here, we show that under identical cell-free reaction conditions, the addition of antibodies specific for BRCA1 and Rad 50 but not Rad51, inhibits end-joining activity. Cell extracts derived from Brca1-deficient mouse embryonic fibroblasts exhibit reduced end-joining activity independent of the endogenous protein amounts of DNA ligase IV, Ku80, and Ku70. The Brca1-dependent NHEJ activity predominates at the lower concentrations of Mg2+ (0.5 mM); elevated Mg2+ or Mn2+ concentrations (10 mM) dramatically increase overall end-joining activity and abrogates the requirement for Brca1, Xrcc4, and Ku70. The addition of partially purified BRCA1, in association with Rad50/Mre11/Nbs1 complex, complements the NHEJ deficiency of Brca1-null fibroblast extracts. These results suggest a role for Brca1 in NHEJ and in the maintenance of genome integrity.

INTRODUCTION

Inactivation of the hereditary breast cancer susceptibility gene, *BRCA1*,[3] leads to genomic instability (1–3). Extensive chromosomal abnormalities have been observed in Brca1-deficient murine fibroblasts (4), as well as the BRCA1-mutant human breast cancer cell line HCC1937 (5). The function of BRCA1 in genome stability is attributable to its central role in the cellular response to DNA damage response, and emerging evidence supports a role for BRCA1 in DNA damage repair. For example, Brca1-deficient murine and human cells are sensitive to DNA-damaging agents, including IR (6–8). Furthermore, HCC1937 cells expressing mutant BRCA1 protein exhibit a reduction in both the rate and extent of DSB repair after IR when compared with cells expressing wild-type BRCA1 protein (9). Finally, BRCA1 physically interacts with the Rad50/Mre11/Nbs1 DSB repair complex and colocalizes to nuclear foci along with this complex after treatment of cells with IR (8).

In eukaryotic cells, DSBs are repaired through two distinct pathways: homologous recombination and NHEJ. BRCA1 has been implicated in homology-based repair because cells expressing a Brca1 exon-11 deletion mutant exhibit defects in gene targeting, single-strand annealing, and gene conversion (10). BRCA1 may also influence NHEJ by virtue of its interaction with the Rad50/Mre11/Nbs1 complex. The orthologous complex in *Saccharomyces cerevisiae* Rad50/Mre11/Xrs2 is critical for NHEJ, sister chromatid recombination, and telomere maintenance. Yeast strains deficient in any of the components of the Rad50/Mre11/Xrs2 complex are 10–100-fold less efficient in nonhomologous joining of DNA ends (11, 12). The Rad50/Mre11/Nbs1 complex is characterized by 3′ to 5′ exonucleolytic activity on double-stranded DNA and endonucleolytic activity on single-stranded DNA and hairpin structures. Furthermore, in the presence of a DNA ligase, Mre11 can facilitate DNA end joining using microhomologies at or near DNA termini (13, 14). Recently, the yeast Rad50/Mre11/Xrs2 complex was found to exhibit DNA end-binding activity and end-bridging activity (15). Thus, the Rad50/Mre11/Nbs1 complex may fulfill a functionally conserved role in NHEJ.

In mammalian cells, a NHEJ pathway has been identified that comprises the heterodimeric DNA end-binding activity Ku70/Ku80 and the DNA-PKcs (reviewed in Ref. 12). Recently, Baumann *et al.* (16) developed a cell-free system that faithfully reflects the genetic requirements for this NHEJ pathway. In this system, accurate intermolecular ligation of DNA ends was found to be dependent on DNA ligase IV/Xrcc4 and requires Ku70, Ku80, and DNA-PKcs. However, the role of Rad50/Mre11/Nbs1 in this NHEJ assay has not been addressed.

We report here the use of this cell-free assay to investigate the role of BRCA1 in DNA end joining. We observed that antibodies specific for BRCA1, Rad50, and Ku70, but not Rad51, inhibit the end-joining activity present in extracts prepared from a human lymphoblastoid cell line. Comparison of extracts derived from Brca1-null MEFs with that from isogenic Brca1-proficient MEFs for their respective abilities to catalyze end joining *in vitro* revealed that Brca1-deficient MEF extracts exhibit a significantly reduced end-joining activity. This deficiency can be complemented by partially purified BRCA1 in association with the Rad50/Mre11/Nbs1 complex. Finally, we found the BRCA1-dependent NHEJ activity in mammalian WCE to be sensitive to the reaction concentration of divalent cations. Elevated concentrations of Mg2+ or Mn2+ (to 10mM) stimulated the overall level of DNA end-joining activity and masked a BRCA1, Ku, and Xrcc4 requirement. These results provide evidence that BRCA1 promote NHEJ in a Mg2+ concentration-dependent manner.

MATERIALS AND METHODS

MEFs and Lymphoblastoid Cell Line. The *Brca1*$^{-/-}$:*p53*$^{-/-}$ and p53$^{-/-}$ MEFs were derived from 9.5-day old embryos of a cross between *Brca1*$^{+/-}$ and *p53*$^{+/-}$ mice as described (17) and cultured in DMEM plus 10% FCS. Human lymphoblastoid cell line, LEM, was immortalized by Epstein-Barr virus and cultured in DMEM plus 10% FCS.

Cell-free NHEJ Assay. Cell extracts were prepared and *in vitro* reactions were performed according to previously described procedure (16). WCEs were normalized for their respective total protein levels using the Bio-Rad protein assay (Bio-Rad, Richmond, CA). Reactions (16 μl) were carried out in 50 mM triethanolamine-HCl (pH 7.5), 0.5 mM $Mg(OAc)_2$, 80 mM potassium acetate, 2 mM ATP, 1 mM DTT, and 100 μg/ml BSA. Cell-free extracts were incubated for 5 min at 37°C before the addition of 5 fmol ^{32}P-labeled DNA. pBSK(+) duplex plasmid DNA (2.96 kb; Stratagene, La Jolla, CA) was linearized with *Eco*RI, dephosphorylated using calf intestinal phosphatase, and was 5′ ^{32}P-end-labeled using polynucleotide kinase. In each reaction, 5 fmol of labeled DNA was used. After incubation at 37°C for 1 h, ^{32}P-labeled DNA products were deproteinized by proteinase K (500 μg/ml) and 1% SDS at 37°C for 20 min and analyzed by electrophoresis through 0.7% agarose gels, followed by autoradiography. Quantitation of DNA end-joining efficiency was carried out

Received 3/12/02; accepted 5/13/02.

The costs of publication of this article were defrayed in part by the payment of page charges. This article must therefore be hereby marked *advertisement* in accordance with 18 U.S.C. Section 1734 solely to indicate this fact.

[1] Supported in part by NIH Grant CA 81020 and 94170 (to W-H. L.) and Grant CA 85605 (to P-L. C.). Q. Z. was supported by a predoctoral training grant from the U.S. Army Medical Research and Materiel Command under DAMD17-99-1-9402.

[2] To whom requests for reprints should be addressed, at E-mail: leew@uthscsa.edu.

[3] The abbreviations used are: *BRCA1*, human breast cancer 1 gene; BRCA1, protein product of *BRCA1*; *Brca1*, mouse breast cancer 1 gene; Brca1, protein product of *Brca1*; IR, ionizing radiation; NHEJ, nonhomologous end joining; DSB, double-strand break; MEF, mouse embryonic fibroblast; WCE, whole cell extract; mAb, monoclonal antibody; RPB1, RNA polymerase II.

by densitometry. For antibody inhibition experiments, cell extracts were preincubated with specific antibodies on ice for 30 min before shifting to 37°C for 5 min, followed by the addition of ^{32}P-labeled DNA.

Antibodies and Antisera. A recombinant protein containing glutathione *S*-transferase fused with mouse Brca1 of amino acids 788-1135 in frame was used as an antigen for the production of antimurine Brca1 mouse polyclonal antisera. Purified goat IgG specific for XRCC4, Ku70, and Ku80 was purchased from Santa Cruz Biotechnology (Santa Cruz, CA). Purified mouse monoclonal antibody specific for BRCA1 (Ab-1) was purchased from Oncogene Research Products (San Diego, CA). Other antibodies specifically against BRCA1, Rad50, and Rad51 have been described (8).

The amounts of the following antibodies were used in NHEJ inhibition experiments: 10 μg of antimouse IgG; 1 μg of purified goat anti-Ku70 IgG; 1 μg of anti-BRCA1 mAb Ab-1; 2 μg of anti-BRCA1 mAb 17F8; 5 μg of anti-Rad50 mAb 13B3; 1 μg of purified rabbit anti-Rad51 IgG; and 1 μg of purified rabbit anti-Xrcc4. Only mAbs and commercial available purified antisera were used in antibody inhibition assays. Most of the polyclonal antisera contain high levels of nuclease activity and cannot be used in the cell-free end-joining assay.

Protein Purification. HeLa cell nuclear extract was subjected to successive phosphocellulose P-11, DEAE-Sepharose, and Superose 6 gel filtration chromatography as described previously (18). Individual fractions derived from Superose 6 chromatography corresponding to the peaks of the Rad50, Mre11, and NBS1 proteins were pooled and designated as fraction C1. The fraction C1 was concentrated on phosphocellulose P-11 by elution with 0.5 M KCl D buffer [20 mM HEPES (pH 7.9), 0.2 mM EDTA, and 20% glycerol], followed by dialysis with 0.1 M KCl in D buffer.

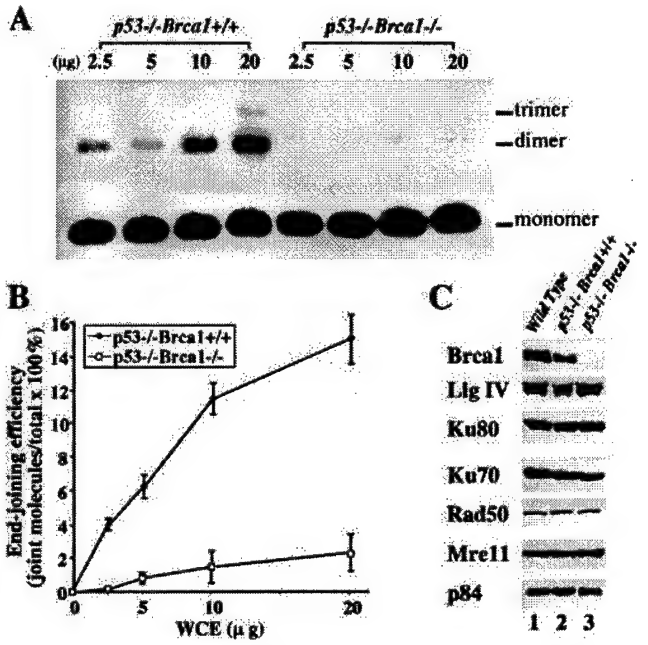

Fig. 2. Deficient end-joining activity in Brca1 mutant MEFs. *A*, end-joining activity of MEF extracts. Increasing amounts of WCE from each of the indicated MEF cell lines were incubated with ^{32}P-end-labeled linear DNA and assayed for end-joining activity. *B*, quantitative analysis by phosphorimaging. End-joining efficiency was calculated as: intensity of end-joining products/total substrate × 100%; *error bars* indicate the experimental deviation. *C*, immunoblot analysis demonstrating equivalent levels of representative NHEJ proteins and an unrelated nuclear matrix protein, p84, in the MEF WCEs assayed for end-joining activity.

RESULTS

To explore the function of BRCA1 in DNA repair, we used an *in vitro* DNA end-joining assay that has been described previously (16). In this system, NHEJ catalyzed by human WCE was observed by rejoining ^{32}P-labeled linear duplex DNA in a reaction that is dependent upon all of the mammalian factors thus far genetically implicated in NHEJ, including DNA ligase IV, Xrcc4, Ku70, Ku80, and DNA-PKcs. We initially tested WCE from a human lymphoblastoid cell line, LEM, for its ability to catalyze NHEJ and observed that 25–35% of the input DNA molecules were rejoined during a 1-h incubation with 20 μg of this cell extract. Under identical reaction conditions, BRCA1-specific antibodies Ab-1 and 17F8, preincubated with LEM WCE before the addition of ^{32}P-end-labeled linear DNA into the reaction, dramatically inhibited end joining (Fig. 1). Antibodies specific for Rad50 also inhibited the end-joining activity present in WCE. Consistent with previous observations, antibodies specific for Ku70 inhibited end-joining activity *in vitro* (16). However, antibodies specific for Rad51 or normal murine IgG did not inhibit end-joining activity. These results indicate that BRCA1 and Rad50, but not Rad51, may be involved in NHEJ in this cell-free system.

To further substantiate the requirement for BRCA1 in NHEJ, we directly compared WCEs derived from *Brca1*$^{-/-}$*p53*$^{-/-}$ MEFs with extracts from both *p53*$^{-/-}$ and wild-type MEFs for their respective NHEJ activities *in vitro*. WCEs from wild-type or *p53*$^{-/-}$ MEFs could rejoin 35–50% of input DNA. Significantly, WCE from *Brca1*$^{-/-}$*p53*$^{-/-}$ MEFs was reduced 3–10-fold consistently, relative to WCE from either *p53*$^{-/-}$ or wild-type MEFs, for end-joining activity (Fig. 2, *A* and *B*). For quantitative standardization, WCEs

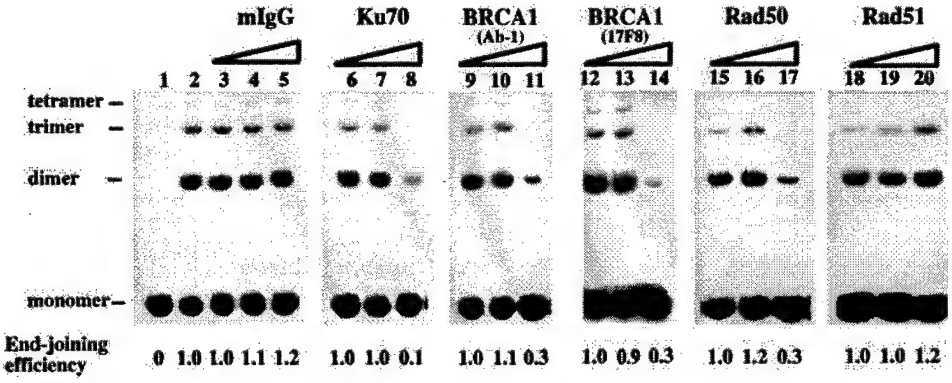

Fig. 1. Antibodies specific for BRCA1, Rad50, and Ku70 inhibit the end-joining activity present in human cell extract. Human lymphoblastoid LEM WCE was preincubated with BRCA1-specific antibodies Ab-1 (*Lanes 9–11*) and 17F8 (*Lanes 12–14*), Ku70-specific antibody (*Lanes 6–8*), Rad50-specific antibody (*Lanes 15–17*), Rad51-specific antibody (*Lanes 18–20*), or control antibody murine IgG (*Lanes 3–5*) before the addition of ^{32}P-end-labeled linear DNA (5 fmol/reaction) and subsequent incubation. Antibodies or antisera were added at 1:6 serial dilutions as follows (the actual amounts were described in the "Materials and Methods" section): straight, *Lanes 5, 8, 11, 14, 17,* and *20*; diluted 1/6, *Lanes 4, 7, 10, 13, 16,* and *19*; diluted 1/36, *Lanes 3, 6, 9, 12, 15,* and *18*. *Lane 1*: no extract. *Lane 2*: LEM extract alone. Note that BRCA1-, Rad50-, and Ku-70-specific, but not control, antibodies inhibited end joining. The end-joining efficiency was calculated as the end-joining activity [intensity of multimers/(multimers + monomer)] in each reaction expressed relative to the end-joining activity in WCEs without antibodies as determined by densitometric analysis.

were first normalized for total protein levels and subsequently analyzed by immunoblot analyses for their respective expression levels of Ku70, Ku80, DNA ligase IV, Rad50, Mre11, or the nuclear matrix protein p84 (19). No significant difference in protein levels could be observed among these WCEs (Fig. 2*C*), excluding the possibility that the reduced end-joining activity in Brca1-null cell extract is because of variations in the expression levels of these NHEJ proteins.

It is known that divalent cations such as Mg2+ and Mn2+ affect NHEJ catalyzed by mammalian WCE *in vitro* (20). Our NHEJ reactions included 0.5 mM Mg2+ and were performed identically to those described initially by Baumann *et al.* (16). To test whether the Brca1-dependent NHEJ activity present in WCEs of MEFs is affected by the concentration of divalent ions, we compared extracts derived from Brca1-deficient and wild-type MEFs for their respective NHEJ activities in the presence of increasing concentrations of Mg2+ or Mn2+. As shown in Fig. 3, augmentation of the Mg2+ or Mn2+ concentration dramatically increased the level of DNA end joining catalyzed by both Brca1-null and wild-type cell extracts and concomitantly abrogated the requirement for Brca1 regardless the amount of WCE used in the reactions. Thus, at reaction concentrations of divalent ions exceeding 1.5 mM Mg2+ or 0.5 mM Mn2+ plus 0.5 mM Mg2+, the difference in NHEJ catalyzed by Brca1-null and wild-type MEF extracts was indistinguishable, possibly indicating the involvement of a Brca1-independent pathway for NHEJ under these conditions.

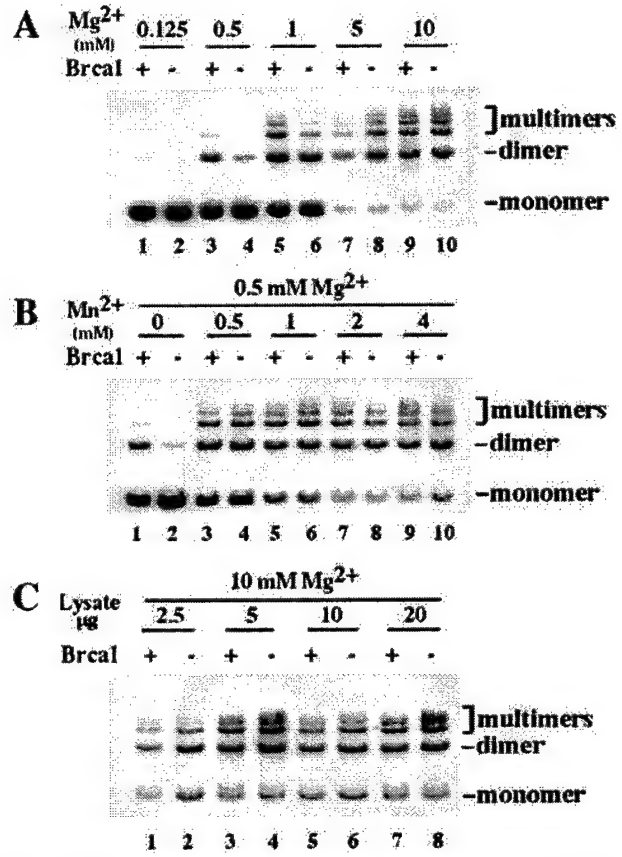

Fig. 3. DNA end-joining activity in cell extracts is sensitive to Mg2+ and Mn2+. *A*, determination of optimal concentration of Mg2+. Cell extracts (10 µg) derived from Brca1-proficient (*odd-numbered lanes*) or Brca1-deficient (*even-numbered lanes*) MEFs were incubated with different concentration of Mg2+ as follows: *Lanes 1–2*, 0.125 mM; *Lanes 3–4*, 0.5 mM; *Lanes 5–6*, 1 mM; *Lanes 7–8*, 5 mM; and *Lanes 9–10*, 10 mM. *B*, determination of the effect of Mn2+. Extract (10 µg) derived from Brca1-proficient (*odd-numbered lanes*) or Brca1-deficient (*even-numbered lanes*) MEFs were incubated at 0.5 mM Mg2+ with different concentration of Mn2+ as follows: *Lanes 1–2*, 0 mM; *Lanes 3–4*, 0.5 mM; *Lanes 5–6*, 1 mM; *Lanes 7–8*, 2 mM; and *Lanes 9–10*, 4 mM. *C*, titration of the amount of cell extracts. In the presence of 10 mM Mg2+, cell extracts (2.5, 5, 10, and 20 µg) derived from Brca1-proficient (*odd-numbered lanes*) or Brca1-deficient (*even-numbered lanes*) MEFs were assayed for DNA end-joining activity.

To explore the relationship between the Brca1-dependent NHEJ activity and known components of the NHEJ pathway, including Xrcc4 and Ku70, at different divalent ion concentrations, we performed reactions with either 0.5 mM or 10 mM Mg2+ (Fig. 4). Addition of Brca1-specific antibody reduced end-joining activity in Brca1 proficient MEFs to the level of Brca1 mutant cells at 0.5 mM Mg2+. Similarly, the addition of antibodies against Ku70 and Xrcc4 completely eliminated end-joining activity of Brca1 deficient or proficient cells. These observations suggest that BRCA1 may function along with Xrcc4 and Ku70 in NHEJ. However, at 10 mM Mg2+, the additions of antibodies against Ku70, Xrcc4, and BRCA1 have no apparent inhibitory function against the robust end-joining activities in both Brca1-proficient and -deficient MEFs (Fig. 4), indicating an existence of an alternative pathway.

To determine whether a cellular fraction containing BRCA1 can complement the diminished NHEJ activity in Brca1-deficient cells, we fractionated human HeLa cell nuclear extract according to the scheme outlined in Fig. 5*A*. The bulk of BRCA1 protein present in a soluble HeLa nuclear extract bound to phosphocellulose PC-11 and eluted predominantly and approximately equally between 0.1–0.3 and 0.3–0.5 M KCl step fractions (fractions B and C, respectively, Fig. 5*A*). The bulk of cellular Rad50 protein was also recovered in the PC-11 B and C fractions, although more eluted in the B fraction than in the C fraction (Fig. 5*A*). Most of the BRCA1 protein present in the PC-11 C fraction bound to, and eluted from, a DEAE-Sepharose anion exchange resin in a 0.1–0.25 M KCl step fraction (fraction CB). After Superose 6 gel filtration chromatography of the CB fraction, BRCA1 was eluted in fractions corresponding to peaks of the Rad50, Mre11, and Nbs1 proteins, indicating cofractionation of BRCA1 with the Rad50/Mre11/Nbs1 protein complex (Fig. 5*A*). Western blot analysis of individual Superose 6 column fractions with antibodies specific for BRCA1 and the large subunit of RPB1 also revealed that the bulk of BRCA1 eluted ahead of RPB1 in a number of high molecular weight fractions (Fig. 5*A*). Reciprocal coimmunoprecipitation of BRCA1 and Rad50 from peak Superose 6 column fractions demonstrated that BRCA1, Rad50, and Nbs1 all reside in a single high molecular weight complex of M_r ~1,000,000 (Fig. 5*B*).

Individual Superose 6 column fractions corresponding to the peak of the BRCA1/Rad50/Mre11/Nbs1 complex were pooled and concentrated on phosphocellulose PC-11 to yield a partially purified protein fraction termed C1. Fraction C1 was tested for its ability to complement WCE of Brca1-deficient MEF for end-joining activity *in vitro*. Although it catalyzed no end-joining activity on its own, the addition of fraction C1 to WCE of Brca1-deficient MEFs increased its end-joining activity about 2.5-fold (Fig. 5, *C* and *D*) to 60% of the end-joining activity catalyzed by WCE derived from Brca1-proficient MEFs. The addition of fraction C1 to WCE of Brca1-proficient MEFs has no effect on end-joining activity (data not shown). These results suggest that the partially purified BRCA1 complex facilitated the BRCA1-dependent NHEJ process.

DISCUSSION

BRCA1 plays an important role in maintaining genomic stability through its participation in DNA repair and cell cycle checkpoint control. For DNA DSB repair, BRCA1 has been shown to be critical for homologous recombination (10). However, it is not known whether BRCA1 has a role in NHEJ. In this study, we showed that under identical cell-free reaction conditions described by Baumann *et al.* (16), the addition of antibodies specific for BRCA1 and Rad50, but not Rad51, inhibits end-joining activity. Cell extracts derived from Brca1-deficient MEFs exhibit reduced end-joining activity independent of the endogenous protein amounts of DNA ligase IV, Ku80, and Ku70. The BRCA1-dependent NHEJ activity predominates at the lower concentra-

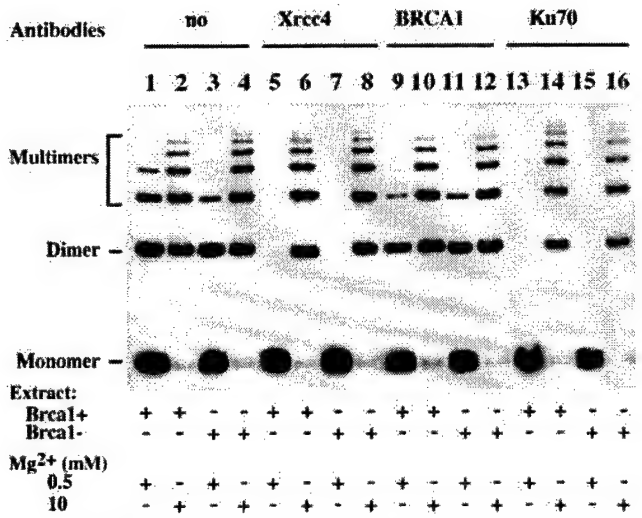

Fig. 4. Antibodies specific against BRCA1, Ku, and Xrcc4 inhibit NHEJ at 0.5 mM, but not at 10 mM, Mg2+. At 0.5 mM Mg2+ (*odd lanes*), antibodies against BRCA1 (*Lanes 9–12*) reduced the end-joining activity in Brca1-proficient MEF extracts (*Lanes 1* and *9*) to the level of Brca1-deficient cells (*Lanes 3* and *11*). Antibodies against Xrcc4 (*Lane 5–8*) or Ku70 (*Lanes 13–16*) completely inhibited the end-joining activity in Brca1-proficient cells (*Lanes 5* and *13*) and the residual activity in Brca1-deficient cells (*lanes 7* and 15). However, at 10 mM Mg2+ (*even lanes*), robust end-joining activity in both Brca1-proficient and Brca1-deficient MEFs is resistant to antibodies against Ku70 (*Lanes 6* and *8*), Xrcc4 (*Lanes 14* and *16*), and BRCA1 (*Lanes 10* and *12*), indicating an existence of an alternative pathway.

tions of 0.5 mM Mg2+; elevated reaction concentrations of Mg2+ or Mn2+ to 10 mM dramatically increases overall end-joining activity and abrogates the requirement for Brca1, Xrcc4, and Ku70. The addition of partially purified BRCA1 in association with Rad50/Mre11/Nbs1 complements the NHEJ deficiency of Brca1-deficient MEF extracts. These results support a role for BRCA1 in NHEJ.

BRCA1 is likely to participate in NHEJ by virtue of its interaction with the Rad50/Mre11/Nbs1 complex. Previous work has demonstrated that BRCA1 interacts physically with the Rad50/Mre11/Nbs1 complex *in vivo* and *in vitro* (8). Furthermore, BRCA1 can be isolated from cells in a high molecular complex with Rad50/Mre11/Nbs1. These observations suggest that the function of BRCA1 in DSB repair may be mediated, at least in part, through its association with the Rad50/Mre11/Nbs1 complex. It is recently shown that the yeast counterpart Rad50/Mre11/Xrs2 has DNA end-binding and bridging activities. Addition of the Ku homologous protein HdfA and B enhances the DNA end-bridging activity of the Rad50/Mre11/Xrs2 complex. The Rad50/Mre11/Xrs2 complex then directly recruits Dnl4/Lif1 (equivalent to mammalian DNA ligase IV and Xrcc4) to complete DNA end ligation (15). Similarly, mammalian Rad50/Mre11NBS1 has also been shown to exhibit DNA end-tethering activity (21, 22). Therefore, NHEJ *in vitro* can be carried out by components, including Rad50/Mre11/Nbs1, Ku homologues, and DNA ligase IV/Xrcc4. Although the precise role of BRCA1 in NHEJ remains unclear, the ability of BRCA1 to form a tight complex with Rad50/Mre11/Nbs1 suggests that BRCA1 may facilitate the NHEJ function of this complex. Recently, a purified recombinant BRCA1 was shown to have a direct DNA-binding activity (23). Whether this DNA-binding activity has a direct contribution to the NHEJ warrants additional investigation.

The cell-free system for NHEJ that we used in this study has been reported to be dependent on a DNA-PK-mediated pathway (16). Nonetheless, substantial evidence accumulated from *in vitro* studies indicates that eukaryotic cells rely on more than one DNA end-joining pathway (24–27). For example, extracts derived from the DNA-PK mutant cell line MO59J have been reported to exhibit wild-type end-joining activity, suggesting the involvement of a DNA-PK-independent end-joining pathway in these cells (27). The relative contribution of a particular pathway to the overall end-joining activity observed in mammalian WCEs likely

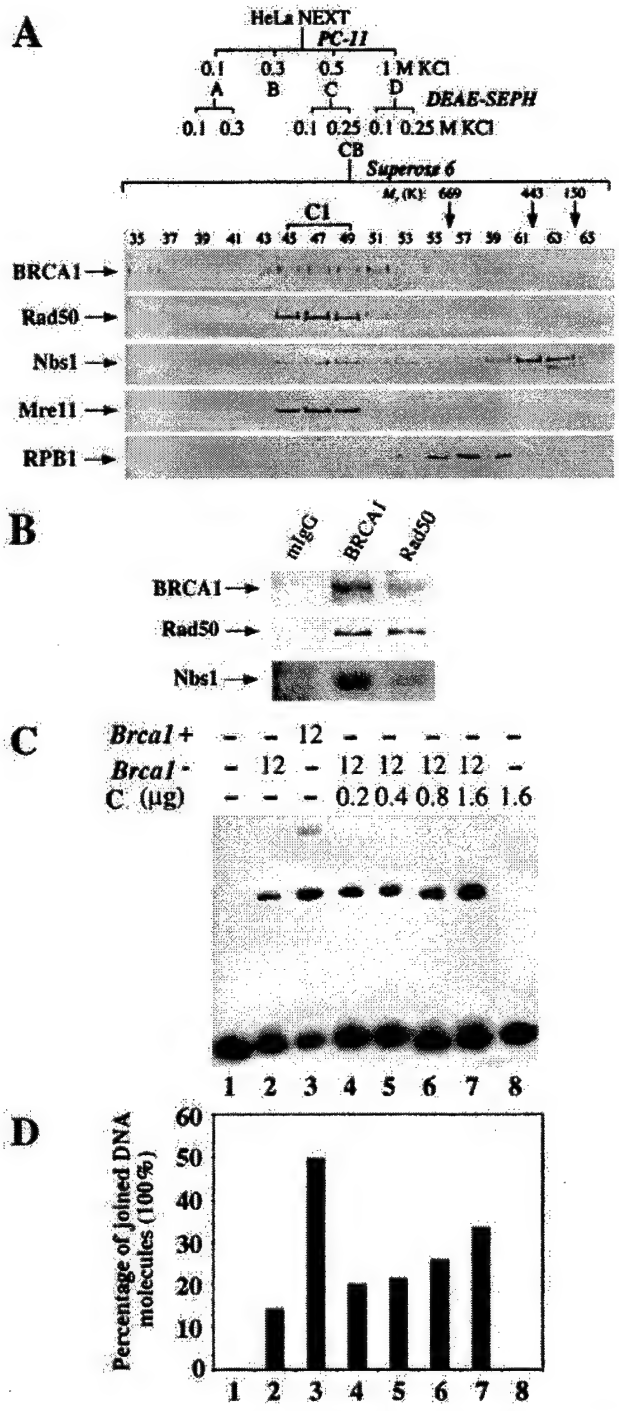

Fig. 5. Complementation of NHEJ activity in BRCA1-deficient cell extracts by exogenous BRCA1. *A*, schematic diagram of purification of a BRCA1/Rad50/Mre11/NBS1-containing complex. HeLa cell nuclear extract (NEXT) was subjected to successive phosphocellulose PC-11, DEAE-Sepharose, and Superose 6 gel filtration chromatography. CB protein fraction (4 mg/ml) was subjected to Superose 6 gel filtration analysis. Individual fractions were resolved by 10% SDS-PAGE and subjected to immunoblot analysis using antibodies specific for the proteins indicated to the *left* of the blot (RPB1: large subunit of RNA polymerase II). *Vertical arrows* above the immunoblot panels indicate marker protein peaks. *B*, coimmunoprecipitation of BRCA1, Rad50, and NBS1 from peak Superose 6 column fractions. Column fractions 45–49 (fraction C1) from the experiment in *A* were pooled, and a portion subjected to immunoprecipitation with the antibodies indicated above the immunoblot (mIgG = murine IgG). Immunoprecipitates were resolved by 10% SDS-PAGE and subjected to immunoblot analysis with antibodies specific for the proteins indicated to the left of the blot. *C*, complementation of Brca1-deficient MEF extracts for end-joining activity by a BRCA1/Rad50/Mre11/Nbs1 complex. Fraction C1 was added as indicated to Brca1-deficient WCE and incubated on ice for 30 min before assay of end-joining activity. Fraction C1 alone (*Lane 8*) does not catalyze end-joining activity. *D*, end-joining activity in *C* was measured as [intensity of multimers/(multimers + monomer) × 100%] by phosphoimage analysis and converted to percentage of joined DNA molecules.

reflects the *in vitro* reaction conditions used. One factor that could alter the relative influence of a particular end-joining pathway in the reaction is the concentration of divalent cations, particularly Mg2+ and Mn2+. In this regard, we observed that the BRCA1-dependent NHEJ activity present in mammalian WCE is sensitive to the reaction concentration of Mg2+ and Mn2+. Elevated concentrations of these divalent cations stimulates overall end-joining activity and masks the requirement for BRCA1, suggesting the involvement of a BRCA1-independent pathway to achieve end joining. A similar phenomenon has recently been reported for DNA ligase IV using ligase IV mutant 180BR cell (20). Elevated reaction concentrations of Mg2+ (10 mM) stimulated DNA end joining through an apparent DNA ligase IV-independent pathway, whereas reduced concentrations of Mg2+ (0.5 mM) revealed a DNA ligase IV dependency for low levels of end-joining activity. Interestingly, we observed that under similar conditions, antibodies specific for Ku70, Xrcc4, and BRCA1 efficiently suppressed DNA end-joining activity at reduced concentrations of Mg2+ (Fig. 4). These observations raise the possibility that BRCA1 works along with Rad50, Ku, and Xrcc4 in NHEJ at a low concentration of Mg 2+. Interestingly, mammalian cell extracts deficient in Fanconi anemia proteins had a 3–9-fold reduction in DNA end-joining activity at high Mg2+ concentration (10 mM) in a pathway independent of DNA-PK/Ku (28). Therefore, it is very likely that multiple NHEJ pathways may exist in mammalian cells.

Previously, BRCA1 has been implicated in homology-based repairs of DNA breaks because cells expressing a Brca1 exon 11-deletion mutant exhibit defects in gene targeting, single-strand annealing, and gene conversion (10). Interestingly, no defects in plasmid integration and nonhomologous repair processes were observed in these Brca1 mutant cells. However, it is possible that the NHEJ activity observed in this previous study described by Moynahan *et al.* (10), reflects the contribution of a BRCA1-independent NHEJ pathway. Alternatively, genetic differences between independently derived Brca1 mutant cell lines may contribute to different conclusions regarding the importance of Brca1 in NHEJ. Our Brca1 mutant allele carries a reverse-oriented neomycin cassette inserted into the 5′ end of Brca1 exon 11, which will lead to premature termination of translation (29). No stable Brca1 protein derivative can be detected in our Brca1$^{-/-}$ MEFs. The embryonic stem (ES) cells previously characterized for defects in homologous and NHEJ repair (10), express a Brca1 exon 11 splice variant (30) and the homozygote embryos derived from these ES cells exhibit a less severe phenotype than our homozygotes (29, 30). Using our Brca1$^{-/-}$ MEFs, we have demonstrated a 50–100-fold reduced efficiency in microhomology-mediated end-joining activity of a defined chromosomal DNA DSB introduced by a rare-cutting endonuclease I-SceI (31). These results further support a role of BRCA1 in NHEJ.

The findings presented here suggest that BRCA1 functions in the repair of DSBs through a novel role in NHEJ, consistent with the recent report that a single mutated BRCA1 allele leads to impaired fidelity of DSB end joining (32). Inefficient or error-prone DNA repair resulting directly from inactivation of BRCA1 could lead to global genomic instability and a concomitant accrual of functionally inactivating mutations at genetic loci involved in breast tumorigenesis. Additional mechanistic studies concerning the role of BRCA1 in DNA damage response and repair should expedite the design and implementation of strategies to delay, and ultimately to prevent, breast cancer formation.

ACKNOWLEDGMENTS

We thank Diane Jones and Chi-Fen Chen for excellent technical assistance.

REFERENCES

1. Chen, Y., Lee, W. H., and Chew, H. K. Emerging roles of BRCA1 in transcriptional regulation and DNA repair. J. Cell. Physiol., *181:* 385–392, 1999.
2. Welcsh, P. L., Owens, K. N., and King, M. C. Insights into the functions of BRCA1 and BRCA2. Trends Genet., *16:* 69–74, 2000.
3. Zheng, L., Li, S., Boyer, T. G., and Lee, W-H. Lessons learned from BRCA1 and BRCA2. Oncogene, *19:* 6159–6175, 2000.
4. Xu, X., Weaver, Z., Linke, S. P., Li, C., Gotay, J., Wang, X. W., Harris, C. C., Ried, T., and Deng, C. X. Centrosome amplification and a defective G_2-M cell cycle checkpoint induce genetic instability in BRCA1 exon 11 isoform-deficient cells. Mol. Cell, *3:* 389–395, 1999.
5. Tomlinson, G. E., Chen, T-L., Stastny, V. A., Virmani, A. K., Spillman, M. A., Tonk, V., Blum, J. L., Schneider, N. R., Wistuba, I. I., Shay, J. W., Minna, J. D., and Gazdar, A. F. Characterization of a breast cancer cell line derived from a germ-line *BRCA1* mutation carrier. Cancer Res., *58:* 3237–3242, 1998.
6. Gowen, L. C., Avrutskaya, A. V., Latour, A. M., Koller, B. H., and Leadon, S. A. BRCA1 required for transcription-coupled repair of oxidative DNA damage. Science (Wash. DC), *281:* 1009–1012, 1998.
7. Cressman, V. L., Backlund, D. C., Avrutskaya, A. V., Leadon, S. A., Godfrey, V., and Koller, B. H. Growth retardation, DNA repair defects, and lack of spermatogenesis in BRCA1-deficient mice. Mol. Cell. Biol., *19:* 7061–7075, 1999.
8. Zhong, Q., Chen, C. F., Li, S., Chen, Y., Wang, C. C., Xiao, J., Chen, P. L., Sharp, Z. D., and Lee, W. H. Association of BRCA1 with the hRad50-hMre11-p95 complex and the DNA damage response. Science (Wash. DC), *285:* 747–750, 1999.
9. Scully, R., Ganesan, S., Vlasakova, K., Chen, J., Socolovsky, M., and Livingston, D. M. Genetic analysis of BRCA1 function in a defined tumor cell line. Mol. Cell, *4:* 1093–1099, 1999.
10. Moynahan, M. E., Chiu, J. W., Koller, B. H., and Jasin, M. Brca1 controls homology-directed DNA repair. Mol. Cell, *4:* 511–518, 1999.
11. Haber, J. E. The many interfaces of Mre11. Cell, *95:* 583–586, 1998.
12. Tsukamoto, Y., and Ikeda, H. Double-strand break repair mediated by DNA end-joining. Genes Cells, *3:* 135–144, 1998.
13. Paull, T. T., and Gellert, M. The 3′ to 5′ exonuclease activity of Mre 11 facilitates repair of DNA double-strand breaks. Mol. Cell, *1:* 969–979, 1998.
14. Paull, T. T., and Gellert, M. A mechanistic basis for Mre11-directed DNA joining at microhomologies. Proc. Natl. Acad. Sci. USA, *97:* 6409–6414, 2000.
15. Chen, L., Trujillo, K., Ramos, W., Sung, P., and Tomkinson, A. E. Promotion of Dnl4-catalyzed DNA end-joining by the Rad50/Mre11/Xrs2 and Hdf1/Hdf2 complexes. Mol. Cell, *8:* 1105–1115, 2001.
16. Baumann, P., and West, S. C. DNA end-joining catalyzed by human cell-free extracts. Proc. Natl. Acad. Sci. USA, *95:* 14066–14070, 1998.
17. Zheng, L., Pan, H., Li, S., Flesken-Nikitin, A., Chen, P. L., Boyer, T. G., and Lee, W. H. Sequence-specific transcriptional corepressor function for BRCA1 through a novel zinc finger protein. ZBRK1. Mol. Cell, *6:* 757–768, 2000.
18. Boyer, T. G., Martin, M. E., Lees, E., Ricciardi, R. P., and Berk, A. J. Mammalian Srb/Mediator complex is targeted by adenovirus E1A protein. Nature (Lond.), *399:* 276–279, 1999.
19. Durfee, T., Mancini, M. A., Jones, D., Elledge, S. J., and Lee, W-H. The amino-terminal region of the retinoblastoma gene product binds a novel nuclear matrix protein that co-localizes to centers for RNA processing. J. Cell Biol., *127:* 609–622, 1994.
20. Wang, H., Zeng, Z. C., Perrault, A. R., Cheng, X., Qin, W., and Iliakis, G. Genetic evidence for the involvement of DNA ligase IV in the DNA-PK-dependent pathway of non-homologous end joining in mammalian cells. Nucleic Acids Res., *29:* 1653–1660, 2001.
21. Huang, J., and Dynan, W. S. Reconstitution of the mammalian DNA double-strand break end-joining reaction reveals a requirement for an Mre11/Rad50/NBS1-containing fraction. Nucleic Acids Res., *30:* 667–674, 2002.
22. de Jager, M., van Noort, J., van Gent, D. C., Dekker, C., Kanaar, R., and Wyman, C. Human Rad50/Mre11 is a flexible complex that can tether DNA ends. Mol. Cell, *8:* 1129–1135, 2001.
23. Paull, T. T., Cortez, D., Bowers, B., Elledge, S. J., and Gellert, M. From the cover: direct DNA binding by Brca1. Proc. Natl. Acad. Sci. USA, *98:* 6086–6091, 2001.
24. North, P., Ganesh, A., and Thacker, J. The rejoining of double-strand breaks in DNA by human cell extracts. Nucleic Acids Res., *18:* 6205–6210, 1990.
25. Johnson, A. P., and Fairman, M. P. The identification and characterization of mammalian proteins involved in the rejoining of DNA double-strand breaks *in vitro*. Mutat. Res., *364:* 103–116, 1996.
26. Feldmann, E., Schmiemann, V., Goedecke, W., Reichenberger, S., and Pfeiffer, P. DNA double-strand break repair in cell-free extracts from Ku80-deficient cells: implications for Ku serving as an alignment factor in non-homologous DNA end joining. Nucleic Acids Res., *28:* 2585–2596, 2000.
27. Cheong, N., Perrault, A. R., Wang, H., Wachsberger, P., Mammen, P., Jackson, I., and Iliakis, G. DNA-PK-independent rejoining of DNA double-strand breaks in human cell extracts *in vitro*. Int. J. Radiat. Biol., *75:* 67–81, 1999.
28. Lundberg, R., Mavinakere, M., and Campbell, C. Deficient DNA end joining activity in extracts from fanconi anemia fibroblasts. J. Biol. Chem., *276:* 9543–9549, 2001.
29. Liu, C. Y., Flesken-Nikitin, A., Li, S., Zeng, Y. Y., and Lee, W-H. Inactivation of the mouse *Brca1* gene leads to failure in the morphogenesis of the egg cylinder in early postimplantation development. Genes Dev., *10:* 1835–1843, 1996.
30. Gowen, L. C., Johnson, B. L., Latour, A. M., Sulik, K. K., and Koller, B. H. Brca1 deficiency results in early embryonic lethality characterized by neuroepithelial abnormalities. Nat. Genet., *12:* 191–194, 1996.
31. Zhong, Q., Chen, C-F., Chen, P-L., and Lee, W-H. BRCA1 facilitates microhomology mediated end-joining of DNA double-strand breaks. J. Biol Chem., in press, 2002.
32. Baldeyron, C., Jacquemin, E., Smith, J., Jacquemont, C., De Oliveira, I., Gad, S., Feunteun, J., Stoppa-Lyonnet, D., and Papadopoulo, D. A single mutated BRCA1 allele leads to impaired fidelity of double strand break end-joining. Oncogene, *21:* 1401–1410, 2002.

THE JOURNAL OF BIOLOGICAL CHEMISTRY
Vol. 277, No. 32, Issue of August 9, pp. 28641–28647, 2002
Printed in U.S.A.

BRCA1 Facilitates Microhomology-mediated End Joining of DNA Double Strand Breaks*

Received for publication, January 23, 2002, and in revised form, May 21, 2002
Published, JBC Papers in Press, May 30, 2002, DOI 10.1074/jbc.M200748200

Qing Zhong‡, Chi-Fen Chen, Phang-Lang Chen, and Wen-Hwa Lee§

From the Department of Molecular Medicine, Institute of Biotechnology, University of Texas Health Science Center at San Antonio, San Antonio, Texas 78245

BRCA1 is critical for the maintenance of genomic stability, in part through its interaction with the Rad50·Mre11·Nbs1 complex, which occupies a central role in DNA double strand break repair mediated by nonhomologous end joining (NHEJ) and homologous recombination. BRCA1 has been shown to be required for homology-directed recombination repair. However, the role of BRCA1 in NHEJ, a critical pathway for the repair of double strand breaks and genome stability in mammalian cells, remains elusive. Here, we established a pair of mouse embryonic fibroblasts (MEFs) derived from 9.5-day-old embryos with genotypes *Brca1*$^{+/+}$:*p53*$^{-/-}$ or *Brca1*$^{-/-}$:*p53*$^{-/-}$. The *Brca1*$^{-/-}$:*p53*$^{-/-}$ MEFs appear to be extremely sensitive to ionizing radiation. The contribution of BRCA1 in NHEJ was evaluated in these cells using three different assay systems. First, transfection of a linearized plasmid in which expression of the reporter gene required precise end joining indicated that *Brca1*$^{-/-}$ MEFs display a moderate deficiency when compared with *Brca1*$^{+/+}$ cells. Second, using a retrovirus infection assay dependent on NHEJ, a 5–10-fold reduction in retroviral integration efficiency was observed in *Brca1*$^{-/-}$ MEFs when compared with the *Brca1*$^{+/+}$ MEFs. Third, *Brca1*$^{-/-}$ MEFs exhibited a 50–100-fold deficiency in microhomology-mediated end-joining activity of a defined chromosomal DNA double strand break introduced by a rare cutting endonuclease I-*Sce*I. These results provide evidence that Brca1 has an essential role in microhomology-mediated end joining and suggest a novel molecular basis for its caretaker role in the maintenance of genome integrity.

Inactivation of the breast cancer susceptibility gene, *BRCA1*, accounts for a significant portion of familial breast cancer (1, 2). Chromosome aneuploidy has been reported in human breast cancer cells, HCC1937, which contain a C-terminal truncated BRCA1 (3). Similarly, murine fibroblasts containing a deletion within exon 11 of BRCA1 display extensive chromosomal abnormality (4). Both Brca1-deficient murine and human cells have been shown to be sensitive to DNA-damaging agents, including ionizing radiation (5–7), suggesting that BRCA1 may play an essential role in DNA double strand break (DSB)[1] repair. DSBs can be repaired through homologous recombination (HR) or nonhomologous end joining (NHEJ) to ensure the maintenance of genome integrity in eukaryotic organisms (8). More significantly, deficiencies in the mammalian NHEJ pathway can lead to an increase in the frequency of chromosomal translocations and the rate of neoplastic transformation (9–13), thus emphasizing the importance of this DSB repair pathway in the maintenance of genome integrity.

BRCA1 binds to the Rad50·Mre11·Nbs1 complex and can form radiation-induced foci with this complex (14). The yeast counterpart of this complex, Rad50·Mre11·Xrs2, is required for both NHEJ and HR (15). BRCA1 has been implicated in homology-based recombination repair (16). In the study described by Moynahan *et al.* (16), a reporter substrate containing two differentially mutated neomycin phosphotransferase gene (*neo*) placed in tandem, with one harboring an I-*Sce*I cleavage site, was integrated into the genome of both wild-type or Brca1 exon 11 deleted embryonic stem (ES) cells. Upon expression of the I-*Sce*I endonuclease, ES cells containing the Brca1 exon 11 deleted mutant, but not wild-type Brca1, showed a deficiency in intra- and interchromosomal recombination (16). Interestingly, these Brca1 mutant cells showed a slight increase in nonhomologous repair processes characterized by nucleotide deletion or addition (16). However, neither precise end joining, which may account for nearly 60% of the end-joining events in the I-*Sce*I-inducible DNA DSB repair (17), nor a microhomology-mediated end-joining activity that may recover a functional *neo* gene independent of gene conversion was taken into consideration in this assay system (16). Moreover, it is likely that repair by HR contributes much more than NHEJ in ES cells because of their relatively short cell cycle duration (18). Thus, the potential role of BRCA1 in NHEJ may not be revealed by this reported assay system (16). In BRCA1-deficient HCC1937 cells, a much slower rate and less extensive amount of DSB repair, as measured by pulse field gel electrophoresis (PFGE) at 6 h after ionizing irradiation, has been observed as compared with the same cells expressing wild-type BRCA1 protein (19). The altered kinetics of the PFGE assay primarily reflects the inefficiency of chromosomal break rejoining, which is commonly observed in mutant cells deficient in NHEJ mutant but not in HR (20). This finding, albeit circumstantial, suggests that BRCA1 may participate in NHEJ.

To address the potential role of BRCA1 in NHEJ, we utilized three independent *in vivo* approaches demonstrating that BRCA1 promotes NHEJ mediated by microhomology. Trans-

* This work was supported by grants from the National Institutes of Health (CA 85605 to P.-L. C. and CA 81020, CA58183, and CA30195 to W.-H. L.). The costs of publication of this article were defrayed in part by the payment of page charges. This article must therefore be hereby marked "*advertisement*" in accordance with 18 U.S.C. Section 1734 solely to indicate this fact.

‡ Supported by a postdoctoral training grant from the United States Army Medical Research and Materiel Command under DAMD17-00-1-0457.

§ To whom correspondence should be addressed: Dept. of Molecular Medicine, Institute of Biotechnology, University of Texas Health Science Center at San Antonio, 15355 Lambda Dr., San Antonio, TX 78245. Tel.: 210-567-7351; Fax: 210-567-7377; E-mail: leew@ uthscsa.edu.

[1] The abbreviations used are: DSB, double strand break; HR, homologous recombination; NHEJ, nonhomologous end joining; m.o.i., multiplicity(s) of infection; ES cells, embryonic stem cells; MEF, mouse embryonic fibroblast; GFP, green fluorescent protein.

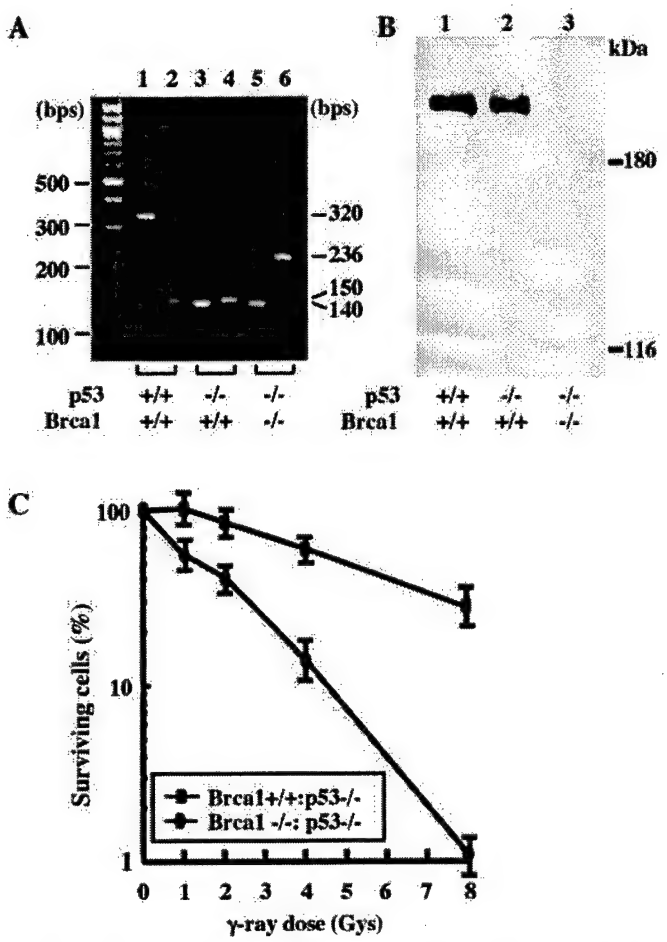

FIG. 1. *A*, genotyping of MEFs. The methods for genotyping wild-type and mutant *p53* or *Brca1* are described under "Materials and Methods." The resulting sizes of the different PCR products serving as diagnostic markers for the different alleles are as follows: 320 bp for wild-type *p53*, 140 bp for mutated *p53*, 150 bp for wild-type *Brca1*, and 236 bp for the mutated *Brca1* allele. *Lanes 1*, *3*, and *5* were PCR products derived from the *p53* locus. *Lanes 2*, *4*, and *6* were derived from the *Brca1* locus. Genomic DNA used in *lanes 1* and *2* was extracted from $Brca1^{+/+}$:$p53^{+/+}$, in *lanes 3* and *4* from $Brca1^{+/+}$:$p53^{-/-}$, and in *lanes 5* and *6* from $Brca1^{-/-}$:$p53^{-/-}$. *B*, expression of Brca1 in wild-type, $Brca1^{+/+}$:$p53^{-/-}$, and $Brca1^{-/-}$:$p53^{-/-}$ MEFs. Cell lysates were prepared from these MEFs for protein analysis by immunoprecipitation followed by Western blotting using anti-mouse Brca1 antibody. In $Brca1^{-/-}$:$p53^{-/-}$ MEFs, the full-length Brca1 protein was not detected. *C*, $Brca1^{-/-}$:$p53^{-/-}$ MEFs are hypersensitive to γ-irradiation. $Brca1^{+/+}$:$p53^{-/-}$and $Brca1^{-/-}$:$p53^{-/-}$ MEFs were either exposed to different doses of γ-irradiation as indicated or mock-exposed. Surviving colonies were counted 10 days later. The results shown represent the mean ± standard deviation of three independent experiments.

fection of a linearized plasmid in which expression of the reporter gene required precise end joining indicated that $Brca1^{-/-}$ MEFs display a moderate deficiency when compared with $Brca1^{+/+}$ MEFs. Further, Brca1 promotes efficient retroviral infection, which depends on an intact NHEJ pathway. Most importantly, Brca1-deficient MEFs exhibit severely impaired end-joining activity mediated by microhomology in response to I-*Sce*I restriction endonuclease induced chromosomal double-stranded DNA break. These results support a role for Brca1 in NHEJ and provide a biochemical basis for the caretaker function of BRCA1 in the maintenance of genome integrity.

MATERIALS AND METHODS

Mouse Embryonic Fibroblast

To prepare $Brca1^{-/-}$:$p53^{-/-}$ and $p53^{-/-}$ mouse embryonic fibroblasts (MEFs), $Brca1^{+/-}$ mice derived from a Brca1-ko(o)3 targeted ES clone (21) were crossed with $p53^{-/-}$ mice (Jackson Laboratory). Brca1-ko(o)3 contained a neo cassette in the opposite orientation within Brca1 exon 11. The resultant F_1 $Brca1^{+/-}$:$p53^{-/-}$ mice were then crossed with each other, and embryos about 9.5 days old were used to prepare MEFs as described (22).

PCR Genotyping

Primers for genotyping *Brca1* were as described (21). In short, a 236-bp PCR product was the diagnostic indicator of the targeted *Brca1* allele, and a 150-bp product was diagnostic of the wild-type allele. For the targeted *p53* allele, a 140-bp PCR product was generated using a sense oligonucleotide, 5′-AGTTCGAGGCCATCTCTGACTACAC-3′ and an antisense oligonucleotide, 5′-CTGTGCTCTAGTAGCTTTACGGAGC-3′, within the *PolII* promoter. A 320-bp PCR product was diagnostic of the wild-type allele using the same sense oligonucleotide and an antisense oligonucleotide, 5′-GAGGGGAGGAGAGTACTGGAAGAGA-3′, within exon 5 of the *p53* gene (23).

Irradiation and Clonogenic Survival Assay

$Brca1^{-/-}$:$p53^{-/-}$ and $p53^{-/-}$ MEFs were seeded in identical plates at 4000 cells/6-cm dish in regular medium for 24 h. Cells were then irradiated with 0, 1, 2, 4, and 8 grays using a Mark I, model 68A, irradiator. After 14 days, the colonies were fixed and stained with 2% methylene blue in 50% ethanol and then counted.

Adenovirus I-SceI Construct

pPGK3XNLS-I-*Sce*I was kindly provided by P. Berg and G. Donoho (Stanford University). The entire I-*Sce*I DNA fragment was digested with *Sal*I and *Pst*I and cloned into the pBluescript vector, referred to as pBSK-I-*Sce*I. This plasmid was then digested with *Not*I and *Xho*I to release I-*Sce*I and inserted into the AdTrack.CMV plasmid (a gift from B. Vogelstein) (24) to form the AdTrack-CMV-I-*Sce*I plasmid. The adenovirus was then produced following the protocol as described (24).

Mouse Brca1 Antibodies, Immunoprecipitation, and Western Blotting

Mouse Brca1 cDNA-encoded amino acids 788–1135 was translationally fused to glutathione *S*-transferase in-frame, and the bacterially generated fusion protein derived from this construct was used as an antigen for producing mouse polyclonal antisera. Immunoprecipitation and Western blotting were performed as described previously (14).

Transfection and Luciferase Activity Assay

pGL2 plasmid (Promega) was completely linearized by restriction endonuclease *Hin*dIII or *Eco*RI and confirmed by agarose gel electrophoresis. The linearized DNA was subjected to phenol/chloroform extraction, ethanol-precipitated, and dissolved in sterilized water. DNA was then transfected into cells with Fugene 6 following the procedures described by the supplier (Roche Molecular Biochemicals). The transfected cells were harvested and assayed for luciferase activity as described (22).

Retroviral Infection Assay

MEFs were plated at 5×10^5/10-cm dish and infected with a 477H recombinant retrovirus carrying a hygromycin resistance gene for 24 h (25). The infected cells were then selected by hygromycin (200 μg/ml) for 10–14 days. The resulting hygromycin-resistant colonies were counted on three plates for each infection titer, and the experiments were repeated three times.

Chromosomal DNA End-joining Assay

Substrate Construction—pBSK-S1hygro was constructed by inserting an endonuclease I-*Sce*I recognition sequence into the unique *Nco*I site of pBSK-PGKhygro as described below. The *Nco*I site was filled in using Klenow fragment and ligated with an 18-bp I-*Sce*I recognition sequence of 5′-CATGATTACCCTGTTTATCCCTA-3′. A DNA cassette containing puromycin resistance gene driven by the SV40 T antigen promoter was then inserted into pBSK-S1hygro. The entire *S1hygro* with puromycin gene was propagated as a plasmid, and the plasmid DNA was then transfected into MEFs followed by a selection with 2 μg/ml puromycin. Cell clones that contained one to two copies of *S1hygro* identified by genomic DNA blotting analysis were selected for further experiments.

S1hygro Retrovirus—The entire *S1hygro* with puromycin gene was released and inserted into an engineered murine leukemia virus (MuLV)-based retroviral vector. The *S1hygro* virus, produced by transfecting the constructed viral vector DNA into Phoenix Ampho packag-

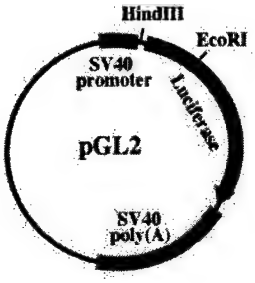

Cell lines	Relative end-joining efficiency	
	HindIII/uncut	EcoRI/uncut
p53-/-Brca1+/+	29.0 ± 2.4%	11.9 ± 0.6%
p53-/-Brca1-/-	31.6 ± 0.1%	7.1 ± 0.2%

FIG. 2. **Plasmid end-joining assay.** The pGL2-control plasmid as illustrated contains two unique restriction sites, *Hin*dIII and *Eco*RI. The relative end-joining efficiency was calculated by comparing luciferase activity expressed in MEFs transfected with *Hin*dIII- or *Eco*RI-digested DNA with that of the uncut plasmid. The results shown were from three independent transfection experiments.

ing cells as described (26), was used to infect MEFs. MEF clones grown out from the selection of puromycin (2 μg/ml) and containing a single copy of proviral DNA of *S1hygro* substrate were used for the end-joining experiments.

Microhomology-mediated End-joining Assay—MEF clones containing a single copy of *S1hygro* substrate were transfected with pPGK3Xnls-I-*Sce*I or infected with I-*Sce*I adenovirus to express I-*Sce*I endonuclease that cleaves the I-*Sce*I site at the proviral hygromycin DNA. The cells were subsequently selected in medium with hygromycin (200 μg/ml) for 14 days, and the hygromycin-resistant colonies were counted. To examine whether these resistant colonies arose from the microhomology-mediated end-joining repair, genomic DNA was extracted for PCR analysis using the primers hygro-4 (5′-CCTGCGGGTAAATAGCTGCGCCGATG-3′) and hygro-5 (5′-CATACAAGC CAACCACGGCCTCCAG-3′) within the hygromycin resistance gene to generate a 595-bp DNA fragment that included the original inactivated *Nco*I and I-*Sce*I sites. Recovery of the *Nco*I site by microhomology-mediated end joining was indicated by the cleavage of the 595-bp fragment into a 379- and a 216-bp fragment following *Nco*I restriction enzyme digestion.

RESULTS

Brca1 Null MEFs Are Hypersensitive to Ionizing Irradiation—Previously, mice carrying a mutated *Brca1* allele with a small 5′ portion of exon 11 replaced by a neomycin gene were generated and shown to be viable (21). However, mice with both alleles mutated were embryonic lethal at postnatal days 5–7 (22). This phenotype was much more severe when compared with mice carrying both alleles of *Brca1* deleted for exon 11, which displayed an extended embryonic life span (4, 27, 28). Therefore, the MEFs derived from our *Brca1* knock-out mouse may be useful in exploring the full function of the *Brca1* gene. Because the mutant Brca1 embryos died too early to generate MEFs, survival of $Brca1^{-/-}$ mutant embryos could be extended with the ablation of the p53 gene (4, 29). MEFs with $Brca1^{-/-}$:$p53^{-/-}$ or $p53^{-/-}$ genotype were then established from E9.5 embryos (Fig. 1*A*) derived from a cross of $Brca1^{+/-}$:$p53^{-/-}$ mice (21). Protein analysis by immunoprecipitation followed by Western blotting revealed no full-length BRCA1 protein in these $Brca1^{-/-}$:$p53^{-/-}$ MEFs (Fig. 1*B*). Importantly, the Brca1-deficient MEFs exhibited hypersensitivity to γ-irradiation when compared with the $p53^{-/-}$ MEFs (Fig. 1*C*). The degree of γ-irradiation sensitivity of this $Brca1^{-/-}$:$p53^{-/-}$ MEF is greater than mouse embryonic stem cells or MEFs carrying a Brca1 exon 11 spliced variant (5, 6).

Brca1 Affects Precise End Joining rather than Overall End Joining—To examine the potential contribution of Brca1 in DSB repair, the established Brca1-deficient MEFs were used in a plasmid end-joining assay utilizing transient transfection of a linearized pGL2 plasmid harboring a luciferase reporter gene. If the reporter plasmid was linearized with restriction endonuclease *Hin*dIII, which cleaved at the linker region between promoter and coding sequence, any end-joining activity with small deletion or insertion would not affect the expression of the luciferase gene and could be considered an overall end-joining activity. However, if the reporter plasmid was digested with *Eco*RI at the luciferase coding region, only precise end joining would restore the original sequence (Fig. 2). Repair efficiency was calculated from the luciferase activities of linearized reporter constructs compared with that of the intact plasmid. We observed no difference in the overall end-joining activity between the $Brca1-/-$:$p53^{-/-}$ and $p53^{-/-}$ MEFs, but Brca1-deficient MEFs exhibited about a 50% reduction in precise end-joining activity (Fig. 2).

BRCA1 Is Required for Efficient Retroviral Infection Mediated by NHEJ—It has been reported that cells deficient in proteins involved in NHEJ show a reduced efficiency of retroviral infection (30, 31), suggesting that NHEJ is critical for the resolution of DNA DSBs that arise during retroviral infection. The first report suggested that NHEJ is required for retroviral DNA integration that proceeds through the repair of gapped intermediates arising from the linkage of viral and host cell DNA in an early reaction catalyzed by the viral integrase protein. The repair of gapped intermediates, which consist of nonjoined viral DNA 5′ ends, results in a 4–6-base pair repeat of host cell DNA flanking each proviral end (30). The second report demonstrated that cells with mutated NHEJ proteins suffer a high level of cell death upon retroviral infection (31) and proposed that, instead of being involved in an early step of retroviral integration, the NHEJ proteins are required to circularize the linear viral DNA to conceal the exposed DSBs to prevent subsequent apoptosis (31). In either case, NHEJ appears to be essential for retroviral infection.

Based on these findings, we decided to examine the efficiency of retroviral infection in the Brca1 deficient cells. Following infection with a retrovirus, 477H, carrying a hygromycin resistance gene (*Hygro*^{r}), the frequency of hygromycin-resistant colonies was found to be 5–10-fold lower in the $Brca1^{-/-}$:$p53^{-/-}$ MEFs as compared with the matched $Brca1^{+/+}$:$p53^{-/-}$ MEFs (Fig 3, *A* and *B*). Similarly, a 3–5-fold reduction in the number of hygromycin-resistant colonies was also observed in infected $Ku80^{-/-}$:$p53^{-/-}$ MEFs (13) as compared with $Ku80^{+/-}$:$p53^{-/-}$ MEFs (Fig. 3*B*). These results are consistent with the notion that DNA end-joining activity is significantly reduced in Brca1-deficient cells.

Brca1 Promotes Nonhomologous End joining of Chromosomal DSBs—In an attempt to further substantiate the contribution of Brca1 in NHEJ, we modified a DSB repair assay system (32) that permitted us to measure the frequency of NHEJ at a defined chromosomal DSB. For this purpose, we established $p53^{-/-}$ and $Brca1^{-/-}$:$p53^{-/-}$ MEF cell lines that carried a single integrated copy of a defined DSB repair substrate. This substrate, *S1hygro*, contained one copy of the hygromycin resistance gene (*Hygro*^{r}) carrying an 18-base pair recognition sequence for the rare cutting restriction endonuclease I-*Sce*I inserted into a naturally occurring *Nco*I site (Fig. 4), therefore leaving 4 bp of CATG microhomologies (residual *Nco*I site) flanking the I-*Sce*I site (Fig. 4*A*). This modification resulted in the inactivation of the hygromycin resistance gene. However, upon I-*Sce*I endonuclease cleavage, hygromycin-resistant activity could be restored, if this defined DSB was resected to a point at which the CATG microhomologies could be detected, and rejoined to restore the *Nco*I site, thereby

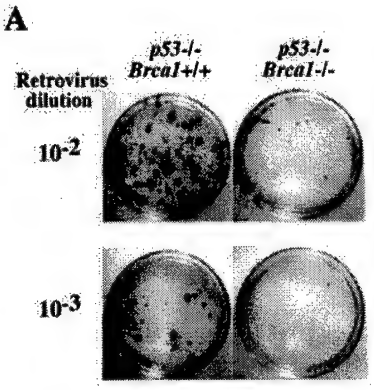

B

Number of Hygro^r colonies		
	Retrovirus dilution	
Cell lines	10^{-2}	10^{-3}
p53-/-Ku+/-	544 ± 21	110 ± 18
p53-/-Ku+/-	557 ± 21	102 ± 3
p53-/-Ku-/-	171 ± 18	37 ± 7
p53-/-Ku-/-	142 ± 39	21 ± 6
p53-/-Brca1+/+	456 ± 21	77 ± 39
p53-/-Brca1-/-	44 ± 7	14 ± 3

1x10^6 cells were used in each experiment.

FIG. 3. **Retroviral infection assay.** *A*, *Brca1*$^{+/+}$:*p53*$^{-/-}$and *Brca1*$^{-/-}$:*p53*$^{-/-}$ MEFs were plated at 5 × 10^5/100-mm dish and infected for 24 h with the indicated dilutions of virus 477H carrying a hygromycin resistance gene. Cells were selected with hygromycin (200 μg/ml) for 10–14 days and stained with methylene blue. Representative plates are shown. *B*, efficiency of retroviral DNA infection in distinct MEFs. The number of hygromycin-resistant colonies was counted from three plates for each assay, and each experiment was repeated three times.

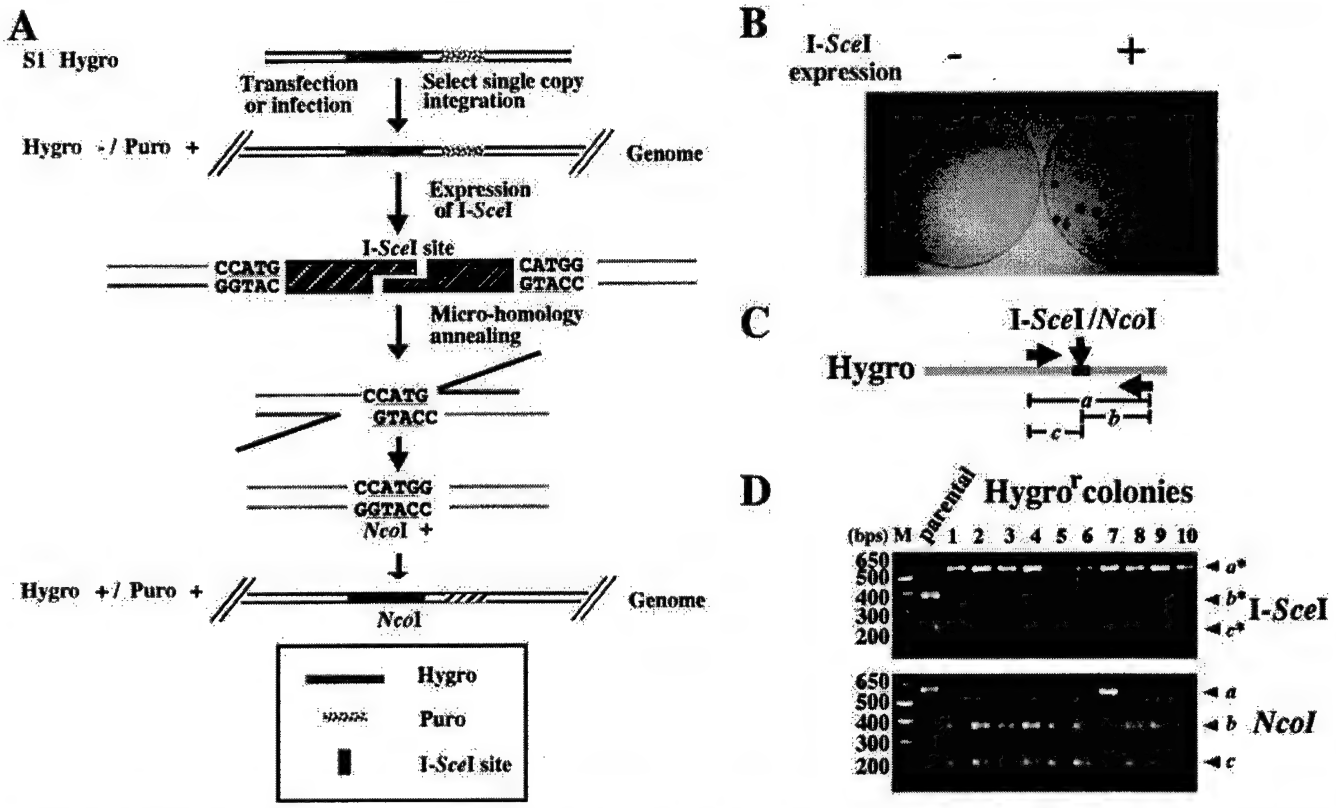

FIG. 4. **Design and analysis of the microhomology-mediated end-joining assay.** *A*, illustration of the scheme for I-*Sce*I-induced chromosomal end-joining reaction using the CATG microhomology sequence of the inactivated *Nco*I site. *B*, expression of I-*Sce*I in *p53*$^{-/-}$ MEFs promotes NHEJ-mediated repair of the *S1hygro* substrate. Two identical plates of MEFs with a single integrated copy of *S1hygro* substrate were transfected with an I-*Sce*I expression vector (+) or control vector (−). The dishes were fixed and stained with methylene blue. Representative dishes are shown. *C*, physical analysis of NHEJ products. PCR reaction using a pair of primers within the hygromycin gene generates a DNA fragment of ~573–595 bp (*a*). If this fragment contained a recovered *Nco*I site, digestion with restriction enzyme *Nco*I would produce two fragments of 368 (*b*) and 205 bp (*c*), respectively. *D*, physical analysis of genomic DNA extracted from both hygromycin-resistant clones (hygro^r) and parental cells containing *S1hygro*. PCR reactions were performed using primers flanking the I-*Sce*I or *Nco*I site as shown in *panel C*. Upon I-*Sce*I endonuclease digestion, the PCR product (*a*) from the parental clone cleaved into two fragments, *b** (379 bp) and *c** (216 bp), indicating the intact I-*Sce*I site. However, I-SceI failed to cleave the PCR fragments (*a**) from the 10 hygromycin-resistant clones (*lanes 1–10*). Conversely, upon *Nco*I restriction digestion, 9 of 10 clones (except *lane 7*) gave rise to the *b* and *c* fragments, which were not seen in the parental clone. Clone 7 apparently went through a different repair mechanism because it lost both the I-*Sce*I and *Nco*I sites but kept hygromycin resistance.

generating an intact hygromycin resistance gene (Fig. 4*A*). The original sequence was unlikely to be restored by homologous recombination due to the absence of homologous sequence. Importantly, this type of NHEJ repair promoted by an I-*Sce*I-induced DSB at the *S1hygro* gene could be assayed by selecting for hygromycin-resistant cell clones and physically analyzing the repair products by genomic DNA blotting or by direct PCR followed by digestion with *Nco*I endonuclease. Using a similar system, the Ku80 protein has been demonstrated to be crucial for NHEJ of a defined chromosomal DSB *in vivo* (32).

The *S1hygro* DSB repair substrate containing a puromycin selection cassette was stably integrated into the genome of wild-type, *p53*$^{-/-}$, and *Brca1*$^{-/-}$:*p53*$^{-/-}$ MEFs by either plasmid transfection or retroviral infection. Puromycin-resistant clones were selected and analyzed by Southern blotting and PCR. MEF clones containing a single copy of *S1hygro* were chosen for the chromosomal DSB-promoted NHEJ repair assay as described above. To generate DSBs, I-*Sce*I endonuclease was introduced by transfection of an I-*Sce*I expression vector (33) into the MEFs. In the mock transfection experiment, few or no hygromycin-resistant colonies were obtained following a selection against hygromycin. However, expression of the I-*Sce*I endonuclease in either the wild-type or the *p53*$^{-/-}$ MEFs pro-

TABLE I
Brca1 promotes NHEJ of Chromosomal DSBs
1×10^6 cells were used in each assay.

Cell line	No. of Hygro^r colonies[a]		
	Genotype	Mock-transfected	I-*Sce*I
WT-1	Wild type	1 ± 1	50 ± 3
p53-3	$p53^{-/-}Brca1^{+/+}$	<1	86 ± 19
p53-4	$p53^{-/-}Brca1^{+/+}$	<1	90 ± 16
1H-5	$p53^{-/-}Brca1^{-/-}$	<1	<1
	Number of Hygro^r colonies[b]		
	Genotype	Mock-transfected	I-*Sce*I
RP-3	$p53^{-/-}Brca1^{+/+}$	<1	45 ± 17
RP-4	$p53^{-/-}Brca1^{+/+}$	<1	82 ± 41
RP-6	$p53^{-/-}Brca1^{+/+}$	<1	45 ± 15
RH-1	$p53^{-/-}Brca1^{-/-}$	<1	<1
RH-3	$p53^{-/-}Brca1^{-/-}$	<1	1 ± 1
RH-6	$p53^{-/-}Brca1^{-/-}$	<1	<1

[a] 1–2 copies of *S1hygro* were introduced into the cells by plasmid transfection.
[b] Single copies of *S1hygro* were introduced into the cells by retroviral DNA integration.

duced numerous hygromycin-resistant colonies (Fig. 4*B* and Table I), indicating that I-*Sce*I cleavage occurred at the *S1hygro* substrate and hygromycin resistance arose almost exclusively from the repair of the I-*Sce*I-cleaved substrates. These results demonstrate that a defined chromosomal DSB can stimulate NHEJ as much as 100-fold above the spontaneous level.

Expression of I-*Sce*I in either wild-type or $p53^{-/-}$ MEFs yielded 45–82 hygromycin-resistant colonies/10^6 cells (4.5×10^{-5}-8.2×10^{-5}). By contrast, only background levels of hygromycin-resistant colonies were obtained after transfection of I-*Sce*I in *Brca1* $^{-/-}$:$p53^{-/-}$ MEFs (Table I). The transfection efficiency of the parental *Brca1* $^{-/-}$:$p53^{-/-}$ MEF was 2-fold lower than *Brca1* wild-type cells. However, each individual clone harboring *S1hygro* had a varied transfection efficiency of between 2-fold lower (RH3) to 3-fold higher (RH1) when compared with the clones derived from *Brca* $^{+/+}$:$p53^{-/-}$ MEF (RP3 and RP4), as measured by a transient transfection assay with a SV40 promoter-driven luciferase reporter (data not shown). Only background levels of hygromycin-resistant colonies were formed in a *Brca1* $^{-/-}$:$p53^{-/-}$ MEF clone (RH1) despite its highest transfection efficiency. Therefore, mutation of *Brca1* decreased the formation of hygromycin-resistant colonies by 1–2 orders of magnitude.

The repair of DSBs by NHEJ in the hygromycin-resistant clones would be expected to restore the naturally occurring *Nco*I restriction site, which was destroyed by the insertion of the 18-bp I-*Sce*I recognition site during construction of the *S1hygro* substrate. To verify that the hygromycin-resistant colonies derived from I-*Sce*I-induced DSB repair did in fact arise from NHEJ, a 595-bp DNA fragment of the hygromycin resistance gene encompassing the inactivated *Nco*I and I-*Sce*I restriction sites was amplified by PCR and subjected to *Nco*I restriction enzyme digestion (Fig. 4*C*). Nine of 10 PCR products generated from the hygromycin-resistant colonies were completely cleaved by *Nco*I but were resistant to I-*Sce*I digestion. In contrast, PCR products derived from parental clones harboring *S1hygro* were readily cleaved by I-*Sce*I but not by *Nco*I (Fig. 4*D*). These results indicated that cleavage followed by end processing must have occurred in these cells to restore the *Nco*I site.

To ensure a high level of I-*Sce*I expression, an adenovirus, AdTrack-CMV-I-*Sce*I, encoding I-*Sce*I and GFP under two distinct promoters was generated (Fig. 5*A*). We then tested this

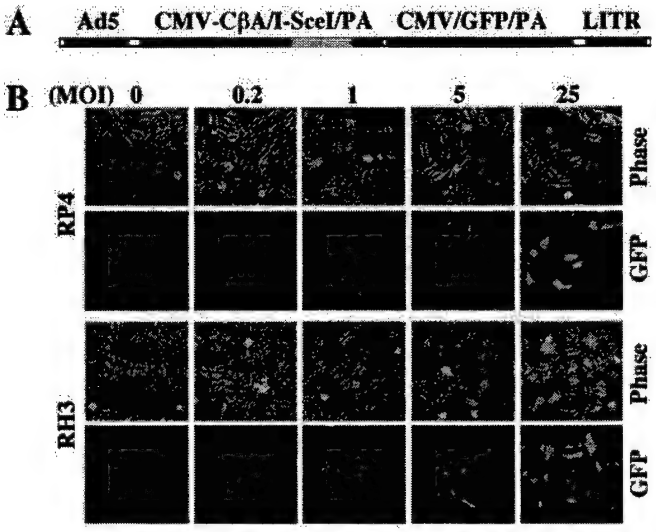

C

Genotype	Number of Hygro^r colonies			
	p53-/-Brca1+/+		*p53-/-Brca1-/-*	
Cell line	RP3	RP4	RH1	RH3
MOI				
Adeno-GFP 25	<1	<1	<1	<1
Adeno-I-SceI				
0.2	2±2	3±1	<1	<1
1	13±4	15±1	<1	1±1
5	35±4	51±5	<1	<1
25	77±7	124±7	<1	<1

FIG. 5. **Efficient expression of I-*Sce*I delivered by adenovirus enhances NHEJ.** *A*, diagram of the adenovirus construct AdTrack-CMV-I-*Sce*I, which contains two distinct expression units for I-*Sce*I under the CMV-CβA promoter (a composite promoter of cytomegalovirus (*CMV*) late gene promoter and chicken β-actin promoter) and for GFP under the CMV promoter. About 2×10^5 Brca1-proficient (RP3 and RP4) or -deficient cells (RH1 and RH3) were infected with the adenovirus AdTrack-CMV-I-*Sce*I at different m.o.i. dosages. *B*, as an example of RH3 and RP4, the number of the GFP-positive cells was proportional to the m.o.i. level as indicated. Cells expressing GFP fluorescence were recorded 48 h post-infection (magnification, 400×). *C*, the corresponding infected cells were grown in medium containing hygromycin for 14 days. As indicated, the number of hygromycin-resistant colonies increased proportionally to the m.o.i. level in RP3 and RP4 but was undetectable in RH3 and RH1 MEFs. Infection with Adeno-I-GFP that expressed only GFP alone did not increase any hygromycin-resistant colonies in either type of MEF.

adenovirus over a series of m.o.i. by tracing the fluorescence derived from GFP to monitor the infection efficiency. As shown in Fig. 5*B*, the expression of GFP in *Brca1* mutant or wild-type MEFs was comparable following the infection of AdTrack-CMV-I-*Sce*I in the range of m.o.i. used, suggesting that there was no significant difference between these two MEFs in terms of adenovirus infection and expression. We observed that the hygromycin-resistant colonies increased in proportion to the amount of m.o.i. infected in *Brca1*$^{+/+}$:$p53^{-/-}$ MEFs compared with *Brca1* $^{-/-}$:$p53^{-/-}$ MEFs, which remained negligible regardless of the high m.o.i. used (Fig. 5*C*). Taken together, these results suggested that the Brca1 mutant cells exhibited a severe defect in the repair of DSBs by microhomology-mediated NHEJ.

To establish that the above described microhomology-mediated end joining preceded independent of drug selection, we examined the repair process of the *S1hygro* substrate in these MEFs upon expression of the I-*Sce*I endonuclease at earlier

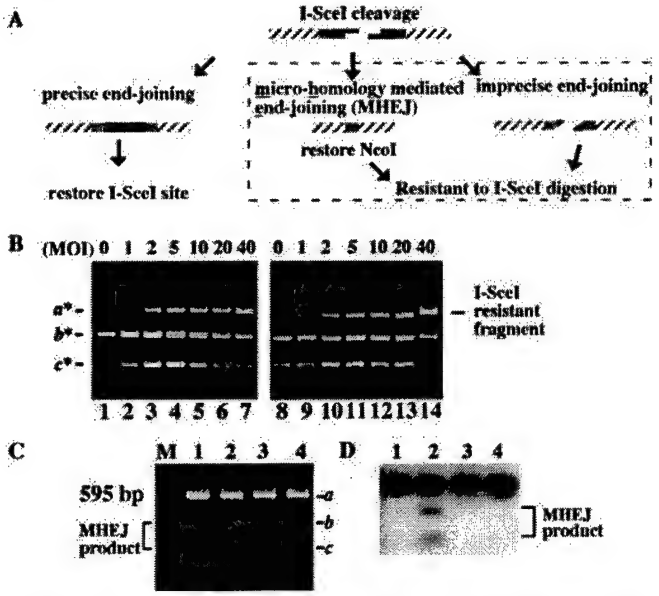

FIG. 6. **Analysis of earlier time points for chromosomal end joining induced by I-*Sce*I DSBs by transient transfection.** *A*, illustration of the potential processes for repairing I-*Sce*I-induced DSB and the properties of the end products derived from each repair process. The first pathway is mediated by a precise end joining that will regenerate the I-*Sce*I site; its end product is indistinguishable from the original substrate. This pathway cannot be analyzed by this method. The second pathway functions through MHEJ, which restores the *Nco*I site. The third pathway is mediated by imprecise end joining, and the end product loses the I-*Sce*I site and does not restore the *Nco*I site. *B*, physical analysis of the nonhomologous end-joining product. Genomic DNA from RP3 (*Brca1*$^{+/+}$:*p53*$^{-/-}$, *lanes 1–7*) or RH1 (*Brca1*$^{-/-}$:*p53*$^{-/-}$, *lanes 8–14*) MEFs infected with different m.o.i. of AdTrack-CMV-I-*Sce*I as indicated were used as templates to generate 573–595-bp PCR fragments as described in Fig 4. The PCR products were digested with I-*Sce*I endonuclease, separated by agarose gel electrophoresis, and stained with ethidium bromide. The presence of the I-*Sce*I-resistant DNA fragments (*a**) in both cell types indicates that they have similar efficiencies in NHEJ after I-*Sce*I expression. *C*, physical analysis of microhomology-mediated end-joining products. Genomic DNA from RP3 (*Brca1*$^{+/+}$:*p53*$^{-/-}$, *lanes 1* and *2*) or RH1 (*Brca1*$^{-/-}$:*p53*$^{-/-}$, *lanes 3* and *4*) MEFs infected with 20 m.o.i. of AdTrack-CMV-I-*Sce*I (*lanes 2* and *4*) or Adeno-I-GFP (*lanes 1* and *3*) were used as templates to generate the PCR fragments as described above. The PCR products (*lanes 2* and *4*) were digested with *Nco*I endonuclease, analyzed by agarose gel electrophoresis, and stained with ethidium bromide. *Lane M* shows the DNA size marker. The appearance of two DNA fragments (*b* and *c*) from *Nco*I digestion (*lane 2*) indicates the presence of the recovered *Nco*I site through microhomology-mediated end joining. *D*, DNA blotting analysis using hygromycin resistance gene cDNA as probe. The gel shown in *C* was analyzed by Southern blotting with p32-labeled cDNA of the hygromycin resistance gene as described (21).

time points. These *Brca1*$^{+/+}$:*p53*$^{-/-}$ and *Brca1* $^{-/-}$:*p53*$^{-/-}$ MEFs were infected with different m.o.i. levels of the adenovirus, AdTrack-CMV-I-*Sce*I, for 36 h. To demonstrate that I-*Sce*I endonuclease was expressed efficiently in both cell types, the genomic DNA of these cells was extracted, and the 595-bp hygromycin DNA fragment was amplified by PCR. The resistance of the 595-bp hygromycin DNA fragment to I-*Sce*I digestion indicates that a NHEJ must occur after I-*Sce*I cleavage. As shown in Fig. 6*B*, the I-*Sce*I-resistant fragment appeared in both Brca1-proficient and -deficient MEFs with very similar kinetics. This result also suggested that a deficiency of Brca1 did not affect the overall NHEJ activity. If NHEJ was to proceed through the designed CATG microhomology, the resulting repair product could be cleaved by the *Nco*I restriction enzyme as described above (Fig. 6*A*). Consistent with our previous observation, a portion of the NHEJ proceeded through the CATG microhomology, thereby restoring the original *Nco*I site in the *Brca1* wild-type cells. Therefore, the 595-bp hygromycin

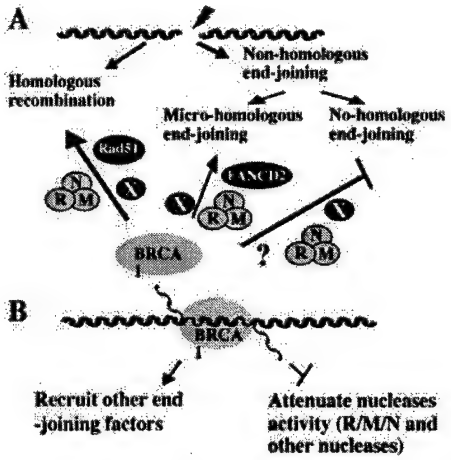

FIG. 7. **Proposed multiple functions of BRCA1 in DNA double strand break repair.** *A*, BRCA1 is important in homology-based repair and microhomology-mediated end joining, possibly through its direct interaction with the Rad50·Mre11·Nbs1 complex (*R/M/N*), and/or indirect association with Rad51, and/or other unknown factors (*X*). BRCA1 may also function in the suppression of nonhomologous end joining through Rad50·Mre11·Nbs1 or other proteins. *B*, BRCA1 may bind to a microhomology-paired double-stranded DNA to stabilize it transiently before recruiting other repair factors involved in further processing.

DNA fragment derived from genomic PCR could be cleaved by *Nco*I into two fragments, as either directly revealed by ethidium bromide staining (Fig. 6*C*) or by DNA blotting using the cDNA of the hygromycin resistance gene as a probe (Fig. 6*D*). This type of NHEJ activity was readily detectable in the Brca1-proficient MEFs but not in Brca1-deficient cells (Fig. 6, *C* and *D*). Taken together, these results suggest that Brca1 plays an important role in microhomology-mediated end-joining activity in the repair of DNA DSBs *in vivo*.

DISCUSSION

BRCA1 plays an essential role in DNA DSB repair either through HR or NHEJ. The results described above suggest that Brca1 may have an important role in NHEJ. Using a plasmid end-joining assay, it was shown that Brca1 plays a moderate role in precise end joining rather than in overall NHEJ. Brca1 was also found to promote efficient retroviral infection, likely reflecting a role in retroviral DNA end-joining activity. Furthermore, repair of a defined chromosomal DSB mediated by microhomology annealing is severely impaired in Brca1-deficient MEFs. Taken together, these observations suggest that BRCA1 has a critical role in microhomology-mediated end joining rather than in overall nonhomologous end-joining activity. These results are consistent with the recent observation that cell extracts derived from Brca1-deficient MEFs significantly reduced end-joining activity with 4-bp homology *in vitro* (34).

Mechanistically speaking, NHEJ can proceed through distinct subpathways determined by the nucleotide sequence immediately surrounding the break site. Often, NHEJ generates junctions with sequence homologies consisting of only a few nucleotides. DNA ends can be joined either precisely, without nucleotide loss through sequence homology at the DNA termini, or imprecisely, through nucleotide deletion or addition, to generate microhomologies flanking the break site. Alternatively, broken DNA ends can be joined without microhomology (15). In an assay for gross chromosomal rearrangements (GCRs), the rate of non-homology-mediated GCRs was increased ~600-fold in yeast *rad50, mre11,* and *xrs2* mutants (35), suggesting that the Rad50·Mre11·Xrs2 complex appears to be important in suppressing non-homology-mediated end-joining processes. Previous work has demonstrated that BRCA1

physically interacts with the Rad50·Mre11·Nbs1 complex *in vivo* and *in vitro* (14). Furthermore, BRCA1 can be isolated from cells in a high molecular complex with Rad50·Mre11·Nbs1 (36). These observations suggest that the function of BRCA1 in DSB repair is mediated, at least in part, through its association with the Rad50·Mre11·Nbs1 complex (Fig. 7*A*), although the possibility exists that BRCA1 functions through other associated repair component such as FANCD2 (37, 38).

The function of the mammalian Rad50·Mre11·Nbs1 complex in DSB repair is not entirely known at present. However, substantial evidence has suggested a functional conservation between the mammalian Rad50·Mre11·Nbs1 and yeast Rad50·Mre11·Xrs2 in NHEJ. It has been shown that the yeast Rad50·Mre11·Xrs2 purified complex can bind and bridge DNA ends together. The addition of the yeast homologues of Ku70/80, HdfA and HdfB, enhances this DNA end-bridging activity of the Rad50·Mre11·Xrs2 complex. The DNA-bound Rad50·Mre11·Xrs2 complex can then directly recruit Dnl4/Lif1 (equivalent to mammalian DNA ligase IV and Xrcc4) to complete the DNA end ligation process (40). Similarly, mammalian Rad50·Mre11·Nbs1 has also been to exhibit DNA end-tethering activity (39, 41, 42). Therefore, purified proteins that include Rad50·Mre11·Nbs1, Ku homologues, and DNA ligase IV/Xrcc4 can carry out NHEJ *in vitro*. These results implicate a potential conservation of these two complexes in nonhomologous end joining.

The NHEJ pathway represents an efficient, energy-saving process to rescue cells following extensive DNA damage. NHEJ can be error-prone in mammalian cells. However, NHEJ may utilize microhomology sequences to minimize error rates. If complimentary sequences are left at the DNA termini, these DNA termini can be joined readily without nucleotide loss by annealing the complementary sequences. Experimental evidence has suggested that this type of error-free NHEJ could represent up to 60% of overall end joining in mammalian cells (17) and more than 90% in yeast when a cohesive overhang is present at the DNA termini (15). On the other hand, microhomology sequences may serve as a platform for stabilizing protein-DNA interactions, attenuating nuclease attack, recruiting other repair factors, and bridging DNA ends together (Fig. 7*B*). BRCA1 has been shown to associate with this type of DNA structure *in vitro*, suggesting that BRCA1 may participate in this process (38). Similar models have been proposed for DNA-PK through structural analytical studies (43, 44). Proper NHEJ contributes significantly to maintain genome stability in mammalian cells. It has been demonstrated that in the presence of multiple chromosomal breaks, homology-directed translocation can be observed at a frequency as high as that of conservative gene conversion (45). In the absence of DNA-PK or ligase IV/Xrcc4, greatly elevated levels of chromosomal translocation can be detected in murine embryonic cells (10–12).

As discussed above, Brca1 may work together with the Rad50·Mre11·Nbs1 complex in NHEJ in addition to homologous recombination. The timing for this complex to function in either pathway may be dependent on the cell cycle status, at which the availability of the other repair factors of these two pathways is critical. Inefficient or error-prone DNA repair resulting directly from mutational inactivation of BRCA1 can lead to global genomic instability and a concomitant accrual of functionally inactivating mutations at genetic loci involved in breast tumorigenesis.

Acknowledgments—We thank Drs. P. Berg and G. Donoho for pPGK3Xnls-I-*Sce*I plasmid, P. Hasty for *Ku* mutant MEFs, N. Ting and S. Vijayakumar for comments, and D. Jones for technical assistance.

REFERENCES

1. Welcsh, P. L., Owens, K. N., and King, M. C. (2000) *Trends Genet.* **16,** 69–74
2. Zheng, L., Li, S., Boyer, T. G., and Lee, W. H. (2000) *Oncogene* **19,** 6159–6175
3. Tomlinson, G. E., Chen, T.-L., Stastny, V. A., Virmani, A. K., Spillman, M. A., Tonk, V., Blum, J. L., Schneider, N. R., Wistuba, I. I., Shay, J. W., Minna, J. D., and Gazdar, A. F. (1998) *Cancer Res.* **58,** 3237–3242
4. Xu, X., Weaver, Z., Linke, S. P., Li, C., Gotay, J., Wang, X. W., Harris, C. C., Ried, T., and Deng, C. X. (1999) *Mol. Cell* **3,** 389–395
5. Gowen, L. C., Avrutskaya, A. V., Latour, A. M., Koller, B. H., and Leadon, S. A. (1998) *Science* **281,** 1009–1012
6. Cressman, V. L., Backlund, D. C., Avrutskaya, A. V., Leadon, S. A., Godfrey, V., and Koller, B. H. (1999) *Mol. Cell. Biol.* **19,** 7061–7075
7. Deng, C. X. (2001) *Mutat. Res.* **477,** 183–189
8. Chu, G. (1997) *J. Biol. Chem.* **272,** 24097–24100
9. Roth, D. B., and Gellert, M. (2000) *Nature* **404,** 823–825
10. Karanjawala, Z. E., Grawunder, U., Hsieh, C. L., and Lieber, M. R. (1999) *Curr. Biol.* **9,** 1501–1504
11. Difilippantonio, M. J., Zhu, J., Chen, H. T., Meffre, E., Nussenzweig, M. C., Max, E. E., Ried, T., and Nussenzweig, A. (2000) *Nature* **404,** 510–514
12. Gao, Y., Ferguson, D. O., Xie, W., Manis, J. P., Sekiguchi, J., Frank, K. M., Chaudhuri, J., Horner, J., DePinho, R. A., and Alt, F. W. (2000) *Nature* **404,** 897–900
13. Lim, D. S., Vogel, H., Willerford, D. M., Sands, A. T., Platt, K. A., and Hasty, P. (2000) *Mol. Cell. Biol.* **20,** 3772–3780
14. Zhong, Q., Chen, C. F., Li, S., Chen, Y., Wang, C. C., Xiao, J., Chen, P. L., Sharp, Z. D., and Lee, W. H. (1999) *Science* **285,** 747–750
15. Tsukamoto, Y., and Ikeda, H. (1998) *Genes Cells* **3,** 135–144
16. Moynahan, M. E., Chiu, J. W., Koller, B. H., and Jasin, M. (1999) *Mol. Cell* **4,** 511–518
17. Lin, Y., Lukacsovich, T., and Waldman, A. S. (1999) *Mol. Cell. Biol.* **19,** 8353–8360
18. Takata, M., Sasaki, M. S., Sonoda, E., Morrison, C., Hashimoto, M., Utsumi, H., Yamaguchi-Iwai, Y., Shinohara, A., and Takeda, S. (1998) *EMBO J.* **17,** 5497–5508
19. Scully, R., Ganesan, S., Vlasakova, K., Chen, J., Socolovsky, M., and Livingston, D. M. (1999) *Mol. Cell* **4,** 1093–1099
20. Pierce, A. J., Stark, J. M., Araujo, F. D., Moynahan, M. E., Berwick, M., and Jasin, M. (2001) *Trends Cell Biol.* **11,** S52–S59
21. Liu, C. Y., Flesken-Nikitin, A., Li, S., Zeng, Y. Y., and Lee, W. H. (1996) *Genes Dev.* **10,** 1835–1843
22. Zheng, L., Pan, H., Li, S., Flesken-Nikitin, A., Chen, P. L., Boyer, T. G., and Lee, W. H. (2000) *Mol. Cell* **6,** 757–768
23. Donehower, L. A., Harvey, M., Slagle, B. L., McArthur, M. J., Montgomery, C. A., Jr., Butel, J. S., and Bradley, A. (1992) *Nature* **356,** 215–221
24. He, T. C., Zhou, S., da Costa, L. T., Yu, J., Kinzler, K. W., and Vogelstein, B. (1998) *Proc. Natl. Acad. Sci. U. S. A.* **95,** 2509–2514
25. Chen, P. L., Chen, Y. M., Bookstein, R., and Lee, W. H. (1990) *Science* **250,** 1576–1580
26. Pear, W. S., Nolan, G. P., Scott, M. L., and Baltimore, D. (1993) *Proc. Natl. Acad. Sci. U. S. A.* **90,** 8392–8396
27. Gowen, L. C., Johnson, B. L., Latour, A. M., Sulik, K. K., and Koller, B. H. (1996) *Nat. Genet.* **12,** 191–194
28. Huber, L. J., Yang, T. W., Sarkisian, C. J., Master, S. R., Deng, C. X., and Chodosh, L. A. (2001) *Mol. Cell. Biol.* **21,** 4005–4015
29. Hakem, R., de la Pompa, J. L., Elia, A., Potter, J., and Mak, T. W. (1997) *Nat. Genet.* **16,** 298–302
30. Daniel, R., Katz, R. A., and Skalka, A. M. (1999) *Science* **284,** 644–647
31. Li, L., Olvera, J. M., Yoder, K. E., Mitchell, R. S., Butler, S. L., Lieber, M., Martin, S. L., and Bushman, F. D. (2001) *EMBO J.* **20,** 3272–3281
32. Liang, F., Romanienko, P. J., Weaver, D. T., Jeggo, P. A., and Jasin, M. (1996) *Proc. Natl. Acad. Sci. U. S. A.* **93,** 8929–8933
33. Donoho, G., Jasin, M., and Berg, P. (1998) *Mol. Cell. Biol.* **18,** 4070–4078
34. Zhong, Q., Boyer, T. G., Chen, P.-L., and Lee, W.-H. (2002) *Cancer Res.*, in press
35. Chen, C., and Kolodner, R. D. (1999) *Nat. Genet.* **23,** 81–85
36. Chiba, N., and Parvin, J. D. (2001) *J. Biol. Chem.* **276,** 38549–38554
37. Garcia-Higuera, I., Taniguchi, T., Ganesan, S., Meyn, M. S., Timmers, C., Hejna, J., Grompe, M., and D'Andrea, A. D. (2001) *Mol. Cell* **7,** 249–262
38. Lundberg, R., Mavinakere, M., and Campbell, C. (2001) *J. Biol. Chem.* **276,** 9543–9549
39. Paull, T. T., and Gellert, M. (2000) *Proc. Natl. Acad. Sci. U. S. A.* **97,** 6409–6414
40. Chen, L., Trujillo, K., Ramos, W., Sung, P., and Tomkinson, A. E. (2001) *Mol. Cell* **8,** 1105–1115
41. Huang, J., and Dynan, W. S. (2002) *Nucleic Acids Res.* **30,** 667–674
42. de Jager, M., van Noort, J., van Gent, D. C., Dekker, C., Kanaar, R., and Wyman, C. (2001) *Mol. Cell* **8,** 1129–1135
43. Leuther, K. K., Hammarsten, O., Kornberg, R. D., and Chu, G. (1999) *EMBO J.* **18,** 1114–1123
44. Walker, J. R., Corpina, R. A., and Goldberg, J. (2001) *Nature* **412,** 607–614
45. Richardson, C., and Jasin, M. (2000) *Nature* **405,** 697–700

THE JOURNAL OF BIOLOGICAL CHEMISTRY
Vol. 277, No. 51, Issue of December 20, pp. 49408–49416, 2002
Printed in U.S.A.

Phosphorylation of the Mitotic Regulator Protein Hec1 by Nek2 Kinase Is Essential for Faithful Chromosome Segregation*

Received for publication, July 15, 2002, and in revised form, October 11, 2002
Published, JBC Papers in Press, October 16, 2002, DOI 10.1074/jbc.M207069200

Yumay Chen‡§, Daniel J. Riley§, Lei Zheng‡, Phang-Lang Chen‡, and Wen-Hwa Lee‡¶

From the Institute of Biotechnology, Departments of ‡Molecular Medicine and §Medicine, University of Texas Health Science Center at San Antonio, San Antonio, Texas 78245-3207

Hec1 (highly expressed in cancer) plays essential roles in chromosome segregation by interacting through its coiled-coil domains with several proteins that modulate the G_2/M phase. Hec1 localizes to kinetochores, and its inactivation either by genetic deletion or antibody neutralization leads to severe and lethal chromosomal segregation errors, indicating that Hec1 plays a critical role in chromosome segregation. The mechanisms by which Hec1 is regulated, however, are not known. Here we show that human Hec1 is a serine phosphoprotein and that it binds specifically to the mitotic regulatory kinase Nek2 during G_2/M. Nek2 phosphorylates Hec1 on serine residue 165, both *in vitro* and *in vivo*. Yeast cells are viable without scNek2/Kin3, a close structural homolog of Nek2 that binds to both human and yeast Hec1. When the same yeasts carry an scNek2/Kin3 (D55G) or Nek2 (E38G) mutation to mimic a similar temperature-sensitive *nima* mutation in *Aspergillus*, their growth is arrested at the nonpermissive temperature, because the scNek2/Kin3 (D55G) mutant binds to Hec1 but fails to phosphorylate it. Whereas wild-type human Hec1 rescues lethality resulting from deletion of Hec1 in *Saccharomyces cerevesiae*, a human Hec1 mutant or yeast Hec1 mutant changing Ser^{165} to Ala or yeast Hec1 mutant changing Ser^{201} to Ala does not. Mutations changing the same Ser residues to Glu, to mimic the negative charge created by phosphorylation, partially rescue lethality but result in a high incidence of errors in chromosomal segregation. These results suggest that cell cycle-regulated serine phosphorylation of Hec1 by Nek2 is essential for faithful chromosome segregation.

Mitosis must be precisely regulated and checked for faithful partitioning of chromosomes during a short but crucial period of the cell division cycle. Since the basic mechanics of chromosome segregation and checkpoint control are conserved in all eukaryotes, yeast and other fungi are excellent tools for dissecting mechanisms that apply to mammalian cell cycle proteins with clear homologs in lower eukaryotes. The novel coiled-coil protein Hec1 plays important roles in chromosome condensation and cohesion by interacting with structural components of the mitotic chromosome, including Smc1 (structure of the mitotic chromosome 1) complexes (1–3) and the kinetochore protein Ctf19p (4). Hec1 also regulates 26 S proteasome activity through interaction with MSS1 (CIM5/subunit 7), p45/Trip1 (Sug1/CIM3/subunit 8), and p44.5 (subunit 9) (5). These Hec1-interacting proteins were first identified in yeast two-hybrid assays using the coiled-coil region of Hec1 as bait (1). The mechanisms by which Hec1 itself is regulated during G_2 and M phases are not yet known, however. Since Hec1 has a structural and functional homolog in *S. cerevesiae* (scHec1, also known as TID3, NDC80, and YIO4) (3, 6), the consequences of its interactions with other proteins can be meaningfully explored in yeast.

Protein kinases have been shown to play important roles regulating G_2/M phase progression. One such kinase, NimA (never in mitosis A), which phosphorylates specific proteins on serine and threonine residues, is vital in *Aspergillus nidulans* for entry into mitosis (7–9). Cells harboring temperature-sensitive mutations of *nima* arrest specifically in G_2 at nonpermissive temperature, but rapidly and synchronously enter mitosis upon shift to permissive temperature (10). The expression of NimA is tightly regulated during the nuclear division cycle, peaking in G_2 and M phases. NimA, like Hec1, has also been shown to influence faithful chromosome segregation (7–9).

Kinases with structural and functional homology to NimA exist in vertebrate cells (11–18). These NimA-related kinases, or Neks, are purported to complement or function in manners similar to those of Cdc2 and other G_2/M phase cyclin-dependent kinases. Nek2, the homolog in human cells with the greatest structural similarity to NimA within the catalytic domain (19), is regulated in yeast in a manner similar to regulation of NimA in *A. nidulans*; its expression and serine/threonine kinase activity are highest during late G_2 phase, when Nek2 is expected to function critically (7, 17, 20). Furthermore, a portion of Nek2 localizes to centrosomes and appears in mammalian cells to play a role similar to NimA in controlling entry into mitosis (17, 21). Nek2 may have more diverse roles during several phases of the cell cycle, from S phase to multiple phases of mitosis, based on its dynamic expression and subcellular localization in cytosol, nucleus, and chromosome portions other than the centrosome (21, 22). Nek2 may therefore have several functions in regulating cell proliferation, not only a role in G_2/M phase progression. In budding yeast, a structural homolog of NimA and Nek2, scNek2/Kin3 (also known as Fun52 and Npk1), has been identified (23–25), but its functional similarity to human Nek2 has not yet been established.

In this report, we demonstrate how the function of Hec1 is regulated during G_2/M phases by characterizing the previously reported interaction between Hec1 and Nek2 (5). We take advantage of Nek2 and Hec1 homologs, specific point mutants, and the ability to assay chromosomal segregation errors in budding yeast to show that Hec1 is phosphorylated by Nek2

* This work was supported by National Institutes of Health Grants EY05758-18, CA58318, and CA81020 (to W. H. L.) and Veterans Affairs Advanced Research Career Development Award 1999-40 (to D. J. R.). The costs of publication of this article were defrayed in part by the payment of page charges. This article must therefore be hereby marked "*advertisement*" in accordance with 18 U.S.C. Section 1734 solely to indicate this fact.

¶ To whom correspondence should be addressed: Institute of Biotechnology, Dept. of Molecular Medicine, University of Texas Health Science Center at San Antonio, 15355 Lambda Dr., San Antonio, TX 78245-3207. Tel.: 210-567-7351; Fax: 210-567-7377; E-mail: leew@uthscsa.edu.

TABLE I
Yeast strains and genotypes

Strain	Genotype	Source
YPH499	Mat a *ura3–52 lys2–801 ade2–101 trp1-Δ63 his3-Δ200 leu2-Δl*	P. Hieter
WHL101	Mat a *ura3–52 lys2–801 ade2–101 trp1-Δ63 his3-Δ200 leu2-Δ1 schec1Δ*::*URA3 hsHEC1* (YcpPA-HSHEC1::*TRP1*)	W-H. Lee
WHL-SE	Mat a *ura3–52 lys2–801 ade2–101 trp1-Δ63 his3-Δ200 leu2-Δ1 schec1Δ*::*URA3 hsHEC1*(YcpPA-hshec1S165E::*TRP1*)	This study
WHL103	Mat a *ura3–52 lys2–801 ade2–101 trp1-Δ63 his3-Δ200 leu2-Δ1 schec1Δ*::*URA3 scHEC1* (YcpPA-scHEC1::*TRP1*)	W-H. Lee
WHL-S201	Mat a *ura3–52 lys2–801 ade2–101 trp1-Δ63 his3-Δ200 leu2-Δ1 schec1Δ*::*URA3 scHEC1* (YcpPA-scHEC1S201E::*TRP1*)	This study
WHL6001	Mat a *ura3–52 lys2–801 ade2–101 trp1-Δ63 his3-Δ200 leu2-Δ1 scnek2Δ*::*URA3* Ycp::LEU2	This study
WHL6009	Mat a *ura3–52 lys2–801 ade2–101 trp1-Δ63 his3-Δ200 leu2-Δ1 scnek2Δ*::*URA3 scNek2*(Ycp-scNek2D55G::*LEU2*)	This study
WHL6010	Mat a *ura3–52 lys2–801 ade2–101 trp1-Δ63 his3-Δ200 leu2-Δ1 scnek2Δ*::*URA3 NEK2*(Ycp-nek2E38G::*TRP1*)	This study
WHL6012	Mat a *ura3–52 lys2–801 ade2–101 trp1-Δ63 his3-Δ200 leu2-Δ1* scNek2(Ycp-scNek2D55G::*LEU2*) *schec1Δ*::*URA3 hsHEC1* (YcpPA-HSHEC1::*TRP1*)	This study
WHL6013	Mat a *ura3–52 lys2–801 ade2–101 trp1-Δ63 his3-Δ200 leu2-Δ1 scnek2Δ*::*URA3 scNek2*(Ycp-scNek2D55G::*LEU*)(Ycp::*TRP1*)	This study
WHL6014	Mat a *ura3–52 lys2–801 ade2–101 trp1-Δ63 his3-Δ200 leu2-Δ1 scnek2Δ*::*URA3 scnek2*(Ycp-scNek2D55G::*LEU*) KIN3(Ycp-scNek2::*TRP1*)	This study
WHL6015	Mat a *ura3–52 lys2–801 ade2–101 trp1-Δ63 his3-Δ200 leu2-Δ1 scnek2Δ*::*URA3 scnek2*(Ycp-scNek2D55G::*LEU*) NEK2(Ycp-NEK2::*TRP1*)	This study
YPH1017	Mat α *ura3–52 lys2–801 ade2–101 trp1-Δ63 his3-Δ200 leu2-Δ1* (CFIII *HIS3 SUP11*)	P. Hieter
WHL2003	Mat a/α *lys2–801/lys2–801 ade2–101/ade2–101 leu2-Δ1/leu2-Δ1* scHEC1/scHEC1 (CFIII *TRP1 SUP11*)	W-H. Lee
WHL4003	Mat a/α *lys2–801/lys2–801 ura3–52/ura3–52 ade2–101/ade2–101 trp1-Δ63/trp1-Δ63 his3-Δ200/his3-Δ200 leu2-Δ1/leu2-Δ1 schec1Δ*::*URA3/schec1Δ*::*URA3 hsHEC1* (YcpPA-HSHEC1::*TRP1*) (CFIII *HIS3 SUP11*)	This study
WHL4001	Mat a/α *lys2–801/lys2–801 ura3–52/ura3–52 ade2–101/ade2–101 trp1-Δ63/trp1-Δ63 his3-Δ200/his3-Δ200 leu2-Δ1/leu2-Δ1 schec1Δ*::*URA3/schec1Δ*::*URA3 hsHEC1* (YcpPA-HSHEC1::*TRP1*) (CFIII *HIS3 SUP11*) *hshec 1S165E* (YcpPA-hshec1S165E::*TRP1*)	This study
WHL6502	Mat a/α *lys2–801/lys2–801 ade2–101/ade2–101 leu2-Δ1/leu2-Δ1 scHEC1/scHEC1* (CFIII *TRP1 SUP11*) *scnek2Δ*::*URA3/scnek2Δ*::*URA3* (CFIII *TRP1 SUP11*)	This study

kinase during G_2 and M phases. This specific modification is vital for Hec1 to coordinate faithful chromosome segregation.

EXPERIMENTAL PROCEDURES

Cell Culture and Synchronization—Human bladder carcinoma T24 cells (American Type Tissue Collection, Manassas, VA) grown in Dulbecco's modified Eagle's medium plus 10% fetal bovine serum were synchronized at G_1 by density arrest and then released at time zero by replating in Dulbecco's modified Eagle's medium plus 10% fetal calf serum at a density of 2×10^6 cells per 10-cm plate. At various time points thereafter (18 h for G_1/S, 22 h for S, 32 h for G_2), the cells were harvested. To obtain a cell population enriched in M phase, nocodazole (0.4 μg/ml) was added to the culture medium for 8 h prior to harvest (26).

Yeast Strains, Reagents, and Media—Yeast strains are described in Table I. Strains used in this study were grown in complete medium (YPD; 1% yeast extract, 2% peptone, and 2% dextrose) or in supplemented minimal medium with appropriate amino acids missing. The chemicals and medium components were purchased from Sigma and BD Industries (Franklin Lakes, NJ).

Immunoprecipitation and Western Blot Analysis—T24 cells resuspended in ice-cold Lysis 250 buffer (50 mM Tris-HCl, pH 7.4, 250 mM NaCl, 5 mM EDTA, 0.1% Nonidet P-40, 50 mM NaF, 1 mM phenylmethylsulfonyl fluoride) were subjected to three freeze/thaw cycles (liquid nitrogen/37 °C) and then centrifuged at 14,000 rpm for 2 min at room temperature. The supernatants were used for immunoprecipitation as described (27). Briefly, anti-Hec1 antibody mAb[1] 9G3 (1 μg) or mouse polyclonal anti-Nek2 antiserum (1 μl) was added to each supernatant. After a 1-h incubation, protein A-Sepharose beads were added, and incubation continued for another 1 h. Beads were collected, washed five times with lysis buffer containing hypertonic NaCl, and then boiled in SDS-loading buffer for immunoblot analysis as described (27). For the double immunoprecipitation experiment, Hec1 was immunoprecipitated from ^{35}S-labeled T24 cells as above. The washed immunocomplex was then incubated at 100 °C for 5 min in 200 μl of disassociation buffer (20 mM Tris, pH 7.4, 50 mM NaCl, 1% SDS, and 5 mM dithiothreitol). The heated immunocomplex was then diluted with 1 ml of cold Lysis 250 and immunoprecipitated again with the same polyclonal anti-Hec1 antibody (26, 27). For the co-immunoprecipitation experiments from yeast cells, yeast cell lysate was prepared as described (3). Briefly, yeast cells were collected by centrifugation and washed twice with cold distilled H_2O. Glass beads were used to break the cells in lysis buffer (50 mM Tris, pH 7.5, 10 mM $MgSO_4$, 1 mM EDTA, 10 mM KOAc, 1 mM dithiothreitol). Clarified yeast cell lysates were then used for co-immunoprecipitation by anti-Hec1 mAb 9G3 or anti-scHec1 polyclonal antiserum as described above. After a 4-h incubation with antibodies and protein A-Sepharose beads, the beads were collected, washed extensively with lysis buffer, and then boiled in SDS-loading buffer. After immunoblotting to Immobilon-P membrane (Millipore Corp., Bedford, MA), blots were probed with anti-scHec1 antibodies, anti-Hec1 mAb 9G3, or anti-scNek2 antibodies. All but one of the immunoblots were developed by 5-bromo-4-chloro-3-indolyl phosphate/nitro blue tetrazolium substrate for alkaline phosphatase-conjugated anti-mouse antibodies. Horseradish peroxidase-conjugated protein A was used to detect anti-scNek2 antibodies. Blots using that antibody were developed using an ECL chemiluminescence kit (Amersham Biosciences), according to the manufacturer's instructions.

Metabolic Labeling—T24 cells grown in Dulbecco's modified Eagle's medium plus 10% fetal calf serum were synchronized at G_1 by density arrest and then released at time 0 by replating in Dulbecco's modified Eagle's medium plus 10% fetal calf serum at a density of 2×10^6 cells/10-cm plate. At various time points thereafter (18 h for G_1/S, 22 h for S, 32 h for G_2), the cells were metabolically labeled with 100 μCi/ml [^{32}P]phosphoric acid (ICN, Costa Mesa, CA) for 3 h and harvested for immunoprecipitation with mAb 9G3 anti-Hec1 antibodies as described above.

Colony Sectoring Assay—Chromosome segregation errors were measured by colony sectoring assay as described (3, 28), except that adenine was added at a concentration of 6 μg/ml instead of 30 μg/ml.

Purification of His-tagged Hec1 Protein—cDNA encoding full-length Hec1 was digested with *Xho*I and fused in-frame to His_6 at the N terminus and expressed in *E. coli* using the PET expression system (29). After induction with 0.1 mM isopropylthiogalactoside, cells were lysed and clarified by centrifugation. The clarified total soluble cellular protein was passed through a DEAE-Sepharose column (Amersham Biosciences). The flow-through from the column was passed through an SP-Sepharose column (Amersham Biosciences) and eluted with a 100–750 mM NaCl gradient. His-Hec1 eluted at fractions between 200 and

[1] The abbreviations used are: mAb, monoclonal antibody; aa, amino acids; GST, glutathione *S*-transferase.

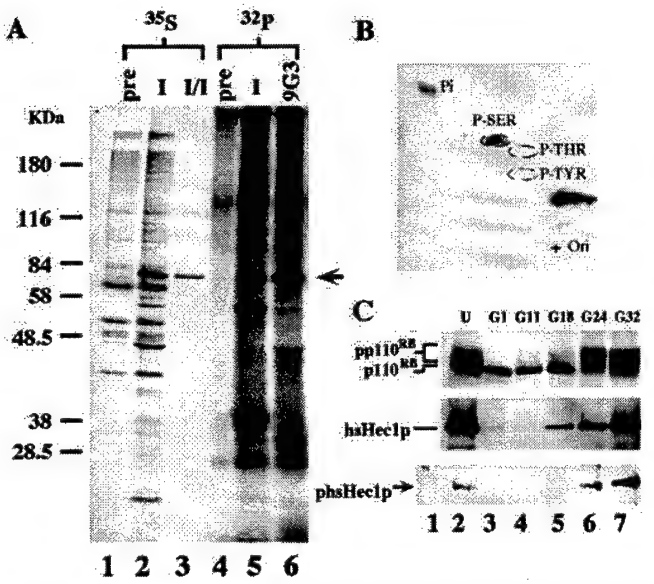

FIG. 1. **Cell cycle-dependent serine phosphorylation of Hec1.** *A*, T24 cells were labeled with either [^{35}S]methionine or [^{32}P]orthophosphate and lysed. Lysates were immunoprecipitated with polyclonal anti-Hec1 antibodies (*lanes 2* and *5*), preimmune sera (*lanes 1* and *4*), or monoclonal anti-Hec1 antibodies (mAb 9G3) (*lane 6*). *Lane 3* was performed as a double immunoprecipitation to eliminate nonspecific and co-immunoprecipitating proteins. The *arrow* indicates migration of the 76-kDa Hec1 protein. *B*, phosphoamino acid analysis of ^{32}P-labeled Hec1. The radioactively labeled protein was isolated and subjected to amino acid hydrolysis. The lysates were analyzed by thin layer chromatography using phosphorylated serine, threonine, and tyrosine as standards. Hec1 is primarily phosphorylated on serine residues. P_i, unincorporated, labeled phosphate; *Ori*, original spot. *C*, cell cycle-dependent phosphorylation of Hecl. T24 cells released from density arrest at G_1 (*lane 3*) were labeled with [^{32}P]orthophosphate, lysed, and immunoprecipitated with mAb 9G3 at time periods corresponding to different phases of the cell cycle. Expression of Hec1 was detected by Western blotting with mAb 9G3, shown in the *middle panel* (*G11*, 11 h after release for G_1; *G18*, 18 h after release for G_1/S; *G24*, S phase; *G32*, for G_2/M phase). Phosphorylation of Hec1 (*phsHec1p*) is evident starting at S phase (*lane 6*, *bottom panel*) and becomes most prominent during M phase (*lane 7*, *bottom panel*). The phosphorylation pattern of p110^{RB} was used to mark cell cycle progression (*top panel*), as previously described (27).

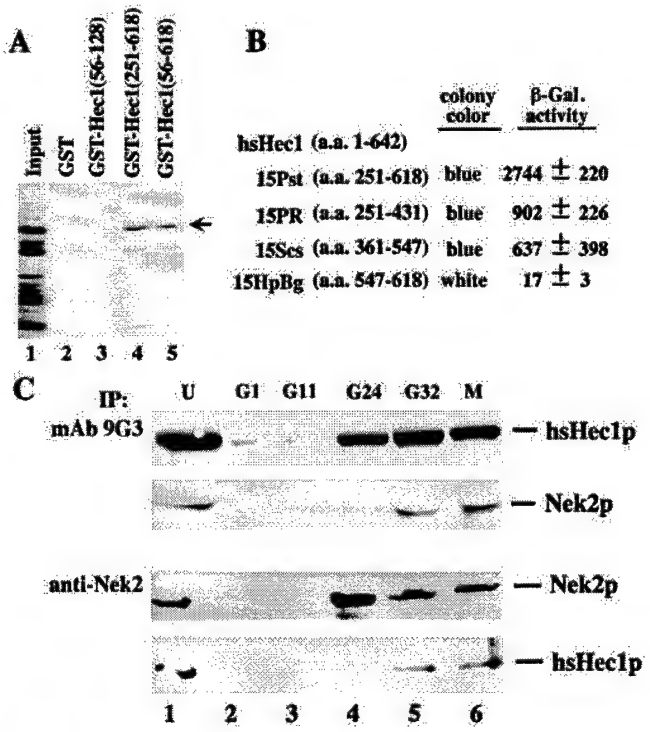

FIG. 2. **Interaction between Nek2 and Hecl by GST pull-down assay.** *A*, Sepharose beads bound with purified GST (*lane 2*) and GST fusions of Hec1 containing amino acids 56–642 (*lane 3*) or 251–618 (*lane 4*) were mixed with *in vitro* translated, [^{35}S]methionine-labeled Nek2 (*lane 1*) and then washed extensively. The binding complexes were separated by SDS-PAGE, dried, and visualized by autoradiography. *B*, specific regions of Hec1 bind to Nek2 by yeast two-hybrid assay. Deletion mutants containing the different coiled-coil domains of Hecl were fused in frame to a GAL4 DNA binding domain. Nek2 was expressed as a GAL4 transactivation domain fusion. Yeast transformants with these two hybrid proteins were grown in liquid cultures and used for *O*-nitrophenyl-β-galactopyranosidase quantification of β-galactosidase activity. The -fold increase in activity compared with the host yeast strain Y153 is indicated. Assays were performed in triplicate for each transformation. *C*, cell cycle-dependent interaction between Hecl and Nek2. T24 bladder carcinoma cells were first density-arrested at G_1 (*lanes 2*) and then released for reentry into the cell cycle. At different time points after release from density arrest (indicated *above* the *lanes*), cells were collected and lysed. The clarified lysates were immunoprecipitated with mAb9G3 anti-Hecl monoclonal antibodies (*upper two panels*) or anti-Nek2 antisera (*lower two panels*). Hecl and Nek2 co-immunoprecipitated at G_2 and M phases (*lanes 5* and *6*).

300 mM NaCl. The fractions from the SP Sepharose column were loaded onto a nickel-Sepharose column (Amersham Biosciences) and eluted with 60 mM imidazole. The Hec1 protein was fractionated by Sephadex 300 to obtain purified protein.

Expression of His-tagged Nek2 in a Baculovirus System—Full-length Nek2 was fused in-frame to His_6 and expressed in a baculovirus system as described (30). 36 h after infection, the infected Sf9 cells were lysed and immunoprecipitated with anti-Nek2 antisera. The resulting immune complexes were used in kinase assays.

In Vitro Kinase Assay—Immunoprecipitated recombinant Nek2 was washed with Lysis 250 buffer five times, followed by washing twice with Tris-buffered saline (10 mM Tris-HCl, pH 7.4, 20 mM NaCl) and once with distilled H_2O. The kinase reactions were carried out for 20 min at 37 °C in Nek2 kinase buffer (0.5 M Hepes, pH 7.5, 50 mM $MnCl_2$, 50 mM NaF, 50 mM β-glycerol phosphate, 10 μM okadaic acid, 10 μg/ml heparin sulfate, 40 μM ATP, and 10 mM dithiothreitol) supplemented with 10 μCi of [γ-^{32}P]ATP. Purified Hec1 proteins (5 μg) were added to the kinase reactions as described (20). Kinase reactions were stopped by adding 2× SDS sample buffer, and proteins were separated by SDS-PAGE. The resulting gel was dried and autoradiographed.

Phosphoamino Acid Analysis—T24 cells were labeled with [^{32}P]orthophosphoric acid for 2 h, followed by immunoprecipitation with mAb 9G3 anti-Hec1 antibody. Immune complexes were separated by SDS-PAGE and transferred to Immobilon-P membrane. Phosphoamino acid analysis was performed as described (31).

Antibody Production—For production of anti-Nek2 antibody, cDNA encoding aa 235–399 of Nek2 was fused to glutathione *S*-transferase (GST) in frame. Purified GST-Nek2 fusion protein was used as antigen to immunize a mouse to produce mouse polyclonal anti-Nek2 antisera. For the anti-scNek2/Kin3 antibody, cDNA encoding full-length scNek2/Kin3 was fused to GST in frame; the fusion protein was purified and used as an antigen. Anti-Hec1 and anti-scHec1 antibodies have been described (1, 3). For anti-phosphorylated Hec1 antibody, a synthetic phosphopeptide (A439; Fig. 3*A*) was coupled to keyhole limpet hemacyanin (KLH) and used as antigen.

RESULTS

HEC1 Is a Serine Phosphoprotein, and Its Phosphorylation Is Cell Cycle-dependent—To explore a potential mechanism by which Hec1 is regulated, we tested whether Hec1 is modified by phosphorylation. T24 cells were labeled with either [^{35}S]methionine or ^{32}P-orthophosphate and lysed. The lysates were immunoprecipitated with polyclonal anti-Hec1 serum, monoclonal anti-Hec1 antibodies (mAb9G3), or preimmune serum and then separated by SDS-PAGE. The 76-kDa Hec1 protein recognized by both polyclonal and monoclonal 9G3 antibodies was labeled by ^{32}P (Fig. 1*A*, *lanes 5* and *6*), showing Hec1 to be a phosphoprotein. Phosphoamino acid analysis showed Hec1 to be phosphorylated only on serine residues (Fig. 1*B*). To determine the cell cycle dependence of Hec1 phosphorylation, T24 cells released from density arrest at G_0 phase for different

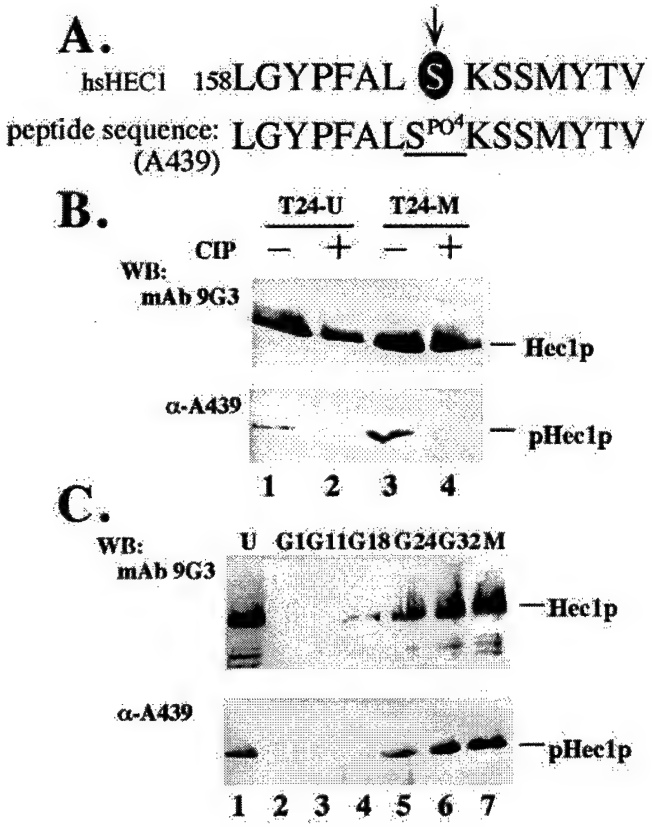

FIG. 3. **Hec1 is phosphorylated on serine 165 *in vivo*.** *A*, potential Nek2 recognition sequence including serine 165 of human Hec1 (hs-Hec1) and the chemically synthesized phosphopeptide (A439) used as antigen for generating specific antibodies. *B*, anti-A439 antibodies specifically recognize phosphorylated Hec1. T24 cells, either unsynchronized (T24-U, *lanes 1* and *2*) or treated with nocadozole to arrest them at G_2/M (T24-M, *lanes 3* and *4*), were lysed and immunoprecipitated with mAb 9G3. The immunoprecipitates were not treated (*lanes 1* and *3*) or treated with calf intestine phosphatase (*CIP*) (*lanes 2* and *4*), separated by SDS-PAGE, and subjected to Western blotting probed with mAb 9G3 (*upper panel*) or anti-A439 antibodies (*lower panel*). Anti-A439 antibodies recognized the untreated but not calf intestine phosphatase-treated Hec1. *C*, expression of the phosphorylated Hec1 detected by anti-A439 antibodies during cell cycle progression. T24 cells in different synchronized stages of the cell cycle were prepared as described above. Hec1 was detected by straight Western blotting with either mAb 9G3 (*upper panel*) (*G11*, 11 h after release for G_1; *G18*, 18 h after release for G_1/S; *G24*, S phase; *G32*, G_2/M phase) or anti-A439 antibodies (*lower panel*).

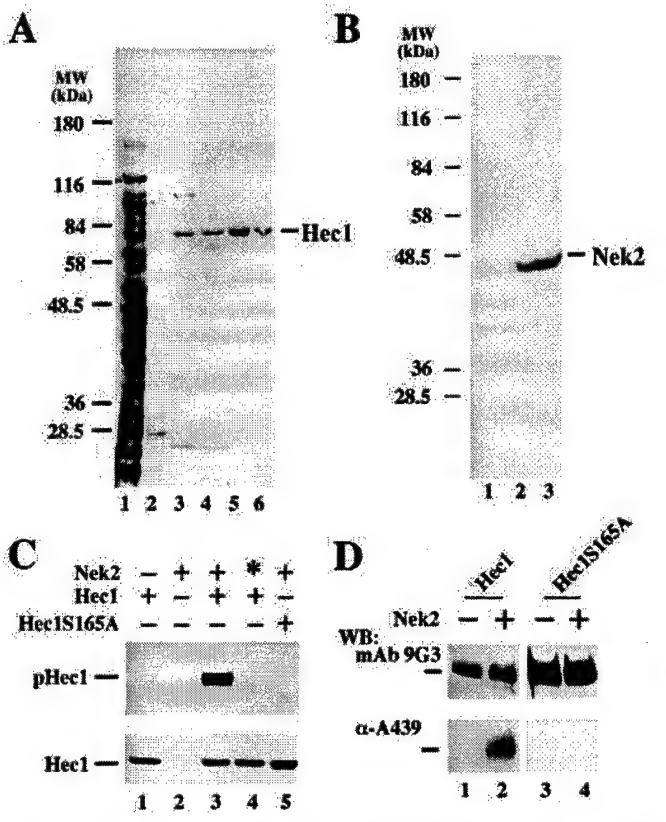

FIG. 4. **Nek2 phosphorylates Hec1 *in vitro*.** *A*, purification of His-tagged Hec1. His_6-tagged full-length Hec1 was expressed in *E. coli* using the PET expression system (29). The total bacterial lysate (*lane 1*) was passed through a DEAE-Sepharose column, and the flow-through (*lane 2*) was then bound to an SP Sepharose column. Hec1 eluted with NaCl gradient fractions between 200 and 300 mM. The eluant was then loaded onto a nickel-Sepharose column and eluted with 60 mM imidazole (*lane 4*). This eluant was loaded onto a Sephadex 300 column (*lane 5*) to obtain nearly pure Hec1. Hec1 from different steps of the purification was subjected to SDS-PAGE and then stained with Coomassie Blue. Hec1S165A was purified by an identical scheme; the final purified product is shown in *lane 6*. *B*, expression of His-tagged Nek2 in a baculovirus system. Baculovirus carrying the His_6 full-length Nek2 was generated as described (30). Cell lysates from infected (*lanes 2* and *3*) or uninfected (*lane 1*) Sf9 cells were probed with anti-Nek2 antibodies to demonstrate the specificity of the anti-Nek2 antibodies. The antibodies specifically recognize the recombinant Nek2 protein but not proteins from uninfected Sf9 cells. *C*, Nek2 phosphorylates Hec1. Kinase reactions were performed with [γ-^{32}P]ATP to assess the activity of immunopurified Nek2 kinase, using either wild-type Hec1 (*lane 3*) or Hec1S165A mutant (*lane 5*) as the substrate. Additional control reactions carried out either by using preimmune antisera to purify the Nek2 (*lane 1*), heat-inactivated Nek2 (*lane 4*), or without substrate (*lane 2*) failed to detect radioactively labeled Hec1 protein. *D*, anti-A439 antibodies recognize Hec1 phosphorylated *in vitro* by Nek2. Purified Hec1 or Hec1S165A was either left unphosphorylated (*lanes 1* and *3*) or phosphorylated with Nek2 (*lanes 2* and *4*), using cold ATP, and analyzed by Western blotting with either mAb 9G3 antibody (*upper panel*) or anti-A439 (*lower panel*). Phosphorylated Hec1 was detected by anti-A439.

periods of time were labeled with [^{32}P]orthophosphate and analyzed. The phosphorylation of Hec1 began during time periods corresponding to S phase and was most prominent during M phase (Fig. 1*C*). These results showed Hec1 to be phosphorylated on serine residues by a cell cycle-regulated serine kinase.

Hec1 Binds to Nek2 Specifically at G_2/M Phase—A candidate kinase for phosphorylating Hec1 is Nek2, which we found in a yeast two-hybrid screen to be a specific interacting protein (1). The binding of Hec1 with Nek2 was further established using GST pull-down assays (Fig. 2*A*). *In vitro* translated Nek2 interacted with the carboxyl-terminal portion of Hec1 (aa 251–618). Using Hec1 deletion constructs and yeast two-hybrid assays, we found that Hec1 interacts with Nek2 via the first (aa 251–431) or second (aa 361–547) coiled-coil domain (Fig. 2*B*).

To determine the cell cycle specificity of the Hec1-Nek2 interaction in living cells, T24 cells released from density arrest at G_0 phase were collected at various subsequent time points. Proteins from cell lysates were immunoprecipitated with either anti-Nek2 serum or with mAb 9G3, which recognizes Hec1. The expression of both Hec1 and Nek2 was regulated during progression of the cell cycle (Fig. 2*C*). Co-immunoprecipitation of Nek2 and Hec1 occurred specifically during G_2 and M phases (Fig. 2*C*, *lanes 5* and *6*). The initiation of Hec1 phosphorylation (Fig. 2*C*, G24, *lane 6*) corresponded to the same time period during which Nek2 was most abundant (Fig. 2*C*, *lane 4*), suggesting that Nek2 may phosphorylate Hec1 *in vivo* during G_2/M phase.

Phosphorylation of Hec1 on Serine 165 in Vivo—We noted that Hec1 has a potential phosphorylation site at serine 165 for both NimA and Nek2 (16, 20, 32) (Fig. 3*A*). To test whether Ser^{165} of Hec1 is the authentic site phosphorylated by Nek2, an

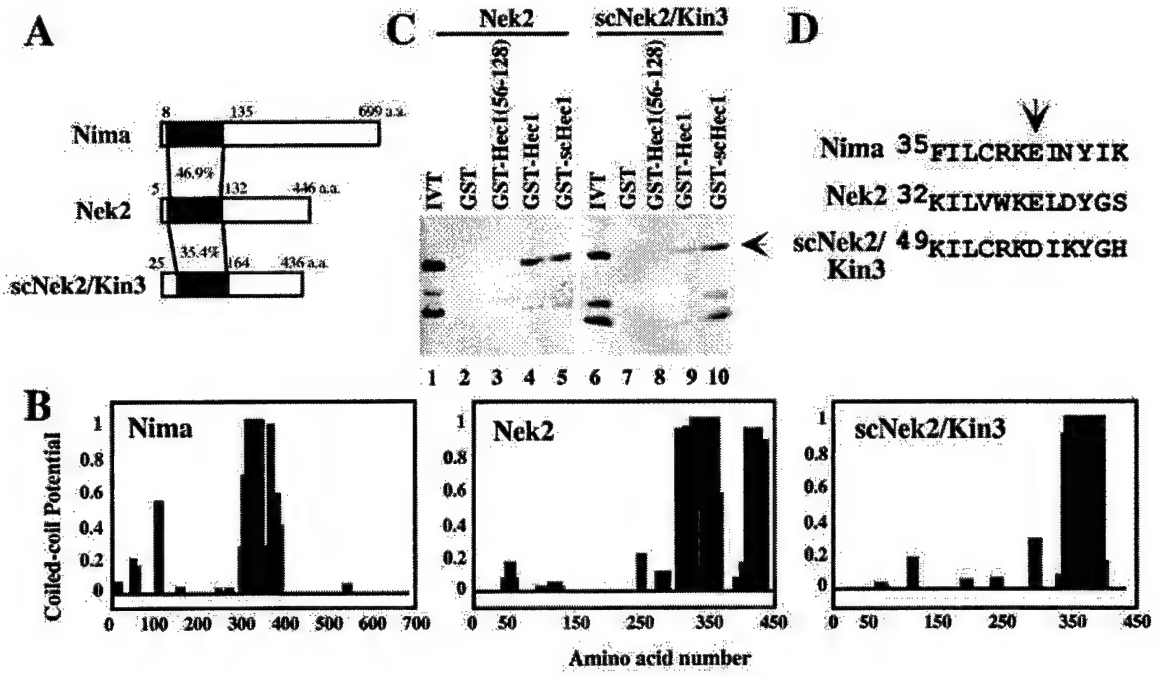

FIG. 5. **Yeast Kin3 shares properties with Nek2.** *A*, primary sequence homology comparison between NimA, Nek2, and scNek2/Kin3. *B*, comparison of the potential coiled-coil regions in NimA, Nek2, and scNek2/Kin3, predicted from primary sequences using a program found on the World Wide Web at www.isrec.isb-sib.ch/software/software.html. *C*, Nek2 or scNek2 binds to hsHec1 and scHec1 by GST pull-down assay. GST (*lanes 2* and *7*), GST fusions of a small N-terminal hsHec1 (GST-Hec1 aa 56–128) (*lanes 3* and *8*), a longer portion of hsHec1 (aa 56–618, GST-Hec1) (*lanes 4* and *9*), and a full-length of scHec1 (aa 1–691, GST-scHec1) (*lanes 4* and *8*) were prepared and used to bind to *in vitro* translated human Nek2 (*lane 1*) or scNek2/Kin3 (*lane 6*). Human Nek2 and scNek2/Kin3 both bind to hsHec1 and scHec1. *D*, partial sequence of NimA showing the glutamic acid residue at amino acid position 41. Comparison of homologous sequences in Nek2 and scNek2/Kin3, with glutamic acid at amino acid residue 38 (Nek2) and aspartic acid at amino acid residue 55 (scNek2/Kin3), is also shown.

antibody specifically recognizing a synthesized Hec1 phosphopeptide (Fig. 3*A*) was generated and used to examine the expression of phosphorylated Hec1 (Fig. 3*B*). Lysates from T24 cells, from cells synchronized at M phase, and from an unsynchronized population were immunoprecipitated with anti-Hec1 antibodies. The anti-A439 antibody recognized the phosphorylated form of Hec1 but did not recognize the unphosphorylated form from lysates treated with calf intestine phosphatase (Fig. 3*B*). In contrast, interaction between Hec1 and mAb 9G3 recognized both phosphorylated and unphosphorylated forms of Hec1 and was not affected by phosphatase treatment (Fig. 3*B*). The phosphorylated form of Hec1 was detected most abundantly by anti-439 in the lysates enriched for mitotic cells (Fig. 3*C*, *lane 3*). This finding is consistent with the ^{32}P labeling experiment shown in Fig. 1*C*, in which the phosphorylated form of Hec1 was most abundant at the G_2/M phase. Together, the results suggest that human Hec1 is phosphorylated on serine 165 *in vivo*.

Nek2 Phosphorylates Hec1 in Vitro—To determine whether Nek2 phosphorylates Hec1 directly, His-tagged, wild-type Hec1 and a specific human Hec1 mutant (hsHec1S165A) changing the putative Nek2 phosphorylation site at serine 165 into a neutral amino acid, alanine, were then expressed and purified to near homogeneity using a PET expression system (Fig. 4*A*). His-tagged Nek2 was expressed in a baculovirus system and immunopurified using anti-Nek2 antibodies (Fig. 4*B*). Kinase reactions were then performed using purified Hec1 and hsHec1S165A mutant as substrates. Nek2 phosphorylated wild-type Hec1 (Fig. 4*C*, *lane 3*) but not hsHec1S165A (*lane 5*). Proteins immunoprecipitated by nonspecific, preimmune antibodies (Fig. 4*C*, *lane 1*) or intentionally heat-inactivated Nek2 (Fig. 4*C*, *lane 4*) failed to phosphorylate Hec1. Furthermore, anti-A439 recognized the phosphorylated form of wild-type Hec1 (Fig. 4*D*, *lane 2*) but not the hsHec1S165A mutant even after the kinase reaction (Fig. 4*D*, *lanes 3* and *4*). Anti-A439 did not recognize the unphosphorylated form of wild-type Hec1 (Fig. 4*D*, *lane 1*). These results confirmed the residue on which Nek2 kinase phosphorylates human Hec1 is serine 165.

Yeast Kin3 Shares Similar Properties with Nek2—Human Hec1 (hsHec1) has a structural and functional homolog in yeast, scHec1/TID3/NDC80/YIO4, and is required for faithful chromosome segregation (3). Since Hec1 is specifically phosphorylated at the G_2 and M phases, phosphorylation of Hec1 by Nek2 may be critical for chromosome segregation. To address this possibility, a yeast model system was employed because well established methods are available to assay chromosome segregation (2, 3, 28, 37). However, we first needed to identify a homolog of Nek2 in yeast that may phosphorylate scHec1. There is an open reading frame in the *S. cerevesiae* genome, *Kin3/scNek2*, which encodes a putative protein and could function as a serine/threonine kinase (23, 24). This protein shares relatively high homology (36.4% identity) with NimA and human Nek2 in the catalytic domain (Fig. 5*A*) and contains a coiled-coil domain in its C-terminal region that is similar to the same domains in the other two proteins (Fig. 5*B*). To test whether these C-terminal regions share similar abilities to physically interact with hsHec1p or scHec1p, Nek2p and scNek2p were synthesized *in vitro* for GST pull-down assays with both GST-hsHec1 and GST-scHec1. Nek2p and scNek2p could bind both human and yeast Hec1p (Fig. 5*C*). These results suggested that scNek2 and Nek2 not only share homology at their N-terminal kinase domain sequences but that they also both have Hec1 binding activity at their C-terminal regions.

Changing glutamic acid 41 of NimA into glycine leads to a temperature-sensitive growth phenotype that arrests the cells in the G_2 phase at the nonpermissive temperature (8, 9). Interestingly, similar acidic residues have been found by other researchers to be highly conserved in the other kinases: residue

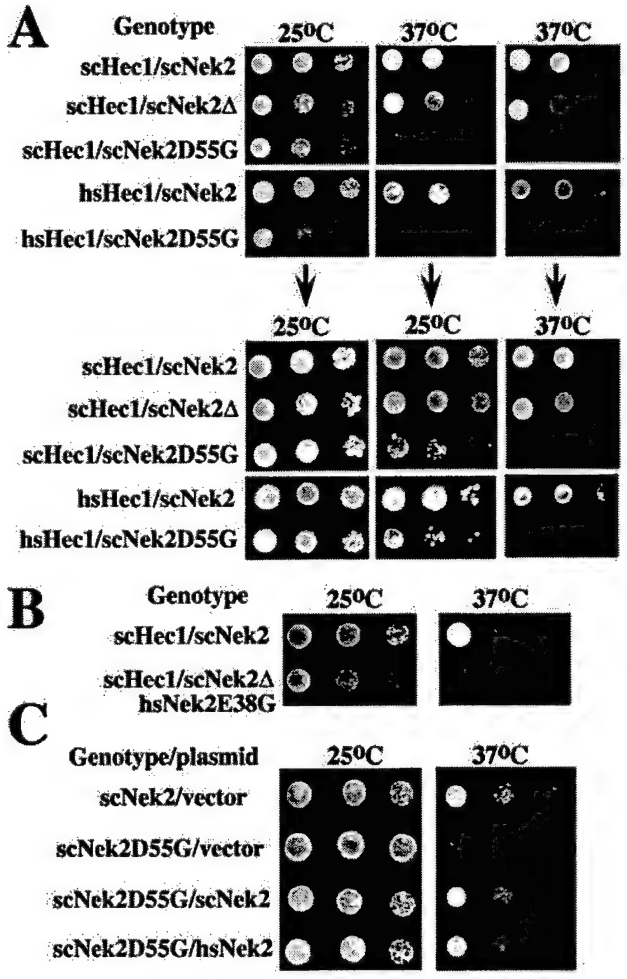

FIG. 6. **Growth properties of the scNek2D55G mutant.** *A*, temperature-sensitive growth of yeast strain carrying scNek2D55G. Yeasts were spotted on triplicate plates and grown at two different temperatures. One of the plates originally maintained at 37 °C was shifted to room temperature (25 °C). Both strains carrying the scNek2D55G mutation were reversibly temperature-sensitive. The growth of these mutant strains was temperature-dependent regardless of the Hec1 status. The ΔscNek2 mutant grew like the wild-type strain. *B*, expression of the Nek2E38G mutant in the ΔscNek2 mutant leads to temperature-sensitive growth. Nek2E38G was introduced into the ΔscNek2 mutant under control of the scNek2 promoter in a CEN.ARS construct to create strain Nek2E38G. The growth of this mutant strain was temperature-sensitive. *C*, overexpression of wild type scNek2 or hsNek2 partially suppressed the temperature sensitivity of the scNek2D55G mutant strain.

38 (glutamic acid) in Nek2 (19), and residue 55 (aspartic acid) in scNek2 (23, 24) (Fig. 5*D*). To test the functional similarity of these key regions among the kinases, glutamic acid 38 of Nek2 and aspartic acid 55 of scNek2 were each changed to glycine. Like the temperature-sensitive *nima* mutant (8, 9), the scNek2D55G mutant grew at 25 °C, arrested at 37 °C, and reentered the cell cycle when shifted back to the 25 °C (Fig. 6*A*). When the Nek2E38G mutant was introduced into scNek2 null cells, growth and propagation of the cells was temperature-sensitive as well (Fig. 6*B*). This temperature-sensitive phenotype was partially suppressed by expression of additional wild-type scNek2 or hsNek2 (Fig. 6*C*). Taken together, these results suggest that scNek2/Kin3 shares several similar functions with hsNek2 and that scNek2/Kin3 might function as an Nek2 homolog in *S. cerevesiae*.

Temperature-sensitive scNek2 Mutant Fails to Phosphorylate Hec1 at the Nonpermissive Temperature—To determine whether scNek2D55G may behave in a dominant negative fashion to arrest cells at nonpermissive temperature, we first generated specific antibodies and examined the physical interaction between scNek2p and scHec1p or scNek2p and hsHec1p, using co-immunoprecipitation (Fig. 7, *A* and *B*). In cells carrying the scNek2D55G mutant, the interaction between scNek2p and scHec1p or scNek2p and hsHec1p (Fig. 7, *C* and *D*) was intact, as it was in wild-type scNek2 cells (Fig. 7, *C* and *D*). Moreover, the phosphorylation of hsHec1p on serine 165 was detected by anti-A439, both in wild-type and in scNek2D55G mutant cells at the permissive temperature, but not in scNek2D55G mutant cells at the nonpermissive temperature (Fig. 7*E*). These results suggest that phosphorylation of Hec1 by scNek2p is essential for cells to continue cycling. scNek2D55G thus appears indeed to be a dominant negative mutant; it can bind to Hec1 but cannot phosphorylate it.

Phosphorylation of hsHec1 Serine 165 Is Critical for Its Function in Chromosome Segregation—To examine whether the phosphorylation of human Hec1 (hsHec1) on serine 165 is important for hsHec1 to function, yeast strains containing specific hsHec1 mutations were created. The homolog of human Hec1 in *S. cerevesiae* (scHec1/TID3/NDC80/YIO4) has been characterized extensively and shown, like its mammalian counterpart, to be essential for chromosome segregation and yeast survival (3, 6). Furthermore, hsHec1 can complement the essential functions of scHec1 (3). Mutant constructs were created in which the critical serine residues phosphorylated by Nek2 in scHec1 (Ser^{201}) and hsHec1 (Ser^{165}) were mutated. scHec1S201A and hsHec1S165A substituted the neutral amino acid alanine for serine; scHec1S201E and hsHec1S165E substituted glutamic acid for serine to mimic the negative charge created by serine phosphorylation (Fig. 8*A*). To test whether these Hec1 mutants could complement scHec1 deficiency, they were introduced into the scHec1 null yeast strain. Both scHec1S201E and Hec1S165E were able to rescue yeast deficient in scHec1, but the scHec1S201A and hsHec1S165A mutants were not (Fig. 8*B*). These results suggest that phosphorylation of serine 165 (or serine 201 in yeast Hec1) is important for the function of Hec1.

To determine whether substituting glutamic acid for serine 165 in hsHec1 could rescue all essential functions of Hec1 in yeast, plating efficiency and chromosome segregation were examined in *schec1* null yeast rescued by either wild-type hsHec1 or hsHec1S165E. The plating efficiency of the schec1Δ/hsHec1S165E strain was only 75% of the efficiency for the strain rescued by wild-type hsHec1 (Fig. 8*C*). This result suggested that the hsHec1S165E mutant was not fully functional in allowing faithful mitosis. To address this possibility, colony sectoring assays (2, 3, 28) were performed in the two yeast strains to monitor chromosome segregation. Yeast cells null for *scHec1* and rescued by the *hsHec1S165E* were 10 times more prone to segregation errors, especially chromosome loss (1:0) events, compared with cells rescued by wild-type hsHec1 (Table II). Yeast cells lacking scNek2, although viable, were thought to have subtle errors in chromosomal segregation. To test this hypothesis directly, *scNek2* null cells were examined by colony sectoring assays. They were found to have 50-fold higher rates of errors of chromosomal losses (1:0 events) and 6-fold higher rates of nondisjunction (2:0 events) (Table II). Taken together, the results suggest that precisely regulated phosphorylation of Hec1 by Nek2 is critical for accurate chromosome segregation during mitosis.

DISCUSSION

In this paper, we have shown that Hec1 binds to Nek2 both *in vitro* and *in vivo* at G_2/M phase. Nek2 specifically phosphorylates human Hec1 on serine residue 165 in a cell cycle-dependent manner, with a peak activity during G_2/M. The phos-

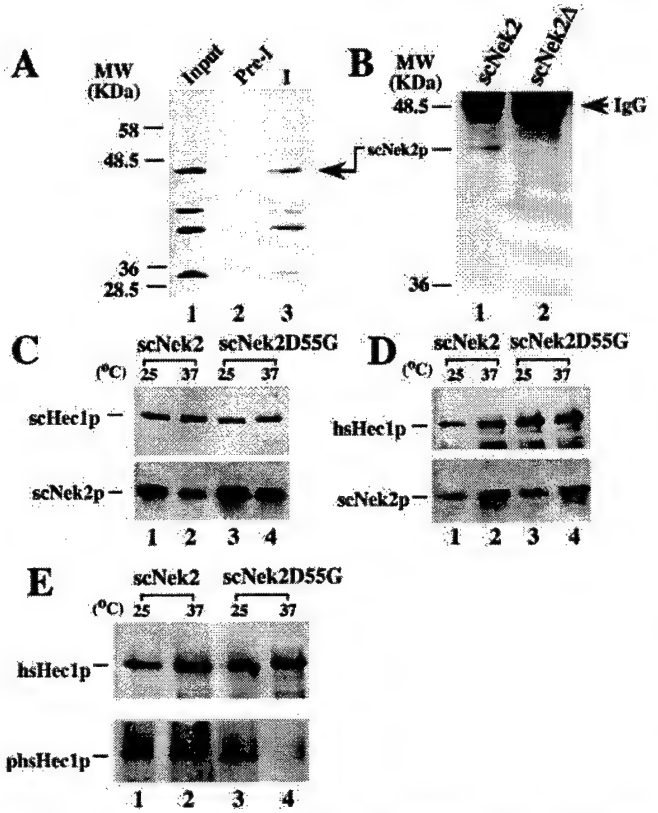

FIG. 7. **Phosphorylation of Hec1 by Nek2.** *A* and *B*, production and specificity of anti-scNek2 antibodies. Full-length *scNek2/Kin3* cDNA was fused to GST in frame, and the resulting GST-scNek2 fusion protein was used to immunize mice. After several boosts, anti-scNek2 antisera were collected and used to immunoprecipitate *in vitro* translated full-length scNek2 protein. Preimmune serum failed to immunoprecipitate *in vitro* translated scNek2 (*A*, *lane 2*), whereas immune serum was able to immunoprecipitate it (*A*, *lane 3*). Detection of scNek2 from wild-type yeast cells using anti-scNek2 serum identified scNek2 as a 46-kDa protein (*B*, *lane 1*). The anti-scNek2 serum was specific for scNek2, since it failed to detect scNek2 in lysate prepared from scNek2 null cells (*B*, *lane 2*). *C*, scHeclp and scNek2 interact at nonpermissive temperature. Wild-type or scNek2D55G mutant strains were grown at 25 °C for 4 h before shifting to 37 °C for an additional 8 h. The cells were harvested and lysed for immunoprecipitation with anti-scHec1 antibodies (*lanes 1–4*) and Western blotted with anti-scHeclp antisera (*upper panel*) or anti-scNek2p antisera (*lower panel*). scHeclp interacts with scNek2p at permissive and nonpermissive temperature in both wild-type and scNek2D55G cells. *D*, interaction between hsHecl and scNek2 at nonpermissive temperature in cells carrying the scNek2D55G mutation. scHec1 null cells rescued by hsHec1 in scNek2 or scNek2D55G mutant background were cultured as described for *C*. Clarified lysates were immunoprecipitated with anti-hsHec1 mAb 9G3 antibodies (*lanes 1–4*) and Western blotted with anti-Hec1p mAb 9G3 antibodies (*upper panel*) or anti-scNek2p antisera (*lower panel*). hsHeclp interacted with scNek2p at permissive and nonpermissive temperatures in both yeast strains. *E*, phosphorylation of Hecl is abolished at nonpermissive temperature in scHec1 null cells rescued by hsHec1 in the scNek2D55G mutant. Cells were prepared as described for *C*. The cells were harvested and lysed in the presence of phosphatase inhibitors. The clarified lysates were immunoprecipitated with mAb 9G3 and Western blotted with mAb 9G3 (*upper panel*) or monoclonal anti-A439 antibodies (*lower panel*). hsHec1 was not phosphorylated in scNek2 mutant cells at the nonpermissive temperature.

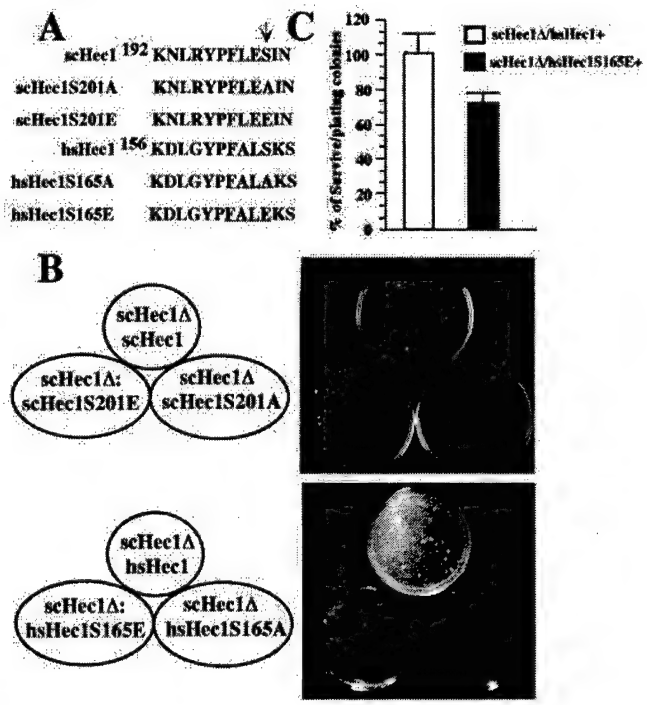

FIG. 8. **Phosphorylation of Hecl by Nek2 is critical for yeast survival.** *A*, Hec1 phosphorylation sites for Nek2. The potential Nek2 Ser phosphorylation sites in scHec1 (Ser^{201}) and hsHec1 (Ser^{165}) were mutated to Ala (S201A,S165A) or Glu (S201E,S165E) (37). *B*, both scHec1S201A and hsHeclS165A failed to rescue cells null for scHec1. Only wild type scHec1 or hsHec1 and the scHec1S201E and hsHec1S165E mutants, in which glutamic acid substitution for serine mimics the negative charge created by serine phosphorylation, were able to rescue yeast deficient for scHecl. *C*, plating efficiency of yeast rescued by wild-type hsHec1 or by hsHeclS165E. Two hundred cells from log phase cultures were plated onto solid plates. The surviving cells were scored for colonies formed on plates after 3 days in culture at 30 °C. The results are shown as means ± S.E. from three independent experiments.

phorylation of Hec1 is necessary for faithful chromosome segregation and cell survival. Nek2 appears to be the primary kinase responsible for Hec1 phosphorylation, and scNek2/Kin3 is a functional homolog of Nek2 in yeast.

The Role of Hec1 in Chromosome Segregation Is Highly Conserved—Hec1, a coiled-coil protein highly expressed in most cancer cells, is crucial for faithful chromosome segregation. Cells microinjected with anti-Hec1 antibodies undergo aberrant mitosis, with grossly inequitable distribution of chromosomes (1). Furthermore, Hec1 associates with several proteins required for G_2/M phase progression, including components of the 26 S proteasome, Smc1/2, and the NimA-like protein kinase Nek2 (5). Nek2 has significant sequence homology with NimA, a serine/threonine kinase required for passage of fungi past G_2 into M phase, exit from M phase, and response to DNA damage (9). To facilitate analysis of the function of Hec1, a yeast homolog scHec1 has been identified and characterized (3, 6). scHec1/NDC80 is essential for yeast survival and plays an important role in chromosome segregation. Moreover, human hsHec1 can serve all essential functions in *S. cerevesiae* null for *scHec1*, suggesting that fundamental mechanisms governing chromosome segregation are highly conserved in evolutionarily divergent species (3).

G_2/M Phase-specific Regulation of Hec1 by Phosphorylation—Regulation of proteins involved in cell cycle progression must occur rapidly and precisely. Such regulation is especially important during the dynamic processes of mitosis, during which replicated chromosomes must align and distribute equally between daughter cells. The many proteins involved in mitosis must be activated and deactivated during a very narrow time window. Phosphorylation is an excellent way to achieve such precise regulation. We have shown here that yeast strains carrying scHec1S201A or hsHec1S165A mutations, which cannot be phosphorylated by Nek2, are unable to rescue the lethal phenotype in scHec1-deficient yeast. Furthermore, an hsHec1S165E mutation that mimics constitutive phosphorylation of Hec1 can only partially rescue faithful chromosome segregation and subsequent viability of daughter cells.

TABLE II

Increased chromosome segregation errors

Yeast cells null for scHec1 and rescued by the hsHec1S165E mutant (strain WHL4001) were susceptible to segregation errors, which were monitored by sectoring assays (2). Chromosome loss errors (1:0) in these hsHec1S165E mutant cells were especially prominent compared with wild-type cells (strain WHL2003) or scHec1 null cells rescued by wild-type hsHec1 (strain WHL4003). Yeast cells without scNek2 (strain WHL6502) had a much higher incidence of chromosome segregation errors compared to cells rescued by wild-type hsHec1 or hsHec1S165E. NS, not significant.

Yeast strain	Genotype	Total colony number	Chromosome segregation events			
			1:0	Significance *versus* weight	2:0	Significance *versus* weight
WHL2003[a]	scHEC1/scHEC1 scNek2/scNek2	10,021	2 (0.02%)		1 (0.01%)	
WHL4003	Δschec1/Δschec1 hsHEC1/hsHEC1 scNek2/scNek2	10,483	2 (0.02%)	X^2 = 0.00203 (NS)	2 (0.02%)	X^2=0.290(NS)
WHL4001	Δschec1/Δschec1 hsHEC(S165E)/ hsHEC1(S165E) scNek2/scNek2	5,748	8 (0.14%)	X^2 = 8.54 (p = 0.0035)	1 (0.02%)	X^2=0.159(NS)
WHL6502	scHEC1/scHEC1 ΔscNek2/ΔscNek2	6,770	502 (7.42%)	X^2 = 756 (p < 0.0001)	4 (0.06%)	X^2=1.83(NS)

[a] Adapted from Ref. 3.

Thus, phosphorylation of Hec1 must be tightly regulated and coordinated along with the cell cycle progression.

Hec1 Is a Substrate of Nek2—Specific phosphorylation during G_2/M is required for Hec1 to function properly and for chromosome segregation to occur faithfully. Our studies have clearly shown Hec1 to be an authentic substrate of Nek2. Failure of Nek2 to phosphorylate Hec1 during G_2/M leads to errors in segregation of chromosomes. Another potential substrate of Nek2, C-Nap1, localizes to centrioles in both mother and daughter cells and has coiled-coil structures appropriate for other protein-protein interactions (33). The structure of C-Nap1 might allow it to connect proximal ends of centrioles to each other, although this concept at present remains speculative (33). Nevertheless, it is interesting to note that both Nek2 substrates, C-Nap1 and Hec1, localize either to centrioles or kinectochores (1, 3, 6, 21). They are therefore positioned precisely at the mitotic apparatus, along with the machinery responsible for chromosome segregation.

Potential Redundant Kinases for Hec1—scNek2/Kin3 has been purported to be the homolog of Nek2 and NimA because the three proteins have significant structural similarities. However, complete deletion of *scNek2* had little influence on yeast survival and led to some suggestions that scNek2 may be functionally different from NimA in fungi. The scNek2D55G mutant in our experiments was generated specifically to mimic the characterized NimA mutants. The growth of cells carrying this scNek2D55G mutant arrested at the nonpermissive temperature, similar to the homologous *nima* mutant. Interestingly, the physical association between Hec1 and scNek2D55G or Nek2E38G remained intact at any temperature, although the kinase activity of the mutants, and therefore their ability to phosphorylate Hec1, was temperature-sensitive. Hec1 appears to be a crucial substrate of Nek2, and the phosphorylation of Hec1 by Nek2 is required for passage through mitosis and for faithful chromosome segregation. These results support the notion that *scNek2/Kin3* is an important gene in yeast with functions similar to *Nek2*.

Surprisingly, a complete lack of Nek2 was not lethal in yeast; another kinase was apparently able to supplant the function of Nek2 in phosphorylating Hec1. To reconcile the apparent paradox of these observations (*i.e.* that precisely phosphorylated Hec1 is essential for yeast mitosis but that the kinase responsible for the phosphorylation is not), the existence other kinases with functions redundant for Nek2 must be postulated. Cdc5, based on its structural similarity with Nek2 and cell cycle expression pattern (34–36), is a potential candidate. A search of GenBank™ showed that Cdc5 shares 35% similarity with NIMA, Nek2, and scNek2/Kin3 in the catalytic domain and, like Nek2, contains a coiled-coil domain near the catalytic domain. Our preliminary results have shown that Cdc5 phosphorylates Hec1 *in vitro* and specifically associates with Hec1 only when Nek2 is unavailable (data not shown). However, Cdc5 seems to have lower affinity for binding to Hec1. It is particularly interesting that the temperature-sensitive scNek2/Kin3 mutants bind to Hec1 but fail to phosphorylate it at the nonpermissive temperature. These preliminary results suggest that binding and kinase activity are two distinct and potentially independent steps in the activation of Hec1 by Nek2. scNek2D55G thus serves as a dominant negative mutant that binds to Hec1 at the nonpermissive temperature. The secondary kinase, perhaps Cdc5, may fail to compete successfully for binding in the presence of wild-type or mutant Nek2. Cells carrying the dominant negative Nek2 mutation are markedly prone to segregation errors, however, particularly chromosomal losses (1:0 errors), perhaps because the redundant kinase for Hec1 is less efficient or less precisely regulated than Nek2. These data provide a reasonable explanation for why yeast cells completely lacking scNek2 are viable but those with the scNek2D55G mutation are growth-arrested at the nonpermissive temperature.

Implications in Higher Organisms and in Cancer—We have demonstrated that Hec1 is an important substrate of hsNek2 and scNek2/Kin3. Hec1 is specifically phosphorylated by these kinases, and such phosphorylation is required for faithful chromosome segregation. Without Hec1, chromosomes distribute to daughter cells in a disordered, ultimately lethal fashion. Without precise regulation through phosphorylation of Hec1 by Nek2 during G_2/M phases, more subtle errors in chromosome segregation, similar to those involved commonly in the progression of cancer in humans, are likely. If we can extrapolate findings in yeast to similar systems controlling mitosis in humans, then phosphorylation of Hec1 by Nek2 in mammalian systems may be a focus for exploring chromosomal mechanisms of carcinogenesis and cancer progression. Because of the abundant expression of Hec1 in cancer cells (1), the specific phosphorylation of Hec1 by Nek2 may also be a potential target for drug development in the treatment of cancers.

Acknowledgments—We thank C.-F. Chen, P. Garza, and D. Jones for technical assistance and P. Heiter for several yeast strains.

REFERENCES

1. Chen, Y., Riley, D. J., Chen, P.-L., and Lee, W.-H. (1997) *Mol. Cell. Biol.* **17**, 6049–6056
2. Zheng, L., Chen, Y., Riley, D. J., Chen, P.-L., and Lee, W.-H. (2000) *Mol. Cell. Biol.* **20**, 3529–3537

3. Zheng, L., Chen, Y., and Lee, W.-H. (1999) *Mol. Cell. Biol.* **19,** 5417–5428
4. Hyland, K. M., Kingsbury, J., Koshland, D., and Hieter, P. (1999) *J. Cell Biol.* **145,** 15–28
5. Chen, Y., Sharp, Z. D., and Lee, W.-H. (1997) *J. Biol. Chem.* **272,** 24081–24087
6. Wigge, P. A., Jensen, O. N., Holmes, S., Soues, S., Mann, M., and Kilmartin, J. V. (1998) *J. Cell Biol.* **141,** 967–977
7. Osmani, S. A., Pu, R. T., and Morris, N. R. (1988) *Cell* **53,** 237–244
8. Osmani, S. A., Engle, D. B., Doonan, J. H., and Morris, N. R. (1988) *Cell* **52,** 241–251
9. Osmani, S. A., May, G. S., and Morris, N. R. (1987) *J. Cell Biol.* **104,** 1495–1504
10. Oakley, B. R., and Morris, N. R. (1983) *J. Cell Biol.* **96,** 1155–1158
11. Chen, A., Yanai, A., Arama, E., Kilfin, G., and Motro, B. (1999) *Gene (Amst.)* **234,** 127–137
12. Holland, P. M., Milne, A., Garka, K., Johnson, R. S., Willis, C., Sims, J. E., Rauch, C. T., Bird, T. A., and Virca, G. D. (2002) *J. Biol. Chem.* **277,** 16229–16240
13. Kandli, M., Feige, E., Chen, A., Kilfin, G., and Motro, B. (2000) *Genomics* **68,** 187–196
14. Letwin, K., Mizzen, L., Motro, B., Ben-David, Y., Bernstein, A., and Pawson, T. (1992) *EMBO J.* **11,** 3521–3531
15. Li, M. Z., Yu, L., Liu, Q., Chu, J. Y., and Zhao, S. Y. (1999) *Cytogenet. Cell Genet.* **87,** 271–272
16. Lu, K. P., and Hunter, T. (1995) *Cell* **81,** 413–424
17. Schultz, S. J., Fry, A. M., Sutterlin, C., Ried, T., and Nigg, E. A. (1994) *Cell Growth Differ.* **5,** 625–635
18. Tanaka, K., and Nigg, E. A. (1999) *J. Biol. Chem.* **274,** 13491–13497
19. Schultz, S. J., and Nigg, E. A. (1993) *Cell Growth Differ.* **4,** 821–830
20. Fry, A. M., Schultz, S. J., Bartek, J., and Nigg, E. A. (1995) *J. Biol. Chem.* **270,** 12899–12905
21. Fry, A. M., Meraldi, P., and Nigg, E. A. (1998) *EMBO J.* **17,** 470–481
22. Kim, Y. H. (2001) *J. Arthroplasty* **16,** 730–739
23. Barton, A. B., Davies, C. J., Hutchison, C. A. D., and Kaback, D. B. (1992) *Gene (Amst.)* **117,** 137–140
24. Jones, D. G., and Rosamond, J. (1990) *Gene (Amst.)* **90,** 87–92
25. Schweitzer, B., and Philippsen, P. (1992) *Mol. Gen. Genet.* **234,** 164–167
26. Chen, Y., Farmer, A. A., Chen, C.-F., Jones, D. C., Chen, P.-L., and Lee, W.-H. (1996) *Cancer Res.* **56,** 3168–3172
27. Chen, P.-L., Scully, P., Shew, J.-Y., Wang, J. Y., and Lee, W.-H. (1989) *Cell* **58,** 1193–1198
28. Koshland, D., and Hieter, P. (1987) *Methods Enzymol.* **155,** 351–372
29. Studier, F. W., and Moffatt, B. A. (1986) *J. Mol. Biol.* **189,** 113–130
30. Smith, G. E., Summers, M. D., and Fraser, M. J. (1983) *Mol. Cell. Biol.* **3,** 2156–2165
31. Boyle, W. J., Van Der Geer, P., and Hunter, T. (1991) *Methods Enzymol.* **201,** 110–152
32. Songyang, Z., Lu, K. P., Kwon, Y. T., Tsai, L. H., Filhol, O., Cochet, C., Brickey, D. A., Soderling, T. R., Bartleson, C., Graves, D. J., DeMaggio, A. J., Hoekstra, M. F., Blenis, J., Hunter, T., and Cantley, L. C. (1996) *Mol. Cell. Biol.* **16,** 6486–6493
33. Fry, A. M., Mayor, T., Meraldi, P., Stierhof, Y. D., Tanaka, K., and Nigg, E. A. (1998) *J. Cell Biol.* **141,** 1563–1574
34. Shirayama, M., Zachariae, W., Ciosk, R., and Nasmyth, K. (1998) *EMBO J.* **17,** 1336–1349
35. Charles, J. F., Jaspersen, S. L., Tinker-Kulberg, R. L., Hwang, L., Szidon, A., and Morgan, D. O. (1998) *Curr. Biol.* **8,** 497–507
36. Cheng, L., Hunke, L., and Hardy, C. F. J. (1998) *Mol. Cell. Biol.* **18,** 7360–7370
37. Kunkel, T. A. (1985) *Proc. Natl. Acad. Sci. U. S. A.* **82,** 488–492

Retinoblastoma Tumor Suppressor and Genome Stability

Lei Zheng and Wen-Hwa Lee*

Department of Molecular Medicine/Institute of Biotechnology, University of Texas Health Science Center at San Antonio, San Antonio, Texas 78245

Retinoblastoma gene (Rb) is the prototype of tumor suppressors. Germline mutation in the retinoblastoma gene is susceptible to cancer and reintroduction of wild-type Rb is able to suppress neoplastic phenotypes. The fundamental cellular functions of Rb in the control of cell growth and differentiation are important for its tumor suppression. In general, cancer susceptibility caused by inactivation of a tumor suppressor gene results from genome instability. Accordingly, Rb may function in the maintenance of chromosome stability by influencing mitotic progression, faithful chromosome segregation, and structural remodeling of mitotic chromosomes. Rb is also implicated in the regulation of replication machinery and in the control of cell cycle checkpoints in response to DNA

*Corresponding author: W.-H. Lee, Tel: 210-567-7351, Fax: 210-567-7377, e-mail:leew@uthscsa.edu

damage, further supporting such a role for Rb. Moreover, the mechanistic basis for Rb-mediated transcriptional repression has revealed its connection to global chromatin remodeling. It is likely that Rb suppresses tumor formation by virtue of its multiple biological activities, and a theme throughout its multiple cellular functions is its central role in controlling activities that involve chromatin remodeling. A model in which Rb controls global genome fluidity is thus proposed. Finally, a recent study provides direct evidence indicating that loss of Rb function leads to genome instability. Therefore, tumor suppressors have a common role in the maintenance of genome stability, and such a role may be pivotal for their functions in tumor suppression.

I. INTRODUCTION

Genetic factors play a fundamental role in the genesis of cancer. The existence of a class of genes that suppresses tumor formation in normal cells has been long conceived (Klein, 1987). The retinoblastoma susceptibility gene (Rb), which is mutated in patients susceptible to the childhood retinal malignancy, was the first human tumor suppressor gene identified (see review by Bookstein and Lee, 1991, and references therein), and its identification marked the beginning of a new era of cancer research. Since then, Rb has been serving as the prototype of this gene class from almost every aspect (reviewed by Zheng and Lee, 2001).

First, it was experimentally demonstrated that reintroduction of a wild-type Rb allele into cells derived from Rb-deficient retinoblastoma and many other human tumors was able to suppress neoplastic phenotypes such as anchorage-independent growth and tumorigenesis in nude mice (Huang *et al.*, 1988; reviewed by Riley *et al.*, 1994). With the development of transgenic mouse and gene targeting techniques, the concept that Rb inactivation led to tumorigenesis was recapitulated (Jacks *et al.*, 1992; Lee *et al.*, 1992). Mice heterozygous for germline Rb mutations developed pituitary tumors with complete penetrance. Other types of tumors such as multiple neuroendocrine neoplasia were also found in these mice (Nikitin *et al.*, 1999). Similar to the loss of heterozygosity observed in Rb-deficient human cancer, homozygous deletions of the remaining wild-type allele occurred in all tumors formed in Rb +/− mice (Jacks *et al.*, 1992; Lee *et al.*, 1992; Nikitin and Lee, 1996).

The importance of the above findings lies not only in the identification of a tumor suppressor, but also in the elucidation of the growth control pathways (see review by Riley *et al.*, 1994, and references therein). An Rb-centered mechanism, which restrains the cell cycle progression through the late G1 phase or maintains the quiescent (G0) state, has thereby been revealed (Goodrich *et al.*, 1991; Hinds *et al.*, 1992). Inactivation of Rb results in improper control of the cell cycle, which is characterized by inadequate response

to the extracellular or intracellular growth-inhibitory signals (reviewed by Hanahan and Weinberg, 2000). It is considered that the growth-inhibitory signals converging onto Rb and the cell cycle are disrupted in one way or another in a majority of human cancers (reviewed by Sherr, 1996). Rb not only regulates the growth signals, but also mediates differentiation signals (reviewed by Chen *et al.,* 1995a). Accumulating evidence suggests that Rb is critical for cellular differentiation and embryonic development (see review by Lipinski and Jacks, 1999, and references therein).

The studies of Rb and other tumor suppressor genes have greatly enriched our knowledge on the control of cell growth and differentiation, which are apparently important for the tumor suppression function of Rb. It remains, however, unclear how inactivation of Rb increases cancer susceptibility, leading to the predisposition to retinoblastoma and other cancers. It is generally recognized that multiple genetic alterations lie in all the tumorigenic processes. However, it is argued that spontaneous mutation rates are so low that multiple genetic alterations are unlikely to occur within the normal human life span (Loeb, 1991). On the other hand, cancer cells are genetically unstable; and genetic instability increases genomic alterations that could contribute to multiple genetic lesions that underlie tumorigenic process.

A major indication of an unstable genome is aneuploidy, which is observed in nearly all cancer cells. The idea that aneuploidy is a key to cancer originated from Theodore Boveri, who, almost a century ago, made the observation that multipolar mitosis causes unequal segregation of chromosome. He formulated the hypothesis that the resultant aneuploidy is the basis of abnormal growth in tumor cells (Boveri, 1902). Aneuploidy, a trait characterized by the numeric changes of chromosomes, is undoubtedly a result of chromosome missegregation. Chromosome structural abnormality, a trait characterized by gross interchromosomal rearrangement, is also frequently observed in cancer cells and is suspected to be attributed to illegitimate recombination following chromosomal breaks (Myung *et al.,* 2001). Both numeric change and structural change of chromosomes are characteristics of chromosomal instability. Genetic instability also occurs at the nucleotide level, comprising nucleotide instability and microsatellite instability, the result of defects in nucleotide excision repair and mismatch repair, respectively (reviewed by Lengauer *et al.,* 1998).

Genome stability is maintained by proper replication and segregation of chromosomes and high fidelity of DNA repair (Flores-Rozas and Kolodner, 2000; Hoeijmakers, 2001; Lengauer *et al.,* 1998). Therefore, genes involved in DNA repair and chromosome replication and segregation are important for genome stability. Moreover, genes responsible for cell cycle checkpoints are also critical for genome stability. When DNA is damaged, replication or mitosis is stalled, then triggers cell cycle checkpoints to arrest cells for

correcting the mistakes, or apoptosis occurs before errors on the genome are duplicated and transmitted to the daughter cells. Thus, genes responsible for DNA damage-induced checkpoints and apoptosis are also important for genome stability (Hartwell *et al.*, 1994).

A functional link between the prototype of tumor suppressors and proteins for the maintenance of chromosome stability would strongly support the role of genetic instability in tumorigenesis. In the past decade, a growing body of evidence has supported a function of Rb in maintaining genome stability through activities involved in the modulation of chromosome behaviors. Interestingly, recent studies have implicated that other functions of Rb such as its role in cell cycle regulation are also mediated through activities intimately associated with the chromatin structures of chromosomes. We shall primarily discuss these issues in this chapter.

II. Rb AND CHROMOSOME SEGREGATION

A. Linking Rb to Mitotic Chromosome Structural Remodeling

1. Rb INTERACTS WITH HEC1 SPECIFICALLY AT G2/M PHASES

It is clear that Rb has multiple cellular functions and resides in multiple protein complexes (see review by Zheng and Lee, 2001, and references therein). Recently, a growing number of M phase players have been found to associate with Rb and form distinct complexes involved in chromosome segregation during M phase (Fig. 1). Such evidence links Rb to maintenance and stability of mitotic chromosomes.

The best-characterized association of Rb with M phase players is between it and human HEC1 (Chen *et al.*, 1997a; Zheng *et al.*, 2000a). HEC1 was originally identified in a yeast two-hybrid screen for proteins that interacted with domains A/B of Rb (Durfee *et al.*, 1993). It was subsequently shown to bind to Rb specifically at the G2/M phases of the cell cycle (Zheng *et al.*, 2000a). To elucidate the function of this novel protein, antibodies specific for HEC1 were injected into cultured human cells and mitosis of these cells was severely disturbed (Chen *et al.*, 1997a). In these cells, chromosomes congressed without properly aligning to the spindle, which subsequently resulted in unequal chromosome segregation and cell death. This result suggested an essential role of HEC1 in mitotic progression and chromosome segregation.

Further studies then revealed that the function of HEC1 is executed by interacting with other proteins. This notion was first suggested by the structure of the C-terminal region of HEC1, which is enriched in leucine-haptad

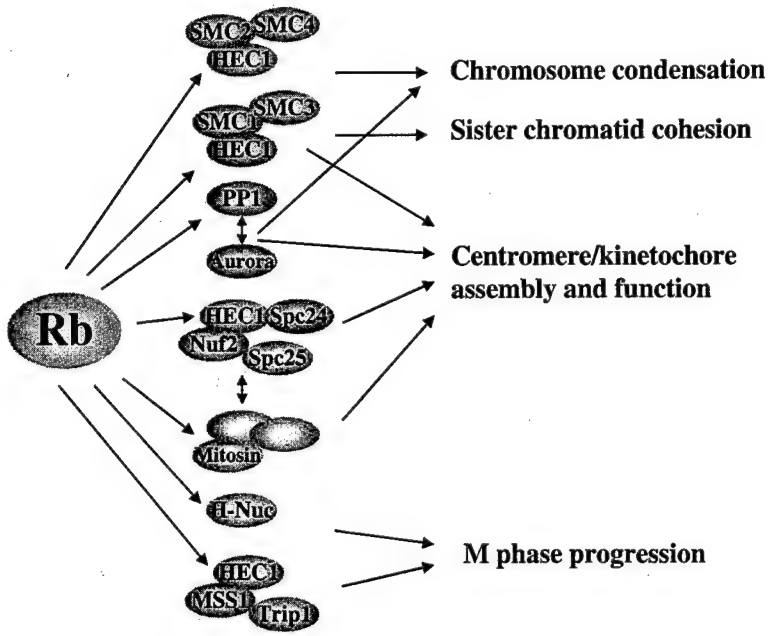

Fig. 1 A paradigm of Rb in the regulation of chromosome segregation and M phase progression.

repeats and forms three discrete coiled-coil domains (Chen *et al.,* 1997a) that were used as a bait to search for HEC1-interacting proteins (Chen *et al.,* 1997a). The majority of putative HEC1-interacting proteins included human structural maintenance of chromosomes (SMC) proteins, the 26S proteasome subunits MSS1 and p45/Trip1, and the mitotic kinase Nek2. These proteins are implicated in either M phase progression or chromosome segregation.

2. HEC1 IS ESSENTIAL FOR CHROMOSOME SEGREGATION AND IS INVOLVED IN MITOTIC CHROMATIN REMODELING

Among HEC1-interacting proteins, SMC1 belongs to a conserved protein family involved in structural maintenance of chromosome. The biological functions of SMC proteins are deduced from studies in various model systems including yeast, *Drosophila,* and *Xenopus* (see reviews by Hirano, 2000; Koshland and Strunnikov, 1996, and references therein). In eukaryotes, there are four subclasses of SMC proteins: SMC1 to SMC4. All four SMC proteins have nearly identical structures and are believed to associate with chromatin. SMC1 and SMC3 form an antiparallel heterodimer, which is present in the cohesin complex and assembles the postreplication chromatin structures for

the establishment of sister chromatin cohesion (reviewed by Koshland and Guacci, 2000; Nasmyth *et al.,* 2000). Sister chromatid cohesion is the linker between the two sister DNA molecules and must be properly established as they are replicated in the S phase, and maintained until the onset of anaphase. At the metaphase to anaphase transition, sister chromatin cohesion is resolved by a protease activity encoded by separin that separates sister chromatids (reviewed by Nasmyth, 1999). Failing to establish or maintain the sister chromatin cohesion would result in premature separation of sister chromatid separation leading to unequal chromosome segregation. Moreover, the G2/M DNA-damage checkpoint or spindle/kinetochore checkpoint would be activated in response to DNA damage, spindle disruption, or kinetochore malfunction. Sister chromatid cohesion should not be resolved until damaged DNA is repaired and the mitotic apparatus is reestablished (see reviews by Nasmyth, 1999; Yanagida, 2000, and references therein). Since the mitotic chromatin structures assembled by SMC1/3 dimer are essential for the establishment and maintenance of sister chromatid cohesion, deficiency of SMC1/3 complex would lead to chromosome missegregation (reviewed by Hirano, 2000; Strunnikov, 1998).

By contrast, SMC2/4 form a heterodimer, which is present in the condensin complex, and is involved in chromosome condensation (reviewed by Hirano, 2000; Koshland and Strunnikov, 1996). Chromosome condensation is another distinct process of mitotic modification of chromatin structure, in which nucleosomes are packaged into more compact forms. Nonetheless, chromosome condensation is established on the basis of the chromatin structures that have been remodeled by SMC1/3. Chromosome condensation, which prevents entanglement of otherwise loose chromatin during chromosome transmission, is essential for the faithful segregation of chromosome, and SMC2/4 deficiency leads to chromosome missegregation (reviewed by Hirano, 2000; Strunnikov, 1998).

A potential role for HEC1 in these SMC protein-mediated structural remodeling processes was revealed in an effort to establish a genetic system for understanding the biological function of the interaction between Rb and HEC1. First, a homologue of HEC1, designated sc*HEC1* or *NDC80,* was identified in *Saccharomyces cerevisiae* (Wigge *et al.,* 1998; Zheng *et al.,* 1999). Null mutation of the budding yeast *HEC1/NDC80* is lethal (Wigge *et al.,* 1998; Zheng *et al.,* 1999), while expression of human *HEC1* under the control of the yeast *HEC1* promoter completely rescues lethality (Zheng *et al.,* 1999). This result indicates that *HEC1* is evolutionarily conserved, and establishes a system in which human *HEC1* can be analyzed in yeast.

To understand the precise functions of HEC1, yeast cells carrying temperature-sensitive mutations of human *HEC1* were isolated and the resultant phenotypes were characterized (Zheng *et al.,* 1999). Meanwhile, the

temperature-sensitive mutations of the yeast *HEC1/NDC80* were also investigated (Wigge *et al.*, 1998). Both studies indicate that HEC1 is essential for chromosome segregation (Wigge *et al.*, 1998; Zheng *et al.*, 1999). Further analysis found that one human *HEC1* mutant, *hshec1-113*, failed to interact with the Smc1 protein in yeast at nonpermissive temperatures, suggesting that chromosome missegregation may result from dissociation of Hec1 and Smc1 (Zheng *et al.*, 1999). Overexpression of *HEC1* partially suppresses the *smc1* mutations at nonpermissive temperatures. Interestingly, Hec1 can also interact with Smc2, and Hec1 overexpression also partially suppresses *smc2* mutations. Given that chromosome missegragation is responsible for the lethality of both *smc1* and *smc2* mutants, the partial suppression of their lethality by *HEC1* could be due to a modulation in chromosome segregation. Taken together, these results indicate that HEC1 and SMC proteins are physically associated and functionally relevant, suggesting a role for HEC1 in modulating chromosome segregation by interacting with SMC proteins.

3. THE Rb–HEC1 INTERACTION MODULATES SMC ACTIVITY

The effect of Rb on chromosome segregation was examined in those yeast cells that have human *HEC1* in place of yeast *HEC1* (Zheng *et al.*, 2000a). Human *HEC1* contains an IxCxE motif, a well-characterized Rb-interacting motif that is essential for interaction with Rb. Interestingly, the yeast Hec1 does not contain this IxCxE motif, and no interaction has been observed between the yeast *Hec1* and Rb. Thus, the human *HEC1* engineered in yeast cells linked Rb to the rest of the cellular structural and regulatory components for chromosome segregation. In this heterologous genetic system, Rb is capable of reducing chromosome segregation errors by partially suppressing the human hs*hec1-113* temperature-sensitive mutation, and by enhancing the ability of wild-type human *HEC1* in suppressing the yeast *smc1* mutation (Zheng *et al.*, 2000a).

To further understand the role of Rb in chromosome segregation, the Hec1–Smc1 complex was characterized. Smc1 has specific activities that binds to structural DNA (Akhmedov *et al.*, 1999), and such activities could be the biochemical basis for the association to the *Smc1*-containing cohesin complex with the specific chromatin regions (Blat and Kleckner, 1999; Saitoh *et al.*, 1995). Our studies suggest that, if *HEC1* is mutated, then the Smc1-DNA binding would be compromised. However, Rb has the capability of enhancing the DNA-binding activity of Smc1 in a Hec1-dependent manner (Zheng *et al.*, 2000a). Interestingly, Rb itself was not present in the complex with DNA-bound Hec1 and Smc1. Thus, Rb does not appear to play a direct role in modulating the *Smc1* activity; instead, it appears to serve as a chaperone-like factor for the Hec1 protein. A chaperone-like activity of

Rb has been previously proposed to enhance the activity of C/EBP β (Chen *et al.*, 1996). Similarly, Rb was not present in the complex with DNA-bound C/EBP β, whereas Rb was able to affect the transactivation activity of C/EBP β on the promoter DNA template. Therefore, Rb might have the capability of modulating the conformation of its associated proteins; and for instance, it might convert the mutated hec1 from a less active form to a more active form. Such a chaperone-like activity of Rb might be also important for the wild-type *HEC1* to maintain an active form of conformation.

The function of Rb in modulating chromosome segregation is apparently dispensable for yeasts, which undergo mitosis properly without Rb. Rb appears to emerge late during evolution in higher organisms that have a more complicated chromosome structure and mitotic apparatus. Thus, due to the complexity of higher eukaryotes, a more active, Rb-dependent form of HEC1 might be required. As described above, cells without HEC1 died of chromosome missegregation. In the absence of Rb, the function of HEC1 would be adequate for the survival of mammalian cells, although not sufficient for the high fidelity of chromosome segregation. Therefore, without Rb, high frequencies of chromosome segregation errors, a trait of chromosomal instability, would be expected.

B. Linking Rb to Centromere Structure Assembly and Kinetochore Function

1. HEC1 AND THE CENTROMERE

HEC1 is apparently a regulator of multiple mitotic events; therefore, Rb may modulate chromosome segregation from multiple aspects. An additional role of HEC1 was revealed by showing its subcellular localization to centromeric regions of chromosomes in mammalian cells (Chen *et al.*, 1997a). The centromere localization of HEC1 and its associated kinetochore complexes in various organisms were recently characterized. A *S. cerevisiae* Ndc80/Hec1 associated complex was isolated in different laboratories by affinity purification of epitope-tagged Ndc80/Hec1 or Spc25 (Janke *et al.*, 2001; Wigge and Kilmartin, 2001). In addition to Ndc80/Hec1, Nuf2, Spc24, and Spc25 were found in this complex. Ndc80/Hec1, Spc24, and Spc25 were previously identified by mass spectrometry from a preparation of highly enriched spindle poles (Wigge *et al.*, 1998), whereas Nuf2 was identified elsewhere as a spindle pole body (SPB)-associated protein (Osborne *et al.*, 1994). Although these proteins appear to localize close to the nuclear sides of the SPB, they were found to associate consistently with a subset of nuclear microtubules, which distinguished them from other components of the SPB that are associated with all of the nuclear microtubules.

To circumvent the limitation of distinguishing between spindle pole bodies and centromeres in budding yeast cells, the localization of homologues of Ndc80/Hec1, Spc24, Spc25, and Nuf2 were examined in *S. pombe* fission yeast cells and human HeLa cells (Wigge and Kilmartin, 2001). It thus became clear that all these proteins are localized to centromeric regions similar to previously identified kinetochore proteins such as human CENP-B and fission yeast sad1. The centromeric association of Ndc80/Hec1 and other components in the complex were further supported by chromatin immunoprecipitation assays showing that *S. cerevisae* centromere DNA was specifically enriched by immunoprecipitation of these proteins (Wigge and Kilmartin, 2001). These results are consistent with the initial observation of centromere localization of HEC1 in mammalian cells and in yeast cells (Chen *et al.,* 1997a; Zheng *et al.,* 1999), indicating that HEC1 is a centromere-associated component.

Despite growing evidence supporting a role of HEC1 in kinetochore function, the nature of such a role remains mysterious. Studies from various laboratories have provided some insightful clues. First, HEC1 localizes to the outer layer of kinetochore (Wigge and Kilmartin, 2001). It was suggested that the three centromere-associated subcomplexes in budding yeast, including the Ndc80/Hec1, Ctf19, and CBF3 subcomplexes, is ordered from centromere DNA to microtubules (Lechner and Carbon, 1991; Ortiz *et al.,* 1999; Wigge and Kilmartin, 2001). The CBF3 subcomplex was known to contact with centromere DNA directly (Espelin *et al.,* 1997). Ctf19 stays in a subcomplex with Mcm21 and Okp1 (Ortiz *et al.,* 1999), and this subcomplex is associated with centromere DNA in a CBF3-dependent, but not a Ndc80 or Spc24-dependent, manner, suggesting that it may hold a position between the Ndc80 and CBF subcomplex. Ndc80/Hec1, with its close relation to the SPB and association with the spindles, was considered to play a role in the spindle attachment of kinetochore, albeit evidence supporting such a role remains circumstantial (Wigge and Kilmartin, 2001; Janke *et al.,* 2001). Genetic interactions between *NDC80/HEC1* and *CTF19* (Hyland *et al.,* 1999), and between *SPC24* and *MCM2,* were observed (Janke *et al.,* 2001). Although a moderate interaction between Spc24 and Mcm21 was detected by yeast two-hybrid binding assays (Janke *et al.,* 2001), no interactions were observed between Ndc80/Hec1 and Ctf19 (Zheng, L., and Lee, W.-H., unpublished results). Moreover, at present, no physical interactions have been detected *in vivo* between the Ndc80 subcomplex and the Ctf19 subcomplex or the CBF3 subcomplex (Wigge and Kilmartin, 2001; Janke *et al.,* 2001), suggesting that other components may mediate the interactions. Alternatively, different subcomplexes, associated with centromeric DNA, may be dynamically connected to each other, and this may explain why no single preparation has identified all the centromere-associated components in one complex.

In fission yeast, *Hec1* was localized to an "anchor" structure that resides between the heterochromatin domain and the spindle pole body (Kniola *et al.*, 2001). In mammalian cells, although it was suggested that HEC1 might also localize to the spindle side of kinetochore, a precise position of HEC1 and its relations with other components in the kinetochore remains to be determined. Human homologs of Nuf2 and Spc24 were also identified and they had localization in mammalian cells similar to their yeast counterparts (Wigge and Kilmartin, 2001); however, more components are likely involved, considering the complexity of human centromeres. Identification of these additional components in the HEC1 complex may assist determining the role of HEC1, particularly the proposed role of HEC1 in spindle attachment to the kinetochore.

The absence of *Smc* proteins in the Ndc80/Hec1 centromere-associated subcomplex is not unexpected. Although it is possible that SMC proteins could be transient components of the Ndc80/Hec1 complex, the HEC1–SMC1 interaction could be independent of the centromere complex. It becomes apparent that HEC1 is a multifunctional regulator and its subcellular localization is not restricted to centromeres; therefore, it is likely that HEC1 can form distinct complexes in the cells. It is known that *Smc1* and the cohesin complex are concentrated at the centromeric regions and that is critical for normal assembly and function of the centromere/kinetochore (Bernard *et al.*, 2001; Blat and Kleckner, 1999; Megee and Koshland, 1999; Tanaka *et al.*, 1999a, 2000). Therefore, it is more likely that the HEC1–SMC1 interaction, as well as their association with Rb, not only functions in the structural remodeling of mitotic chromosomes, but also in centromere/kinetochore function.

2. Rb AND MITOSIN

Rb is linked to the centromere/kinetochore function by other kinetochore components. Mitosin/CENP-F, a structural component of the outer layer of kinetochore (Liao *et al.*, 1995; Zhu *et al.*, 1995), was initially isolated as both a Rb-interacting protein and an antigen recognized by autoimmune antibodies. It was suggested that yeast Okp1 might be the homolog of Mitosin/CENP-F though the homology is quite limited (Ortiz *et al.*, 1999). Nonetheless, similar localization of these two proteins supports that the Ctf19–Mcm21–Okp1 complex is the counterpart of the Mitosin-associated complex. Considering the intimate relations between the HEC1 and the Ctf19–Mcm21–Okp1 subcomplex as described above, it would be conceivable that Rb may coordinate the organization and activity of both subcomplexes. However, at present, the *in vivo* interaction between Rb and Mitosin has not been established. Similar to the interaction between different centromere-associated subcomplexes, the association between a regulator like Rb and a structural protein like Mitosin may be difficult to find due to

its dynamic nature. A technical improvement in discerning the composition of the centromere-associated complex and the connections between different subcomplexes may be necessary for exploring the role of Rb in kinetochore function.

C. Linking Rb to Mitotic Cyclin Degradation and G2/M Phase Progression

An early study has suggested a role for Rb in G2/M progression. It showed that overexpression of Rb in S phase arrested cells at G2 (Karantza *et al.*, 1993). Indeed, all mitotic events including postreplicative chromosome remodeling, M phase entry, sister chromatid separation, spindle alignment and elongation, and M phase exit are regulated in a timely and orderly fashion and in concert with the G2/M phase cell cycle progression. A major mechanism that regulates G2/M phase progression is the anaphase-promoting complex (APC)- and the 26S proteasome-mediated ubiquitin-dependent protein degradation pathways (reviewed by Page and Hieter, 1999). Ubiqutin-dependent proteolytic activities, which control the turnover of specific regulators such as Pds1, Ase1, and mitotic cyclins, are critical for sister chromatid separation and M phase exit. By contrast, the synthesis and accumulation of the mitotic cyclin, cyclin B, is necessary for M phase entry, which, in part, is assumed to be achieved by inhibiting the ubiquitin ligase activity of APC.

Although Rb does not appear to regulate the synthesis of cyclin B directly, Rb/E2F-mediated G1 phase regulation may coordinate with the mechanism that controls G2/M transition (Lukas *et al.*, 1999). It was suggested that Rb/E2F represses the transcription of another mitotic cyclin, cyclin A in the G1 phase, and this repression activity of Rb persists when cells have entered S phase. This result was highlighted by a more recent study showing that Rb recruits human polycomb group proteins to repress the transcription of cyclin A and cdc2 (Dahiya *et al.*, 2001). In S phase, cyclin A/cdk2 phosphorylates Cdh1, the substrate-specific activator of APC, thereby blocking the activity of this ubiquitin ligase in degrading cyclin B. Conversely, repression of cyclin A synthesis leads to the activation of the APC complex, which in turn degrades cyclin B, presumably creating a low-cyclin B environment for the later induction of cyclin B during M phase entry. It can be predicted that further phosphorylation of Rb by cyclin E/cdk2 would relieve the repression of cyclin A expression, leading to the inhibition of APC and, eventually, accumulation of cyclin B (Lukas *et al.*, 1999). Therefore, Rb is capable of coordinating the regulatory machinery in G1 to that in S, G2, and M phase by orchestrating a cascade of cyclin induction and cdk activation.

In addition to an indirect role in regulating the function of APC, Rb may directly interact with APC. Rb interacts with H-nuc/Cdc27, an essential component of APC (Chen *et al.*, 1995a). Moreover, Rb may influence the activity

of the 26S proteasome since HEC1 directly interacts with 26S proteasome subunits. The interaction between HEC1 and two 26S proteasome subunits, MSS1 and p45/Trip1, was identified in a yeast two-hybrid screen (Chen *et al.*, 1997b). MSS1 and p45/Trip1 are the S7 and S8 subunits of 26S proteasome, respectively, and both have ATPase activity (reviewed by Baumeister *et al.*, 1998). The interaction between HEC1 and MSS1 was characterized in detail, serving as a paradigm for understanding the role of HEC1 in 26S proteasome-dependent proteolysis (Chen *et al.*, 1997b). Previously, both subunits were found important for G2/M progression in a study showing that temperature-sensitive (ts) mutants of their homologue in budding yeast, *SUG1/CIM3* and *CIM5*, respectively, arrested at metaphase at nonpermissive temperatures. A defect in the degradation of yeast B-type cyclins was observed in these mutants and was proposed to lie in the ts phenotypes (Ghislain *et al.*, 1993). This early study implicated a role of HEC1 in the regulation of mitotic cyclins. In agreement with this prediction, ectopic expression of the C-terminal region of HEC1 in mammalian cells inhibited the degradation of cyclin A and cyclin B when cells progressed from metaphase to anaphase (Chen *et al.*, 1997b). Consistently, purified HEC1 protein was capable of modulating the ATPase activity of MSS1 *in vitro*. A potential role of HEC1 in metaphase to anaphase transition was therefore suggested. How this HEC1-mediated regulation of mitotic cyclins influences the cell cycle progression, and how HEC1 cross talks with other pathways in cyclin degradation, however, remains to be elucidated. Moreover, whether Rb plays any role in this function of HEC1 awaits to be investigated.

Proper control of mitosis exit also appears to involve Rb. When treated with microtubule-destabilizing agents, cells lacking functional Rb do not finish mitosis properly, but exit M phase without chromosome separation and cytokinesis and undergo a new cycle of DNA replication, leading to hyperploidy (Di Leonardo *et al.*, 1997; Khan and Wahl, 1998). In contrast, normal mammalian cells treated with microtubule-destabilizing agents for the same period of time also transverse to G1 phase without cytokinesis, a process designated "adaptation," albeit no rereplication occurs. The precise mechanism underlying adaptation and rereplication has not yet been elucidated; however, a potential role of Rb in preventing hyperploidy is suggested.

D. Rb and Protein Phosphatase 1α Interacts at M Phase

The phosphorylation of Rb is oscillated throughout the cell cycle. Hypophosphorylated forms of Rb are functional, predominate at G1 phase, and reappear at G2 and M phases (Chen *et al.*, 1989; DeCaprio *et al.*, 1989; Ludlow *et al.*, 1990). Hyperphosphorylated forms of Rb predominate at

S phase; albeit recent studies suggest that hypophosphorylated forms of Rb are also present at S phase (Knudsen *et al.,* 2000; Ludlow *et al.,* 1993; Yen and Sturgill, 1998). Presumably, the function of Rb at G2/M phase relies on it being hypophosphorylated because all the known Rb partners interact with the hypophosphorylated forms, although it still cannot be excluded that hyperphosphorylated forms of Rb exhibit certain activities.

Protein phosphatase 1α (PP1α) interacts with Rb specifically at M phase, leading to the hypothesis that PP1α is responsible for the dephosphorylation of Rb (Durfee *et al.,* 1993). The enzyme–substrate relation between PP1α and Rb has been established *in vitro* (Ludlow *et al.,* 1993; Nelson and Ludlow, 1997), and a cellular complex formed between PP1 and hyperphosphorylated forms of Rb has been isolated (Tamrakar *et al.,* 1999). However, the major forms of Rb that interact with PP1α are hypophosphorylated (Durfee *et al.,* 1993; Nelson and Ludlow, 1997), suggesting that the PP1–Rb complex may have other distinct functions. Consistent with this notion, it was shown that Rb can modulate the enzymatic activity of PP1 (Tamrakar and Ludlow, 2000), suggesting that Rb may serve as a regulator of the cellular functions of PP1.

PP1 is a conserved enzyme involved in diverse cellular functions. An important feature of PP1 is to regulate mitosis. Mutations of PP1 orthologs in diverse organisms exhibit defects in M phase progression, chromosome segregation, and kinetochore functions (Francisco *et al.,* 1994; Hisamoto *et al.,* 1994; Kinoshita *et al.,* 1990; Tung *et al.,* 1995; Zhang *et al.,* 1995). It was thought that mutations in *GLC7,* the budding yeast PP1, causes a defect in kinetochore functions, and therefore activates the kinetochore/spindle checkpoint which in turn arrests the mutant cells at G2/M phase (Bloecher and Tatchell, 1999; Sassoon *et al.,* 1999). This phosphatase does not work alone, but coordinates with Ipl1, a serine-threonine kinase originally identified in a genetic screen for mutants that increase in ploidy (Chan and Botstein, 1993). Ipl1 homologs have been reported in various species (Bischoff and Plowman, 1999), for instance, aurora in *Drosophila* (Glover *et al.,* 1995). Its homologs in mammalian cells gained extra attention because they are overexpressed in a variety of human cancers (Bischoff *et al.,* 1998; Gopalan *et al.,* 1997; Sen *et al.,* 1997; Tanaka *et al.,* 1999a; Tatsuka *et al.,* 1998; Zhou *et al.,* 1998). In yeast, Ipl1 acts in opposition to Glc7 in regulating chromosome segregation (Francisco *et al.,* 1994), suggesting that a balance of opposing actions from Ipl1/aurora and Glc7/PP1 is important for chromosome segregation.

Although substrates of Ipl1/aurora and Glc7/PP1 in kinetochore remain to be revealed, a study indicates that histone H3 is a substrate for both Ipl1 and Glc7 on yeast chromosome structures (Hsu *et al.,* 2000). Phosphorylation of histone H3 is essential for proper chromosome segregation and condensation during mitosis and meiosis in a wide range of organisms, and a point mutation of serine 10 leads to abnormal chromosome segregation and

extensive chromosome loss (Hendzel *et al.*, 1997; Wei *et al.*, 1998, 1999). Both Ipl1/aurora and Glc7/PP1 act in opposition to each other in regulating histone H3 phosphorylation, and presumably are required for its balance during mitosis in *S. cerevisiae* and *C. elegans* (Hsu *et al.*, 2000), although a causal link between two enzymatic activities remains to be demonstrated.

Therefore, the Rb-PP1 complex might participate in the regulation of kinetochore function and chromosome condensation. The presence of both hypophosphorylated Rb and hyperphosphorylated Rb complexes with PP1 may be critical for a balance of Rb phosphorylation. Like coregulation of histone H3 phosphorylation by PP1 and aurora, the balance of Rb phosphorylation may also be important for M phase progression, though it is merely speculative at the present time.

III. Rb AND CHROMOSOME REPLICATION

A. Rb Regulates the Replication Origin Activity

Chromosome replication must also be properly controlled to maintain genomic stability. Although a role of Rb in replication has long been proposed, it is thought to be mediated by E2F in the transcription regulation of genes necessary for entering S phase and initiating replication. The E2F family is a group of transcription factors that regulate transcription through binding to specific sequences, namely E2F sites, on promoters (see reviews by Dyson, 1998; Nevins, 1998, and references therein). Recent studies revealed a role of Rb directly involved in the replication machinery. In these studies, activating replication origins to initiate DNA synthesis is visualized *in situ* using the *Drosophila chorion* gene loci as a model metazoan replication origin (Bosco *et al.*, 2001). In response to developmental signals in ovarian follicle cells, the *chorion* gene clusters amplify by repeatedly initiating DNA replication from specific replication origins in each cluster. *Drosophila melanogaster* origin recognition complex (DmORC) localizes *in vivo* to *chorion* replication origins, binds amplification control elements (ACE) within the origins, and supports DNA replication *in vitro* (Austin *et al.*, 1999; Chesnokov *et al.*, 1999; Royzman *et al.*, 1999). This model replication origin was used to investigate the roles of *Drosophila* orthologs of E2F1 and Rb (dE2F1 and Rbf, respectively) in controlling initiation of DNA replication. These studies showed that a complex containing Rbf, dE2F1, and *Drosophila* DP1 bind near DmORC (Bosco *et al.*, 2001). Potential dE2F-binding sites were found adjacent to ACE; and the heterodimer of E2F1-DP1 was proposed to bind to these E2F sites near DmORC. The complex formation between dDP1, dE2F1, Rbf, and DmORC is detectable in the cell extract.

Truncation of the C-terminal Rb-binding region of dE2F1 eliminates the formation of the dDP–dE2F1–Rbf–DmORC complex, and in this truncation mutant, DmORC is localized to the replication origin, but increased amplification occurs. Reduced levels of Rbf results in increased gene amplification levels and genomic replication without measurable effects on transcription of dE2F target genes. These results therefore suggest that Rb represses the activity of DmORC through the origin-bound dDP1–dE2F1–Rbf–DmORC complex; moreover, release of Rb from the origin-bound complex permits DmORC to initiate origin firing when cells receive proper signals to commence DNA replication.

It remains to be shown that Rb and E2F1 play a role in global DNA replication in *Drosophila,* and particularly in mammalian cells. Human Rb and associated histone deacetylases (HDACs) had been shown to immunologically colocalize to BrdU foci in early S phase of mammalian cells, suggesting that Rb is localized to the active replication sites (Kennedy *et al.,* 2000). It will be of greater value to determine whether mammalian E2F–Rb complexes can interact with ORC to support a direct role of Rb in replication origins in mammalian cells.

A recent study provides evidence that E2F binds to replication origins in human cells (Maser *et al.,* 2001). Chromatin immunoprecipitation assays indicate that E2F family proteins bound near Epstein–Barr virus later origin of replication, oriP, in Raji cells containing an oriP episome. Two E2F binding sites were identified within 400 bp of oriP. Moreover, E2Fs bound at chromosomal E2F sites in the vicinity of the c-myc promoter, a region that has been shown to contain replication origin activity. Whether Rb plays a role in regulating the activity of these mammalian replication origins, and in particular whether this proposed role of Rb is important for tumor suppression, awaits elucidation.

B. Mechanisms for Regulatory Roles of Rb in Replication Origin

The mechanism by which Rb controls the activity of replication origin has not been clarified. A possible mechanism is that Rb directly inhibits the activity of the ORC subunits. Alternatively, Rb might inhibit loading of other replication factors at origins such as the MCM7 protein, which has been demonstrated to interact with Rb physically (Sterner *et al.,* 1998). Nonetheless, a more attractive model is that Rb may alter the chromatin configuration of replication origins, for example through recruiting HDACs and/or the SWI/SNF ATP-dependent chromatin remodeling complex (Harbour and Dean, 2000), and thereby affect the assembly of replication origin complex and replication origin firing. Chromatin remodeling activities have been

suggested to underlie the Rb-mediated transcription regulation. Moreover, it may be involved in a wide spectrum of chromosome metabolic processes including DNA replication, recombination, and repair.

C. Biological Role of Rb in Replication

A role for Rb in the control of replication initiation could account for its function in cell growth and cell cycle regulation. Such a role would directly involve Rb in the control of chromosomal stability during replication. The role of Rb in replication may not be restricted to regulating replication initiation at early S phase of the normal cell cycle. Rb may be continuously required for proper control of replication processes throughout the S phase. More importantly, Rb may be required for inhibiting repeated replication origin firing, inhibiting replication origin firing at non-S phase cell cycle stages, or inhibiting replication when the cell cycle is arrested, for example, in response to DNA damage. A growing body of evidence suggests that Rb is required to monitor S progression and involved in S phase response to DNA damage (Knudsen *et al.*, 1998, 2000). Loss of Rb function results in endoreplication in cells arrested at the G1/S and G2/M boundaries by DNA damage agents (Niculescu *et al.*, 1998), suggesting that Rb is required for inhibiting replication in cells arrested by the G1/S and G2/M checkpoints. Such functions of Rb may be closely related to its role in regulating replication initiation and replication machinery. A potential role of Rb in the DNA damage checkpoint is discussed below.

IV. Rb AND DNA DAMAGE RESPONSE

Mechanisms for DNA damage response include sensing DNA lesions, transducing DNA damage signals, arresting cell cycle progression, and activating either the process of DNA repair or the process of apoptosis. Accumulated evidence suggests that Rb is important for the cellular response to DNA damage.

A. Rb and G1/S and G2/M Checkpoints

Rb occupies a central position in mediating growth inhibitory signals, not only from outside the cell but also from inside the cell. Upon DNA damage by exogenous genotoxic agents or endogenous metabolic by-products, signaling

cascades are activated to transmit growth inhibitory signals to arrest cell cycle progression, presumably from damaged sites inside nuclei to the cell cycle regulators. Although no evidence suggests a direct response of Rb to DNA damage signaling, cell cycle arrest is eventually mediated by Rb function. In agreement with this notion, specific phosphorylation of Rb by cdk2 is inhibited by ionizing radiation in a manner dependent on the cdk2 inhibitor, p21 (Brugarolas *et al.,* 1999). It has been well established that p21 is induced transcriptionally by DNA damage and arrests cells at G1/S transition through inhibiting cdk2 (reviewed by el-Deiry, 1998). This result therefore suggests that Rb is a component of p21-mediated G1/S DNA damage checkpoint control pathway and that p21 arrests the cell cycle through inhibiting cdk2 phosphorylation of Rb (Brugarolas *et al.,* 1999). Consistent with this notion, Rb-deficient cells fail to arrest at G1/S in response to DNA damage and inappropriately activate E2F-target genes (Harrington *et al.,* 1998).

A role for Rb in the G2/M checkpoint control has also been proposed. It was shown that p53-mediated G2/M arrest in response to DNA damage is dependent on Rb (Flatt *et al.,* 2000). This is consistent with the role of Rb in the G2/M cell cycle regulation as mentioned, although the underlying mechanism remains to be explored.

B. Rb and the S Phase Checkpoint

As described above, a potential role of Rb in the S phase DNA damage checkpoint has been implicated (Knudsen *et al.,* 2000). The study showing that E2F bound to replication origins in mammalian cells provides some clues to understanding these underlying mechanisms (Maser *et al.,* 2001). The Mre11–Rad50–Nbs1 complex, important for DNA recombination and repair following DNA double-strand breakage (Haber, 1998), binds to the E2F sites at replication origins through a direct interaction between Nbs1 and E2F1. The association between Nbs1 and E2F sites was significantly enhanced when cells progressed from early S phase to mid-S phase. Mre11 and Nbs1 have also been implicated in the S phase checkpoint control, which is thought to inhibit DNA synthesis when DNA is damaged during S phase (reviewed by Petrini, 2000). The association of the Mre11 complex with replication origins can then explain how Mre11 and Nbs1 may inhibit DNA synthesis. Here, the involvement of the Mre11–Rad50–Nbs1 complex may be beneficial for an efficient repair of DNA breakage, which resulted from stalled replication forks and would otherwise lead to chromosome structural abnormality (Chen and Kolodner, 1999; Flores-Rozas and Kolodner, 2000; Myung *et al.,* 2001).

How the Mre11 complex influences the replication origin firing and whether Rb is involved in this regulation have not yet been addressed. It

was proposed that the Mre11 complex could affect DNA replication origins by influencing local chromatin architecture. It is reasonable to further conceive that Rb, which is able to recruit histone modification or chromatin remodeling factors, participates in this regulation. Nonetheless, whether Rb is physically localized to the E2F sites at the mammalian replication origins and whether the Rb-E2F complex interacts with the Mre11 complex, and more importantly, whether loss of Rb function would affect the function of the Mre11 complex, remain to be explored.

C. Rb and Other Mechanisms for DNA Damage Response

In another study, the large subunit of replication factor C (RF-C) is shown to promote cell survival after UV-induced DNA damage in a Rb-dependent manner (Pennaneach *et al.,* 2001). RF-C is a complex of five polypeptides important for both DNA replication and DNA damage repair (reviewed by Mossi and Hubscher, 1998). This RF-Cp145 subunit binds to Rb through the LxCxE motif. The cell survival-promoting function of ectopically expressed RF-Cp145 is dependent on Rb. However, since no apparent DNA repair defect has been observed in Rb-deficient cells, the Rb-RF-C interaction was suggested to contribute to a role in DNA damage checkpoint control (Pennaneach *et al.,* 2001). Considering that these observations were based on the ectopic expression of RC-F, a future study with experimental manipulation of RF-C at physiological levels would be necessary to deduce the precise role of the Rb–RC-F interaction.

It is worthwhile to note that the N-terminal region of Rb contains a BRCT domain, which is a protein–protein interaction motif present in a number of proteins implicated in DNA damage response (Bork *et al.,* 1997). Although the A/B domains and the C-terminal region of Rb mediate the interaction with most of its associated proteins and fulfill most of the activities associated with Rb *in vitro,* there is evidence suggesting that the N-terminal region of Rb is also important for tumor suppression. For instance, transgenic expression of N-terminally deleted human Rb is not able to rescue Rb−/− mice completely from embryonic lethality; and moreover, it delays, but does not prevent, pituitary tumors formed in Rb+/− mice (Riley *et al.,* 1997). Mutations in the N-terminal region of Rb, including a deletion mutation that specifically disrupts the BRCT domain, are associated with human low-penetrance retinoblastoma families (Otterson *et al.,* 1997; Sellers *et al.,* 1998). Therefore, it will be valuable to explore the function of the N-terminal region, in particular, the BRCT domain of Rb, which may provide insights into how Rb participates in the DNA damage response.

V. GLOBAL CONNECTIONS OF Rb AND CHROMATIN

A. Connections of Rb and Basic Chromatin Structures

Rb is involved in maintaining genome stability from multiple aspects and is intimately associated with activities that take place on chromosomes. These activities include maintenance and reconfiguration of mitotic chromosome structures, organization of a special chromatin structure such as a centromere, replication origin assembly and firing, and cellular responses to damaged chromosomal DNA. Many of these activities involve remodeling of high-level chromatin structures; however, the connections of Rb to chromatin extend beyond specialized chromatin structures previously discussed (sister chromatid cohesion, centromere, replication origin, and condensed mitotic chromatin). By studying mechanisms for Rb-mediated transcription repression, Rb is connected to remodeling of basic chromatin structures, which directly involves modification and positioning of nucleosomes. These connections occur at different levels as follows.

1. Rb AND HDACs

Rb interacts with HDAC1, HDAC2, and HDAC3, which modify nucleosomes and modulate local chromatin structures (Brehm *et al.*, 1998; Lai *et al.*, 1999; Luo *et al.*, 1998; Magnaghi-Jaulin *et al.*, 1998). HDAC1 and HDAC2 form a complex with RbAp48 and RbAp46 (Alland *et al.*, 1997; Heinzel *et al.*, 1997; Laherty *et al.*, 1997; Nagy *et al.*, 1997; Zhang *et al.*, 1997), which were originally identified as Rb-associated proteins (Qian *et al.*, 1993). HDAC3 is present in a distinct histone deacetylase complex (Guenther *et al.*, 2000; Urnov *et al.*, 2000; Wen *et al.*, 2000). Histone deacetylases remove acetyl groups from histone tails and promote nucleosome formation (reviewed by Wolffe, 1996). They act in opposition to histone acetyltransferses (HAT) that add acetyl groups. These acetyl groups neutralize the positive charge on lysine residues on histone tails and lead to the disruption of nucleosome structure, and the unwrapping of chromosomal DNA thus allows access to transcription factors. Accordingly, histone deacetylases inhibit access of transcription factor. The Rb–E2F complex is thought to repress the transcription of E2F-target genes by recruiting HDACs (Brehm *et al.*, 1998; Luo *et al.*, 1998; Magnaghi-Jaulin *et al.*, 1998). The HDAC–Rb complex is disrupted by phosphorylation of Rb by cyclin D/cdk4, leading to the relief of repression and consequently transcription of genes such as cyclin E, which further phosphorylates Rb and eventually leads to S phase entry (Zhang *et al.*, 2000).

2. Rb AND SWI/SNF

Rb interacts with BRG1 and hBRM, which are components of the human SWI/SNF complex (Dunaief *et al.*, 1994; Strober *et al.*, 1996; Trouche *et al.*, 1997; Zhang *et al.*, 2000). Human SWI/SNF complex has ATPase-dependent chromatin remodeling activity, which is thought to modulate high-order chromatin structures (see reviews by Kingston and Narlikar, 1999; Peterson and Workman, 2000; Winston and Carlson, 1992, and references therein). *In vitro,* this complex was shown to be capable of changing the relative positions of nucleosomes on a DNA template and catalyzing the transfer of nucleosomes from one DNA template to another. The SWI/SNF complex appears to participate in both transcriptional activation and repression (Holstege *et al.*, 1998). The BRG1–Rb complex is thought to repress the transcription of a group of E2F-target genes, which appear to be different from those targeted by the HDAC–Rb complex. Release of repression on this group of E2F-target genes is also achieved by disruption of the BRG1–Rb complex; however, disruption of the BRG1–Rb complex requires not only the phosphorylation of Rb by cyclin D/cdk4, but also the further phosphorylation of Rb by cyclin E/cdk2 (Zhang *et al.*, 2000).

3. Rb AND POLYCOMB GROUP

Rb forms a complex with HPC2 of polycomb group proteins (PcG) (Dahiya *et al.*, 2001). The PcG complex is proposed to have distinct activities that direct high-order chromatin remodeling and maintain gene silencing by inhibiting general transcription factor-mediated activation of transcription (Breiling *et al.*, 2001; Francis *et al.*, 2001; Saurin *et al.*, 2001). The Rb–HPC2 complex was suggested to specifically repress expression of cyclin A and cdc2, but not cyclin E (Dahiya *et al.*, 2001). More interestingly, HPC2 and Rb coordinate to arrest cells at G2/M phases. HPC2 and Rb are mutually required for repression of cyclin A and cdc2 and cell cycle arrest at G2/M phases.

4. Rb AND HISTONE METHYLTRANSFERASE

Rb forms a complex with SUV39H1 and HP1 (Nielsen *et al.*, 2001). SUV39H1 is a histone methyltransferase that methylates lysine 9 of histone H3, creating a binding site on H3 for the chromo domain of HP1 (Bannister *et al.*, 2001; Lachner *et al.*, 2001; Nakayama *et al.*, 2001). HP1 is a heterochromatin-associated protein proposed to direct promoter silencing by translocating its associated promoters to the vicinity of heterochromatin regions or packaging the promoter-associated euchromatin into heterochromatin-like structures. SUV39H1 cooperates with Rb to repress

the cyclin E promoter, and Rb is necessary to direct methylation of histone H3, and necessary for binding of HP1 to the cyclin E promoter (Nielsen *et al.*, 2001). This study thus suggests that both SUV39H1 and HP1 are involved in the repressive function of Rb.

5. Rb AND DNA METHYLTRANSFERASE

Rb copurifies with DNMT1, E2F1, and HDAC1 (Robertson *et al.*, 2000). DNMT1 is the predominant form of mammalian DNA methyltransferase. Methylation of CpG islands by DNMTs is associated with transcriptional silencing and the formation of chromatin structures enriched in hypoacetylated histones (see reviews by Ng and Bird, 1999; Razin, 1998, and references therein). It is thought that methylation of CpG leads to the binding of methyl-CpG-binding proteins such as MeCP2, which may then recruit histone deacetylases to direct transcriptional repression (Jones *et al.*, 1998; Nan *et al.*, 1998). In agreement with this idea, DNMT1 cooperates with Rb to repress transcription from promoters containing E2F-binding sites (Robertson *et al.*, 2000).

B. Do the Rb/Chromatin Connections Go Global?

Chromatin remodeling activities are involved not only in transcription regulation, but are also important for processes other than transcription, such as DNA replication, homologous recombination, transcription-coupled repair, mitotic chromosome segregation, centromere assembly, and global chromatin assembly. Moreover, diverse chromatin remodeling activities or factors involved in transcriptional regulation can participate in various processes. It is conceivable that the chromatin remodeling activities utilized by Rb in transcription repression are similarly recruited by Rb to modulate chromosome replication, mitotic chromosome dynamics, DNA recombination, and repair. The association of Rb with chromatin-remodeling factors thus may be important for maintaining genome stability.

Indeed, genetic ablation of chromatin remodeling factors leads to genome instability and in some cases to cancer formation. For example, the SNF5/INI1 component of human SWI/SNF complex is mutated in sporadic rhabdoid tumors, and germline mutations confer an autosomal dominant syndrome that predisposes to a variety of rhabdoid cancers (Versteege *et al.*, 1998). In both sporadic and hereditory cancers, biallelic loss-of-function mutations in SNF5/INI1 were found. Mutations in SNF5/INI1 are also associated with acute leukemia (Sevenet *et al.*, 1999). Rhabdoid tumorigenesis was also observed in mice with genetic ablation of SNF5/INI1 (Guidi *et al.*,

2001; Roberts *et al.,* 2000). Consistently, mutations in human BRG1, another subunit of the SWI/SNF complex, are associated with multiple types of cancers (Wong *et al.,* 2000). More recent studies have shown that mice with genetic ablation of both histone methyltransferases, Suv39h1 and Suv39h2, display severely impaired viability and aneuploidy, and are associated with an increased risk of B cell lymphomas (Peters *et al.,* 2001). Moreover, illegitimate paring of nonhomologous chromosomes, impaired synapse, premature chromosome separation, and chromosome missegregation were also observed in Suv39h-deficient spermatocytes (Peters *et al.,* 2001). These studies provide compelling evidence suggesting a role for chromatin remodeling factors in maintaining genome stability and in tumor suppression.

Conversely, it is conceivable that these Rb-associated chromatin-remodeling factors fail to maintain genome stability in Rb-deficient cells, thereby contributing to tumor development. This notion is highlighted by the evidence showing differences in complex formation and subnuclear distribution of polycomb group proteins in Rb-deficient cells compared with Rb-proficient cells (Dahiya *et al.,* 2001); thus indicating that Rb globally influences the function of at least some chromatin remodeling factors.

In addition, Rb may modulate global chromosome organization through a connection with DNA Topoisomerase IIα (Bhat *et al.,* 1999). DNA Topo II is an essential nuclear enzyme that plays a key role in the topological modification of DNA during replication, recombination, and chromosome condensation and segregation (see review by Warburton and Earnshaw, 1997, and references therein). Mutation of Topo II in *S. pombe* and *S. cerevisiae* cells leads to chromosome breakage and a high frequency of chromosome nondisjunction (Holm *et al.,* 1985, 1989; Rose *et al.,* 1990; Uemura *et al.,* 1986, 1987). Studies in mammalian cells also reveal that Topo II inhibitors block chromosome segregation at the metaphase–anaphase transition (Ishida *et al.,* 1994). The DNA modification activity of Topo II is apparently important for the modulation of chromatin structures. Topo II is essential for chromosome condensation, which is unambiguously supported by genetic and biochemical studies in a variety of species (Adachi *et al.,* 1991; Uemura *et al.,* 1987; Wood and Earnshaw, 1990). Although still controversial, considerable evidence suggests that Topo II plays an important role in chromatin assembly and maintenance of essential chromosome structures (Hirano and Mitchison, 1991; Sealy *et al.,* 1986; Sekiguchi and Kmiec, 1988). The interaction between Rb and Topo IIα, the major form of Topo II in the mammalian cells was shown *in vivo* to be mediated by the A/B domains of Rb. Transient expression of the wild-type but not the mutant Rb in Rb-deficient cancer cells inhibits the Topo II enzymatic activity in cell extracts. Purified recombinant Rb also inhibits Topo II activity *in vitro*. The biological significance, however, has not been established at present for the Rb–Topo II interaction and the inhibitory activity of Rb on Topo II. Nevertheless, the

biological functions of the Rb–Topo II could be globally involved in virtually every activity of Topo II conducted on chromosomes, including replication, transcription, and recombination (reviewed by Warburton and Earnshaw, 1997).

C. Rb and Global Genome Fluidity

It has been conceived that genomic DNA must retain a degree of fluidity at interphase for the processes of DNA replication, recombination, repair, and transcription and other DNA metabolic activities (see reviews by Kingston and Narlikar, 1999, and references therein). Apparently, such genome fluidity must be properly controlled to facilitate DNA metabolism and to keep the genome stable. How genome fluidity is controlled has not been studied. The connections between Rb and remodeling factors that either modify histone conformation or rearrange nucleosome positions may lie in this regulation. Given that HEC1 functions in part through interacting with the SMC proteins, Rb is also potentially important for the reorganization and dynamics of postreplication chromosomes. Taken together, Rb may control genome fluidity by influencing the global activities of chromatin remodeling factors at multiple levels (Fig. 2).

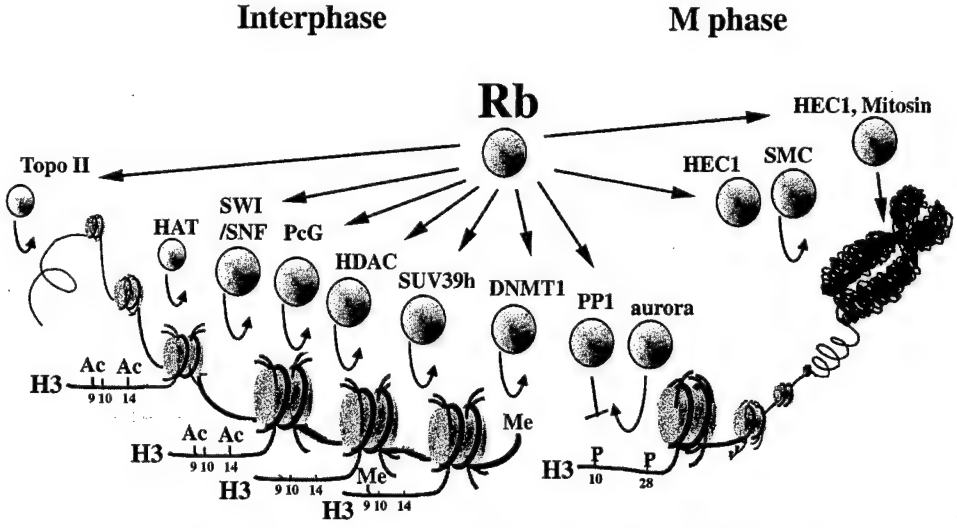

Fig. 2 A model of Rb in regulating genome fluidity. The amino-terminal tail of histone H3 is shown. Numbers indicate the positions of residues that are acetylated, methylated, or phosphorylated. Ac, acetylation; Me, methylation; P, phosphorylation.

VI. HAPLOINSUFFICIENCY OF Rb IN MAINTAINING GENOME STABILITY

Although Rb is apparently involved in multiple cellular functions important for maintaining genome stability, direct evidence supporting a role of Rb in the maintenance of genetic stability remains scarce; namely, the question remains whether loss of Rb function leads to genome instability. This question has not been answered partly due to limited methods used to measure chromosome instability. To circumvent this limitation, a method was recently developed to examine the level of chromosome instability by using a retrovirus carrying both a positive and a negative selectable marker that can integrate randomly into individual chromosomes (Zheng *et al.*, 2002). With this method, frequency of loss of this selectable chromosomal marker (LOM) was measured, and the results showed that normal mouse embryonic stem (ES) cells have a very low frequency of LOM, which was less than 10^{-8}/cell/generation. In mouse ES cells with homozygous Rb null mutation, the frequency was increased to approximately 10^{-5}/cell/generation, while in Rb-heterozygous ES cells, the frequency was approximately 10^{-7}/cell/generation. Further analysis indicated that LOM was mainly mediated through chromosomal mechanisms instead of point mutations. These results reveal that Rb+/− cells are haploinsufficient and that Rb plays a critical role in the maintenance of chromosome stability (Zheng *et al.*, 2002).

The average frequency of LOM observed in Rb−/− cells is approximately 10^{-5}. Classical methods such as multiplex fluorescent *in situ* hybridization (FISH) and spectral karyotyping (SKY) would not be able to discern any aberrance if vast numbers of cells were not subjected to these experiments (Lengauer *et al.*, 1997; Liyanage *et al.*, 1996). Because of the complexity of those methods, it is impractical to examine a large number of cells. By contrast, this method is more sensitive in evaluating chromosome instability, although, unlike FISH or SKY, it cannot tell the types of chromosome aberrations directly. It remains necessary to employ the traditional polymorphism marker analysis on the viral integrated chromosome to examine which type(s) of chromosome mechanisms are involved.

Although nondisjunction is apparently a result of improper chromosome segregation, how the other types of chromosome aberrations occur remains unknown. Chromosome mechanisms underlying LOM in Rb-deficient cells are most likely composed of multiple types of chromosome aberrance since Rb appears to be capable of modulating chromosome metabolism from different, but intimately linked, aspects including chromosome replication, segregation, and structural maintenance. With this newly developed method,

it will be interesting to study how the association of Rb with these different chromosome mechanisms maintains chromosome stability.

The low level of chromosome instability in Rb-deficient cells is not unexpected since severe chromosome abnormality would lead to cell growth arrest or cell death. Otherwise, additional molecular events are necessary for cells to bypass the checkpoint control or apoptosis. Therefore, acquired p53 mutations have been frequently observed in tumors developed from cells with severe defects in genetic stability. It is considered that p53 mutations abolish DNA damage checkpoint or apoptosis control, thereby allowing the accumulation of genetic alterations. By contrast, p53 mutations or loss of heterozygosity at chromosome 17 are not as frequently detected in human retinoblastoma as in other tumors (Kato *et al.,* 1996), although mutations in other checkpoint control or apoptosis pathways cannot be excluded, particularly in the advanced stages of tumor development. Similarly, genome instability caused by other tumor suppressor genes may also occur at a low level, which previous studies could have easily overlooked.

Genomic instability in Rb-deficient cells could be responsible for further genetic alterations involved in cancer development. Germline mutations in one Rb allele leads to the development of retinoblastoma in human and pituitary tumors in mouse at very early ages and with nearly complete penetrance (Knudson, 1971; Lee *et al.,* 1992). The remaining wild-type allele is lost as a somatic event and, as suggested, mainly through chromosomal mechanisms (Cavenee *et al.,* 1985; Hagstrom and Dryja, 1999). It has been estimated previously, based on the mean number of tumors occurring in carriers of retinoblastoma, that the mutation rates in both events are nearly equal (Knudson, 1971). In the recent study, by directly accessing the mutation rate, it was suggested that the mutation rate increased when the first Rb allele is inactivated (Zheng *et al.,* 2002). Chromosome instability in Rb-heterozygous cells could explain the high penetrance of tumor development with loss of the remaining wild-type allele. Nonetheless, the loss of the second Rb allele appears to be the threshold event in tumor development, given that it results in much greater instability, which might account for all of the subsequent genetic alterations essential for tumorigenesis.

Although loss of heterozygosity is the major mechanism underlying the inactivation of a tumor suppressor gene, functional haploinsufficiency of a tumor suppressor gene was previously observed in mice with heterozygous null mutation of p27, which encodes a cdk2 inhibitor and functions mainly as a negative regulator of cell cycle. These mice had increased risk of developing tumors without loss of the remaining wild-type allele (Fero *et al.,* 1998), suggesting that p27 is a tumor suppressor gene with haploinsufficiency in tumor suppression. Although it still holds true that loss of the remaining

wild-type allele for classical tumor suppressor genes is a threshold event in tumor development, heterozygosity of tumor suppressor genes may not be sufficient to maintain genome stability, thereby attributing to the loss of heterozygosity.

VII. PERSPECTIVES

A substantial amount of evidence has revealed the links between genes functionally important for genome stability and cancer. For example, mutations in genes (XPA-XPG) involved in nucleotide excision repair (NER) are predisposed to *xeroderma pigmentosum* (XP), a human hereditary disease characterized by hypersensitivity to UV light and a high incidence of skin tumors (reviewed by Berneburg and Lehmann, 2001). The hereditary nonpolyposis colon cancer (HNPCC) genes are involved in mismatch repair (reviewed by Kinzler and Vogelstein, 1996). Genes, such as ATM, NBS1, BLM, FACNA to FACNE, etc., responsible for more complicated hereditary disease syndromes including ataxia telangiectasia, Nimenjin's syndrome, Bloom's syndrome, Fanconi's anemia, etc., have also been identified (reviewed by Carney, 1999; Ellis and German, 1996; Joenje and Patel, 2001; Lavin and Shiloh, 1997). Mutations in these genes cause cellular defects in DNA damage response and repair pathways, and mutation carriers are prone to various cancers as well as other diseases. Taken together, HNPCC genes, XP genes, as well as ATM, BLM, NBS, etc., constitute a unique group of cancer susceptibility genes, which are mainly involved in DNA damage signaling and repair pathways. Genes of this group are apparently important for maintaining genome stability, but do not suppress tumor formation after being reintroduced into the cell, for example, MSH2-deficient cancer cells (reviewed by Kinzler and Vogelstein, 1997). Moreover, mutations in this group of genes contribute to only a small percentage of human cancers, and mostly the hereditary cancers.

By contrast, cancer susceptibility genes such as Rb, p53, WT1, APC, p16, ARF, PTEN, etc., whose mutations are frequently observed in human cancers, exhibit tumor suppression activities (Baker *et al.,* 1990; Chen *et al.,* 1990; Furnari *et al.,* 1997; Groden *et al.,* 1995; Haber *et al.,* 1993). From this aspect, they are considered to be *bona fide* tumor suppressor genes. Although the mechanistic basis of tumor suppression has not been completely clarified, we can attribute it at least in part to their function in the control of cell growth and differentiation in normal cells. As discussed above, a role in maintaining genome stability is necessary for them to reduce cancer susceptibility. Thus, it is important to understand how these *bona fide* tumor suppressors function in maintaining genome stability.

It has been suggested that p53 is involved in DNA damage-induced checkpoint and apoptosis control, and in centrosome duplication (reviewed by Bates and Vousden, 1996; Fukasawa *et al.,* 1996; reviewed by Hartwell and Kastan, 1994). p53-deficient cells are characterized by aneuploidy, chromosome instability, and gene amplification (Fukasawa *et al.,* 1996; Livingstone *et al.,* 1992; Shao *et al.,* 2000; Yin *et al.,* 1992). Germline p53 mutations in Li–Fraumani syndrome could be attributed to genome instability that leads to cancer formation in this familial disease (Malkin *et al.,* 1990; Srivastava *et al.,* 1990). Recently, APC was found to be critical for chromosome segregation and chromosome stability (Fodde *et al.,* 2001; Kaplan *et al.,* 2001), further highlighting a role of *bona fide* tumor suppressors in maintaining genome stability. It is therefore of great value to examine the role of other tumor suppressors in maintaining chromosome stability, and Rb may serve as a prototype for such an exploration.

It is conceivable that tumor suppressors share a common role in the maintenance of genome stability. Thus, the next question is what is the central mechanism shared by tumor suppressors for maintaining genome stability. Tumor suppressors could directly participate in DNA repair or other aspects of chromosome metabolism. For instance, the familial breast cancer susceptibility genes BRCA1 and BRCA2 are potentially *bona fide* tumor suppressors by playing significant roles in cell growth and differentiation. BRCA1 and BRCA2 have been implicated in both DNA damage-induced checkpoint control and DNA double-strand break repair (see review by Zheng *et al.,* 2000b, and references therein). However, many tumor suppressors are not known for a direct role in DNA repair or any other aspects of chromosome metabolism. DNA repair, replication, and chromosome segregation continue in the absence of tumor suppressors, and no gross abnormality in cells is observed as a result of defects in these chromosome metabolic processes. Although Rb is involved in many aspects of chromosome metabolism, it does not directly participate in any of these activities; instead, it serves as a modulator. Chromatin remodeling activity appears to be mediated by this regulatory role of Rb. On the other hand, all the chromosome metabolic processes take place on the chromatin template. For an efficient and accurate process of DNA repair and any other form of chromosome metabolism, the chromatin template must be properly configured. Without a proper configuration of chromatin structures and fluidity, one would expect that chromosome metabolic processes continue, provided that cellular machinery for chromosome metabolism is intact. Consequently, no gross chromosomal abnormality would result. Nonetheless, the efficiency and accuracy of these processes would be affected, which would result in genome instability. Thus, it is not surprising that most known tumor suppressors maintain genome stability without direct participation in DNA repair, replication, or chromosome segregation and that no obvious genome

aberrations have so far been observed in noncancerous cells with deficiency in most tumor suppressors. However, it does not preclude the existence of a low degree of genome instability in these cells that may be attributable to a defect in chromatin remodeling mechanism. It is, therefore, likely that control of chromatin fluidity may be the central mechanism shared by Rb and other tumor suppressors in maintaining genome stability.

ACKNOWLEDGMENTS

Work performed in this laboratory was supported by grants from the NIH (EY05758, CA 58318) and A. P. McDermott endowment fund. We thank Paul Hasty for his comments and suggestions.

REFERENCES

Adachi, Y., Luke, M., and Laemmli, U. K. (1991). Chromosome assembly in vitro: Topoisomerase II is required for condensation. *Cell* **64,** 137–148.

Akhmedov, A. T., Gross, B., and Jessberger, R. (1999). Mammalian SMC3 C-terminal and coiled-coil protein domains specifically bind palindromic DNA, do not block DNA ends, and prevent DNA bending. *J. Biol. Chem.* **274,** 38,216–38,224.

Alland, L., Muhle, R., Hou, H., Jr., Potes, J., Chin, L., Schreiber-Agus, N., and DePinho, R. A. (1997). Role for N-CoR and histone deacetylase in Sin3-mediated transcriptional repression. *Nature* **387,** 49–55.

Austin, R. J., Orr-Weaver, T. L., and Bell, S. P. (1999). Drosophila ORC specifically binds to ACE3, an origin of DNA replication control element. *Genes Dev.* **13,** 2639–2649.

Baker, S. J., Markowitz, S., Fearon, E. R., Willson, J. K., and Vogelstein, B. (1990). Suppression of human colorectal carcinoma cell growth by wild-type p53. *Science* **249,** 912–915.

Bannister, A. J., Zegerman, P., Partridge, J. F., Miska, E. A., Thomas, J. O., Allshire, R. C., and Kouzarides, T. (2001). Selective recognition of methylated lysine 9 on histone H3 by the HP1 chromo domain. *Nature* **410,** 120–124.

Bates, S., and Vousden, K. H. (1996). p53 in signaling checkpoint arrest or apoptosis. *Curr. Opin. Genet. Dev.* **6,** 12–18.

Baumeister, W., Walz, J., Zuhl, F., and Seemuller, E. (1998). The proteasome: Paradigm of a self-compartmentalizing protease. *Cell* **92,** 367–380.

Bernard, P., Maure, J. F., Partridge, J. F., Genier, S., Javerzat, J. P., and Allshire, R. C. (2001). Requirement of heterochromatin for cohesion at centromeres. *Science* **11,** 11.

Berneburg, M., and Lehmann, A. R. (2001). Xeroderma pigmentosum and related disorders: Defects in DNA repair and transcription. *Adv. Genet.* **43,** 71–102.

Bhat, U. G., Raychaudhuri, P., and Beck, W. T. (1999). Functional interaction between human Topoisomerase IIalpha and retinoblastoma protein. *Proc. Natl. Acad. Sci. USA* **96,** 7859–7864.

Bischoff, J. R., Anderson, L., Zhu, Y., Mossie, K., Ng, L., Souza, B., Schryver, B., Flanagan, P., Clairvoyant, F., Ginther, C., Chan, C. S., Novotny, M., Slamon, D. J., and Plowman, G. D. (1998). A homologue of Drosophila aurora kinase is oncogenic and amplified in human colorectal cancers. *EMBO J.* **17,** 3052–3065.

Bischoff, J. R., and Plowman, G. D. (1999). The Aurora/Ipl1p kinase family: Regulators of chromosome segregation and cytokinesis. *Trends Cell. Biol.* **9,** 454–459.

Blat, Y., and Kleckner, N. (1999). Cohesins bind to preferential sites along yeast chromosome III, with differential regulation along arms versus the centric region. *Cell* **98,** 249–259.

Bloecher, A., and Tatchell, K. (1999). Defects in Saccharomyces cerevisiae protein phosphatase type I activate the spindle/kinetochore checkpoint. *Genes Dev.* **13,** 517–522.

Bookstein, R., and Lee, W. H. (1991). Molecular genetics of the retinoblastoma suppressor gene. *Crit. Rev. Oncogen.* **2,** 211–227.

Bork, P., Hofmann, K., Bucher, P., Neuwald, A. F., Altschul, S. F., and Koonin, E. V. (1997). A superfamily of conserved domains in DNA damage-responsive cell cycle checkpoint proteins. *FASEB J.* **11,** 68–76.

Bosco, G., Du, W., and Orr-Weaver, T. L. (2001). DNA replication control through interaction of E2F-RB and the origin recognition complex. *Nat. Cell Biol.* **3,** 289–295.

Boveri, T. (1902). Uber mehrpolige mitosen als mittel zur analyse des zellkerns. *Verh. D. Phys. Med. Ges. Wurzberg N.F.* **35,** 67–69.

Brehm, A., Miska, E. A., McCance, D. J., Reid, J. L., Bannister, A. J., and Kouzarides, T. (1998). Retinoblastoma protein recruits histone deacetylase to repress transcription. *Nature* **391,** 597–601.

Breiling, A., Turner, B. M., Bianchi, M. E., and Orlando, V. (2001). General transcription factors bind promoters repressed by Polycomb group proteins. *Nature* **412,** 651–655.

Brugarolas, J., Moberg, K., Boyd, S. D., Taya, Y., Jacks, T., and Lees, J. A. (1999). Inhibition of cyclin-dependent kinase 2 by p21 is necessary for retinoblastoma protein-mediated G1 arrest after gamma-irradiation. *Proc. Natl. Acad. Sci. USA* **96,** 1002–1007.

Carney, J. P. (1999). Chromosomal breakage syndromes. *Curr. Opin. Immunol.* **11,** 443–447.

Cavenee, W. K., Hansen, M. F., Nordenskjold, M., Kock, E., Maumenee, I., Squire, J. A. P., and Gallie, B. L. (1985). Genetic origin of mutations predisposing to retinoblastoma. *Science* **228,** 501–503.

Chan, C. S., and Botstein, D. (1993). Isolation and characterization of chromosome-gain and increase-in-ploidy mutants in yeast. *Genetics* **135,** 677–691.

Chen, C., and Kolodner, R. D. (1999). Gross chromosomal rearrangements in Saccharomyces cerevisiae replication and recombination defective mutants. *Nat. Genet.* **23,** 81–85.

Chen, P.-L., Riley, D. J., Chen, Y., and Lee, W.-H. (1996). Retinoblastoma protein positively regulates terminal adipocyte differentiation through direct interaction with C/EBPs. *Genes Dev.* **10,** 2794–2804.

Chen, P. L., Chen, Y. M., Bookstein, R., and Lee, W. H. (1990). Genetic mechanisms of tumor suppression by the human p53 gene. *Science* **250,** 1576–1580.

Chen, P. L., Riley, D. J., and Lee, W. H. (1995a). The retinoblastoma protein as a fundamental mediator of growth and differentiation signals. *Crit. Rev. Eukaryotic Gene Expression* **5,** 79–95.

Chen, P. L., Scully, P., Shew, J. Y., Wang, J. Y., and Lee, W. H. (1989). Phosphorylation of the retinoblastoma gene product is modulated during the cell cycle and cellular differentiation. *Cell* **58,** 1193–1198.

Chen, P. L., Ueng, Y. C., Durfee, T., Chen, K. C., Yang-Feng, T., and Lee, W. H. (1995b). Identification of a human homologue of yeast nuc2 which interacts with the retinoblastoma protein in a specific manner. *Cell Growth Differ.* **6,** 199–210.

Chen, Y., Riley, D. J., Chen, P. L., and Lee, W. H. (1997a). HEC, a novel nuclear protein rich in leucine heptad repeats specifically involved in mitosis. *Mol. Cell. Biol.* **17,** 6049–6056.

Chen, Y., Sharp, Z. D., and Lee, W. H. (1997b). HEC binds to the seventh regulatory subunit of the 26S proteasome and modulates the proteolysis of mitotic cyclins. *J. Biol. Chem.* **272,** 24,081–24,087.

Chesnokov, I., Gossen, M., Remus, D., and Botchan, M. (1999). Assembly of functionally active Drosophila origin recognition complex from recombinant proteins. *Genes Dev.* **13**, 1289–1296.

Dahiya, A., Wong, S., Gonzalo, S., Gavin, M., and Dean, D. C. (2001). Linking the Rb and polycomb pathways. *Mol. Cell* **8**, 557–569.

DeCaprio, J. A., Ludlow, J. W., Lynch, D., Furukawa, Y., Griffin, J., Piwnica-Worms, H., Huang, C. M., and Livingston, D. M. (1989). The product of the retinoblastoma susceptibility gene has properties of a cell cycle regulatory element. *Cell* **58**, 1085–1095.

Di Leonardo, A., Khan, S. H., Linke, S. P., Greco, V., Seidita, G., and Wahl, G. M. (1997). DNA rereplication in the presence of mitotic spindle inhibitors in human and mouse fibroblasts lacking either p53 or pRb function. *Cancer Res.* **57**, 1013–1019.

Dunaief, J. L., Strober, B. E., Guha, S., Khavari, P. A., Alin, K., Luban, J., Crabtree, G. R., and Goff, S. P. (1994). The retinoblastoma protein and BRG1 form a complex and cooperate to induce cell cycle arrest. *Cell* **79**, 119–130.

Durfee, T., Becherer, K., Chen, P.-L., Yeh, S.-H., Yang, Y., Kilburn, A. E., Lee, W.-H., and Elledge, S. J. (1993). The retinoblastoma protein associates with the protein phosphatase type 1 catalytic subunit. *Genes Dev.* **7**, 555–569.

Dyson, N. (1998). The regulation of E2F by pRB-family proteins. *Genes Dev.* **12**, 2245–2262.

el-Deiry, W. S. (1998). p21/p53, cellular growth control and genomic integrity. *Curr. Top. Microbiol. Immunol.* **227**, 121–137.

Ellis, N. A., and German, J. (1996). Molecular genetics of Bloom's syndrome. *Hum. Mol. Genet.* **5**, 1457–1463.

Espelin, C. W., Kaplan, K. B., and Sorger, P. K. (1997). Probing the architecture of a simple kinetochore using DNA-protein crosslinking. *J. Cell Biol.* **139**, 1383–1396.

Fero, M. L., Randel, E., Gurley, K. E., Roberts, J. M., and Kemp, C. J. (1998). The murine gene p27Kip1 is haplo-insufficient for tumour suppression. *Nature* **396**, 177–180.

Flatt, P. M., Tang, L. J., Scatena, C. D., Szak, S. T., and Pietenpol, J. A. (2000). p53 regulation of G(2) checkpoint is retinoblastoma protein dependent. *Mol. Cell. Biol.* **20**, 4210–4223.

Flores-Rozas, H., and Kolodner, R. D. (2000). Links between replication, recombination and genome instability in eukaryotes. *Trends Biochem. Sci.* **25**, 196–200.

Fodde, R., Kuipers, J., Rosenberg, C., Smits, R., Kielman, M., Gaspar, C., van Es, J. H., Breukel, C., Wiegant, J., Giles, R. H., and Clevers, H. (2001). Mutations in the APC tumour suppressor gene cause chromosomal instability. *Nat. Cell Biol.* **3**, 433–438.

Francis, N. J., Saurin, A. J., Shao, Z., and Kingston, R. E. (2001). Reconstitution of a functional core polycomb repressive complex. *Mol. Cell* **8**, 545–556.

Francisco, L., Wang, W., and Chan, C. S. (1994). Type 1 protein phosphatase acts in opposition to IpL1 protein kinase in regulating yeast chromosome segregation. *Mol. Cell. Biol.* **14**, 4731–4740.

Fukasawa, K., Choi, T., Kuriyama, R., Rulong, S., and Vande Woude, G. F. (1996). Abnormal centrosome amplification in the absence of p53. *Science* **271**, 1744–1747.

Furnari, F. B., Lin, H., Huang, H. S., and Cavenee, W. K. (1997). Growth suppression of glioma cells by PTEN requires a functional phosphatase catalytic domain. *Proc. Natl. Acad. Sci. USA* **94**, 12,479–12,484.

Ghislain, M., Udvardy, A., and Mann, C. (1993). S. cerevisiae 26S protease mutants arrest cell division in G2/metaphase. *Nature* **366**, 358–362.

Glover, D. M., Leibowitz, M. H., McLean, D. A., and Parry, H. (1995). Mutations in aurora prevent centrosome separation leading to the formation of monopolar spindles. *Cell* **81**, 95–105.

Goodrich, D. W., Wang, N. P., Qian, Y.-W., Lee, E. Y.-H. P., and Lee, W.-H. (1991). The retinoblastoma gene product regulates progression through the G1 phase of the cell cycle. *Cell* **67**, 293–302.

Gopalan, G., Chan, C. S., and Donovan, P. J. (1997). A novel mammalian, mitotic spindle-associated kinase is related to yeast and fly chromosome segregation regulators. *J. Cell Biol.* **138,** 643–656.

Groden, J., Joslyn, G., Samowitz, W., Jones, D., Bhattacharyya, N., Spirio, L., Thliveris, A., Robertson, M., Egan, S., Meuth, M., *et al.* (1995). Response of colon cancer cell lines to the introduction of APC, a colon-specific tumor suppressor gene. *Cancer Res.* **55,** 1531–1539.

Guenther, M. G., Lane, W. S., Fischle, W., Verdin, E., Lazar, M. A., and Shiekhattar, R. (2000). A core SMRT corepressor complex containing HDAC3 and TBL1, a WD40-repeat protein linked to deafness. *Genes Dev.* **14,** 1048–1057.

Guidi, C. J., Sands, A. T., Zambrowicz, B. P., Turner, T. K., Demers, D. A., Webster, W., Smith, T. W., Imbalzano, A. N., and Jones, S. N. (2001). Disruption of Ini1 leads to peri-implantation lethality and tumorigenesis in mice. *Mol. Cell. Biol.* **21,** 3598–3603.

Haber, D. A., Park, S., Maheswaran, S., Englert, C., Re, G. G., Hazen-Martin, D. J., Sens, D. A., and Garvin, A. J. (1993). WT1-mediated growth suppression of Wilms tumor cells expressing a WT1 splicing variant. *Science* **262,** 2057–2059.

Haber, J. E. (1998). The many interfaces of Mre11. *Cell* **95,** 583–586.

Hagstrom, S. A., and Dryja, T. P. (1999). Mitotic recombination map of 13cen-13q14 derived from an investigation of loss of heterozygosity in retinoblastomas. *Proc. Natl. Acad. Sci. USA* **96,** 2952–2957.

Hanahan, D., and Weinberg, R. A. (2000). The hallmarks of cancer. *Cell* **100,** 57–70.

Harbour, J. W., and Dean, D. C. (2000). Chromatin remodeling and Rb activity. *Curr. Opin. Cell Biol.* **12,** 685–689.

Harrington, E. A., Bruce, J. L., Harlow, E., and Dyson, N. (1998). pRB plays an essential role in cell cycle arrest induced by DNA damage. *Proc. Natl. Acad. Sci. USA* **95,** 11,945–11,950.

Hartwell, L., Weinert, T., Kadyk, L., and Garvik, B. (1994). Cell cycle checkpoints, genomic integrity, and cancer. *Cold Spring Harbor Symp. Quant. Biol.* **59,** 259–263.

Hartwell, L. H., and Kastan, M. B. (1994). Cell cycle control and cancer. *Science* **266,** 1821–1828.

Heinzel, T., Lavinsky, R. M., Mullen, T. M., Soderstrom, M., Laherty, C. D., Torchia, J., Yang, W. M., Brard, G., Ngo, S. D., Davie, J. R., Seto, E., Eisenman, R. N., Rose, D. W., Glass, C. K., and Rosenfeld, M. G. (1997). A complex containing N-CoR, mSin3 and histone deacetylase mediates transcriptional repression. *Nature* **387,** 43–48.

Hendzel, M. J., Wei, Y., Mancini, M. A., Van Hooser, A., Ranalli, T., Brinkley, B. R., Bazett-Jones, D. P., and Allis, C. D. (1997). Mitosis-specific phosphorylation of histone H3 initiates primarily within pericentromeric heterochromatin during G2 and spreads in an ordered fashion coincident with mitotic chromosome condensation. *Chromosoma* **106,** 348–360.

Hinds, P. W., Mittnacht, S., Dulic, V., Arnold, A., Reed, S. I., and Weinberg, R. A. (1992). Regulation of retinoblastoma protein functions by ectopic expression of human cyclins. *Cell* **70,** 993–1006.

Hirano, T. (2000). Chromosome cohesion, condensation, and separation. *Annu. Rev. Biochem.* **69,** 115–144.

Hirano, T., and Mitchison, T. J. (1991). Cell cycle control of higher-order chromatin assembly around naked DNA in vitro. *J. Cell Biol.* **115,** 1479–1489.

Hisamoto, N., Sugimoto, K., and Matsumoto, K. (1994). The Glc7 type 1 protein phosphatase of Saccharomyces cerevisiae is required for cell cycle progression in G2/M. *Mol. Cell. Biol.* **14,** 3158–165.

Hoeijmakers, J. H. (2001). Genome maintenance mechanisms for preventing cancer. *Nature* **411,** 366–374.

Holm, C., Goto, T., Wang, J. C., and Botstein, D. (1985). DNA Topoisomerase II is required at the time of mitosis in yeast. *Cell* **41,** 553–563.

Holm, C., Stearns, T., and Botstein, D. (1989). DNA Topoisomerase II must act at mitosis to prevent nondisjunction and chromosome breakage. *Mol. Cell. Biol.* **9**, 159–168.

Holstege, F. C., Jennings, E. G., Wyrick, J. J., Lee, T. I., Hengartner, C. J., Green, M. R., Golub, T. R., Lander, E. S., and Young, R. A. (1998). Dissecting the regulatory circuitry of a eukaryotic genome. *Cell* **95**, 717–728.

Hsu, J. Y., Sun, Z. W., Li, X., Reuben, M., Tatchell, K., Bishop, D. K., Grushcow, J. M., Brame, C. J., Caldwell, J. A., Hunt, D. F., Lin, R., Smith, M. M., and Allis, C. D. (2000). Mitotic phosphorylation of histone H3 is governed by Ipl1/aurora kinase and Glc7/PP1 phosphatase in budding yeast and nematodes. *Cell* **102**, 279–291.

Huang, H. J., Yee, J. K., Shew, J. Y., Chen, P. L., Bookstein, R., Friedmann, T., Lee, E. Y.-P., and Lee, W. H. (1988). Suppression of the neoplastic phenotype by replacement of the RB gene in human cancer cells. *Science* **242**, 1563–1566.

Hyland, K. M., Kingsbury, J., Koshland, D., and Hieter, P. (1999). Ctf19p: A novel kinetochore protein in Saccharomyces cerevisiae and a potential link between the kinetochore and mitotic spindle. *J. Cell Biol.* **145**, 15–28.

Ishida, R., Sato, M., Narita, T., Utsumi, K. R., Nishimoto, T., Morita, T., Nagata, H., and Andoh, T. (1994). Inhibition of DNA Topoisomerase II by ICRF-193 induces polyploidization by uncoupling chromosome dynamics from other cell cycle events. *J. Cell Biol.* **126**, 1341–1351.

Jacks, T., Fazeli, A., Schmitt, E. M., Bronson, R. T., Goodell, M. A., and Weinberg, R. A. (1992). Effects of an Rb mutation in the mouse. *Nature* **359**, 295–300.

Janke, C., Ortiz, J., Lechner, J., Shevchenko, A., Magiera, M. M., Schramm, C., and Schiebel, E. (2001). The budding yeast proteins Spc24p and Spc25p interact with Ndc80p and Nuf2p at the kinetochore and are important for kinetochore clustering and checkpoint control. *EMBO J.* **20**, 777–791.

Joenje, H., and Patel, K. J. (2001). The emerging genetic and molecular basis of Fanconi anaemia. *Nat. Rev. Genet.* **2**, 446–457.

Jones, P. L., Veenstra, G. J., Wade, P. A., Vermaak, D., Kass, S. U., Landsberger, N., Strouboulis, J., and Wolffe, A. P. (1998). Methylated DNA and MeCP2 recruit histone deacetylase to repress transcription. *Nat. Genet.* **19**, 187–191.

Kaplan, K. B., Burds, A. A., Swedlow, J. R., Bekir, S. S., Sorger, P. K., and Nathke, I. S. (2001). A role for the Adenomatous Polyposis Coli protein in chromosome segregation. *Nat. Cell Biol.* **3**, 429–432.

Karantza, V., Maroo, A., Fay, D., and Sedivy, J. M. (1993). Overproduction of Rb protein after the G1/S boundary causes G2 arrest. *Mol. Cell. Biol.* **13**, 6640–6652.

Kato, M. V., Shimizu, T., Ishizaki, K., Kaneko, A., Yandell, D. W., Toguchida, J., and Sasaki, M. S. (1996). Loss of heterozygosity on chromosome 17 and mutation of the p53 gene in retinoblastoma. *Cancer Lett.* **106**, 75–82.

Kennedy, B. K., Barbie, D. A., Classon, M., Dyson, N., and Harlow, E. (2000). Nuclear organization of DNA replication in primary mammalian cells. *Genes Dev.* **14**, 2855–2868.

Khan, S. H., and Wahl, G. M. (1998). p53 and pRb prevent rereplication in response to microtubule inhibitors by mediating a reversible G1 arrest. *Cancer Res.* **58**, 396–401.

Kingston, R. E., and Narlikar, G. J. (1999). ATP-dependent remodeling and acetylation as regulators of chromatin fluidity. *Genes Dev.* **13**, 2339–2352.

Kinoshita, N., Ohkura, H., and Yanagida, M. (1990). Distinct, essential roles of type 1 and 2A protein phosphatases in the control of the fission yeast cell division cycle. *Cell* **63**, 405–415.

Kinzler, K. W., and Vogelstein, B. (1997). Cancer-susceptibility genes. Gatekeepers and caretakers. *Nature* **386**, 763.

Kinzler, K. W., and Vogelstein, B. (1996). Lessons from hereditary colorectal cancer. *Cell* **87**, 159–170.

Klein, G. (1987). The approaching era of the tumor suppressor genes. *Science* **238**, 1539–1545.

Kniola, B., O'Toole, E., McIntosh, J. R., Mellone, B., Allshire, R., Mengarelli, S., Hultenby, K., and Ekwall, K. (2001). The domain structure of centromeres is conserved from fission yeast to humans. *Mol. Biol. Cell* **12,** 2767–2775.

Knudsen, E. S., Buckmaster, C., Chen, T. T., Feramisco, J. R., and Wang, J. Y. (1998). Inhibition of DNA synthesis by RB: effects on G1/S transition and S-phase progression. *Genes Dev.* **12,** 2278–2292.

Knudsen, K. E., Booth, D., Naderi, S., Sever-Chroneos, Z., Fribourg, A. F., Hunton, I. C., Feramisco, J. R., Wang, J. Y., and Knudsen, E. S. (2000). RB-dependent S-phase response to DNA damage. *Mol. Cell. Biol.* **20,** 7751–7763.

Knudson, A. G., Jr. (1971). Mutation and cancer: Statistical study of retinoblastoma. *Proc. Natl. Acad. Sci. USA* **68,** 820–823.

Koshland, D., and Strunnikov, A. (1996). Mitotic chromosome condensation. *Annu. Rev. Cell. Dev. Biol.* **12,** 305–333.

Koshland, D. E., and Guacci, V. (2000). Sister chromatid cohesion: The beginning of a long and beautiful relationship. *Curr. Opin. Cell Biol.* **12,** 297–301.

Lachner, M., O'Carroll, D., Rea, S., Mechtler, K., and Jenuwein, T. (2001). Methylation of histone H3 lysine 9 creates a binding site for HP1 proteins. *Nature* **410,** 116–120.

Laherty, C. D., Yang, W. M., Sun, J. M., Davie, J. R., Seto, E., and Eisenman, R. N. (1997). Histone deacetylases associated with the mSin3 corepressor mediate mad transcriptional repression. *Cell* **89,** 349–356.

Lai, A., Lee, J. M., Yang, W. M., DeCaprio, J. A., Kaelin, W. G., Jr., Seto, E., and Branton, P. E. (1999). RBP1 recruits both histone deacetylase-dependent and -independent repression activities to retinoblastoma family proteins. *Mol. Cell. Biol.* **19,** 6632–6641.

Lavin, M. F., and Shiloh, Y. (1997). The genetic defect in ataxia-telangiectasia. *Annu. Rev. Immunol.* **15,** 177–202.

Lechner, J., and Carbon, J. (1991). A 240 kd multisubunit protein complex, CBF3, is a major component of the budding yeast centromere. *Cell* **64,** 717–725.

Lee, E. Y., Chang, C.-Y., Hu, N., Wang, Y.-C., Lai, C.-C., Herrup, K., Lee, W.-H., and Bradley, A. (1992). Mice deficient for Rb are nonviable and show defects in neurogenesis and haematopoiesis. *Nature* **359,** 288–294.

Lengauer, C., Kinzler, K. W., and Vogelstein, B. (1998). Genetic instabilities in human cancers. *Nature* **396,** 643–649.

Lengauer, C., Kinzler, K. W., and Vogelstein, B. (1997). Genetic instability in colorectal cancers. *Nature* **386,** 623–627.

Liao, H., Winkfein, R. J., Mack, G., Rattner, J. B., and Yen, T. J. (1995). CENP-F is a protein of the nuclear matrix that assembles onto kinetochores at late G2 and is rapidly degraded after mitosis. *J. Cell Biol.* **130,** 507–518.

Lipinski, M. M., and Jacks, T. (1999). The retinoblastoma gene family in differentiation and development. *Oncogene* **18,** 7873–7882.

Livingstone, L. R., White, A., Sprouse, J., Livanos, E., Jacks, T., and Tlsty, T. D. (1992). Altered cell cycle arrest and gene amplification potential accompany loss of wild-type p53. *Cell* **70,** 923–935.

Liyanage, M., Coleman, A., du Manoir, S., Veldman, T., McCormack, S., Dickson, R. B., Barlow, C., Wynshaw-Boris, A., Janz, S., Wienberg, J., Ferguson-Smith, M. A., Schrock, E., and Ried, T. (1996). Multicolour spectral karyotyping of mouse chromosomes. *Nat. Genet.* **14,** 312–315.

Loeb, L. A. (1991). Mutator phenotype may be required for multistage carcinogenesis. *Cancer Res.* **51,** 3075–3079.

Ludlow, J. W., Howell, R. L., and Smith, H. C. (1993). Hypoxic stress induces reversible hypophosphorylation of pRB and reduction in cyclin A abundance independent of cell cycle progression. *Oncogene* **8,** 331–339.

Ludlow, J. W., Shon, J., Pipas, J. M., Livingston, D. M., and DeCaprio, J. A. (1990). The retinoblastoma susceptibility gene product undergoes cell cycle-dependent dephosphorylation and binding to and release from SV40 large T. *Cell* **60**, 387–396.

Lukas, C., Sorensen, C. S., Kramer, E., Santoni-Rugiu, E., Lindeneg, C., Peters, J. M., Bartek, J., and Lukas, J. (1999). Accumulation of cyclin B1 requires E2F and cyclin-A-dependent rearrangement of the anaphase-promoting complex. *Nature* **401**, 815–818.

Luo, R. X., Postigo, A. A., and Dean, D. C. (1998). Rb interacts with histone deacetylase to repress transcription. *Cell* **92**, 463–473.

Magnaghi-Jaulin, L., Groisman, R., Naguibneva, I., Robin, P., Lorain, S., Le Villain, J. P., Troalen, F., Trouche, D., and Harel-Bellan, A. (1998). Retinoblastoma protein represses transcription by recruiting a histone deacetylase. *Nature* **391**, 601–605.

Malkin, D., Li, F. P., Strong, L. C., Fraumeni, J. F., Jr., Nelson, C. E., Kim, D. H., Kassel, J., Gryka, M. A., Bischoff, F. Z., Tainsky, M. A., *et al.* (1990). Germ line p53 mutations in a familial syndrome of breast cancer, sarcomas, and other neoplasms. *Science* **250**, 1233–1238.

Maser, R. S., Mirzoeva, O. K., Wells, J., Olivares, H., Williams, B. R., Zinkel, R. A., Farnham, P. J., and Petrini, J. H. (2001). Mre11 complex and DNA replication: Linkage to E2F and sites of DNA synthesis. *Mol. Cell. Biol.* **21**, 6006–6016.

Megee, P. C., and Koshland, D. (1999). A functional assay for centromere-associated sister chromatid cohesion. *Science* **285**, 254–257.

Mossi, R., and Hubscher, U. (1998). Clamping down on clamps and clamp loaders—The eukaryotic replication factor C. *Eur. J. Biochem.* **254**, 209–216.

Myung, K., Chen, C., and Kolodner, R. D. (2001). Multiple pathways cooperate in the suppression of genome instability in Saccharomyces cerevisiae. *Nature* **411**, 1073–1076.

Nagy, L., Kao, H. Y., Chakravarti, D., Lin, R. J., Hassig, C. A., Ayer, D. E., Schreiber, S. L., and Evans, R. M. (1997). Nuclear receptor repression mediated by a complex containing SMRT, mSin3A, and histone deacetylase. *Cell* **89**, 373–380.

Nakayama, J., Rice, J. C., Strahl, B. D., Allis, C. D., and Grewal, S. I. (2001). Role of histone H3 lysine 9 methylation in epigenetic control of heterochromatin assembly. *Science* **292**, 110–113.

Nan, X., Ng, H. H., Johnson, C. A., Laherty, C. D., Turner, B. M., Eisenman, R. N., and Bird, A. (1998). Transcriptional repression by the methyl-CpG-binding protein MeCP2 involves a histone deacetylase complex. *Nature* **393**, 386–389.

Nasmyth, K. (1999). Separating sister chromatids. *Trends Biochem. Sci.* **24**, 98–104.

Nasmyth, K., Peters, J. M., and Uhlmann, F. (2000). Splitting the chromosome: Cutting the ties that bind sister chromatids. *Science* **288**, 1379–1385.

Nelson, D. A., and Ludlow, J. W. (1997). Characterization of the mitotic phase pRb-directed protein phosphatase activity. *Oncogene* **14**, 2407–2415.

Nevins, J. R. (1998). Toward an understanding of the functional complexity of the E2F and retinoblastoma families. *Cell. Growth Differ.* **9**, 585–593.

Ng, H. H., and Bird, A. (1999). DNA methylation and chromatin modification. *Curr. Opin. Genet. Dev.* **9**, 158–163.

Niculescu, A. B., 3rd, Chen, X., Smeets, M., Hengst, L., Prives, C., and Reed, S. I. (1998). Effects of p21(Cip1/Waf1) at both the G1/S and the G2/M cell cycle transitions: pRb is a critical determinant in blocking DNA replication and in preventing endoreduplication. *Mol. Cell. Biol.* **18**, 629–643.

Nielsen, S. J., Schneider, R., Bauer, U. M., Bannister, A. J., Morrison, A., O'Carroll, D., Firestein, R., Cleary, M., Jenuwein, T., Herrera, R. E., and Kouzarides, T. (2001). Rb targets histone H3 methylation and HP1 to promoters. *Nature* **412**, 561–565.

Nikitin, A. Y., Juarez-Perez, M. I., Li, S., Huang, L., and Lee, W. H. (1999). RB-mediated suppression of spontaneous multiple neuroendocrine neoplasia and lung metastases in Rb+/− mice. *Proc. Natl. Acad. Sci. USA* **96**, 3916–3921.

Nikitin, A. Y., and Lee, W.-H. (1996). Early loss of the retinoblastoma gene is associated with impaired growth inhibitory innervation during melanotroph carcinogenesis in $Rb^{+/-}$ mice. *Genes Dev.* **10,** 1870–1879.

Ortiz, J., Stemmann, O., Rank, S., and Lechner, J. (1999). A putative protein complex consisting of Ctf19, Mcm21, and Okp1 represents a missing link in the budding yeast kinetochore. *Genes Dev.* **13,** 1140–55.

Osborne, M. A., Schlenstedt, G., Jinks, T., and Silver, P. A. (1994). Nuf2, a spindle pole body-associated protein required for nuclear division in yeast. *J. Cell Biol.* **125,** 853–866.

Otterson, G. A., Chen, W. D., Coxon, A. B., Khleif, S. N., and Kaye, F. J. (1997). Incomplete penetrance of familial retinoblastoma linked to germ-line mutations that result in partial loss of RB function. *Proc. Natl. Acad. Sci. USA* **94,** 12,036–12,040.

Page, A. M., and Hieter, P. (1999). The anaphase-promoting complex: New subunits and regulators. *Annu. Rev. Biochem.* **68,** 583–609.

Pennaneach, V., Salles-Passador, I., Munshi, A., Brickner, H., Regazzoni, K., Dick, F., Dyson, N., Chen, T. T., Wang, J. Y., Fotedar, R., and Fotedar, A. (2001). The large subunit of replication factor C promotes cell survival after DNA damage in an LxCxE motif- and Rb-dependent manner. *Mol. Cell* **7,** 715–27.

Peters, A. H., O'Carroll, D., Scherthan, H., Mechtler, K., Sauer, S., Schofer, C., Weipoltshammer, K., Pagani, M., Lachner, M., Kohlmaier, A., Opravil, S., Doyle, M., Sibilia, M., and Jenuwein, T. (2001). Loss of the suv39h histone methyltransferases impairs mammalian heterochromatin and genome stability. *Cell* **107,** 323–337.

Peterson, C. L., and Workman, J. L. (2000). Promoter targeting and chromatin remodeling by the SWI/SNF complex. *Curr. Opin. Genet. Dev.* **10,** 187–192.

Petrini, J. H. (2000). The Mre11 complex and ATM: Collaborating to navigate S phase. *Curr. Opin. Cell Biol.* **12,** 293–296.

Qian, Y. W., Wang, Y. C., Hollingsworth, R. E., Jr., Jones, D., Ling, N., and Lee, E. Y. (1993). A retinoblastoma-binding protein related to a negative regulator of Ras in yeast. *Nature* **364,** 648–652.

Razin, A. (1998). CpG methylation, chromatin structure and gene silencing—A three-way connection. *EMBO J.* **17,** 4905–4908.

Riley, D. J., Lee, E. Y., and Lee, W. H. (1994). The retinoblastoma protein: More than a tumor suppressor. *Annu. Rev. Cell Biol.* **10,** 1–29.

Riley, D. J., Liu, C. Y., and Lee, W. H. (1997). Mutations of N-terminal regions render the retinoblastoma protein insufficient for functions in development and tumor suppression. *Mol. Cell. Biol.* **17,** 7342–7352.

Roberts, C. W., Galusha, S. A., McMenamin, M. E., Fletcher, C. D., and Orkin, S. H. (2000). Haploinsufficiency of Snf5 (integrase interactor 1) predisposes to malignant rhabdoid tumors in mice. *Proc. Natl. Acad. Sci. USA* **97,** 13,796–13,800.

Robertson, K. D., Ait-Si-Ali, S., Yokochi, T., Wade, P. A., Jones, P. L., and Wolffe, A. P. (2000). DNMT1 forms a complex with Rb, E2F1 and HDAC1 and represses transcription from E2F-responsive promoters. *Nat. Genet.* **25,** 338–342.

Rose, D., Thomas, W., and Holm, C. (1990). Segregation of recombined chromosomes in meiosis I requires DNA Topoisomerase II. *Cell* **60,** 1009–1017.

Royzman, I., Austin, R. J., Bosco, G., Bell, S. P., and Orr-Weaver, T. L. (1999). ORC localization in Drosophila follicle cells and the effects of mutations in dE2F and dDP. *Genes Dev.* **13,** 827–840.

Saitoh, N., Goldberg, I., and Earnshaw, W. C. (1995). The SMC proteins and the coming of age of the chromosome scaffold hypothesis. *Bioessays* **17,** 759–766.

Sassoon, I., Severin, F. F., Andrews, P. D., Taba, M. R., Kaplan, K. B., Ashford, A. J., Stark, M. J., Sorger, P. K., and Hyman, A. A. (1999). Regulation of Saccharomyces cerevisiae kinetochores by the type 1 phosphatase Glc7p. *Genes Dev.* **13,** 545–555.

Saurin, A. J., Shao, Z., Erdjument-Bromage, H., Tempst, P., and Kingston, R. E. (2001). A Drosophila Polycomb group complex includes Zeste and dTAFII proteins. *Nature* **412**, 655–660.

Sealy, L., Cotten, M., and Chalkley, R. (1986). Novobiocin inhibits passive chromatin assembly in vitro. *EMBO J.* **5**, 3305–3311.

Sekiguchi, J. A., and Kmiec, E. B. (1988). Studies on DNA Topoisomerase activity during in vitro chromatin assembly. *Mol. Cell. Biochem.* **83**, 195–205.

Sellers, W. R., Novitch, B. G., Miyake, S., Heith, A., Otterson, G. A., Kaye, F. J., Lassar, A. B., and Kaelin, W. G., Jr. (1998). Stable binding to E2F is not required for the retinoblastoma protein to activate transcription, promote differentiation, and suppress tumor cell growth. *Genes Dev.* **12**, 95–106.

Sen, S., Zhou, H., and White, R. A. (1997). A putative serine/threonine kinase encoding gene BTAK on chromosome 20q13 is amplified and overexpressed in human breast cancer cell lines. *Oncogene* **14**, 2195–2200.

Sevenet, N., Sheridan, E., Amram, D., Schneider, P., Handgretinger, R., and Delattre, O. (1999). Constitutional mutations of the hSNF5/INI1 gene predispose to a variety of cancers. *Am. J. Hum. Genet.* **65**, 1342–1348.

Shao, C., Deng, L., Henegariu, O., Liang, L., Stambrook, P. J., and Tischfield, J. A. (2000). Chromosome instability contributes to loss of heterozygosity in mice lacking p53. *Proc. Natl. Acad. Sci. USA* **97**, 7405–7410.

Sherr, C. J. (1996). Cancer cell cycles. *Science* **274**, 1672–1677.

Srivastava, S., Zou, Z. Q., Pirollo, K., Blattner, W., and Chang, E. H. (1990). Germ-line transmission of a mutated p53 gene in a cancer-prone family with Li–Fraumeni syndrome. *Nature* **348**, 747–749.

Sterner, J. M., Dew-Knight, S., Musahl, C., Kornbluth, S., and Horowitz, J. M. (1998). Negative regulation of DNA replication by the retinoblastoma protein is mediated by its association with MCM7. *Mol. Cell. Biol.* **18**, 2748–2757.

Strober, B. E., Dunaief, J. L., Guha, S., and Goff, S. P. (1996). Functional interactions between the hBRM/hBRG1 transcriptional activators and the pRB family of proteins. *Mol. Cell. Biol.* **16**, 1576–1583.

Strunnikov, A. V. (1998). SMC proteins and chromosome structure. *Trends Cell Biol.* **8**, 454–459.

Tamrakar, S., and Ludlow, J. W. (2000). The carboxyl-terminal region of the retinoblastoma protein binds non-competitively to protein phosphatase type 1alpha and inhibits catalytic activity. *J. Biol. Chem.* **275**, 27784–27789.

Tamrakar, S., Mittnacht, S., and Ludlow, J. W. (1999). Binding of select forms of pRB to protein phosphatase type 1 independent of catalytic activity. *Oncogene* **18**, 7803–7809.

Tanaka, T., Cosma, M. P., Wirth, K., and Nasmyth, K. (1999a). Identification of cohesin association sites at centromeres and along chromosome arms. *Cell* **98**, 847–858.

Tanaka, T., Fuchs, J., Loidl, J., and Nasmyth, K. (2000). Cohesin ensures bipolar attachment of microtubules to sister centromeres and resists their precocious separation. *Nat. Cell Biol.* **2**, 492–499.

Tanaka, T., Kimura, M., Matsunaga, K., Fukada, D., Mori, H., and Okano, Y. (1999b). Centrosomal kinase AIK1 is overexpressed in invasive ductal carcinoma of the breast. *Cancer Res.* **59**, 2041–2044.

Tatsuka, M., Katayama, H., Ota, T., Tanaka, T., Odashima, S., Suzuki, F., and Terada, Y. (1998). Multinuclearity and increased ploidy caused by overexpression of the aurora- and Ipl1-like midbody-associated protein mitotic kinase in human cancer cells. *Cancer Res.* **58**, 4811–4816.

Trouche, D., Le Chalony, C., Muchardt, C., Yaniv, M., and Kouzarides, T. (1997). RB and hbrm cooperate to repress the activation functions of E2F1. *Proc. Natl. Acad. Sci. USA* **94**, 11,268–11,273.

Tung, H. Y., Wang, W., and Chan, C. S. (1995). Regulation of chromosome segregation by Glc8p, a structural homolog of mammalian inhibitor 2 that functions as both an activator and an inhibitor of yeast protein phosphatase 1. *Mol. Cell. Biol.* **15,** 6064–6074.

Uemura, T., Morikawa, K., and Yanagida, M. (1986). The nucleotide sequence of the fission yeast DNA Topoisomerase II gene: Structural and functional relationships to other DNA Topoisomerases. *EMBO J.* **5,** 2355–2361.

Uemura, T., Ohkura, H., Adachi, Y., Morino, K., Shiozaki, K., and Yanagida, M. (1987). DNA Topoisomerase II is required for condensation and separation of mitotic chromosomes in S. pombe. *Cell* **50,** 917–925.

Urnov, F. D., Yee, J., Sachs, L., Collingwood, T. N., Bauer, A., Beug, H., Shi, Y. B., and Wolffe, A. P. (2000). Targeting of N-CoR and histone deacetylase 3 by the oncoprotein v-erbA yields a chromatin infrastructure-dependent transcriptional repression pathway. *EMBO J.* **19,** 4074–4090.

Versteege, I., Sevenet, N., Lange, J., Rousseau-Merck, M. F., Ambros, P., Handgretinger, R., Aurias, A., and Delattre, O. (1998). Truncating mutations of hSNF5/INI1 in aggressive paediatric cancer. *Nature* **394,** 203–206.

Warburton, P. E., and Earnshaw, W. C. (1997). Untangling the role of DNA Topoisomerase II in mitotic chromosome structure and function. *Bioessays* **19,** 97–99.

Wei, Y., Mizzen, C. A., Cook, R. G., Gorovsky, M. A., and Allis, C. D. (1998). Phosphorylation of histone H3 at serine 10 is correlated with chromosome condensation during mitosis and meiosis in Tetrahymena. *Proc. Natl. Acad. Sci. USA* **95,** 7480–7484.

Wei, Y., Yu, L., Bowen, J., Gorovsky, M. A., and Allis, C. D. (1999). Phosphorylation of histone H3 is required for proper chromosome condensation and segregation. *Cell* **97,** 99–109.

Wen, Y. D., Perissi, V., Staszewski, L. M., Yang, W. M., Krones, A., Glass, C. K., Rosenfeld, M. G., and Seto, E. (2000). The histone deacetylase-3 complex contains nuclear receptor corepressors. *Proc. Natl. Acad. Sci. USA* **97,** 7202–7207.

Wigge, P. A., Jensen, O. N., Holmes, S., Soues, S., Mann, M., and Kilmartin, J. V. (1998). Analysis of the Saccharomyces spindle pole by matrix-assisted laser desorption/ionization (MALDI) mass spectrometry. *J. Cell Biol.* **141,** 967–977.

Wigge, P. A., and Kilmartin, J. V. (2001). The Ndc80p complex from Saccharomyces cerevisiae contains conserved centromere components and has a function in chromosome segregation. *J. Cell Biol.* **152,** 349–360.

Winston, F., and Carlson, M. (1992). Yeast SNF/SWI transcriptional activators and the SPT/SIN chromatin connection. *Trends Genet.* **8,** 387–391.

Wolffe, A. P. (1996). Histone deacetylase: A regulator of transcription. *Science* **272,** 371–372.

Wong, A. K., Shanahan, F., Chen, Y., Lian, L., Ha, P., Hendricks, K., Ghaffari, S., Iliev, D., Penn, B., Woodland, A. M., Smith, R., Salada, G., Carillo, A., Laity, K., Gupte, J., Swedlund, B., Tavtigian, S. V., Teng, D. H., and Lees, E. (2000). BRG1, a component of the SWI-SNF complex, is mutated in multiple human tumor cell lines. *Cancer Res.* **60,** 6171–6177.

Wood, E. R., and Earnshaw, W. C. (1990). Mitotic chromatin condensation in vitro using somatic cell extracts and nuclei with variable levels of endogenous Topoisomerase II. *J. Cell Biol.* **111,** 2839–2850.

Yanagida, M. (2000). Cell cycle mechanisms of sister chromatid separation; roles of Cut1/separin and Cut2/securin. *Genes Cells* **5,** 1–8.

Yen, A., and Sturgill, R. (1998). Hypophosphorylation of the RB protein in S and G2 as well as G1 during growth arrest. *Exp. Cell Res.* **241,** 324–331.

Yin, Y., Tainsky, M. A., Bischoff, F. Z., Strong, L. C., and Wahl, G. M. (1992). Wild-type p53 restores cell cycle control and inhibits gene amplification in cells with mutant p53 alleles. *Cell* **70,** 937–948.

Zhang, H. S., Gavin, M., Dahiya, A., Postigo, A. A., Ma, D., Luo, R. X., Harbour, J. W., and Dean, D. C. (2000). Exit from G1 and S phase of the cell cycle is regulated by repressor complexes containing HDAC-Rb-hSWI/SNF and Rb-hSWI/SNF. *Cell* **101,** 79–89.

Zhang, S., Guha, S., and Volkert, F. C. (1995). The Saccharomyces SHP1 gene, which encodes a regulator of phosphoprotein phosphatase 1 with differential effects on glycogen metabolism, meiotic differentiation, and mitotic cell cycle progression. *Mol. Cell. Biol.* **15**, 2037–2050.

Zhang, Y., Iratni, R., Erdjument-Bromage, H., Tempst, P., and Reinberg, D. (1997). Histone deacetylases and SAP18, a novel polypeptide, are components of a human Sin3 complex. *Cell* **89**, 357–364.

Zheng, L., Chen, Y., and Lee, W. H. (1999). Hec1p, an evolutionarily conserved coiled-coil protein, modulates chromosome segregation through interaction with SMC proteins. *Mol. Cell. Biol.* **19**, 5417–5428.

Zheng, L., Chen, Y., Riley, D. J., Chen, P. L., and Lee, W. H. (2000a). Retinoblastoma protein enhances the fidelity of chromosome segregation mediated by hsHec1p. *Mol. Cell. Biol.* **20**, 3529–3537.

Zheng, L., and Lee, W. H. (2001). The retinoblastoma gene: A prototypic and multifunctional tumor suppressor. *Exp. Cell Res.* **264**, 2–18.

Zheng, L., Li, S., Boyer, T. G., and Lee, W. H. (2000b). Lessons learned from BRCA1 and BRCA2. *Oncogene* **19**, 6159–6175.

Zheng, L., Flesken-Nikitin, N., Chen, P.-L., and Lee, W.-H. (2002). Deficiency of Retinoblastoma gene in mouse embryonic stem cells leads to genetic instability. *Cancer Res.* **62**, 2498–2502.

Zhou, H., Kuang, J., Zhong, L., Kuo, W. L., Gray, J. W., Sahin, A., Brinkley, B. R., and Sen, S. (1998). Tumour amplified kinase STK15/BTAK induces centrosome amplification, aneuploidy and transformation. *Nat. Genet.* **20**, 189–193.

Zhu, X., Mancini, M. A., Chang, K.-H., Liu, C.-Y., Chen, C.-F., Shan, B., Jones, D., Yang-Feng, T. L., and Lee, W.-H. (1995). Characterization of a novel 350-kilodalton nuclear phosphoprotein that is specifically involved in mitotic-phase progression. *Mol. Cell. Biol.* **15**, 5017–5029.

[CANCER RESEARCH 62, 3773–3781, July 1, 2002]

A Common DNA-binding Site for SZF1 and the BRCA1-associated Zinc Finger Protein, ZBRK1[1]

Hongzhuang Peng, Lei Zheng,[2] Wen-Hwa Lee, John J. Rux, and Frank J. Rauscher III[3]

The Wistar Institute, Philadelphia, Pennsylvania 19104 [H. P., J. J. R., F. J. R.], and Department of Molecular Medicine and Institute of Biotechnology, University of Texas Health Science Center at San Antonio, San Antonio, Texas 78245 [L. Z., W-H. L.]

ABSTRACT

More than 220 Kruppel-associated box-zinc finger protein (KRAB-ZFP) genes are encoded in the human genome. KRAB-ZFPs function as transcriptional repressors by binding DNA through their tandem zinc finger motifs. Gene silencing is mediated by the highly conserved KRAB domain, which recruits histone deacetylase complexes, histone methylases, and heterochromatin proteins. However, little is known of the biological programs regulated by KRAB-ZFPs, in large part because of the difficulty in identifying DNA-binding sites recognized by long arrays of zinc fingers. In an attempt to identify the natural target genes for a KRAB-ZFP, we chose SZF1, a hematopoietic progenitor-restricted, KRAB-ZFP that contains only four C_2H_2 zinc finger motifs. Using recombinant SZF1 protein and a PCR-based binding site selection strategy, we identified a 15-bp consensus DNA sequence recognized by SZF1. Remarkably, this sequence is similar to the core DNA-binding site described recently for ZBRK1, a KRAB-ZFP that binds to BRCA1 and is involved in coordinating the cellular DNA damage response. The SZF1 and ZBRK1 proteins bind to both the experimentally derived SZF1 site and the canonical ZBRK1 site. The KRAB domain from SZF1 bound directly to the KAP-1 corepressor and displayed intrinsic silencing activity. Moreover, full-length SZF1 repressed a promoter containing ZBRK1 recognition sequences. Thus, SZF1 and ZBRK1 may regulate a common set of target genes *in vivo*.

INTRODUCTION

The ~220 KRAB-ZFP[4] genes in the human genome have been proposed to have important regulatory roles during cell differentiation and development. Each KRAB-ZFP is composed of a 75-amino acid KRAB domain at the NH_2 terminus and tandem C_2H_2 class zinc fingers at the COOH terminus (Fig. 1). The tandem zinc finger modules can number from 3 to upwards of 40 in a single protein and presumably participate in DNA recognition. The KRAB domain was originally identified as a conserved motif at the NH_2 terminus of ZFPs (1) and was shown to be a potent, DNA binding-dependent transcriptional repression module (2–4). The KRAB domain only occurs in higher vertebrates and can be classified into three subfamilies based on amino acid sequence alignment (5, 6): subfamilies containing a KRAB A box alone, both A and B boxes, or A box with a divergent B box. The KRAB domain consists of ~75 amino acid residues and is predicted to fold into two amphipathic helices that are involved in protein/protein interactions (Fig. 1*B*; Refs. 1, 7). Silencing mediated by the KRAB domain occurs through recruitment of the corepressor protein, KAP-1 (8–10), which in turn recruits the NURD histone deacetylase complex, histone methylases, and the HP1 family of heterochromatin proteins (11–13). Thus, although much is known of the KRAB silencing mechanism, comparatively little is known about KRAB-ZFP function in the organism.

The spatial and temporal expression of KRAB-containing zinc finger transcription factors suggests that their biological functions could include influences on embryonic development, cell differentiation, and cell transformation (1, 14–18). For example, some KRAB-containing ZFPs are mainly restricted to lymphoid cells and may play a specific role in lymphoid differentiation (14, 19), whereas others are expressed and specifically down-regulated during myeloid differentiation (1). A number of KRAB-ZFPs are candidate genes for human diseases based on their chromosomal locations (20, 21). There are more than 40 KRAB-ZFP-encoding genes that have been identified on chromosome 19p13 and >10 KRAB-ZFP genes clustered on chromosome 19q13 (22, 23), many of which exhibit hematopoietic-specific expression (24). Intriguingly, some of the KRAB-ZFPs in these clusters are coordinately regulated in specific cell lineages (24).

The tandem C_2H_2 zinc fingers in KRAB-ZFPs are presumed to recognize specific DNA targets. The analyses of two crystal structures of the C_2H_2 zinc finger proteins, Zif268/Egr1 and GLI-1, with their cognate DNA-binding sites have provided some rules about DNA recognition by zinc finger domains (25–28). Each finger has a conserved $\beta\beta\alpha$ structure, and amino acids on the surface of the α-helix contact bases of the DNA. Each finger recognizes a three-nucleotide sequence along the major groove of the DNA helix. In the case of GLI-1, not all of the five zinc finger domains contact the DNA, suggesting that not all zinc finger domains contribute equally to DNA recognition. The linker region that separates neighboring C_2H_2 zinc fingers is usually of the form TGEKPYX (X representing any amino acid), is an important structural element that helps control the spacing of the fingers along the DNA site, and is required for high-affinity DNA binding (28–31).

Thus, the crystal structures of 3- and 5-fingered proteins have clearly provided a preliminary set of rules for zinc finger DNA interaction. However, the great challenge lies in determining whether these rules will also govern the binding of long array zinc finger arrays, *e.g.*, 10–20 tandem units. Only a few target DNA consensus sequences have been identified for the long array KRAB-ZFP family, and these already suggest that the rules may be different. For instance, the 8-fingered ZBRK1 protein binds a consensus of GGGxxx-CAGxxxTTT (32). The 8-fingered ZNF202 protein binds a consensus of GGGGT (17), and the 10-fingered KS1 protein binds the 27-bp consensus TCCTACAGTACCAACCCTACAGAGTAA (33). These results suggest that: (*a*) not all fingers bind DNA; and (*b*) not all fingers contribute specificity for sequence recognition.

To simplify the problem of identifying target sequences (and promoters) regulated by KRAB-ZFPs, we have chosen a short array, lineage-restricted KRAB-ZFP, SZF1. SZF1 is a KRAB-zinc finger gene expressed predominantly in $CD34^+$ stem/progenitor cells. The gene was isolated by screening a cDNA library prepared from human

Received 1/10/02; accepted 4/26/02.

The costs of publication of this article were defrayed in part by the payment of page charges. This article must therefore be hereby marked *advertisement* in accordance with 18 U.S.C. Section 1734 solely to indicate this fact.

[1] H. P. is supported by Wistar Basic Cancer Research Training Grant CA09171. F. J. R. is supported, in part, by NIH Grants CA 92088, Core Grant CA 10815, GM 54220, DAMD 17-96-1-6141, the Irving A. Hansen Memorial Foundation, the Mary A. Rumsey Memorial Foundation, and the Susan G. Komen Breast Cancer Foundation. J. J. R and the Wistar Institute Bioinformatics Facility are supported, in part, by NIH Core Grant CA 10815 and Grant AI 17279.

[2] Present address: Laboratory of Biochemistry and Molecular Biology, The Rockefeller University, New York, NY 10021.

[3] To whom requests for reprints should be addressed, at The Wistar Institute, 3601 Spruce Street, Philadelphia, PA 19104. Phone: (215) 898-0995; Fax: (215) 898-3929; E-mail: rauscher@wistar.upenn.edu.

[4] The abbreviations used are: KRAB-ZPF, Kruppel-associated box-zinc finger protein; EMSA, electrophoretic mobility shift analysis; UAS, upstream activating sequence; GST, glutathione *S*-transferase.

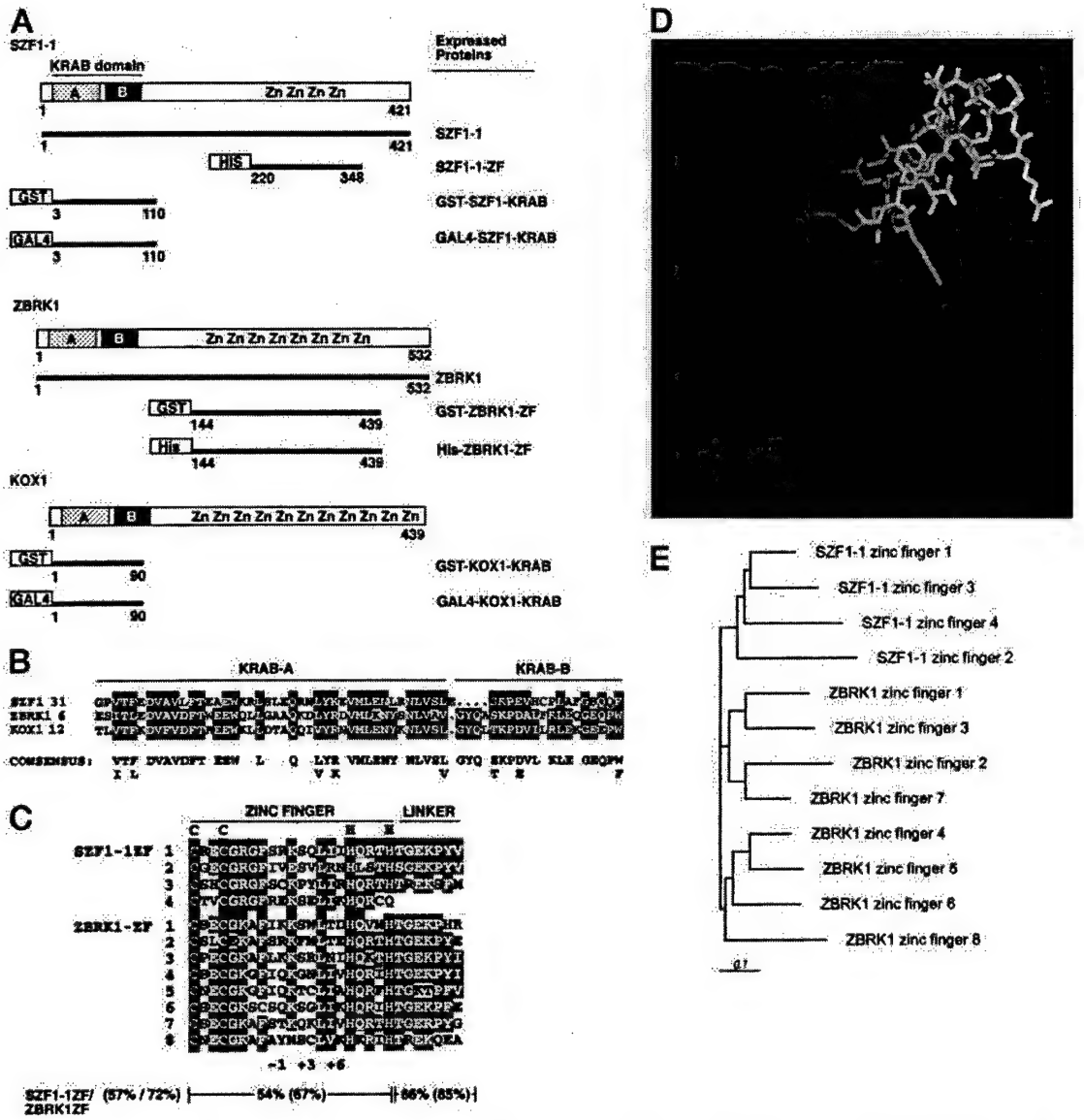

Fig. 1. *A*, a diagram illustrating the architecture of the KRAB-ZFPs, including SZF1-1, ZBRK1, and KOX1. The numbers represent amino acid positions. *ZF* or *Zn* refers to a zinc finger motif. *Column* to the *right*, expressed proteins. Database accession numbers are: SZF1-1 (AF114816); ZBRK1 (AF295096); and KOX1 (XP_031850). *B*, amino acid alignment of the KRAB domains from SZF1, ZBRK1, and KOX1 proteins. The numbers refer to amino acid positions in the corresponding proteins. The KRAB domain consensus residues are highlighted in *black*. The *periods* represent spaces introduced to obtain maximal alignment. The consensus sequence was previously derived (35). *C*, amino acid alignment of the zinc finger motifs from SZF1-1 and ZBRK1 proteins. The numbers on the *left* of the alignment refer to the orders of the zinc finger motifs within each protein. The numbers (−1, +3, and +6) under the alignment refer to the position of the amino acids within the α-helical region of each zinc finger. The consensus Cys_2-His_2 (C_2H_2) residues of each zinc finger are highlighted in *black*. The other consensus residues of zinc fingers and linker regions are highlighted in *gray*. The identity and similarity of zinc finger and linker regions between SZF1-1 and ZBRK1 are indicated under the alignment. *D*, homology model of the first zinc finger domain of SZF1-1 (*yellow*) bound to DNA (*red*) highlighting the −1, +3, and +6 positions of the zinc finger (*green*). The model was prepared with the Swiss-PdbViewer protein-modeling environment (40) and is based upon the closely related Zif268-DNA complex structure (26). *E*, the phylogenetic tree of zinc finger motifs of SZF1-1 and ZBRK1 proteins. The unrooted tree was calculated with the program CLUSTALX (45, 46) using the distance algorithm of Kimura (47) and displayed with Tree View (48). Branch lengths are proportional to the number of substitutions, and the *scale bar* represents 10 mutations per 100 sequence positions.

bone marrow $CD34^+$ cells (16). It encodes a protein containing a canonical KRAB domain at the NH_2 terminus and four contiguous zinc fingers of the C_2H_2 type at the COOH terminus. Two alternatively spliced transcripts were isolated; SZF1-1 is a truncated form resulting in an apparently incomplete fourth zinc finger (Fig. 1*C*) and is expressed only in $CD34^+$ cells; SZF1-2 encodes a consensus fourth zinc finger, a novel COOH terminus, and is ubiquitously expressed. Both forms showed the potential for transcriptional repression of a $CD34^+$-specific promoter (16). Our experimental strategy was to define the DNA site recognized by SZF1 zinc fingers as a means to identify potential target genes regulated in $CD34^+$ hematopoietic cells.

MATERIALS AND METHODS

Construction of Expression Plasmids. The bacterial expression plasmid for His-SZF1-1-ZF (amino acids 220–348) was created by PCR using the primers SZF1-1-ZFfor (*Bam*HI) 5′-CGC AGG ATC CGC TTT TAA CCA GAA GTC AAA C-3′ and SZF1-1-ZFrev (*Sal*I) 5′-CAC TGG TCG ACT CAC TGG TGC TTA ATG AGC TCT GAC-3′. GST-SZF1-KRAB (amino acids 3–110) and GAL4-SZF1-KRAB (amino acids 3–110) were created by PCR using the primers SZF1-KBfor (*Bam*HI) 5′-CTG CGG ATC CGA TTT TCA AAT GTT GAA CCA G-3′ and SZF1-KBrev (*Sal*I) 5′-GAG GTC GTC GAC TCA TCC TGC ATG GAA ACC TGG-3′. The resulting PCR products were digested with the restriction endonucleases indicated in brackets and cloned into the corresponding sites of the pQE30 vector (Qiagen) for His-SZF1-1-ZF,

the pGEX-4T-1 vector (Amersham Pharmacia Biotech) for GST-SZF1-KRAB, and the pM2 vector for GAL4-SZF1-KRAB. All plasmids generated by PCR were confirmed by DNA sequencing on both strands to verify the appropriate reading frame and the integrity of flanking sequences. The pNeoSZF1-1 (amino acids 1–421) expression plasmid was kindly provided by Donald Small (The Johns Hopkins Oncology Center, The Johns Hopkins University School of Medicine, Baltimore, MD). The pCHPL-ZBRK1 (amino acids 1–532) and the GST-ZBRK1-ZF (amino acids 144–439) expression plasmids have been described previously (32). The bacterial expression plasmid for His-ZBRK1-ZF (amino acids 144–439) was created by PCR using the primers ZBRK1-ZFfor (*Bam*HI) 5′-GCA CGA GGA TCC AAC CAG AGC AAA GGC TAT GAA A-3′ and ZBRK1-ZFrev (*Hin*dIII) 5′-CAG CGA AAG CTT TCA TGC AGG AGG ATT TTC CAC CTT-3′. The GST-KOX1-KRAB (amino acids 1–90) and the GAL4-KOX1-KRAB (amino acids 1–90) expression plasmids have been described previously (2, 8).

Purification of Recombinant Proteins. *Escherichia coli* SG13009 cells (Qiagen) bearing the desired plasmid were propagated with aeration at 37°C in 1 liter of Luria broth to an A_{600} of ~0.6. isopropyl-1-thio-β-D-galactopyranoside was added to 1 mM, and $ZnSO_4$ was added to 100 μM. The growth at 18°C was continued for 20 h. The cells were harvested by centrifugation. The His-SZF1-1-ZF and the His-ZBRK1-ZF proteins expressed from bacteria were purified at 4°C using nondenaturing conditions as recommended by the manufacturer (Qiagen). Briefly, the bacterial pellet was resuspended in P300 buffer (pH 7.0), 10% (v/v) glycerol, 10 mM imidazole, and lysed by sonication (34). The cell extract was centrifuged at 12,000 × *g* for 20 min. The supernatant fraction containing soluble protein was incubated in batch with Ni-NTA resin for 1 h. The resin was washed four times with P300 buffer, 10% glycerol, and for the last wash, the imidazole was increased to 40 mM. The resin was loaded into a column, and the protein was eluted with P300 buffer, 10% glycerol, and 300 mM imidazole. The eluted protein was dialyzed against three changes of P300, 10% glycerol, 20 μM $ZnSO_4$, and 0.5 mM DTT.

GST Association Assays. The preparation of the GST fusion proteins and the GST association assays were performed essentially as described previously (35, 36). Briefly, 5 μg of freshly prepared GST fusion protein immobilized on glutathione-Sepharose were incubated with 5 μg of Ni-NTA-purified recombinant His-tagged protein in 100 μl of BB500 buffer [20 mM Tris (pH 7.9), 500 mM NaCl, 0.2 mM EDTA, 10% glycerol, 0.2% NP40, 1 mM phenylmethylsulfonyl fluoride, 500 μg of BSA (BSA; fraction V)] for 1 h at room temperature. The protein complexes were washed four times with BB750 [20 mM Tris (pH 7.9), 750 mM NaCl, 0.2 mM EDTA, 10% glycerol, 0.2% NP40, and 1 mM phenylmethylsulfonyl fluoride], and the bound proteins were eluted in 5× Laemmli buffer, resolved by SDS-PAGE, and visualized with Coomassie Blue stain.

Generation of Oligonucleotide Library and Binding Site Selection. A single-stranded oligonucleotide 5′-AGACGGATCCATTGCA-N14-CTGTAGGAATTCGGA-3′ bearing 15- and 16-nucleotide fixed-end sequences flanking 14 random nucleotides was synthesized. Recognition sequences for the *Bam*HI and *Eco*RI restriction enzymes (underlined) were incorporated to facilitate the cloning of the binding sites. The oligonucleotides were amplified by PCR using primers complementary to the fixed-end sequences, and the resulting double-stranded DNA library was purified by electrophoresis on a 12% native polyacrylamide gel, followed by elution and precipitation. The purified oligonucleotide library was end-labeled with [^{32}P]ATP and incubated with the purified recombinant SZF1-1-ZF protein. The selection and amplification of the binding site was performed as described previously (37). The DNA-protein binding reactions were performed in a buffer containing 20 mM HEPES (pH 7.6), 50 mM NaCl, 50 μM $ZnSO_4$, 0.5 mM $MgCl_2$, 0.5 mM DTT, 10% glycerol, 0.5 μg deoxyinosinic-deoxycytidylic acid in a total volume of 15 μl (38).

DNA Sequencing and Analysis of Selected Oligonucleotides. After three rounds of EMSA selection and PCR amplification, the affinity-selected oligonucleotides were extensively digested with *Bam*HI and *Eco*RI and ligated into the pGEM7Zf+ plasmid (Promega) at the corresponding sites. After bacterial transformation and clone selection, the DNAs were sequenced. The degenerate positions of the oligonucleotide were aligned using the GCG sequence analysis Pileup program (39).

EMSA and Binding Site Competitions. Increasing amounts of purified SZF1-1-ZF and ZBRK1-ZF proteins in binding buffer were incubated with a ^{32}P-end-labeled synthetic oligonucleotide containing the binding sites for either the wild-type or the mutant probe for 10 min. The wild-type probes include the SZF1-1-ZF (designated as SZF1 probe, 5′-GATCCCAGGGTAACAGCCGTTTG-3′) and the ZBRK1-ZF (designated as ZBRK1 probe, 5′-GATCCACGGGACGCAGGTGTTTTGTGCCG-3′). Three sets of mutant SZF1 oligonucleotides were synthesized. The triplet GGG was mutated to CTC in the first set (designated as SZF1-mut1 probe, 5′-GATCCCACTCTAACAGCCGTTTG-3′). The triplet CAG was mutated to TTC in the second set (designated as SZF1-mut2 probe, 5′-GATCCCAGGGTAATTCCCGTTTG-3′). Both triplets GGG and CAG were mutated to AAA in the third set (designated as SZF1-mut3 probe, 5′-GATCCCAAAATAAAAACCGTTTG-3′). In competition assays, 1 μg of SZF1-1-ZF or 400 ng of ZBRK1-ZF protein were incubated with a mixture of ^{32}P-end-labeled oligonucleotide and a 25–100-fold molar excess of unlabeled oligonucleotide for 15 min at 30°C. The DNA-protein complexes were analyzed on a native polyacrylamide gel in 0.5× TBE running buffer. The gels were dried and visualized by autoradiography.

Transient Transfection Luciferase Assays. Transient transfection and luciferase assays were performed with NIH/3T3 cells as described previously (36). Briefly, NIH/3T3 cells were transiently cotransfected with a luciferase reporter plasmid, a pcDNA3-β-galactosidase expression plasmid, and effector plasmids for 5 h. For reporter assays with GAL4 fusion proteins, the luciferase reporter plasmids consisted of either 0 or 5 copies of the GAL4 UAS in front of a minimal herpes simplex virus TK promoter. Reporter assays with ZBRK1 and SZF1 used the pGL3p-E reporter plasmid, which contains four copies of the ZBRK1 consensus binding site upstream of the SV40 promoter driving expression of a luciferase gene as described previously (32). At 18 h after transfection, the cells were collected and assayed for luciferase activity using the Luciferase Assay System (Promega), and values were normalized for transfection efficiency using β-galactosidase activity.

RESULTS

Domain Analysis for KRAB-ZFPs and Purification of Recombinant Proteins. KRAB-ZFP genes are very abundant in the human genome. However, only a few detailed biochemical and biophysical analyses of KRAB-ZFP function have been undertaken (34, 35). The potential target sequences have been identified for only a few members of the KRAB-ZFP family (17, 32, 33). We began our studies by aligning and analyzing the protein domains for the members of the KRAB-ZFPs, including SZF1, ZBRK1, and KOX1 (Fig. 1). As expected, the KRAB domain shows remarkable homology among the members (Fig. 1*B*). In KRAB-ZFPs, the zinc fingers conform to a "classic" C_2H_2 zinc finger motif first described in the Kruppel protein in *Drosophila*. SZF1-1 encodes four consecutive zinc finger motifs, whereas ZBRK1 encodes eight consecutive zinc finger motifs (Fig. 1*C*). Both proteins contain the canonical linker region between fingers composed of the sequence TGEKPYX. Because the zinc finger regions are the determinant for DNA-binding specificity (Fig. 1*D*; Ref. 40), comparisons of the SZF1-1 and ZBRK1 zinc finger region sequences were made. As expected, the zinc finger motifs are closely related; comparative analyses indicate that SZF1-1 displays 57% identity and 72% similarity with ZBRK1 over the zinc finger motifs (Fig. 1*C*). A distance-based phylogenetic analysis of zinc finger sequences was performed (Fig. 1*E*). That the sequences are all closely related is evident from the similarity of the distances between the sequences. However, an examination of the branching pattern reveals that the sequences cluster into three groups of four sequences each. In addition, all four SZF1-1 zinc fingers completely segregate from those of ZBRK1, indicating that they are more similar to one another than they are to those of ZBRK1. Finally, it is also interesting to note that in both SZF1-1 and ZBRK1, the first and third zinc finger domains cluster together, whereas second finger is always more divergent. The degree to which this pattern relates to the observed overlap in DNA-binding specificity of these proteins is not yet known and will require further study.

For the binding site selection experiments, recombinant protein

containing four zinc fingers of SZF1-1 was produced by cloning the DNA encoding the four zinc fingers (amino acids 220–348) into a protein expression vector (designated as SZF1-1-ZF; Fig. 1*A*). The recombinant SZF1-1-ZF protein was expressed in *Escherichia coli* as a 6-histidine fusion protein and purified by Ni-NTA chromatography under nondenaturing conditions. SDS-PAGE analysis showed that the protein was purified to near homogeneity (Fig. 2*A*). Recombinant protein containing eight zinc fingers of ZBRK1 was produced by cloning the DNA encoding amino acids 144–439 into a GST fusion protein expression vector (designed as GST-ZBRK1-ZF; Fig. 1*A*). The recombinant GST-ZBRK1-ZF protein was expressed in *E. coli*, purified by GST chromatography, and examined by SDS-PAGE (Fig. 2*A*). These purified SZF1-1-ZF and GST-ZBRK1-ZF proteins were used in binding site selection experiments.

Identification of a Consensus SZF1-1 DNA Binding Sequence. On the basis of the fact that one zinc finger module has the capability of binding to 3 bp of DNA (26), the four zinc fingers of SZF1-1 would be predicted to bind to a minimum of 12 bp of DNA. Therefore, a library of double-stranded DNA was designed to contain 14 bp of random sequence, flanked by sequences containing restriction enzyme sites and which were complementary to the PCR primers. Purified, recombinant SZF1-1-ZF protein was then used to affinity-select DNA sequences from the library by using successive rounds of EMSA. At each step, the bound oligonucleotides were recovered and subjected to PCR amplification. The first round of affinity selection with SZF1-1-ZF protein produced a significant enrichment of sequences in the heterogeneous oligonucleotide library that bound to the protein (Fig. 2*B*). However, the second and the third rounds of selection produced little further enrichment of DNA-binding activity. Therefore, after three rounds of selection, the affinity-selected oligonucleotides were subcloned and sequenced. A consensus sequence of 5′-CCA**GGG**-TAA**CAG**CCG-3′ was derived from sequence alignment of individual subclones (shown in Fig. 2*C* are 12 sequences of 80 individual subclones). Surprisingly, the selected consensus sequence for SZF1-1 is very similar to the consensus binding site recently described for ZBRK1 (5′-CAC**GGGACGCAGGTGTTT**-3′; Fig. 2*D*). Both consensus sequences share the same core binding site, 5′-**GGG**xxx-**CAG**xxx-3′. By comparison of the sequence selected from SZF1-1-ZF protein binding and the reported STK-140 promoter sequence (16), we found that the STK-140 promoter has only a partial SZF1-1 consensus sequence (**CAGGG**xxxxx**GCCG**). This finding is consistent with the fact that SZF1-1 has a weaker repression activity with the STK-140 promoter reporter than SZF1-2. Consideration that SZF1-1 has more activity on the ZBRK-like site suggests that the alternate splicing that generates SZF1-1 may select for a different set of target genes, although this has not been thoroughly examined.

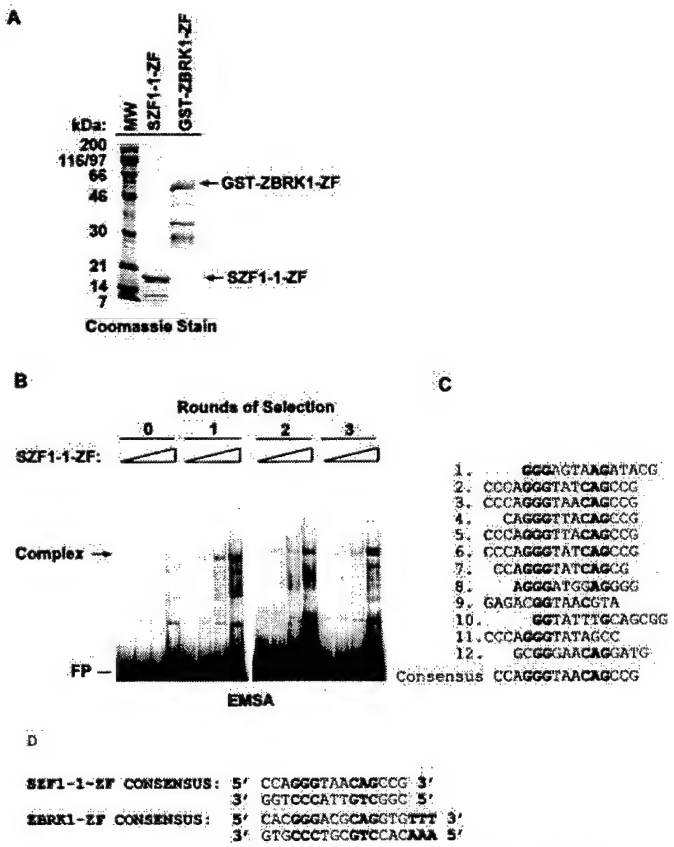

Fig. 2. *A*, expression and detection of recombinant SZF1-1 protein containing four zinc fingers (SZF1-1-ZF) and ZBRK1 protein containing eight zinc fingers (GST-ZBRK1-ZF) in *E. coli*. Coomassie Blue-stained SDS-PAGE of the purified recombinant SZF1-1-ZF and GST-ZBRK1-ZF proteins (5 μg) is shown. *B*, selection and amplification of a SZF1-1-ZF binding site. Equivalent amounts (cpm of each probe) of PCR-amplified DNA from each round (0–3) of affinity selection were subjected to EMSA using 0, 0.5, 1, and 2 μg of recombinant SZF1-1-ZF protein. DNA-protein complexes were analyzed on a native 4.5% polyacrylamide gel. *Arrow*, protein-DNA complex. *FP*, free probe. *C*, alignment of individual DNA sequences selected after the third round of selection by SZF1-1-ZF using a binding site selection strategy. The deduced consensus SZF1-1 DNA-binding sequence is indicated below the individually aligned sequences. The residues in *boldface* show the most frequently selected consensus residues. *D*, comparison of consensus sequences selected by SZF1-1-ZF and ZBRK1-ZF proteins.

To determine whether SZF1-1 and ZBRK1 proteins specifically bind to both consensus binding site DNA sequences selected from both proteins, oligonucleotides that contain the selected consensus binding sites for SZF1-1-ZF and ZBRK1-ZF proteins were synthesized (Fig. 3*A*) and used as probes in the EMSA analysis. Because the SZF1 site is a subset of the site required for ZBRK1 binding, we added the additional three nucleotides, **TTT** to the 3′ end of the core SZF1-1 consensus. The SZF1-1-ZF protein was tested by EMSA for its ability to bind to the SZF1 probe (5′-GATCCCA**GGG**TAA-**CAGCCGTTTG**-3′) and to the ZBRK1 probe (5′-GATCCAC**GG**-**GACGCAGGTGTTT**TGTGCCG-3′). As shown in Fig. 3*B, left panel*, the SZF1-1-ZF protein bound to both consensus probes to form protein-DNA complexes and yields the mobility shifts indicated by the *arrow*. The binding ability of SZF1-1-ZF protein to both probes is comparable and occurs in a protein concentration-dependent manner (Fig. 3*B, left panel*). The ZBRK1-ZF also bound to both consensus probes to form DNA-protein complexes (Fig. 3*B, right panel*), and the apparent binding affinity of the ZBRK1-ZF protein to both of the probes is comparable. Thus, both SZF1-1-ZF and ZBRK1-ZF proteins select similar core DNA binding sites from a heterogeneous population of oligonucleotides.

To address the specificity for the SZF1-1-ZF and ZBRK1-ZF proteins binding to their consensus sequences, we used three sets of mutant SZF1 oligonucleotides to bind to both His-tagged SZF1-1-ZF and ZBRK1-ZF proteins (Fig. 3, *A* and *C*). The triplet GGG was mutated to CTC (SZF1-mut1), the triplet CAG was mutated to TTC (SZF1-mut2), and both GGG and CAG mutated to AAA (SZF1-mut3). We observed that these sets of mutant oligonucleotides significantly reduced but did not completely abolish the binding of SZF1-1-ZF protein in the EMSA assay (Fig. 3*C, left panel*). These data indicate the specificity of the SZF1-1-ZF protein in the recognition of the consensus sequence, the GGG and CAG triplets. However, the SZF1-1-ZF protein may also interact with the bp between the triplet GGG and CAG or other triplets in the sequence because mutations of both GGG and CAG did not completely abolish the binding of SZF1-1-ZF protein. We also observed that the three sets of mutant oligonucleotides completely abolished the binding of ZBRK1-ZF protein in the EMSA assay (Fig. 3*C, right panel*). The data are consistent with the previous observation in competition EMSA assay

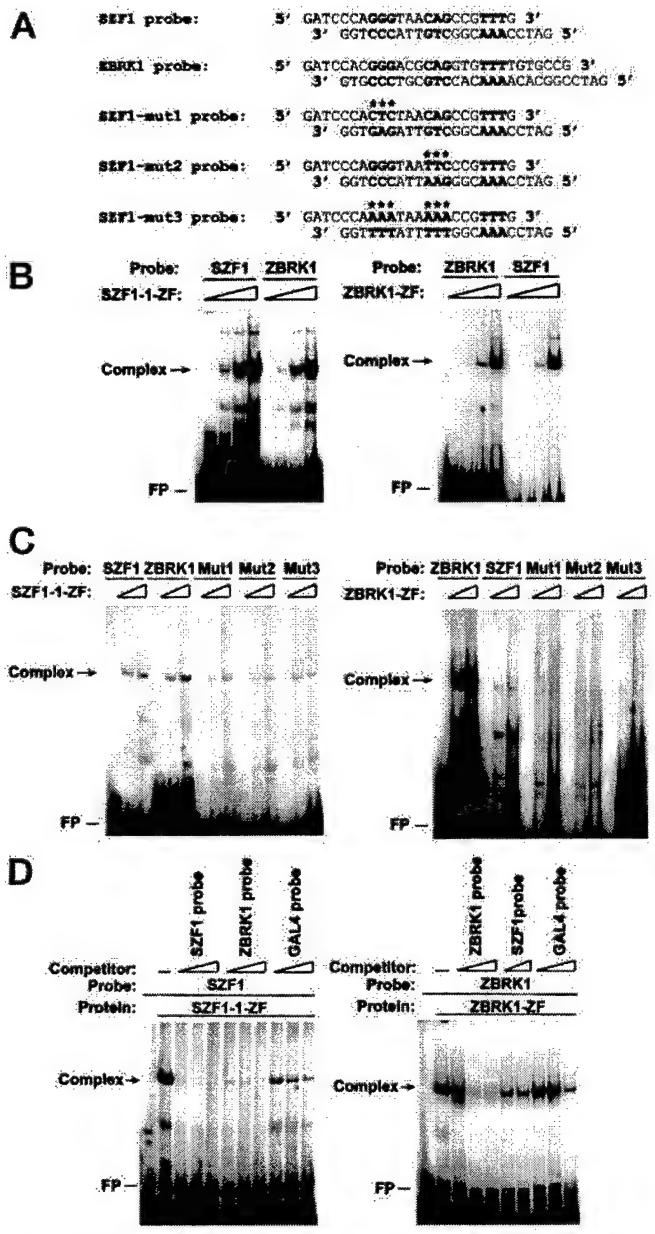

Fig. 3. SZF1-1 and ZBRK1 proteins recognize a similar core DNA-binding site. *A*, experimentally derived SZF1-1-ZF and ZBRK1-ZF binding DNA sequences (wild-type and mutant) used as probes in the EMSA and competition assays are shown in *B–D*. For *B–D*, the DNA-protein complexes were resolved in native polyacrylamide gels. *Arrows*, DNA-protein complex. *FP*, free probe. *B*, SZF1-1-ZF and ZBRK1-ZF proteins specifically recognize both consensus binding site DNA sequences selected from both proteins. EMSA was performed with ^{32}P-labeled probes (SZF1 probe and ZBRK1 probe) and increasing amounts of either SZF1-1-ZF protein (*left panel*) or ZBRK1-ZF protein (*right panel*). *C*, the mutant oligonucleotides significantly reduced the binding of SZF1-1-ZF protein and completely abolished the binding of ZBRK1-ZF protein in EMSA assays. EMSA was performed with ^{32}P-labeled probes (wild-type and mutant probes including SZF1-mut1, SZF1-mut2, and SZF1-mut3 probes) and increasing amounts of either the His-tagged SZF1-1-ZF protein (*left panel*) or His-tagged ZBRK1-ZF protein (*right panel*). *D*, competition EMSA assays. *Left panel:* EMSA assay was performed with ^{32}P-labeled SZF1 probe and a constant amount of SZF1-1-ZF protein. A 25-, 50-, and 100-fold molar excess of unlabeled SZF1 probe, ZBRK1 probe, or GAL4 probe was added to binding reactions, respectively. *Right panel:* EMSA assay was also performed with ^{32}P-labeled ZBRK1 probe and a constant amount of ZBRK1-ZF protein. A 25-, 50-, and 100-fold molar excess of unlabeled ZBRK1 probe, GAL4 probe, or 25- and 50-fold molar excess of unlabeled SZF1 probe was added to binding reactions, respectively.

with a mutant probe using GST-ZBRK1-ZF protein (32). The data indicate that the ZBRK1-ZF protein more specifically recognizes the triplets **GGGxxxCAGxxxTTT** in the sequence.

The specificity of SZF1-1-ZF and ZBRK1-ZF protein binding to their consensus sequence was further revealed by testing the ability of a molar excess (25–100-fold) of unlabeled probes to compete for binding to the labeled probes. The results of these competition EMSA analyses indicated that the SZF1 probe and the ZBRK1 probe, but not the GAL4 probe, could effectively compete for SZF1-1-ZF protein binding to its consensus sequence (Fig. 3*D, left panel*). A similar result was obtained for the ZBRK1-ZF protein (Fig. 3*D, right panel*). Therefore, these data suggest that both SZF1-1 zinc fingers and the ZBRK1 zinc fingers comprise sequence-specific DNA-binding domains that specifically recognize similar core consensus DNA sequences.

Direct Interaction between the SZF1-KRAB Domain and KAP-1-RBCC Domain. Previous studies had shown the potential for SZF1 in transcriptional repression of a CD34$^+$-specific promoter (16). The KRAB domain of SZF1 shows a high degree of homology with the KRAB domain of other KRAB-ZFPs (Fig. 1*B*). Thus, it would be expected that the SZF1-KRAB domain would confer transcription repression activity via KAP-1 binding, as demonstrated for other KRAB proteins (8, 34, 35). To confirm this, we analyzed the KRAB domain of SZF1 using biochemical approaches. We have shown previously that the *E. coli*-expressed KOX1-KRAB domain was able to directly bind to the RBCC (RING-B box-Coiled-coil) domain of the KAP-1 protein in GST association and in EMSA analyses (34, 35). We used the GST association assay to test the ability of SZF1-KRAB to bind to the purified KAP-1-RBCC protein. Significant binding of the KAP-1-RBCC protein was observed for the GST-SZF1-KRAB protein but was negative for the control GST protein (Fig. 4). The affinity of the SZF1-KRAB protein for binding to the KAP-1-RBCC protein is comparable with that of the KOX1-KRAB protein, supporting our previous results demonstrating that the interaction between the KRAB domain and the RBCC domain of KAP-1 is direct and specific.

Assessment of SZF1-KRAB Transcriptional Regulation with GAL4 Reporter Assays. Previous studies demonstrate that the KRAB domains from other zinc finger proteins repressed transcription when fused to a heterologous DNA-binding domain (2, 4, 41). To assess the transcriptional regulatory properties of SZF1-KRAB, the KRAB domain of SZF1 was fused to a heterologous GAL4 DNA-binding domain. The GAL4-SZF1-KRAB expression plasmid was cotransfected with a 5xGAL4-TK-Luc reporter plasmid into NIH/3T3 cells. As a positive control for transcriptional repression, the GAL4-KOX1-KRAB plasmid was cotransfected into NIH/3T3 cells with the 5xGAL4-TK-Luc reporter plasmid. The GAL4-KOX1-KRAB protein strongly repressed luciferase activity in a dose-dependent manner (Fig. 5*B*). The GAL4-SZF1-KRAB protein also strongly repressed luciferase activity (17-fold over vector alone, at the highest input level

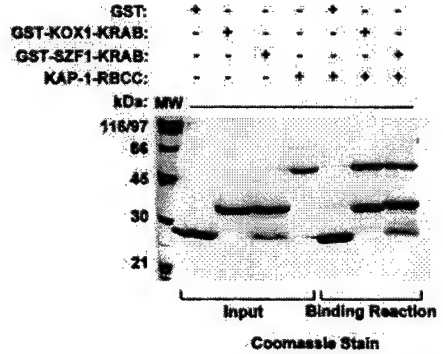

Fig. 4. Direct interaction between the SZF1-KRAB domain and the KAP-1-RBCC domain. The binding of the GST-SZF1-KRAB and GST-KOX1-KRAB proteins to a purified KAP-1-RBCC protein is detected by GST association assay. The input lanes represent 5 μg of each purified protein. Five μg of purified KAP-1-RBCC protein were added to each binding reaction mixture. No binding was detected for GST alone.

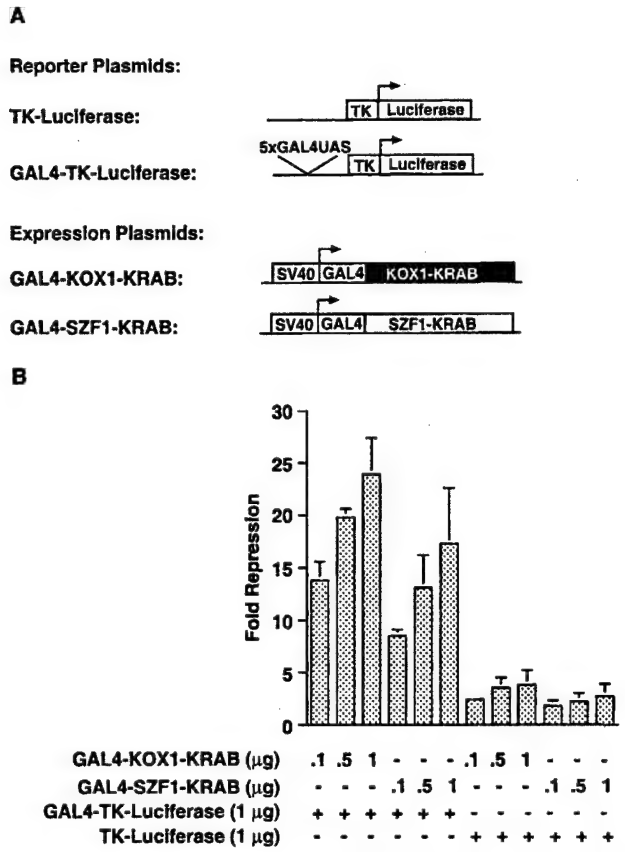

Fig. 5. The GAL4-SZF1-KRAB protein expression confers dose-dependent and binding site-dependent transcriptional repression of a GAL4 TK luciferase reporter plasmid. *A*, schematic diagram of the TK luciferase reporter plasmids with and without five copies of GAL4 UAS site and of the GAL4-KOX1-KRAB and GAL4-SZF1-KRAB expression plasmids. *B*, NIH/3T3 cells were transiently transfected with the indicated microgram amounts of expression plasmids along with constant amounts of a CMV-β-D-galactosidase plasmids and a TK luciferase reporter plasmid containing either no or five GAL4 UAS binding sites. *Fold Repression*, ratio of luciferase activities of empty expression vector relative to that obtained with the indicated expression plasmids. All activities were normalized for transfection efficiency based on β-D-galactosidase activity. *Bars*, SD for three independent transfections.

of GAL4-SZF1-KRAB tested; Fig. 5*B*). On the basis of the similar levels of expression in mammalian cells (data not shown), the repression activity by GAL4-SZF1-KRAB is comparable with the repression activity by GAL4-KOX1-KRAB.

SZF1 Is a Sequence-specific Transcriptional Repressor. The studies of the GAL4-SZF1-KRAB chimera illustrate the transcriptional repression activity of the SZF1-KRAB domain, and the EMSA analysis indicated that the SZF1-1-ZF and the ZBRK1-ZF proteins specifically bind to similar consensus sequences. To evaluate the ability of SZF1-1 to regulate transcription according to its intrinsic DNA-binding activity, the SZF1-1 expression vector was cotransfected with the pGL3p-E luciferase reporter plasmid into NIH/3T3 cells. This luciferase reporter plasmid contains four copies of the ZBRK1 consensus binding site upstream of the SV40 promoter driving expression of a luciferase reporter gene (32). As a positive control for transcriptional repression, the ZBRK1 expression vector was cotransfected with the pGL3p-E luciferase reporter plasmid into NIH/3T3 cells. The expression of ZBRK1 conferred a dose-dependent repression of luciferase activity from the reporter carrying ZBRK1-binding sites but had no effect on a control luciferase reporter that lacks the binding sites (Fig. 6*B* and data not shown), consistent with previous reports (32). As shown in Fig. 6*B*, expression of SZF1-1 also conferred a dose-dependent repression of luciferase activity from the reporter carrying ZBRK1-binding sites but had no effect on a control luciferase reporter that lacks the binding sites, suggesting that the repression activity of SZF1-1 is mediated through its cognate recognition sequence. This result is also consistent with the GAL4 studies described above. Therefore, in NIH/3T3 cells the full-length SZF1-1 functions as a DNA binding-dependent transcriptional repressor on the consensus binding sequences selected for *in vitro* by the SZF1-1-ZF and the ZBRK1-ZF domain proteins.

DISCUSSION

A mandatory prerequisite for understanding the function of a putative transcription factor (or family of transcription factors) is to identify the DNA sequence recognized by the cognate DNA-binding domain in the protein. This key discovery allows application of a myriad of experimental approaches, including the ability to predict target genes and pathways, to detect binding activity in complex mixtures and to test the potential of the protein as an activator or repressor of gene expression *in vivo*. This principle is well illustrated by the studies of the MYC-MAX, FOS-JUN, and HOMEODOMAIN protein families wherein identification of core DNA-binding consensus sequences was the key catalyst that allowed full characterization of their functions. A paradigm that emerged from these studies is that often multiple members of families that contain a common type of DNA-binding domain will recognize a common DNA-binding site. For example, the FOS-JUN-CREB family of bZIP proteins has the capability of forming >100 biologically distinct complexes via combinatorial heterodimerization; yet, all of them bind to subtle variants of the AP1 site. A great challenge has been to determine whether this paradigm will extend to other classes of DNA-binding proteins.

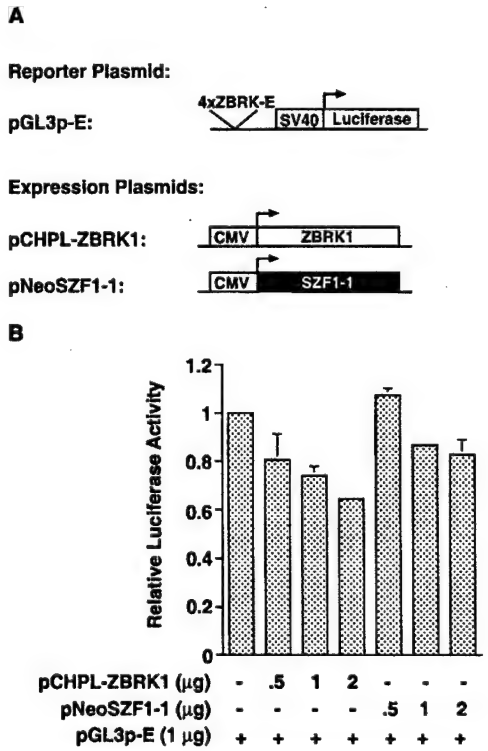

Fig. 6. SZF1-1 is a sequence-specific and dose-dependent transcriptional repressor. *A*, schematic diagram of the pGL3p-E luciferase reporter plasmid and the ZBRK1 and SZF1-1 expression plasmids. *B*, reporter assays with the ZBRK1 and the SZF1-1 expression plasmids were conducted using the pGL3p-E luciferase reporter plasmid containing four copies of the ZBRK1 consensus binding site. Assays were performed in NIH/3T3 cells as described in Fig. 5 and are plotted as relative luciferase activity that refers to the ratio of the activity for the indicated expression plasmids to the activity with the empty vector (~4×10^5 relative light units). SZF1 shows a similar dose-dependent transcriptional repression potential as ZBRK1. *Bars*, SD.

We have been studying the C_2H_2 zinc finger class of DNA-binding proteins. The C_2H_2 finger is the second most abundant motif found in the human genome (6, 42). This 24–30 amino acid motif, which contains tandem cysteine and histidine residues, functions by chelating a zinc atom resulting in a tightly folded modular unit. In most zinc finger proteins, these modules are found arranged in tandem arrays from 3 to upwards of 40 zinc finger units. Crystal structures of 3- and 5-fingered proteins have suggested that each module recognizes ~3 bp of DNA (26, 27). Thus, in a many-fingered protein, there is a potential for tremendous DNA-binding specificity and target affinity. Unfortunately, these predictions have not been thoroughly tested because only a few DNA-binding sites for multifingered proteins have been identified.

To simplify this problem, we have focused on a subclass of C_2H_2 zinc finger proteins, the KRAB-ZFPs. In this study, we have presented evidence for sequence-specific DNA binding by the KRAB-ZFP, SZF1. We chose SZF1 for a number of reasons: (*a*) it encodes only four zinc fingers, which should limit the complexity of the DNA recognition sequence; (*b*) SZF1 is predominantly expressed in $CD34^+$ hematopoietic progenitor cells, which should serve to limit the number of potential target genes; and (*c*) elucidation of its function may shed light on the generation or maintenance of hematopoietic stem cells.

The data shown in this study allow the following conclusions: (*a*) the KRAB-ZFP, SZF1 is a sequence-specific DNA-binding protein that recognizes the consensus sequence 5′-CCAGGGTAACAG-CCG-3′; (*b*) this sequence is a subset of the recently derived consensus DNA-binding site for the KRAB-ZFP, ZBRK1; (*c*) purified, recombinant zinc finger regions from either SZF1 or ZBRK1 bind both consensus sequences; (*d*) the binding is sequence specific because competition for binding can be demonstrated with homologous but not heterologous DNA binding sites; (*e*) the KRAB domain from SZF1 forms a strong, modular repression domain that binds to the universal KRAB domain corepressor, KAP-1; and (*f*) full-length SZF1 functions as a sequence-specific repressor on target genes that contain consensus ZBRK1 sites.

From the standpoint of understanding DNA recognition by zinc finger proteins, this study highlights the need for the experimental derivation of binding sequences as opposed to their empirical prediction. Structural and functional studies of many zinc finger proteins, including both arrays and single fingers, have suggested that there is a "code" for DNA recognition. This code is largely determined by the identity of the −1, +3, and +6 amino acids (Fig. 1, *C* and *D*) within the α-helical region of each finger (26–28). Although it is likely to be incomplete, this code was simply unable to predict a consensus sequence for SZF1 binding.[5] Moreover, the well-established amino acid code of "FSRSD" in the recognition helix for recognizing the 5′-GGG-3′ sequence is not present in any of the SZF1 fingers, although this bp triplet is strongly selected for in the binding assay. Furthermore, although there is little identity at the −1, +3, and +6 position when comparing individual fingers of SZF1 to ZBRK1, clearly they are able to bind similar DNA sequences. It is also noteworthy that the phylogenetic analysis indicates a clustering pattern that is common to the SZF1 fingers and the NH_2-terminal ZBRK1 fingers that is not present in the COOH-terminal fingers of ZBRK1. This observation is consistent with the functions of ZBRK1. The NH_2-terminal fingers appear to be required for DNA binding, whereas the COOH-terminal fingers appear to participate in binding to BRCA1. Thus, even with the caveat that we do not know which fingers bind which bp in the consensus, it is a reasonable conclusion that each protein will probably use different modes of molecular recognition to accomplish binding the same sequence. Solving these types of comparative molecular recognition problems (via atomic structure determination) will certainly be a great aid in correcting and extending the code hypothesis for zinc finger DNA recognition.

A key finding of this study is that SZF1 and ZBRK1 show a common binding site. By analogy to the known functions of ZBRK1, this finding immediately suggests both potential target genes for SZF1 and physiological functions. ZBRK1 was cloned in a two-hybrid screen for proteins that interact with the BRCA1 protein (32). BRCA1 is the familial breast/ovarian cancer tumor suppressor, and germ-line mutations in the gene account for ~50% of this inherited cancer predisposition syndrome. The BRCA1 protein is a nuclear protein, the abundance, posttranslational modification, and intranuclear location of which is dynamically regulated by many different cellular stimuli. Roles for BRCA1 in direct DNA repair, DNA damage sensing, transcriptional regulation/chromatin remodeling, and DNA replication have emerged (43). Most likely, BRCA1 serves as a scaffolding protein that coordinates these diverse activities in response to DNA damage stimuli. Although BRCA1 is a nuclear protein with gene-specific regulatory effects, it contains no apparent intrinsic DNA-binding activity or recognition domain. The key issue of how BRCA1 is tethered to DNA was partly resolved by the cloning of ZBRK1 as a BRCA1-binding protein. Moreover, the discovery that ZBRK1 bound the consensus sequence 5′-GGGxxxCAGxxxTTT-3′ found in many genes regulated by stress and DNA damage further suggested the relevance of ZBRK1 to BRCA1 function. BRCA1 has been shown to function as a corepressor for ZBRK1, and it was suggested that DNA damage-induced phosphorylation could relieve repression, thereby leading to activation of DNA damage response genes (43, 44). Whether the KAP-1 corepressor is involved in the ZBRK1/BRCA1 complex remains to be clarified.

How does SZF1 fit into this model? It is critical to determine whether SZF1 also binds to BRCA1. Although these experiments are ongoing, we think it is highly unlikely: (*a*) the COOH terminus of zinc fingers of ZBRK1, which contributes to the BRCA1 binding surface, are the most divergent in sequence when compared with the SZF1 fingers; (*b*) there is no significant homology between the COOH-terminal, non-finger region of ZBRK1 and the COOH terminus of either SZF1-1 or SZF1-2. In ZBRK1, this COOH-terminal extension in addition to the zinc fingers are required for BRCA1 binding (32). Thus, we think it unlikely that there is direct cross-talk between ZBRK1 and SZF1 for BRCA1 binding. A more likely scenario *in vivo* may simply be competition for binding at promoters containing these recognition sequences. Because the SZF1 consensus is shorter than the full ZBRK1 consensus, theoretically SZF1 has the capability for binding every ZBRK1 target gene. It should also be noted that ZBRK1 will also bind the shorter SZF1 consensus, albeit with lower apparent affinity (data not shown). It will be interesting to determine whether the protein with the longer array of fingers (ZBRK1) is able to functionally displace a SZF1 bound to a consensus sequence *in vivo*.

The current model for ZBRK1 function suggests that the protein is very stable when bound to target genes *in vivo* and that various cellular stress/DNA damage signals regulate the association of coactivator or corepressor complexes with the bound ZBRK1 protein, thereby regulating gene activation or repression. That BRCA1 is found in both types of regulatory complexes *in vivo* is consistent with this. However, ZBRK1 isolated from cells appears to be stably associated with both BRCA1 and KAP-1 (the caveat to this result being that there may be separate pools of ZBRK1 in the cells indistinguishable in the assays used). If indeed a ternary KAP-1:ZBRK1:BRCA1 complex is formed, it will be quite interesting to determine how BRCA1 when functioning as a coactivator in this complex can over-

[5] Unpublished data.

ride gene silencing that is presumably mediated by the KAP-1 corepressor, which is bound to the spatially separate KRAB domain on ZBRK1. One hypothesis is that SZF1 is functioning at ZBRK1 targets as a pure repressor; it does not toggle between activation and repression (similar to ZBRK1), because it probably does not bind BRCA1 (or presumably other coactivator complexes). In this context, the SZF1-ZBRK1 system may be functioning like other binary regulation systems whereby basal (repressed) gene activity is controlled by a DNA-binding protein with less specificity, whereas derepression is controlled by a complex with a DNA-binding subunit with more specificity (*i.e.,* a large number of zinc fingers) that contains coactivators. To resolve this, it will be critical to determine whether SZF1 and ZBRK1 regulate the same or overlapping sets of target genes, experiments that are currently underway using cDNA microarrays.

In summary, this discovery sheds new light on a potential mechanism for regulating target genes under the control of BRCA1.

ACKNOWLEDGMENTS

We thank D. Small for the SZF1 plasmids and W. J. Fredericks, D. C. Schultz, and M. S. Lechner for helpful discussions. We thank the Wistar Institute DNA Core Facility for DNA sequencing.

REFERENCES

1. Bellefroid, E. J., Poncelet, D. A., Lecocq, P. J., Revelant, O., and Martial, J. A. The evolutionarily conserved Kruppel-associated box domain defines a subfamily of eukaryotic multifingered proteins. Proc. Natl. Acad. Sci. USA, *88:* 3608–3612, 1991.
2. Margolin, J. F., Friedman, J. R., Meyer, W. K., Vissing, H., Theisen, H. J., and Rauscher, F. J., III. Kruppel-associated boxes are potent transcriptional repression domains. Proc. Natl. Acad. Sci. USA, *91:* 4509–4513, 1994.
3. Vissing, H., Meyer, W. K., Aagaard, L., Tommerup, N., and Thiesen, H. J. Repression of transcriptional activity by heterologous KRAB domains present in zinc finger proteins. FEBS Lett., *369:* 153–157, 1995.
4. Witzgall, R., O'Leary, E., Leaf, A., Onaldi, D., and Bonventre, J. V. The Kruppel-associated box-A (KRAB-A) domain of zinc finger proteins mediates transcriptional repression. Proc. Natl. Acad. Sci. USA, *91:* 4514–4518, 1994.
5. Mark, C., Abrink, M., and Hellman, L. Comparative analysis of KRAB zinc finger proteins in rodents and man: evidence for several evolutionarily distinct subfamilies of KRAB zinc finger genes. DNA Cell Biol., *18:* 381–396, 1999.
6. Venter, J. C., Adams, M. D., Myers, E. W., Li, P. W., Mural, R. J., Sutton, G. G., Smith, H. O., Yandell, M., Evans, C. A., Holt, R. A., Gocayne, J. D., Amanatides, P., Ballew, R. M., Huson, D. H., Wortman, J. R., Zhang, Q., Kodira, C. D., Zheng, X. H., Chen, L., Skupski, M., Subramanian, G., Thomas, P. D., Zhang, J., Gabor Miklos, G. L., Nelson, C., Broder, S., Clark, A. G., Nadeau, J., McKusick, V. A., Zinder, N., Levine, A. J., Roberts, R. J., Simon, M., Slayman, C., Hunkapiller, M., Bolanos, R., Delcher, A., Dew, I., Fasulo, D., Flanigan, M., Florea, L., Halpern, A., Hannenhalli, S., Kravitz, S., Levy, S., Mobarry, C., Reinert, K., Remington, K., Abu-Threideh, J., Beasley, E., Biddick, K., Bonazzi, V., Brandon, R., Cargill, M., Chandramouliswaran, I., Charlab, R., Chaturvedi, K., Deng, Z., Di Francesco, V., Dunn, P., Eilbeck, K., Evangelista, C., Gabrielian, A. E., Gan, W., Ge, W., Gong, F., Gu, Z., Guan, P., Heiman, T. J., Higgins, M. E., Ji, R. R., Ke, Z., Ketchum, K. A., Lai, Z., Lei, Y., Li, Z., Li, J., Liang, Y., Lin, X., Lu, F., Merkulov, G. V., Milshina, N., Moore, H. M., Naik, A. K., Narayan, V. A., Neelam, B., Nusskern, D., Rusch, D. B., Salzberg, S., Shao, W., Shue, B., Sun, J., Wang, Z., Wang, A., Wang, X., Wang, J., Wei, M., Wides, R., Xiao, C., Yan, C., *et al.* The sequence of the human genome. Science (Wash. DC), *291:* 1304–1351, 2001.
7. Rosati, M., Marino, M., Franze, A., Tramontano, A., and Grimaldi, G. Members of the zinc finger protein gene family sharing a conserved N-terminal module. Nucleic Acids Res., *19:* 5661–5667, 1991.
8. Friedman, J. R., Fredericks, W. J., Jensen, D. E., Speicher, D. W., Huang, X. P., Neilson, E. G., and Rauscher, F. J., III. KAP-1, a novel corepressor for the highly conserved KRAB repression domain. Genes Dev., *10:* 2067–2078, 1996.
9. Kim, S. S., Chen, Y. M., O'Leary, E., Witzgall, R., Vidal, M., and Bonventre, J. V. A novel member of the RING finger family. KRIP-1, associates with the KRAB-A transcriptional repressor domain of zinc finger proteins. Proc. Natl. Acad. Sci. USA, *93:* 15299–15304, 1996.
10. Moosmann, P., Georgiev, O., Le Douarin, B., Bourquin, J. P., and Schaffner, W. Transcriptional repression by RING finger protein TIF1β that interacts with the KRAB repressor domain of KOX1. Nucleic Acids Res., *24:* 4859–4867, 1996.
11. Lechner, M. S., Begg, G. E., Speicher, D. W., and Rauscher, F. J., III. Molecular determinants for targeting heterochromatin protein 1-mediated gene silencing: direct chromoshadow domain-KAP-1 corepressor interaction is essential. Mol. Cell. Biol., *20:* 6449–6465, 2000.
12. Schultz, D. C., Friedman, J. R., and Rauscher, F. J., III. Targeting histone deacetylase complexes via KRAB-zinc finger proteins: the PHD and bromodomains of KAP-1 form a cooperative unit that recruits a novel isoform of the Mi-2α subunit of NuRD. Genes Dev., *15:* 428–443, 2001.
13. Schultz, D. C., Ayyanathan, K., Negorev, D., Maul, G. G., and Rauscher, F. J., III. SETDB1: a novel KAP-1-associated histone H3, lysine 9-specific methyltransferase that contributes to HP1-mediated silencing of euchromatic genes by KRAB zinc-finger proteins. Genes Dev., *16:* 919–932, 2002.
14. Bellefroid, E. J., Marine, J. C., Ried, T., Lecocq, P. J., Riviere, M., Amemiya, C., Poncelet, D. A., Coulie, P. G., de Jong, P., Szpirer, C., *et al.* Clustered organization of homologous KRAB zinc-finger genes with enhanced expression in human T lymphoid cells. EMBO J., *12:* 1363–1374, 1993.
15. Gebelein, B., Fernandez-Zapico, M., Imoto, M., and Urrutia, R. KRAB-independent suppression of neoplastic cell growth by the novel zinc finger transcription factor KS1. J. Clin. Investig., *102:* 1911–1919, 1998.
16. Liu, C., Levenstein, M., Chen, J., Tsifrina, E., Yonescu, R., Griffin, C., Civin, C. I., and Small, D. SZF1: a novel KRAB-zinc finger gene expressed in CD34+ stem/progenitor cells. Exp. Hematol., *27:* 313–325, 1999.
17. Wagner, S., Hess, M. A., Ormonde-Hanson, P., Malandro, J., Hu, H., Chen, M., Kehrer, R., Frodsham, M., Schumacher, C., Beluch, M., Honer, C., Skolnick, M., Ballinger, D., and Bowen, B. R. A broad role for the zinc finger protein ZNF202 in human lipid metabolism. J. Biol. Chem., *275:* 15685–15690, 2000.
18. Jheon, A. H., Ganss, B., Cheifetz, S., and Sodek, J. Characterization of a novel KRAB/C2H2 zinc finger transcription factor involved in bone development. J. Biol. Chem., *276:* 18282–18289, 2001.
19. Lovering, R., and Trowsdale, J. A gene encoding 22 highly related zinc fingers is expressed in lymphoid cell lines. Nucleic Acids Res., *19:* 2921–2928, 1991.
20. Crew, A. J., Clark, J., Fisher, C., Gill, S., Grimer, R., Chand, A., Shipley, J., Gusterson, B. A., and Cooper, C. S. Fusion of SYT to two genes, *SSX1* and *SSX2*, encoding proteins with homology to the Kruppel-associated box in human synovial sarcoma. EMBO J., *14:* 2333–2340, 1995.
21. Tommerup, N., Aagaard, L., Lund, C. L., Boel, E., Baxendale, S., Bates, G. P., Lehrach, H., and Vissing, H. A zinc-finger gene *ZNF141* mapping at 4p16.3. *D4S90* is a candidate gene for the Wolf-Hirschhorn (4p-) syndrome. Hum. Mol. Genet., *2:* 1571–1575, 1993.
22. Bellefroid, E. J., Lecocq, P. J., Benhida, A., Poncelet, D. A., Belayew, A., and Martial, J. A. The human genome contains hundreds of genes coding for finger proteins of the Kruppel type. DNA, *8:* 377–387, 1989.
23. Shannon, M., Ashworth, L. K., Mucenski, M. L., Lamerdin, J. E., Branscomb, E., and Stubbs, L. Comparative analysis of a conserved zinc finger gene cluster on human chromosome 19q and mouse chromosome 7. Genomics, *33:* 112–120, 1996.
24. Han, Z. G., Zhang, Q. H., Ye, M., Kan, L. X., Gu, B. W., He, K. L., Shi, S. L., Zhou, J., Fu, G., Mao, M., Chen, S. J., Yu, L., and Chen, Z. Molecular cloning of six novel Kruppel-like zinc finger genes from hematopoietic cells and identification of a novel transregulatory domain KRNB. J. Biol. Chem., *274:* 35741–35748, 1999.
25. Pabo, C. O., Peisach, E., and Grant, R. A. Design and selection of novel Cys2His2 zinc finger proteins. Annu. Rev. Biochem., *70:* 313–340, 2001.
26. Pavletich, N. P., and Pabo, C. O. Zinc finger-DNA recognition: crystal structure of a Zif268-DNA complex at 2.1 A. Science (Wash. DC), *252:* 809–817, 1991.
27. Pavletich, N. P., and Pabo, C. O. Crystal structure of a five-finger GLI-DNA complex: new perspectives on zinc fingers. Science (Wash. DC), *261:* 1701–1707, 1993.
28. Wolfe, S. A., Nekludova, L., and Pabo, C. O. DNA recognition by Cys2His2 zinc finger proteins. Annu. Rev. Biophys. Biomol. Struct., *29:* 183–212, 2000.
29. Crozatier, M., Kongsuwan, K., Ferrer, P., Merriam, J. R., Lengyel, J. A., and Vincent, A. Single amino acid exchanges in separate domains of the *Drosophila* serendipity δ zinc finger protein cause embryonic and sex biased lethality. Genetics, *131:* 905–916, 1992.
30. Gaul, U., Redemann, N., and Jackle, H. Single amino acid exchanges in the finger domain impair the function of the *Drosophila* gene *Kruppel* (*Kr*). Proc. Natl. Acad. Sci. USA, *86:* 4599–4603, 1989.
31. Laity, J. H., Lee, B. M., and Wright, P. E. Zinc finger proteins: new insights into structural and functional diversity. Curr. Opin. Struct. Biol., *11:* 39–46, 2001.
32. Zheng, L., Pan, H., Li, S., Flesken-Nikitin, A., Chen, P. L., Boyer, T. G., and Lee, W. H. Sequence-specific transcriptional corepressor function for BRCA1 through a novel zinc finger protein, ZBRK1. Mol. Cell, *6:* 757–768, 2000.
33. Gebelein, B., and Urrutia, R. Sequence-specific transcriptional repression by KS1, a multiple-zinc-finger-Kruppel-associated box protein. Mol. Cell. Biol., *21:* 928–939, 2001.
34. Peng, H., Begg, G. E., Schultz, D. C., Friedman, J. R., Jensen, D. E., Speicher, D. W., and Rauscher, F. J., III. Reconstitution of the KRAB-KAP-1 repressor complex: a model system for defining the molecular anatomy of RING-B box-coiled-coil domain-mediated protein-protein interactions. J. Mol. Biol., *295:* 1139–1162, 2000.
35. Peng, H., Begg, G. E., Harper, S. L., Friedman, J. R., Speicher, D. W., and Rauscher, F. J., III. Biochemical analysis of the Kruppel-associated box (KRAB) transcriptional repression domain. J. Biol. Chem., *275:* 18000–18010, 2000.
36. Ryan, R. F., Schultz, D. C., Ayyanathan, K., Singh, P. B., Friedman, J. R., Fredericks, W. J., and Rauscher, F. J., III. KAP-1 corepressor protein interacts and colocalizes with heterochromatic and euchromatic HP1 proteins: a potential role for Kruppel-associated box-zinc finger proteins in heterochromatin-mediated gene silencing. Mol. Cell. Biol., *19:* 4366–4378, 1999.
37. Morris, J. F., Hromas, R., and Rauscher, F. J., III. Characterization of the DNA-binding properties of the myeloid zinc finger protein MZF1: two independent DNA-binding domains recognize two DNA consensus sequences with a common G-rich core. Mol. Cell. Biol., *14:* 1786–1795, 1994.
38. Fredericks, W. J., Galili, N., Mukhopadhyay, S., Rovera, G., Bennicelli, J., Barr, F. G., and Rauscher, F. J., III. The PAX3-FKHR fusion protein created by the t(2;13) translocation in alveolar rhabdomyosarcomas is a more potent transcriptional activator than PAX3. Mol. Cell. Biol., *15:* 1522–1535, 1995.

39. Feng, D. F., and Doolittle, R. F. Progressive sequence alignment as a prerequisite to correct phylogenetic trees. J. Mol. Evol., *25:* 351–360, 1987.
40. Guex, N., and Peitsch, M. C. SWISS-MODEL and the Swiss-PdbViewer: an environment for comparative protein modeling. Electrophoresis, *18:* 2714–2723, 1997.
41. Pengue, G., Calabro, V., Bartoli, P. C., Pagliuca, A., and Lania, L. Repression of transcriptional activity at a distance by the evolutionarily conserved KRAB domain present in a subfamily of zinc finger proteins. Nucleic Acids Res., *22:* 2908–2914, 1994.
42. Lander, E. S., Linton, L. M., Birren, B., Nusbaum, C., Zody, M. C., Baldwin, J., Devon, K., Dewar, K., Doyle, M., FitzHugh. W., Funke, R., Gage, D., Harris, K., Heaford, A., Howland, J., Kann, L., Lehoczky, J., LeVine, R., McEwan, P., McKernan, K., Meldrim, J., Mesirov, J. P., Miranda, C., Morris, W., Naylor, J., Raymond, C., Rosetti, M., Santos, R., Sheridan, A., Sougnez, C., Stange-Thomann, N., Stojanovic, N., Subramanian, A., Wyman, D., Rogers, J., Sulston, J., Ainscough, R., Beck, S., Bentley, D., Burton, J., Clee, C., Carter, N., Coulson, A., Deadman, R., Deloukas, P., Dunham, A., Dunham, I., Durbin, R., French, L., Grafham, D., Gregory, S., Hubbard, T., Humphray, S., Hunt, A., Jones, M., Lloyd, C., McMurray, A., Matthews, L., Mercer, S., Milne, S., Mullikin, J. C., Mungall, A., Plumb, R., Ross, M., Shownkeen, R., Sims, S., Waterston, R. H., Wilson, R. K., Hillier, L. W., McPherson, J. D., Marra, M. A., Mardis, E. R., Fulton, L. A., Chinwalla, A. T., Pepin, K. H., Gish, W. R., Chissoe, S. L., Wendl, M. C., Delehaunty, K. D., Miner, T. L., Delehaunty, A., Kramer, J. B., Cook, L. L., Fulton, R. S., Johnson, D. L., Minx, P. J., Clifton, S. W., Hawkins, T., Branscomb, E., Predki, P., Richardson, P., Wenning, S., Slezak, T., Doggett, N., Cheng, J. F., Olsen, A., Lucas, S., Elkin, C., Uberbacher, E., Frazier, M., *et al.* Initial sequencing and analysis of the human genome. Nature (Lond.), *409:* 860–921, 2001.
43. Zheng, L., Li, S., Boyer, T. G., and Lee, W. H. Lessons learned from BRCA1 and BRCA2. Oncogene, *19:* 6159–6175, 2000.
44. Li, S., Ting, N. S., Zheng, L., Chen, P. L., Ziv, Y., Shiloh, Y., Lee, E. Y., and Lee, W. H. Functional link of *BRCA1* and ataxia telangiectasia gene product in DNA damage response. Nature (Lond.), *406:* 210–215, 2000.
45. Thompson, J. D., Higgins, D. G., and Gibson, T. J. CLUSTAL W: improving the sensitivity of progressive multiple sequence alignment through sequence weighting, position-specific gap penalties and weight matrix choice. Nucleic Acids Res., *22:* 4673–4680, 1994.
46. Thompson, J. D., Gibson, T. J., Plewniak, F., Jeanmougin, F., and Higgins, D. G. The CLUSTAL_X windows interface: flexible strategies for multiple sequence alignment aided by quality analysis tools. Nucleic Acids Res., *25:* 4876–4882, 1997.
47. Kimura, M. Rare variant alleles in the light of the neutral theory. Mol. Biol. Evol., *1:* 84–93, 1983.
48. Page, R. D. TreeView: an application to display phylogenetic trees on personal computers. Comput. Appl. Biosci., *12:* 357–358, 1996.

[CANCER RESEARCH 62, 2498–2502, May 1, 2002]

Advances in Brief

Deficiency of *Retinoblastoma* Gene in Mouse Embryonic Stem Cells Leads to Genetic Instability[1]

Lei Zheng, Andrea Flesken-Nikitin, Phang-Lang Chen, and Wen-Hwa Lee[2]

Department of Molecular Medicine and Institute of Biotechnology, University of Texas Health Science Center at San Antonio, San Antonio, Texas 78245

Abstract

Genetic instability has been recognized as a hallmark of human cancers. Retinoblastoma (Rb) tumor suppressor protein has an essential role in modulating cell cycle progression. However, there is no direct evidence supporting its role in maintaining genetic stability. Here, we developed a sensitive method to examine the level of chromosome instability by using retrovirus carrying both positive and negative selectable markers that integrated randomly into individual chromosomes, and the frequency of loss of this selectable chromosomal marker (LOM) in normal mammalian cells was measured. Our results showed that normal mouse embryonic stem (ES) cells had a very low frequency of LOMs, which was less than 10^{-8}/cell/generation. In Rb−/− mouse ES cells, the frequency was increased to approximately 10^{-5}/cell/generation, whereas in Rb+/− ES cells, the frequency was approximately 10^{-7}/cell/generation. LOMs was mediated mainly through chromosomal mechanisms and not through point mutations. These results, therefore, revealed that Rb, with a haploinsufficiency, plays a critical role in the maintenance of chromosome stability. The mystery of why Rb heterozygous carriers have early-onset tumor formation with high penetrance can be, at least, partially explained by this novel activity.

Introduction

Genetic instability is one of the most important hallmarks of cancer (1). Associations of tumor suppressors with the process of chromosome behavior provide possible links between carcinogenesis and genetic instability. Aneuploidy, chromosome structural rearrangements, centrosome amplification, and gene amplification have been observed in p53-deficient cells (2) and, more recently, in APC-deficient cells (3), which supports a potential role of tumor suppressors in the maintenance of genetic stability.

The roles of Rb[3] in cell cycle regulation and differentiation are well established and can explain how Rb suppresses tumor growth, but do not completely explain why cancer susceptibility results from loss of Rb function (4). In particular, the mystery as to why the inactivation of Rb leads to multiple genetic alterations that predispose cells to the process of tumorigenesis remains unsolved. In addition to its role in G_1 progression, several lines of evidence suggest that Rb also plays a significant role at G_2-M phases. First, the hypophosphorylated form of Rb, the functional form, is present in these cell cycle stages. It appears that Rb becomes dephosphorylated as Rb interacts with protein phosphatase 1α specifically during G_2-M phases (5). The yeast homologue of protein phosphatase 1α has been shown to be essential for kinetochore function, execution of mitotic kinetochore/spindle checkpoint, and faithful chromosome segregation (6). A regulatory role in the activity of protein phosphatase 1α mediated by Rb would be consistent with other potential activities of Rb in G_2-M progression. Second, phosphorylation of Rb in G_1-S phases has a coordinated effect on mitotic cyclin induction and degradation in G_2-M phases (7). Third, overexpression of Rb in S phase arrests cells at G_2 phase (8). Fourth, when treated with microtubule-destabilizing agents, cells lacking functional Rb do not finish mitosis properly but exit M phase and undergo a new cycle of DNA replication, leading to hyperploidy (9). Finally, p53-mediated G_2-M arrest in response to DNA damage requires the presence of functional Rb (10). Taken together, these results suggest that mitotic division cannot be completed in a controlled manner without functional Rb.

Rb may also directly modulate chromosome segregation. Rb has been shown to associate with Hec1, a conserved regulator of multiple mitotic events (11, 12). Hec1 interacts with the SMC family of proteins, which are chromosome structural proteins essential for establishment of sister chromatid cohesion and chromosome condensation (13). Inactivation of Hec1 in either mammalian cells or yeast cells, either by microinjection of specific anti-Hec1 antibodies or by introducing genetic mutations, leads to severe chromosome missegregation resulting in lethality (11, 14). This essential function of Hec1 appears to be mediated in part by its interaction with the SMC family of protein (14). The interaction between Rb and Hec1 occurs specifically in G_2-M phase (12). It has been demonstrated that the fidelity of chromosome segregation in yeast cells is enhanced on induced expression of exogenous human Rb, and this activity requires the specific interaction between Rb and Hec1 (12). However, the role of Rb for maintaining genetic stability in mammalian cells remains to be shown.

Here, we developed a sensitive method for examining the level of chromosome instability in normal mammalian cells by using a retroviral system to integrate randomly a selectable marker on individual chromosomes. The frequency of LOMs was measured, and our results showed increased frequency of LOMs (to ~10^{-5}/cell/generation) in mouse Rb−/− ES cells compared with that in Rb+/+ cells. The frequency of LOMs in Rb+/− cells was also moderately increased. Further analysis indicated that the loss of the fusion genes is most likely caused by gross chromosomal changes.

Materials and Methods

Isolation, Culture, and Genotyping of Mouse ES Cells. Rb +/+, Rb+/− and Rb−/− ES cells were isolated from blastocysts of the same litter of mouse embryos taken from pregnant intercrossed Rb+/− mice (15) following a previously described procedure (16). Briefly, blastocysts were harvested from pregnant mice on embryonic day 3.5 and cultured on a feeder layer derived from mouse embryonic fibroblasts. The embryos were allowed to hatch for 4–6 days and the inner cell mass was moved away from the trophoblast cells, disaggregated, and cultured on the feeder layer in the medium containing DMEM, 15% fetal bovine serum, and leukemia- inhibitory factors. The pluripotential individual ES colonies were picked, transferred onto a freshly

Received 12/6/01; accepted 3/13/02.

The costs of publication of this article were defrayed in part by the payment of page charges. This article must therefore be hereby marked *advertisement* in accordance with 18 U.S.C. Section 1734 solely to indicate this fact.

[1] Supported in part by NIH Grants EY 05758 and CA58318.

[2] To whom requests for reprints should be addressed, at Department of Molecular Medicine and Institute of Biotechnology, University of Texas Health Science Center at San Antonio, 15355 Lambda Drive, San Antonio, Texas 78245. Phone: (210) 567-7351; Fax: (210) 567-7377; E-mail: leew@uthscsa.edu.

[3] The abbreviations used are: Rb, retinoblastoma; LOM, loss of chromosomal marker; ES, embryonic stem; HygTK, fusion gene (or virus) of the *hygromycin phosphotransferase* gene and thymidine kinase; SMC, structural maintenance of chromosomes; LTR, long terminal repeat.

prepared feeder layer, and amplified. To determine the genotype of the ES cells, genomic DNA was extracted, and PCR was performed as described previously (17). The selected three genotypes of the ES cells were karyotyped and had apparently normal chromosome pattern.

Selection of Individual ES Clones Infected with HygTK Retrovirus. The *HygTK* fusion gene (18) was inserted between the two LTRs derived from Moloney murine leukemia virus in a previously described vector (19). The resultant vector pLHL1-HygTK was transfected into the retroviral packaging cell lines and the HygTK virus was harvested. Approximately 2×10^6 ES cells, isolated as above, described at the 12th passage with the genotype of Rb+/+, Rb+/−, and Rb−/−, respectively, were grown on a hygromycin-resistant feeder layer derived from embryonic fibroblasts of transgenic mice expressing the *hygromycin phosphotransferase* gene (The Jackson Laboratory). Cells were infected by the HygTK virus for 24 h in the presence of Polybrene and subsequently treated with 250 μg/ml hygromycin after another 24 h. Hygromycin-resistant clones were picked after 9 days of selection and afterward maintained in the ES cell culture medium containing 200 μg/ml hygromycin. Clones were individually amplified, and PCR analysis indicated that all of the hygromycin-resistant colonies carried the integration of the *HygTK* fusion gene (data not shown).

Results

Establishing a Method for Measuring the Globally Genetic Instability in Mammalian Cell. To follow the dynamic changes of individual chromosomes, a selectable marker was permanently integrated on the chromosome by retrovirus-mediated gene transfer, which would be expected to harbor a single copy of this marker randomly on individual chromosomes (19). By tracing this marker in multiple virally infected clones, one would have a global view of genetic alterations on chromosomes in general rather than at one specific locus. For the feasibility of detecting the presence or absence of the marker, we chose a fusion gene that combines the *hygromycin phosphotransferase* (*Hyg*) gene and herpes simplex virus type 1 *thymidine kinase* gene (*TK*) in frame. Translation of this fusion gene into a single bifunctional enzyme protein (designated hereafter as HygTK) confers both resistance to hygromycin and sensitivity to ganciclovir (18), which provides both positive and negative selectivity.

The *HygTK* fusion gene was inserted between two LTRs derived from Moloney murine leukemia virus (19); and thereby, its expression was under the control of the LTR promoter (Fig. 1*A*). In an attempt to explore the overall frequencies of LOMs regardless of the viral integration loci, more than 50 individual hygromycin-resistant colonies with approximately equal number of cells were mixed together. The mixture of cells was maintained in the hygromycin-containing medium, and then transferred to a selection-free medium in which the cells were to be propagated for about 10 generations. Before this propagation step, 1×10^7 cells were removed from the hygromycin-containing medium and immediately seeded in the ganciclovir-containing medium, and the ganciclovir-resistant colonies were counted to obtain *Eo* (Fig. 1*B*). After the propagation (in the selection-free medium), the cell number was counted; the number of generations through which the cells had been propagated was calculated (usually between 9 and 10 generations); 1×10^7 cells were seeded in the ganciclovir-containing medium; and, after 12 days of ganciclovir-selection, the ganciclovir-resistant colonies were counted to obtain *Ep* (Fig. 1*B*).

The ganciclovir-resistant colonies that arose were from those cells that had lost the functional *TK* gene and, thus, were no longer sensitive to ganciclovir. Maintaining the cells in the hygromycin-containing medium would have prevented the loss of the entire *HygTK* gene; therefore, ganciclovir-resistant cells were not detected or were detected at a frequency less than 10^{-8}. The appearance of ganciclovir-resistant cells before the cells were propagated in nonselective medium would be expected, because the accumulation of mutations during this long-term culture could have inactivated the *TK* gene in some hygromycin-resistant cells. This frequency, however, was subtracted from that of ganciclovir-resistant cells analyzed after the propagation, and the resultant subtraction represented the frequency of cells that had the *TK* gene inactivated during the propagation. Finally, this subtraction was sequentially divided by the total cell number and by the generation numbers to deduce the frequency of LOMs at the *HygTK*-integrated loci in one cell per division generation (Fig. 1*C*).

Loss of *Rb* Gene Increases Frequency of LOMs. The above method is ideal for cells with high colony forming efficiency. Normal human fibroblasts and mouse embryonic fibroblasts have poor colony-forming efficiency, at about 10^{-3} to 10^{-4}. Therefore, it requires a substantial amount of cells for measuring LOMs by this method. Any immortalized cell lines, including cancer cell lines, are prone to genetic changes. The selection process in this procedure may create a bias toward certain changes and generate artifacts for this measuring. To circumvent these difficulties, we used ES cells to perform this experiment because of their normalcy and high colony-forming efficiency. Three mouse ES cell lines with normal karyotype from the same litter were used; one with the wild-type *Rb*, the other with one allele of *Rb* mutated at exon 20, and another one with both alleles mutated at exon 20 (15). Our results indicated that the LOM frequency of Rb+/+ cells was lower than 10^{-8}, the frequency of Rb+/− cells was between $10^{-7}$and 10^{-6}, and the frequency of Rb−/− cells was higher than 10^{-5} (Fig. 2). These results, therefore, suggest that the frequency of LOMs is increased in cells homozygous for the null mutation of Rb and moderately increased in cells heterozygous for Rb.

To determine whether the experiments with mixed viral-infected colonies would reveal the average frequencies of LOMs regardless of the viral integration loci, we examined the LOM frequencies at individual integration loci. Viral-infected cells were selected by hygromycin and hygromycin-resistant clones were randomly picked and individually cultured. PCR analysis indicated that all of the selected clones carried the integration of the *HygTK* fusion gene (as shown

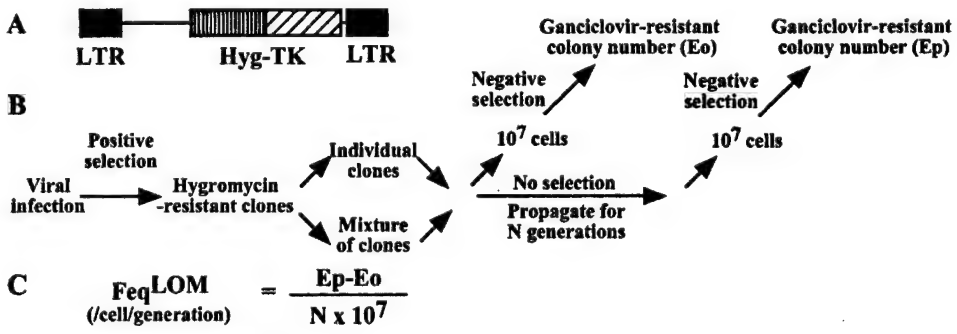

Fig. 1. A method for measuring the frequency of LOMs using the retroviral-integrated *HygTK* fusion gene as reporter. A, schematic structure of the retrovirus carried the *HygTK* fusion gene. *B*, experimental steps outlined for measuring the frequency of loss of heterozygosity. *C*, formula for calculating the frequency of loss of heterozygosity. Feq^{LOM} is the frequency of loss of the marker per cell per generation. Ep and Eo are designated as in *B*. *n*, the number of generations.

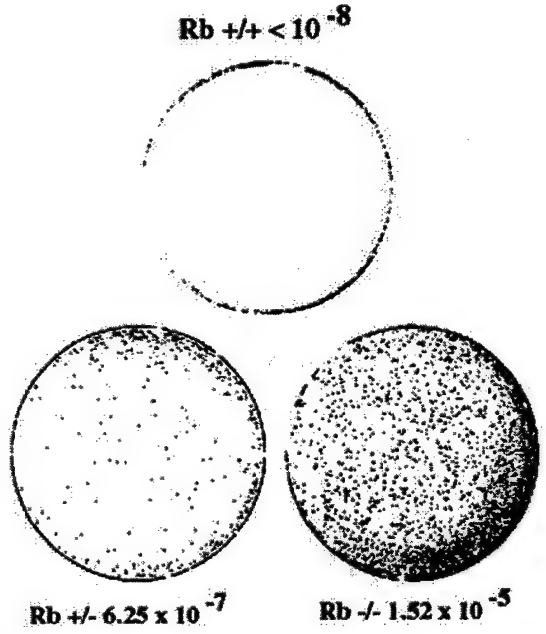

Fig. 2. Increased frequency of LOMs in Rb-deficient ES cells. Three representative dishes selected for ganciclovir-resistant colonies are shown. A mixture of more than 50 individual hygromycin-resistant clones of ES cells infected with the HygTK retrovirus was propagated about 10 generations without any selection. About 10^7 cells of each genotype were seeded on 10-cm dishes and selected for ganciclovir-resistant colonies. Pictures were taken after 12 days of selection. The frequencies of LOMs were calculated based on the results collected from multiple dishes

later in Fig. 4). The ES cells carrying the *HygTK* fusion gene were maintained in hygromycin-containing medium for at least 6 days before LOM frequency was analyzed following the same procedures for the experiments with the mixed clones.

More than 20 individual clones of each genotype were analyzed to cover approximately one haploid number of chromosomes. The results indicated that individually viral-infected clones, although derived from the same parental cells, have different frequency of LOMs at the *HygTK* loci. A similar frequency of LOMs was observed with the same clone in repeated experiments. Considering that retroviral infection tends to integrate the *HygTK* marker in different chromosomal loci, we inferred from these results that different chromosomal loci vary in the frequency of LOMs. We summarized the number of clones with the frequency of LOMs that fell in the same logarithm range (Fig. 3*A*). Results from both sources of Rb+/+ ES cells were combined and showed that ~90% of the Rb+/+ clones had a frequency of LOMs lower than 10^{-8}, and the rest of the clones had a frequency of LOMs between 10^{-8} and 10^{-6} (Fig. 3*B*). However, 80–90% of the Rb−/− clones had a frequency of LOMs higher than 10^{-6}, and a number of clones (~30%) had a frequency of LOMs higher than 10^{-4}. Karyotyping of these clones that had a frequency of LOMs higher than 10^{-3} revealed that they had an aneuploidy tendency (~10% of the cell population). Interestingly, although none of the Rb+/− clones had this LOM frequency higher than 10^{-4}, ~60% of these clones had a LOM frequency between 10^{-7} and 10^{-5}. These results suggested again that Rb-deficient cells have a significantly higher frequency of LOMs compared with that of wild-type cells. As shown in Fig. 3*B*, the majority of clones had a frequency of LOMs similar to that of the mixed clones (Fig. 2), which suggests that the assay with the mixed clones was able to reveal an overall frequency of LOMs that closely represented the stability of the whole genome. It should be noted that the frequency determined by this procedure could be overestimated because the mutated cells may continue to propagate in nonselection medium. However, the relative frequencies of these three different genotype cells are consistent, regardless of the different procedures.

Loss of the Marker Involves Larger Deletion of Chromosomal Event Instead of Point Mutation. To explore the mechanisms underlying the loss of functional *TK* gene, we examined the status of the *HygTK* fusion gene in the ganciclovir-resistant cells by PCR. As shown in Fig. 4, *A* and *B*, PCR was not able to amplify any fragments of the *HygTK* fusion from genomic DNA of the ganciclovir-resistant clones that were randomly picked. This result indicated that ~90% of ganciclovir-resistant clones had lost the entire *HygTK* fusion gene physically. It also suggested that point mutations or small deletions that could have inactivated the *TK* gene occurred at a low frequency (~10%). As suggested previously, potential mechanisms attributed to the loss of a whole gene include chromosomal loss, mitotic recombination, and interchromosomal rearrangement, which are all chromosome mechanisms (20). Therefore, increased frequency of LOMs observed in Rb−/− cells suggests that Rb-deficiency would lead to chromosome instability.

Interestingly, retaining one wild-type *Rb* allele does not appear to be sufficient for the maintenance of chromosome stability, because Rb+/− cells also have a moderately increased frequency of LOMs compared with the wild-type cells. It would, however, be possible that chromosome instability is a consequence of the loss of the remaining wild-type *Rb* allele. To examine this possibility, these ganciclovir-resistant clones derived from Rb+/− cells were genotyped for the wild-type *Rb* allele by PCR. The result indicated the clones picked randomly all retained one wild-type *Rb* allele (Fig. 4*C*), which suggested the haploinsufficiency of Rb in maintaining chromosome stability.

Discussion

Genetic instability in Rb-deficient cells could be responsible for further genetic alterations involved in cancer development. Germ-line

A

Freq LOM	Numbers of clones		
	Rb-/-	Rb+/-	Rb+/+
$<10^{-8}$	2	7	20
~10^{-8}	0	4	1
~10^{-7}	1	6	0
~10^{-6}	7	4	1
~10^{-5}	11	4	0
~10^{-4}	6	0	0
~10^{-3}	4	0	0
Total	31	25	22

B

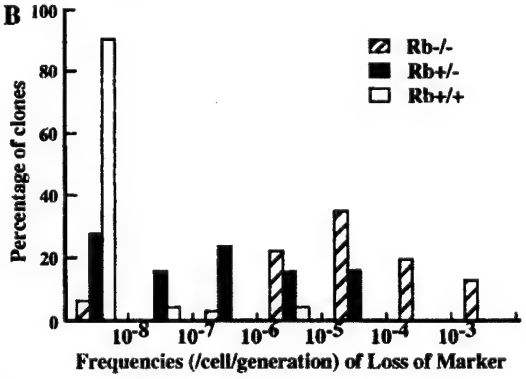

Fig. 3. Frequencies of LOMs in individual infected clones. *A*, number of clones of each genotype of ES cells is listed in the table (*A*) with frequencies of LOMs falling in each indicated logarithm range. *B*, histogram shows the percentage of clones falling in each indicated logarithm range deduced from *A*.

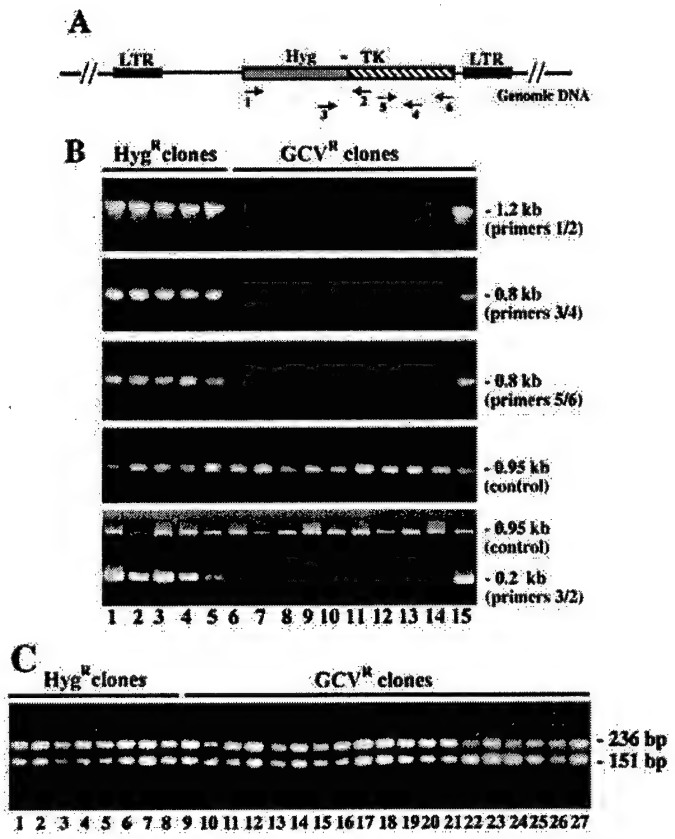

Fig. 4. Genotyping PCR of the *HygTK* fusion gene and the *Rb* allele. *A*, schematic diagram of the genomic structure of the *HygTK*-integrated loci. PCR primers for amplifying various regions of the *HygTK* gene are indicated at their relative positions. *B*, genotyping PCR of the *HygTK* gene. *Lanes 1–5*, representatives of the hygromycin-resistant clones that carry the *HygTK* fusion gene; *Lanes 6–15*, representatives of ganciclovir-resistant clones. The approximate size of PCR products and corresponding primers used are indicated. *Bottom panel*, two pairs of primers as indicated were used in the same reaction. Primers amplifying a region of the *Brca1* genome were used as control. *C*, genotyping PCR showed that the heterozygosity of the *Rb* allele was retained. *Lanes 1–8*, representatives of hygromycin-resistant clones of Rb+/− ES cells that carry the *HygTK* fusion gene; *Lanes 9–27*, representative of ganciclovir resistant clones of Rb+/− ES cells that have lost the *HygTK* fusion gene. *236 bp*, PCR products derived from the target allele; *151 bp*, products derived from the wild-type *Rb* allele.

mutations in one *Rb* allele lead to the development of retinoblastoma in human and pituitary tumors in mice at very early ages and with nearly complete penetrance (15, 21). The remaining wild-type allele is lost as a somatic event and, as suggested, mainly through chromosome mechanisms (20, 22). It has been estimated previously, based on the mean number of tumors occurring in carriers of Rb, that the mutation rates in both events are nearly equal (21).

In this study, by directly accessing the mutation rate, one view suggested that the mutation rate increases when the first *Rb* allele is inactivated. Chromosome instability in Rb-heterozygous cells could explain the high penetrance of tumor development with loss of the remaining wild-type allele. Nonetheless, the loss of the second *Rb* allele appears to be the threshold event in tumor development, given that it results in much more severe genetic instability, which might account for all of the following genetic alterations essential for tumorigenesis.

The possibility cannot be excluded that Rb could also suppress the frequency of point mutations or small deletions, considering that the *HygTK* gene may not serve as an appropriate reporter for small nucleotide changes. However, our observations implicating a low frequency of point mutations or small deletions in Rb-deficient cells is consistent with previous reports indicating that the loss of the remaining *Rb* allele in the majority of Rbs is mediated by chromosome mechanisms (20, 22). In addition, chromosome mechanisms appear to be the major cause of loss of heterozygosity during tumorigenesis based on studies with different tumor suppressor genes (23).

In previous studies, reporters such as the *adenine phosphoribosyltransferase* (*APRT*) gene at a specific chromosome locus have been used to evaluate the frequency of LOMs (23, 24). The new method used in this study, by using retroviral infection to integrate the reporter randomly on different chromosomes, allows us to access comprehensively all of the chromosome behaviors in a cell. In addition, the loss of reporter is prevented by positive selectivity conferred by the same reporter gene; thus, the new method is able to evaluate precisely the level of chromosome instability.

Chromosome abnormality in Rb-deficient fibroblasts has not yet been reported. The average frequency of LOMs observed in Rb−/− cells is approximately 10^{-5}. Classical methods such as multiplex fluorescent *in situ* hybridization and spectral karyotyping (25) would not be able to catch any aberrance if vast numbers of cells were not subjected to such analysis. By contrast, the new method appears to be more sensitive in evaluating the chromosome instability. However, unlike fluorescent *in situ* hybridization or spectral karyotyping, this new method does not reveal the types of chromosome aberrance directly. Our method has to be followed by traditional polymorphism marker analysis on the viral-integrated chromosome if one is interested in what types of chromosome mechanisms are involved.

Although nondisjunction is apparently a result of improper chromosome segregation, how other types of chromosome aberrance occur remains to be clarified. Chromosome mechanisms underlying LOMs in Rb-deficient cells are most likely comprised of multiple types of chromosome aberrance because Rb appears to be capable of modulating chromosome metabolisms from different, but intimately related, aspects including chromosome replication, segregation, and structural maintenance (4). Given that Rb is regarded as the prototype for tumor suppressors, it will be even more interesting to examine the role of other tumor suppressors in maintaining chromosome stability by this new method. It is conceivable that the other tumor suppressors have a common role in the maintenance of chromosome stability, and such a role may be pivotal for their functions in tumor suppression.

Acknowledgments

We thank Dr. Stanley Cohen (Stanford University) for his generosity in providing pLLTX plasmid and Dr. Nicholas Ting for his critical reading of the manuscript.

References

1. Lengauer, C., Kinzler, K. W., and Vogelstein, B., Genetic instabilities in human cancers. Nature (Lond.), *396:* 643–649, 1998.
2. Livingstone, L. R., White, A., Sprouse, J., Livanos, E., Jacks, T., and Tlsty, T. D. Altered cell cycle arrest and gene amplification potential accompany loss of wild-type p53. Cell, *70:* 923–935, 1992.
3. Kaplan, K. B., Burds, A. A., Swedlow, J. R., Bekir, S. S., Sorger, P. K., and Nathke, I. S. A role for the adenomatous polyposis coli protein in chromosome segregation. Nat. Cell Biol., *3:* 429–432, 2001.
4. Zheng, L., and Lee, W-H. The *retinoblastoma* gene: a prototypic and multifunctional tumor suppressor. Exp. Cell Res. *264:* 2–18, 2001.
5. Durfee, T., Becherer, K., Chen, P-L., Yeh, S-H., Yang, Y., Kilburn, A. E., Lee, W-H., and Elledge, S. J. The retinoblastoma protein associates with the protein phosphatase type 1 catalytic subunit. Genes Dev., *7:* 555–569, 1993.
6. Sassoon, I., Severin, F. F., Andrews, P. D., Taba, M. R., Kaplan, K. B., Ashford, A. J., Stark, M. J., Sorger, P. K., and Hyman, A. A. Regulation of *Saccharomyces cerevisiae* kinetochores by the type 1 phosphatase Glc7p. Genes Dev. *13:* 545–555, 1999.
7. Lukas, C., Sorensen, C. S., Kramer, E., Santoni-Rugiu, E., Lindeneg, C., Peters, J. M., Bartek, J., and Lukas, J. Accumulation of cyclin B1 requires E2F and cyclin-A-dependent rearrangement of the anaphase-promoting complex. Nature (Lond.), *401:* 815–818, 1999.
8. Karantza, V., Maroo, A., Fay, D., and Sedivy, J. M. Overproduction of Rb protein after the G_1/S boundary causes G_2 arrest. Mol. Cell. Biol., *13:* 6640–6652, 1993.
9. Di Leonardo, A., Khan, S. H., Linke, S. P., Greco, V., Seidita, G., and Wahl, G. M. DNA rereplication in the presence of mitotic spindle inhibitors in human and mouse fibroblasts lacking either p53 or pRb function. Cancer Res, *57:* 1013–1019, 1997.

10. Flatt, P. M., Tang, L. J., Scatena, C. D., Szak, S. T., and Pietenpol, J. A. p53 regulation of G_2 checkpoint is retinoblastoma protein dependent. Mol. Cell. Biol. *20:* 4210–4223, 2000.
11. Chen, Y., Riley, D. J., Chen, P-L., and Lee, W-H. HEC, a novel nuclear protein rich in leucine heptad repeats specifically involved in mitosis. Mol. Cell. Biol. *17:* 6049–6056, 1997.
12. Zheng, L., Chen, Y., Riley, D. J., Chen, P-L., and Lee, W-H. Retinoblastoma protein enhances the fidelity of chromosome segregation mediated by hsHec1p. Mol. Cell. Biol. *20:* 3529–3537, 2000.
13. Koshland, D., and Strunnikov, A. Mitotic chromosome condensation. Annu. Rev. Cell Dev. Biol. *12:* 305–333, 1996.
14. Zheng, L., Chen, Y., and Lee, W-H. Hec1p, an evolutionarily conserved coiled-coil protein, modulates chromosome segregation through interaction with SMC proteins. Mol. Cell. Biol. *19:* 5417–5428, 1999.
15. Lee, E. Y., Chang, C-Y., Hu, N., Wang, Y-C., Lai, C-C., Herrup, K., Lee, W-H., and Bradley, A. A. Mice deficient for Rb are nonviable and show defects in neurogenesis and haematopoiesis. Nature (Lond.), *359:* 288–294, 1992.
16. Robertson, E. J. Embryo-derived stem cell lines. *In:* E. J. Robertson (ed.), Teratocarcinoma and Embryonic Stem Cells: A Practical Approach, pp. 71–112. Oxford, England: IRL Press, 1987.
17. Nikitin, A. Y., and Lee, W-H. Early loss of the *retinoblastoma* gene is associated with impaired growth inhibitory innervation during melanotroph carcinogenesis in Rb+/− mice. Genes Dev., *10:* 1870–1879, 1996.
18. Lupton, S. D., Brunton, L. L., Kalberg, V. A., and Overell, R. W. Dominant positive and negative selection using a *hygromycin phosphotransferase-thymidine kinase* fusion gene. Mol. Cell. Biol., *11:* 3374–3378, 1991.
19. Chen, P-L., Chen, Y., Bookstein, R., and Lee, W-H. Genetic mechanisms of tumor suppression by the human *p53* gene. Science (Wash. DC), *250:* 1576–1580, 1990.
20. Hagstrom, S. A., and Dryja, T. P. Mitotic recombination map of 13cen-13q14 derived from an investigation of loss of heterozygosity in retinoblastoma. Proc. Natl. Acad. Sci. USA, *96:* 2952–2957, 1999.
21. Knudson, A. G. Mutation and cancer: statistical study of retinoblastoma. Proc. Natl. Acad. Sci. USA, *68:* 820–823, 1971.
22. Cavenee, W. K., Dryja, T. P., Phillips, R. A., Benedict, W. F., Godbout, R., Gallie, B. L., Murphree, A. L., Strong, L. C., and White, R. L. Expression of recessive alleles by chromosomal mechanisms in retinoblastoma. Nature (Lond.), *305:* 779–784, 1983.
23. Shao C., Deng, L., Henegariu, O., Liang, L., Stambrook, P. J., and Tischfield J. A. Chromosome instability contributes to loss of heterozygosity in mice lacking p53. Proc. Natl. Acad. Sci. USA, *97:* 7405–7410, 2000.
24. Gupta, P. K., Sahota, A., Boyadjiev, S. A., Bye, S., Shao, C., O'Neill, J. P., Hunter, T. C., Albertini, R. J., Stambrook, P. J., and Tishfield, J. A. High frequency *in vivo* loss of heterozygosity is primarily a consequence of mitotic recombination. Cancer Res., *57:* 1188–1193, 1997.
25. Liyanage, M., Coleman, A., du Manoir, S., Veldman, T., McCormack, S., Dickson, R. B., Barlow, C., Wynshaw-Boris, A., Janz, S., Wienberg, J., Ferguson-Smith, M. A., Schrock, E., and Ried, T. Multicolour spectral karyotyping of mouse chromosomes. Nat. Genet., *14:* 312–315, 1996.

THE JOURNAL OF BIOLOGICAL CHEMISTRY
Vol. 277, No. 46, Issue of November 15, pp. 43578–43587, 2002
Printed in U.S.A.

Functional Cross-talk among Rad51, Rad54, and Replication Protein A in Heteroduplex DNA Joint Formation*

Received for publication, June 12, 2002, and in revised form, September 3, 2002
Published, JBC Papers in Press, September 10, 2002, DOI 10.1074/jbc.M205864200

Stephen Van Komen‡, Galina Petukhova§, Stefan Sigurdsson¶, and Patrick Sung‖

From the Department of Molecular Medicine/Institute of Biotechnology, University of Texas Health Science Center at San Antonio, San Antonio, Texas 78245-3207

Saccharomyces cerevisiae **Rad51, Rad54, and replication protein A (RPA) proteins work in concert to make heteroduplex DNA joints during homologous recombination. With plasmid length DNA substrates, maximal DNA joint formation is observed with amounts of Rad51 substantially below what is needed to saturate the initiating single-stranded DNA template, and, relative to Rad51, Rad54 is needed in only catalytic quantities. RPA is still indispensable for optimal reaction efficiency, but its role in this instance is to sequester free single-stranded DNA, which otherwise inhibits Rad51 and Rad54 functions. We also demonstrate that Rad54 helps overcome various reaction constraints in DNA joint formation. These results thus shed light on the function of Rad54 in the Rad51-mediated homologous DNA pairing reaction and also reveal a novel role of RPA in the presynaptic stage of this reaction.**

Aside from contributing to the creation of genetic diversity, homologous recombination is indispensable for DNA double-stranded break repair, meiosis I, and for various aspects of telomere homeostasis. Genetic studies in *Saccharomyces cerevisiae* have been chiefly responsible for identifying the components of the recombination machinery. These recombination genes (*RAD50*, *RAD51*, *RAD52*, *RAD54*, *RAD55*, *RAD57*, *RAD59*, *RDH54/TID1*, *MRE11*, and *XRS2*) are collectively referred to as the *RAD52* epistasis group. Gene cloning, genetic analyses, and biochemical studies have revealed a remarkable degree of conservation of the *RAD52* group, from yeast to humans (1–4). In mammals, members of the *RAD52* group interact with the tumor suppressors BRCA1 and BRCA2, which in turn influence the activities of their partner recombination factors and the efficiency of recombination (5–8). The latter observations underscore the importance for deciphering the functions of individual recombination factors and the mechanism of the protein machine comprising these factors.

Results from combined genetic and biochemical studies have suggested the following sequence of events in recombination. Following the introduction of a DNA double-stranded break, the ends of the break are processed nucleolytically to generate long single-stranded tails that have a 3′ extremity. Mre11, working in conjunction with Rad50 and Xrs2, provides the nuclease function for the formation of the 3′ ssDNA[1] tails. Rad51, the eukaryotic equivalent of the *Escherichia coli* general recombinase RecA, nucleates onto the ssDNA tails to form a right-handed nucleoprotein filament. The Rad51-ssDNA nucleoprotein filament then conducts a search for a chromosomal homolog, either the sister chromatid or the homologous chromosome. Pairing between the initiating ssDNA tails and the complementary strand in the duplex partner yields heteroduplex DNA joints, followed by extension of the joints by branch migration. The biochemical reaction responsible for DNA homology search and the formation of heteroduplex DNA joints is commonly called "homologous DNA pairing and strand exchange" (1, 4, 9).

In the homologous DNA pairing and strand exchange reaction, the assembly of the Rad51-ssDNA nucleoprotein filament is referred to as the presynaptic phase. Rad52 and the Rad55-Rad57 complex are recombination mediators that promote the assembly of the Rad51-ssDNA presynaptic nucleoprotein filament (4, 10, 11). In the post-synaptic phase, the Rad51-ssDNA nucleoprotein filament cooperates with Rad54 and Rdh54 (also called Tid1) to form DNA joints (12, 13). Rad54 and Rdh54, both members of the Swi2/Snf2 protein family (4), utilize the free energy from ATP hydrolysis to produce compensatory negative and positive supercoils in duplex DNA, which probably result from a tracking motion of these proteins on DNA (13–15). The negative supercoils produced by Rad54 and Rdh54 lead to transient DNA strand opening, believed to be germane for the promotion of DNA joint formation (15). Interestingly, Rad51 enhances the DNA supercoiling and DNA strand opening activities of Rad54 (15, 16).

Whereas a good body of information concerning the biochemical properties of the *RAD52* group proteins has accumulated in recent years, the manner in which these recombination factors functionally interact with one another and with the DNA substrates to achieve the maximal efficiency of DNA joint formation has remained mysterious. Here we present results that shed light on the synergistic interactions among Rad51, Rad54, RPA, and the ssDNA substrate in the initial stages of recombination. The results also reveal a new role of RPA in the homologous DNA pairing reaction.

EXPERIMENTAL PROCEDURES

Recombination Proteins—Rad51 and Rad54 proteins were overexpressed in yeast cells and purified to near homogeneity as described

* This work was supported by United States Public Health Service Grants RO1ES07061 and RO1GM57814. The costs of publication of this article were defrayed in part by the payment of page charges. This article must therefore be hereby marked "*advertisement*" in accordance with 18 U.S.C. Section 1734 solely to indicate this fact.

‡ Supported in part by United States Army Predoctoral Fellowship DAMD17-01-1-0414.

§ Present Address: NIDDK, National Institutes of Health, Bldg. 10, Rm. 9D17, 9000 Rockville Pike, Bethesda, MD 20892.

¶ Supported in part by United States Army Training Grant DAMD17-99-1-9402 and Predoctoral Fellowship DAMD17-01-1-0412.

‖ To whom correspondence should be addressed: Dept. of Molecular Medicine/Institute of Biotechnology, University of Texas Health Science Center at San Antonio, 15355 Lambda Dr., San Antonio, TX 78245-3207. Tel.: 210-567-7216; Fax: 210-567-7277; E-mail: sung@uthscsa.edu.

[1] The abbreviations used are: ssDNA, single-stranded DNA; RPA, replication protein A.

previously (12, 17). RPA was overexpressed in yeast using three plasmids that code for the three subunits of RPA (18) and purified to near homogeneity as described (19). The concentrations of Rad51 and RPA were determined using extinction coefficients of 1.29×10^4 and 8.8×10^4 at 280 nm, respectively (20). The concentration of Rad54 was determined by densitometric scanning of SDS-PAGE gels of multiple loadings of purified Rad54 against known quantities of bovine serum albumin and ovalbumin.

DNA Substrates—The ϕX174 (+) strand and replicative form I DNA were purchased from New England Biolabs and Invitrogen, respectively. The replicative form DNA was linearized by treatment with *Apa*LI or *Stu*I to yield linear duplex substrates that have either 3′ 4-base overhangs or blunt ends, respectively. Linearization of the viral (+) strand was done by hybridizing a 26-mer oligonucleotide to create a *Pst*I site, followed by treatment with *Pst*I (12). The pBluescript (+) strand and replicative form DNA were prepared as described previously (21). The pBluescript dsDNA used in Fig. 4*B* was a 1712-bp fragment generated from the replicative form by treatment with *Apa*LI and *Bsa*I; it was purified from 0.9% agarose gels as above. The pBluescript dsDNA used in Fig. 5*C* was full-length replicative form DNA linearized with *Bsa*I. The 90-mer oligonucleotide (5′-AAATCAATCTAAAGTATATATGAGTAAACTTGGTCTGACAGTTACCAATGCTTAATCAGTGAGGCACCTATCTCAGCGATCTGTCTATTT-3′) used for D-loop formation in Fig. 8 is complementary to pBluescript SK DNA from position 1932 to 2022. The oligonucleotide was 5′-end-labeled with T4 polynucleotide kinase (Promega) and [γ-^{32}P]ATP (Amersham Biosciences) and then purified using the MERmaid Spin Kit (Bio 101). All of the DNA substrates were stored in TE (10 mM Tris-HCl, pH 7.0, 0.5 mM EDTA).

DNA Strand Exchange Reaction—Unless stated otherwise, the reactions containing Rad54 were carried out at 23 °C, and the reactions without Rad54 were carried out at 37 °C. In the standard reaction (12.5-μl final volume), circular ϕX (+)-strand (19.6 μM nucleotides) was incubated for 4 min in 10 μl of buffer R (35 mM Tris-HCl, pH 7.2, 60 mM KCl, 2.5 mM ATP, 3 mM $MgCl_2$, 1 mM dithiothreitol, and an ATP-regenerating system consisting of 20 mM creatine phosphate and 300 ng of creatine kinase) with the indicated amounts of Rad51 added in 0.5 μl of storage buffer. Following the incorporation of RPA in 0.5 μl of storage buffer and the indicated amounts of Rad54 in 0.3 μl of storage buffer and an additional 4-min incubation, *Apa*LI linearized dsDNA in 0.7 μl, and 1 μl of 50 mM spermidine hydrochloride (4 mM final concentration) was added to complete the reaction. For time course experiments, the reactions were scaled up accordingly, and unless stated otherwise, the same order of addition of reaction components was used. At the times indicated, 5-μl portions of the reaction mixtures were mixed with an equal volume of 1% SDS and then treated with proteinase K (0.5 mg/ml) for 10 min at 37 °C before being run in 0.9% agarose gels in TAE buffer (40 mM Tris acetate, pH 7.4, 0.5 mM EDTA) at 23 °C. The gels were stained with ethidium bromide and recorded in a Nucleotech gel documentation system. Quantitation of the data was done using the Gel Expert software.

L-loop Reactions with Plasmid Length ssDNA—The standard D-loop reaction was assembled by preincubating *Pst*I-linearized ϕX ssDNA with Rad51 for 3 min, followed by the incorporation of RPA and an additional 3-min incubation. Rad54 was then added, and, following a 2-min incubation, ϕX replicative form DNA was incorporated to complete the reaction. All of the incubations were carried out at 23 °C, and the reaction mixtures were processed for electrophoresis as described above. Other details are given in the figure legends.

D-loop Reactions with Oligonucleotide as Single-stranded Substrate—Unless stated otherwise, Rad51 (2 μM) and the indicated amounts of Rad54 were incubated with the 5′-end-labeled 90-mer oligonucleotide (6 μM nucleotides or 67 nM oligonucleotide) in 11.5 μl of buffer R. The protein/DNA mixture was incubated for 10 min at either 23 or 37 °C, and D-loop formation was initiated by the addition of pBluescript SK replicative form DNA (65 μM base pairs or 22 nM plasmid molecules) in 1 μl. The reaction mixtures were incubated for 5 min at 23 °C and arrested by the addition of an equal volume of 1% SDS. The reactions were deproteinized with proteinase K as above before being subjected to electrophoresis in 0.9% agarose gels in TAE buffer at 23 °C. The gels were dried, and the level of D-loop was quantified in a Personal FX phosphor imager with Quantity One software (Bio-Rad). The results were plotted as the percentage of oligonucleotide that had been incorporated into the D-loop. For the order of addition experiments in Fig. 8*D*, the reactions were scaled up accordingly with the indicated amounts of components.

Inhibition of DNA Pairing and Strand Exchange by ssDNA and Reversal by RPA—In Fig. 4*B*, *panels I* and *II*, the reaction mixtures (final volume of 14.5 μl) were assembled as described for the standard D-loop reaction, except that increasing concentrations of pBluescript circular ssDNA or linear duplex were added with the ϕX replicative form I DNA substrate in 3 μl of TE. In Fig. 4*B*, *panel III*, the reaction mixtures (final volume of 14.5 μl) were assembled as described for *panels I* and *II*, except that the pBluescript ssDNA competitor (150 μM nucleotides) had been preincubated with RPA (9 μM) at 37 °C for 3 min in buffer R. The RPA-coated ssDNA competitor was then diluted with buffer R to the desired concentrations and added in 2 μl with the replicative form I DNA in 1 μl to the D-loop reactions. In Fig. 5, *A* and *C*, the reaction mixtures (final volume of 14.5 μl) were assembled as described for the model DNA strand exchange reaction, except that increasing concentrations of pBluescript ssDNA (Fig. 5*A*, *lanes 3–6*) or pBluescript linear duplex (Fig. 5*C*, *lanes 3–6* and *9–12*) was added with the ϕX linear duplex in 3 μl of TE. In Fig. 5*A*, *lanes 7–10*, the pBluescript ssDNA competitor (150 μM nucleotides) had been preincubated with RPA (9 μM), as described above for Fig. 4*B*, and then added in 2 μl with the ϕX linear duplex in 1 μl of TE to the reaction.

ATPase Assay—In Fig. 1*A*, Rad54 (150 nM), in 8 μl of buffer A (30 mM Tris-HCl, pH 7.2, 1 mM dithiothreitol, 5 mM $MgCl_2$, 45 mM KCl, and 200 μg/ml bovine serum albumin), that had or had not been preincubated either at 37 or 23 °C was mixed with ϕX replicative form DNA (30 μM base pairs) and 1.5 mM [γ-^{32}P]ATP (Amersham Biosciences) in 2 μl. Where indicated, dsDNA or ATP was also present during the preincubation of Rad54 at 37 °C. The reactions (10 μl) were incubated at 23 °C, and at the indicated times a 1.5-μl aliquot was removed and mixed with an equal volume of 500 mM EDTA to halt the reaction. The amount of ATP hydrolysis was determined by thin layer chromatography, as described (12). To examine the effect of Rad51 on the thermal stability of Rad54 (Fig. 1*B*), the combination of Rad51 (2 μM) and Rad54 (75 nM), in 8 μl of buffer A, that had or had not been preincubated at 23 °C or 37 °C as above was mixed with ϕX replicative form DNA (30 μM base pairs) and 1.5 mM [γ-^{32}P] ATP in 2 μl.

In Fig. 5*D*, Rad54 (150 nM) was incubated for 15 min at 23 °C with 1.5 mM [γ-^{32}P]ATP and the indicated amounts of ssDNA (0.9, 3.6, 7.2, 14.4, or 28.7 μM nucleotides) in 10 μl of buffer A. Rad54 (150 nM) was also similarly incubated with ϕX replicative form DNA (30 μM base pairs) and the indicated amounts of pBluescript ssDNA (0.9, 3.6, 7.2, 14.4, and 28.7 μM nucleotides). To examine the effect of precoating the pBluescript ssDNA competitor with RPA, the ssDNA (150 μM nucleotides) was incubated with RPA (9 μM) at 37 °C for 5 min in buffer A, diluted with the appropriate volume of buffer A, before being incorporated with the ϕX replicative form DNA (30 μM base pairs) in 2 μl into the ATPase reactions. The completed reactions (10 μl) were incubated at 23 °C for 15 min.

In Fig. 3*A*, *panel III*, the ATPase assay was performed as described for the model D-loop reaction with 660 nM Rad54, 1.4 μM Rad51, 1.3 μM RPA, and [γ-^{32}P]ATP, either with or without the ATP-regenerating system consisting of 20 mM creatine phosphate and 300 ng of creatine kinase.

RESULTS

Rad54 Is Prone to Thermal Inactivation—The rate of dsDNA-activated ATP hydrolysis by Rad54 was linear with time for at least 12 min at 23 °C (Fig. 1*A*). Preincubation of Rad54 at 37 °C in the absence of ATP and dsDNA for brief periods caused a dramatic decrease in ATP hydrolysis in reactions conducted at 23 °C, whereas preincubation of Rad54 at 23 °C had no effect on the ATPase activity (Fig. 1*A*). These results indicate that the Rad54 ATPase function is prone to denaturation at 37 °C. Whereas ATP had only a very slight protective effect against thermal denaturation of Rad54 (Fig. 1*A*), dsDNA exhibited a modest protective effect (Fig. 1*A*). Although Rad51 physically interacts with Rad54 (12, 22, 23) and stimulates the Rad54 ATPase and DNA supercoiling activities (15, 16), it did not prevent thermal denaturation of Rad54 (Fig. 1*A*).

In the homologous DNA pairing reaction, preincubation of Rad54 or the combination of Rad51 and Rad54 at 37 °C for brief periods also greatly diminished the extent of the reaction (see below). By contrast, Rad51 is stable for at least 30 min at 37 °C, as gauged by its ATPase and homologous DNA pairing and strand exchange activities (data not shown). Thus, Rad54 is quite unstable at 37 °C, and because of this, all of the reactions involving Rad54 were routinely carried out at 23 °C, where it is

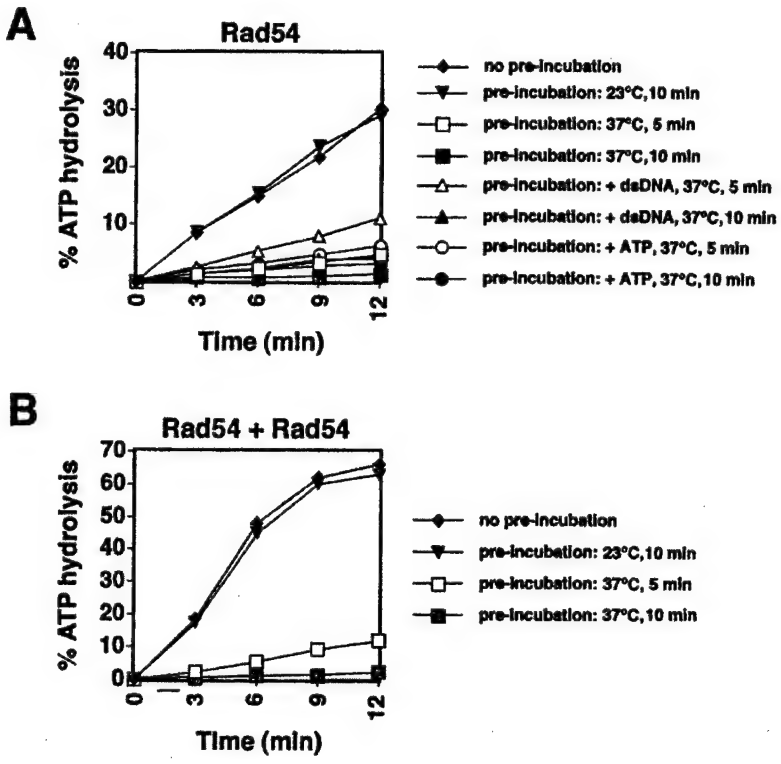

FIG. 1. **Thermal inactivation of Rad54 ATPase activity.** *A*, Rad54 (150 nM) was incubated with ϕX dsDNA (30 μM base pairs) and 1.5 mM [γ-^{32}P]ATP (*dark diamonds*) at 23 °C for the indicated times. Alternatively, the same amount of Rad54 was preincubated at 23 °C for 10 min (*gray inverted triangles*), at 37 °C for 5 min (*open squares*) or 10 min (*gray squares*), with the dsDNA at 37 °C for 5 min (*open triangles*) or 10 min (*gray triangles*), and with ATP at 37 °C for 5 min (*open circles*) or 10 min (*gray circles*), prior to mixing with the remaining reaction components and continuing the incubation at 23 °C for the indicated times. *B*, graphical representation of time courses of ATP hydrolysis by Rad54 (75 nM), Rad51 (2 μM), and ϕX dsDNA (30 μM base pairs) with no preincubation (*dark diamonds*) or preincubation at 23 °C for 10 min (*gray inverted triangles*) and at 37 °C for 5 min (*open squares*) or 10 min (*gray squares*), as done in *A*.

much more stable. Furthermore, since homologous pairing by Rad51 and Rad54 occurs efficiently, the use of a relatively low reaction temperature also allowed us to follow the reaction kinetics with greater ease.

With Rad54, a Contiguous Rad51-ssDNA Nucleoprotein Filament Is Not Needed for Homologous Pairing—In the model homologous DNA pairing and strand exchange reaction that employs circular ssDNA and linear duplex (see Fig. 2*A*, *panel I*, for schematic) but contains no Rad54, maximal reaction efficiency is observed at 3 nucleotides per Rad51 monomer (Fig. 2*B*, *panels I* and *III*) (20, 24). The optimal ratio of Rad51 to ssDNA in this model reaction corresponds to the ssDNA binding site size of Rad51 (25). Based on these observations, it has been generally assumed that a contiguous Rad51-ssDNA nucleoprotein filament is needed for achieving maximal homologous DNA pairing and strand exchange.

The stoichiometric relationship between Rad51 and the ssDNA substrate in the D-loop reaction (see Fig. 2*A*, *panel II*, for schematic) was examined here. Amounts of Rad51 varying from 30 to 3.2 nucleotides of ssDNA per protein monomer (0.66–6.1 μM Rad51 and 19.6 μM nucleotides of ssDNA) were used with a concentration of Rad54 (150 nM) sufficient to afford robust homologous DNA pairing. Surprisingly, maximal homologous pairing (see Fig. 2*B*, *panels II* and *III*) occurred over the range of 15 to 9 nucleotides/Rad51 monomer, which is substantially below the ratio of 3 nucleotides/Rad51 monomer needed for the formation of a contiguous Rad51 filament. In fact, increasing the Rad51 amount to 3 nucleotides/protein monomer consistently led to a greater than 3-fold decrease in the amount of D-loop (Fig. 2*B*, *panels II* and *III*). We note that whereas at 30 nucleotides/Rad51 monomer a substantial level of D-loop was obtained (Fig. 2*B*, *panel II*, *lane 2*), only a trace of reaction product was formed by an amount of Rad51 corresponding to 7.4 nucleotides/Rad51 monomer in the model reaction that did not contain Rad54 (Fig. 2*B*, *panel I*, *lane 2*). We have also examined the dependence of D-loop formation on the Rad51 amount with concentrations of Rad54 higher and lower than that used in the experiment above. Under those conditions, we again found that Rad51 amounts from ~15 to 9 nucleotides per protein monomer were optimal and that increasing the Rad51 level beyond this optimal range resulted in a similar degree of reduction of D-loop as in Fig. 2*B* (data not shown).

Turnover of RecA from the bound ssDNA occurs when the ssDNA is linear (9). If there had been sufficient Rad51 dissociating from the linear ssDNA substrate in the D-loop reaction, the free Rad51 pool could have sequestered the dsDNA from pairing with the ssDNA (24). To help eliminate this caveat, we examined the pairing between a circular ssDNA with linear duplex (Fig. 2*A*, *panel I*) in the presence of Rad54. In this case, the stoichiometric relationship between Rad51 and the ssDNA (Fig. 2*C*) closely resembled that seen in the D-loop experiment (Fig. 2*B*, *panel II*) (*i.e.* with the optimal concentration range of Rad51 at ~15 to 9 nucleotides per protein monomer and the reaction efficiency gradually decreasing with elevating Rad51 amounts).

In aggregate, the new data demonstrate that homologous pairing catalyzed by the combination of Rad51 and Rad54 does not require a contiguous Rad51 filament. In fact, suppression of DNA joint formation occurs when a full Rad51 filament is allowed to assemble.

Rad54 Is Required in Only Catalytic Amounts—Although a quantity of Rad54 substoichiometric to Rad51 affords a robust homologous pairing reaction (12, 15, 26) (see Fig. 2), we examined whether higher amounts of Rad54 would further enhance the reaction. Although an ATP-regenerating system was included in the pairing assays, to ensure that the increased amounts of Rad54 did not cause a depletion of the ATP pool, we also monitored the level of free ATP by thin layer chromatography. As shown in Fig. 3*A*, *panels I* and *II*, the optimal level of Rad54 was between 82.5 and 300 nM, substantially below that of Rad51 (1.4 μM) used. Importantly, increasing the amount of Rad54 to 660 nM in fact suppressed joint formation greatly. For example, after 2.5 min of incubation, whereas ~40% of the replicative form DNA had been converted to D loop at 82.5 nM of Rad54, a ratio of Rad51/Rad54 of 17 (Fig. 3*A*, *panel I*, *lane 3*; *panel II*), only ~4% of D-loop formation was observed at 660 nM

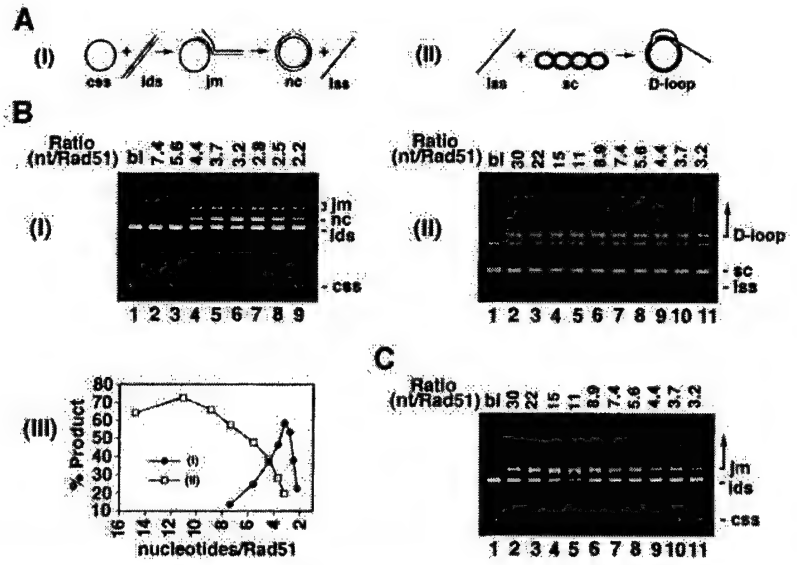

FIG. 2. **Subsaturating Rad51 amounts give maximal DNA pairing.** *A*, the pairing systems used. In *I*, pairing between the circular ssDNA and the linear duplex yields a joint molecule, which has the potential of generating a nicked circular duplex and a linear single strand as products, if branch migration of the DNA joint is successful over the 5.4 kb of ϕX ssDNA. *css*, circular single strand; *lds*, linear duplex; *jm*, joint molecules; *nc*, nicked circular duplex; *lss*, linear single strand. In *II*, pairing of linear ssDNA with the homologous replicative form I DNA gives a D-loop. *lss*, linear single-stranded DNA; *sc*, replicative form I DNA. *B*, stoichiometric relationship between Rad51 and ssDNA in homologous DNA pairing and strand exchange. In *panel I*, circular ϕX ssDNA (19.6 μM nucleotides) was first incubated with Rad51 (2.6, 3.5, 4.5, 5.3, 6.1, 7, 7.8, and 8.9 μM in *lanes 2–9*, respectively) and then with RPA (1.3 μM) at 37 °C, before the linear duplex (10 μM base pairs) was incorporated to complete the reaction, which was stopped after 50 min of incubation at 37 °C. In *panel II*, linear ϕX ssDNA (19.6 μM nucleotides) was incubated with Rad51 (0.66, 0.88, 1.3, 1.7, 2.2, 2.6, 3.5, 4.5, 5.3, and 6.1 μM in *lanes 2–11*, respectively) at 23 °C and then with RPA (1.3 μM) and Rad54 (150 nM) at 23 °C, before the ϕX replicative form I DNA (12.3 μM base pairs) was added to complete the reaction. The completed reaction mixtures were incubated at 23 °C for 5 min before electrophoresis. The efficiency of joint formation is plotted against the nucleotides (*nt*) to Rad51 monomer ratio in *panel III*. *Closed circles*, results from *panel I* of *B*; *open squares*, results from *panel II*. *C*, circular ϕX ssDNA (19.6 μM nucleotides) was incubated with Rad51 (0.66, 0.88, 1.3, 1.7, 2.2, 2.6, 3.5, 4.5, 5.3, and 6.1 μM in *lanes 2–11*, respectively) at 23 °C and then with RPA (1.3 μM) and Rad54 (150 nM) at 23 °C before the linear ϕX duplex (10 μM base pairs) was added. The completed reaction mixtures were incubated at 23 °C for 10 min before electrophoresis.

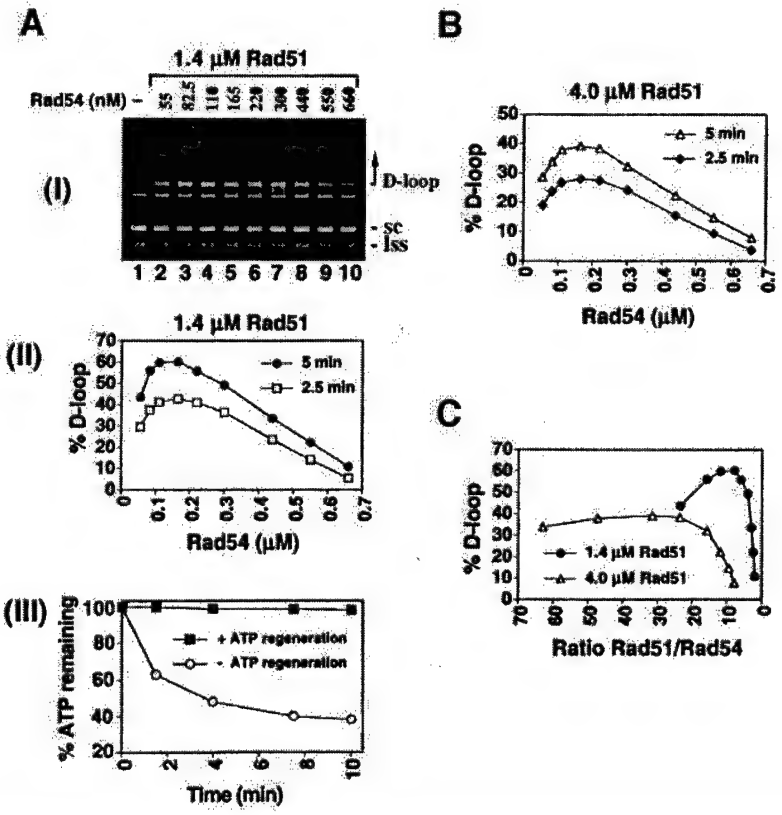

FIG. 3. **Catalytic amounts of Rad54 are sufficient for maximal DNA joint formation.** *A*, all of the steps were carried out at 23 °C. In *panel I*, linear ϕX ssDNA (19.6 μM nucleotides) was incubated with Rad51 (1.4 μM) and then with RPA (1.3 μM) and the indicated concentrations of Rad54 before the ϕX replicative form I DNA (12.3 μM base pairs) was incorporated. After 2.5 min and 5 min of incubation, a 5-μl aliquot was withdrawn and processed for electrophoresis. The agarose gel containing the samples from the 2.5-min time point is shown. *lss*, linear single-strand DNA; *sc*, replicative form DNA. The results are graphed in *panel II*. *Panel III* shows the level of ATP in D-loop reactions containing 660 nM Rad54 either with (*open squares*) or without (*closed circles*) the ATP-regenerating system. The reaction mixtures in *panel III* contained [γ-^{32}P]ATP and were assembled in the same manner as those in *panel I*. *B*, the results from another series of D-loop reactions that contained 4 μM Rad51, 1.3 μM RPA, and varying amounts of Rad54 are graphed. *C*, the results from the 5-min time point in *panel I* of *A* (*closed circles*) and in *B* (*open triangles*) are plotted as percentage of D-loop against the Rad51/Rad54 ratio.

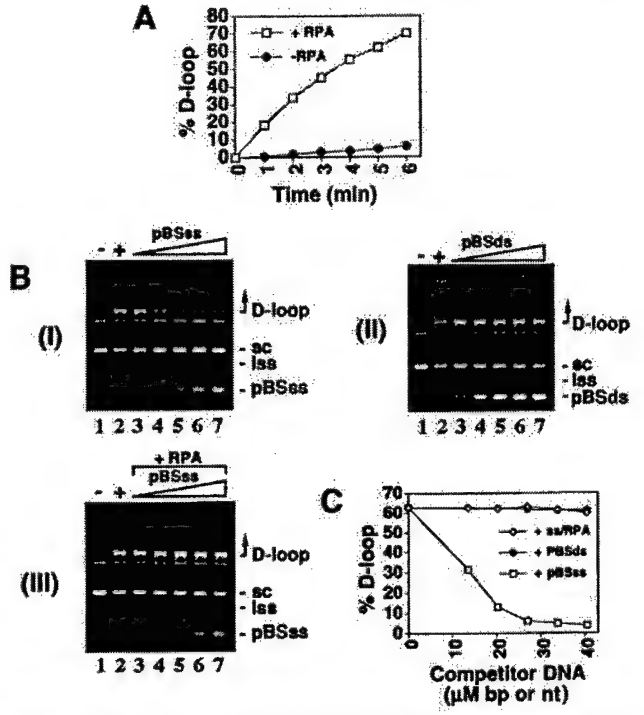

FIG. 4. **Role of RPA in DNA joint formation.** *A*, D-loop reactions containing Rad51 (1.4 μM) and Rad54 (150 nM) with (*open squares*) or without RPA (*closed circles*; 1.3 μM) were assembled and incubated as described under "D-loop Reactions with Plasmid Length ssDNA." The reaction mixtures had a final volume of 37.5 μl, and aliquots of 5 μl were withdrawn at the indicated times and analyzed. *B*, D-loop formation is specifically inhibited by free ssDNA. Reactions containing the same amounts of Rad51, Rad54, RPA, and φX DNA substrates as in *A* and also pBluescript ssDNA (in *panel I*, 13.5, 20, 27, 34, and 40.5 μM nucleotides in *lanes 3–7*, respectively) or pBluescript linear dsDNA (in *panel II*, 13.5, 20, 27, 34, and 40.5 μM base pairs in *lanes 3–7*, respectively) were assembled as described under "Experimental Procedures." In *panel III*, the pBluescript ssDNA competitor (13.5, 20, 27, 33.75, and 40.5 μM nucleotides) was precoated with RPA at a ratio of 17 nucleotides/RPA monomer before being added to the pairing reaction. The incubation time for these experiments was 5 min. *lss*, φX linear single-stranded DNA; *sc*, φX replicative form I DNA; *pBSss*, pBluescript ssDNA; *pBSds*, pBluescript linear duplex. *C*, graphical representation of the results in *panels I* (*open squares*), *II* (*closed circles*), and *III* (*open diamonds*) of *B*.

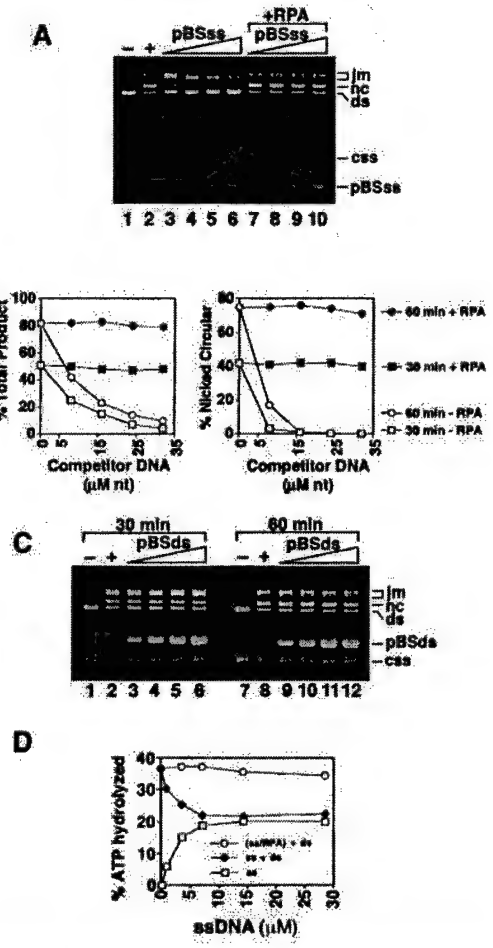

FIG. 5. **Effect of ssDNA on Rad51 and Rad54 functions.** *A*, all of the incubations were carried out at 37 °C. In *panel I*, φX circular ssDNA (19.6 μM nucleotides) was incubated first with Rad51 (6.5 μM) and then with RPA (1.3 μM). At the time of incorporation of the φX linear duplex (10 μM base pairs), increasing amounts of pBluescript circular ssDNA (8, 16, 24, and 32 μM nucleotides in *lanes 3–6*) or the same concentrations of pBluescript ssDNA precoated with RPA at a ratio of 17 nucleotides/RPA (*lanes 7–10*) was also added. Aliquots were withdrawn from the reactions after 30 and 60 min and subjected to electrophoresis. The agarose gel containing the samples from the 60-min time point is shown. *css*, circular φX ssDNA; *ds*, φX linear duplex; *jm*, φX DNA joint molecules; *nc*, φX nicked circular duplex; *pBSss*, pBluescript ssDNA. *B*, graphical representation of the results from the experiment in *A*. The total products (sum of joint molecules and nicked circular DNA; *left panel*) or percentage of nicked circular DNA (*right panel*) are plotted against increasing amounts of competitor pBluescript ssDNA. *Open circles*, results from *A* (*lanes 2–6*); *closed circles*, results from *A* (*lanes 2* and *7–10*); *open squares*, results from the 30-min time point with increasing amounts of competitor pBluescript ssDNA; *closed squares*, results from the 30-min time point with the pBluescript ssDNA competitor precoated with RPA. *C*, DNA strand exchange reactions were set up as described for *A*, except that linear pBluescript duplex DNA (12, 24, 36, and 48 μM base pairs in *lanes 3–6* and *lanes 9–12*, respectively) was added to the reaction mixtures at the time of incorporation of the φX linear duplex (10 μM base pairs). *Symbols* are as described for *A*; *pBSds*, pBluescript dsDNA. *D*, Rad54 (150 nM) was incubated with [γ-^{32}P]ATP, φX dsDNA (30 μM base pairs), and increasing concentrations of pBluescript ssDNA (0.9–28.7 μM nucleotides) with precoating of the ssDNA with RPA (*open circles*) or without (*closed diamonds*). ATPase activity (*open squares*) with 150 nM Rad54 was also determined for the same concentration range of pBluescript ssDNA (0.9–28.7 μM nucleotides). All of the reactions were incubated at 23 °C for 15 min.

Rad54, a ratio of Rad51/Rad54 of 2.1 (Fig. 3*A*, *panel I*, *lane 10*; *panel II*). Even at the highest concentration of Rad54, the ATP level never dropped below 98% of the nucleotide pool (Fig. 3*A*, *panel III*).

We also investigated whether maximal D-loop formation would require more Rad54 at a Rad51 concentration (4 μM) significantly higher than that used in Fig. 3*A* (1.4 μM). However, even with the increased Rad51 amount, the optimal concentration range of Rad54 (Fig. 3*B*) remained essentially the same as that observed before (Fig. 3*A*). Once again, elevating the Rad54 amount above the optimal range resulted in a precipitous decrease in DNA joint formation (Fig. 3*B*). It is important to note that in this particular instance (Fig. 3*B*), optimal D-loop formation was at ratios of Rad51/Rad54 of 48 to 16 (Fig. 3, *B* and *C*).

Taken together, we were able to conclude that only a catalytic quantity of Rad54 is needed for robust DNA joint formation and that there does not appear to be a formal stoichiometric relationship between Rad51 and Rad54 in order to achieve maximal reaction efficiency. We will discuss under "Discussion" why D-loop formation is suppressed by relatively high Rad54 concentrations.

RPA Shields the Presynaptic Complex from Free ssDNA—In the model reaction, RPA is indispensable for maximal reaction efficiency. By helping minimize secondary structure in the ssDNA template, RPA allows for the assembly of a contiguous Rad51-ssDNA nucleoprotein filament (20, 24). The results in Fig. 2 have shown that in the D-loop reaction, Rad51 amounts

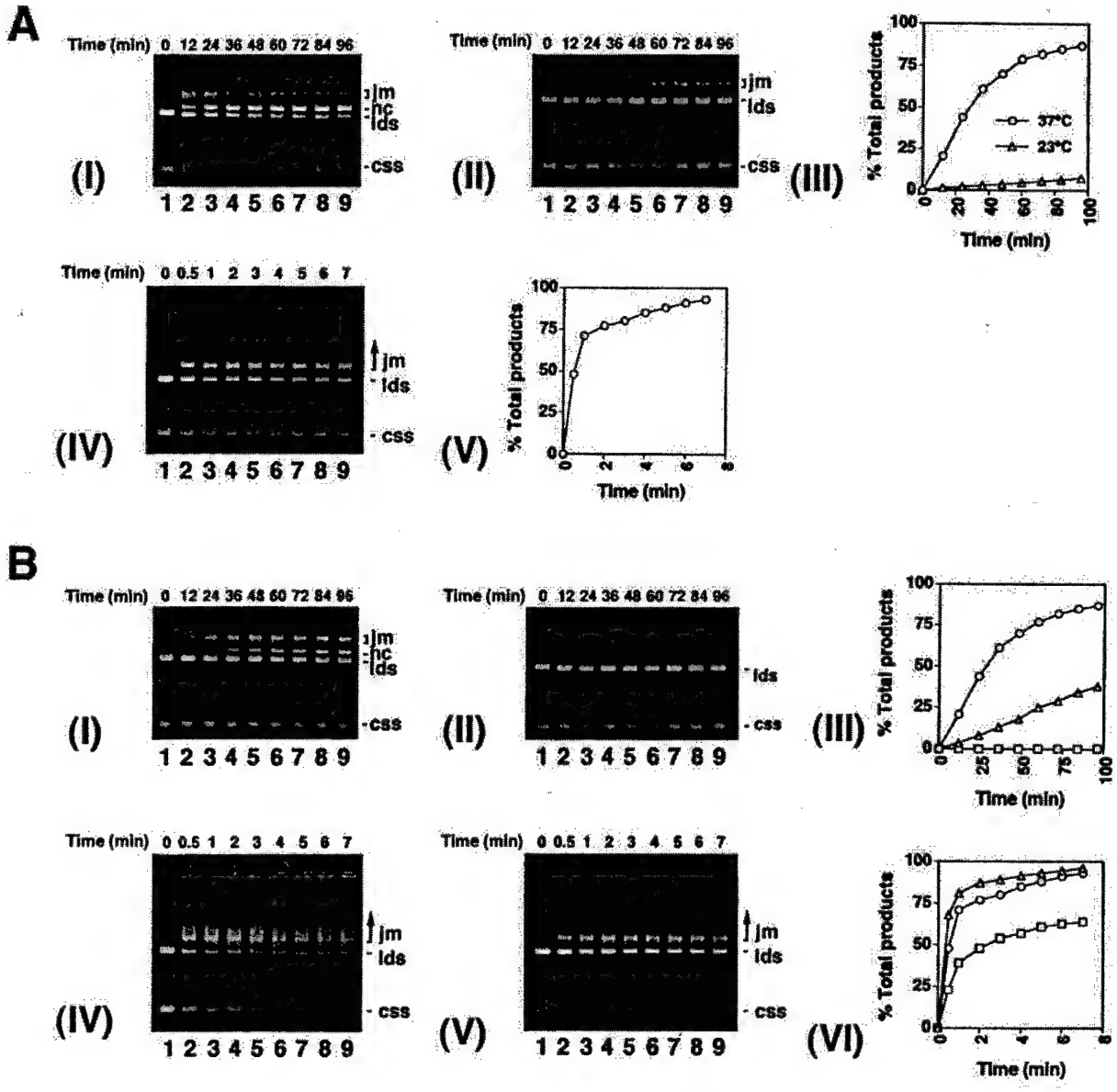

FIG. 6. **Rad54 overcomes various reaction impediments in Rad51-mediated DNA joint formation.** *A*, in *panels I* and *II*, circular ϕX ssDNA (19.6 μM nucleotides) was incubated for 4 min with Rad51 (6.1 μM) and then for an additional 4 min with RPA (1.3 μM) at 37 °C, followed by the addition of *Apa*LI-linearized ϕX duplex (10 μM base pairs) and 4 mM spermidine hydrochloride to complete the reaction mixture, which was further incubated either at 37 °C (*panel I*) or 23 °C (*panel II*) for the indicated times. *Panel III*, graphical representation of the reaction products (joint molecules and nicked circular duplex) in *panel I* (*open circles*) and *panel II* (*open triangles*). In *panel IV*, circular ϕX ssDNA (19.6 μM nucleotides) was incubated for 4 min with Rad51 (1.4 μM) and then for an additional 4 min with RPA (1.3 μM) and Rad54 (150 nM) at 23 °C, before *Apa*LI-linearized ϕX duplex (10 μM base pairs) and 4 mM spermidine hydrochloride were incorporated to complete the reaction mixture, which was incubated at 23 °C for the indicated times. *Panel V*, graphical representation of the reaction products (joint molecules and nicked circular duplex) in *panel IV*. *B*, the reactions in *panels I* and *II* were assembled in exactly the same manner as that in *panel I* of *A*, except that spermidine hydrochloride was substituted with either magnesium chloride (7.5 mM) in *panel I* or with water in *panel II*. *Panel III* is the graphical representation of the total reaction products (joint molecules and nicked circular duplex) in *panel I* (*open triangles*) and panel II (*open squares*); the results from *panel I* of *A* (*open circles*) are also included for comparison. The reactions in *panels IV* and *V* were assembled in exactly the same manner as that in *panel IV* of *A*, except that spermidine hydrochloride was substituted with either magnesium chloride (7.5 mM) in *panel IV* or with water in *panel V*. *Panel VI* is the graphical representation of the total reaction products (joint molecules and nicked circular duplex) in *panel IV* (*open triangles*) and *panel V* (*open squares*); the results from *panel IV* of *A* (*open circles*) are also included for comparison.

substantially below that required to saturate the ssDNA template in fact yield significantly more D-loop than when a saturating amount of Rad51 is used. As shown in Fig. 4*A*, at these low Rad51 concentrations, RPA was still needed for maximal DNA joint formation. Specifically, while greater than 60% of the input substrate had been converted into D-loop after 5 min, less than 5% of D-loop was seen with the omission of RPA.

In the optimized D-loop reaction there is insufficient Rad51 to make a contiguous nucleoprotein filament, yet RPA is still needed for optimal efficiency. Therefore, we concluded that RPA probably plays another role in this reaction. We considered the possibility that perhaps by sequestering free ssDNA left uncovered by Rad51, RPA might prevent the naked ssDNA from interfering with the homologous pairing reaction. To test this hypothesis directly, we carried out a reaction in which the ϕX ssDNA was incubated with Rad51, Rad54, and RPA as before (*e.g.* Fig. 2*B*, *panel II*), but an increasing amount of the unrelated pBluescript ssDNA was added with the ϕX replicative form. Severe inhibition of DNA loop formation by the pBluescript ssDNA was seen (Fig. 4, *B* (*panel I*) and *C*). For

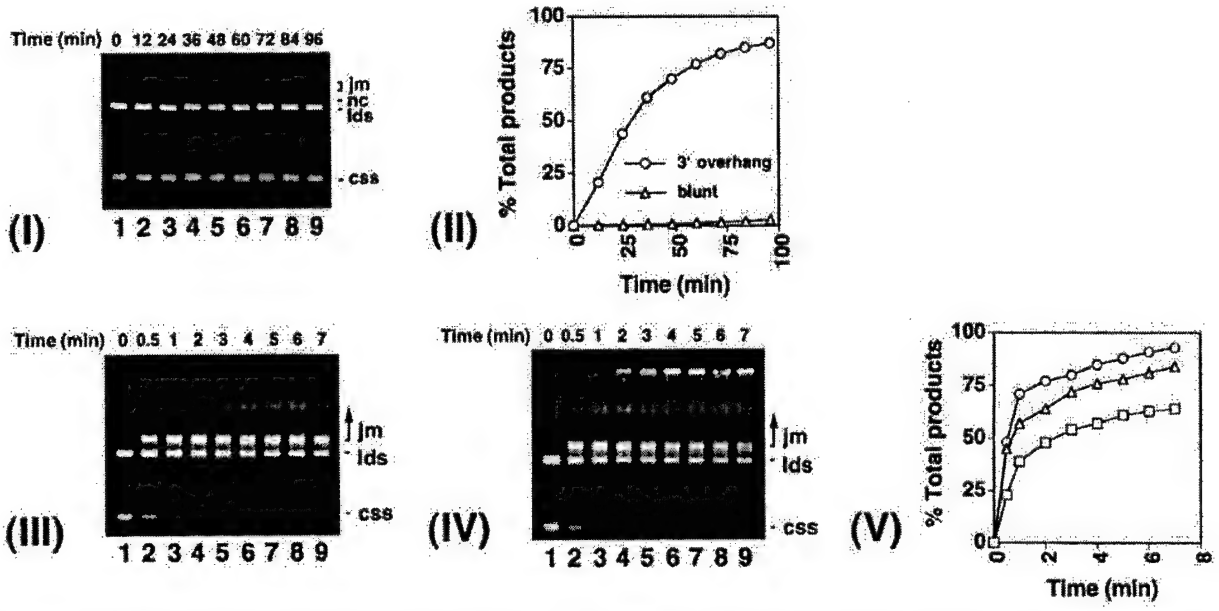

FIG. 7. **Rad51/Rad54 can utilize a blunt-ended substrate for homologous pairing.** The reaction in *panel I* contained Rad51 and RPA and was assembled in the same manner as that in *panel I* of Fig. 6*A*, except that *Stu*I-linearized blunt-ended dsDNA ϕX (10 μM base pairs) was used. *Panel II*, graphical representation of the reaction products (joint molecules and nicked circular duplex) in *panel I* (*open triangles*); the results in *panel I* of Fig. 6*A* (*open circles*) are also included for comparison. The reactions in *panels III* and *IV* contained Rad51, Rad54, and RPA and used *Stu*I-linearized blunt-ended DNA as substrate. Both of these reactions were assembled in the same manner as that in *panel IV* of Fig. 6*A*, except that in *panel IV*, magnesium chloride (7.5 mM) replaced spermidine hydrochloride. *Panel V* is the graphical representation of the total reaction products (joint molecules and nicked circular duplex) in *panel III* (*open squares*) and panel IV (*open triangles*); the results in *panel IV* of Fig. 6*A* (*open circles*) are also included for comparison.

instance, the level of D-loop was reduced from ~60% (Fig. 4*B*, *panel I*, *lane 2*) after 5 min of reaction to 11 and 4% by 20 and 34 μM of the pBluescript ssDNA, respectively (Fig. 4, *B* (*panel I*, *lanes 4* and *6*, respectively) and *C*). By contrast, the addition of equivalent amounts of pBluescript dsDNA did not cause inhibition of the D-loop reaction (Fig. 4, *B* (*panel II*) and *C*). Importantly, preincubation of the pBluescript ssDNA competitor with an amount of RPA sufficient to completely coat the ssDNA competitor proved to be highly effective in ablating the inhibitory effect of the DNA (Fig. 4, *B* (*panel III*) and *C*). Taken together, the results support the notion that free ssDNA left uncovered by Rad51/Rad54 constitutes a strong inhibitor of homologous pairing. The data also lent credence to the suggestion that the main role of RPA in the D-loop reaction is to sequester protein-free ssDNA and prevent inhibition of the pairing reaction by the DNA.

Single-stranded DNA Compromises Rad51 and Rad54 Functions—The results above indicated that naked ssDNA inhibits the D-loop reaction markedly but did not address whether the ssDNA inhibitor compromises the functional integrity of the Rad51 presynaptic filament and/or Rad54 function. To identify the target(s) of inhibition by ssDNA, we first tested the effect of ssDNA on the Rad51-mediated strand exchange reaction that used ϕX174 DNA substrates. As shown in Fig. 5, *A* (*lanes 3–6*) and *B*, the addition of free pBluescript ssDNA strongly inhibited strand exchange between the ϕX DNA substrates. By contrast, equivalent amounts of free pBluescript dsDNA had little or no effect on the reaction efficiency (Fig. 5*C*). Once again, preincubation of the ssDNA competitor with RPA (Fig. 5, *A* (*lanes 7–10*) and *B*) was sufficient to ablate its inhibitory effect.

Rad54 has a robust ATPase activity that is dependent on DNA for activation, and dsDNA is more effective than ssDNA in supporting ATP hydrolysis (12, 27). To assess whether ssDNA can also interfere with the binding of dsDNA by Rad54, we examined the effect of adding ssDNA on the Rad54 dsDNA-dependent ATPase activity. The results, as summarized in Fig. 5*D*, indicated that ATP hydrolysis by Rad54 was suppressed by concentrations of ssDNA (0.9–7.2 μM nucleotides) substantially below that of the duplex (30 μM base pairs). Here too, incubating the ssDNA with RPA can effectively reverse the suppression by ssDNA (Fig. 5*D*). In control experiments, the addition of extra dsDNA (45 μM base pairs) had no effect on the level of ATP hydrolysis (data not shown). Taken together, the results indicated that the Rad54 dsDNA-activated ATPase activity is strongly inhibited by ssDNA. Other experiments have found that Rad54 in fact has a higher affinity for ssDNA, which, when present, prevents Rad54 from binding to dsDNA (data not shown).

Rad54 Helps Overcome Various Reaction Constraints—The Rad51-mediated homologous DNA pairing and strand exchange reaction is normally conducted at 37 °C (Fig. 6*A*, *panel I*), since lowering the reaction temperature to 23 °C greatly diminishes product formation (Fig. 6*A*, *panels II* and *III*). As demonstrated before (15) and reiterated here (Figs. 6 and 7), homologous DNA pairing reactions that contain Rad54 proceed efficiently at 23 °C. In the reaction that does not contain Rad54, a low level of magnesium is present during the preincubation of Rad51 with ssDNA, but the addition of either spermidine or extra magnesium with the duplex substrate is critical for robust pairing and strand exchange (17, 19) (Fig. 6*B*, *panels I*, *II*, and *III*), with spermidine being more effective than magnesium in this regard (Fig. 6*B*, *panel III*). With the inclusion of Rad54, even in the absence of spermidine or additional magnesium, a highly significant amount of DNA joints is obtained (Fig. 6*B*, *panels V* and *VI*). Interestingly, with Rad54, higher rates of homologous pairing are seen with the addition of magnesium (Fig. 6*B*, *panels IV* and *VI*) than spermidine (Fig. 6*A*, *panel IV*). The duplex substrate used in the standard DNA strand exchange reaction has either 3′ or 5′ overhangs, since Rad51 has very limited capacity to utilize duplex DNA with blunt ends (28) (Fig. 7, *panel I*). By contrast, with Rad54 in the reaction, a blunt-ended DNA substrate is efficiently used for homologous pairing (Fig. 7, *panels III*, *IV*, and *V*).

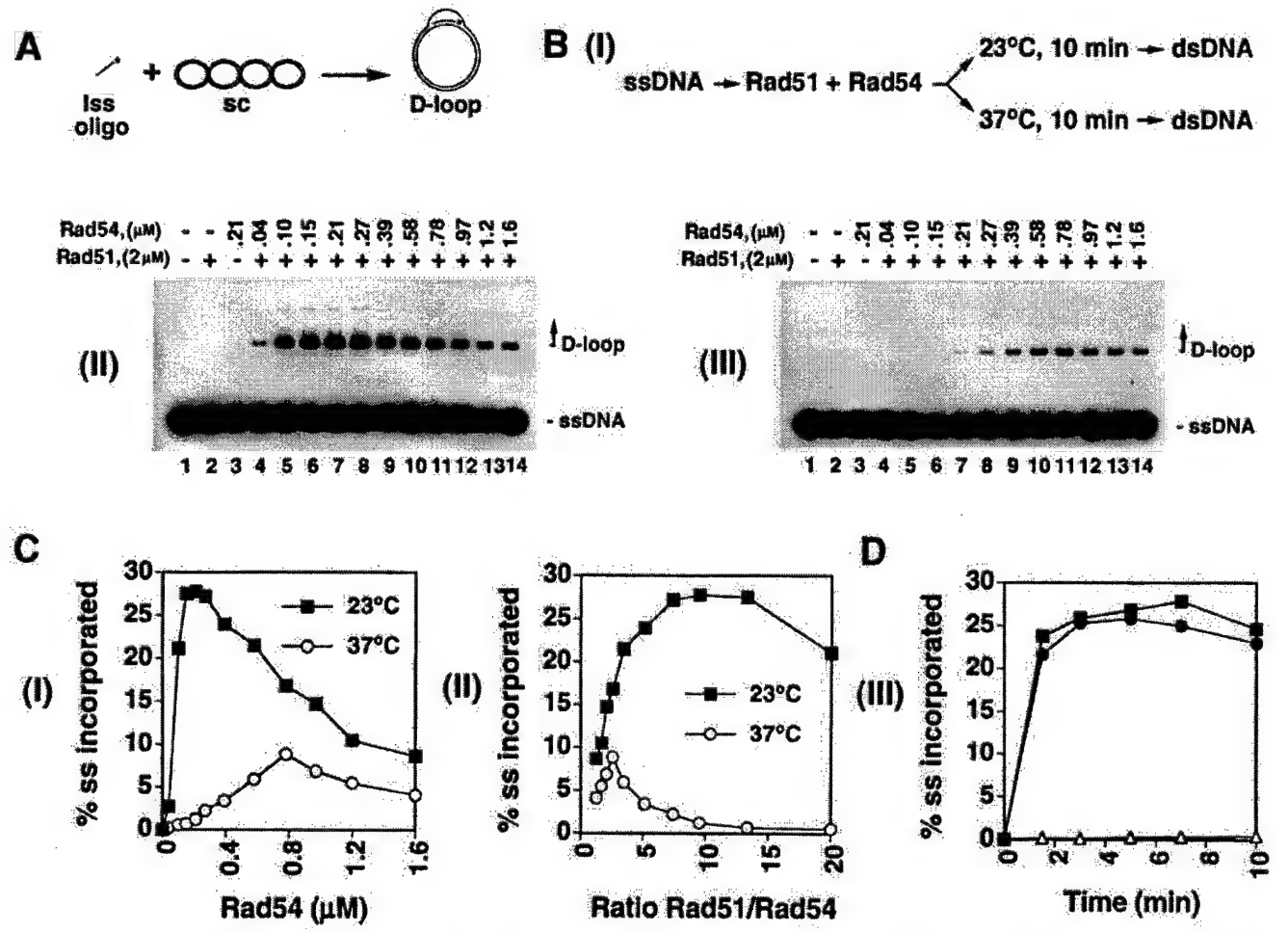

FIG. 8. **Characteristics of the D-loop reaction with an oligonucleotide as initiating substrate.** *A*, schematic of assay. A 90-mer ^{32}P-labeled oligonucleotide (*lss oligo*) is paired with its homologous supercoiled DNA target (*sc*) to yield a D-loop. *B*, *panel I*, reaction schematic. The combination of Rad51 (2 μM) and Rad54 (0.04–1.6 μM) was mixed with the 90-mer oligonucleotide (6 μM nucleotides) in the presence of ATP. The reactions were preincubated for 10 min at either 23 or 37 °C prior to the addition of target duplex. The completed reaction mixtures were incubated at 23 °C for 5 min and processed for electrophoresis in 0.9% agarose gels. *Panel II* displays the reactions in which Rad51 and Rad54 were preincubated with the 90-mer oligonucleotide at 23 °C, whereas *panel III* shows the reaction with the preincubation step done at 37 °C. *C*, the results in *panels II* (*lanes 5–14*) and *III* (*lanes 5–14*) of *B* are graphed as a function of Rad54 concentration and against the Rad51/Rad54 ratio, as shown. The level of reaction product is expressed as the percentage of the input single-stranded oligonucleotide incorporated into the D-loop structure. *D*, in one reaction (*shaded squares*), Rad51 was incubated with the 90-mer oligonucleotide for 8 min at 23 °C, followed by the addition of Rad54 and a 2-min incubation at 23 °C, before the pBluescript DNA was incorporated to complete the reaction mixture. In another reaction (*closed circle*), Rad51 and Rad54 were coincubated with the oligonucleotide for 10 min at 23 °C, and then the pBluescript DNA was incorporated to complete the reaction. In the third reaction (*open triangles*), Rad51 and Rad54 were coincubated with the oligonucleotide for 10 min at 37 °C, and then the pBluescript DNA was incorporated to complete the reaction. In all three cases, the completed reaction mixture was incubated at 23 °C, and aliquots were withdrawn at the indicated times and analyzed as described for *B*. The concentrations of reaction components were as follows: Rad51, 2 μM; Rad54, 150 nM; 90-mer oligonucleotide, 6 μM nucleotides or 67 nM oligonucleotides; pBluescript DNA, 65 μM base pairs or 22 nM plasmid molecules.

D-loop Reaction with an Oligonucleotide as Initiating Substrate—Recently, Mazin *et al.* (16) reported that maximal D-loop formation required an amount of Rad54 equivalent to that of Rad51. In this work, the D-loop reaction was carried out with an oligonucleotide as the initiating substrate (see Fig. 8*A* for schematic). In addition, a fusion of Rad54 to glutathione *S*-transferase (GST-Rad54) and a reaction temperature of 37 °C were employed (16). With our histidine-tagged Rad54 and 23 °C as the reaction temperature, even when an oligonucleotide was used (Fig. 8), optimal D-loop formation occurred at a Rad51/Rad54 ratio of ≥10 (Fig. 8, *B* (*panel II*) and *C* (*panel II*)), which is congruent with results obtained with plasmid length ssDNA (see Fig. 3). As with the plasmid length ssDNA substrate (see Fig. 3), when an oligonucleotide was used, elevating Rad54 beyond the optimal range resulted in suppression of the D-loop reaction (Fig. 8, *B* (*panel II*) and *C* (*panel I*)).

Mazin *et al.* (16) also suggested that GST-Rad54 was targeted to the site of homologous pairing by the Rad51-ssDNA nucleoprotein filament. This conclusion was drawn from experiments in which the order of addition of GST-Rad54, Rad51, and ssDNA was varied. Specifically, preincubation of GST-Rad54 with the ssDNA substrate at 37 °C for 10 min, regardless of whether Rad51 was present, resulted in a substantial drop in reaction efficiency, as compared with the addition of GST-Rad54 after the formation of the Rad51 presynaptic complex (16). We wished to reexamine this issue, since we know that Rad54 is quite unstable at 37 °C (Fig. 1), which was the reaction temperature used in the work of Mazin *et al.* (16). Importantly, when all the reaction steps were carried out at 23 °C, preincubation of Rad51, Rad54, and the oligonucleotide resulted in nearly identical levels of D-loop as when Rad54 was added to a preassembled Rad51-ssDNA nucleoprotein complex (Fig. 8*D*). In sharp contrast, preincubation of Rad51, Rad54, and the oligonucleotide at 37 °C resulted in almost complete

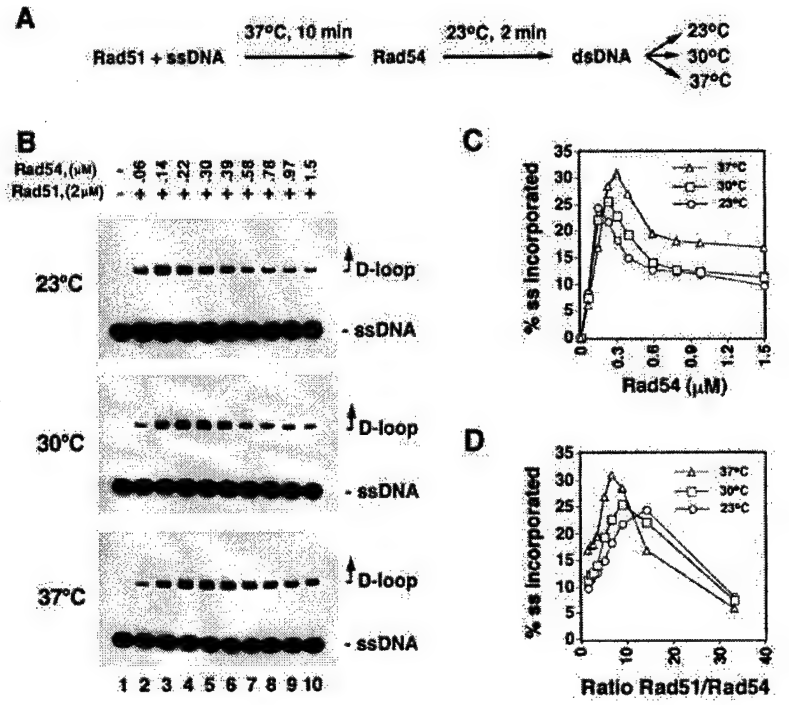

FIG. 9. **Stoichiometric relationship of Rad51/Rad54 at different reaction temperatures.** A series of D-loop reactions were set up in which Rad51 (2 μM) was incubated with the 90-mer oligonucleotide (6 μM nucleotides) for 10 min at 37 °C in the presence of ATP, followed by mixing with Rad54 (0.06–1.5 μM) and a 2-min incubation at 23 °C. At this stage, the reaction mixtures were divided into three equal portions, with each being mixed with the supercoiled DNA substrate and then continuing the incubation at 23, 30, or 37 °C for 5 min, respectively. The reaction mixtures (6 μl each) were processed for electrophoresis in 0.9% agarose gels. The reaction scheme is summarized in *A*, and the autoradiograms containing the reaction mixtures are presented in *B*. The results in *B* are shown graphically as percentage of ssDNA (*ss*) incorporated into D-loop as a function of the Rad54 concentration (*C*) and as a function of the Rad51/Rad54 molar ratio (*D*).

ablation of D-loop formation (Fig. 8, B (*panel III, lane 6*) and *D*). The lack of D-loop formation in this instance was due to thermal inactivation of Rad54, since incubating Rad51 with the ssDNA at 37 °C for 20 min before adding Rad54 and then continuing the incubation at 23 °C did not result in inhibition of the D-loop reaction (data not shown).

We have also investigated whether increasing amounts of Rad54 would at least partially compensate for the thermal denaturation of Rad54. Although some D-loop was seen with higher concentrations of Rad54 preincubated at 37 °C (Fig. 8, *B* (*panel III*) and *C* (*panel I*)), its final level was substantially lower than what was attained when the preincubation step was done at 23 °C (Fig. 8, *B* (*panel II*) and *C* (*panel I*)). Importantly, with plasmid length ssDNA, preincubation of Rad51 and Rad54 with the ssDNA at 23 °C also did not diminish the efficiency of the D-loop reaction, whereas when 37 °C was used as the preincubation temperature, a dramatic decrease in the level of D-loop was again seen (data not shown).

To further delineate the stoichiometric relationship between Rad51 and Rad54 as a function of the reaction temperature, we carried out another series of experiments in which the Rad51 presynaptic filament was preassembled at 37 °C and then mixed with Rad54 that had not previously been exposed to 37 °C, with the actual D-loop reactions being carried out at 23, 30, and 37 °C, respectively (Fig. 9). At all three reaction temperatures, maximal D-loop formation occurred at amounts of Rad54 substoichiometric to that of Rad51. Interestingly, significantly more Rad54 was needed to achieve maximal D-loop formation at 37 °C than at 23 °C; this could be due to rapid thermal denaturation of Rad54 that was offset by increasing amounts of this protein.

Taken together, the results clearly indicate that Rad54 is equally effective in homologous pairing whether it is added with Rad51 to the ssDNA or to a preformed Rad51-ssDNA nucleoprotein complex. Our results also provide evidence that the decrease in D-loop formation seen with preincubation of Rad54 with Rad51 and the ssDNA substrate as reported by Mazin *et al.* (16) was probably due to thermal inactivation of Rad54.

DISCUSSION

Stoichiometric Relationship among Rad51, Rad54, and the ssDNA Substrate—We have demonstrated that in the Rad51/Rad54/RPA-mediated homologous DNA pairing reaction that utilizes plasmid length DNA substrates, a contiguous Rad51-ssDNA filament is not needed for maximal DNA joint formation. In fact, the reaction efficiency decreases significantly when an amount of Rad51 sufficient to yield a contiguous filament is used. Equally important, our results indicate that amounts of Rad54 substantially below that of Rad51 can achieve highly robust DNA joint formation and that increasing the Rad54 concentration beyond the optimal level results in a lower reaction efficiency.

Our observation that catalytic amounts of Rad54 are sufficient for attaining the maximal rate of homologous pairing is seemingly at odds with the work of Mazin *et al.* (16), who suggested that the assembly of a 1:1 complex of Rad51 and Rad54 was required for maximal efficiency of DNA joint formation. We do not yet have a definitive answer to this discrepancy between the two studies, but it is possible that the GST-Rad54 used in the work of Mazin *et al.* behaves differently than the six histidine-tagged Rad54 employed in our work. In addition, the different purification protocols used in the two studies could have resulted in Rad54 preparations with different specific activities. Last, it remains possible that the GST-Rad54 protein is even more prone to thermal denaturation than our histidine-tagged Rad54, such that higher amounts of the GST-Rad54 fusion protein could be needed for achieving optimal homologous pairing at the reaction temperature of 37 °C. Regardless of the reason(s) for the discrepancy between the two studies, we note that in the work of Mazin *et al.* (16), significant D-loop formation was seen at levels of Rad54 severalfold below that of Rad51 (16). Together with our results reported here and elsewhere (12, 15), it seems clear that efficient homologous pairing is not contingent upon the assembly of an equimolar complex of Rad51 and Rad54.

Mazin *et al.* (16) also reported that incubation of Rad54 with the ssDNA led to a greatly diminished reaction efficiency. By contrast, we find that with both plasmid length ssDNA and an

oligonucleotide, Rad54 is just as active in the D-loop reaction whether it is added to the ssDNA or to a preassembled Rad51-ssDNA nucleoprotein complex. Furthermore, our results have provided compelling evidence that the diminished ability of Rad54 to promote homologous pairing when used in conjunction with the ssDNA substrate (16) was probably due to thermal inactivation of this protein.

Modulation of Homologous DNA Pairing Efficiency by ssDNA and RPA—RPA is known to promote Rad51 presynaptic filament assembly by effecting the removal of secondary structure in the DNA (20, 24). We have found that free ssDNA greatly diminishes the ability of a preassembled Rad51-ssDNA nucleoprotein filament to conduct the homologous DNA pairing and strand exchange reaction. Our data have shown that this strong suppressive effect of free ssDNA can be ablated by RPA. Based on the paradigm established with RecA (1, 29), we propose that free ssDNA exerts its inhibitory effect by occupying the "secondary" DNA binding site in the Rad51-ssDNA presynaptic filament and thereby excluding the homologous duplex molecule from being recognized by the presynaptic filament. Our results thus reveal a novel role of RPA, not in the removal of secondary DNA structure in the ssDNA template, but in sequestering ssDNA and preventing it from occupying the secondary DNA binding site in the Rad51-ssDNA nucleoprotein filament. In addition, RPA could effect the sequestering of Rad51 molecules at the end of the linear single strand, which would enhance the probability for the formation of a stable DNA joint with the homologous duplex.

We have also asked whether ssDNA affects Rad54 functions. At the expense of ATP hydrolysis, Rad54 tracks on duplex DNA and generates negatively and positively supercoiled domains in the DNA (14, 15). Furthermore, as a result of negative superhelical stress, the DNA strands in the duplex molecule undergo transient separation, resulting in a marked sensitivity to the single-stranded specific nuclease P1 (15). Regretfully, we have been unable to ascertain whether free ssDNA inhibits Rad54-mediated DNA supercoiling and DNA strand opening, because the *E. coli* topoisomerase I used in monitoring DNA supercoiling is completely inhibited by ssDNA, and the P1 nuclease employed in the detection of DNA strand opening digests the ssDNA competitor rapidly. However, since both DNA supercoiling and DNA strand opening by Rad54 are strictly coupled to the hydrolysis of ATP, it seems reasonable to suggest that free ssDNA would also adversely affect the ability of Rad54 to supercoil and transiently unwind duplex DNA.

A Model for DNA Strand Invasion—The available results indicate that Rad54 tracks on the incoming duplex, producing compensatory negative and positive supercoils (14, 15). The tracking motion probably enhances the rate at which the incoming duplex molecule can be sampled for homology by the presynaptic complex. The negative supercoils produced lead to transient opening of the DNA strands that is thought to facilitate the formation of the nascent DNA joint upon locating DNA homology (14, 15).

Although it can be expected that long heteroduplex joints may only occur with a contiguous Rad51 filament, our results strongly suggest that a nascent DNA joint can be made before a contiguous filament of Rad51 is assembled on the initiating ssDNA substrate. In fact, as indicated from our biochemical experiments, the assembly of a contiguous Rad51 nucleoprotein filament at the very initial stage of the recombination reaction may compromise the formation of the nascent DNA joint. We speculate that extensive interactions between the incoming duplex and the "secondary" DNA binding site within the presynaptic Rad51 filament may actually impede scanning of the duplex molecule for DNA homology and DNA supercoiling by Rad54. We envision that at a later stage of the recombination reaction, the branch migration of the nascent DNA joint to extend the region of heteroduplex DNA will probably require the assembly of a contiguous Rad51 nucleoprotein filament. The assembly of a contiguous Rad51 nucleoprotein filament is expected to depend on the mediator function of Rad52 and the Rad55-Rad57 heterodimer (4).

Our results have shown that an excess of Rad54 is inhibitory to DNA joint formation, suggesting that uncoordinated movement of the incoming duplex molecule relative to the presynaptic nucleoprotein complex may diminish the ability of the nucleoprotein complex to conduct DNA homology search and joint formation. Alternatively, or in addition, the ssDNA that results from extensive unwinding of the DNA duplex by Rad54 may inhibit DNA joint formation by compromising the functional integrity of the presynaptic protein complex through inhibition of Rad51 and Rad54 functions.

Acknowledgments—We are grateful to Lumir Krejci and Kelly Trujillo for reading the manuscript.

REFERENCES

1. Bianco, P. R., Tracy, R. B., and Kowalczykowski, S. C. (1998) *Front. Biosci.* **3,** 570–603
2. Cromie, G. A., Connelly, J. C., and Leach, D. R. (2001) *Mol. Cell* **8,** 1163–1174
3. Paques, F., and Haber, J. E. (1999) *Microbiol. Mol. Biol. Rev.* **63,** 349–404
4. Sung, P., Trujillo, K. M., and Van Komen, S. (2000) *Mutat. Res.* **451,** 257–275
5. Dasika, G. K., Lin, S. C., Zhao, S., Sung, P., Tomkinson, A., and Lee, E. Y. (1999) *Oncogene* **18,** 7883–7899
6. Moynahan, M. E., Chiu, J. W., Koller, B. H., and Jasin, M. (1999) *Mol. Cell* **4,** 511–518
7. Moynahan, M. E., Pierce, A. J., and Jasin, M. (2001) *Mol. Cell* **7,** 263–272
8. Pierce, A. J., Stark, J. M., Araujo, F. D., Moynahan, M. E., Berwick, M. B., and Jasin M. (2001) *Trends Cell Biol.* **11,** 52–59
9. Roca, A. I., and Cox, M. M. (1997) *Prog. Nucleic Acids Res. Mol. Biol.* **56,** 129–223
10. Beernink, H. T., and Morrical, S. W. (1999) *Trends Biochem. Sci.* **24,** 385–389
11. Kanaar, R., Hoeijmakers, J. H., and van Gent, D. C. (1998) *Trends Cell Biol.* **8,** 483–489
12. Petukhova, G., Stratton, S., and Sung, P. (1998) *Nature* **393,** 91–94
13. Petukhova, G., Sung, P., and Klein, H. (2000) *Genes Dev.* **14,** 2206–2215
14. Ristic, D., Wyman, C., Paulusma, C., and Kanaar, R. (2001) *Proc. Natl. Acad. Sci. U. S. A.* **98,** 8454–8460
15. Van Komen, S., Petukhova, G., Sigurdsson, S., Stratton, S., and Sung, P. (2000) *Mol. Cell* **6,** 563–572
16. Mazin, A. V., Bornarth, C. J., Solinger, J. A., Heyer, W. D., and Kowalczykowski, S. C. (2000) *Mol. Cell* **6,** 583–592
17. Sung, P. (1994) *Science* **265,** 1241–1243
18. Nakagawa, T., Flores-Rozas, H., and Kolodner, R. D. (2001) *J. Biol. Chem.* **276,** 31487–31493
19. Sung, P. (1997) *Genes Dev.* **11,** 1111–1121
20. Sugiyama, T., Zaitseva, E. M., and Kowalczykowski, S. C. (1997) *J. Biol. Chem.* **272,** 7940–7945
21. Petukhova, G., Stratton, S. A., and Sung, P. (1999) *J. Biol. Chem.* **274,** 33839–33842
22. Jiang, H., Xie, Y., Houston, P., Stemke-Hale, K., Mortensen, U. H., Rothstein, R., and Kodadek, T. (1996) *J. Biol. Chem.* **271,** 33181–33186
23. Clever, B., Interthal, H., Schmuckli-Maurer, J., King, J., Sigrist, M., and Heyer, W. D. (1997) *EMBO J.* **16,** 2535–2544
24. Sung, P., and Robberson, D. L. (1995) *Cell* **82,** 453–461
25. Zaitseva, E. M., Zaitsev, E. N., and Kowalczykowski, S. C. (1999) *J. Biol. Chem.* **274,** 2907–2915
26. Petukhova, G., Van Komen, S., Vergano, S., Klein, H., and Sung, P. (1999) *J. Biol. Chem.* **274,** 29453–29462
27. Swagemakers, S. M., Essers, J., de Wit, J., Hoeijmakers, J. H., and Kanaar, R. (1998) *J. Biol. Chem.* **273,** 28292–28297
28. Namsaraev, E. A., and Berg, P. (1997) *Mol. Cell Biol.* **17,** 5359–5368
29. Mazin, A. V., and Kowalczykowski, S. C. (1998) *EMBO J.* **17,** 1161–1168

THE JOURNAL OF BIOLOGICAL CHEMISTRY
Vol. 277, No. 45, Issue of November 8, pp. 42790–42794, 2002
Printed in U.S.A.

Homologous DNA Pairing by Human Recombination Factors Rad51 and Rad54*

Received for publication, August 6, 2002
Published, JBC Papers in Press, August 29, 2002, DOI 10.1074/jbc.M208004200

Stefan Sigurdsson‡, Stephen Van Komen§, Galina Petukhova¶, and Patrick Sung‖

From the Department of Molecular Medicine and Institute of Biotechnology, University of Texas Health Science Center, San Antonio, Texas 78254-3207

Human Rad51 (hRad51) and Rad54 proteins are key members of the *RAD52* group required for homologous recombination. We show an ability of hRad54 to promote transient separation of the strands in duplex DNA via its ATP hydrolysis-driven DNA supercoiling function. The ATPase, DNA supercoiling, and DNA strand opening activities of hRad54 are greatly stimulated through an interaction with hRad51. Importantly, we demonstrate that hRad51 and hRad54 functionally cooperate in the homologous DNA pairing reaction that forms recombination DNA intermediates. Our results should provide a biochemical model for dissecting the role of hRad51 and hRad54 in recombination reactions in human cells.

In eukaryotic organisms, the repair of DNA double-stranded breaks by homologous recombination is mediated by a group of evolutionarily conserved genes known as the *RAD52* epistasis group. Members of the *RAD52* group (*RAD51*, *RAD52*, *RAD54*, *RAD55*, *RAD57*, *RAD59*, and *RDH54/TID1*) were first uncovered in genetic screens in the budding yeast *Saccharomyces cerevisiae* (1, 2). In mammals, the efficiency of homology-directed recombinational DNA repair is modulated by the tumor suppressors BRCA1 and BRCA2 (3), providing a compelling link between this DNA repair pathway and the suppression of tumor formation. The involvement of the homologous recombination machinery in the maintenance of genome stability and tumor suppression underscores the need for deciphering the action mechanism of this machinery.

During the recombinational repair of DNA double-stranded breaks, a single-stranded DNA intermediate is utilized by the recombination machinery to invade a DNA homolog, most often the sister chromatid, to form a DNA joint molecule referred to as a D-loop (2). D-Loop formation is critical for subsequent steps in the recombination reaction, which include repair DNA synthesis and resolution of recombination intermediates (1, 2), that lead to the restoration of the integrity of the injured chromosome.

In the past several years, biochemical studies have begun to shed light on the functions of the human *RAD52* group proteins in DNA joint formation. Much of the published work has centered on the human Rad51 (hRad51)[1] protein, which is structurally related to the *Escherichia coli* recombinase enzyme RecA (4). Like RecA, hRad51 assembles into a right-handed filament on single-stranded (ss) DNA in a reaction that is dependent on ATP binding (reviewed in Ref. 5). Importantly, hRad51 protein has been shown to have DNA pairing and strand exchange activities that yield DNA joints between homologous ssDNA and double-stranded DNA substrates (6–8). The homologous pairing and strand exchange function of hRad51 is augmented by replication protein A (RPA), a heterotrimeric single-stranded DNA binding factor (6, 8), by hRad52 protein (9), and by the Rad51B-Rad51C heterodimeric complex (10), which is the functional equivalent of the yeast Rad55-Rad57 complex (11).

The *RAD54* encoded product belongs to the Swi2/Snf2 protein family (12). Purified hRad54 exhibits DNA-dependent ATPase and DNA supercoiling activities (13–15). However, the manner in which hRad54 influences the hRad51-mediated recombination reaction has remained mysterious. Here we report our biochemical studies that show functional interactions between hRad51 and hRad54 in DNA supercoiling and homologous DNA pairing reactions. We discuss how hRad51 and hRad54 cooperate to make DNA joints during recombination processes.

EXPERIMENTAL PROCEDURES

Anti-Rad54 Antibodies—The first 238 amino acid residues of the human Rad54 protein were fused to glutathione *S*-transferase in the vector pGEX-3X. The fusion protein was expressed in *E. coli* strain BL21 (DE3) and purified from inclusion bodies by preparative denaturing polyacrylamide gel electrophoresis and used as antigen for raising polyclonal antibodies in rabbits. The same antigen was covalently conjugated to cyanogen bromide-activated Sepharose 4B and used as affinity matrix to purify the antibodies from rabbit antisera, as described (16).

Rad54 Expression and Purification—A recombinant baculovirus containing the cloned *hRad54* cDNA with an added FLAG epitope at the C terminus was generated. HighFive insect cells were infected with the recombinant baculovirus at a multiplicity of infection of 10 and harvested after 48 h of incubation. An extract was prepared from 500 ml of insect cell culture (5×10^8 cells) using a French Press in 60 ml of cell breakage buffer (50 mM Tris-HCl, pH 7.5, 2 mM EDTA, 10% sucrose, 200 mM KCl, 1 mM dithiothreitol, 1 mM phenylmethylsulfonyl fluoride, and the following protease inhibitors at 3 μg/ml each: aprotinin, chymostatin, leupeptin, and pepstatin). After centrifugation (100,000 × *g* for 60 min), the clarified extract was loaded onto a Q-Sepharose column (10-ml matrix). The flow-through fraction from the Q column was fractionated in a sulfopropyl-Sepharose column (10-ml matrix) with a 50-ml, 0–700

* This work was supported in part by National Institutes of Health Grants GM57814 and CA81020. The costs of publication of this article were defrayed in part by the payment of page charges. This article must therefore be hereby marked "*advertisement*" in accordance with 18 U.S.C. Section 1734 solely to indicate this fact.

‡ Supported in part by United States Army Predoctoral Fellowship DAMD17-01-1-0412.

§ Supported in part by United States Army Predoctoral Fellowship DAMD17-01-1-0414.

¶ Supported in part by National Institutes of Health Training Grant T32AG00165. Present address: NIDDK, National Institutes of Health, Bldg. 10, Rm. 9D17, 9000 Rockville Pike, Bethesda, MD 20892.

‖ To whom correspondence should be addressed. Tel.: 210-567-7216; Fax: 210-567-7277; E-mail: sung@uthscsa.edu.

[1] The abbreviations used are: hRad51, human Rad51; yRad51, yeast Rad51; ss, single-stranded; BSA, bovine serum albumin; AMP-PNP, adenosine 5′-(β,γ-imino)triphosphate; ATPγS, adenosine 5′-3-*O*-(thio)-triphosphate.

mM KCl gradient in K buffer (20 mM KH_2PO_4 at pH 7.4, 0.5 mM EDTA, 1 mM dithiothreitol, and 10% glycerol). Fractions containing the peak of hRad54 were pooled and loaded onto a 1-ml Macro-hydroxyapatite (Bio-Rad) column, which was eluted with 30 ml of 0–300 mM KH_2PO_4 in K buffer. The peak fractions were pooled and mixed with 1.5 ml of Anti-FLAG M2 agarose (Sigma) and rocked for 3 h at 4 °C. The FLAG agarose was washed three times with 3 ml of 150 mM KCl in buffer K before eluting hRad54 using the same buffer containing 1 mg/ml of the FLAG peptide (Sigma). hRad54 (~1 mg) eluted from the FLAG matrix was concentrated in a Centricon-30 microconcentrator to 5 mg/ml and stored in small aliquots at −70 °C.

Rad51 and hrad51 K133R Proteins—The hRad51 protein was expressed in the *E. coli* RecA-deficient strain BLR (DE3) and purified to near homogeneity using our previously described procedure (8). The hrad51 K133R mutant was expressed and purified to near homogeneity in exactly the same way.

Topoisomerase I—*E. coli* topoisomerase I was purified to near homogeneity from the *E. coli* strain JM101 with plasmid pJW312-sal containing the *topA* gene under the Lac promoter, as described (17).

Binding of hRad54 to Affi-hRad51 Beads—Purified hRad51 and bovine serum albumin (BSA) were coupled to Affi-Gel 15 beads at 4 °C following the instructions of the manufacturer (Bio-Rad). The resulting matrices contained 4 and 12 mg/ml hRad51 and BSA, respectively. Purified hRad54 (1.2 μg) was mixed with 5 μl of Affi-Rad51 or Affi-BSA at 4 °C for 30 min in 30 μl of buffer containing 100 mM KCl and 0.1% Triton X-100 by constant tapping. The beads were washed twice with 50 μl of the same buffer before being treated with 30 μl of 2% SDS at 37 °C for 5 min to elute the bound hRad54. The various fractions (4 μl each) were analyzed by immunoblotting to determine their content of hRad54.

DNA Substrates—Topologically relaxed φX174 DNA was prepared as described (18), and pBluescript SK DNA was made in *E. coli* DH5α and purified as described (19). The oligonucleotide used in the D-loop reaction is complementary to positions 1932–2022 of the pBluescript SK DNA and had the sequence 5′-AAATCAATCTAAAGTATATATGAGTAAACTTGGTCTGACAGTTACCAATGCTTAATCAGTGAGGCACCTATCTCAGCGATCTGTCTATTT-3′. This oligonucleotide was 5′ end-labeled with [γ-^{32}P]ATP and T4 polynucleotide kinase.

ATPase Assay—The hRad54 protein (60 nM) was incubated with replicative form I φX174 DNA (30 μM base pairs) and 1.5 mM [γ-^{32}P]ATP with or without 400 nM hRad51 or yRad51 in 10 μl of reaction buffer (20 mM Tris-HCl, pH 7.4, 25 mM KCl, 1 mM dithiothreitol, 4 mM $MgCl_2$, 100 μg/ml BSA) at 30 °C for the indicated times. The level of ATP hydrolysis was determined by thin layer chromatography, as described (19).

DNA Supercoiling and DNA Strand-opening Reactions—Increasing amounts of hRad54 were incubated with 80 ng of relaxed φX174 DNA (12 μM nucleotides) for 2 min at 23 °C in 12 μl of reaction buffer (20 mM Tris-HCl, pH 7.4, 5 mM $MgCl_2$, 1 mM dithiothreitol, 100 μM ATP, and an ATP-regenerating system consisting of 10 mM creatine phosphatase and 28 μg/ml creatine kinase). Following the addition of 100 ng of *E. coli* topoisomerase I in 0.5 μl, the reactions were incubated for 10 min at 23 °C and then deproteinized by treatment with 0.5% SDS and proteinase K (0.5 mg/ml) for 10 min at 37 °C. Samples were run on 1% agarose gels in TAE buffer (35 mM Tris acetate, pH 7.4, 0.5 mM EDTA) at 23 °C and then stained with ethidium bromide. In the experiment in Fig. 4*B*, the relaxed DNA was incubated with the indicated amounts of hRad51 and hRad54 for 2 min at 23 °C, followed by the addition of topoisomerase and a 10-min incubation at 23 °C. For the P1 sensitivity experiments in Figs. 3*C* and 4*C*, the reactions were assembled in the same manner except that 0.4 unit of P1 nuclease (Roche) was used instead of topoisomerase. The DNA species were resolved in a 1% agarose gel containing 10 μM ethidium bromide in TAE buffer.

D-Loop Reaction—For the time course reactions (25 μl, final volume) in Fig. 5, hRad51 or hrad51 K133R (800 nM) was incubated with the 5′-labeled ss oligonucleotide (2.5 μM nucleotides) for 3 min at 37 °C in 22 μl of reaction buffer (20 mM Tris-HCl, pH 7.4, 100 μg/ml BSA, 1.5 mM $MgCl_2$, 2 mM ATP, and the ATP-generating system described above). This was followed by the addition of hRad54 (120 nM) in 1 μl and incubation at 23 °C for 2 min. The reaction was completed by adding the pBluescript SK replicative form DNA (35 μM base pairs) in 2 μl. The reaction mixture was incubated at 30 °C, and 3.8-μl aliquots were withdrawn at the indicated times, deproteinized, and run in 1% agarose gels in TAE buffer. The gels were dried and the levels of D-loop were quantified by phosphorimage analysis. The reactions in which ATP, hRad51, or hRad54 was omitted or ATP was replaced by ATPγS or AMP-PNP were scaled down 2-fold to a 12.5-μl final volume, but they were otherwise assembled and processed in exactly the same manner.

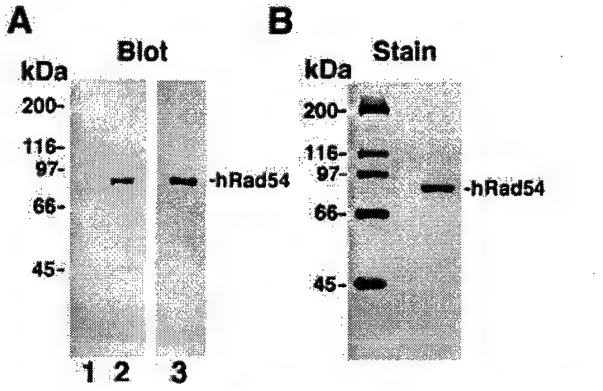

FIG. 1. **Purification of hRad54.** *A*, expression of hRad54 in insect cells. Extracts from uninfected insect cells (*lane 1*) and from insect cells infected with the recombinant hRad54 baculovirus (*lane 2*) were probed with affinity-purified anti-hRad54 antibodies. In *lane 3*, 100 ng of purified hRad54 was also subjected to immunoblotting. *B*, purified hRad54 protein (1 μg) was run in an 8% denaturing polyacrylamide gel and stained with Coomassie Blue.

RESULTS

Human Recombination Factors—Human Rad51 was expressed in a recA-*E. coli* strain and purified to near homogeneity as described previously (8). The hrad51 K133R mutant, which harbors the change of the conserved lysine residue in the Walker type A nucleotide binding motif to arginine, was also similarly expressed and purified. In agreement with previously published results (20), hrad51 K133R has negligible ATPase activity compared with wild type hRad51 (data not shown). We cloned the human *RAD54* cDNA from a testis cDNA library using the polymerase chain reaction. The entire cloned *hRAD54* cDNA was sequenced to ensure that it agreed with the published sequence (21). We tagged hRad54 protein with a FLAG epitope at the carboxyl terminus and expressed it in insect cells by the use of a recombinant baculovirus (Fig. 1*A*). We obtained ~1 mg of nearly homogeneous hRad54 (Fig. 1*B*) from 500 ml of insect cell culture by a combination of conventional column chromatography and affinity binding to an antibody specific for the FLAG epitope. The purified hRad54 has a level of DNA-dependent ATPase very similar to that described in the literature (13) (see later).

hRad54 Physically Interacts with hRad51—Golub *et al.* (22) found that the amino terminus of hRad54 can bind hRad51 in *in vitro* analyses and also in the yeast two-hybrid system. However, in mouse embryonic stem cells, association of mRad51 and mRad54 requires prior treatment of cells with a DNA damaging agent (14). To examine whether purified hRad54 physically interacts with hRad51, we coupled hRad51 to Affi-Gel beads to use as affinity matrix for binding hRad54. As shown in Fig. 2, purified hRad54 was efficiently retained on Affi-hRad51 beads but not on Affi-beads that contained BSA. When a less purified hRad54 fraction (~25% hRad54) was used, hRad54, but not the contaminating protein species, bound to the Affi-hRad51 beads (data not shown). The results thus indicate a direct and specific interaction between hRad51 and hRad54.

DNA Supercoiling and DNA Strand Opening by hRad54—Tan *et al.* (14) showed an ability of hRad54 to alter the DNA linking number of a nicked plasmid in the presence of DNA ligase. The induction of DNA linking number change was dependent on ATP hydrolysis by hRad54 (14). The same group also used scanning force microscopy to provide evidence that hRad54 tracks on DNA when ATP is hydrolyzed (15). A schematic depicting the basis for tracking-induced DNA supercoiling by hRad54 is given in Fig. 3*A*.

The yRad54 protein also tracks on DNA and, as a result,

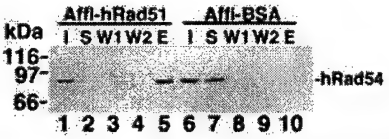

FIG. 2. **hRad54 interacts with hRad51.** Purified hRad54 (1.2 μg) was mixed with Affi-beads containing either BSA (Affi-BSA) or hRad51 (Affi-Rad51) in 30 μl and washed twice with 50 μl buffer, followed by treatment of the beads with 30 μl of SDS to elute bound hRad54. The starting material (*I*), supernatant (*S*), the two washes (*W1* and *W2*), and the SDS eluate (*E*), 4 μl each, were subjected to immunoblotting to determine their hRad54 content.

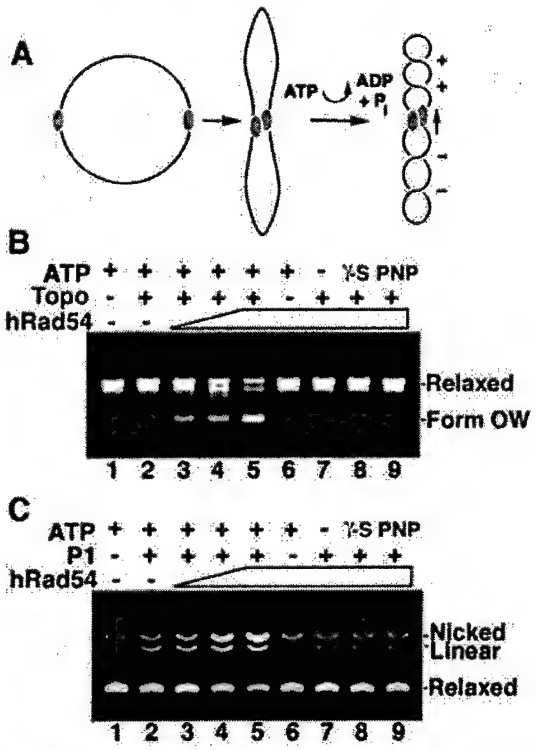

FIG. 3. **hRad54 supercoils DNA and promotes DNA strand opening.** *A*, basis for hRad54-induced supercoiling, as per Ristic *et al.* (15) and Van Komen *et al.* (18). The free energy from ATP hydrolysis fuels the tracking of a hRad54 oligomer on DNA, producing a positively supercoiled domain ahead of protein movement and a negatively supercoiled domain behind. *B*, increasing amounts of hRad54 (200, 400, and 750 nM in *lanes 3–5*, respectively) were incubated with topologically relaxed DNA (20 μM nucleotides) and *E. coli* topoisomerase I in buffer that contained ATP. The highest amount of hRad54 (750 nM) was also incubated with the DNA substrate in the absence of topoisomerase (*lane 6*) and in the presence of topoisomerase but with the omission of ATP (*lane 7*) or the substitution of ATP by ATPγS (*γ-S*; *lane 8*) and AMP-PNP (*PNP*; *lane 9*). DNA alone (*lane 1*) or DNA incubated with topoisomerase (*lane 2*) was also included. The reaction mixtures were run in a 1% agarose gel, which was treated with ethidium bromide to reveal the DNA species. *C*, increasing amounts of hRad54 (200, 400, and 750 nM in *lanes 3–5*, respectively) were incubated with topologically relaxed DNA (20 μM nucleotides) and P1 nuclease in buffer that contained ATP. The highest amount of hRad54 (750 nM) was also incubated with the DNA substrate in the absence of P1 (*lane 6*) and in the presence of P1 but with the omission of ATP (*lane 7*) or the substitution of ATP by ATPγS (*γ-S*; *lane 8*) and AMP-PNP (*PNP*; *lane 9*). DNA alone (*lane 1*) and DNA incubated with P1 in the absence of hRad54 (*lane 2*) were also included. The reaction mixtures were run in a 1% agarose gel containing 10 μM ethidium bromide.

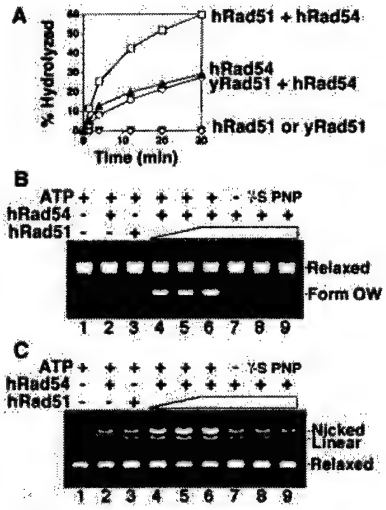

FIG. 4. **The hRad54 activities are stimulated by hRad51.** *A*, hRad54 was incubated with ϕX replicative form I DNA (30 μM nucleotides) and 1.5 mM [γ-^{32}P]ATP for the indicated times, and the level of ATP hydrolysis was quantified by thin layer chromatography. ATPase activity was also measured for hRad51 alone, yRad51 alone, and the combinations of hRad54/hRad51 and hRad54/yRad51. The protein concentrations were as follows: hRad54, 60 nM; hRad51, 400 nM; yRad51, 400 nM. In every case, negligible ATP hydrolysis was seen when DNA was omitted (data not shown). *B*, relaxed DNA (20 μM nucleotides) was incubated with hRad54 (75 nM in *lanes 2* and *4–9*) and hRad51 (80, 160, and 240 nM in *lanes 4–6*, respectively) in the presence of ATP and *E. coli* topoisomerase I. The highest amount of hRad51 (240 nM) was incubated with substrate and topoisomerase I but without hRad54 (*lane 3*) and also with hRad54 (75 nM) but with the omission of ATP (*lane 7*) or its substitution with ATPγS (*γ-S*; *lane 8*) or AMP-PNP (*PNP*; *lane 9*). DNA alone was analyzed in *lane 1*. After deproteinization, the reaction mixtures were run in a 1% agarose gel, which was treated with ethidium bromide to stain the DNA species. *C*, relaxed DNA was incubated with hRad54 (75 nM in *lanes 2* and *4–9*) and hRad51 (80, 160, and 240 nM in *lanes 4–6*, respectively) in the presence of ATP and P1 nuclease. The highest amount of hRad51 (240 nM) was incubated with substrate and P1 but without hRad54 (*lane 3*) and also with hRad54 (75 nM) but with the omission of ATP (*lane 7*) or its substitution with ATPγS (*γ-S*; *lane 8*) or AMP-PNP (*PNP*; *lane 9*). DNA alone was run in *lane 1*. Analysis was carried out in a 1% agarose gel that contained 10 μM ethidium bromide.

generates positive and negative supercoils in the DNA substrate. Removal of the negative supercoils by treatment with *E. coli* topoisomerase I leads to the accumulation of positive supercoils and the formation of an overwound DNA species called Form OW (18). Here we used the same strategy to examine the ability of hRad54 to supercoil DNA. As shown in Fig. 3*B*, in the presence of topoisomerase, purified hRad54 protein readily induces a linking number change in the DNA (18). The DNA supercoiling reaction is dependent on ATP hydrolysis, as revealed by its omission or substitution with a nonhydrolyzable analogue (ATPγS or AMP-PNP) (Fig. 3*B*).

We asked whether the negative supercoils generated as a result of hRad54 tracking on the DNA substrate (15) (Fig. 3, *A* and *B*) leads to transient DNA strand opening by examining the sensitivity of a relaxed DNA template to the single-strand specific nuclease P1, as per Van Komen *et al.* (18). Fig. 3*C* shows that incubation of topologically relaxed DNA with hRad54 rendered the relaxed DNA substrate sensitive to P1 nuclease, as indicated by the accumulation of nicked circular and linear DNA forms. The DNA strand opening reaction is also completely dependent on ATP hydrolysis (Fig. 3*C*).

Activities of hRad54 Are Stimulated by hRad51—The results presented here (Fig. 2) and elsewhere (22) have unveiled a specific interaction between hRad51 and hRad54. We examined whether the hRad54 ATPase would be enhanced upon interaction with hRad51. As shown in Fig. 4*A*, a much higher rate of ATP hydrolysis was seen when hRad54 was combined with hRad51. The fact that yRad51 was ineffective in this reaction (Fig. 4*A*) indicates that the action of hRad51 is specific. Although hRad51 is known to have a weak ATPase activity (23), the fact that the hrad51 K133R mutant protein, which binds but does not hydrolyze ATP (20), was just as effective in

promoting ATP hydrolysis (data not shown) strongly indicated that the increase in ATP hydrolysis was because of enhancement of the hRad54 ATPase function.

We next asked whether the DNA supercoiling activity of hRad54 would also be up-regulated by hRad51. The results showed that hRad51 stimulates the supercoiling reaction, as indicated by a much higher level of Form OW DNA (Fig. 4*B*). Because negative supercoiling generated by hRad54 leads to DNA strand opening (Fig. 3*C*), we thought that hRad51 might also promote this activity. Indeed, the inclusion of hRad51 greatly elevated the nicking of the relaxed DNA substrate by P1 nuclease (Fig. 4*C*). Even with the inclusion of hRad51, no Form OW DNA or nicking of DNA was seen when ATP was omitted or substituted by the nonhydrolyzable analogues ATPγS and AMP-PNP (Fig. 4, *B* and *C*). Thus, the results revealed that hRad51 markedly stimulates the ability of Rad54 to supercoil DNA and unwind DNA strands. The hrad51 K133R protein was just as effective as wild type hRad51 in enhancing the DNA supercoiling and strand opening activities of hRad54 (data not shown). Furthermore, we found that yRad51 does not stimulate the hRad54 activities (data not shown), thus indicating a high degree of specificity in the hRad51 action.

hRad51 and hRad54 Cooperate in Homologous DNA Pairing—The RecA/Rad51 class of general recombinases is central to recombination processes by virtue of their ability to catalyze the homologous DNA pairing reaction that yields heteroduplex DNA joints (2, 24). Because hRad51 and hRad54 physically interact (22) (Fig. 2) and hRad51 enhances the various activities of hRad54 (Fig. 4), it was of considerable interest to examine the influence of hRad54 on hRad51-mediated homologous DNA pairing.

The homologous pairing assay monitors the incorporation of a ^{32}P-labeled single-stranded oligonucleotide into a homologous supercoiled target (pBluescript) to give a D-loop structure (Fig. 5*A*). As reported before (25) and reiterated here (Fig. 5*B*), hRad51 by itself is not particularly adept at forming D-loop. Importantly, the inclusion of hRad54 rendered D-loop formation possible. D-Loop formation by the combination of hRad51 and hRad54 requires ATP hydrolysis, because no D-loop was seen when ATP was omitted or when it was replaced by either ATPγS or AMP-PNP (Fig. 5*B*). Significantly, the time course revealed a cycle of rapid formation and disruption of D-loop, such that the D-loop level reached its maximum by 1 min but declined rapidly thereafter (Fig. 5, *B* and *D*). In fact, by the reaction end point of 6 min, little or no D-loop remained (Fig. 5, *B* and *D*). Such a cycle of D-loop synthesis and reversal seems to be a general characteristic for the RecA/Rad51 class of recombinases (26, 27). Because the RecA-ssDNA nucleoprotein filament disassembles upon ATP hydrolysis (24), we considered the possibility that the dissociation of D-loop seen here (Fig. 5*B*) could be related to ATP hydrolysis-mediated turnover of hRad51. To test this premise, we used the hrad51 K133R mutant protein, which binds but does not hydrolyze ATP (20), with hRad54 in the D-loop assay. True to prediction, with hrad51 K133R, the D-loop amount increased with time, reaching a much higher final level than when hRad51 was used (Fig. 5, *B–D*); by 4 min, 23% of the input ssDNA or 55% of the pBluescript plasmid DNA had been incorporated into the D-loop structure. As expected, with both hRad51/hRad54 and hrad51 K133R/hRad54, formation of D-loop required both the 90-mer substrate and the pBluescript target, and substitution of the pBluescript DNA with the heterologous φX174 DNA completely abolished D-loop formation (data not shown).

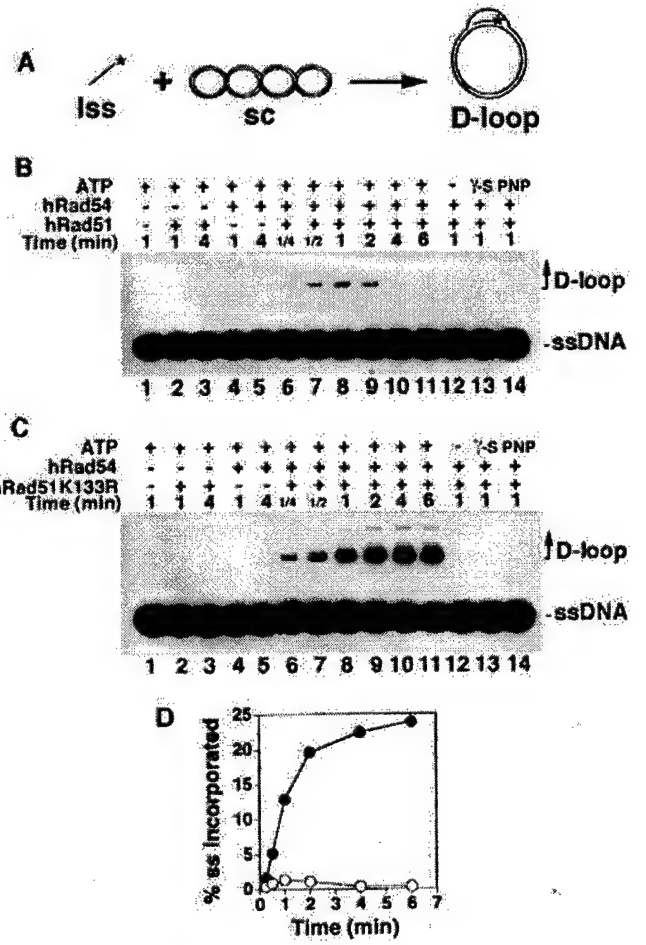

FIG. 5. **D-Loop formation by hRad51 and hRad54.** *A*, schematic of assay. A radiolabeled 90-mer DNA pairs with a homologous duplex target to yield a D-loop. *B*, hRad51 alone (*lanes 2* and *3*), hRad54 alone (*lanes 4* and *5*), and the combination of hRad51 and hRad54 (*lanes 6–14*) were incubated at 30 °C for the indicated times with the DNA substrates in the presence of ATP (*lanes 2–11*), ATPγS (*γS*; *lane 13*), or AMP-PNP (*PNP*; *lane 14*) or in the absence of nucleotide (*lane 12*). In *lane 1*, the DNA substrates were incubated in buffer without protein. The protein and DNA concentrations were as follows: hRad51, 800 nM; hRad54, 120 nM; 90-mer oligonucleotide, 2.5 μM nucleotides or 27.7 nM oligonucleotide; pBluescript supercoiled DNA, 35 μM base pairs or 11.6 nM plasmid. *C*, the homologous pairing activity of hrad51 K133R was examined with hRad54 as described for hRad51 above. *D*, the results in *lanes 6–11* of *B* (○) and *C* (●) were graphed.

positive supercoils ahead of the protein movement and negative supercoils tailing it (15, 18). As a result of interaction with hRad51, the ATPase, DNA supercoiling, and DNA strand opening activities of Rad54 are greatly enhanced (this work). Petukhova *et al.* (19) first reported that yRad54 enhances homologous DNA pairing by yRad51. Here we have presented biochemical evidence that hRad51 and hRad54 also work in concert to make DNA joints. Interestingly, the hRad51/hRad54-mediated D-loop reaction undergoes a rapid cycle of joint formation and dissociation. We have speculated that ATP hydrolysis by hRad51 could have resulted in its turnover from the bound ssDNA. This might have led to the transfer of hRad51/hRad54 to the displaced strand in the D-loop to initiate a second round of homologous pairing with the newly formed DNA joint. The presumed secondary pairing reaction could have accounted for the dissociation of the initial D-loop. Consistent with this hypothesis, the ATP hydrolysis-defective hrad51 K133R mutant is much more adept at forming D-loop than the wild type protein. Previously, studies in yeast and chicken DT40 cells with the same Rad51 ATPase mutant have

DISCUSSION

It has been deduced from biochemical and scanning force microscopy analyses that Rad54 tracks on DNA, producing

shown that it is biologically active but that an increased level of this mutant is needed for full complementation of the various phenotypes of Rad51-deficient cells (20, 28). The fact that the hrad51 K133R mutant is even more effective than the wild type protein in the D-loop reaction strongly suggests that the slighted biological efficacy (20, 28) and observed dominance (29) of this protein are because of a reason other than a diminished ability to mediate homologous pairing. The hrad51 K133R mutant may form a highly stable complex with DNA, thus reducing the effective concentration of free protein available for recombination reactions. Importantly, our biochemical results predict that other members of the *RAD52* group may function to prevent reversal of the D-loop reaction catalyzed by hRad51/hRad54.

Inactivation of the hRad54 ATPase activity impairs the ability to carry out recombination *in vivo* (14), consistent with the premise that the ATP hydrolysis-dependent DNA supercoiling and DNA strand opening activities of hRad54 are germane for recombination. As discussed here and elsewhere (15, 18, 30), it is likely that the DNA strand opening activity of hRad54 promotes the acquisition of an unwound DNA structure conducive for the formation of the nascent DNA joint that links recombining chromosomes. The ability of hRad54 to pull the incoming duplex molecule through its fold (*i.e.* tracking) is also expected to enhance the rate at which the duplex can be sampled by the hRad51-ssDNA nucleoprotein filament for homology. Finally, it remains a distinct possibility that the dynamic DNA topological changes induced by the combination of hRad51 and hRad54 are critical for the remodeling of chromatin during recombination.

Acknowledgment—We thank Toshiyuki Habu for helping with plasmid constructions.

REFERENCES

1. Paques, F., and Haber, J. E. (1999) *Microbiol. Mol. Biol. Rev.* **63,** 349–404
2. Sung, P., Trujillo, K., and Van Komen, S. (2000) *Mutat. Res.* **451,** 257–275
3. Pierce, A. J., Stark, J. M., Araujo, F. D., Moynahan, M. E., Berwick, M., and Jasin, M. (2001) *Trends Cell Biol.* **11,** S52–59
4. Shinohara, A., Ogawa, H., Matsuda, Y., Ushio, N., Ikeo, K., and Ogawa, T. (1993) *Nat. Genet.* **4,** 239–243
5. Yu, X., Jacobs, S. A., West, S. C., Ogawa, T., and Egelman, E. H. (2001) *Proc. Natl. Acad. Sci. U. S. A.* **17,** 8419–8424
6. Baumann, P., Benson, F. E., and West, S. C. (1996) *Cell* **87,** 757–766
7. Gupta, R. C., Bazemore, L. R., Golub, E. I., and Radding, C. M. (1997) *Proc. Natl. Acad. Sci. U. S. A.* **94,** 463–468
8. Sigurdsson, S., Trujillo, K., Song, B.-W., Stratton, S., and Sung P. (2001) *J. Biol. Chem.* **276,** 8798–8806
9. Benson, F. E., Baumann, P., and West, S. C. (1998) *Nature* **391,** 401–404
10. Sigurdsson, S., Van Komen, S., Bussen, W., Schild, D., Albala, J. S., and Sung, P. (2001) *Genes Dev.* **15,** 3308–3318
11. Sung, P. (1997) *Genes Dev.* **11,** 1111–1121
12. Eisen, J. A., Sweder, K. S., and Hanawalt, P. C. (1995) *Nucleic Acids Res.* **23,** 2715–2723
13. Swagemakers, S. M. A., Essers, J., de Wit, J., Hoeijmakers, J. H. J., and Kanaar, R. (1998) *J. Biol. Chem.* **273,** 28292–28297
14. Tan, T. L., Essers, J., Citterio, E., Swagemakers, S. M., de Wit, J., Benson, F. E., Hoeijmakers, J. H., and Kanaar, R. (1999) *Curr. Biol.* **9,** 325–328
15. Ristic, D., Wyman, C., Paulusma, C., and Kanaar, R. (2001) *Proc. Natl. Acad. Sci. U. S. A.* **84,** 8454–8460
16. Sung, P., Prakash, L., Matson, S. W., and Prakash, S. (1987) *Proc. Natl. Acad. Sci. U. S. A.* **84,** 8951–8955
17. Lynn, R. M., and Wang, J. C. (1989) *Proteins* **6,** 231–239
18. Van Komen, S., Petukhova, G., Sigurdsson, S., Stratton, S., and Sung, P. (2000) *Mol. Cell* **6,** 563–572
19. Petukhova, G., Stratton, S., and Sung, P. (1998) *Nature* **393,** 91–94
20. Morrison, C., Shinohara, A., Sonoda, E., Yamaguchi-Iwai, Y., Takata, M., Weichselbaum, R. R., and Takeda, S. (1999) *Mol. Cell. Biol.* **19,** 6891–6897
21. Kanaar, R., Troelstra, C., Swagemakers, S. M., Essers, J., Smit, B., Franssen, J. H., Pastink, A., Bezzubova, O. Y., Buerstedde, J. M., Clever, B., Heyer, W. D., and Hoeijmakers, J. H. (1996) *Curr. Biol.* **6,** 828–838
22. Golub, E. I., Kovalenko, O. V., Gupta, R. C., Ward, D. C., and Radding, C. M. (1997) *Nucleic Acids Res.* **25,** 4106–4110
23. Benson, F. E., Stasiak, A., and West, S. C. (1994) *EMBO J.* **13,** 5764–5771
24. Bianco, P. R., Tracy, R. B., and Kowalczykowski, S. C. (1998) *Front. Biosci.* **3,** D580–603
25. Mazin, A. V., Zaitseva, E., Sung, P., and Kowalczykowski, S. C. (2000) *EMBO J.* **19,** 1148–1156
26. Shibata, T., Ohtani, T., Iwabuchi, M., and Ando, T. (1982) *J. Biol. Chem.* **10,** 13981–13986
27. McIlwraith, M. J., Van Dyck, E., Masson, J. Y., Stasiak, A. Z., Stasiak, A., and West, S. C. (2000) *J. Mol. Biol.* **304,** 151–164
28. Sung, P., and Stratton, S. A. (1996) *J. Biol. Chem.* **271,** 27983–27986
29. Stark, J. M., Hu, P., Pierce, A. J., Moynahan, M. E., Ellis, N., and Jasin, M. (2002) *J. Biol. Chem.* **277,** 20185–20194
30. Mazin, A. V., Bornarth, C. J., Solinger, J. A., Heyer, W. D., and Kowalczykowski, S. C. (2000) *Mol. Cell* **6,** 583–592

Mediator function of the human Rad51B–Rad51C complex in Rad51/RPA-catalyzed DNA strand exchange

Stefan Sigurdsson,[1] Stephen Van Komen,[1] Wendy Bussen,[1] David Schild,[2] Joanna S. Albala,[3] and Patrick Sung[1,4]

[1]Department of Molecular Medicine/Institute of Biotechnology, University of Texas Health Science Center at San Antonio, San Antonio, Texas 78245-3207, USA; [2]Life Science Division, Lawrence Berkeley National Laboratory, Berkeley, California 94720, USA; [3]Biology and Biotechnology Research Program, Lawrence Livermore National Laboratory, Livermore, California 94551-0808, USA

Five Rad51-like proteins, referred to as Rad51 paralogs, have been described in vertebrates. We show that two of them, Rad51B and Rad51C, are associated in a stable complex. Rad51B–Rad51C complex has ssDNA binding and ssDNA-stimulated ATPase activities. We also examined the functional interaction of Rad51B–Rad51C with Rad51 and RPA. Even though RPA enhances Rad51-catalyzed DNA joint formation via removal of secondary structure in the ssDNA substrate, it can also compete with Rad51 for binding to the substrate, leading to suppressed reaction efficiency. The competition by RPA for substrate binding can be partially alleviated by Rad51B–Rad51C. This recombination mediator function of Rad51B–Rad51C is likely required for the assembly of the Rad51-ssDNA nucleoprotein filament in vivo.

[*Key Words:* DNA double-strand break repair; tumor suppression]

Received August 7, 2001; revised version accepted October 17, 2001.

Studies in *Saccharomyces cerevisiae* have identified a large number of genetic loci required for mitotic and meiotic recombination. These genes, comprising *RAD50, RAD51, RAD52, RAD54, RAD55, RAD57, RAD59, RDH54/TID1, MRE11,* and *XRS2* are collectively known as the *RAD52* epistasis group. The *RAD52* group of genes are also intimately involved in the repair of DNA double-strand breaks induced by exogenous agents such as ionizing radiation (Paques and Haber 1999; Sung et al. 2000) and for telomere maintenance in the absence of telomerase.

Cloning, genetic, and biochemical studies have indicated that the structure and function of the *RAD52* group genes are highly conserved among eukaryotes, from yeast to humans (Sung et al. 2000; Thompson and Schild 2001). Interestingly, in mammals, the efficiency of recombination and DNA double-strand break repair is contingent upon the integrity of the tumor suppressors BRCA1 and BRCA2 (Dasika et al. 1999; Moynahan et al. 1999, 2001; Thompson and Schild 2001), underscoring the importance for deciphering the mechanistic basis of the recombination machinery.

[4]**Corresponding author.**
E-MAIL sung@uthscsa.edu; FAX (210) 567-7277.
Article and publication are at http://www.genesdev.org/cgi/doi/10.1101/gad.935501.

In recombination processes that involve the formation of a DNA double-strand break, the ends of the DNA break are processed to yield single-stranded DNA tails. These DNA tails are utilized by the *RAD52* group recombination factors for the formation of DNA joints with a homologous DNA template, contained within the sister chromatid or the chromosomal homolog. The nascent DNA joints are then extended in length by branch migration, followed by resolution of DNA intermediates to complete the recombination process (Paques and Haber 1999; Sung et al. 2000).

The *RAD51* encoded product is the functional homolog of *Escherichia coli* RecA protein, and like RecA, possesses the ability to promote the homologous DNA pairing and strand exchange reaction that forms heteroduplex DNA joints. In mediating homologous DNA pairing and strand exchange, Rad51 must first assemble onto ssDNA as a nucleoprotein filament, in which the DNA is held in a highly extended conformation (Ogawa et al. 1993; Benson et al. 1994; Sung and Robberson 1995). Assembly of the Rad51-ssDNA nucleoprotein filament is rate-limiting and strongly inhibited by secondary structure in the ssDNA template. The removal of secondary structure can be effected by the single-strand DNA binding protein RPA, which has proved to be indispensable for homologous DNA pairing and strand exchange effi-

ciency, especially when a plasmid-length ssDNA template is used as the initiating substrate (Sung et al. 2000; Sigurdsson et al. 2001).

Even though RPA is an important accessory factor for Rad51-mediated homologous DNA pairing and strand exchange, it can also compete with Rad51 for binding sites on the ssDNA template, which, when allowed to occur, suppresses pairing and strand exchange efficiency markedly (Sung et al. 2000). Here we demonstrate that the stoichiometric complex of the human Rad51B and Rad51C proteins, homologs of the *S. cerevisiae* Rad55 and Rad57 proteins (Sung et al. 2000), can partially overcome the suppressive effect of hRPA on hRad51-catalyzed DNA pairing and strand exchange, thus identifying the Rad51B–Rad51C complex as a mediator of recombination.

Results

Rad51B and Rad51C are associated in a stable complex

Because Rad51B and Rad51C interact in two-hybrid studies (Schild et al. 2000), we wished to address whether they are associated in human cells. For detecting Rad51B and Rad51C, we raised antibodies against these proteins expressed in *E. coli* and purified from inclusion bodies by preparative SDS-PAGE. The specificity of the anti-Rad51B and anti-Rad51C antibodies is shown in Figure 1A, in the left and right panels, in which extracts from yeast cells harboring the empty protein expression vector and plasmids expressing Rad51B and Rad51C were probed with the antibodies. A single 40-kD Rad51B and 42-kD Rad51C species was detected. The observed sizes of Rad51B and Rad51C are in good agreement with the predicted values of 39 kD for Rad51B and 42 kD for Rad51C. Furthermore, Rad51B and Rad51C endogenous to human HeLa cells have the same gel sizes as proteins expressed in yeast cells (see below). In both the immunoblot analysis (Fig. 1A) and immunoprecipitation (data not shown), the anti-Rad51B antibodies did not cross-react with Rad51C protein, nor did the anti-Rad51C antibodies cross-react with Rad51B protein.

To identify Rad51B and Rad51C endogenous to human cells, an extract from HeLa cells was fractionated in a Q Sepharose column, and the column fractions were subjected to immunoblotting analysis. In this analysis, we used extracts from yeast cells expressing Rad51B and Rad51C (Fig. 1B, lane 10 in both panels) to aid in the identification of the endogenous proteins. The results (Fig. 1B) showed that Rad51B and Rad51C coeluted from Q Sepharose precisely, from fractions 8 to 16. To investigate whether Rad51B and Rad51C in the Q Sepharose fractions were stably associated, we examined whether they could be coimmunoprecipitated. As shown in Figure 1C, anti-Rad51B antibodies precipitated not only Rad51B, but also Rad51C. Similarly, Rad51B coprecipitated with Rad51C in the anti-Rad51C immunoprecipitation (Fig. 1C). Importantly, the quantity of Rad51B and Rad51C that coprecipitated with the other protein was similar to the amount of these proteins precipitated by their cognate antibodies, suggesting that Rad51B and Rad51C in the Q column fractions were associated as a stable complex. Neither Rad51B nor Rad51C was precipitated by control antibodies raised against yeast Srs2 protein (Fig. 1C). Rad51C also forms a complex with XRCC3 (Schild et al. 2000; Kurumizaka et al. 2001; Mas-

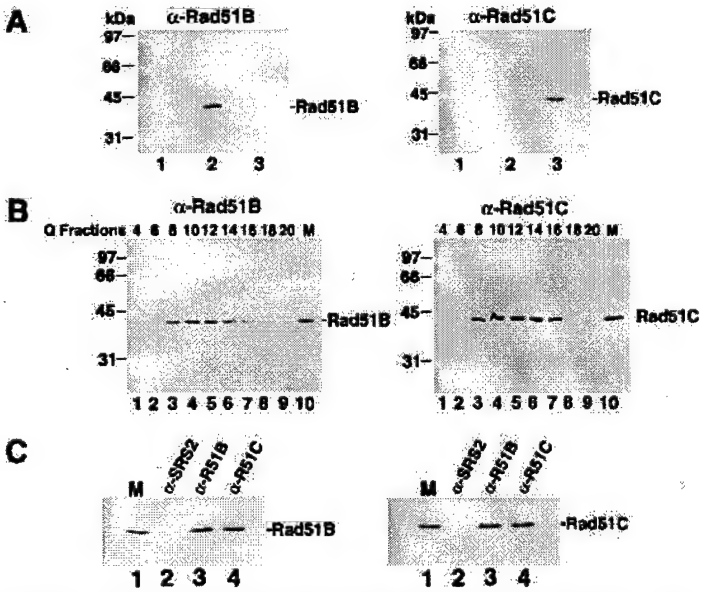

Figure 1. Rad51B and Rad51C form a stable complex. (*A*) Specificity of antibodies. Yeast cells harboring the empty expression vector pPM231 (*2μ, GAL-PGK;* lane *1*), the Rad51B expression plasmid pR51B.1 (*2μ, GAL-PGK-RAD51B;* lane *2*), and the Rad51C expression plasmid pR51C.1 (*2μ, PGK-RAD51C;* lane *3*) were run in an 11% polyacrylamide gel and then subjected to immunoblot analysis with either anti-Rad51B (αRad51B; *left* panel) or anti-Rad51C antibodies (αRad51C; *right* panel). (*B*) Rad51B and Rad51C are associated in a complex in human cells. HeLa cell extract was fractionated in a Q Sepharose column, and the indicated fractions were run in an 11% gel and then subjected to immunoblot analysis with anti-Rad51B antibodies (α-Rad51B; *left* panel) or anti-Rad51C antibodies (α-Rad51C; *right* panel). Yeast extracts containing Rad51B (lane *10* in *left* panel, marked M) or Rad51C (lane *10* in *right* panel, marked M) were used to help identify these proteins in the Q column fractions. (*C*) Coimmunoprecipitation of Rad51B and Rad51C from the Q column fractions. The Q Sepharose pool (fractions 8–16) was subjected to immunoprecipitation with protein A beads containing anti-ySrs2 antibodies (α-SRS2), anti-Rad51B antibodies (α-R51B) and anti-Rad51C antibodies (α-R51C). Proteins bound to the various immunobeads were eluted by SDS treatment and analyzed for their content of Rad51B (*left* panel) and Rad51C (*right* panel).

son et al. 2001), and it remains possible that a portion of Rad51C in the Q Sepharose fractions was bound to XRCC3 or that the XRCC3-Rad51C complex was not retained on the Q column.

The results above indicated that Rad51B and Rad51C are associated in a stable complex in HeLa cell extract, but they could not address whether association of these two proteins was due to direct interaction between them or whether an intermediary is required. To determine whether Rad51B and Rad51C interact directly, we carried out immunoprecipitation using extracts from yeast cells that expressed these two factors. As expected, Rad51B and Rad51C were precipitated by their cognate antibodies but not by antibodies specific for the other protein (data not shown). Importantly, upon mixing of the extracts containing Rad51B and Rad51C, coprecipitation of the two proteins occurred (data not shown). Direct interaction between Rad51B and Rad51C was demonstrated another way. In this case, we constructed recombinant baculoviruses that encoded a six-histidine-tagged form of Rad51B and an untagged form of Rad51C. The expression of Rad51B and Rad51C in insect cells infected separately with these baculoviruses was verified by immunoblotting (Fig. 2A). Because Rad51B was tagged with a six-histidine sequence, we could in this instance use affinity binding of the six-histidine tag to nickel-NTA agarose as criterion for protein–protein interaction when extracts were mixed. As summarized in Figure 2B, untagged Rad51C alone did not bind the nickel matrix, whereas a significant portion of it was retained on the affinity matrix in the presence of six-histidine-tagged Rad51B. Taken together, these results made it clear that Rad51B and Rad51C form a stable complex via direct interaction. The results presented below further indicated that the complex of Rad51B and Rad51C is highly stable, and contains stoichiometric amounts of the two proteins.

Rad51C expressed in insect cells consists of two closely spaced species (Fig. 2A,B), with the top band having the same gel mobility as Rad51C seen in extract from HeLa cells or yeast cells expressing this protein (data not shown). The slower migrating species of the two Rad51C immunoreactive bands is likely full-size Rad51C, whereas the faster migrating form, which represents ~60% of the total Rad51C amount, could be a proteolytic product or the result of an aberrant expression in insect cells.

Expression and purification of the Rad51B–Rad51C complex

We used insect cells as the medium for the purification of the Rad51B–Rad51C complex for the following two reasons: (1) much larger amounts of Rad51B–Rad51C complex can be obtained from insect cells infected with the recombinant baculoviruses than from HeLa cell extract or yeast cells harboring the Rad51B and Rad51C expression plasmids, and (2) the six-histidine tag engineered in the recombinant Rad51B baculovirus allowed

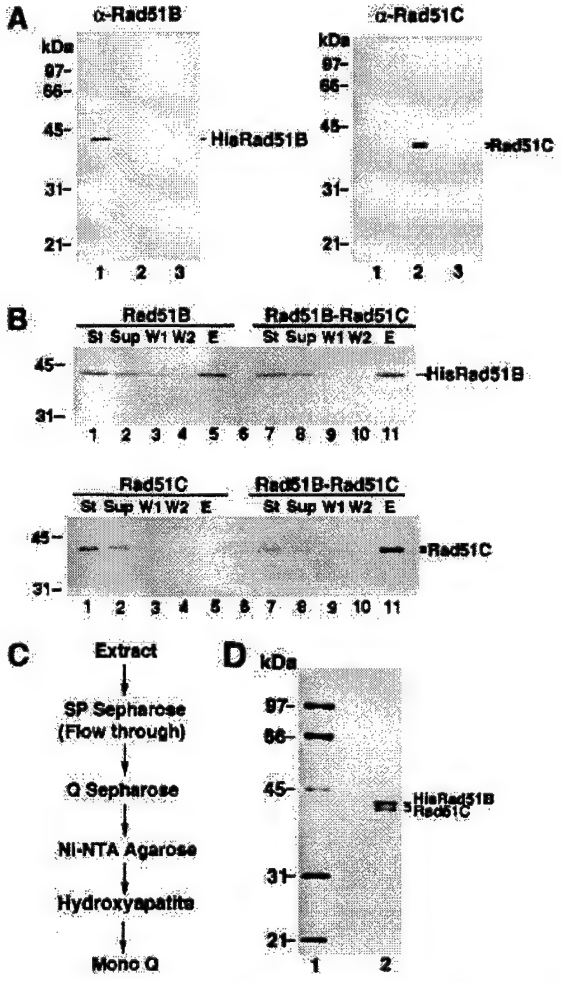

Figure 2. Purification of Rad51B and Rad51C from insect cells. (*A*) Expression of six-histidine-tagged Rad51B and Rad51C in insect cells. Nitrocellulose blots containing extracts from insect cells without any baculovirus (lane *3* of both panels) and infected with the recombinant 6His-tagged Rad51B baculovirus (lane *1* of both panels) or Rad51C baculovirus (lane *2* of both panels) were probed with either anti-Rad51B antibodies (αRad51B; *left* panel) or anti-Rad51C antibodies (αRad51C; *right* panel). (*B*) Complex formation between 6His-tagged Rad51B and Rad51C. Extracts from insect cells expressing 6His-tagged Rad51B (Rad51B), Rad51C (Rad51C), and the mixture of these extracts (Rad51B–Rad51C) were incubated with nickel-NTA agarose beads, which were washed with 10 mM, 20 mM, and then with 150 mM imadazole. The starting fractions (St), the supernatants containing unbound proteins (Sup), the 10 mM (W1) and 20 mM (W2) imidazole washes, and the 150 mM imidazole eluate (E) were subjected to immunoblotting to determine their content of Rad51B (*upper* panel) and Rad51C (*lower* panel). (*C*) Purification scheme for Rad51B–Rad51C complex. (*D*) Purity analysis. The purified Rad51B–Rad51C complex, 1.5 μg in lane *2*, was run alongside molecular size markers (lane *1*) in an 11% denaturing polyacrylamide gel and stained with Coomassie blue.

us to use nickel-NTA agarose as an affinity step to facilitate the purification of this complex.

We initially attempted to purify Rad51B and Rad51C individually, but our efforts were hampered by the complications that a significant portion (>75%) of these two proteins was insoluble and the soluble portion gave broad peaks during chromatographic fractionation procedures. To determine whether the Rad51B–Rad51C complex might be more amenable to purification than the individual components, we coinfected the Rad51B and Rad51C recombinant baculoviruses into insect cells. Interestingly, coexpression of Rad51B and Rad51C improved the solubility of these two proteins, even though the overall protein amounts in the infected insect cells remained relatively unchanged (data not shown). Importantly, the Rad51B–Rad51C complex eluted from various chromatographic matrices as relatively well defined peaks, thus enabling us to obtain substantial purification of the complex. Through many small-scale trials, a procedure was devised to encompass fractionation of insect cell extract containing the Rad51B–Rad51C complex in SP Sepharose, Q Sepharose, Hydroxyapatite, Mono Q, and affinity chromatography on nickel-NTA agarose (Fig. 2C) to purify this complex to near homogeneity (Fig. 2D). Stoichiometric amounts of Rad51B and Rad51C cofractionated during the entire purification procedure, indicating a high degree of stability of the complex. Using the aforementioned purification protocol, we could obtain about 100 μg of Rad51B–Rad51C complex from one liter of insect cell culture. Three independent preparations of Rad51B–Rad51C complex gave similar results in the experiments described below.

Rad51B–Rad51C complex binds DNA and hydrolyzes ATP

Because Rad51B and Rad51C are involved in recombination, we tested the purified Rad51B–Rad51C complex for binding to DNA. For this, an increasing amount of Rad51B–Rad51C complex was incubated with either ϕX ssDNA or dsDNA. The reaction mixtures were run in agarose gels, followed by staining with ethidium bromide to detect shifting of the DNA species. As shown in Figure 3A, while clear shifting of the ssDNA occurred at the lowest Rad51B–Rad51C concentration of 0.15 μM (DNA to protein ratio of 80 nucleotides/protein complex; see lane 2 of panel I), no shifting of the dsDNA was seen until the Rad51B–Rad51C concentration reached 0.6 μM (7 base pairs/protein complex; see lane 5 of panel II). These observations suggested that Rad51B–Rad51C complex binds ssDNA readily but has a lower affinity for dsDNA. To validate this conclusion, we repeated the DNA binding experiment by coincubating the ssDNA and dsDNA with the same concentration range of Rad51B–Rad51C used before. The results (Fig. 3A, panel III) revealed that Rad51B–Rad51C complex preferentially shifted the ssDNA without binding significantly to the dsDNA. In these experiments, ATP was included in the buffer used for the binding reaction, but the exclusion of ATP or its substitution with the nonhydrolyzable ATP-γ-S did not affect the binding results appreciably (data not shown). Taken together, these findings led us to conclude that the Rad51B–Rad51C complex binds ssDNA preferentially. We also examined ssDNA binding by Rad51B–Rad51C as a function of the ionic strength. To

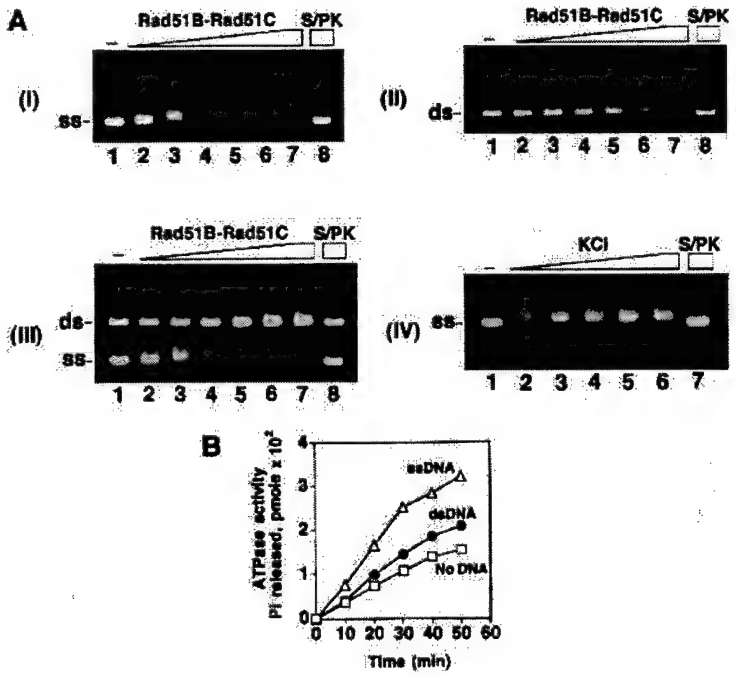

Figure 3. Rad51B–Rad51C binds DNA and hydrolyzes ATP. (*A*) Rad51B–Rad51C complex (0.15, 0.3, 0.45, 0.6, 0.75, and 0.9 μM in lanes *2–7*, respectively) was incubated with ϕX ssDNA (12 μM nucleotides in panel *I*; designated as ss), ϕX dsDNA (4 μM base pair in panel *II*; designated as ds), or with both the ssDNA and dsDNA (panel *III*) for 10 min at 37°C and then run in a 0.9% agarose gel. The DNA species were stained with ethidium bromide. In lane *8* of all three panels, the nucleoprotein complex formed with 0.9 μM of Rad51B–Rad51C complex was treated with 0.5% SDS and 500 μg/mL proteinase K at 37°C for 5 min before loading onto the agarose gel. In lane *1* of all three panels, DNA was incubated in buffer without protein. In panel *IV*, Rad51B–Rad51C complex (0.3 μM) was incubated with ssDNA (12 μM nucleotides) in the presence of increasing concentrations (50, 100, 150, 200, and 250 mM in lanes *2–6*, respectively) of KCl at 37°C for 10 min and then analyzed. (*B*) Rad51B–Rad51C, 1.8 μM, was incubated with 1 mM ATP in the absence of DNA (designated by the squares) and in the presence of ssDNA (20 μM nucleotides; designated by the triangles) or dsDNA (20 μM base pairs; designated by the closed circles) for the indicated times at 37°C.

do this, a fixed quantity of Rad51B–Rad51C complex (0.3 μM) was incubated with the ssDNA (12 μM nucleotides) in the presence of increasing concentrations (50, 100, 150, 200, and 250 mM) of KCl. The results (Fig. 3A, panel IV) showed that ssDNA binding was not diminished significantly by even the highest concentration of KCl (250 mM), indicating a high degree of avidity of Rad51B–Rad51C complex for the DNA.

Both Rad51B and Rad51C contain Walker ATP binding motifs, suggestive of an ability to bind and hydrolyze ATP (Sung et al. 2000; Thompson and Schild 2001). For this reason, we examined the purified Rad51B–Rad51C complex for ATPase activity. As shown in Figure 3B, Rad51B–Rad51C complex possesses an ATP hydrolytic activity that is stimulated by DNA. Reproducibly, ssDNA was more effective at stimulating ATP hydrolysis than was dsDNA. The kcat values for the Rad51B–Rad51C ATPase were found to be 0.15/min in the absence of DNA, and 0.19/min and 0.3/min in the presence of dsDNA and ssDNA, respectively.

Effects of RPA on Rad51-mediated DNA joint formation

Human Rad51 (hRad51) can make joints between homologous single-stranded and double-stranded DNA molecules, but was thought to have only limited DNA strand exchange activity (Baumann and West 1997, 1999; Gupta et al. 1997). We recently described a DNA strand exchange system (Fig. 4A) wherein hRad51 mediates a substantial amount of DNA strand exchange (Sigurdsson et al. 2001). In this new system, the efficiency of homologous DNA pairing and strand exchange is strongly dependent on the heterotrimeric ssDNA binding factor RPA. To assemble the reaction, hRad51 is preincubated with circular ssDNA at the optimal ratio of 4 nucleotides per protein monomer, followed by the addition of

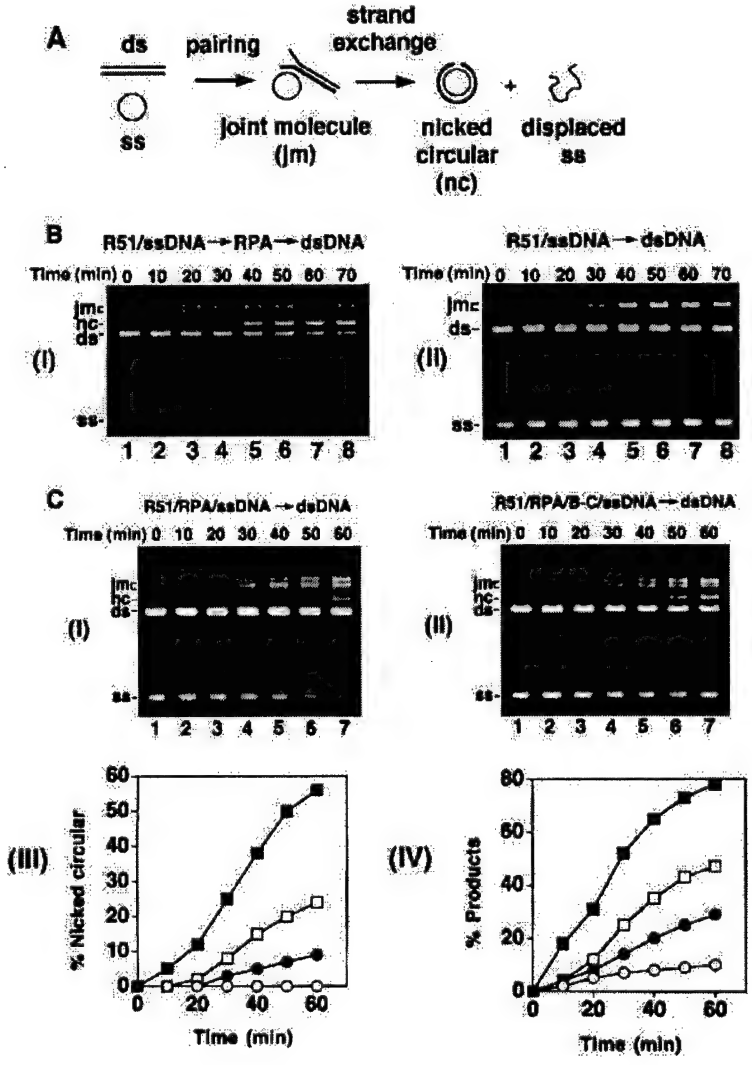

Figure 4. Mediator function of Rad51B–Rad51C. (*A*) Schematic of the homologous DNA pairing and strand exchange reaction using ϕX174 DNA substrates. Linear duplex is paired with the homologous ssDNA circle to yield a joint molecule. DNA strand exchange, if successful over the length (5.4 kb) of the DNA molecules, results in the formation of the nicked circular duplex. (*B*) Rad51-mediated DNA pairing and strand exchange was carried out with RPA (panel *I*) or without it (panel *II*). In panel *I*, the ssDNA was preincubated with Rad51 (R51) before RPA was added. The concentrations of the reaction components were: Rad51, 7.5 μM; RPA, 1.5 μM; ssDNA, 30 μM nucleotides; linear duplex, 15 μM base pairs. (*C*) In the DNA strand exchange reaction in panel *I*, the ssDNA was incubated with both Rad51 (R51) and RPA simultaneously, and in the reaction in panel *II*, the ssDNA was incubated with Rad51, RPA and Rad51B–Rad51C (*B–C*) simultaneously. The concentration of Rad51B–Rad51C was 0.8 μM, while the concentrations of the other components were exactly as those in *B*. In panel *III*, the amounts of nicked circular duplex in the reactions represented in *B* panel *I* (filled squares) and panel *II* (open circles) and in *C* panel *I* (filled circles) and panel *II* (open squares) are plotted. In panel *IV*, the amounts of total reaction products (sum of joint molecules and nicked circular duplex) in the reactions represented in *B* panel *I* (filled squares) and panel *II* (open circles) and in *C* panel *I* (filled circles) and panel *II* (open squares) are plotted.

hRPA at 20 nucleotides per protein monomer and the homologous linear duplex substrate (Fig. 4A). The reaction products, that is, joint molecules and nicked circular duplex (Fig. 4A), are separated from the input substrates by agarose gel electrophoresis and visualized by staining with ethidium bromide. An example of this reaction is shown in Figure 4B, panel I. As reported earlier (Sigurdsson et al. 2001) and reiterated here, omission of RPA from the reaction reduced the amount of products markedly (Fig. 4B, panel II). Importantly, little or no nicked circular duplex, the product of full strand exchange, was generated in the reaction that did not contain RPA (Fig. 4B, panel II).

Interestingly, coaddition of RPA with Rad51 to the ssDNA to mimic what may be expected to occur in vivo resulted in a marked reduction in reaction efficiency (Fig. 4C, panels I, III, and IV). Specifically, while ~38% and ~56% of the input linear duplex substrate had been converted into nicked circular duplex after 40 min and 60 min in the standard reaction (Fig. 4B, panel I and 4C, panel III), coaddition of hRPA with hRad51 to the ssDNA yielded only 5% and 9% of nicked circular duplex after these reaction time (Fig. 4C, panels I and III). In the homologous DNA pairing and strand exchange reaction mediated by *E. coli* RecA or yeast Rad51, SSB/yRPA added to the ssDNA template before or at the same time as the recombinase causes a notable suppression of the reaction as well (Umezu et al. 1993; Sung 1997a; New et al. 1998; Shinohara and Ogawa 1998). In these cases, suppression of the reaction efficiency by SSB/yRPA is due to competition of these ssDNA binding factors with RecA/yRad51 for sites on the ssDNA template. Based on the paradigm established with the *E. coli* and yeast recombination systems (Bianco et al. 1998; Sung et al. 2000), we also attribute the suppression of hRad51-mediated DNA pairing and strand exchange by hRPA to the exclusion of hRad51 from the ssDNA template.

Rad51B–Rad51C complex has a presynaptic mediator function

Rad51B and Rad51C are both required for recombination and DNA double-strand break repair in vivo. In chicken DT40 cells deleted for either Rad51B or Rad51C, the assembly of Rad51 nuclear foci in response to DNA damage is compromised (Takata et al. 2000, 2001). Based on these results, we wished to test whether Rad51B–Rad51C could promote homologous DNA pairing and strand exchange by Rad51 with RPA competing for binding sites on the initiating ssDNA substrate. To do this, we added Rad51B–Rad51C complex (0.8 μM) with Rad51 (7.5 μM) and RPA (1.5 μM) during the preincubation with ssDNA (30 μM), and then completed the reaction mixture by adding the homologous duplex. Importantly, upon inclusion of the Rad51B–Rad51C complex, significantly higher amounts of the reaction products were seen (Fig. 4C, panels II, III, and IV). In particular, the level of the nicked circular duplex, product of complete strand exchange (see Fig. 4A), was formed at a significantly higher rate than in the absence of Rad51B–Rad51C (Fig. 4C, panels II and III). We also examined whether amounts of Rad51B–Rad51C below and above that used before would lead to different levels of homologous DNA pairing and strand exchange. As shown in Figure 5, the optimal concentration of Rad51B–Rad51C was from 0.4 to 1.0 μM, and amounts of Rad51B–Rad51C above the optimal level in fact led to gradual inhibition of the reaction (Fig. 5; data not shown).

One possible explanation for the stimulatory effect of Rad51B–Rad51C complex (Fig. 5) is that this protein complex promotes homologous DNA pairing and strand exchange regardless of the order of addition of RPA. To test this possibility, we used the same amount of Rad51B–Rad51C complex (0.8 μM) that afforded the maximal restoration of DNA pairing and strand exchange (see Fig. 5A,B) in reactions wherein the protein complex was (1) added with Rad51 to the ssDNA substrate, followed by RPA; (2) added with RPA after Rad51 had already nucleated onto the ssDNA substrate; and (3) added after the ssDNA had first been incubated with Rad51 and then with RPA. No measurable effect of the Rad51B–Rad51C complex on the rate of formation of joint molecules and nicked circular duplex was recorded in any of these experiments (data not shown). We also tested whether the inclusion of Rad51B–Rad51C complex would alter the concentration of Rad51 needed for optimal pairing and strand exchange, determined previously to be from 3 to 4 nucleotides per Rad51 monomer (Baumann and West 1997, 1999; Gupta et al. 1997; Sigurdsson et al. 2001). However, Rad51B–Rad51C did not change the concentration of Rad51 needed for optimal reaction efficiency (data not shown).

To examine whether the Rad51B–Rad51C complex can substitute for RPA in the DNA pairing and strand exchange reaction, we used a range of Rad51B–Rad51C concentrations (0.4, 0.8, 1.2, and 2.0 μM) with a fixed concentration of Rad51 (7.5 μM) and ssDNA (30 μM) without RPA. Rad51B–Rad51C did not promote the formation of nicked circular duplex (Fig. 6) even after 60 min of reaction (data not shown), showing that it cannot substitute for RPA, which is highly effective in enabling Rad51 to make nicked circular duplex (Fig. 4; Sigurdsson et al. 2001). Interestingly, we observed an increase in joint molecules at 0.8 and 1.2 μM of Rad51B–Rad51C complex (Fig. 6). Specifically, after 30 min, the level of DNA joint molecules increased from ~5% in the absence of Rad51B–Rad51C to ~10% upon the inclusion of 1.2 μM Rad51B–Rad51C. As with the earlier strand exchange restoration experiment (Fig. 5), suppression of DNA joint molecule formation was seen at higher concentrations of the Rad51B–Rad51C complex (Fig. 6A,B; data not shown). In other experiments, over the range of Rad51B–Rad51C concentration from 3 to 45 nucleotides/protein complex, we did not detect any DNA joint molecule with the ϕX substrates, regardless of whether RPA was present (data not shown). These observations suggested that the Rad51B–Rad51C complex is devoid of homologous DNA pairing activity.

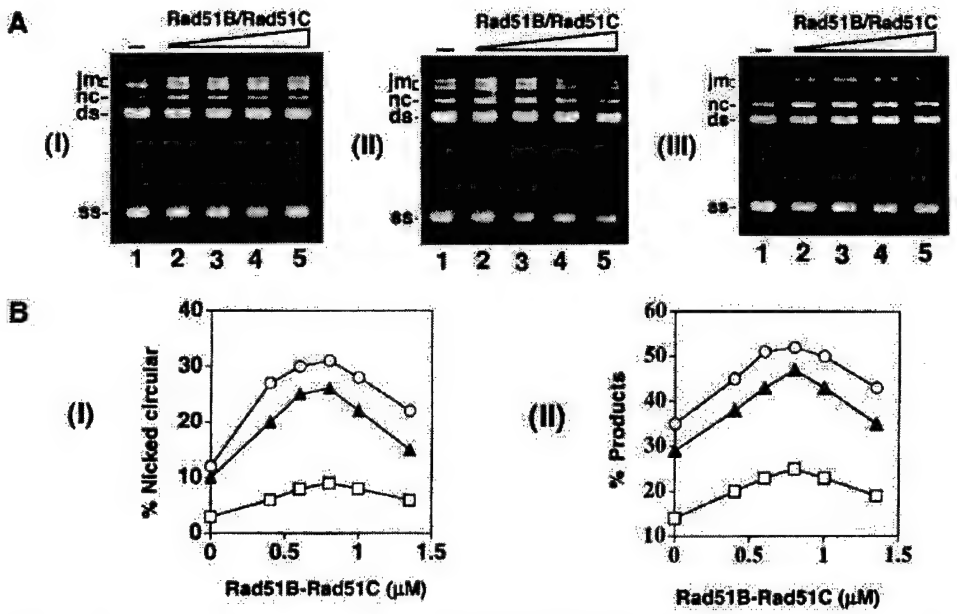

Figure 5. Mediator activity as a function of Rad51B–Rad51C concentration. (*A*) The ϕX174 ssDNA template (30 μM nucleotides) was incubated with Rad51 (7.5 μM), RPA (1.5 μM), and increasing concentrations of Rad51B–Rad51C (0, 0.6, 0.8, 1.0, and 1.4 μM in lanes *1–5*, respectively) for 10 min before the ϕX174 linear duplex (15 μM base pairs) was incorporated to complete the reaction mixtures. Portions of the reaction mixtures were withdrawn at 30 min (panel *I*), 60 min (panel *II*), and 80 min (panel *III*) and then processed for agarose gel electrophoresis. (*B*) The results from *A* and from two other independent experiments performed under the same reaction conditions were compiled and graphed. Symbols: results from the 30 min timepoint (squares), the 60 min timepoint (filled triangles), and the 80 min timepoint (circles). Panel *I* shows the levels of nicked circular duplex formed, and panel *II* shows the amounts of total reaction products (joint molecules and nicked circular duplex).

Discussion

Paradoxical effects of RPA on homologous DNA pairing and strand exchange

Like other members of the RecA/Rad51 class of recombinases (Ogawa et al. 1993; Sung and Robberson 1995; Roca and Cox 1997; Bianco et al. 1998), hRad51 assembles onto ssDNA to form a nucleoprotein filament in an ATP-dependent manner (Benson et al. 1994). Extensive biochemical studies with RecA have indicated that the search for DNA homology, DNA joint formation, and DNA strand exchange all occur within the confines of the RecA-ssDNA nucleoprotein filament. The assembly of the recombinase-ssDNA nucleoprotein filament is therefore the critical first step in the homologous DNA pairing and strand exchange reaction, and is generally referred to as the presynaptic phase of this reaction (Roca and Cox 1997; Bianco et al. 1998; Sung et al. 2000).

For RecA and yeast Rad51, the assembly of the presynaptic filament on plasmid-length DNA molecules is dependent on the cognate single-strand binding protein, *E. coli* SSB or yeast RPA, which acts to minimize the secondary structure in the DNA template and hence renders extension of the nascent nucleoprotein filament facile. In most experimental systems, the single-strand DNA binding factor is added subsequent to the recombinase, that is, after nucleation of the recombinase onto the ssDNA substrate has already commenced. Interestingly, precoating of the ssDNA template with the single-strand binding protein (Umezu et al. 1993; Sugiyama et al. 1997; New et al. 1998; Shinohara and Ogawa 1998) or coincubation of RPA, Rad51, and the ssDNA substrate (Sung 1997a,b) results in pronounced suppression of the reaction efficiency. We have shown in the present study that the hRad51 recombinase activity is similarly suppressed by RPA during the presynaptic phase. Taken together, the results indicate that the single-strand binding protein, while important for secondary structure removal in the ssDNA template, can interfere with the nucleation of the recombinase onto the DNA template and can thus prevent the formation of a contiguous presynaptic filament.

Mediator function in the Rad51B–Rad51C complex

Exploiting the paradoxical behavior of the single-strand DNA binding protein in the assembly of the presynaptic recombinase filament, various recombination mediator proteins capable of overcoming the suppressive effect of the single-strand binding protein have been identified in prokaryotes and yeast cells (Umezu et al. 1993; Sung 1997a,b; New et al. 1998; Shinohara and Ogawa 1998; Beernink and Morrical 1999). In yeast, two such mediators—Rad52 and the Rad55–Rad57 complex—have been

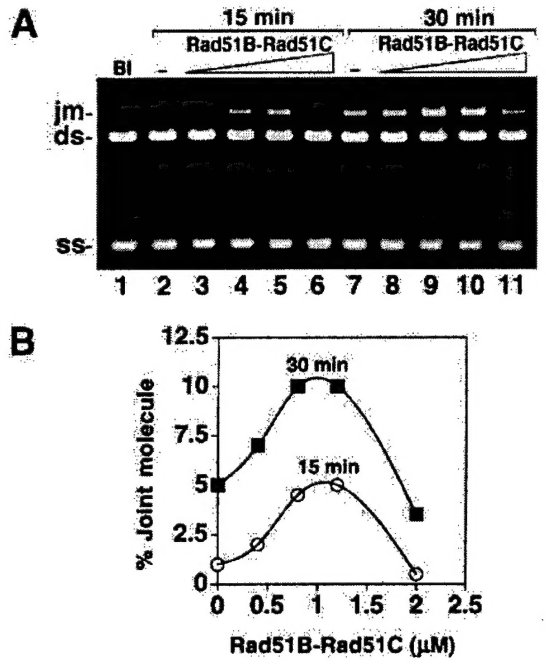

Figure 6. Rad51B–Rad51C stimulates DNA joint formation but does not replace RPA in DNA strand exchange. (*A*) Rad51 and Rad51B–Rad51C were used in the homologous DNA pairing and strand exchange reaction without RPA. The concentrations of the reaction components were: Rad51, 7.5 μM; Rad51B–Rad51C, 0.4 to 2 μM, as indicated; ssDNA, 30 μM nucleotides; linear duplex, 15 μM base pairs. (*B*) Graphic representation of the results from the experiment in *A*.

described. Rad55 and Rad57 are similar to Rad51B and Rad51C in that they too exhibit homology to Rad51 and form a stable stoichiometric complex via direct interaction (Sung et al. 2000). Importantly, both Rad51B–Rad51C and Rad55–Rad57 complexes are needed for the assembly of Rad51 nuclear foci in response to DNA damaging treatment (Gasior et al. 1998, 2001; Takata et al. 2000, 2001), which are thought to correspond to the sites of ongoing DNA damage repair.

We show here that purified Rad51B–Rad51C complex has single-strand DNA binding and ssDNA-stimulated ATPase activities. Importantly, Rad51B–Rad51C can promote the Rad51-mediated homologous DNA pairing and strand exchange reaction under conditions wherein Rad51 must contend with the competition by RPA for binding sites on the initiating ssDNA substrate. In addition, DNA joint formation by Rad51 in the absence of RPA is also enhanced by Rad51B–Rad51C. We asked whether Rad51B–Rad51C could stimulate the rate of DNA pairing and strand exchange, but did not uncover a postsynaptic role (Roca and Cox 1997; Bianco et al. 1998; Sung et al. 2000) in this protein complex. Rad51B–Rad51C complex did not pair the ϕX DNA substrates used, nor did it lower the concentration of Rad51 needed to attain optimal reaction efficiency. Thus, the results of our study suggest a specific role of Rad51B–Rad51C in promoting the assembly of the presynaptic Rad51 filament, identifying it as a mediator of recombination, in a manner analogous to what has been described for the yeast Rad55–Rad57 complex (Sung et al. 2000). Given that both Rad51B and Rad51C are indispensable for recombination and DNA repair and needed for the normal assembly of Rad51 nuclear foci after DNA damaging treatment, we surmise that the Rad51B–Rad51C mediator function likely contributes to the recruitment of hRad51 to sites of recombination and DNA damage repair.

Role of other Rad51 paralogs in recombination processes

Aside from Rad51B and Rad51C, three additional Rad51 paralogs, namely, XRCC2, XRCC3, and Rad51D, have been described (Thompson and Schild 2001). XRCC3 and Rad51C also form a stable complex that has DNA binding activity (Kurumizaka et al. 2001; Masson et al. 2001). Rad51D (also called Rad51L3) has DNA binding and ssDNA-stimulated ATPase activities, and it forms a stable complex with XRCC2 (Braybrooke et al. 2000). Whether the XRCC2–Rad51D and XRCC3–Rad51C complexes also have a recombination mediator function remains to be determined. However, that the formation of DNA damage-induced Rad51 nuclear foci is impaired in mutants of all five of the Rad51 paralogs would seem to suggest that they all play a role in the delivery of Rad51 to DNA lesions in vivo. It thus seems possible that some combination of complexes of the Rad51 paralogs could have an enhanced mediator function in the Rad51-catalyzed homologous DNA pairing and strand exchange reaction. In fact, our observation that Rad51B–Rad51C only partially overcomes the suppressive effect of RPA is consistent with such a scenario. It remains to be seen whether the other two Rad51 paralog pairs, either by themselves or in combination with each other and with Rad51B–Rad51C, may also function in the postsynaptic phase of the pairing and strand exchange reaction by enhancing the efficiency of DNA joint formation and promoting DNA branch migration.

Materials and methods

Antibodies

Rad51B protein was expressed in *E. coli* BL21 (DE3) using the T7 promoter in the vector pET11a. The insoluble Rad51B protein was purified by preparative SDS-PAGE, dialyzed into phosphate-buffered saline (10 mM NaH_2PO_4 at pH 7.2, 150 mM NaCl), and then used as antigen for production of antisera in rabbits. A GST–Rad51C fusion protein was expressed in *E. coli* BL21 (DE3) using the vector pGEX-2T. The GST–Rad51C fusion protein is also insoluble and was purified for antibody production in rabbits as described for Rad51B. The antigens were covalently conjugated to cyanogen bromide activated Sepharose 4B (Pharmacia-LKB) for use as affinity matrices to purify monospecific antibodies from rabbit antisera (Sung et al. 1987).

DNA substrates

ϕX174 viral (+) strand was purchased from New England Biolabs, and the ϕX174 replicative form I DNA was from GIBCO BRL. The replicative form I DNA was linearized with *Apa*LI. All of the DNA substrates were stored in TE (10 mM Tris-HCl at pH 7.5, 0.5 mM EDTA).

Fractionation of HeLa cell extract

To make extract, 10.4 g of HeLa S3 cells (National Cell Culture Center) was suspended in 15 mL of cell breakage buffer (50 mM Tris/HCl at pH 7.5, 2 mM EDTA, 10% sucrose, 100 mM KCl, 1 mM dithiothreitol and the following protease inhibitors: aprotinin, chymostatin, leupeptin, pepstatin, all at 3 μg/mL, and 1 mM phenylmethylsulfonyl fluoride) and passed through a French Press at 20,000 psi. After centrifugation (100,000*g* for 1 h), the clarified extract (20 mL) was loaded onto a column of Q-Sepharose (4 mL), which was fractionated with a 45 mL gradient of KCl from 100 to 600 mM in K buffer (20 mM KH_2PO_4 at pH 7.4, 0.5 mM EDTA, 1 mM DTT, and 10% glycerol) collecting 30 fractions. To identify the Rad51B and Rad51C proteins, the Q-Sepharose fractions (8 μL) were subjected to immunoblot analyses with anti-Rad51B and anti-Rad51C antibodies after SDS-PAGE in 11% gels.

Expression of Rad51B and Rad51C in yeast cells

The *RAD51B* gene was placed under the control of the *GAL-PGK* promoter in vector pPM231 (*2μ, GAL-PGK, LEU2d*) to yield pRad51B.1 (*2μ, GAL-PGK-RAD51B, LEU2d*) and *RAD51C* were placed under the control of the *PGK* promoter in vector pPM255 (*2μ, PGK, URA3*) to yield pRad51C.1 (*2μ, PGK-RAD51C, URA3*). The empty expression vector, pR51B.1, and pR51C.1 were introduced into the protease-deficient yeast strain BJ5464 (*MATα, ura3-52, trp-1, leu2Δ1, his3Δ200, pep4::HIS3, prbΔ1.6R*). Induction of Rad51B and Rad51C followed the protocol of Petukhova et al. (2000). Extracts (2 mL of buffer per gram of yeast cells) were prepared using a French press and clarified by centrifugation, as described above.

Purification of the Rad51B–Rad51C complex

Six-histidine (6His)-tagged Rad51B and untagged Rad51C recombinant baculoviruses were constructed by cloning the cDNAs for these proteins into the baculovirus transfer vector pVL1393 (Invitrogen). Amplification of the recombinant viruses was carried out in Sf9 cells and for protein expression, High-Five insect cells (Invitrogen) were infected with the 6His-tagged Rad51B and Rad51C baculoviruses at an MOI of 5. The insect cells were harvested 36–48 h postinfection. For the purification of the Rad51B–Rad51C complex, High-Five cells were coinfected with the Rad51B and Rad51C baculoviruses at an MOI of 5 for both viruses. The insect cells were harvested 36–48 h postinfection.

All the protein purification steps were carried out at 0 to 4°C. Cell lysate was prepared from 1 L of insect cell culture (15 g) using a French press in 60 mL of cell breakage buffer. The lysate was clarified by centrifugation (100,000*g* for 1 h) and the supernatant was applied on a 10 mL SP-Sepharose column. The flow-through from SP-Sepharose was then fractionated in a column of Q-Sepharose (10 mL of matrix) with a 30 mL, 100 to 600 mM KCl gradient in buffer K. Rad51B–Rad51C eluted from 200–300 mM KCl, and the peak fractions were pooled and mixed with 0.6 mL of Ni-NTA agarose for 2 h, followed by fractionation with a 15 mL, 0 to 250 mM imidazole in buffer K. The Rad51B–Rad51C peak fractions were pooled and further fractionated in a column of Macro-hydroxyapatite (0.5 mL matrix) with a 15 mL, 0 to 180 mM KH_2PO_4 gradient in buffer K. The peak fractions were pooled and dialyzed against buffer K with 50 mM KCl and applied onto a Mono Q column (HR5/5), which was developed with a 15 mL gradient from 100 to 800 mM KCl in buffer K. Rad51B–Rad51C from the Mono Q step was concentrated in a Centricon-30 microconcentrator to 2 mg/mL and stored at −70°C.

Immunoprecipitation

Affinity-purified anti-Rad51B, anti-Rad51C, and anti-ySrs2 antibodies, 1.0 mg each, were coupled to 300 μL protein A agarose beads as described previously (Sung 1997a). In Figure 1C, 0.3 mL of the Q-Sepharose pool (fractions 8 to 16) containing the Rad51B–Rad51C peak was mixed with 10 μL of protein A beads containing anti-Rad51B, anti-Rad51C, or anti-ySrs2 antibodies at 4°C for 5 h. The beads were washed twice with 200 μL of buffer K containing 1 M KCl and once with 200 μL of buffer K, before being eluted with 20 μL of 2% SDS at 37°C for 10 min. The SDS eluates, 2 μL each, were analyzed by immunoblotting to reveal their content of Rad51B and Rad51C.

Affinity binding of the Rad51B–Rad51C complex to nickel-NTA agarose

Extract from 0.5 mL packed cell volume of High-Five insect cells harboring either the six-histidine-tagged Rad51B or Rad51C recombinant baculovirus was prepared as described above, using 3 mL of cell breakage buffer. After ultracentrifugation (100,000*g* for 1 h), 0.25 mL of the Rad51B and Rad51C containing extracts were mixed either with each other or with 0.25 mL of extract from insect cells that did not contain any recombinant baculovirus. After incubation on ice for 1 h, the various mixtures were subjected to ultracentrifugation (100,000*g* for 1h), and then rocked gently with 50 μL of nickel-NTA agarose beads (QIAGEN) at 4°C for 3 h. The beads were washed sequentially with 0.2 mL of 10 mM and 20 mM imidazole, and then with 0.1 mL of 150 mM imidazole. The starting fractions, supernatants after nickel-binding, and the three imidazole washes, 5 μL each, were subjected to immunoblot analysis to determine their content of Rad51B and Rad51C.

Other recombination proteins

Human Rad51 (hRad51 Lys^{313}) was expressed in and purified from *E. coli* as described (Sigurdsson et al. 2001). Human RPA was purified from *E. coli* cells transformed with a plasmid that co-overexpresses the three subunits of this factor (Henricksen et al. 1994), as described (Sigurdsson et al. 2001). Both hRad51 and hRPA were nearly homogeneous.

Homologous DNA pairing and strand exchange reactions

All the reaction steps were carried out at 37°C. The reaction buffer was 40 mM Tris-HCl (pH 7.8), 2 mM ATP, 1 mM $MgCl_2$, and 1 mM DTT, and contained an ATP regenerating system consisting of 8 mM creatine phosphate and 28 μg/mL creatine kinase. The standard reaction had a final volume of 12.5 μL, and was assembled by first incubating hRad51 (7.5 μM) added in 0.5 μL of storage buffer and ϕX174 viral (+) strand (30 μM nucleotides) added in 1 μL for 5 min. After this, hRPA (1.5 μM) in 0.5 μL of storage buffer was added and following a 5 min incubation, 1.25 μL of ammonium sulfate (1 M stock, final concentration of

100 mM) was incorporated. Immediately afterward, linear ϕX174 replicative form I DNA (15 μM base pairs) in 1 μL was added to complete the reaction. At the indicated times, 5 μL portions were withdrawn, mixed with 7.5 μL of 0.8% SDS and 800 μg/mL proteinase K, incubated for 15 min at 37°C, before being run in 0.9% agarose gels in TAE buffer (40 mM Tris acetate at pH 7.4, 0.5 mM EDTA). The gels were stained in ethidium bromide (2 μg/mL in H_2O) for 1 h, destained for 12 to 18 h in a large volume of water at 4°C, and then subjected to image analysis in a NucleoTech gel documentation station equipped with a CCD camera. In some experiments, the reaction was scaled up appropriately to accommodate the increased number of timepoints used. In Figure 4B, panel II, storage buffer was added instead of RPA, but otherwise the reaction was assembled in exactly the same manner as the standard reaction. In Figure 5A, panel I, Rad51 and RPA were added together to ssDNA at the beginning of the reaction and incubated for 10 min with the latter, but otherwise the additions of the ammonium sulfate and linear ϕX duplex followed the procedure described for the standard reaction. In Figure 5A, panel II and in Figure 5B, Rad51, RPA, and the indicated amounts of Rad51B–Rad51C were incubated with the ssDNA for 10 min, but otherwise the additions of the ammonium sulfate and linear ϕX duplex followed the procedure described for the standard reaction. In Figure 6, Rad51 and the indicated amounts of Rad51B–Rad51C were incubated with the ssDNA for 10 min, but otherwise the additions of the ammonium sulfate and linear ϕX duplex followed the procedure described for the standard reaction.

DNA mobility shift and ATPase assays

The indicated amounts of Rad51B–Rad51C complex were incubated with ϕX ssDNA (12 μM nucleotides), dsDNA (4 μM base pairs), or both ssDNA (12 μM nucleotides) and dsDNA (4 μM base pairs) in reaction buffer (50 mM Tris-HCl at pH 7.8, 1 mM DTT, 100 μg/mL BSA, 1 mM $MgCl_2$, 1 mM ATP, and 100 mM KCl) for 10 min at 37°C. After electrophoresis in 0.9% agarose gels in TAE buffer at 4°C, the gels were stained in ethidium bromide (2 μg/mL in H_2O) for 1 h and destained at 4°C for 12 to 18 h, before being subjected to image analysis in the gel documentation station.

Rad51B–Rad51C (1.8 μM) was incubated in the absence or presence of ssDNA (20 μM nucleotides) or dsDNA (20 μM base pairs) in 10 μL of reaction buffer (50 mM Tris-HCl at pH 7.8, 1 mM DTT, 1 mM $MgCl_2$) containing 1 mM [γ-^{32}P]ATP for the indicated times at 37°C. The level of ATP hydrolysis was determined by thin layer chromatography as described previously (Petukhova et al. 2000).

Acknowledgments

We thank Susie Zhang for constructing the Rad51C recombinant baculovirus. This work was supported by Public Health Service grants PO1CA81020, GM57814, ES07061, GM30990, CA81019-01 and by California Breast Cancer Research Program grant 5KB-0123. S.S. was supported in part by U.S. Army Training Grant DAMD17-99-1-9402 and Predoctoral Fellowship DAMD-17-01-1-0412. S.V.K. was supported in part by U.S. Army Predoctoral Fellowship DAMD-17-01-1-0414.

The publication costs of this article were defrayed in part by payment of page charges. This article must therefore be hereby marked "advertisement" in accordance with 18 USC section 1734 solely to indicate this fact.

References

Baumann, P. and West, S.C. 1997. The human Rad51 protein: Polarity of strand transfer and stimulation by hRP-A. *EMBO J.* **16:** 5198–5206.

———. 1999. Heteroduplex formation by human Rad51 protein: Effects of DNA end-structure, hRP-A and hRad52. *J. Mol. Biol.* **291:** 363–374.

Beernink, H.T. and Morrical, S.W. 1999. RMPs: Recombination/replication mediator proteins. *Trends. Biochem. Sci.* **24:** 385–389.

Benson, F.E., Stasiak, A., and West, S.C. 1994. Purification and characterization of the human Rad51 protein, an analogue of *E. coli* RecA. *EMBO J.* **23:** 5764–5771.

Bianco, P.R., Tracy, R.B., and Kowalczykowski, S.C. 1998. DNA strand exchange proteins: A biochemical and physical comparison. *Front. Biosci.* **3:** D570–D603.

Braybrooke, J.P., Spink, K.G., Thacker, J., and Hickson, I.D. 2000. The Rad51 family member, Rad51L3, is a DNA-stimulated ATPase that forms a complex with XRCC2. *J. Biol. Chem.* **275:** 29100–29106.

Dasika, G.K., Lin, S.C., Zhao, S., Sung, P., Tomkinson, A., and Lee, E.Y. 1999. DNA damage-induced cell cycle checkpoints and DNA strand break repair in development and tumorigenesis. *Oncogene* **18:** 7883–7899.

Gasior, S.L., Wong, A.K., Kora, Y., Shinohara, A., and Bishop, D.K. 1998. Rad52 associates with RPA and functions with rad55 and rad57 to assemble meiotic recombination complexes. *Genes & Dev.* **12:** 2208–2221.

Gasior, S.L., Olivares, H., Ear, U., Hari, D.M., Weichselbaum, R., and Bishop, D.K. 2001. Assembly of RecA-like recombinases: Distinct roles for mediator proteins in mitosis and meiosis. *Proc. Natl. Acad. Sci.* **98:** 8411–8418.

Gupta, R.C., Bazemore, L.R., Golub, E.I., and Radding, C.M. 1997. Activities of human recombination protein Rad51. *Proc. Natl. Acad. Sci.* **94:** 463–468.

Henricksen, L.A., Umbricht, C.B., and Wold, M.S. 1994. Recombinant replication protein A: Expression, complex formation, and functional characterization. *J. Biol. Chem.* **269:** 11121–11132.

Kurumizaka, H., Ikawa, S., Nakada, M., Eda, K., Kagawa, W., Takata, M., Takeda, S., Yokoyama, S., and Shibata, T. 2001. Homologous-pairing activity of the human DNA-repair proteins Xrcc3–Rad51C. *Proc. Natl. Acad. Sci.* **98:** 5538–5543.

Masson, J.Y., Stasiak, A.Z., Stasiak, A., Benson, F.E., and West, S.C. 2001. Complex formation by the human Rad51C and XRCC3 recombination repair proteins. *Proc. Natl. Acad. Sci.* **98:** 8440–8446.

Moynahan, M.E., Chiu, J.W., Koller, B.H., and Jasin, M. 1999. Brca1 controls homology-directed DNA repair. *Mol. Cell* **4:** 511–518.

Moynahan, M.E., Pierce, A.J., and Jasin, M. 2001. BRCA2 is required for homology-directed repair of chromosomal breaks. *Mol. Cell* **2:** 263–272.

New, J.H., Sugiyama, T., Zaitseva, E., and Kowalczykowski, S.C. 1998. Rad52 protein stimulates DNA strand exchange by Rad51 and replication protein A. *Nature* **391:** 407–410.

Ogawa, T., Yu, X., Shinohara, A., and Egelman, E.H. 1993. Similarity of the yeast RAD51 filament to the bacterial RecA filament. *Science* **259:** 1896–1899.

Paques, F. and Haber, J.E. 1999. Multiple pathways of recombination induced by double-strand breaks in *Saccharomyces cerevisiae*. *Microbiol. Mol. Biol. Rev.* **63:** 349–404.

Petukhova, G., Sung, P., and Klein, H. 2000. Promotion of Rad51-dependent D-loop formation by yeast recombination factor Rdh54/Tid1. *Genes & Dev.* **14:** 2206–2215.

Roca, A.I., and Cox, M.M. 1997. RecA protein: Structure, function, and role in recombinational DNA repair. *Prog. Nucleic. Acid. Res. Mol. Biol.* **56:** 129–223.

Schild, D., Lio, Y., Collins, D.W., Tsomondo, T., and Chen, D.J. 2000. Evidence for simultaneous protein interactions between human Rad51 paralogs. *J. Biol. Chem.* **275:** 16443–16449.

Shinohara, A. and Ogawa, T. 1998. Stimulation by Rad52 of yeast Rad51-mediated recombination. *Nature* **391:** 404–407.

Sigurdsson, S., Trujillo, K., Song, B., Stratton, S., and Sung, P. 2001. Basis for avid homologous DNA strand exchange by human Rad51 and RPA. *J. Biol. Chem.* **276:** 8798–8806.

Sugiyama, T., Zaitseva, E.M., and Kowalczykowski, S.C. 1997. A single-stranded DNA-binding protein is needed for efficient presynaptic complex formation by the *Saccharomyces cerevisiae* Rad51 protein. *J. Biol. Chem.* **272:** 7940–7945.

Sung, P. 1997a. Function of yeast Rad52 protein as a mediator between replication protein A and the Rad51 recombinase. *J. Biol. Chem.* **272:** 28194–28197.

———. 1997b. Yeast Rad55 and Rad57 proteins form a heterodimer that functions with replication protein A to promote DNA strand exchange by Rad51 recombinase. *Genes & Dev.* **11:** 1111–1121.

Sung, P. and Robberson, D.L. 1995. DNA strand exchange mediated by a RAD51-ssDNA nucleoprotein filament with polarity opposite to that of RecA. *Cell* **82:** 453–461.

Sung, P., Prakash, L., Matson, S.W., and Prakash, S. 1987. RAD3 protein of *Saccharomyces cerevisiae* is a DNA helicase. *Proc. Natl. Acad. Sci.* **84:** 8951–8955.

Sung, P., Trujillo, K., and Van Komen, S. 2000. Recombination factors of *Saccharomyces cerevisiae*. *Mutat. Res.* **451:** 257–275.

Takata, M., Sasaki, M.S., Sonoda, E., Fukushima, T., Morrison, C., Albala, J.S., Swagemakers, M.A., Kanaar, R., Thompson, L.H., and Takeda, S. 2000. The Rad51 paralog Rad51B promotes homologous recombinational repair. *Mol. Cell. Biol.* **20:** 6476–6482.

Takata, M., Sasaki, M.S., Tachiiri, S., Fukushima, T., Sonoda, E., Schild, D., Thompson, L.H., and Takeda, S. 2001. Chromosome instability and defective recombinational repair in knockout mutants of the five Rad51 paralogs. *Mol. Cell. Biol.* **21:** 2858–2866.

Thompson L.H. and Schild, D. 2001. Homologous recombinational repair of DNA ensures mammalian chromosome stability. *Mutat. Res.* **477:** 131–153.

Umezu, K., Chi, N.W., and Kolodner, R.D. 1993. Biochemical interaction of the *Escherichia coli* RecF, RecO, and RecR proteins with RecA protein and single-stranded DNA binding protein. *Proc. Natl. Acad. Sci.* **90:** 3875–3879.